Contents

CHAPTER 5

Acknowledgements

The author wishes to thank everyone who was so graciously helpful to me. Special mention goes to my promotor, Prof. Jannie Swarts, for his assistance, skilful guidance and special effort during the course of this study and the writing of this thesis. Thanks go to my co-promotor, Prof. Gert Lamprecht, for his guidance during this study and his assistance in reading this thesis.

My thanks to all the staff of the Department of Chemistry, who somehow or other contributed to the success of this study. In this regard I would like to make special mention of Prof. André Roodt.

My thanks to my family and friends for their motivation, sacrifice and support during the years of my study. A special word of thanks goes to my father, Hans Koorts, who read this thesis for language editing.

Soli deo gloria!

Jeanet Conradie

December 1999.

List of Abbreviations

Ligands

CO	carbonyl ligand or carbonmonoxide
cod	1,5-cyclooctadiene
Fc	ferrocene, *bis*(pentahaptocyclopentadienyl)iron, $[(\eta^5\text{-}C_5H_5)_2Fe]$
fc	ferrocenyl ligand
Fc^+	ferrocenium.
Hacac	2,4-pentanedione, acetylacetone
Hanmetha	4-methoxy-N-methylbenzothiohydroxamate
Hba	1-phenyl-1,3-butanedione, benzoylacetone
Hbfcm	1-ferrocenyl-3-phenylpropane-1,3-dione, benzoylferrocenoylmethane
Hbpha	N-benzoyl-N-phenyl-hydroxylamine
Hbzaa	3-benzyl-2,4-pentanedione, di-acetylbenzylmethane
Hcacsm	methyl(2-cyclohexylamino-1-cyclopentene-1-dithiocarboxylate)
Hcupf	N-hydroxy-N-nitroso-benzeneamine, cupferron
Hdbbtu	N,N-dibenzyl-N'-benzoylthiourea
Hdbm	1,3-diphenyl-1,3-propanedione, dibenzoylmethane
Hdfcm	1,3-diferrocenylpropane-1,3-dione, diferrocenoylmethane
Hdmavk	dimethylaminovinylketone
Hfca	1-ferrocenylbutane-1,3-dione, ferrocenoylacetone
Hfch	2-ferrocenoyl-etan-1-al, ferrocenoylaldehyde
Hfctca	1-ferrocenyl-4,4,4-trichlorobutane-1,3-dione, ferrocenoyltrichloroacetone
Hfctfa	1-ferrocenyl-4,4,4-trifluorobutane-1,3-dione, ferrocenoyltrifluoroacetone
Hhacsm	methyl(2-amino-1-cyclopentene-1-dithiocarboxylate)
Hhfaa	1,1,1,5,5,5-hexafluoro-2,4-pentanedione, hexafluoroacetylacetone
Hhpt	1-hydroxy-2-piridinethione
Hmacsm	methyl(2-methyl-amino-1-cyclopentene-1-dithiocarboxylate)
Hmnt	maleonitriledithiolate
Hneocup	N-nitroso-N-naphthylhydroxylamine, neocupferron
Hox	8-hydroxyquinoline, oxine
Hpic	2-picolinic acid
Hquin	2-carboxyquinoline
Hsacac	thioacetylacetone
Hsalnr	N-o-tolylsalicylaldimine
Hstsc	salicylaldehydethiosemicarbazose
Htfaa	1,1,1-trifluoro-2,4-pentanedione, trifluoroacetylacetone
Htfba	1,1,1-trifluoro-4-phenyl-2,4-butanedione, trifluorobenzoylacetone
Htfdma	1,1,1-trifluoro-5-methyl-2,4-hexanedione
Htfhd	1,1,1-trifluoro-2,4-hexanedione
Htftma	1,1,1-trifluoro-5,5-dimethyl-2,4-hexanedione
Htrop	tropolone
Htta	thenoyltrifluoroacetone, 2-thenoyltrifluoroacetonate
L, L'-BID	mono anionic bidentate ligand
L	one of two donor atoms of the bidentate ligand L,L'-BID
L'	the second donor atom of the bidentate ligand L,L'-BID
$P(OPh)_3$	triphenyl phosphite
phen	1,10-phenanthroline
PPh_3	triphenyl phosphine
PR_3	tertiary phosphine with substituents R

$P(OCH_2)_3CCH_3$

$$P \begin{cases} O-CH_2 \\ O-CH_2 \\ O-CH_2 \end{cases} C-CH_3$$
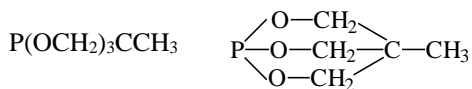
Solvents

DMF   dimethylformamide
DMSO   dimethylsulfoxide
THF   tetrahydrofuran

Groups

Bu n-buthyl
Cp   cyclopentadienyl, $(\pi\text{-}C_5H_5)$
Cy   cyclohexyl
Et   Ethyl
Et   ethyl
Pr^i isopropyl
Me   methyl
Ph   phenyl
$LiNPr^i_2$ lithium diisopropylamide

Other

A   absorbance
ε dielectric constant*
ε molar extinction coefficient*
ν_{CO} infrared stretching frequency of carbonyl
IR   infrared spectroscopy
NMR   nuclear magnetic resonance
pK_a $-\log[H^+]$, K_a = acid dissociation constant
T   temperature
UV   ultraviolet spectroscopy
χ_R group electronegativity of group R

* The same symbol is used for dielectric constant and molar extinction coefficient. The reader is asked to use the correct symbol in the contents of the paragraph.

Cyclic voltammetry.

CV   Cyclic voltammetry
NHE   normal hydrogen reference electrode
SCE   saturated calomel reference electrode
$E^{0'}$ formal electrode potential
ΔE_p separation of peak anodic and peak cathodic potentials
E_{pa} peak anodic potential
E_{pc} peak cathodic potential
i_{pa} peak anodic current
i_{pc} peak cathodic current
Fc   ferrocene
Fc^+ ferrocenium

1 Introduction

1.1   Co-ordination compounds in catalytic processes.

Of the platinum group transition metal complexes, complexes of rhodium and iridium are amongst the most often used as homogeneous catalysts. Hydroformylation and alcohol carbonylation are major industrial processes involving metal catalysts.[1] Each catalytic cycle is composed of several steps; the hydroformylation of C_2H_4 by $[HRh(CO)_2(PPh_3)_2]$ to liberate ethyl aldehyde, $C_2H_5(O)H$, can serve as an example:[1]

$[HRh(CO)_2(PPh_3)_2] + C_2H_4 \square [HRh(CO)_2(PPh_3)(C_2H_4)] + PPh_3$ **1**

$[HRh(CO)_2(PPh_3)(C_2H_4)] \square [C_2H_5Rh(CO)_2(PPh_3)]$ **2**

$[C_2H_5Rh(CO)_2(PPh_3)] + PPh_3 \square [C_2H_5Rh(CO)_2(PPh_3)_2]$ **3**

$[C_2H_5Rh(CO)_2(PPh_3)_2] \square [C_2H_5C(O)Rh(CO)(PPh_3)_2]$ **4**

$[C_2H_5C(O)Rh(CO)(PPh_3)_2] + H_2 \square [C_2H_5C(O)Rh(CO)(PPh_3)_2(H_2)]$ **5**

$[C_2H_5C(O)Rh(CO)(PPh_3)_2(H_2)] \rightarrow [HRh(CO)(PPh_3)_2] + C_2H_5C(O)H$ **6**

$[HRh(CO)(PPh_3)_2] + CO \square [HRh(CO)_2(PPh_3)_2]$ **7**
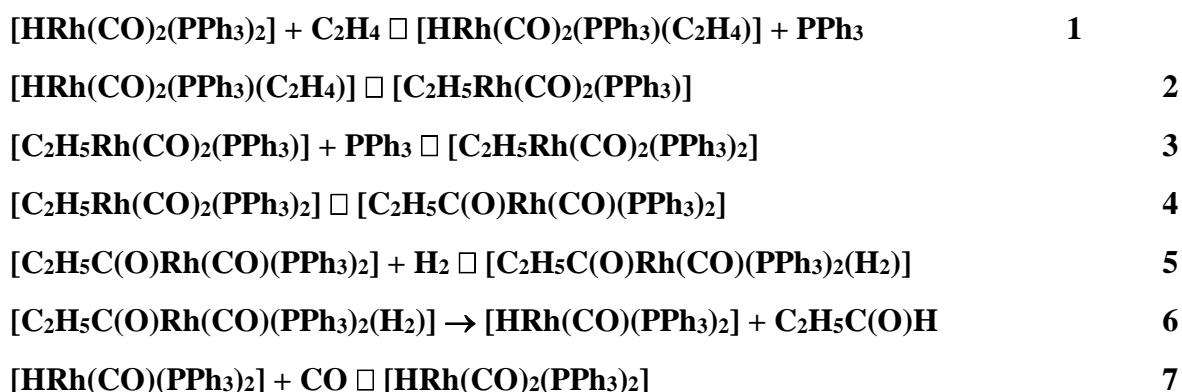
The above reactions may be classified as ligand addition to the sixteen electron metal complex (reactions 3 and 7), ligand substitution (reaction 1), insertion within the co-ordination sphere (reactions 2 and 4), oxidative addition (reaction 5) and reductive elimination (reaction 6). During catalysis, reactions such as 1 – 7 often occur so rapidly that they may not be individually observed. Thus, the importance of model complexes to demonstrate and study the individual steps of catalytic reactions is apparent. Towards this end, reactions 1, 2, 4 and 5 in the above sequence are all examples of general classes of reactions that were investigated kinetically during the course of this study (aims (iii) and (iv) on page 5).

---

[1] Atwood, J.D., *Coord. Chem. Rev.*, **83**, 93 (1988).

Other important processes involving organometallic compounds include:[2, 3, 4, 5]

(i)   Hydrogenation of olefins in the presence of complexes of low-valent transition metals such as rhodium (*e.g.* Wilkinson's catalyst [RhCl(PPh$_3$)$_3$]).

(ii)   Hydroformylation of olefins using a cobalt or rhodium catalyst (oxo process).

(iii)   Oxidation of olefins to aldehydes and ketones (Wacker process).

(iv)   Polymerisation of propylene using an organoaluminium-titanium catalyst (Ziegler-Natta catalyst) to give stereoregular polymers.

(v)   Olefin isomerization using nickel catalysts.

(vi)   Cyclooligomerisation of acetylenes using nickel catalysts (Reppe's or Wilke's catalysts).

(vii)   Carbonylation of methanol (rhodium(III) catalyst, Monsanto process).[6]

(viii) Carbonylation of methanol (iridium(III)-methanol catalyst, Cativa process).[7, 6]

The processes described above represents to a greater or lesser extent several of the fundamental reactions that transition metal complexes undergo, reactions such as oxidative addition, insertion, substitution and reductive elimination. Thus, a better understanding of catalytic cycles is primarily dependant on the study of these fundamental reactions utilising transition metal complexes that are as closely related as possible to those used in any particular catalytic reaction.

The rhodium and iodide-catalysed carbonylation of methanol to acetic acid is to date probably the most successful example of an industrial process catalysed by a metal complex in solution.[6] A survey estimated that in 1993 *ca.* 60% of the world production of acetic acid (*ca.* 5.5 million tonnes per year) was manufactured in this way.[8] **Scheme 1.1** illustrates the cycle for the [Rh(CO)$_2$I$_2$]$^-$ and iodide-catalysed carbonylation of methanol to acetic acid as well as for the [Ir(CO)$_2$I$_2$]$^-$ catalysed Cativa process.[6, 9, 10]

[2] Purcell, K.F. and Kotz, J.C., *Inorganic Chemistry,* W.B. Saunders Company, Philadelphia, 1977, p. 962 – 979.

[3] Halpern, J., *Inorg. Chim. Acta.,* **50**, 11 (1981).

[4] Cotton, F.A. and Wilkinson, G., *Advanced Inorganic Chemistry,* John Wiley & Sons, New York, 1988, Ch. 30.

[5] Herrmamm, W.A. and Cornils, B., *Angew. Chem. Int. Ed. Engl.,* **36**, 1048 (1997).

[6] Maitlis, P.M., Haynes, A., Sunley, G.J. and Howard, M.J., *J. Chem. Soc., Dalton Trans.,* 2187 (1996).

[7] Foster, D., *J. Chem. Soc., Dalton Trans.,* 1639, (1979).

[8] Howard, M.J., Jones, M.D., Roberts, M.S. and Taylor, S.A., *Catal. Today,* **18**, 325 (1993).

[9] Haynes, A., Mann, B.E., Gulliver, D.J., Morris, G.E. and Maitlis, P.M., *J. Am. Chem. Soc.,* **113**, 8567 (1991).

[10] Haynes, A., Mann, B.E., Morris, G.E. and Maitlis, P.M., *J. Am. Chem. Soc.,* **115**, 4093 (1993).
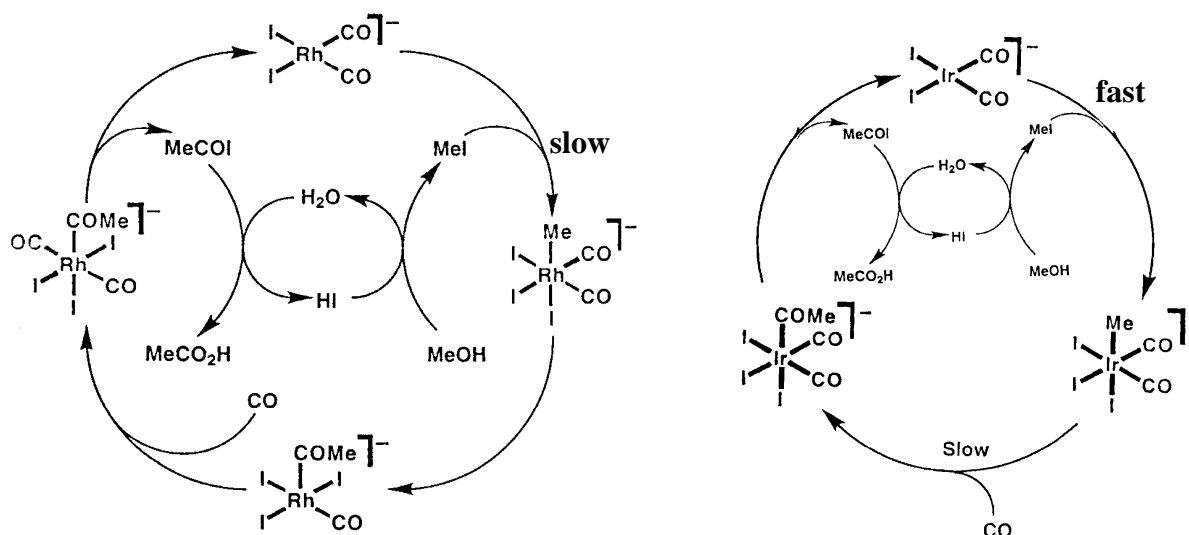
Scheme 1.1: Cycle for the [Rh(CO)$_2$I$_2$]$^-$ and iodide-catalysed carbonylation of methanol to yield acetic acid, left, and the corresponding [Ir(CO)$_2$I$_2$]$^-$ process on the right.[6]

The rate-determining step in the rhodium-iodide catalysed reaction is the oxidative addition of methyl iodide to [Rh(CO)$_2$I$_2$]$^-$. In contrast, during iridium-catalysed carbonylation, CO insertion in [MeIr(CO)$_2$I$_3$]$^-$ to give [(MeCO)Ir(CO)$_2$I$_3$]$^-$ is rate determining. Model studies show that while k_{Rh}/k_{Ir} is *ca.* 1/150 for the oxidative addition, it is *ca.* 10^5-10^6 / 1 for migratory CO insertions. CO insertions in iridium complexes can be substantially accelerated by adding small amounts of methanol (*e.g.* 1% v/v).[11] The iridium-methanol catalysed process has several advantages over the existing rhodium process including higher catalyst solubility and stability. They can also tolerate a wide range of process compositions and they allow higher rates of reactions than rhodium complexes. Not surprisingly, they have already been implemented industrially.[12]

1.2 Transition metals in medical applications.

Ferrocene {*bis*(η^5cyclopentadienyl)iron or [(η^5-C$_5$H$_5$)$_2$Fe]} and its derivatives have been the subject of many different studies because of their use as colour pigments,[13] high burning rate catalysts[14] in solid fuels, liquid fuel combustion catalysts,[15] smoke suppressant additives[16] and as

[11] Pearson, J.M., Haynes, A., Morris, G.E., Sunley, G.J. and Maitlis, P.M., *J. Chem. Soc., Chem. Comm.,* 1045 (1995).

[12] Ellis, P.R., *Platinum Metals Rev.,* **41**, 8 (1997).

[13] Nesmeyanov, A.N. and Kotchetkova, N.S., *Russ. Chem. Rev.,* **43**, 710 (1974).

[14] Tompa, A.S., *Thermochim. Acta,* **77**, 133 (1984).

antineoplastic agents in cancer treatment.[17, 18] Good-to-excellent cure rates against Erlich ascite murine tumour lines were determined for certain ferricenium salts. Some of these ferricenium salts showed favourable 50% lethal dosage (LD_{50}) values compared to the well known chemotherapeutic agent, *cisplatin* [*cis*-diamminedichloroplatinum(II)].

The unexpected discovery of the antitumor activity of *cisplatin* has opened up the 'era of inorganic cytostatics'.[17] It has stimulated a broad search for other inorganic or organometallic compounds with antitumor activity and initiated a series of developments. In the search for new organometallic compounds or inorganic coordination complexes with antitumor properties, it was found that some rhodium(I) and iridium(I) complexes showed antineoplastic activity comparable to or ever better than that of *cisplatin*.[19] In particular, [Rh(acac)(cod)] (acetylacetonate-1,5-cyclooctadienerhodium(I)), showed activities comparable with that of *cis*platin against Ehrlich ascite carcinomas but histological damage, in contrast to what was found for cisplatin, was virtually absent.[20]

To combat the negative aspects, such as the inability to distinguish between healthy and cancerous cells, surrounding *cisplatin* and other chemotherapeutic drugs, new antineoplastic materials are continuously being synthesised and evaluated. New methods of delivering an active drug to cancerous growths are being developed and combination therapy has been investigated in the hope of finding synergistic effects. Experiments involving the combination of ferricenium tetrachloroferrate and *cisplatin* showed the combination of the effects of the drugs to be additive.[18] Tests involving combinations of platinum complexes and other chemotherapeutic drugs showed unexpected synergistic activity, *i. e.* therapeutic effects better than adding the individual effects of each component in the drug mixture, during the treatment of mice with advanced L1210 leukemia.[21] Since the ferrocene containing rhodium(I) chelates obtained in this

[15] Chittawadgi, B.S. and Voinof, A.N., *Indian J. Technol.*, **6**, 83 (1968).

[16] Neuse, E.W., Woodhouse, J.R., Montaudo, G. and Puglisi, C., *Appl. Organomet. Chem.,* **2**, 53 (1988).

[17] Köpf-Maier, P., Köpf, H. and Neuse, E.W., *J. Cancer Res. Clin. Oncol.*, **108**, 336 (1984).

[18] Neuse, E.W. and Kanzawa, *Appl. Organomet. Chem.*, **4**, 19 (1990).

[19] Sava, G., Zorzet, S., Perissin, L., Mestroni, G., Zassinovich, G. and Bontempi, A., *Inorg. Chim. Acta*, **137**, 69 (1987).

[20] Giraldi, T., Sava, G., Bertoli, G., Mestroni, G. and Zassinovich, G., *Cancer Res.*, **37**, 2662 (1977).

[21] (i) Gale, G.R., Atkins, L.M. and Meischen, S.J., *Cancer Treat Rep.*, **61**, 445 (1977).

study are constructed from more than one antineoplastic moiety, rhodium and ferrocene, within the same molecule, they hold the promise of displaying synergistic effects in chemotherapy without the need of administering two or more types of antineoplastic drugs simultaneously to a tumour-bearing mammal.

1.3 Aims of this study.

With this background the following goals were set for this study:

(i) The optimised synthesis and characterisation of new β-diketonate rhodium(I) and iridium(I) complexes of the type [Rh(FcCOCHCOR)(CO)$_2$], [Rh(FcCOCHCOR)(CO)(PPh$_3$)] and [Ir(FcCOCHCOR)(cod)], with Fc = ferrocenyl and R = alkyl or aromatic groups.

(ii) The use of X-ray crystallography to determine the molecular structure of selected synthesised complexes.

(iii) The determination of a general mechanism for the oxidative addition of MeI to [Rh(FcCOCHCOR)(CO)(PPh$_3$)] complexes by means of detailed kinetic studies utilising UV, IR, ^{1}H NMR and ^{31}P NMR techniques. Results of this part of the study can serve as kinetic models for reactions 2,4 and 5 on page 1 and the first two steps in **Scheme 1.1**.

(iv) The determination of a mechanism for the substitution of FcCOCHCOR ligands with 1,10-phenantroline from [M(FcCOCHCOR)(cod)] complexes by means of stopped flow kinetic techniques, M = Rh or Ir. These results may be used as a kinetic model for substitution reactions involving bidentate ligands.

(v) An electrochemical study utilising cyclic voltammetry and bulk electrolysis to determine the formal oxidation potentials of the electrochemical irreversible co-ordinated rhodium and iridium ions, as well as of the formal reduction potentials of the iron core of the ferrocenyl fragment in the β-diketonate ligand for all the complexes synthesised.

(vi) The determination of the relationships between the physical quantities rate constants, reduction potentials, pK$_a$-values, group electronegativities, IR stretching frequencies, NMR data and crystallographic bond lengths.

(ii) Gale, G.R., Atkins, L.M., Meischen, S.J. and Schwartz, P., *Cancer,* **41**, 1230 (1978).

2 Literature survey and fundamental aspects.

2.1 Stereochemical and electronic aspects of square planar complexes of Rh(I) and Ir(I).

2.1.1 The basic bonding structure of Rh(I) and Ir(I) square planar complexes.

Rh and Ir are transition metals with respective electron configurations $[Kr]4d^85s^1$ and $[Xe]4f^{14}5d^76s^2$. A characteristic feature of transition metal atoms is their ability to form complexes with a variety of neutral ligands such as carbon monoxide, substituted phosphines (PR_3), arsines, stibines, nitric oxide, and various molecules with delocalized π orbitals, such as pyridine, 2,2'-bipyridine and 1,10-phenanthroline.[1] In many of these complexes, the metal atoms are in low-positive, zero or even negative formal oxidation states. It is a characteristic feature of the above mentioned ligands that they stabilize low oxidation states. Stabilizing of metals in low oxidation states is associated with the fact that these ligands have vacant π* orbitals in addition to lone-pair electrons. Vacant π* orbitals accept electron density from filled metal orbitals to form a π bond that supplements the σ bond arising from lone-pair donation. High electron density on the metal atom can thus be delocalized into the empty π* orbitals of the ligands, also called π acid ligands.

This study is concerned with:

a) square planar complexes of Rh(I) of general formula [Rh(β-diketonato)(CO)(PPh₃)] where PPh₃ = triphenyl phosphine,

b) square planar complexes of Rh(I) of the general formula [Rh(β-diketonato)(cod)] where cod = 1,5-cyclo-octadiene and

c) square planar complexes of Ir(I) of the general formula [Ir(β-diketonato)(cod)].

---

[1] Cotton, F.A. and Wilkinson, G., *Basic Inorganic Chemistry,* John Wiley & Sons, New York, 1976, p. 473 – 480.

The carbonyl ligand serves well to explain the bonding characteristics of π acid ligands. The metal-carbon bond consists of the following:[1, 2, 3]

(a)   A filled σ orbital of the carbonyl ligand that overlaps with an empty dsp^2 orbital (σ type orbital) of the metal (**Figure 2.1**(a)).

(b)   An overlap of a filled d orbital of the metal with an empty π* orbital of the carbonyl ligand which represents a flow of electron density from the metal to the carbonyl, a process called back bonding (**Figure 2.1**(b)).

The result of this two-way electron flow is a mutual strengthening of the CO-to-M σ bond and the M-to-CO π bond to produce a M-CO bond stronger than the sum of the two bonds acting individually (known as a synergistic effect).[4]
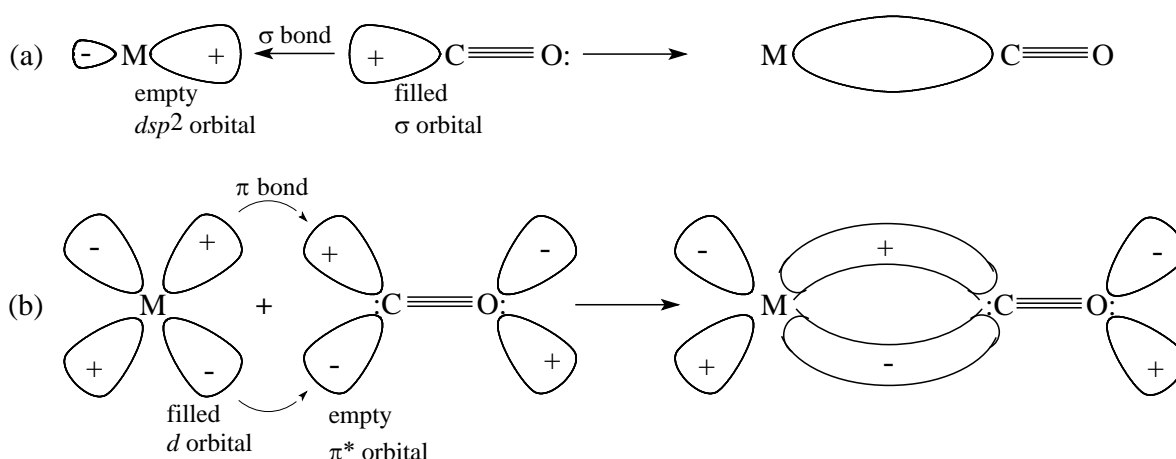
Figure 2.1:   **The molecular orbital view of carbon metal bonding:**
(a)   Formation of carbon → metal σ bond using an unshared pair on the C atom.
(b)   Formation of metal → carbon π bond. The other orbitals on the CO are omitted for clarity. (The direction of electron flow is indicated by the direction of the arrow.)

According to the preceding description of M-CO bonding, the influence of additional ligands simultaneously coordinated to M on the components of the M-C≡O bond may theoretically be summarised as follows: increased electron density on the metal centre of a square planar complex containing a carbonyl ligand would imply more electron donating capability from the metal d- orbital into the π* orbital of the carbonyl ligand. As the extent of back donating from M to

---

[2] Gerloch, M. and Constable, E.C., *Transition Metal Chemistry,* Weinheim, New York, 1994, p. 122.

[3] Mathey, F. and Sevin, A., *Molecular Chemistry of the Transition Elements,* John Wiley & Sons, Chichester, 1996, p15.

[4] Purcell, K.F. and Kotz, J.C., *Inorganic Chemistry,* W.B. Saunders Company, Philadelphia, 1977, p.861.

CO increases, the M-C bond becomes stronger (shorter bond length) and the C-O bond of the carbonyl should become weaker. In practice the C-O bond lengths are very slightly influenced by the electron density on M, but M-C bonds in selective compounds are appreciably shortened consistent with the π bonding concept[1]. The bonding between a metal and C=C double bond (alkenes eg. ethylene or cod) is illustrated in **Figure 2.2**. The bonding consists of the following two independent components:[2, 5, 6]

(a)   The donation of the π electron density of the double bond of C=C to the vacant σ type acceptor orbital on the metal atom (**Figure 2.2**(a)).

(b)   A back bond resulting from a flow of electron density from filled metal d_{xz} or other $d\pi$-$p\pi$ hybrid orbitals into the empty π^* antibonding orbital of the carbon atoms (**Figure 2.2**(b)).

(a)   (b)
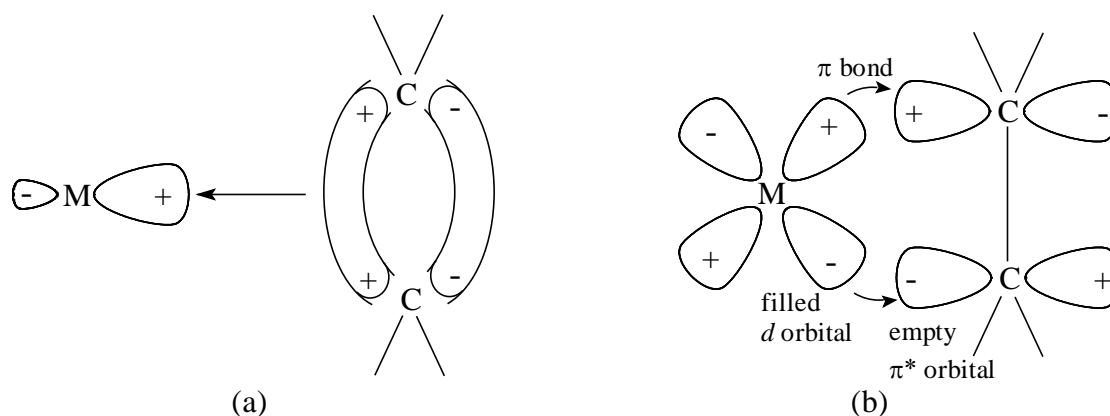
Figure 2.2: The molecular orbital view of alkene metal bonding. The direction of electron flow is indicated by the direction of the arrow.
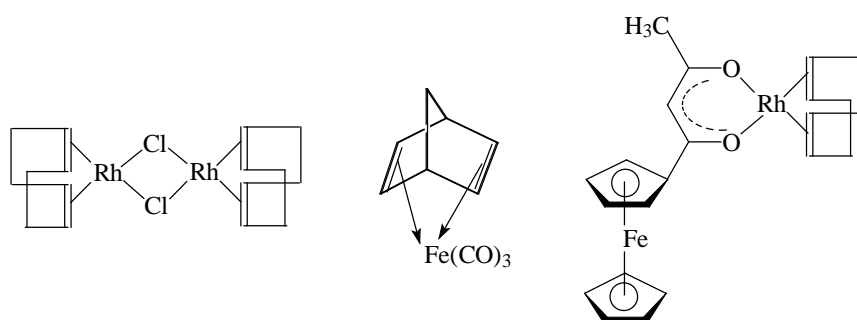
Figure 2.3: Alkenes with unconjugated double bonds form independent linkages to the metal atom.

[5] Cotton, F.A. and Wilkinson, G., *Basic Inorganic Chemistry,* John Wiley & Sons, New York, 1976, p. 514.

[6] Purcell, K.F. and Kotz, J.C., *Inorganic Chemistry,* W.B. Saunders Company, Philadelphia, 1977, p. 866-876.

The bond between M and C=C is thus similar to the bonding of M to C=O and implies the retention of an appreciable "double bond" character in the alkene. Alkenes with unconjugated double bonds can form independent linkages to the metal atom. Representative complexes of cod and norbornadiene are shown in **Figure 2.3**.

2.1.2 *Influence of electron density manipulation on the metal centre on the infrared vibrational spectra of metal carbonyls*.[1]

Infrared vibrational spectra (IR) are widely used in the study of metal carbonyls since stretching frequencies of CO are strong sharp absorption bands well separated from other vibrational modes of any other ligands that may also be present. In this discussion the position of infrared absorption will be referred to as infrared stretching frequencies, expressed in cm^{-1}.

The CO molecule has an infrared stretching frequency (ν_{CO}) of 2143 cm^{-1}. Terminal CO groups in neutral metal carbonyl complexes are found in the range 2125 to 1850 cm^{-1}. The lowering in the obtained stretching frequency when moving from molecular CO to coordinative CO is associated with a reduction in CO bond order. Increased electron density on the metal centre results in lower CO infrared stretching frequencies (see **Table 2.1**): the infrared frequency for $Cr(CO)_6$ is *ca*. 2000 cm^{-1} (exact values vary with phase and solvent), whereas, when three CO's are replaced by amine groups which have no ability to back-accept electron density as in $Cr(CO)_3(dien)$, (dien = $NH(CH_2CH_2NH_2)_2$) two infrared CO stretching modes with frequencies of *ca*. 1900 and 1760 cm^{-1} are observed. Similarly, for the anionic species $V(CO)_6^-$, which contains a very high electron density on the metal atom, a band is found at *ca*. 1860 cm^{-1}. This band is shifted 140 cm^{-1} compared to the one found at *ca*. 2000 cm^{-1} in neutral $Cr(CO)_6$. For the cationic species $Mn(CO)_6^+$ with a relative low electron density on the metal, the CO stretching frequency is found at *ca*. 2090 cm^{-1}.

In complexes of the type $[Rh(R_1COCHCOR_2)(CO)(PPh_3)]$ ($R_1COCHCOR_2$ = β-diketonato ligand with substituents R_1 and R_2) and $[Rh(R_1COCHCOR_2)(CH_3)(I)(CO)(PPh_3)]$, the infrared CO stretching frequency ν_{CO} also increased as R_1 and R_2 were replaced by more electron

withdrawing groups[7], see **Table 2.2**. (The group electronegativity χ_R of CH_3 and CF_3 is 2.34 and 3.01 (Gordy scale) respectively.[8])

Table 2.1: **Illustration of increased electron density on the metal centre (from top to bottom in table) resulting in lower CO infrared stretching frequencies:**[1]

complex	ν_{CO} / cm^{-1}	complex	ν_{CO} / cm^{-1}
$Mn(CO)_6^+$	~2090	$Mn(CO)_3(dien)^+$	~2020 and ~1900
$Cr(CO)_6$	~2000	$Cr(CO)_3(dien)$	~1900 and ~1760
$V(CO)_6^-$,	~1860	-	-

Table 2.2: Infrared carbonyl stretching frequencies, ν_{CO}, in 1,2 dichloroethane of rhodium complexes[7].

Substituents		ν_{CO} / cm^{-1}	
R_1	R_2	[$Rh^I(R_1COCHCOR_2)(CO)(PPh_3)$]	[$Rh^{III}(R_1COCHCOR_2)(CH_3)(I)(CO)(PPh_3)$]
CF_3	CF_3	2000	2070
CF_3	CH_3	1996	2062
CH_3	CH_3	1988	2045

2.1.3   *The influence of tertiary phosphines on metal-carbonyl bonding.*

2.1.3.1 Electronic effect of tertiary phosphines.[9 – 15]

The electronic effect is a result of electron withdrawing or electron donating properties of atoms or groups (*e.g.* CF_3) *via* chemical bonds. Compounds of trivalent phosphorous (*e.g.* PPh_3) with electron configuration $[Ne]3s^2$ can form complexes with transition metals.[9,10] A σ bond is formed by the donation of the electron pair from the phosphorous atom to the metal and a π bond by back-acceptance from a filled metal *d* orbital to an empty phosphorous 3*d* orbital.

---

[7] Basson, S.S., Leipoldt, J.G., and Nel, J.T., *Inorg. Chim. Acta,* **84**, 167 (1984).

[8] du Plessis, W.C., Erasmus, J.J.C., Lamprecht, G.J., Conradie, J., Cameron, T.S., Aquino, M.A.S. and Swarts, J.C., *Can. J. Chem.*, **77**, 1 (1999).

[9] Cotton, F.A. and Wilkinson, G., *Basic Inorganic Chemistry,* John Wiley & Sons, New York, 1976, p. 489.

[10] Emsley, J. and Hall, D., *The Chemistry of Phosphorous,* Harper & Row Publishers, London, 178 (1976).
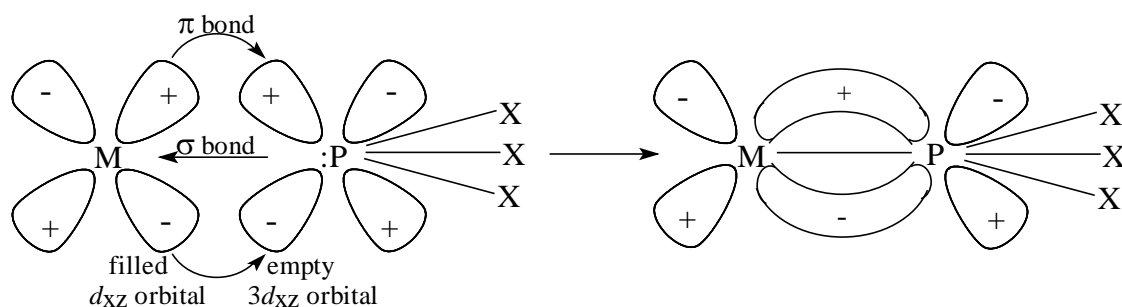
Figure 2.4: **The molecular orbital view of tertiary phosphine metal bonding. The direction of electron flow is indicated by the direction of the arrow.**

In the case where tertiary phosphines ($PX_1X_2X_3$ with groups X_1, X_2 and X_3) are ligands in transition metal complexes, their electron donating capabilities will determine the electron density on the metal and this will have an effect on other possible ligands such as CO. The effect of tertiary phosphines with different electron donating-acceptor capabilities was illustrated by Tolman[11], measuring the CO stretching frequency ν_{CO} of a carbonyl group *trans* to the tertiary phosphines in 70 complexes of Ni(0) with the formula $[Ni(CO)_3(PX_3)]$ (**Table 2.3**). The almost constant increase in CO stretching frequency by successive replacement of one substituent of phosphorus by another, made it possibile to assign to each substituent on the phosphorus a contribution χ_i to the CO stretching frequency given by the ligand:

For any $[Ni(CO)_3(PX_1X_2X_3)]$: $\qquad \nu_{CO} = 2056.1 + \sum_{i=1}^{3} \chi_i$ cm^{-1}

There is an excellent correlation between Tolman's substituent parameter χ_i (based on the CO stretching frequencies) and Kabachnik's σ value[12] (a parameter based on the electronic effect of groups attached to phosphorus, on the phosphorus), as well as the pK_a's of the phosphonium ions. The latter correlations prevails a method for determining electron donor-acceptor properties of the triply substituted phosphorus ligands $PX_1X_2X_3$ from the ν_{CO} of $[Ni(CO)_3(PX_1X_2X_3)]$.

---

[11] Tolman, C.A., *J. Am. Chem. Soc.,* **92,** 2953 (1970).

[12] Kabachnik, M.I., *Dokl. Akad. Nauk. USSR.,* **110**, 393 (1956); *Proc. Acad. Sci. USSR, Chem. Sect.,* **110**, 577 (1956).

Table 2.3: The relation between CO stretching frequencies, ν_{CO},[11] Tolman's substituent parameter χ_i[11] and pK$_a$ values of phosphonium ions[13] in 0.05 M solutions of [Ni(CO)$_3$(PX$_3$)] in CH$_2$Cl$_2$.

Tertiary phosphine ligand	ν_{CO} /cm^{-1}	χ_i/cm^{-1} of X	pK$_a$	Tertiary phosphine ligand	ν_{CO} /cm^{-1}	χ_i/cm^{-1} of X	pK$_a$
P(*t*-Bu)$_3$	2056.1	0.0	11.40	P(*p*-F-Ph)$_3$	2071.3	5.0	1.97
PCy$_3$	2056.4	0.1	9.65	P(*p*-Cl-Ph)$_3$	2072.8	5.6	1.03
PMe$_3$	2064.1	2.6	8.65	P(OMe)$_3$	2079.8	7.7	-
P(*p*-MeO-Ph)$_3$	2066.1	3.4	4.57	PH$_3$	2083.2	8.3	-
P(*p*-Me-Ph)$_3$	2066.7	3.5	3.84	P(OPh)$_3$	2085.3	9.7	
P(*m*-Me-Ph)$_3$	2067.2	3.7	3.30	PCl$_3$	2097.0	14.8	-
PPh$_3$	2068.9	4.3	2.73	PF$_3$	2110.8	18.2	-

In general, groups (X in PX$_3$) with better electron donating capability will increase the Lewis basicity of tertiary phosphines PX$_3$, thereby increasing the pK$_a$ of the phosphines[13]. This has been well illustrated by Allmann and Goel[14] for a series of triaryl- and trialkylphosphines (see **Table 2.4**). The measured pK$_a$'s correlate well with Kabachnik's σ value[12], Tolmann's χ_i parameters[11] (and therefore with ν of the [Ni(CO)$_3$(PX$_3$)] complexes) as well as with the lone-pair ionisation potentials for members of a series of similar phosphines. Since pK$_a$ therefore can directly be linked to the electron donating properties of the group attached to P, **Table 2.4** gives a rough estimate of the electron donating capabilities of the X group attached to P. This should be:

(most electron donating) *t*-Bu > Cy > *p*-(Me)$_2$NPh > *p*-MeO-Ph > *p*-Me-Ph > *m*-Me-Ph

> *o*-Me-Ph > Ph > *p*-F-Ph > *p*-Cl-Ph (least electron donating)

More electron donating substituents on P are expected to give a shorter M-P bond length because they put more phosphorous *s* character into the bond (implying the M-P bond strengthens). This is clearly shown by the 0.075 Å contraction (2.481 to 2.406 Å) in the Mo-P distance on going from [*trans*-CpMo(CO)$_2$PPh$_3$][15] to [*trans*-CpMo(CO)$_2$[P(OMe)$_3$]][16]. OMe is a poorer electron donor than Ph, based on ν_{CO} of [Ni(CO)$_3$(PR$_3$)], **Table 2.3**.

[13] Wilkinson, G., *Comprehensive Coordination Chemistry,* Pergamon Press, New York, 1987, vol 2, p. 1030.

[14] Allmann, T. and Goel, R.G., *Can. J. Chem.,* **60,** 716 (1982).

[15] Bush, M.A., Hardy, A.D.U., Manojlovic-Muir, Lj. and Sim, G.A. *J. Chem. Soc. A,* 1003 (1971).

[16] Hardy, A.D.U., and Sim, G.A.., *J. Chem. Soc., Dalton Trans.,* 1900 (1972).

Table 2.4: **Basicities of tertiary phosphines**[14].

Tertiary phosphines	pK$_a$	Tertiary phosphines	pK$_a$
P(*t*-Bu)$_3$	11.40	P(*m*-Me-Ph)$_3$	3.30
PCy$_3$	9.65	P(*o*-Me-Ph)$_3$	3.08
P(*p*-(Me)$_2$-N-Ph)$_3$	8.65	PPh$_3$	2.73
P(*p*-MeO-Ph)$_3$	4.57	P(*p*-F-Ph)$_3$	1.97
P(*p*-Me-Ph)$_3$	3.84	P(*p*-Cl-Ph)$_3$	1.03

2.1.3.2 Steric effect of substituents X in tertiary phosphines PX$_3$.[17 – 20]

The steric effect in a molecule is the result of forces (usually non-bonding) between parts of a molecule, for example changing from P(*p*-Me-Ph)$_3$ to the more bulky P(*o*-Me-Ph)$_3$. Tolman[17] defined the cone angle θ for tertiary phosphines as a parameter of their bulkiness. The steric parameter θ for symmetrical ligands (all three X-groups the same) is the apex angle of a cylindrical cone, centered 2.28 Å from the centre of the P atom, which just touches the van der Waals radii of the outermost atoms of the model, **Figure 2.5**(a). For values of θ over 180°, measurements may be made by trigonometry. An effective cone angle for unsymmetrical ligands PX$_1$X$_2$X$_3$ (Xi = substituents on tertiary phosphine PX$_1$X$_2$X$_3$) can be calculated by:[18]

$$\theta = \frac{2}{3}\sum_{i=1}^{3}\frac{\theta_i}{2}$$
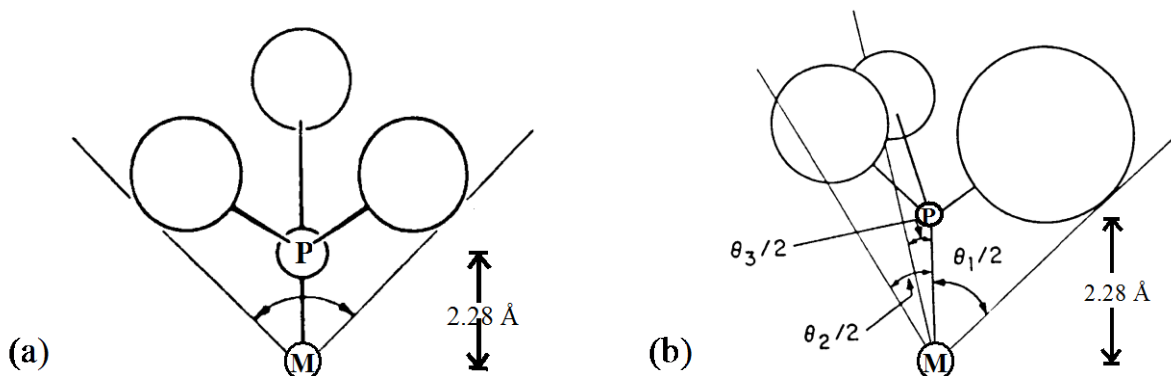
Figure 2.5: **(a) Cone angle θ for symmetrical tertiary phosphines (M = metal). (b) Method of measuring cone angles of unsymmetrical ligands of a tertiary phosphine PX$_1$X$_2$X$_3$.**

[17] Tolman, C.A., C*hem. Rev,* **77,** 313 (1977).

[18] Tolman, C.A., Seidel, W.C., and Gosser, L.W., *J. Am. Chem. Soc.,* **96,** 53 (1974).

The role of the steric effect is evident in **Table 2.5** where the Co-P bond length increases in order of ligand size, not electron-acceptance character.[17]

Table 2.5: Steric effect on Co-P bond lengths[17] (d = bond length, θ = cone angle of tertiary phosphine).

Compound	d(Co-P)/Å	θ[19]
CpNi(μ-CO)$_2$Co(CO)$_2$PEt$_3$	2.236(1)	132
CpNi(μ-CO)$_2$Co(CO)$_2$P(p-C$_6$H$_4$F)$_3$	2.242(3)	145
π-MeC$_5$H$_4$Ni(μ-CO)$_2$Co(CO)$_2$PPh$_2$Cy	2.269(2)	153

It is important to realize that steric effects can have electronic consequences and *vice versa*. For example, increasing the angles between the X-groups of the phosphine will decrease the percentage of the *s* character in the phosphorous lone electron pair,[17] making them less available for strong bonds. Changing the electron donating properties of the atoms can also affect bond distances and angles.[20] Thus electronic and steric effects are intimately related and difficult to separate. A practical and useful separation can be made through the parameters ν and θ.[17]

2.1.4 Bidentate ligands in Rh(I)-complexes.

2.1.4.1 The *trans*-influence.[21 – 26]

The thermodynamic *trans*-influence[21] is a ground state phenomenon, which can be defined as the ability of a ligand to weaken the metal-ligand bond *trans* to it. This means that certain ligands give rise to substitution of ligands *trans* to it by weakening the metal-ligand bond *trans* to it. The *trans*-influence of a wide variety of ligands has been "measured" with techniques such as X-ray crystallography, IR, NMR, nuclear quadrupole resonance, photoelectron and Mössbauer spectroscopy.[22, 23] For example, consider the Pt-Cl bond length in the following [PtCl$_3$L] complexes:[24]

---

[19] Wilkinson, G., *Comprehensive Coordination Chemistry,* Pergamon Press, New York, 1987, vol 2, p. 1017.

[20] Bent, H.A., C*hem. Rev,* **61,** 275 (1961).

[21] Pidcock, A., Richards, R.E. and Venanzi, L.M., *J. Chem. Soc.,* **A,** 1707 (1966).

[22] Bancroft, G.M. and Butler, K.D., *J. Am. Chem. Soc.,* **96,** 7208 (1974).
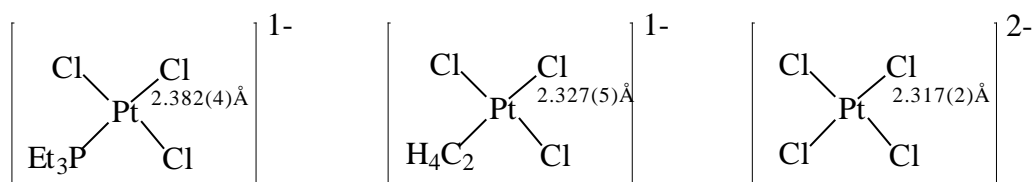
Scheme 2.1: **Illustration of thermodynamic *trans*-influence by measuring the metal-ligand bond length of a common ligand, here Cl⁻, trans to a series of ligands, here PEt₃, C₂H₄ and Cl.**

The decrease in Pt-Cl bond length implies an increase in bond strength illustrating the decrease of *trans*-influence in the order:

(largest *trans*-influence) PR_3 > alkene ≈ Cl^- (smallest *trans*-influence)

Based on more extensive data, the thermodynamic *trans*-influence order obtained from structure determinations has been given as:[25]

(largest *trans*-influence) σ-R ≈ H^- ≥ carbenes ≈ PR_3 > AsR_3 >

CO ≈ RNC ≈ $C=C$ ≈ Cl^- ≈ NH_3 (smallest *trans*-influence)

(a)   (b)
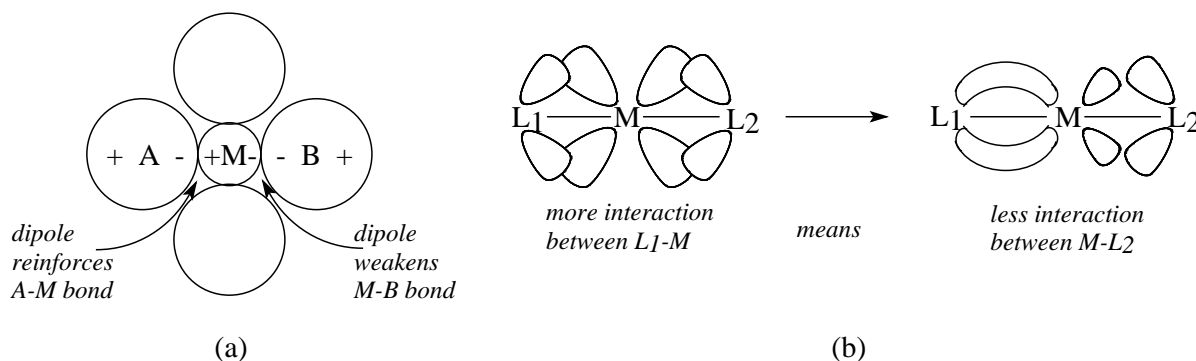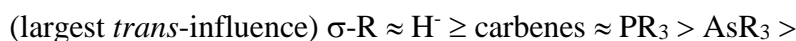
Figure 2.6: **(a) The polarisation theory of Grinberg and (b) the static π bond theory to explain the thermodynamic *trans*-influence.**

Grinberg[26] proposed that the thermodynamic *trans*-influence was purely electrostatic (polarisation theory). A strong dipole interaction between a ligand and the central metal atom would tend to weaken the attachment of the ligand *trans* to it by a mis-match of dipoles

[23] Langford, C.H. and Gray, H.B., *Ligand Substitution Processes,* W.A. Benjamin Inc., New York (1965).

[24] Bushnell, G.W., Pidcock, A. and Smith, M.A.R., *J. Chem. Soc. Dalton,* 572 (1975).

[25] Purcell K.F. and Kotz, J.C., *Inorganic Chemistry,* W.B. Saunders Company, Philadelphia, p 700 - 708 (1977).

[26] Grinberg, A.A., *Acta Physiochim,* USSR, **3**, 573 (1935).

(**Figure 2.6** (a)). A second theory is the static π bonding theory,[27] which is based on the competition between *trans*-ligands for the same *d*-orbital. Unequal utilization of these metal *d*-orbitals will lead to decreased availability to form a metal-ligand π bond from one side of the metal to the other. (See **Figure 2.6** (b).)

2.1.4.2 The *trans*- and *cis*-effect.[25 – 30]

Where the *trans*-influence discussed in paragraph 2.1.4.1 is a thermodynamically based phenomenon, the *trans*-effect is a kinetic phenomenon and is defined as the effect of a coordinated ligand on the substitution rate of the ligand opposite to it.[28] The order of ligands to exert the *trans*-effect depends on two factors: a) the *trans*-influence (i.e. the effect of the group on the strength of the metal-ligand bond *trans* to itself) and b) the stabilisation of the trigonal bipyramidal transition state which is commonly found in substitution reactions in square planar complexes of Pt(I), Rh(I) and Ir(I).[29] The *cis*-effect is similar in origin to the *trans*-effect, but when quantified is found to be a much smaller effect than the *trans*-effect.[25] For example,[30] consider the *trans*-effect in the substitution reaction

$$[PtClL(PEt_3)_2] + \text{pyridine} \,\square\, [PtL(py)(PEt_3)_2]^+ + Cl^-$$

of **Scheme 2.2** (L = T) *versus* the *cis*-effect in the reaction of **Scheme 2.3** (L = C). In **Scheme 2.2** different ligands T are arranged in relative order from largest *trans* effect to smallest *trans* effect by comparing the rate of substitution of the ligand *trans* to T expressed relatively to the rate of substitution as influences by T = Cl (in ethanol at 25°C). Rate constants, expressed as the ratio k(T)/k(Cl), are given in brackets after each T (T = ligand exerting the *trans* effect). In **Scheme 2.3** ligands C are arranged in relative order from largest *cis* effect to smallest *cis* effect by comparing the rate of substitution of the ligand *cis* to C expressed relatively to the rate of substitution as influences by C = Cl (in ethanol at 0°C). Rate constants, expressed as the ratio

---

[27] Emsley, J. and Hall, D., *The Chemistry of Phosphorous,* Harper & Row Publishers, London, 199 (1976).

[28] Cotton, F.A. and Wilkinson, G., *Basic Inorganic Chemistry,* John Wiley & Sons, New York, 1976, p. 151.

[29] Amstrong, D.R., Fortune, R. and Perkins, P.G., *Inorg. Chim. Acta, 9*, 9 (1974).

[30] Basolo, F., Chatt, J., Gray, H.B., Pearson R.G. and Shaw, B.L., *J. Chem. Soc.,* 2207 (1961).

k(C)/k(Cl), are given in brackets after each C (C = ligand exerting the *cis* effect). Both σ and π-electronic effects are important in explaining the kinetic *trans*-effect.[23]

$$\text{Et}_3\text{P}\underset{\text{T}}{\overset{\text{Cl}}{\diagdown}}\text{Pt}\underset{\text{PEt}_3}{\diagup} + \text{ pyridine} \xrightarrow{\text{EtOH}} \left[\ \text{Et}_3\text{P}\overset{N}{\diagdown}\text{Pt}\diagup \text{PEt}_3\ \right]^+ + \ \text{Cl}^-$$

(largest *trans*-effect) T = H⁻ (>10⁴) > CH₃⁻ (170)

> C₆H₅⁻ (40) > Cl⁻ (1) (smallest *trans*-effect)
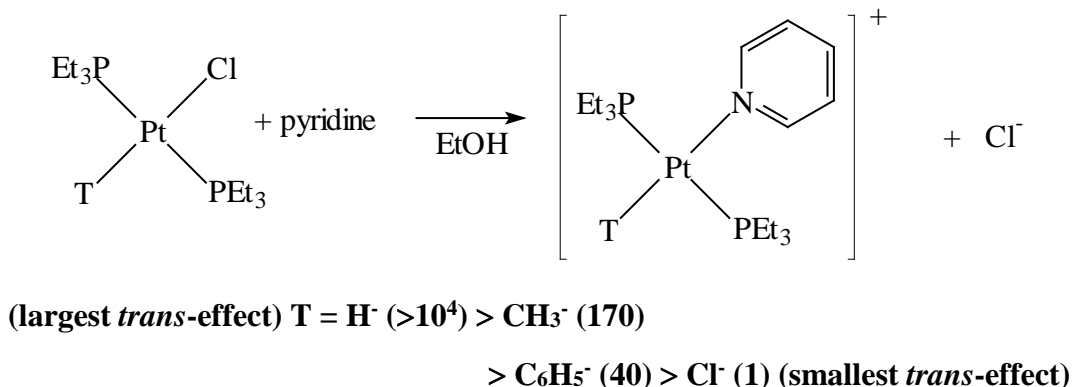
Scheme 2.2: Illustration of *trans*-effect by measuring the kinetic substitution rate. T = ligand exerting the *trans* effect. Rate constants, expressed as the ratio k(T)/k(Cl), are given in brackets after each T.

$$\text{Et}_3\text{P}\underset{\text{Et}_3\text{P}}{\overset{\text{Cl}}{\diagdown}}\text{Pt}\underset{\text{C}}{\diagup} + \text{ pyridine} \xrightarrow{\text{EtOH}} \left[\ \text{Et}_3\text{P}\overset{N}{\diagdown}\text{Pt}\diagup \text{C}\ \right]^+ + \ \text{Cl}^-$$

(largest *cis*-effect) C = CH₃⁻ (3.6) > C₆H₅⁻ (2.3) > Cl⁻ (1) (smallest *cis*-effect)
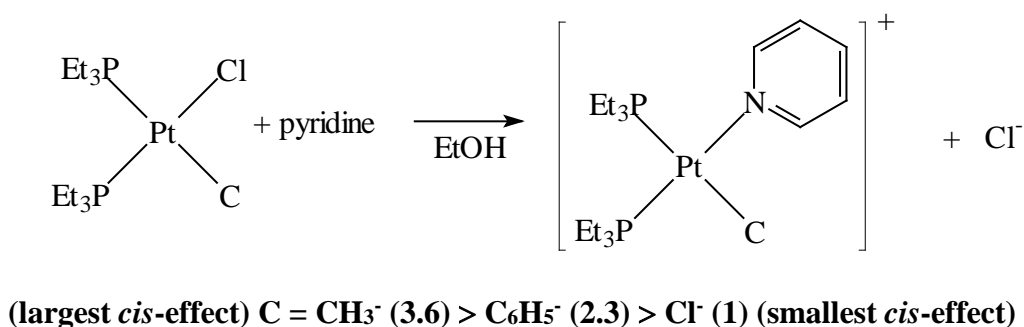
Scheme 2.3: Illustration of *cis*-effect by measuring the kinetic substitution rate. C = ligand exerting the *cis* effect. Rate constants, expressed as the ratio k(C)/k(Cl), are given in brackets after each C.

(i)   *The σ trans-effect.*

Of the four metal valence orbitals involved in strong σ bonding in a square planar complex, only the *p* orbitals have *trans* directional properties. That is, the *trans* group and the leaving group must share the same *p* orbital. If the *trans* group has a particularly strong σ interaction with the *p* orbital, the bond to the leaving group may be relatively weaker. The driving force is then to provide more *p* orbital overlap to the *trans* group by moving the leaving group out of the region of strong overlap while the entering group moves in as shown schematically in **Figure 2.7**. The available p_z orbital is used to help attach both the entering group and the leaving group to the central metal in the five-coordinate transition state. Since the entering and the leaving groups now share the available p_z orbital, the *trans* group owns much more than one-half of the p_z orbital in the transition state. This means that the difference in the energies of the ground state and the

transitional states should be relatively small for good $\sigma \rightarrow$ metal(p) donor ligands. The high *trans*-effects of H⁻, PR₃, Me⁻, -SCN⁻ and I⁻ are due to large σ *trans*-effect contributions.
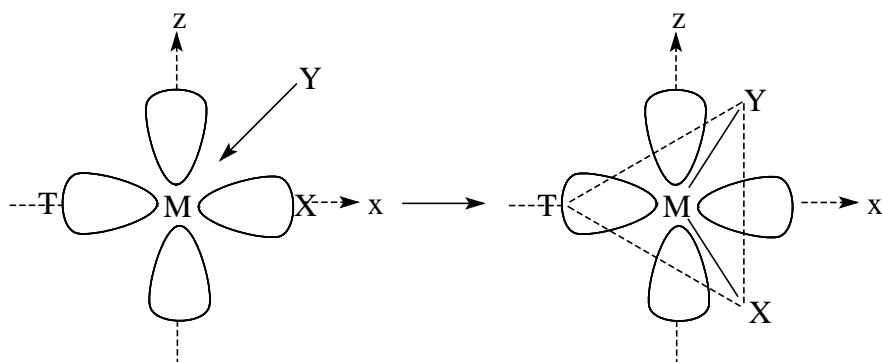
Figure 2.7: Change in the metal p_σ orbital structure in square planar substitution reaction of X with Y illustrating the σ *trans*-effect.

(ii)   *The π trans-effect.*

In a square planar complex three d orbitals have proper symmetries for π interaction, namely d_{xy}, d_{xz}, and d_{yz}. For the purpose of this discussion, we assume that the coordinate system is as shown in **Figure 2.8**. The d_{xz} orbital is shared by the *trans* ligand, T, and the leaving ligand, L.
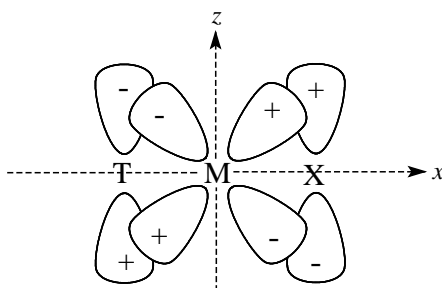
Figure 2.8: π interaction of the *trans* d_{xz} orbital with the *trans* (T) and leaving (L) groups illustrating the π *trans*-effect.

On the formation of the trigonal bipyramid the four d orbitals namely d_{xy}, d_{xz}, d_{yz} and $d_{x^2-y^2}$ are of the right symmetries for π interaction. It is significant that all these orbitals are shared in π interaction with the ligands in the trigonal plane, namely the *trans* group, the entering group and the leaving group. Thus the trigonal-bipyramidal transitional state is greatly stabilised if the *trans* group possesses empty, reasonably stable, π symmetry orbitals, since an interaction of empty ligand π orbitals with the filled metal $d(\pi^*)$ orbitals delocalizes electronic charge to the *trans* ligand and lowers the energy of the system. In simple terms, the *trans* ligand helps to accommodate the excess electronic charge added to the central metal by the entering ligand.

Thus the effect of a good π acceptor *trans* group is to lower the over-all activation energy which we call the π *trans*-effect. Ligands that are very high in π *trans*-effect are CO, CN$^-$ and
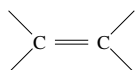
2.1.4.3 The *trans*-influence of bidentate ligands.

Bonati and Wilkinson[31] first prepared compounds of the type [Rh(L,L'-BID)(CO)$_2$] (L,L'-BID = mono anionic bidentate ligand with donor atoms L and L'). They showed that the carbonyl groups could be replaced by olefins, and in part by triphenylphosphine (PPh$_3$) and -arsine (AsPh$_3$). This characteristic makes it possible to study the relative thermodynamic *trans*-influence of the bonding atoms in bidentate ligands[32], since it was assumed that the carbonyl group *trans* to the donor atom with the largest *trans*-influence will be substituted by the PPh$_3$ ligand, resulting in a complex with the general formula [Rh(L,L'-BID)(CO)(PPh$_3$)]:
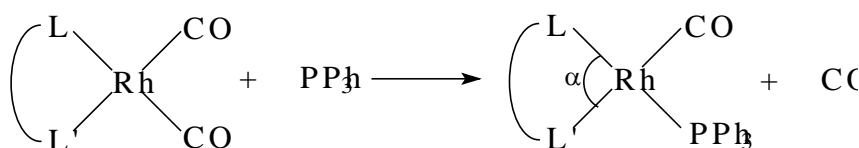
Scheme 2.4: The CO group *trans* to the donor group with the largest *trans*-influence is substituted by the PPh$_3$ ligand. L has a larger *trans*-influence than L' in the above example. α = bite angle.

In general, the *trans*-influence of bidentate ligands in compounds of the type [Rh(L,L'-BID)(CO)(PPh$_3$)] (see **Scheme 2.4**) is a function of at least the following three variables:

(i)   The relative influence of PPh$_3$ and CO on the bidentate ligand L,L'-BID.

(ii)   The relative influence of the donor atoms L and L' of the L,L'-BID on the Rh-P bond length.

(iii)   The influence of the bite angle α of bidentate ligand L-Rh-L' (see **Scheme 2.4**) on the Rh-P bond length.

---

[31] Bonati, F. and Wilkinson, G., *J. Chem. Soc.,* 3156 (1964).

[32] Graham, D.E., Lamprecht, G.J., Potgieter, I.M., Roodt, A. and Leipoldt, J.G., *Transition Met. Chem.,* **16**, 193 (1991).

For [Rh(L,L'-BID)(CO)$_2$] complexes with symmetrical L,L'-BID ligands such as deprotonated 2,4-pentanedione[33] (acac or acetylacetonato), deprotonated di-asetylbenzylmethane[34] (bzaa or 3-benzyl-2,4-pentanedionato), tropolone[35] (trop) and deprotonated dibenzoylmethane[36] (dbm or 1,3-diphenyl-1,3-propanedionato), the two carbonyl groups are chemically equivalent and substitution of any one of the two with PPh$_3$ (**Scheme 2.4**), will yield the same isomer, see **Figure 2.9**. The different Rh-O bond lengths in the resulting complexes [Rh(L,L-BID)(CO)(PPh$_3$)] were determined very accurately by crystallographic methods. In all these cases the Rh-O bond length *trans* to PPh$_3$ was larger than the Rh-O bond length *cis* to PPh$_3$, illustrating the larger *trans*-influence of PPh$_3$ compared with a carbonyl group (see **Table 2.6**).
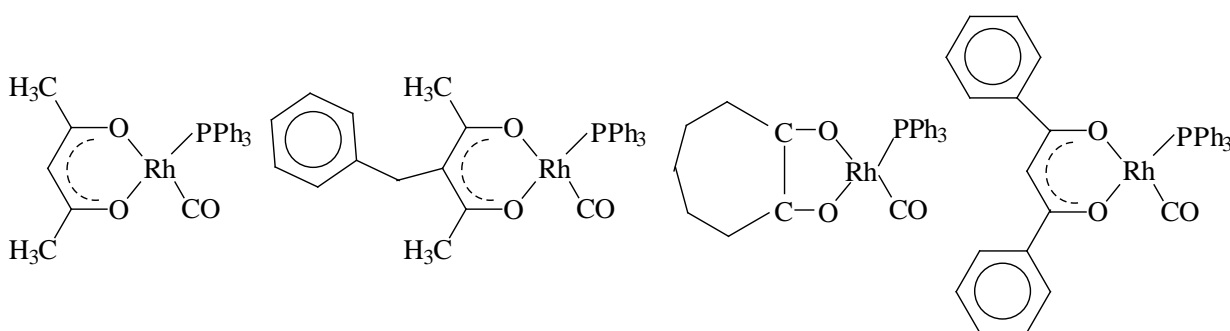
Figure 2.9: Structures of [Rh(acac)(CO)(PPh$_3$)][33], [Rh(bzaa)(CO)(PPh$_3$)][34], [Rh(trop)(CO)(PPh$_3$)][35] and [Rh(dbm)(CO)(PPh$_3$)][36].

Table 2.6: Selected bond lengths of some [Rh(L,L-BID)(CO)(PPh$_3$)] complexes with symmetrical L,L-BID, illustrating the larger *trans*-influence of PPh$_3$ compared with a carbonyl group on L,L-BID.[33 - 36]

L,L-BID	bond length of Rh-O *trans* to PPh$_3$/Å	bond length of Rh-O *trans* to CO/Å
acac	2.087(4)	2.029(5)
bzaa	2.048(2)	2.016(2)
trop	2.081(7)	2.034(7)
dbm	2.081(9)	2.038(10)

In the case where the L,L'-BID ligand is unsymmetrical, the resulting [Rh(L,L'-BID)(CO)(PPh$_3$)] complex after substitution of one of the CO groups in [Rh(L,L'-BID)(CO)$_2$] by PPh$_3$

[33] Leipoldt, J.G., Basson, S.S., Bok, L.D.C. and Gerber, T.I.A., *Inorg. Chim. Acta,* **26**, L35 (1978).

[34] Roodt, A., Leipoldt J.G., Swarts, J.C. and Steyn, G.J.J., *Acta Cryst.,* **C48**, 547 (1992).

[35] Leipoldt, J.G., Bok, L.D.C., Basson, S.S. and Meyer, H., *Inorg. Chim. Acta,* **42**, 105 (1980).

[36] Lamprecht, D., Lamprecht, G.J., Botha, J.M., Umakoshi, K. and Sasaki, Y., *Acta Cryst.,* **C53**, 1403 (1997).

(**Scheme 2.4**) has been used to study the relative *trans*-influence of the donor atom in different L,L'-BID ligands, using the Rh-P bond distance as an indication of the relative *trans*-influence of the donor atom *trans* to PPh$_3$.[32, 37 - 42, 44 - 55] For the purpose of this discussion, the following two general cases are to be dealt with:

(a)   L,L'-BID ligand is unsymmetrical because of different substituents, but L = L' = O (data in **Table 2.7** page 25 with structures as in **Figure 2.11** and **Figure 2.12**)

(b)   L,L'-BID ligand is unsymmetrical, with different L, L' atoms, i.e. N and O, S and O or S and N (data in **Table 2.8** page 27 with the structures as in **Figure 2.14** page 26).

An example of an unsymmetrical L,L'-BID with L = L' = O (case (a)) is the ligand tta in the complex [Rh(tta)(CO)(PPh$_3$)] (Htta = thenoyltrifluoroacetone) illustrated in **Figure 2.10**. The L,L'-BID is unsymmetrical because of the terminal substituents CF$_3$ and C$_4$H$_3$S on the L,L'-BID. The substituents CF$_3$ and C$_4$H$_3$S exert a different electronic influence on the two carbonyl groups CO1 and CO2 respectively because of the different electron donating properties of CF$_3$ and C$_4$H$_3$S. The result of the different electronic influence on the two carbonyl groups is that O1 and O2 have a different *trans* influence in the metal complex.
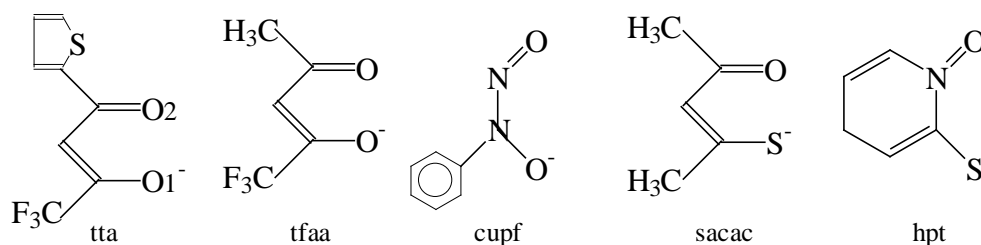
Figure 2.10: **Examples of unsymmetrical monoanionic bidentate ligands L,L'-BID with (a) L = L' = O *e.g.* tta, tfaa and cupf, and (b) L ≠ L' (L and L' = O, S, or N) *e.g.* sacac and hpt.**

In case (a) (L,L'-BID ligand is unsymmetrical, L = L' = O) the carbonyl ligand *trans* to the oxygen atom with the largest *trans* influence should be substituted by PPh$_3$ (**Scheme 2.4** page 19).

$$[Rh(L,L'\text{-BID})(CO)_2] + PPh_3 \rightarrow [Rh(L,L'\text{-BID})(CO)(PPh_3)] + CO$$
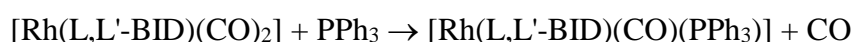
Consider the structures of $[Rh(tta)(CO)(PPh_3)]$[37] (Htta = thenoyltrifluoroacetone), $[Rh(bpha)(CO)(PPh_3)]$[38] (Hbpha = N-benzoyl-N-phenyl-hydroxylamine) and $[Rh(cupf)(CO)(PPh_3)]$[39] (Hcupf = N-hydroxy-N-nitroso-benzeneamine) shown in **Figure 2.11**.
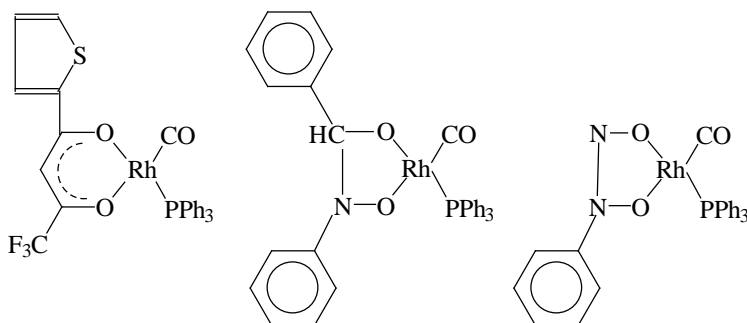
Figure 2.11: Structures of $[Rh(tta)(CO)(PPh_3)]$[37], $[Rh(bpha)(CO)(PPh_3)]$[38] and $[Rh(cupf)(CO)(PPh_3)]$[39].

These results indicate that the oxygen atom nearest to an electron attracting group of the chelate ring, such as CF_3, has the smallest *trans* influence. This is in agreement with the polarisation theory[26] and the σ-*trans* effect[23], since the oxygen nearest to the CF_3 group will be the least polarizable and a weaker σ-donor as a result of the electron attraction by the CF_3 group. In the case of $[Rh(tfaa)(CO)(P(p\text{-}Cl\text{-}Ph)_3)]$[40] (Htfaa = 1,1,1-trifluoro-2,4-pentanedione) where one CO-group has been replaced by the tertiary phosphine $P(p\text{-}Cl\text{-}Ph)_3$, the expected isomer was also formed with $P(p\text{-}Cl\text{-}Ph)_3$ *trans* to the oxygen atom (nearest to the CH_3 group) with the largest *trans* influence.

Steric factors sometimes dominate the above mentioned electronic *trans*-influence. This was found in the crystal structure determinations of $[Rh(tfhd)(CO)(PPh_3)]$,[40] $[Rh(tfdma)(CO)(PPh_3)]$[41] and $[Rh(tftma)(CO)(PPh_3)]$,[42] (Htfhd = 1,1,1-trifluoro-2,4-hexanedione; Htfdma = 1,1,1-trifluoro-5-methyl-2,4-hexanedione; Htftma = 1,1,1-trifluoro-5,5-dimethyl-2,4-hexanedione). The CO ligand *trans* to the oxygen atom nearest to the CF_3 group

[37] Leipoldt, J.G., Bok, L.D.C., van Vollenhoven, J.S. and Pieterse, A.I., *J. Inorg. Nucl. Chem.,* **40**, 61 (1978).

[38] Leipoldt, J.G. and Grobler, E.C., *Inorg. Chim. Acta,* **60** 141 (1982).

[39] Basson, S.S., Leipoldt, J.G., Roodt, A. and Venter, J.A., *Inorg. Chim. Acta,* **118**, L45 (1986).

[40] Steynberg, E.C., Lamprecht, G.J. and Leipoldt, J.G., *Inorg. Chim. Acta,* **133**, 33 (1987).

[41] Leipoldt, J.G., Basson, S.S., and Nel, J.T., *Inorg. Chim. Acta,* **74**, 85 (1983).

[42] Leipoldt, J.G., Basson, S.S., and Potgieter, J.H., *Inorg. Chim. Acta,* **117**, L3 (1986).

was substituted by PPh₃, although the group closer to the other oxygen still has the better electron donating power compared to the CF₃ group, see **Figure 2.12**.
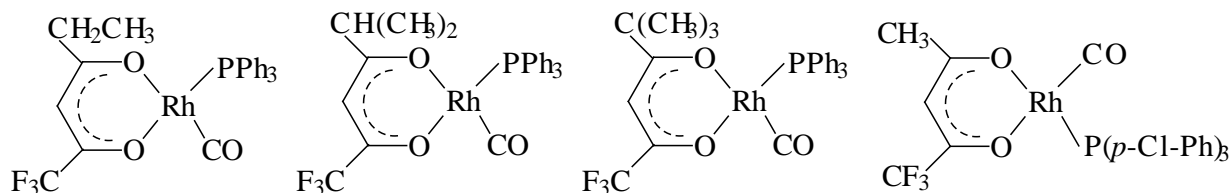
Figure 2.12: Structures of [Rh(tfhd)(CO)(PPh₃)][40], [Rh(tfdma)(CO)(PPh₃)][41], [Rh(tftma)(CO)(PPh₃)][42] and [Rh(tfaa)(CO)(P(*p*-Cl-Ph)₃)].[40]

Above substitution pattern were explained by considering the structure of the the transition state during the course of the substitution reaction:[40]

Reaction 2.1:   [Rh(L,L'-BID)(CO)₂] + PPh₃ → [Rh(L,L'-BID)(CO)(PPh₃)] +CO

A kinetic study of the substitution of the CO ligands in [Rh(L,L'-BID)(CO)₂] with cod (1,5-cyclooctadiene) where L,L'-BID = β-diketonato, indicated an associative mechanism.[43] Such square planar substitution reactions involve a trigonal bipyramidal transition state wherein the entering ligand (PPh₃ in the case of **Reaction 2.1**), the leaving group (CO) and the group *trans* to the leaving group (oxygen) occupy the same trigonal plane of the trigonal bipyramid, with the other two remaining ligands in the apical positions.[23] If the expected isomers, according to electronic considerations, were to be formed, the oxygen nearest to the sterically hindered groups (-CH₂CH₃, -CH(CH₃)₂ and –C(CH₃)₃), the leaving CO and the incoming PPh₃ ligand would have to share the limited space of the trigonal plane, resulting in a relative unstable intermediate. It is thus more likely that the other isomer, with PPh₃, CO and oxygen nearest to the less bulky CF₃ group in the trigonal plane will be formed. **Figure 2.13** gives a schematic presentation of the trigonal bipyramidal transition state of the associative mechanism of the substitution of the carbonyl group in [Rh(tftma)(CO)₂] by PPh₃ illustrating the larger steric interaction expected between the PPh₃ and Buᵗ if the expected isomers according to electronic considerations were to be formed (structure B in **Figure 2.13**). (See paragraph 2.2.4.2 (ii) and **Scheme 2.27** on page 76 for a discussion on the associative mechanism of square planar substitution reactions.) The

structure of $[Rh(tfaa)(CO)(P(p\text{-}Cl\text{-}Ph)_3)]$[40] indicated that the expected isomer according to electronic considerations was formed with $P(p\text{-}Cl\text{-}Ph)_3$ *trans* to the oxygen atom (the oxygen atom nearest to the relative small CH_3 group) with the largest *trans* influence and *cis* to the oxygen atom nearest to a more electron attracting group of the chelate ring CF_3 (**Figure 2.12**).
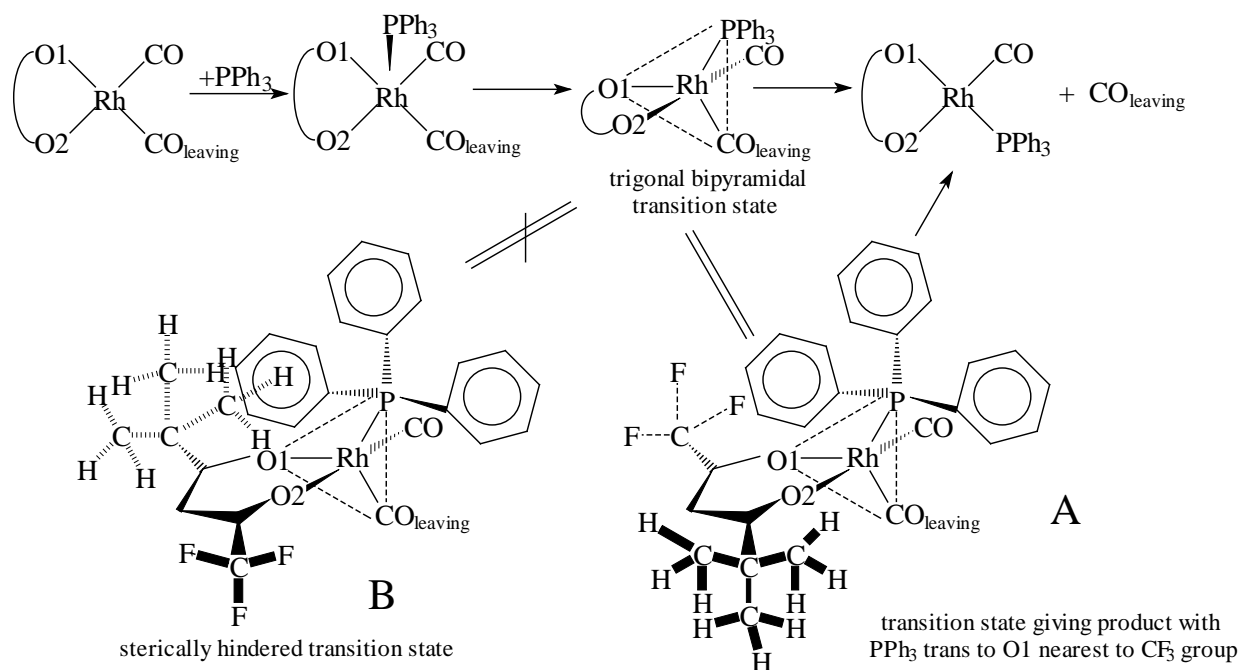
Figure 2.13: Schematic presentation of the trigonal bipyramidal transition state of the associative mechanism of the substitution of the carbonyl group in $[Rh(tftma)(CO)_2]$ by PPh_3. The trigonal bipyramidal transition state, TBP, is expexted to have the structure A with the tertiary butyl group Bu^t above the trigonal plane and far away from the PPh_3 substituents. Transition state B is not expected because of the larger steric interaction expected between the PPh_3 and Bu^t which are here either completely below the trigonal plane (Bu^t) or partially below the trigonal plane (the tetrahedrically PPh_3 group). H-atoms on the phenyl groups are omitted for clarity but in B they enhance steric interaction.

Table 2.7 gives a summary of selected crystallographic data for complexes $[Rh(L,L'\text{-}BID)(CO)(PPh_3)]$ containing L,L'-BID ligands with L = L' = O. L' is the oxygen atom nearest to the strongest electron attracting group of the chelate ring and is expected to show the smallest *trans* influence in the absence of steric factors. Substitution labeled by T (*trans* L and *cis* to L') represents the expected isomer for CO substitution by PPh_3 from $[Rh(L,L'\text{-}BID)(CO)_2]$.

[43] Leipoldt, J.G., Basson, S.S., Schlebusch, J.J.J. and Grobler, E.C., *Inorg. Chim. Acta,* **62**, 113 (1982).

Table 2.7: **Selected crystallographic data for complexes [Rh(L,L'-BID)(CO)(PPh₃)] containing L,L'-BID ligands with donor atom L = L' = O. L' is the oxygen atom nearest to the strongest electron attracting group of the chelate ring. The structures of these complexes is given in Figure 2.9, Figure 2.11, Figure 2.12 and Figure 2.16.**

L,L'-BID	Ring-size	Bite angle /degree	PPh₃ *trans* or *cis* to L	Rh-P distance /(Å)	L,L'-BID	Ring-size	Bite angle /degree	PPh₃ *trans* or *cis* to L	Rh-P distance /(Å)
dbm	6	88.5	equivalent	2.237(7)[36]	tftma	6	88.1	C	2.238(3)[42]
acac	6	87.9	equivalent	2.244(2)[33]	ba	6	88.1, 86.2	T, C	2.249(3), 2.248(3) [44]
bzaa	6	86.8	equivalent	2.243(1)[34]	bpha	5	78.4	T	2.232(2)[38]
tta	6	87.5	T	2.245(3)[37]	trop	5	77.8	equivalent	2.232(2)[35]
tfhd	6	87.5(4)	C	2.252(3)[40]	cupf	5	76.6	T	2.232(2)[39]
tfdma	6	87.5	C	2.239(2)[41]	tfaa[a]	6	88.9(2)	T	2.231(3)[40]

a) data for P(*p*-Cl-Ph)₃ complex

Complexes of the type [Rh(L,L'-BID)(CO)(PPh₃)] containing L,L'-BID ligands with different L, L' donor atoms, i.e. N and O, S and O or S and N will now be considered. This type of complexes is summarised in **Table 2.8** ((case (b) mentioned on page 21) with structures as in **Figure 2.14**.

The order of increasing electronegativity (in brackets after each donor atom) of the donor atoms is S (2.4) < N (3.1) < O (3.5)[45] which is the inverse order of the expected *trans* influence of the donor atoms according to electronic considerations. The more electronegative donor atom L' is expected to have the smallest *trans* influence. Substitutions labeled by T represents the expected isomer for CO substitution by PPh₃ *trans* to L (the donor atom with the smallest electronegativity and the largest *trans* influence) from [Rh(L,L'-BID)(CO)₂].

The crystallographic data from **Table 2.8** reveals the expected decreasing order of the *trans* influence of the donor atoms: S > N > O for all complexes except for [Rh(macsm)(CO)(PPh₃)] and [Rh(cacsm)(CO)(PPh₃)]. (Hmacsm = methyl(2-methyl-amino-1-cyclopentene-1-dithiocarboxylate) and Hcacsm = methyl(2-cyclohexylamino-1-cyclopentene-1-dithiocarboxylate)). The unexpected substitution pattern (according to the electronic *trans*-influence) of the [Rh(macsm)(CO)(PPh₃)] and [Rh(cacsm)(CO)(PPh₃)] complexes was explained

---

[44] Purcell. W., Basson, S.S., Leipoldt, J.G., Roodt, A. and Preston, H. *Inorg. Chim. Acta,* **234**, 153 (1995).

[45] Purcell, K.F. and Kotz, J.C., *Inorganic Chemistry,* W.B. Saunders Company, Philadelphia, 1977, p.59.

by the much larger steric demand of the methyl and cyclohexyl groups on the donor nitrogen atom in the macsm and cacsm ligands respectively, since it is expected that the trigonal bipyramidal transitional state with the sulphur in the apical position would be much more stable (less steric interaction with PPh$_3$) than the nitrogen side of the macsm and cacsm ligands.[55]
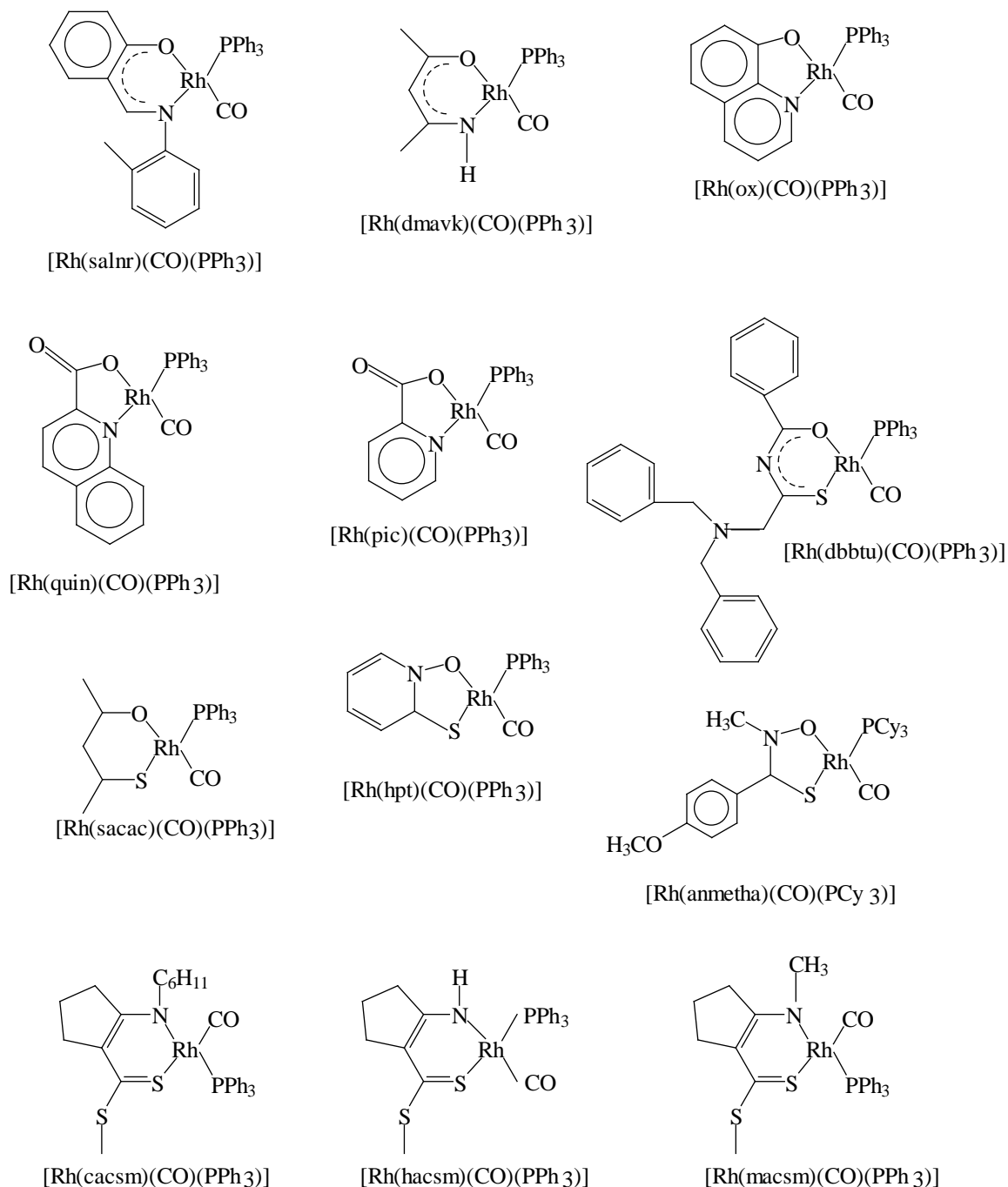
Figure 2.14: Structures of complexes [Rh(L,L'-BID)(CO)(PPh$_3$)], with L,L'-BID = salnr[46] dmavk,[47] ox,[48] quin,[32] pic,[49] dbbtu,[52] sacac,[50] hpt,[51] anmetha,[51] cacsm,[53] hacsm[54] and macsm.[55]

Table 2.8: Selected crystallographic data for complexes [Rh(L,L'-BID)(CO)(PPh₃)] containing L,L'-BID ligands with different donor atoms L and L' = O, N and S. L' is more electronegative than L.

L,L'-BID	L, L'	Ring-size	Bite angle /degree	PPh₃ *trans* (T) or *cis* (C) to L	Rh-P distance/(Å)
salnr	N, O	6	88.7	T	2.281(2)[46]
dmavk	N, O	6	87.4	T	2.275(1)[47]
ox	N, O	5	80.0	T	2.261(2)[48]
quin	N, O	5	78.9	T	2.258(2)[32]
pic	N, O	5	78.9	T	2.262(2)[49]
sacac	S, O	6	91.7	T	2.300(2)[50]
hpt	S, O	5	83.9	T	2.278(1)[51]
dbbtu	S, O	6	90.11(2)	T	2.282(1)[52]
cacsm	S, N	6	93.5	C	2.268(1)[53]
hacsm	S, N	6	91.32(11)	T	2.283(1)[54]
macsm	S, N	6	93.8	C	2.269(1)[55]
anmetha[a]	S, O	5	83.4(1)	T	2.290(1)[51]

a) data for PCy₃ complex

Consider the average Rh-P bond lengths of the different groups of [Rh(L,L'-BID)(CO)(PPh₃)] complexes in **Table 2.9** obtained from the crystallographic data in **Table 2.7**[33 – 42, 44] and **Table 2.8**[32, 46 – 55]. The definite lengthening in the average Rh-P bond length in the order O < N < S confirms the increasing order of the *trans* influence of the donor atoms: O < N < S in complexes of the type [Rh(L,L'-BID)(CO)(PPh₃)].

[46] Leipoldt, J.G., Basson, S.S., Grobler, E.C.and Roodt, A., *Inorg. Chim. Acta,* **99**, 13 (1985).

[47] Damoense, L.J., Purcell, W., Roodt, A. and Leipoldt, J.G., *Rhodium Ex.,* **5**, 10 (1994).

[48] Leipoldt, J.G., Basson, S.S. and Dennis, C.R., *Inorg. Chim. Acta,* **50**, 121 (1981).

[49] Leipoldt, J.G., Lamprecht, G.J. and Graham, D.E., *Inorg. Chim. Acta,* **101**, 123 (1985).

[50] Botha, L.J., Basson, S.S. and Leipoldt, *Inorg. Chim. Acta,* **126**, 25 (1987).

[51] Preston, H., *"Specific isomer formation and oxidative addition behavior of rhodium(I)thiolato complexes"*, *Ph.D. Thesis*, University of the Orange Free State, R.S.A., 1993.

[52] Roodt, A., Leipoldt, J.G., Koch, K.R. and Matoetoe, M., *Rhodium Ex.,* **7-8**, 39 (1994).

[53] Steyn, G.J.J., Roodt, A., Poletaeva, I. and Varshavsky, Y.S., *J. Organomet. Chem.,* **536**, 197 (1997).

[54] Steyn, G.J.J., *"Mechanistic study of Nitrogen/Sulphur Donor Atom Bidentate Ligand Influence on the Iodomethane Oxidative Addition to Carbonylphosphinerhodium(I) Complexes", Ph.D. Thesis*, University of the Orange Free State, R.S.A., 1994.

[55] Steyn, G.J.J., Roodt, A. and Leipoldt, J.G., *Inorg. Chem.,* **31**, 3477 (1992).

Table 2.9: Average Rh-P bond lengths in complexes of the type [Rh(L,L'-BID)(CO)(PPh₃)].

Donor atom L (L' = O)	Electronegativity of L	Rh-P bond lengths / Å	
		Five-membered chelate ring	**Six-membered chelate ring**
O	3.5	2.232(2)	2.244(2)
N	3.1	2.260(2)	2.278(2)
S	2.4	2.278(1)	2.291(2)

The influence of the size of the chelate ring on the *trans* influence of the donor atom in the ring was seen by considering the average Rh-P bond lengths of the different groups of [Rh(L,L'-BID)(CO)(PPh₃)] complexes in **Table 2.9**. A definite lengthening of the Rh-P bond was observed from five- to six-membered chelate rings for all three different donor atom entries in **Table 2.9**. The smaller bite angle of a five-membered chelate ring, 79,2°, (average for the 7 structures with a five-membered chelate ring referred to in **Table 2.7** and **Table 2.8**) decreases the *trans* influence of the donor atom in the ring relative to the same donor atom in a six-membered chelate ring. The average bite angle for six-membered chelate rings is 89.0° (average of the 16 structures with a six- membered chelate ring referred to in **Table 2.7** and **Table 2.8**). The explanation for the lengthening of the Rh-P bond lies in the effective overlap of the relevant σ-orbitals of the L,L'-BID ligand with the *dsp²*-hybrid orbitals of the metal. Theoretically a bite angle of 90° will allow for the most effective overlap of the σ-orbitals of the L,L'-BID ligand (**Figure 2.15**). Any deviation from a 90° bite angle will inhibit the electron donating power of the donor atom to the metal, decreasing its effective *trans* influence.
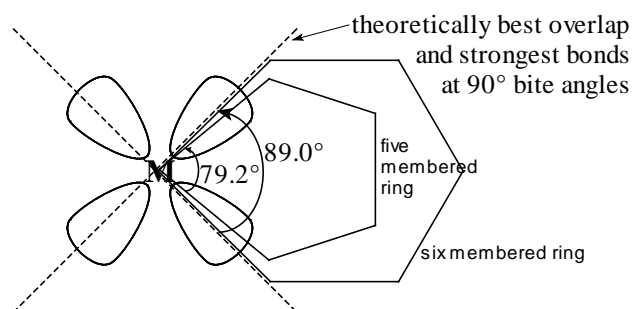
Figure 2.15: Overlap of the *dsp²*-hybrid orbitals of metal M with the relevant σ-orbitals of the L,L'-BID ligand of a five- and six-membered chelate ring. Strongest bonds are obtained where the bite angles approaches 90º, because the best orbital overlap is then obtained.

The discussion on the *trans* influence of bidentate ligands was thus far based on single isomers that crystallized from solutions. However for [Rh(ba)(CO)(PPh₃)][44] (Hba = benzoylacetone or

1-phenyl-1,3-butanedione) both the isomers were isolated with a ratio 1:1. (see **Figure 2.16**). ¹H-NMR showed the ratio isomer1 : isomer2 = 2:1 in a deuterated chloroform solution. ¹³C, ³¹P[56] and ¹H-NMR[57] showed two isomers in solution for [Rh(tta)(CO)(PPh₃)] (structure in **Figure 2.11**) and that the ratio of the two isomers is solvent dependant.
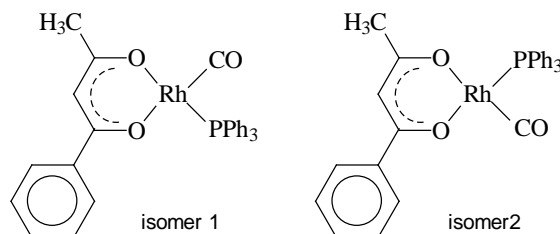
Figure 2.16: Structures of the two isomers of [Rh(ba)(CO)(PPh₃)].

The use of NMR is however not limited to indicate the presence of isomers. Steyn *et. al.*[53] showed that there exists an inverse proportion between the coupling constant $^1J(^{31}P\text{-}^{103}Rh)$ for ³¹P NMR and the P-Rh bond length in [Rh(L,L'-BID)(CO)(PPh₃)] complexes. NMR can therefore be used to "measure" the relative *trans* influence of donor atoms.

The discussion on the structure of the observed [Rh(L,L'-BID)(CO)(PPh₃)] isomer that crystallised from solution after the substitution of one of the CO groups in [Rh(L,L'-BID)(CO)₂] by PPh₃, [Rh(L,L'-BID)(CO)₂] + PPh₃ → [Rh(L,L'-BID)(CO)(PPh₃)], was based on electronic considerations (*trans* influence) and the steric implications of the transition state during the substitution reaction. In all cases no consideration was given to the possibility that the observed isomer simply crystallised because it had a more favourable crystallisation energy. Evidence of more than one isomer in solution, for the [Rh(ba)(CO)(PPh₃)][44] and [Rh(tta)(CO)(PPh₃)][57] complexes, indicate however, that thermodynamic factors such as energy of crystallisation may also play a role in determining which isomer will crystallise from solution. The discussion on electronic considerations (*trans* influence) and steric factors would only represent the complete explanation if the energy of the same isomer was always the highest (or lowest) both in solution and in the solid crystal phase. The isomer that dominates in solution, will definitely be the one that is thermodynamically more stable in solution. It is however also true that the isomer that dominates in solution will not necessarily be the one that crystallises from solution, because the crystallisation energy of the isomers is not necessarily the same. The isomer with the lowest

---

[56] Poletaeva, I.A., Cherkasova, T.G, Osetrova, L.V., Varshavsky, Y.S. and Roodt, A., *Rhodium Ex.,* **3,** 21 (1994).

[57] Varshavsky, Y.S., Poletaeva, I.A., Cherkasova, T.G. and Podkorytov, I.S., *Rhodium Ex.,* **14,** 10 (1995).

crystallisation energy will be the one which will crystallise first from solution. It is not necessarily the same isomer that also satisfies the electronic (*trans* influence) and steric considerations as discussed.

Evidence will be presented in this thesis (chapter 3) that crystallisation energy in some cases determines which isomer crystallises from solution. Results will be backed up by single crystal X-ray-crystallography as well as by ^{31}P NMR.

2.1.4.4 The kinetic *trans*-effect of bidentate ligands.

The kinetic *trans*-effect, the effect of a coordinated ligand on the substitution rate of the ligand opposite to it, were observed in substitution **Reaction 2.2**[43] (in a methanol medium) and in **Reaction 2.3**[58] (in dichloroethane, P(OPh)$_3$ = triphenyl phosphite):

Reaction 2.2: [Rh(β-diketonato)(CO)$_2$] + cod $\rightarrow$ [Rh(β-diketonato)(cod)] + 2CO

Reaction 2.3: [Rh(β-diketonato)(cod)] + 2P(OPh)$_3$ $\rightarrow$ [Rh(β-diketonato)(P(OPh)$_3$)$_2$] + cod
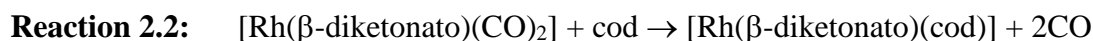
for β-diketonato = acac, ba, dbm, tfaa, tfba and hfaa (abbreviations are defined in List of Abbreviations). Results summarised in **Table 2.10** illustrate the effect of the terminal substituents R$_1$ and R$_2$ on the β-diketonato ligand R$_1$COCHCOR$_2$ on the kinetic *trans*-effect of the β-diketonato ligand during the substitution of CO or of cod. The relative rate of substitution is:

(smallest rate of substitution) acac < ba < dbm << tfaa

< tfba << hfaa (highest rate of substitution)
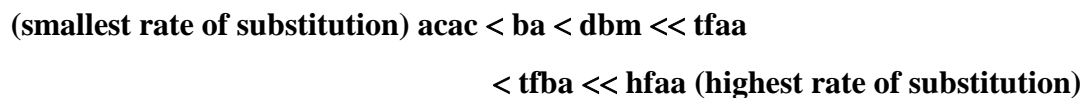
The indicated order of substitution rates shows that the influence of the terminal substituents CH$_3$, Ph and CF$_3$ of the various β-diketonatos on the kinetic *trans*-effect of the co-ordinating O-atoms of the β-diketonato ligands are

(smallest influence) CH$_3$ $\approx$ Ph < CF$_3$ (largest influence)

---

[58] Leipoldt, J.G., Lamprecht, G.J. and Steynberg, E.C. *J. Organomet. Chem.,* **397**, 239 (1990).

The term kinetic *trans*-effect is used because the kinetic *trans*-effect is usually much larger than the kinetic *cis*-effect (see page 16).

Table 2.10: Reaction rate constants for substitution reactions of CO in square planar [Rh(β-diketonato)(CO)$_2$] and [Rh(β-diketonato)(cod)] complexes to illustrate the *trans*-effect of the various β-diketonato ligands R$_1$COCHCOR$_2$.

β-dike-tone	R$_1$	R$_2$	k$_2$ / dm^3 mol^{-1} s^{-1} for substitution reaction	
			[Rh(β-diketonato)(CO)$_2$] + cod → [Rh(β-diketonato)(cod)] + 2CO	[Rh(β-diketonato)(cod)] + 2P(OPh)$_3$ → [Rh(β-diketonato)(P(OPh)$_3$)$_2$] + cod
acac	CH$_3$	CH$_3$	-	48.4
ba	CH$_3$	C$_6$H$_5$	0.10	57.4
dbm	C$_6$H$_5$	C$_6$H$_5$	0.36	58.7
tfaa	CH$_3$	CF$_3$	2.30	610
tfba	C$_6$H$_5$	CF$_3$	4.10	620
hfaa	CF$_3$	CF$_3$	200	1170

It was elsewhere reported[8] that the group electronegativity, χ, of the CF$_3$, phenyl and methyl groups are 3.01, 2.21 and 2.34 respectively. It follows therefore that the influence of the terminal side groups of the β-diketono ligands have on the kinetic *trans*-effect on the adjacent co-ordinating O atoms are directly proportional to the group electronegativity of the side groups. The larger kinetic *trans*-effect caused by the more electronegative groups can be explained by their ability to withdraw electron-density from the metal ion and thus stabilise the five co-ordinated transitional state in an associative mechanism.

To conclude, it is important to remember that during a kinetic study of the substitution of a carbonyl group in complexes of the type [Rh(L,L'-BID)(CO)$_2$] by PPh$_3$ (**Reaction 2.1**) one must distinguish between the thermodynamic *trans*-influence and the kinetic *trans*-effect. The former may determine the specific isomer that will be formed during the substitution of only one of the PPh$_3$ groups (provided energy of crystallisation has no influence on which isomer crystallises - see paragraph 2.1.4.3 above) and the latter determines the reactivity of these complexes towards substitution reactions.

Reaction 2.1 :   [Rh(L,L'-BID)(CO)$_2$] + PPh$_3$ → [Rh(L,L'-BID)(CO)(PPh$_3$)] +CO
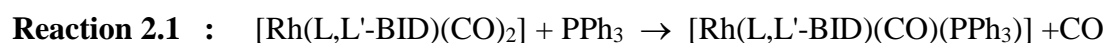
2.2 Oxidative addition, insertion and substitution reactions.

2.2.1 Introduction

Most transition metal complexes obey the 18 electron rule namely: *stable compounds of the transition elements will have a total of 18 electrons around the metal.*[59] The following inverse relationship exists between the coordination number, CN, and the amount of *d*-electrons for diamagnetic, mononuclear transition metal complexes:[60]

$$(CN)_{max} = \frac{18 - n}{2}$$

where $(CN)_{max}$ = maximum amount of ligands to be bonded to the metal provided that the electrons have like spin and n = amount of even non-bonding metal *d* valence electrons. That is, metals (M) with three electron pairs of their own require the presence of six ligand (L) bond pairs and structures of such complexes (ML_6) will be expected to be roughly octahedral (**Figure 2.17**a). Metals with four electron pairs of their own require the presence of five ligand bond pairs and these complexes (ML_5) should exhibit structures based on the trigonal bipyramid or square pyramid (**Figure 2.17**b)). In the case of metals with five electron pairs, ML_4 complexes posessing tetrahedral or square planar structures (by acquisition of four ligand electron pairs) should be obtained (**Figure 2.17**c)).

Well-defined exceptions to the 18 electron rule are found in complexes having only 16 valence electrons which are often just as stable, or even more stable than, 18 electron molecules of the same metal.[59] This is especially true of the platinum group metals, e.g. Rh(I), Pt(0), Pt(II) and Ir(I). Such complexes are invariably based on d^8 metal ions and are square planar (four ligand bond pairs), or they are based on d^{10} metal atoms with three ligands (three ligand bond pairs) and are presumably trigonal. Examples include those shown in **Figure 2.18**.

---

[59] Purcell, K.F. and Kotz, J.C., *Inorganic Chemistry,* W.B. Saunders Company, Philadelphia, 1977, p.794 – 807.

[60] Collman, J.P. and Hegedus, L.S., *Principles and Applications of Organotransition Metal Chemistry,* University Science Books, Mill Valley, California, 1980, p. 17 - 19.

a) $ML_6 = d^6$ + 6 ligand bond pairs   b) $ML_5 = d^8$ + 5 ligand bond pairs   c) $ML_4 = d^{10}$ + 4 ligand bond pairs

e.g. $M = Mn^+$, Fe^{+2}, Rh^{+3}.   *e.g.* $M = Mn^-$, Fe^0, Co^+.   *e.g.* $M = Co^-$, Ni^0, Cu^+.
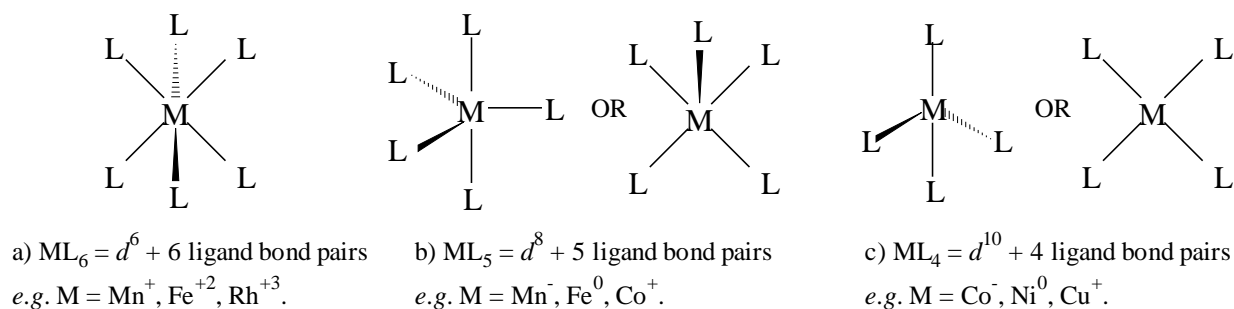
Figure 2.17: **Illustration of the 18 electron rule for the transition metal complexes ML$_n$ (n = number of ligands L bonded to metal M).**

a) $ML_4 = d^8$ + 4 ligand bond pairs.   b) $ML_3 = d^{10}$ + 3 ligand bond pairs.
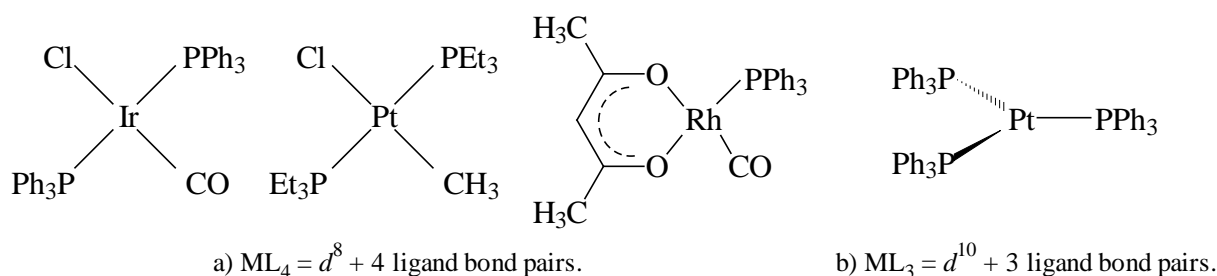
Figure 2.18: Platinum group metal complexes obeying the 16 electron rule.

The great majority of reactions with transition metal complexes can be grouped to a limited number of basic processes. These involve oxidative addition and its inverse reductive elimination, insertion and its reverse elimination, ligand substitution and a nucleophilic or electrophilic attack upon ligands within a metal coordination sphere.[61]

2.2.2 *Oxidative addition reactions*

2.2.2.1 Definition of oxidative addition reactions

The process oxidative addition in transition metal chemistry is used to describe the addition of neutral molecules (X-Y) to transition metal complexes having no more than 16 valence electrons.[61] Oxidative addition can be represented by **Scheme 2.5** below where the forward reaction is oxidative addition and the reverse reaction is reductive elimination:

---

[61] Mathey, F. and Sevin, A., *Molecular Chemistry of the Transition Elements,* John Wiley & Sons, Chichester, 1996, p28 - 50.

$$L_nM^{(m)} + XY \rightleftharpoons L_nM^{(m+2)} \overset{X \quad Y}{}$$
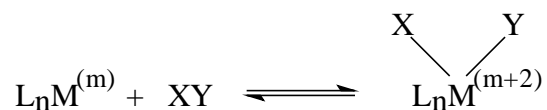
Scheme 2.5: Oxidative addition of the neutral molecule XY to the transition metal complex $L_nM^{(m)}$ with n = number of ligands (L) bonded to the metal (M) and m = the oxidation state of M before oxidative addition.

In the oxidative addition reaction of XY to the transition metal complex L_nM, the metal is oxidised to an oxidation state two units higher and the coordination number of the metal complex increases by two. The group XY is thus reduced during the process while the metal is oxidised. The metal may thus be seen as acting both as a Lewis base (donating of non-bonding electron density) and as a Lewis acid (the metal is co-ordinatively unsaturated and possesses vacant coordination sites). From this general definition of an oxidative addition reaction the metal complex will have to satisfy three basic conditions before oxidative addition can take place:

i)   there must exist non-bonding electron density on the metal,

ii)   there must exist two vacant coordination sites on the metal complex $L_nM^{(m)}$ to allow formation of two new bonds to X and Y, and

iii)   the oxidation state of the central metal atom has to be two units lower than the most stable oxidation state of the metal.[62]

Coordinatively unsaturated d^8 and d^{10} complexes generally undergo oxidative addition reactions. In general the oxidative addition to unsaturated square planar, 16 electron, d^8 complexes gives six-coordinate, 18 electron, d^6 complexes (**Scheme 2.6** (a)). One of the original ligands however, must be lost in the oxidative addition of two new ligands to a coordinatively saturated five-coordinate, 18 electron, d^8 complex to give a six-coordinate, 18 electron, d^6 complex as the final product (**Scheme 2.6** (b)).[63] Coordinatively saturated d^8 compounds are typically less reactive and usually add only the more strongly oxidising addenda XY.[64] Frequently d^{10} complexes are coordinatively unsaturated, being only three or four-coordinate, so addition occurs readily (example in **Scheme 2.6**(c)).[65, 66]

---

[62] Cotton, F.A. and Wilkinson, G., *Basic Inorganic Chemistry,* John Wiley & Sons, New York, 1976, p.529 – 547.

[63] Purcell, K.F. and Kotz, J.C., *Inorganic Chemistry,* W.B. Saunders Company, Philadelphia, 1977, p.938 – 948.

[64] Collman, J.P. and Hegedus, L.S., *Principles and Applications of Organotransition Metal Chemistry,* University Science Books, Mill Valley, California, 1980, p. 176 - 258.

[65] Birk, J.P., Halpern, J. and Pichard, A.L., *J. Amer. Chem. Soc.,* **90**, 4491 (1968).

[66] Ugo R., *Coord. Chem. Rev.,* **3**, 319 (1968).
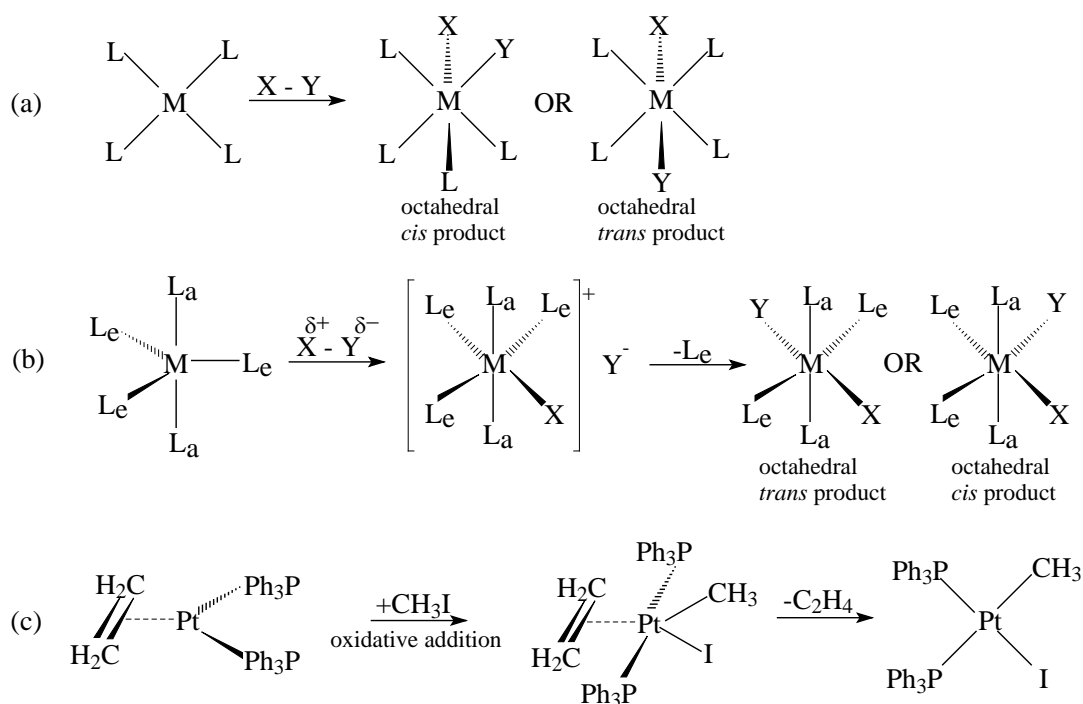
Scheme 2.6: **(a) Oxidative addition to unsaturated square planar d^8 complex ML$_4$ with metal M and ligands L. (b) Oxidative addition to saturated trigonal bipyramidal d^8 complex (L$_a$ = an axial ligand, L$_e$ = an equatorial ligand)**[64]**. (c) Oxidative addition to coodinatively unsaturated d^{10} complex.**[65]

2.2.2.2 Mechanism of oxidative addition reactions

Four main mechanisms govern oxidative addition reactions,[61, 62, 67, 68] namely

- (i) the one step concerted three centre mechanism,
- (ii) The two step S_N2 mechanism,
- (iii) the radical mechanism and
- (iv) the ionic mechanism.

(i) *The one step concerted three centre mechanism.*

The one step concerted three centre mechanism[67] is a process where filled d_{xy} or d_{yz} orbitals on the metal interact with antibonding orbitals of the addending molecule XY to produce a cyclic three centre transition state (**Scheme 2.7**). The product formed by this route will have a *cis*

[67] Dickson, R.S., *Organometallic chemistry of rhodium and iridium,* Academic Press, London, 1983, p.70 - 79

[68] Cross, R.J., *Chem. Soc. Rev.,* **14**, 197 (1985)

arrangement of the groups X and Y if there is no subsequent arrangement, since concerted *trans* addition is a symmetry forbidden process.[69] , [70] The concerted three centre mechanism is usually ascribed to the oxidative addition of a homonuclear molecule such as O_2, H_2 or C_2H_4 and when the reaction is performed under weak or non-polar conditions, *e.g.* in benzene solution.

three centre transition state   *cis* product
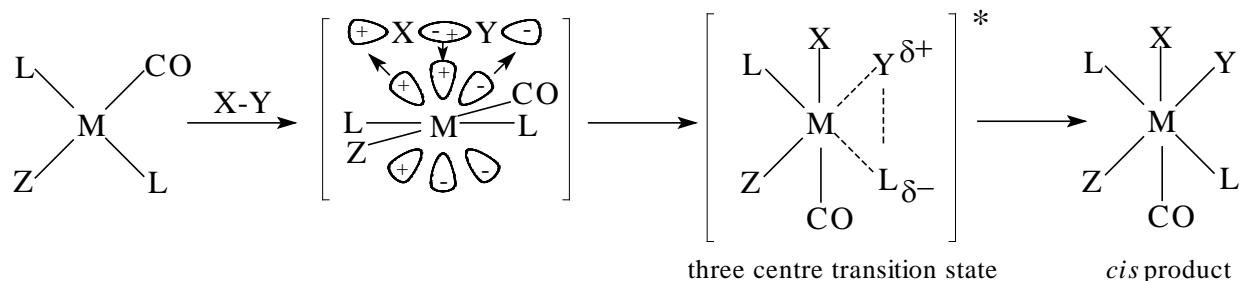
Scheme 2.7: **Reaction pathway for a concerted three centre mechanism for the oxidative addition of a non polar molecule XY to the metal complex [ML₂Z(CO)]. M = metal with four ligands L, L, Z and CO bonded to M.**

A concerted three centre mechanism was proposed for the oxidative addition of $Hg(CN)_2$ to [Rh(β-diketonato)(P(OPh)₃)₂] [71] and [Ir(β-diketonato)(COD)][72] in an acetone medium for various β-diketono ligands (acac, ba, dbm, tfaa, tfba, hfaa). *Cis* addition was proposed with the aid of IR (infrared spectroscopy), ^{1}H-, ^{13}C- and ^{31}P-NMR (nuclear magnetic resonance) spectra. The X-ray structure determination of the oxidative addition product of I_2 to [Rh(TFAA)(P(OPh₃))₂] indicated a *trans* product.[73] It was proposed that the *cis* addition of I_2 was followed by an isomerisation reaction to give the final *trans* diiodo product.

(ii)   *The two step S$_N$2 mechanism.*

The two step S$_N$2 mechanism is described as a nucleophilic attack of the metal centre on the α-carbon of a polar addending molecule R-X (such as alkyl- and acyl halides) with the consequent formation of a polar, five-coordinated transitional state.[62] *Trans* addition is favoured

[69] Pearson, R.G., *Symmetry rules for Chemical reactions,* Wiley Interscience, New York, (1976) p.280 -353, 405 – 413.

[70] Braterman, P.S. and Cross, R.J., *Chem. Soc. Rev.,* **2**, 271 (1973).

[71] van Zyl, G.J., Lamprecht, G.J., and Leipoldt J.G., *Trans. Met. Chem.,* **15**, 170 (1990).

[72] Steyn, G.J.J., Basson, S.S., Leipoldt, J.G. and van Zyl, G.J., *J. Organomet. Chem.,* **418**, 113 (1991).

[73] van Zyl, G.J., Lamprecht, G.J. and Leipoldt, J.G., *Inorg. Chim. Acta,* **122**, 75 (1986).

according to the molecular orbital considerations, but isomerisation may lead to the formation of *cis*-products (**Scheme 2.8**).[68]
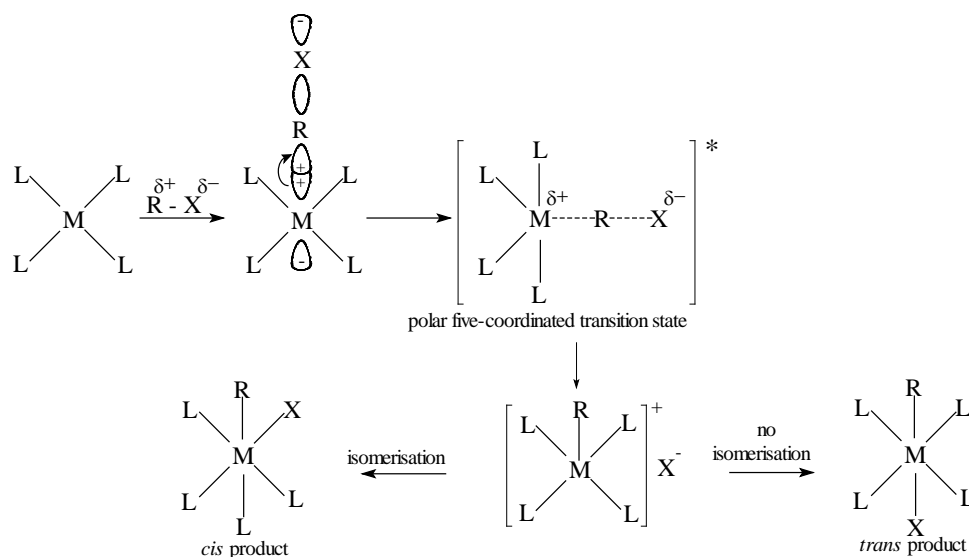
Scheme 2.8: Reaction pathway for a two-step S_N2 mechanism for the oxidative addition of polar molecule RX to the metal complex [ML4]. M = metal with four ligands L bonded to M.

In general, reactions following the two-step S_N2 mechanism, are first order in both reactants, the entropy of activation is usually large negative, the activation parameters are dependant on the solvent polarity, and the rate is dependant on the apparent nucleophilicity of the metal complex.[63]

Based on structural determinations, kinetic data, as well as ΔS^* and ΔV^* values, a two-step S_N2 reaction pathway was proposed for the oxidative addition of CH_3I to [Rh(β-diketonato)(P(OPh)$_3$)$_2$] in acetone for various β-diketonato ligands (acac, ba, dbm, tfaa, tfba, hfaa).[74]

(iii)   *The free radical mechanism.*

The two main free radical mechanisms of importance with respect to coordinatively unsaturated complexes such as d^8 square planar complexes, are

(a) the inner-sphere transfer mechanism and
(b) the radical chain reaction.

---

[74] van Zyl, G.J., Lamprecht, G.J., Leipoldt, J.G. and Swaddle, T.W., *Inorg. Chim. Acta.,* **143**, 223 (1988).

(a) The inner-sphere transfer free radical mechanism.

In the inner-sphere transfer free radical mechanism an organic halide first coordinates to the metal. Electron transfer then gives a radical pair consisting of R· and a metal halide complex. The combination of the metal halide complex with the radical pair gives the final oxidative addition product, but escape of the free radicals may form byproducts. (The free radical, R·, can also react with the original metal complex to initiate a radical chain oxidative addition reaction). This mechanism is represented in **Scheme 2.9**:

$$L_nM^{(m)} + RX \rightleftharpoons L_nM^{(m)}\cdots X\text{-}R \rightleftharpoons [L_nM^{(m+1)} \overset{\bullet}{X} + \overset{\bullet}{R}\,] \xrightarrow{\text{combination}} RL_nM^{(m+2)}X$$

$$\downarrow \text{escape}$$

$$R^{\bullet} + L_nM^{(m+2)}X \longrightarrow \text{byproducts}$$
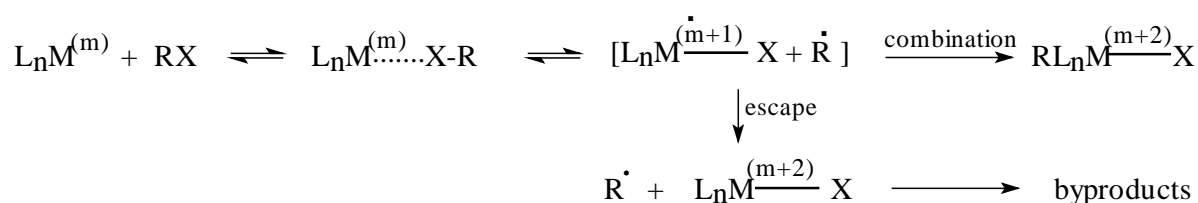
Scheme 2.9: The mechanism of the inner-sphere transfer free radical mechanism. $L_nM^{(m)}$ = transition metal complex with n = number of ligands (L) bonded to the metal (M) and m = the oxidation state of M before oxidative addition.

(b) The radical chain reaction.

The radical chain reaction requires a source of initiator radicals (In·) of which possible sources include trace impurities, traces of light (hυ), trace O_2 or peroxides and the substrate RX itself (especially when RX is a strong reducing agent).[61, 63] This mechanism may be represented as follows (**Scheme 2.10**):

$$In^{\cdot} + X\text{-}R \rightarrow In\text{-}X + R^{\cdot} \qquad \text{(initiation)}$$

$$R^{\cdot} + L_nM^{(m)} \rightarrow L_n \notin^{(m+1)}\text{-}R \qquad \text{(propagation)}$$

$$L_n \notin^{(m+1)}\text{-}R + X^{\cdot\cdot}R \rightarrow X\text{-}L_nM^{(m+2)}\text{-}R + R^{\cdot} \qquad \text{(propagation)}$$
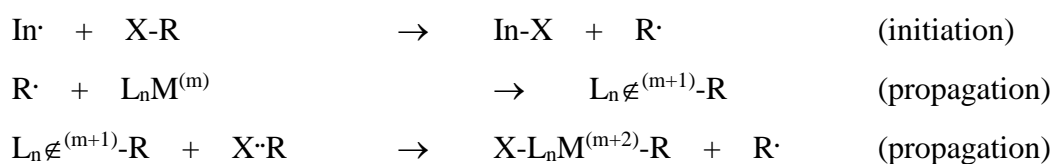
Scheme 2.10: The mechanism of the radical chain reaction. $L_nM^{(m)}$ = transition metal complex with n = number of ligands (L) bonded to the metal (M) and m = the oxidation state of M before oxidative addition.

(iv)   *The ionic mechanism.*

The ionic mechanism generally requires the presence of a strongly dissociated protic acid H-X (*e.g.* HCl or HBr) as a reagent; this means a highly polar solvent like dimethylformamide is required.[61] The first step of an ionic mechanism for the oxidative addition is an electrophilic

attack of the solvated cation on the metal centre to form a five-coordinated cationic square pyramidal complex. The five-coordinated cationic complex may react directly with the anion (:X$^-$) to form a *trans* M(H)(X) product, but intramolecular exchange reactions involving a five-coordinate intermediate could easily generate the *cis* addition product (**Scheme 2.11**).[67] Mixtures of *cis* and *trans* products were found for the oxidative addition of hydrogen halide to *trans*-halobis(arylphosphine)-carbonyliridium(I) complexes in the presence of polar solvents such as methanol, acetonitrile, water and dimethylformamide.[75]
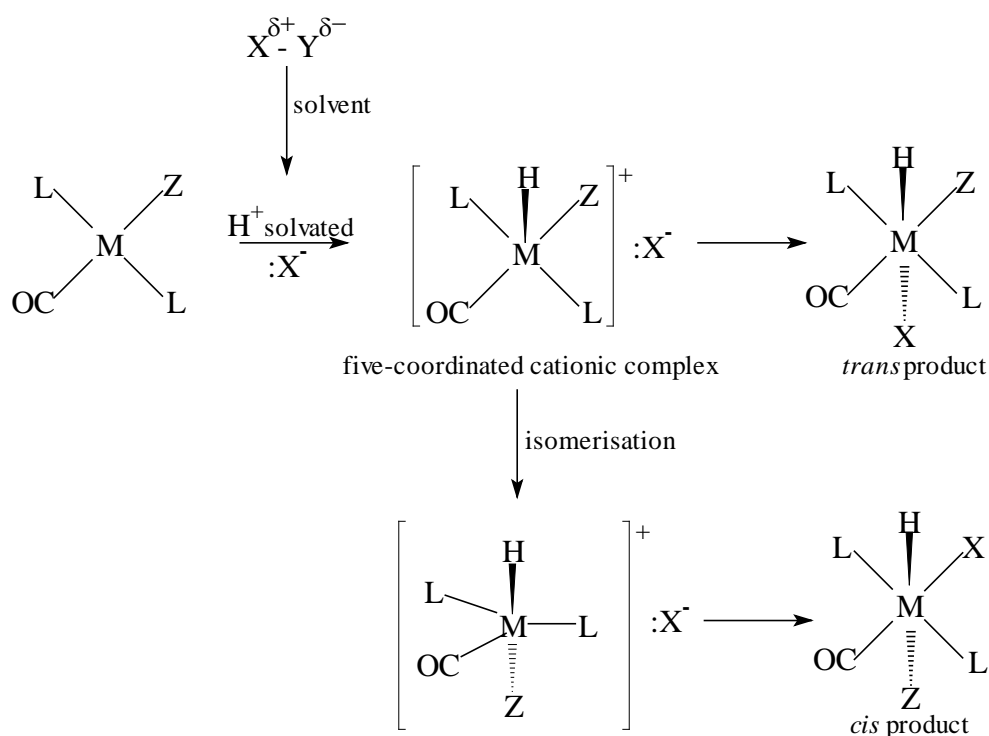
Scheme 2.11: The ionic reaction mechanism for the oxidative addition of strongly dissociated protic acid H-X to the transition metal complex [ML$_2$(CO)Z]. M = metal with four ligands L, L, Z and CO bonded to M.

(v)   *Differentiation between the mechanisms of oxidative addition.*

Based on the symmetry rules for oxidative addition reactions, Pearson[69] stated that the most definitive series of experiments which differentiates between the concerted -, the S$_N$2 – and the free radical mechanisms for oxidative addition is stereochemical investigations. A set of predictions made by him is summarised in **Table 2.11**. The factors selecting each mechanism

[75] Blake, D.M. and Kubota, M., *Inorg. Chem.,* **9**, 989 (1970)

are discernible in most of the known cases. See paragraph 2.2.2.4 for a further discussion on the stereochemistry of oxidative addition reactions.

Table 2.11: Stereochemical prediction for three mechanisms of oxidative addition reactions.

Mechanism	Stereochemistry at metal	Stereochemistry at X or R[a]
Concerted	*cis*	retention
S_N2 two step	*trans*[b]	inversion
Free radical	*trans*[b]	racemization

[a] RX or XY = molecule that oxidative adds to transition metal complex.
[b] *trans* products are most probable, but rearrangements leading to *cis* products cannot be ruled out.

2.2.2.3 Factors influencing oxidative addition reactions

Consider the general form of an oxidative addition reaction(**Scheme 2.5**):

$$L_nM^{(m)} \quad + \quad XY \quad \square \quad L_nM^{(m+2)}XY$$

Whether the equilibrium lies on the reduced or the oxidised side depends on[62, 63]

> (i)   the nature of the metal M,
>
> (ii) the nature of the ligands L in the complex,
>
> (iii) the nature of the added molecule XY (and of the M-X and M-Y bonds so formed) and
>
> (iv) the medium in which the reaction is conducted.

(i)   *The nature of the central metal atom.*

When a transition metal undergoes a oxidative addition reaction, the metal acts as a nucleophile (paragraph 2.2.2.2). It is to be expected that anything that affects the nucleophilicity (or basicity) of the metal will therefore influence the course of the oxidative addition reaction. The basicity of the metal can be affected by the electronic and steric properties of the ligands bonded to the metal and the electronic and steric properties of the addend (the electrophile XY) added during

the oxidative addition reaction. The general trend[63] for metals to undergo oxidative addition[59, 76, 77, 78] is as shown in **Figure 2.19**: *the largest metals in the lowest oxidation state show the greatest relative rate of oxidative addition.* It must be noted that there are exceptions on the rule.[69(ii), 78, 79]

$$
\begin{array}{lll}
Fe(0) & Co(I) & Ni(II) \\
Ru(0) & Rh(I) & Pd(II) \\
Os(0) & Ir(I) & Pt(II)
\end{array}
$$

increasing relative rate of oxidative addition

increasing relative rate of oxidative addition
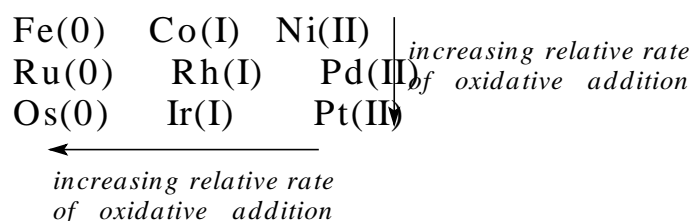
Figure 2.19: Relative rate of oxidative addition to square planar d^8 complexes of transition metals.

It is, however, usually not possible to make comparisons between three different transition metals in the same periodic group, or between metals in adjacent groups. The problem in making such comparisons is that there are few complete isostructural series of complexes.[64] There are, nevertheless, cases in which comparisons can be made between isostructural complexes of the second- and third-row elements of **Figure 2.19**. See **Table 2.12** for selected examples.

Table 2.12: Comparison of the relative rates of oxidative addition to square planar transition metal complexes with different metal centres M = Co, Rh and Ir.

Complex	Addendum	Relative rate of oxidative addition
$[(\eta^5\text{-}C_5H_5)M(CO)PPh_3]$[78] M = Co, Rh, Ir	CH_3I, C_2H_5I	$Co(1.0) < Rh(1.4) < Ir(8)$ for CH_3I $Co^*(2) > Rh(1) < Ir(6)$ for C_2H_5I
$[MX(CO)(PPh_3)_2]$[77] M = Rh, Ir X = Cl, Br, I	PhN_3	$Rh(1) < Ir(1.4)$ for X = Cl $Rh(1) < Ir(1.8)$ for X = Br $Rh(1) < Ir(1.3)$ for X = I
$[M(cis\text{-}(C_6H_5)_2PCHCHP(C_6H_5)_2)_2][B(C_6H_4)_4]$[79] M = Co, Rh, Ir	O_2	$Rh(1) < Ir(4) < Co^*(10^5)$
$[MCl(CO)(PPh_3)_2]$[76]	$HgCl_2$	$Rh < Ir$

* unexpected order

[76] Nyholm, R.S. and Vrieze, K., *J. Chem. Soc.,* 5337 (1965).

[77] Collman, J.P., Kubota, M., Vastine, F.D., Sun, J.Y. and Wang, J.W., *J. Am. Chem. Soc.*, **90**, 5430 (1968).

[78] Hart-Davis, A.J. and Graham, W.A.G., *Inorg. Chem.*, **9**, 2658 (1970).

[79] Vaska, L., Chen, L.S. and Miller, W.V., *J. Am. Chem. Soc.,* **93**, 6671 (1971).

(ii)   *The role of the ligands in the complex.*

Any influence of a ligand bonded to the metal, that will increase the electron density on the metal centre, will lead to an increased rate of oxidative addition, assuming all other influences, factors and parameters remain constant. The σ- and π-bonding properties of bonded ligands largely influence the electron density (the nucleophility) of the metal centre: ligands with good σ donating properties increase the electron density on the metal centre and the increased nucleophilicity of the metal enhances the oxidative addition rates. On the other hand, ligands with good π accepting properties decrease the electron density on the metal centre and inhibit reactivity. The effect of ligands with good σ donating properties on the oxidative addition rates is illustrated by the oxidative addition of iodomethane to [Rh(acac)(CO)(PR₃)][80], to [Rh(sacac)(CO)(PR₃)][81], to [Rh(cacsm)(CO)(PR₃)][54], to [Rh(cupf)(CO)(PR₃)][82] and to [Rh(ox)(CO)(PR₃)][83], (R = *p*-Cl-Ph, Ph and *p*-MeO-Ph) see **Table 2.13**.

Table 2.13: Comparison of the relative rates of the oxidative addition reaction of CH₃I to [Rh(L,L'-BID)(CO)(PR₃)] complexes[54, 80 – 83] with different tertiary phosphines PR₃, R = *p*-Cl-Ph, Ph and *p*-MeO-Ph (L,L'-BID = acac, sacac, cacsm, cupf, and ox).

PR₃	pKₐ of phos-phonium ion[13]	νCO of [Rh(sacac)(CO)(PR₃)] complex (KBr)	$10^3 k_1$ / mol⁻¹dm³s⁻¹				
			[Rh(acac)(CO)(PR₃)] complex[a]	[Rh(sacac)(CO)(PR₃)] complex[a]	[Rh(cacsm)(CO)(PR₃)] complex[b]	[Rh(cupf)(CO)(PR₃)] complex[c]	[Rh(ox)(CO)(PR₃)] complex[c]
P(*p*-Cl-Ph)₃	1.03	1981	3.46(9)	1.10(5)	10(1)	0.193(8)	0.069(1)
PPh₃	2.73	1978	24(3)	5.52(8)	55.9(6)	1.22(2)	0.369(3)
P(*p*-MeO-Ph)₃	4.53	1968	138(3)	11.9(3)	117(4)	4.20(8)	1.04(1)

Reaction in (a) 1,2-dichloroethane, (b) chloroform and (c) acetone

The phosphines are isosteric with a common cone angle of 145°[17, 84] and thus no steric influence on the rate is expected. In both cases the rate of oxidative addition increased in the order of

[80] Basson, S.S., Leipoldt, J.G., Roodt, A., Venter, J.A., and van der Walt, T.J., *Inorg. Chim. Acta,* **119**, 35 (1986).

[81] Leipoldt, J.G, Basson, S.S., and Botha, L.J., *Inorg. Chim. Acta.,* **168**, 215 (1990).

[82] Basson, S.S., Leipoldt, J.G., Roodt, A. and Venter, J.A., *Inorg. Chim. Acta.,* **128**, 31 (1987).

[83] Van Aswegen, K.G., *Kinetic and structural aspects of the oxidative addition reactions of rhodium(I) complexes with iodomethane (in Afrikaans), M.Sc. Thesis,* University of the Orange Free State, R.S.A., 1990.

[84] Giering, W.P., Golouin, M.N., Rahman, M.M. and Belmonte, J.E., *Organometallics,* **4**, 1981 (1985)

P(p-Cl-Ph)$_3$ < PPh$_3$ <P(p-MeO-Ph)$_3$ in accordance with the increased electron donating power of the three tertiary phosphines (ν_{CO} and pK$_a$ here give an indication of the electron density on the metal centre as discussed in paragraph 2.1.3.1). The increased electron donating power of the phosphines (with bigger pK$_a$) increases the electron density on the metal, rendering it a better nucleophile, increasing the oxidative addition rates.

The aspect of the steric influence that ligands in a transition metal complex have on the rate of oxidative addition is illustrated in **Table 2.14** with the example of the addition of H$_2$, O$_2$ and HCl to Vaska's complex *trans*-[Ir(Cl)(CO)(PR$_3$)$_2$] containing tertiary phosphines with different cone angles (thus different steric bulkines) but comparable electron donating power (according to their IR data).[85] It was found that as the cone angle of the tertiary phosphine increased from $\theta = 145°$ (for P(p-Me-Ph)$_3$) to $\theta = 194°$ (for P(o-Me-Ph)$_3$), the oxidative addition rate decreased to such an extent that in the case of P(o-Me-Ph)$_3$, no reaction at all was observed for the oxidative addition of H$_2$ and O$_2$.

Table 2.14: Steric influence of tertiary phosphines on the rate of oxidative addition of H$_2$, O$_2$ and HCl to Vaska's complex *trans*-[Ir(Cl)(CO)(PR$_3$)$_2$][85] (R = P(p-Me-Ph)$_3$, P(m-Me-Ph)$_3$, PCy$_3$ and P(o-Me-Ph)$_3$) in chlorobenzene at 30°.

PR$_3$	pK$_a$ of phosphonium ion[13]	ν_{CO}/cm^{-1} (CHCl$_3$)	θ/deg[17]	k$_2$/mol^{-1}dm^{3}s^{-1} for addition of		
				H$_2$	O$_2$	HCl[(b)]
P(p-Me-Ph)$_3$	3.84	1962	145	1.7	0.096	24000
P(m-Me-Ph)$_3$	3.30	1964	145< θ < 194	0.69	0.044	2700
PCy$_3$	9.65	1931[(a)]	170	0.0066[(c)]	0.00038	≤4.0
P(o-Me-Ph)$_3$	3.08	1960	194	no reaction in 3h at 740 mmHg	no reaction in 18 days at 700 mmHg	0.79

(a) in C$_6$H$_5$Cl (b) k$_2$ in benzene (c) at 40°

The following example (**Table 2.15**) of the oxidative addition of benzoic acid to *trans*-[Ir(Cl)(CO)(L)$_2$] for a series of tertiary phosphines L[86], clearly indicates the effect of increasing steric hinderance and decreasing basicity of the various tertiary phosphines on the rate of oxidative addition.

---

[85] Brady, R., DeCamp, W.H., Flynn, B.R., Schneider, M.L., Scott, J.D., Vaska, L. and Werneke, M.F., *Inorg. Chem.,* **14**, 2669 (1975).

[86] Deeming, A.J. and Shaw, B.L., *J. Chem. Soc.*, **(A)**, 1802 (1969).

Table 2.15: Steric and electronic influence on the rate of oxidative addition of benzoic acid to *trans*-[Ir(Cl)(CO)(L)₂] for a series of tertiary phosphines L.[86]

L	pK$_a$ of phosphonium ion[13]	θ/deg[17]	ν_{CO}/cm^{-1} (a)	relative k
PMe₃	8.65	118	2064.1	370
PMe₂Ph	6.49	122	2065.2	100
PMePh₂	-	136	2067.0	10
PPh₃	2.73	145	2068.9	1

(a) ν_{CO} in CH₂Cl₂ of the tertiary phosphines L of 0.05 M solutions of [Ni(CO)₃(L)] complexes[17]

Both the electronic and steric influence of tertiary phosphines bonded to a transition metal complex are to be considered when the transition metal complex undergoes a oxidative addition reaction and can generally be summarise as follow:

(1)   Increasing electron donating power of the tertiary phosphine, as measured by increasing pK$_a$ and/or by decreasing ν_{CO} of the a metal complex with the tertiary phosphine as ligand, increases the relative rate of oxidative addition.

(2)   Increasing steric hindrance, as measured by the Tolman angle θ, decreases the relative rate of oxidative addition.

Carbonyl ligands, ligands with good π accepting properties, decrease the electron density on the metal centre due to metal to carbonyl backbonding.

The electronegativity, χ_X, of halogen ligands (X) bonded to a transition metal complex, directly influence the basicity of the metal and therefore its reactivity towards oxidative addition. The most electronegative halogen should exhibit the smallest reaction rate. **Table 2.16** gives the relative rates of addition of O₂[87], of H₂[88], of PhN₃[77] and of benzoic acid[86] to Vaska's compound *trans*-[Ir(X)(CO)(L)₂] (X = F, Cl, Br and I; L = PPh₃ for the addition of O₂, H₂, PhN₃ and L = PMe₂Ph for the addition of benzoic acid). It is clear that the rate of oxidative addition decreases as the halogen is changed in the order of increasing electronegativity, namely: I > Br > Cl > F (most electronegative). An exception to this order is the reaction of *trans*-

---

[87] Vaska, L., *Science,* **174**, 587 (1971)

[88] Chock, P.B. and Halpern, J., *J. Am. Chem. Soc.*, **88**, 3511 (1966).

44

[Ir(X)(CO)(PPh$_3$)$_2$] with CH$_3$I following the opposite order of dependence on the nature of the halogen, namely F > Cl > Br. > I.[88, 89, 90] It has been suggested that steric interactions are responsible for the reversal in dependance on the halogen.[91] For the oxidative addition of CH$_3$I to *trans*-[Rh(X)(CO)(PPh$_3$)$_2$] however, the correct order (according to electronegativity) on the rate dependence was found namely I > Cl.[92]

Table 2.16: Comparison of the relative rates of addition of O$_2$,[87] H$_2$[88], PhN$_3$[77] and benzoic acid (C$_6$H$_5$COOH)[86] to Vaska's compound *trans*-[Ir(X)(CO)(L)$_2$], X = F, Cl, Br and I.

X	χ_X (Pauling scale)[93]	relative rate of addition of O$_2$[(a)]	relative rate of addition of H$_2$[(b)]	relative rate of addition of PhN$_3$[(c)]	relative rate of addition of benzoic acid[(d)]
F	4.0	0.15[(e)]	-	-	-
Cl	3.0	1	1	1	1
Br	2.8	2	15	1.7	5.8
I	2.5	7	100	2.3	9.0

(a) – (c) tertiary phosphine L = PPh$_3$ (d) tertiary phosphine L = PMe$_2$Ph
(a) 40°C in chlorobenzene (b) 30°C in benzene (c) 30°C in chloroform (d) 25°C in benzene
(e) 40°C in benzene (F react with chlorobenzene)

The influence of different β-diketonato ligands, R$_1$COCHCOR$_2$, bonded to a transition metal complex on the rate of oxidative addition, is illustrated in **Table 2.17** for the oxidative addition reaction of CH$_3$I to [Rh(β-diketonato)(CO)(PPh$_3$)].[7] It is obvious that the reaction rate decreases as R$_1$ and R$_2$ are replaced by more electron withdrawing groups from top to bottom in **Table 2.17**, decreasing the electron density on the metal centre (ν_{CO} of the complex, an indication of the electron density on the metal centre, increases as the electron density on the metal centre decreases. See paragraph 2.1.3.1 page 10).

The effect of the substituents R$_1$ of the β-diketonato ligands (R$_1$COCHCOR$_2$) on the reaction rate, may be explained using **Figure 2.20**. The π* orbitals of the two CO groups of the β-diketone is of the correct symmetry for interaction with a filled d_{xz} or d_{yz} orbital of the metal.

[89] Kubota, M., Kiefer, G.W., Ishikawa, R.M. and Bencala, K.E., *Inorg. Chim. Acta,* **7**, 195 (1973).

[90] Collman, J.P. and Sears, C.J., Jr., *Inorg. Chem.*, **7**, 27 (1968).

[91] Atwood, J.D., *Coord. Chem. Rev.*, **83**, 93 (1988).

[92] Douek, I.C. and Wilkinson, G., *J. Chem. Soc.*, **(A)**, 2004 (1969).

[93] March, J., *Advanced Organic Chemistry Reactions, Mechanisms and Structure,* John Wiley and Sons, New York, 1985, p. 13.

Because of this interaction, electron density flows from the filled d_{xz} or d_{yz} orbital of the metal into the empty π^* orbital of the CO groups of the β-diketone. This backbonding from the metal will increase as the substituent R_1 is replaced by more electron withdrawing groups resulting in a lower electron density on the metal centre with a subsequent smaller reaction rate of oxidative addition.

Table 2.17: Influence of different β-diketonato ligands (R_1COCHCOR$_2$ with substituents R_1 and R_2) on the rate of oxidative addition of CH$_3$I to [Rh(β-diketonato)(CO)(PPh$_3$)].[7]

β-diketonato	R_1	R_2	pK_a of β-diketone[(b)]	ν_{CO}/cm^{-1} [(a)]	relative k_2
acac	CH$_3$	CH$_3$	8.9	1988	1.0
tfaa	CH$_3$	CF$_3$	6.3	1996	.24
tfdmaa	CH(CH$_3$)$_2$	CF$_3$	6.8	1998	.22
hfaa	CF$_3$	CF$_3$	4.4	2000	.02

(a) ν_{CO} in 1,2-dichloroethane   (b) pK_a from ref. 7
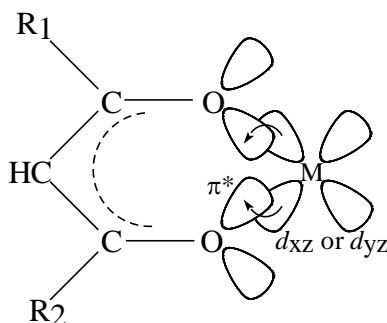
Figure 2.20: Illustration of the backbonding between a filled d_{xz} or d_{yz} orbital of the metal M and the π^* orbitals of both CO groups of the β-diketonato ligand R_1COCHCOR$_2$ in a square planar complex of the type [M(β-diketonato)(CO)(PPh$_3$)].

(iii)   *The nature of the incoming oxidising molecule.*

The incoming oxidising molecule influences the mechanism, stereochemistry and type of products formed during an oxidative addition reaction. A general distinction between three types of incoming oxidising molecules can be made (R = alkyl, X = halogen):[64]

(a)   polar, electrophilic reagents (*e.g.* X_2 (halogens), HX (halogen acids), RSCl, RSO_2CL, RX (alkylating agents), RCOX (acylating agents), RCN),

(b)   those which remain jointed by a bond in the adduction (*e.g.* O_2, S_2, $RC{\equiv}CR$, $RCH{\equiv}CHR$, CH_2O) and

(c)   non-polar addenda (*e.g.* H_2, RH, RCHO).

Molecules of group (a) generally react *via* a polar S_N2 mechanism leading to *cis* and *trans* products. The molecules of group (b) retain at least one bond in the adductions. Thus the two new coordinating bonds to the metal are necessarily *cis*. The non-polar molecules of group (c) usually react only with coordinatively unsaturated complexes and the overall addition to the metal is almost always stereo-specifically *cis*.[64]

Table 2.18:   Oxidative addition of alkyl halides (RX) to square planar Rh(I) and Ir(I) complexes. Influence of halide X to give the general rate profile RI > RBr > RCl.

Complex	Incoming oxidising molecule (RX)	Relative rate of addition
$[RhCl(CO)(PPh_3)_2]$[92]	MeX X = I, Br	RI > RBr (R = Me)
$[C_5H_5Rh(CO)(PPh_3)]$[96]	$C_6H_5CH_2X$ X = I, Br, Cl	RI > RBr >> RCl (R = $C_6H_5CH_2$) (10^4 : 500 : 1)
trans $[IrCl(CO)(PEt_nPh_{3-n})_2]$[94] n = 0, 1, 2	$C_6H_5CH_2X$ X = Br, Cl	RBr < RCl* (R = $C_6H_5CH_2$) (1.2 : 1 for n = 0)
unsaturated d^8 macrocyclic Rh(I) complex[97]	RX R = I, Br, Cl X = $CH_3(CH_2)_3$, $CH_3(CH_2)_4$	RI > RBr > RCl (200 : 1 : -) for R = $CH_3(CH_2)_3$ (10^5 : - : 1) for R = $CH_3(CH_2)_4$

* unexpected order

The reactivity of different alkyl halides (RX) towards square planar transition metal complexes depends mainly on the inductive effect of X and the positive character of the carbon to be attacked by the metal, the C-X dissociation energy and the donar properties of the halogen.[92] **Table 2.18** illustrates that the general rate profile of various halogens bonded to the same alkylgroup (though not without exception[94]) is RI > RBr > RCl.[64, 92, 95, 96, 97] The general order

---

[94] Ugo, R., Pasini, A., Fusi, A. and Cenini, S., *J. Am. Chem. Soc.,* **94**, 7364 (1972).

[95] Stille, J.K. and Lau, K.S.Y., *Acc. Chem. Res.*, **10**, 434 (1977).

[96] Davis, A.J.H.. and Graham, W.A.G., *Inorg. Chem.,* **10**, 1653 (1971).

of the rate dependence of alkyl-halides for various alkyl groups bonded to the same halogen, is methyl > ethyl > secondary > cyclohexyl [78, 7, 97] See **Table 2.19**.

Table 2.19: Oxidative addition of alkyl halides (RX) to square planar Rh(I) and Ir(I) complexes.   Influence of alkyl R to give a general order of rate dependence: methyl > ethyl > secondary > cyclohexyl.

Complex	Incoming oxidising molecule (alkyl halide)	Relative rate of addition
$[C_5H_5M(CO)(PPh_3)]$ [78] M = Rh, Ir	RI R = Me, Et	MeI >> EtI (10^3 : 1)
$[Rh(acac)(CO)(PPh_3)]$[7]	RI R = Me, Et	MeI > EtI (120 : 1)
unsaturated d^8 macrocyclic Rh(I) complex[97]	RI and RBr R = CH_3, CH_3CH_2, $CH_3(CH_2)_3$, $(CH_3)_2CH$, cyclohexyl	methyl > ethyl > n-Bu > secondary >> cyclohexyl

(iv)   *The role of the reaction medium.*

The medium or solvent in which an oxidative addition reaction takes place, influences the rate, the stereochemistry and the mechanism of the reaction. Solvents can arbitarily be divided into three categories:[98]

(a)   protic solvents (*e.g.* fluoro alcohols, water, methanol, hydrogen fluoride, formamide, ammonia) that are capable of strong hydrogen bond formation, including both proton donors and acceptors,

(b)   polar aprotic solvents (*e.g.* acetone, acetonitrile, dimethylformamide (DMF), dimethylacetamide (DMAC), dimethyl sulfoxide (DMSO), nitromethane, nitrobenzene, benzonitrile) are highly polar with dielectric constant > 15, but with very weak hydrogen-bond donors[99] and

(c)   aprotic solvents (*e.g.* carbon tetrachloride) having neither acidic nor basic properties.

---

[97] Collman, J.P. and MacLaury, M.R., *J. Am. Chem. Soc.,* **96**, 3019 (1974).

[98] Wilkins, R.G., *Kinetics and Mechanism of Reactions of Transition Metal Complexes,* 2nd thoroughly revised edition, VCH, Weinheim, 1991, p.116.

[99] Parker, A.J., *Chem. Rev.*, **69**, 1 (1969).

The effect of the solvent on the rates and mechanism of reactions has been extensively explored with variable success. There are basically two ways in which the solvent may be regarded:

A) the solvent may be regarded as an "inert" medium in which case the dielectric constant, ε, of the solvent is the most important parameter (although viscosity may also play an important role) and

B) the solvent may act as a nucleophile and an active participator in the reaction.[98]

Polar solvents generally enhance the rate of oxidative addition for both polar and non-polar molecules to transition complexes, though the observed solvent effects on rate did not exactly parallel the change in solvent polarity.[68] See **Table 2.20** for selected examples of the solvent effect on the relative rate of oxidative addition of CH_3I to Co, Rh and Ir transition complexes.

Table 2.20: Solvent effect on the relative rate of oxidative addition of CH_3I to selected Co, Rh and Ir transition complexes, $\varepsilon_{25°C}$ given in brackets after the solvent, T = 25°C.

Complex	Relative rate of addition
$[C_5H_5Co(CO)(PPh_3)]$[78]	tetrahydrofuran(7.6) < acetone(20.7) < dichloromethane(8.64)* < acetonitrile(38.0)
$[C_5H_5Rh(CO)(PPh_3)]$[78]	toluene(2.40) < dichloromethane(8.64)
trans-$[IrCl(CO)(PPh_3)_2]$[94]	benzene(2.27) < chlorobenzene(5.62) < tetrahydrofuran(7.6) < acetonitrile(38.0)* < DMF(36.1)
trans-$[RhCl(CO)_2(PPh_3)]$[100]	benzene(2.27)< 1,2-dichloroethane(10.36) < DMF(36.1)
$[Rh(tfaa)(CO)(PPh_3)]$[7]	toluene(2.40) < chlorobenzene(5.62) < 1,2-dichloroethane(10.36) < acetone(20.7)
$[Rh(acac)(P(OPh)_3)_2]$[74]	benzene(2.27) < chlorobenzene(5.62) < 1,2-dichloroethane(10.36) < acetone(20.7)
$[Rh(cupf)(CO)(PPh_3)]$[82]	benzene(2.27) < ethyl acetate(6.02) < acetone(20.7) < methanol(32.6) < acetonitrile(38.0) < DMSO(45.0)
$[Rh(sacac)(CO)(PPh_3)]$[81]	toluene(2.40) < ethyl acetate(6.02)* < chlorobenzene(5.62) < acetone(20.7) < 1,2-dichloroethane(10.36)* < acetonitrile(38.0)
$[Rh(bpha)(P(OPh)_3)_2]$[101]	benzene(2.27) < ethyl acetate(6.02) < acetone(20.7)
$[Rh(hpt)(CO)(PPh_3)]$[51]	benzene(2.27) < ethyl acetate(6.02) < acetone(20.7) < acetonitrile(38.0) < DMSO(45.0)
$[Rh(anmetha)(CO)(PPh_3)]$[51]	benzene(2.27) = ethyl acetate(6.02) < acetone(20.7) < acetonitrile(38.0) < DMSO(45.0)

* unexpected order according to dielectric constant ε value

[100] Uguagliati, P., Palazzi, A., Deganello, G. and Belluco, U., *Inorg. Chem.,* **9**, 725 (1970).

[101] Lamprecht, G.J., and Beetge, J.H., *S. Afr. J. Chem.,* **40(2)**, 131 (1987).

The increasing order of the rate of oxidative addition in the different solvents follows the same pattern as the increase in the dielectric constant $\varepsilon_{25°C}$[102] (given in brackets) of the solvent. The dielectric constant ε of the solvent can thus be used as an indication of the polarity of the solvent. The order is as follows:

(smallest ε) benzene (2.27) < toluene (2.40) < chlorobenzene (5.62) < ethyl acetate (6.02) < tetrahydrofuran (7.6) < dichloromethane (8.64) < 1,2-dichloeoethane (10.36) < acetone (20.7) < methanol (32.6) < DMF (36.1) < acetonitrile (38.0) < DMSO(45.0) (largest ε)

The dependence of oxidative addition reaction rates on solvent polarity may be explained in terms of solvent coordination to both reactants. Polar solvents will easily solvate to metal complexes (since the metallic nucleus is partially positively charged) as well as to the polar incoming moieties, $R^{\delta+}-X^{\delta-}$. This solvation will result in slight changes in the M-L bond lengths as well as small structural changes around M. Consequently the metallic centre of the complex becomes more accessible to the incoming oxidising R-X groups to form any of the transitional states shown in **Figure 2.21**, probably as a result of fast solvent-solvent and solvent-RX exchange equilibrium steps. Therefore, the net effect of solvation of polar solvents is to lower the energy barrier to the formation of a transition state, which manifest in faster reaction rates. Non-polar groups, such as H_2 (H-H) also benefits from polar solvents because solvation to the metal complex is not changed and also because of the formation of temporary dipoles in the H_2 molecule (*i.e.* the result of London and dipole-dipole forces.)

(a)   (b)   (c)
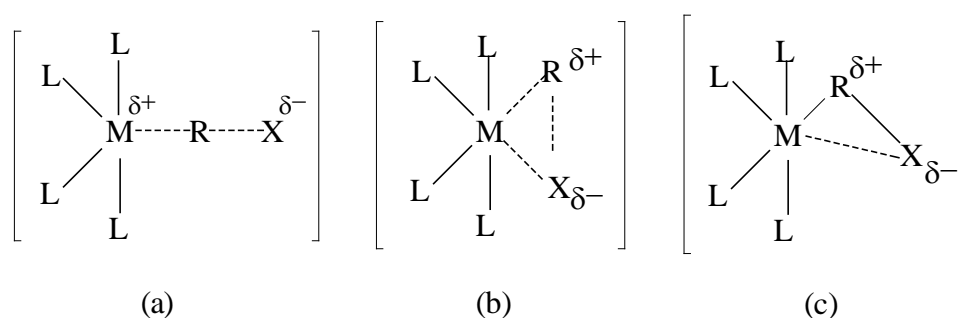
Figure 2.21: Possible transitional states for oxidative addition reactions.

---

[102] i) Weast, R.C., *Handbook of Chemistry and Physics,* 49th edition, The Chemical Rubber Co., Ohio, P. E59.

ii) Gutman, V., *Angew.Chem. Internat. Edit.,* **9**, 843 (1970)

The dependence of the stereochemistry of oxidative addition products on the solvent used for the reaction is clearly illustrated by the addition of hydrogen halides (HX) to *trans*-halobis(arylphosphine)-carbonyliridium(I) complexes. Stereospecifically *cis* products are obtained in benzene or chloroform. Mixtures of *cis* and *trans* isomers are formed in solvents such as methanol, acetonitrile, water or DMF.[75]

2.2.2.4 Stereochemistry of oxidative addition reactions.

The stereochemistry of oxidative addition plays an important, although not conclusive, role in formulating possible transitional states existing during oxidative addition reactions. Non-polar molecules (*e.g.* H_2 and O_2) following a one step concerted three centre mechanism, usually add to square planar complexes in such a way that the fragments of the addend molecule are *cis* to one another in the octahedral complex, *e.g.* the oxidative addition of H_2 to Vaska's complex [IrCl(CO)(PPh$_3$)$_2$][103]. Isomerisation of the oxidative addition product however can lead to a *trans* product, *e.g.* [Rh(tfaa)(I)$_2$(P(OPh$_3$))$_2$] with the two iodide ligands in the *trans* positions[73] (see paragraph 2.2.2.2 (i) on page 35). Polar molecules (*e.g.* CH$_3$I) on the other hand, usually following a S_N2 mechanism, add *trans* to one another, *e.g. trans* addition was found for the product of oxidative addition of CH$_3$I to the square planar complex [Rh(acac)(P(OPh)$_3$)$_2$] (determined by the ^{1}H NMR spectra of the oxidative addition product).[74] Many other examples have also shown *trans* addition of polar molecules to square planar complexes, but cases where *cis* addition of polar molecules took place, are also known *e.g.* the product of oxidative addition of CH$_3$I to the square planar complex [Rh(cupf)(CO)(PPh)$_3$].[82] See **Table 2.21** for the stereochemistry of selected products of oxidative addition to square planar Rh(I) and Ir(I) complexes. The stereochemistry of the oxidative addition products is also dependent on the solvent used for the reaction as was pointed out in paragraph 2.2.2.3 (iv).

The stereochemistry of the products of oxidative addition therefore cannot conclusively indicate whether the reaction took place *via* a three-centre or a linear transitional state.

---

[103] Vaska, L. and DiLuzio,J.W., *J. Am. Chem. Soc.*, **84**, 679 (1962) and **83**, 2784 (1961).

Table 2.21: Stereochemistry of selected octahedral Rh(III) and Ir(III) oxidative addition products as investigated by X-ray structures or NMR*.

Oxidative addition reaction	Product of oxidative addition isolated	*cis/trans addition*
$[Rh(acac)(PPh_3)_2] + I_2$	$[Rh(acac)(I)_2(PPh_3)_2]$[104]	*cis*
$[IrCl(CO)(PPh_3)_2] + H_2$	$[IrCl(CO)(H)_2(PPh_3)_2]$[103]	*cis*
$[Rh(tfaa)(P(OPh_3))_2] + I_2$	$[Rh(tfaa)(I)_2(P(OPh_3))_2]$[73]	*trans*
$[Rh(acac)(PPh_3)_2] + CH_3I$	$[Rh(acac)(CH_3)(I)(PPh_3)_2]$[105]	*cis*
$[Rh(cupf)(CO)(PPh_3)] + CH_3I$	$[Rh(cupf)(CO)(CH_3)(I)(PPh_3)]$[82]	*cis*
$[Rh(neocup)(CO)(PPh_3)] + CH_3I$	$[Rh(neocup)(CO)(CH_3)(I)(PPh_3)]$[106]	*cis*
$[Rh(quin)(CO)(P(4-CH_3-C_6H_4)_3)] + CH_3I$	$[Rh(quin)(CO)(CH_3)(I)(P(4-CH_3-C_6H_4)_3)]$[107]	*cis*
$[Rh(bpha)(P(OPh_3))_2] + CH_3I$	$[Rh(bpha)(CH_3)(I)(P(OPh_3))_2]$[108]	*trans*
$[Rh(dmavk)(CO)(PPh_3)] + CH_3I$	$[Rh(dmavk)(CH_3)(I)(CO)(PPh_3)]$[109]	*trans*
$[Rh(ox)(CO)(PPh_3)] + CH_3I$	$[Rh(ox)(CO)(CH_3)(I)(PPh_3)]$[110]	*trans*
$[Ir(acac)(cod)] + CH_3I$	$[Ir(sacac)(cod)(CH_3)(I)]$[111]	*trans*
$[Ir(sacac)(cod)] + CH_3I$	$[Ir(sacac)(cod)(CH_3)(I)]$[112]	*trans*
$[Rh(acac)(P(OPh)_3)_2] + CH_3I$	$[Rh(acac)(CH_3)(I)(P(OPh)_3)_2]$[74]	*trans**
$[Rh(acac)(PPh_3)_2] + CH_3I$	$[Rh(acac)(CH_3)(I)(PPh_3)_2]$[113]	*cis**
$[Rh(tfaa)(PPh_3)_2] + CH_3I$	$[Rh(tfaa)(CH_3)(I)(PPh_3)_2]$[113]	*cis**
$[Rh(hfaa)(PPh_3)_2] + CH_3I$	$[Rh(hfaa)(CH_3)(I)(PPh_3)_2]$[113]	*cis**
$[Ir(acac)(cod)] + Hg(CN)_2$	$[Ir(acac)(cod)(HgCN)(CN)]$[72]	*cis**

* stereochemistry characterisation from NMR .

[104] Basson, S.S., Leipoldt, J.G., Potgieter, I.M., Roodt, A. and van der Walt, T.J., *Inorg. Chim. Acta,* **119**, L9 (1968).

[105] Roodt, A., Botha, J.M., Otto, S., Shestakova, E.P. and Varshavsky, Y.S., R*hodium Ex.,* **17**, 4 (1996).

[106] Basson, S.S., Venter, J.A. and Roodt, A., *Manuscript in preparation.*

[107] Cano, M., Heras, J.V., Lobo, M.A., Pinilla, E. and Monge, M.A., *Polyhedron*, **11**, 2679 (1992).

[108] Lamprecht, G.J., van Zyl, G.J. and Leipoldt, J.G., *Inorg. Chim. Acta,* **164,** 69 (1989).

[109] Damoense, L.J., Roodt, A., Purcell, W., Galding, M.R. and Varshavsky, Y.S. *Manuscript in preparation.*

[110] van Aswegen, K.G., Leipoldt, J.G., Potgieter, I.M., Lamprecht, G.J., Roodt, A. and van Zyl, G.J., *Trans. Met. Chem.,* **16**, 369 (1991).

[111] Basson, S.S., Leipoldt, J.G., Purcell, W. and Schoeman, J.B., *Acta Cryst.*, **C45**, 2000 (1989).

[112] Terblans. Y.M., Basson, S.S., Purcell, W. and Lamprecht. G.J., *Acta Cryst.*, **C51**, 1748 (1995).

[113] Shestakova, E.P., Cherkasova, T.G., Osetrova L.V., Varshavsky, Y.S., Leipoldt, J.G. and Roodt. A., *Rhodium Ex.,* **7-8**, 24 (1994).

2.2.3   Insertion reactions

2.2.3.1 Definition of insertion reactions.

An insertion reaction can be defined as the incorporation of an unsaturated two-electron ligand (A=B) into a M-X σ bond (X being a one-electron ligand) of a transition metal complex L_nM-X. Of the various classifications of insertion reactions two are considered here:

(i)   Insertion types (1,1) and (1,2) etc. depending on how the addition between M and X to A=B takes place. Each proceeds through two distinct steps. The first involves incorporating A=B as a ligand within the metal coordination sphere. (L_nM-X must have no more than 16 electrons because the reaction requires a vacant coordination site.) The second step, often called migratory-insertion, incorporates A=B into the M-X bond.[114] See **Scheme 2.12**.

$$L_nM\text{ - }X\ +\ A=B\ \longrightarrow\ L_nM\text{ - }A=B\ \ (\overset{X}{|})\ \longrightarrow\ L_nM\text{ - }\overset{\overset{X}{|}}{A}=B\qquad (1,1)\text{-insertion}$$

$$L_nM\text{ - }X\ +\ A=B\ \longrightarrow\ L_nM\text{ -}\overset{\overset{X}{|}}{\underset{B}{\|}}{}^{A}\ \longrightarrow\ L_nM\text{ - A - B - X}\qquad (1,2)\text{-insertion}$$
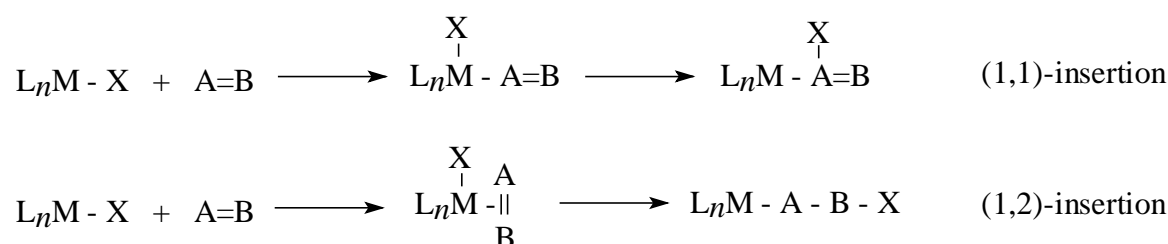
Scheme 2.12: **(1,1) and (1,2) insertion reactions of an unsaturated two-electron ligand (A=B) into a M-X σ bond (X being a one-electron ligand).**

In both the (1,1)- and (1,2)-insertion reactions the metal oxidation state remains unchanged. The migration of X to A=B (or A=B to X) requires that these ligands adopt a *cis* geometry within the metal sphere. During the migratory-insertion, the number of electrons and the metal coordination number decrease by two units and one unit respectively. The addition of a two-electron ligand is often required to stabilise the complex that is produced. Carbon monoxide CO is the ligand that most commonly undergoes (1,1) insertions. Alkenes and alkynes invariably give (1,2) insertions.

(ii)   The insertion processes can also be classified as intramolecular "migratory insertions" or as intermolecular "nucleophilic additions". The intramolecular "migratory insertions" take place

---

[114] Mathey, F. and Sevin, A., *Molecular Chemistry of the Transition Elements,* John Wiley & Sons, Chichester, 1996, p34 - 38.

by the combination of X and A=B while both are coordinated to the metal[115] (the second step of both insertion reactions of **Scheme 2.12**). See **Figure 2.22** for examples of intra[116]- and intermolecular[117] insertion reactions. The reaction $MeMn(CO)_5$ + ^{13}CO → $MeCOMn(CO)_4(^{13}CO)$ is considered as an intramolecular "migratory insertion" since the carbonyl insertion took place by a CO group already coordinated to $MeMn(CO)_5$, and not by the ^{13}CO group (see also paragraph 2.2.3.2).

$$\text{intra:} \quad MeMn(CO)_5 \ + \ ^{13}CO \ \longrightarrow \ \underset{\displaystyle \overset{O}{\|}}{Me\overset{}{C}} - Mn(CO)_4(^{13}CO)$$

$$\text{inter:} \quad CpMo(CO)_3CH_2Ph \ + \ C_6H_{11}NC \ \longrightarrow \ \underset{\displaystyle \underset{C=NC_6H_{11}}{\overset{PhCH_2}{|}}}{CpMo(CO)_3}$$
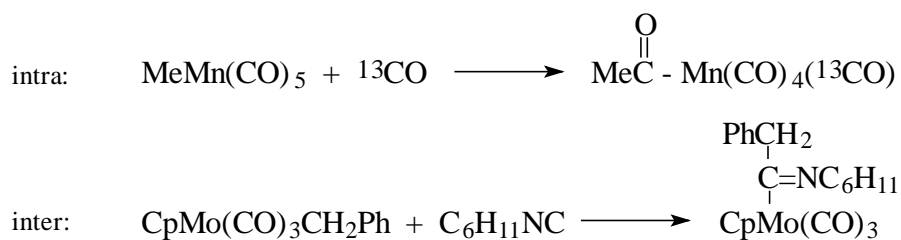
Figure 2.22: **Example of an intra- and an intermolecular insertion reaction.**

The rest of this discussion will be limited to the carbonyl insertion reactions into α-bonds of square planar complexes. Generally speaking, a carbonyl insertion reaction is regarded as known when any one of the following stoichiometric reactions has been fully characterised:[118]

(a) $R\text{-}M + CO \quad \rightarrow \quad RCO\text{-}M$ CO insertion into the metal-carbon σ-bond of a metal complex which may or may not contain carbonyl groups.

(b) $R\text{-}M(CO) \quad \rightarrow \quad RCO\text{-}M$ Conversion of a coordinated CO group into an acyl (or aroyl) group.

(c) $R\text{-}M(CO) + L \rightarrow \quad RCO\text{-}M(L)$ CO insertion into a metal carbonyl complex promoted by a Lewis base L.

(L = two-electron ligand, R is an alkyl or related σ-bonded group.)

---

[115] Collman, J.P. and Hegedus, L.S., *Principles and Applications of Organotransition Metal Chemistry,* University Science Books, Mill Valley, California, 1980, p. 259 - 298.

[116] Noack, K. and Calderazzo, F., *J. Organomet. Chem.,* **10**, 101 (1967)

[117] Yamamato, Y., and Yamazaki, H., *J. Organomet. Chem.,* **24**, 717 (1970)

[118] Calderazzo, F., *Angew. Chem. Int. Ed. Engl.,* **16**, 299 (1977).

2.2.3.2 Carbonyl insertion reactions.

Carbonyl insertion reactions for square planar complexes may be represented as follows, see **Scheme 2.13**, where [MR(CO)] is a reactant or an intermediate, R is an alkyl or related σ-bonded group, L stands for any ligand including CO and M represents a metal *together* with its ancillary ligands:
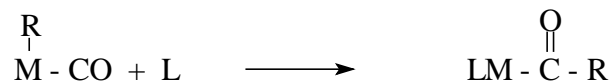
Scheme 2.13: Carbonyl (CO) insertion reactions for square planar complexes.

The question whether CO insertion takes place or whether the R group migrates was investigated for the complex $CH_3Mn(CO)_5$.[116], [119] With ^{13}CO as incoming ligand, the following were determined for the migratory insertion reaction:

(i)   The CO molecule that becomes the acyl-carbonyl is not derived from the external CO but is one already coordinated to the metal atom.

(ii)   The incoming CO is added *cis* to the acyl group (see **Scheme 2.14**).
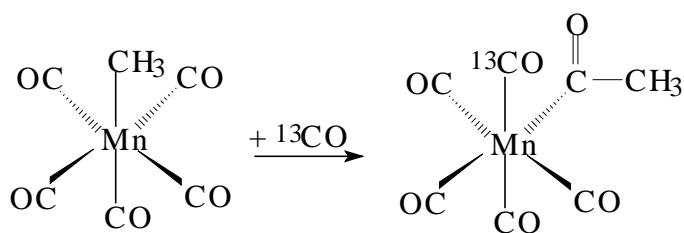
Scheme 2.14: Migratory insertion with ^{13}CO as incoming ligand to [CH$_3$Mn(CO)$_5$]. The acetyl group is formed by migration of the CH$_3$ group to one of the *cis* CO ligands.

(iii)   The conversion of alkyl into acyl can be affected by addition of ligands other than CO, see **Scheme 2.15**.

---

[119] Cotton, F.A. and Wilkinson, G., *Advanced Inorganic Chemistry,* John Wiley & Sons, New York, 1980, p 1248 – 1257.
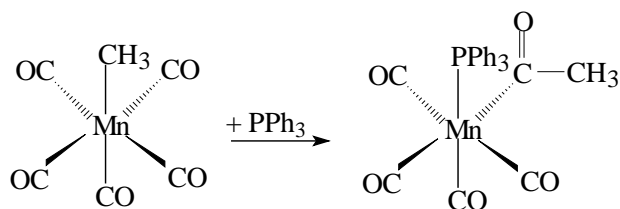
Scheme 2.15: Conversion of alkyl to acyl by addition of PPh₃ to [CH₃Mn(CO)₅].

(iv)   Kinetic studies of the above reaction (**Scheme 2.15**) showed that the first step involves an equilibrium between the octahedral alkyl and a 5-coordinate acyl species. The incoming ligand L (L = CO, PPh₃, *etc.*) then added to the 5-coordinate acyl species to re-form an octahedral complex. See **Scheme 2.16** .
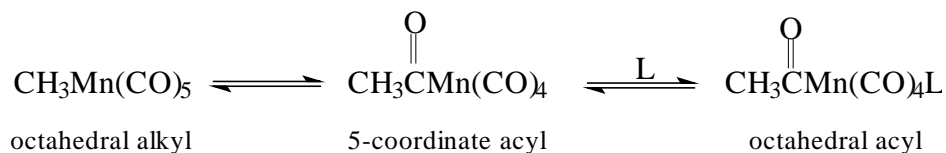
Scheme 2.16:   Addition of a ligand L to octahedral [CH₃Mn(CO)₅] alkyl in equilibrium with its 5-coordinate acyl species.

(v)   Polar solvents can participate in pre-equilibrium (**Scheme 2.17**) and give up to a factor 10^4 increase in the rate of the CO insertion reaction.[120]
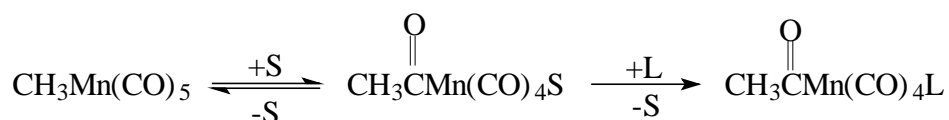
Scheme 2.17: Polar solvent participating in pre-equilibrium of a CO insertion reaction.

(vi)   Since the 5-coordinate species can undergo intramolecular rearrangements, more than one isomer of the final product may be formed.[121] See **Scheme 2.18** which also contains a relevant suggestion about the nature of the acyl intermediate.[118]

[120] Collman, J.P., Finke, R.G., Cawse, N.C. and Brauman, J.I., *J. Am. Chem. Soc.,* **100**, 4766 (1978).

[121] Noack, K., Ruch, M. and Calderazzo, F., *Inorg. Chem.*, **7**, 345 (1968).
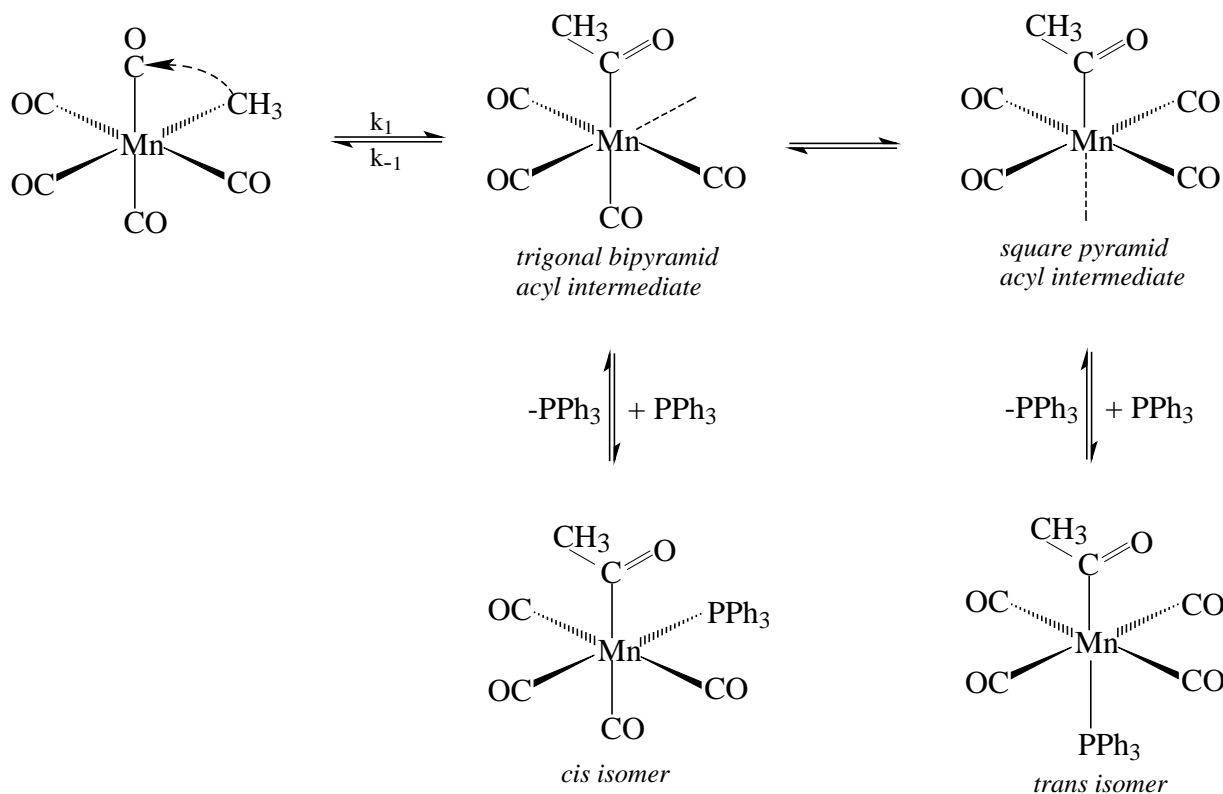
Scheme 2.18: Addition of a ligand PPh₃ to octahedral [CH₃Mn(CO)₅] alkyl giving *cis* and *trans* isomers of [CH₃COMn(CO)₄(PPh₃)][118]. Evidence (Scheme 2.14) indicate that CO insertion really takes place by alkyl migration. The orbital indicated with ------ is vacant.

The insertion reaction is thus best considered as an intramolecular alkyl migration to a coordinated carbon monoxide ligand in a *cis*-position, and the migration probably proceeds through a three-centre transitional state.[122] See **Scheme 2.19**.
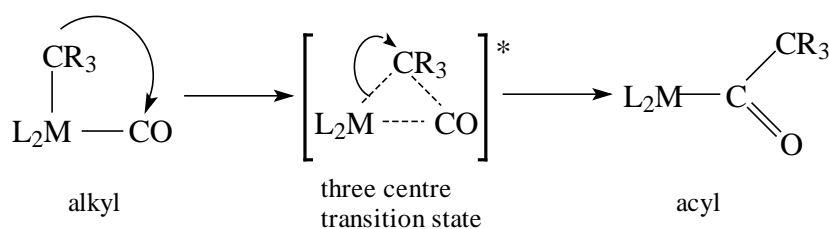
Scheme 2.19: Three-centre transition state proposed for carbonyl insertion reaction.

The requirement that carbonyl insertions (with the name not indicating any specific mechanism for the process in the rest of this presentation) proceed *via* an intramolecular alkyl migration to a coordinated carbon monoxide ligand in a *cis*-position is also illustrated by the fact that both the

---

[122] Cotton, F.A. and Wilkinson, G., *Advanced Inorganic Chemistry,* John Wiley & Sons, New York, 1980, p 1248 - 1257

alkyl and acyl derivatives of the rhodium(III) macrocyclic complex of **Figure 2.23** exist as stable compounds, but conversion of one into the other does not take place. Macrocyclic ligands effectively block the four planar coordination sites and therefore do not allow the two axial ligands to become adjacent to each other. The weakly bonded acetonitrile ligand dissociates readily to give vacant coordination site *trans* to the alkyl and acyl moieties in **Figure 2.23**, but no CO insertion from the *trans* position or decarbonylation (the inverse process of CO insertion) to the *trans* position takes place.[123]
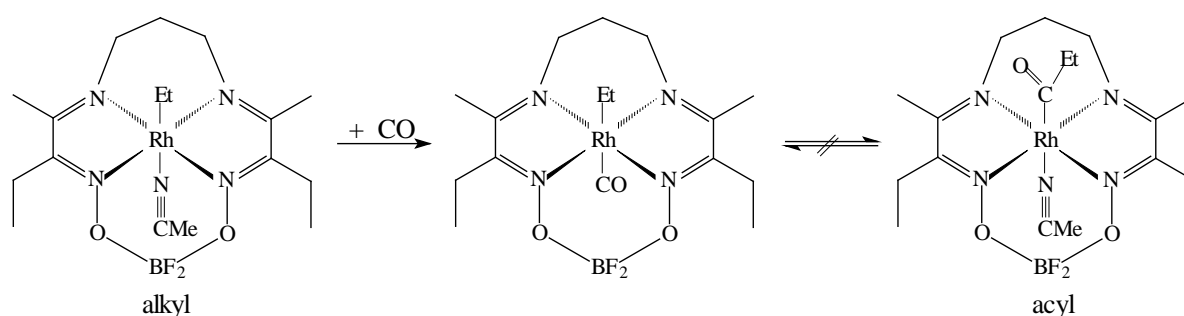
Figure 2.23: **An example of a stable macrocyclic rhodium(III) alkyl and acyl complex which can not be interconverted by carbonylation or decarbonylation.**[123]

Elimination of carbon monoxide accompanied by the conversion of an acyl group to the corresponding alkyl moiety has been termed decarbonylation. The decarbonylation can be affected thermally, photolytically or chemically. Acyl complexes can also rearrange in solution to alkyl complexes *e.g.* [[IrCl$_2$(COCH$_2$Ph)(PPh$_3$)$_2$] in benzene[124] (**Scheme 2.20**(a)), [RhCl$_2$(COCH$_3$)(PMe$_2$Ph)$_3$] with the addition of the ligand NH$_4$PF$_6$[125] (**Scheme 2.20**(b)) and the acyl product formed from an oxidative addition of iodomethane to [Rh(acac)(CO)(PX$_3$)] (in 1,2-dichloroethane) which slowly (10^{-4} s^{-1}) forms an alkyl as final product[80] (**Scheme 2.20**(c)).

---

[123] i) Collman, J.P. and Hegedus, L.S., *Principles and Applications of Organotransition Metal Chemistry,* University Science Books, Mill Valley, California, 1980, p. 285.

   ii) MacLaury, M., *Ph. D. dissertation*, Stanford University (1974)

[124] Kubota, M., Blake, D.M. and Smith, S.A., *Inorg. Chem.,* **10**, 1430 (1971).

[125] Bennet, M.A. Jeffery, J.C. and Robertson, G.B., *Inorg. Chem.,* **20**, 323 (1981).

(a)

(b)

(c)
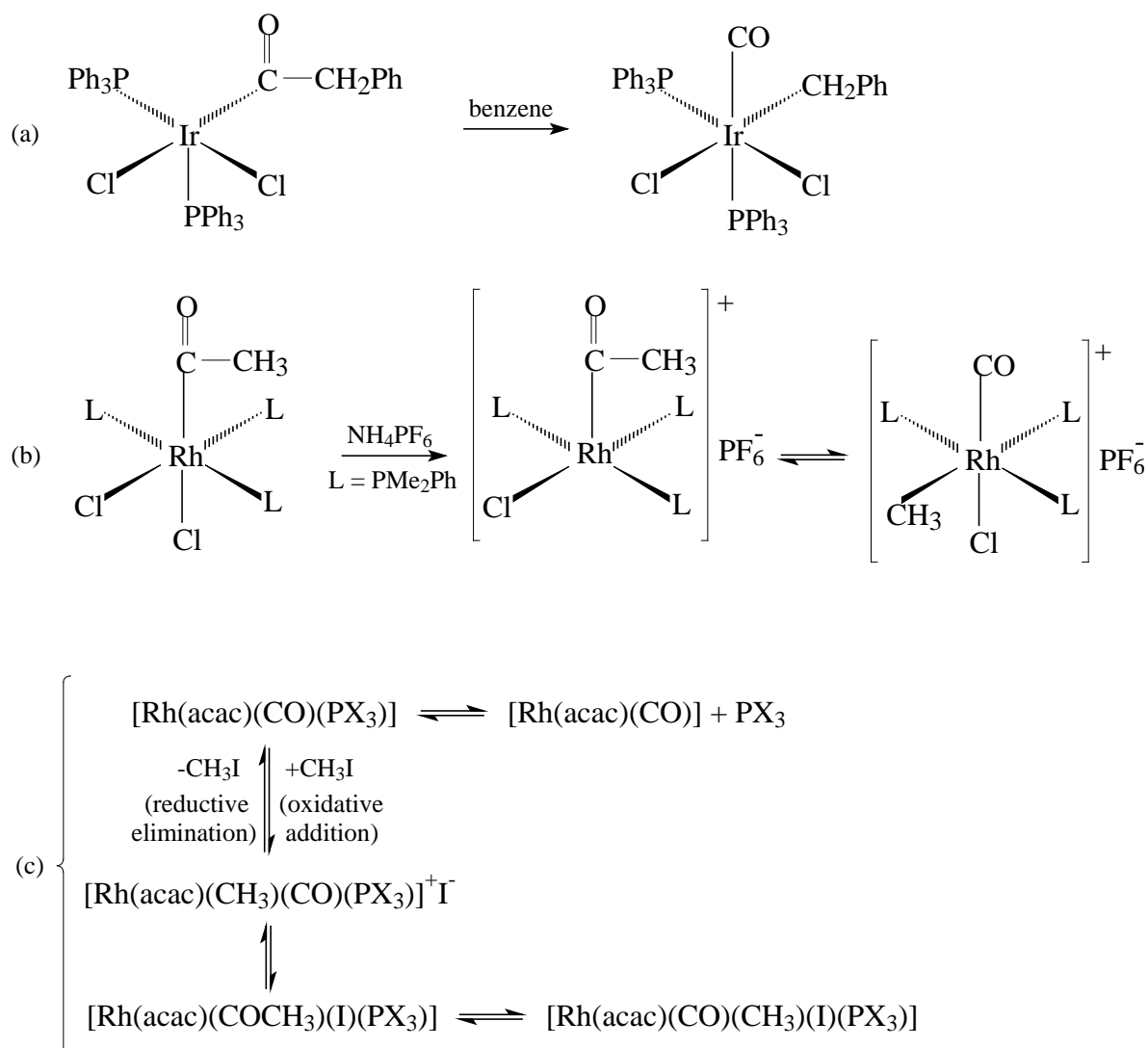
Scheme 2.20: **Decarbonylation of acyl complexes to the corresponding alkyl moieties.**

Structures of several acyl metal complexes have been determined by X-ray crystallography. Where such direct evidence is not available, the infrared and/or proton NMR spectra usually serve as reliable guides in ascertaining the nature of these products. Examples of crystal structures of the Rh(III) acyl-products isolated after the oxidative addition of CH_3I or CH_3CH_2I to square planar rhodium complexes of the type [Rh(L,L'-BIB)(CO)(PX$_3$)] is summarised in **Table 2.22**. The presentations of the structures of the complexes in **Figure 2.24** reveals the presence of the acyl moiety in the apical position of a distorted square pyramidal geometry around the rhodium centre. Although to the knowledge of the author there never have been recorded acyl bonds in the plane for Rh(III) acyl complexes with a bidentate ligand, it is possible to find acyl bonds in the plane for monodentate ligands.[126],[127]

---

[126] Hoffman, R. and Rossi, A.R., *Inorg. Chem.,* **14**, 365 (1975).

Table 2.22: Crystal structures of selected acyl complexes of rhodium.

Complex	L,L'-BIB
[Rh(stsc)(COCH$_3$)(I)(PCy$_3$)][54]	Hstsc = salicylaldehydethiosemicarbazose
[Rh(macsm)(COCH$_3$)(R)(PPh$_3$)][128]	Hmacsm = methyl(2-methyl-amino-1-cyclopentene-1-dithiocarboxylate)
[Rh(dmavk)(COCH$_3$)(I)(PPh$_3$)][129]	Hdmavk = dimethylaminovinylketone
[Rh(mnt)(COCH$_2$CH$_3$)(I)(PPh$_3$)]$^-$[130]	Hmnt = maleonitriledithiolate
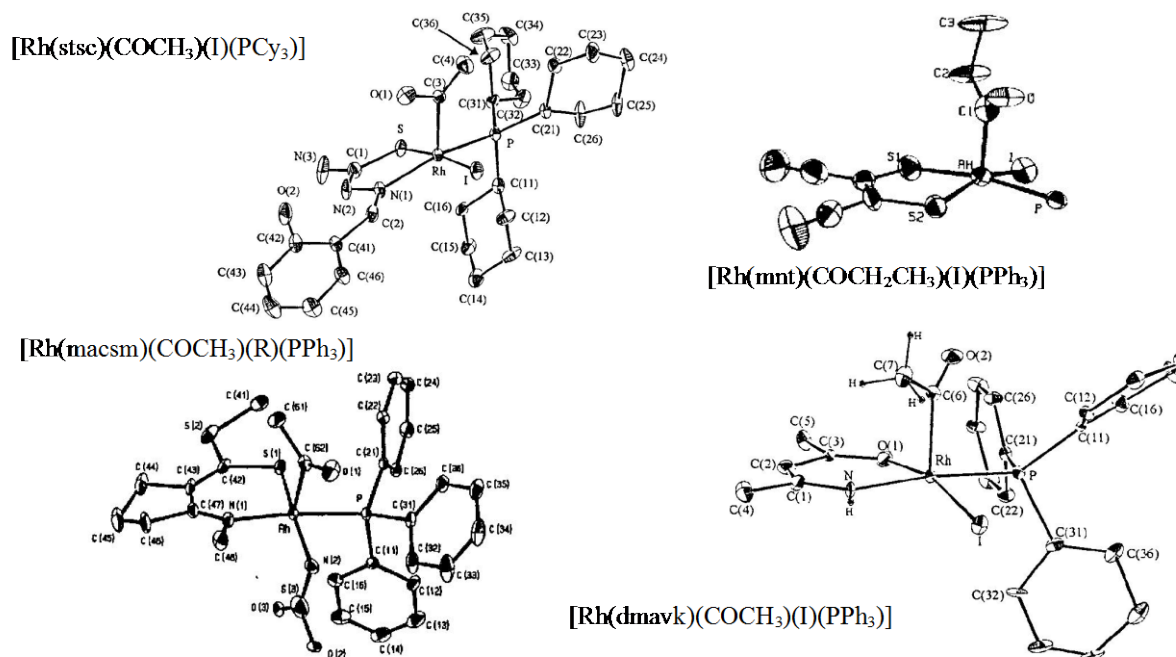
Figure 2.24: Examples of Rh(III) acyl-complexes of the type [Rh(L,L'-BIB)(COR)(I)(PX$_3$)].

2.2.3.3 Mechanism of insertion reactions.

CO insertion can take place without the addition of an external ligand. It is however important to take into account that the conversion of an alkyl to an acyl species, is often affected by the addition of ligands other than CO *e.g.* tertiary phosphines and phosphites, arsines, stibines, organic amines and iodide. Any general mechanism will thus have to reflect the interaction of

[127] Adamson, G.W., Daly, J.J. and Forster, D., *J. Organomet. Chem.,* **71**, C17 (1974).

[128] Steyn, G.J.J., Roodt, A. and Leipoldt, J.G., *Rhodium Ex.,* **0**, 11 (1993).

[129] Damoense, L.J., Purcell, W., and Roodt, A., *Rhodium Ex.,* **14**, 4 (1995).

[130] Cheng, C., Spivack B.D. and Eisenberg, R., *J. Am. Chem. Soc.,* **99**, 3003 (1977).

such ligands in the insertion process. A general mechanism for the CO insertion reaction may be represented as in **Scheme 2.21**.[131]

$$\begin{array}{ccc} \overset{R}{\underset{|}{M}} - CO & \underset{\underset{-L \quad k_{-4}}{\xleftarrow{\quad}}}{\overset{+L \quad k_4}{\xrightarrow{\quad}}} & (L)M - \overset{\overset{O}{||}}{C} - R \\ \underset{k_{-2}}{\overset{k_2}{\searrow}} & & \underset{k_{-3}}{\overset{+L \quad -L}{k_3}} \\ & [intermediate]^* & \end{array}$$
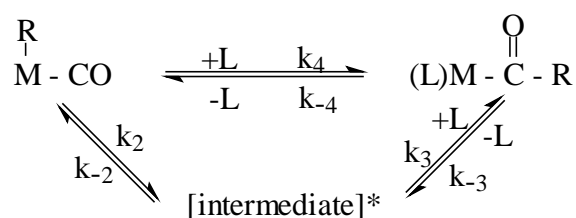
Scheme 2.21: **A general mechanism for the carbonyl (CO) insertion reaction. The other ligands are omitted for clarity.**

In this study the acyl formation from octahedral rhodium(III) alkyl complexes (formed from the oxidative addition of iodomethane to square planar rhodium(I) complexes) is considered. In this case the CO insertion reactions are of the type where no formal incoming ligand is involved for the insertion to take place and a general mechanism may be presented as follows (**Scheme 2.22**):

$$\left\{ \begin{array}{l} [Rh(L,L'\text{-}BID)(CO)(PPh_3)] \ + \ CH_3I \\ \\ \quad k_{-1} \ {\Big\updownarrow} \ k_1 \qquad \text{oxidative addition step} \\ \\ [Rh(L,L'\text{-}BID)(CO)(CH_3)(I)(PPh_3)] \qquad \text{alkyl} \\ \\ \qquad {\Big\downarrow} \ k_2 \qquad\qquad \text{CO insertion} \\ \\ [Rh(L,L'\text{-}BID)(COCH_3)(I)(PPh_3)] \qquad \text{acyl} \end{array} \right.$$

$$OR \quad Rh(I) + CH_3I \ \underset{k_{-1}}{\overset{k_1}{\rightleftharpoons}} \ Rh(III) \ alkyl \ \overset{k_2}{\longrightarrow} \ Rh(III) \ acyl$$
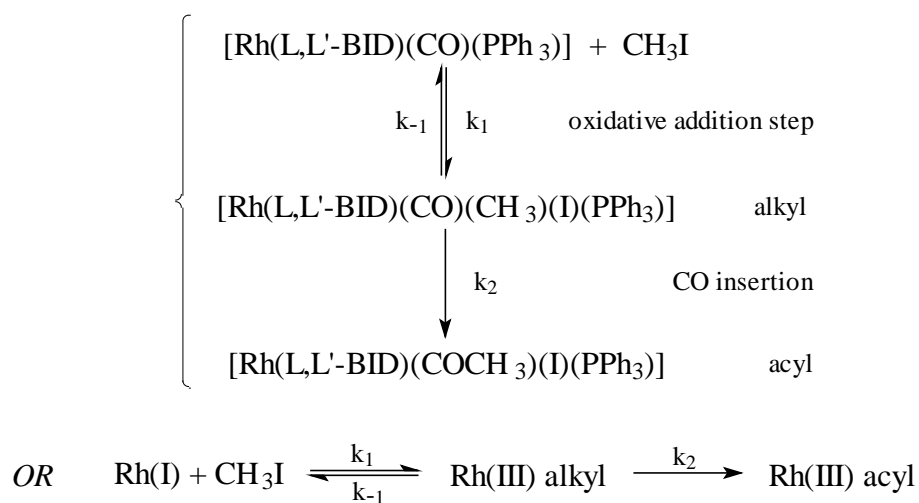
Scheme 2.22: **A mechanism including a carbonyl insertion step proceeding without a formal incoming ligand. This mechanism is just intramolecular isomerisation.**

For the reaction of the type of **Scheme 2.22**, namely

$$A + B \ \underset{k_{-1}}{\overset{k_1}{\rightleftharpoons}} \ C \ \overset{k_2}{\longrightarrow} \ D$$
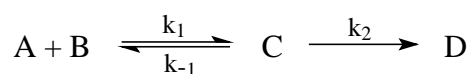
the following equation can be derived for the observed rate of formation of the acyl product:[132]

---

[131] Wojcicki, A., *Adv. Organometal. Chem.,* **11**, 87 (1973).

Equation 2.1: $$k_{obs\ acyl} = \frac{k_2 K_1 [B]}{1 + K_1 [B]} = \frac{k_2 K_1 [CH_3I]}{1 + K_1 [CH_3I]}$$

with the equilibrium constant $K_1 = k_1/k_{-1}$.

The latter equation can be interpreted in terms of the following considerations:[54]

(i)   If $k_1[CH_3I]$, $k_{-1} \gg k_2$, then the first step is a fast equilibrium and **Equation 2.1** keeps its form, with $k_{obsd} = k_2 K_1 [CH_3I]/(1+K_1[CH_3I])$. k_{obsd} thus increases with increasing $[CH_3I]$, reaching a limiting value at high concentrations of iodomethane.

(ii)   If $k_1[CH_3I] \gg k_{-1} \gg k_2$, the equilibrium is shifted to the right so that K_1 is large and thus $(1+K_1[CH_3I]) \cong K_1[CH_3I]$, which in turn reduces **Equation 2.1** to $k_{obsd} = k_2$. The latter predicts that the rate at which CO insertion takes place is independent of $[CH_3I]$. A plot of k_{obsd} *v.s.* $[CH_3I]$ will thus show a straight line parallel to the $[CH_3I]$ axis and only at very low concentrations of iodomethane will k_{obsd} decrease toward a theoretical value of zero at $[CH_3I] = 0$ mol dm^{-3}.

(iii)   If $k_{-1} \gg k_1[CH_3I] \gg k_2$, the equilibrium is shifted to the left so that K_1 is small and thus $(1+K_1[CH_3I]) \cong 1$, which in this case reduces **Equation 2.1** to $k_{obsd} = k_2 K_1 [CH_3I]$. There will thus exist a linear relationship (with zero intercept) between k_{obsd} and $[CH_3I]$ in this case.

2.2.3.4 Factors influencing insertion reactions.

(i)   *Role of the metal centre.*

Few comparative kinetic studies have been made on the same carbonyl system for two members of a given transition metal group. Qualitative data show that the reactivity of transition metal alkyls towards carbonyl insertion reactions usually decreases with a descent of the same subgroup or traid. That is, alkyls of first-row transition metals are more reactive than those of the second-row transition metals, which are more reactive than those of third-row metals:

[132] Wilkins, R.G., *Kinetics and Mechanism of Reactions of Transition Metal Complexes,* 2nd thoroughly revised edition, VCH, Weinheim, 1991, p.24

$3d > 4d > 5d$.[131] This is illustrated by the reaction of complexes of the type [MCl(CO)(PPh$_3$)] (M = Ir(5d) and Rh(4d)) with iodomethane according to **Scheme 2.23**. For M = Rh the complete reaction scheme was applicable.[92] In the case where M = Ir, infrared spectroscopy indicated that the alkyl procuct formed 'immediately' but with no evidence of isomerisation to an acyl product within several days.[88, 92] This tendency probably reflects the greater stability of the Ir-C over the Rh-C σ bond (stronger 5d transition metal-carbon σ bond over the 4d transition metal-carbon σ bond).[115, 118] Examples of the relative reactivity of carbonyl insertion reactions of isostrutural transition metal complexes in a given group of the transition metals are summarised in **Table 2.23**.
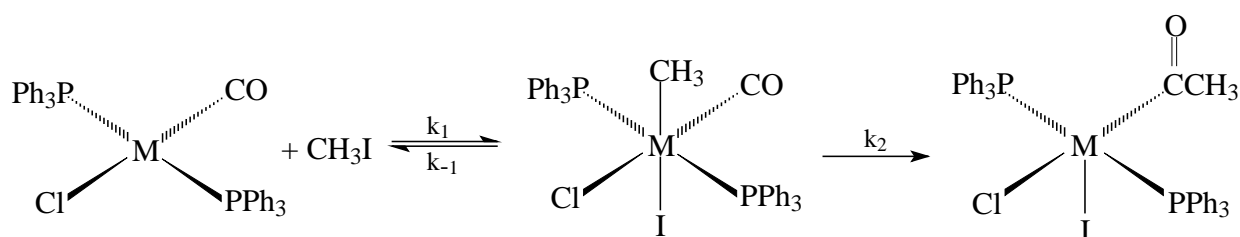
Scheme 2.23: **Mechanism for the reaction of [MCl(CO)(PPh₃)] with iodomethane.**

Table 2.23: Comparison of the relative reactivity of carbonyl insertion of isostructural series of 3d, 4d and 5d transition metal (M) complexes.

Group	Reaction*	Acyl product	Relative reactivity
Cr, Co, Ni	[CpM(CO)$_3$(R)] + PPh$_3$	[CpM(CO)$_2$(COR)(PPh$_3$)]	W(5d) << Mo(4d) ≈ Cr(3d)[115, 118, 131]
Mn, Tc, Re	[RM(CO)$_5$] + L	-	Re(5d) < Mn(3d)[115, 118]
Fe, Ru, Os	[CpM(CO)$_2$(CH$_3$)] + PPh$_3$	[CpM(CO)(COCH$_3$)(PPh$_3$)]	Os(5d) << Ru(4d)[133] < Fe(3d)[134] (Ru needs higher temperature to react than Fe. Os fails to react under the same conditions)[115 131]
Co, Rh, Ir	[MCl(CO)(PPh$_3$)$_2$] + CH$_3$I	[MCl(COCH$_3$)(I)(PPh$_3$)$_2$]	Ir(5d)[88] <<< Rh(4d)[92] (no acyl product for Ir)[92]
Ni, Pd, Pt	*trans*[M(PEt$_3$)$_2$(Me)X] + CO X = Cl, Br	*trans*[M(PEt$_3$)$_2$(COMe)X]	Pt(5d) < Pd(4d)[131] (80 atm and 90°C required for Pt to react *v.s.* 1-3 atm and room temperature for Pd)[131, 135]

* M = transition metal of the given group.

[133] Green, M.L.H., Mitchard, L.C. and Swanwick, M.G., *J. Chem. Soc.,* **A**, 794 (1971).

[134] Green, M., and Westlake, D.J., *J. Chem. Soc.*, **A**, 367 (1971).

[135] Booth, G. and Chatt, J., *J. Chem. Soc.,* **A**, 634 (1966).

(ii)   *Effect of the migrating group (R).*

Electron releasing groups R bonded to a transition metal complex, enhance the rate of acyl formation of the complex involved.   The opposite occurs for electron withdrawing (more electronegative) R groups.[131] The effect of more electronegative groups retarding the rate of acyl formation probably derives from the increase in alkyl to metal bond strength brought about by an increase in electronegativity of R.[115]   See **Table 2.24** for examples where electron-releasing groups R (in most of the cases) enhance the rate of acyl formation.

Table 2.24: Examples illustrating the influence of the migrating group R (bonded to the transition metal complex) on the relative rate of acyl formation of the transition metal complex involved. (This order parallel in most cases the order of electronegativity R.)

Reaction*	Acyl product	Relative rate of acyl formation
$[(C_5Me_5)RhR(CO)I] + PPh_3$	$[(C_5Me_5)Rh(COR)(PPh_3)I]$	$R = p\text{-}MeC_6H_4 > Ph > p\text{-}ClC_6H_4 > p\text{-}OHCC_6H_4 > p\text{-}NCC_6H_4 \approx p\text{-}O_2NC_6H_4$ [136], $R = Ph > Me$ [136]
$[RhR(CO)(PPh_3)_2Cl_2] \square [Rh(COR)(PPh_3)_2Cl_2]$	$[Rh(COR)(PPh_3)_2Cl_2]$	$R = Me > Ph$ [137]
$[RIr(CO)_2(AsPh_3)Cl_2] + AsPh_3$	$[Ir(CO)(COR)(AsPh_3)_2Cl_2]$	$Et > Me$ [138]
$[RMn(CO)_5] + CO$	$[(RCO)Mn(CO)_5]$	$R = n\text{-}Pr > Et > Ph > Me >> CH_2Ph$ and CF_3 [131, 139]
$[RFe(CO)_2(C_p)] + PPh_3$	$[(COR)Fe(CO)(PPh_3)(C_p)]$	$R = i\text{-}Pr > Et > Me$ [134]
$[RMo(CO)_3(C_p)] + L$ $L = PPh_3, P(OCH_2)_3CMe, P(OMe)_3$	$[(COR)Mo(CO)_2(L)(C_p)]$	$R = Et > Me > CH_2Ph > CH_2CH=CH_2$ [140, 141]
$[RMn(CO)_5] \rightarrow [(COR)Mn(CO)_4]$	$[(COR)Mn(CO)_4]$	$R = CH_3 > H^{**}$ [142]

* R = migrating group
** from a theoretical study ΔH^*(for methyl migration) $< \Delta H^*$(for hydride migration)

---

[136] Bassetti, M., Sunley, G.J., Fanizzi F.P. and Maitlis, P.M., *J. Chem. Soc. Dalton Trans.*, 1799 (1990).

[137] Egglestone, D.L., Baird, M.C., Lock, C.J.L. and Tuner, G., *J. Chem. Soc. Dalton Trans.,* 1576 (1977).

[138] Glyde, R.W. and Mawby, R.J., *Inorg. Chim. Acta.,* **4**, 331 (1970).

[139] Calderazzo, F. and Cotton, F.A., *Abst. Int. Conf. Coordination Chem., Stockholm,* Paper 6H7 (1962).

[140] Craig, P.J. and Green, M., *J. Chem. Soc.*, **A**, 1978 (1968).

[141] Craig, P.J. and Green, M., *J. Chem. Soc.*, **A**, 157 (1969).

[142] Ziegler, T., Verluis, L. and Tschinke, V., *J. Am. Chem. Soc.*, **108**, 612 (1986).

(iii)   *Role of the solvent.*

Transition metal alkyls can be divided into two categories with respect to solvent dependence of their CO insertions:[131]

(a)   Transition metal alkyls whose reactions depend on the nature of the solvent.

(b)   Transition metal alkyls that react by the k_2 path (**Scheme 2.21** page 61) and are not influenced by the solvent employed.

A number of representative data of both categories are given in **Table 2.25**. *E.g.* the rate of $[MeMn(CO)_5]$ with $[C_6H_{11}NH_2]$[143] belonging to group (a) varies markedly with the dielectric constant and with the nucleophilic power of the solvent (up to a factor 10^4). The increase in the rate constant parallels the increase in donicity, showing that in general a more polar solvent aids the reaction (**Table 2.25** (a)). However, the fact that k_2 is considerably larger for methanol than for nitromethane, although the latter has a higher dielectric constant, suggests that the coordinating ability of the solvent may also be important.   The kinetics of carbonylation of $[EtPt(CO)(AsPh_3)Cl]$[144] and of $[EtIrCl_2(CO)_2(AsPh_3)]$[138] were interpreted as involving only little solvent assistance if any, although an acyl intermediate was considered to be operative also in these cases (**Table 2.25** (b)).

The role of the solvent on the mechanism of CO insertion can thus be reflected in the influence to reactivity as well as the coordinating ability of the solvent. The question still remains as to how solvent assistance takes place. There are two conflicting explanations[145] for this type of solvent effects on carbonyl insertion reactions:

(A) The solvent, especially polar ones, may lower the energy barrier to the formation of a transition state during carbonyl insertion (possibly three centre as in **Scheme 2.19** page 57) by solvation.

---

[143] Mawby, R., Basolo, F. and Pearson, R.G., *J. Am. Chem. Soc.,* **86**, 3994 (1964).

[144] Glyde, R.W. and Mawby, R.J., *Inorg. Chem.,* **10**, 854 (1971).

[145] Flood, T.C., Jensen, J. and Statler, J.A., *J. Am. Chem. Soc.*, **103**, 4410 (1981).

(B) Direct attack on the metal centre by the solvent (solvents with high donocity) will increase the electron density on the metal centre and subsequently lead to a decrease in Rh-R bond strength increasing the migratory ability of the coordinated R group to the carbonyl.

Table 2.25: Influence of solvent on rates of CO insertion. (Note that the table continues on the next page and that the explanations of the superscripts are at the end of the table).

Solvent	k_2 / s^{-1} [a]	k_4 / mol^{-1} dm^{+3} s^{-1} [a]	ε (dielectric constant)
(a) Solvent dependant [b]			
[MeMn(CO)$_5$] + [C$_6$H$_{11}$NH$_2$] → [(MeCO)Mn(CO)$_4$(C$_6$H$_{11}$NH$_2$)][143] (T = 25.5 °C)			
DMF	> 1.5 x 10^{-2}	-	26.6
methanol	6.33 x 10^{-3}	-	31.2
nitromethane	1.66 x 10^{-3}	-	37.4
THF	9.63 x 10^{-4}	-	7.70
mesitylene	2.18 x 10^{-6}	1.11 x 10^{-4}	2.27
hexane	to small, if any	2.70 x 10^{-5}	1.91
[Rh(cupf)(CO)(CH$_3$)(PPh$_3$)I] ↔ [Rh(cupf)(COCH$_3$)(PPh$_3$)(I)][146]			
DMSO	36.7(4) x 10^{-4}	-	45.0
acetonitrile	17.0(7) x 10^{-4}	-	38.0
nitromethane	15.8(9) x 10^{-4}	-	35.9
acetone	13.5(1) x 10^{-4}	-	20.7
ethyl acetate	12.5(2) x 10^{-4}	-	6.0
THF	11.2(2) x 10^{-4}	-	7.6
benzene	9.96(1) x 10^{-4}	-	2.3
(b) Not influenced by solvent[c]			
[EtPt(CO)(AsPh$_3$)Cl] + AsPh$_3$ → [(COEt)Pt(CO)(AsPh$_3$)$_2$Cl][144] (T = 40.0 °C)			
1,2-dichloroethane	14.0 x 10^{-4}	-	10.4
nitrobenzene	11.4 x 10^{-4}	-	34.8
cyclohexanone	8.20 x 10^{-4}	-	18.3
chlorobenzene	7.57 x 10^{-4}	-	5.6
diethyl ketone	6.60 x 10^{-4}	-	17.0
THF	4.92 x 10^{-4}	-	7.70
[Rh(cacsm)(CO)(CH$_3$)(P(*p*-MeOPh)$_3$)I] → [Rh(cacsm)(COCH$_3$)(P(*p*-MeOPh)$_3$)(I)][d] [54] (T = 25 °C)			
ethyl acetate	0.017(1)	-	6.0
acetone	0.0094(3)	-	20.7
chloroform	0.0029(1)	-	4.9

146 Basson, S.S., Leipoldt, J.G. and Venter, J.A., South African Chemical Institute 31 st Convention, Grahamstad, Poster G7 (1991).

(c) Steric influence of the solvent.[e]					
$[Rh(cupf)(CO)(CH_3)(PPh_3)I] \leftrightarrow [Rh(cupf)(COCH_3)(PPh_3)(I)]$[146]					
Solvent	k_2 / s^{-1} [a]	k_4 / mol^{-1} dm^{+3} s^{-1} [a]	ε	E_Γ [f]	D_n [f]
THF	11.2(2) x 10^{-4}	-	7.6	37.4	20.0
2-Me-THF	10.3(2) x 10^{-4}	-		36.5	12.0
2,5-Me$_2$-THF	9.12(1) x 10^{-4}	-			
acetone (CH$_3$COCH$_3$)	13.5(1) x 10^{-4}	-	20.7	42.2	17.0
methyl-tert.-buthyl ketone (CH$_3$COC(CH$_3$)$_3$)	4.2(6) x 10^{-4}	-			

[a] k_2 and k_4 refer to the different reaction pathways presented in **Scheme 2.21** page 61.

[b] Analogous trends were observed for the insertion reactions: (solvents given in decreasing order of influence on the rate of CO insertion with ε given in brackets after each solvent)

(I) $[CpMo(CO)_3CH_3] + [P(n\text{-}OC_4H_9)_3] \rightarrow [CpMo(CO)_2(COCH_3)P(n\text{-}OC_4H_9)_3]$[147]
        (DMF (26.6) > THF (7.70) $\geq$ nitromethane (37.4) > toluene (2.40))

(II) $[MeMn(CO)_5] + [P(OCH_2)_3CCH_3] \rightarrow [(MeCO)Mn(CO)_4(P(OCH_2)_3CCH_3)]$[148]
        (acetonitrile (38.0) >> acetone (20.7) > THF (7.70) > chloroform (4.9) > benzene (2.28))

(III) $[MeMn(CO)_5] + CO \rightarrow [(MeCO)Mn(CO)_5]$[149]
        (DMF (26.6) > β,β'-dichlorodiethyl ether (21.2) > β,β'-diethoxydiethyl ether (5.68) > n-octhyl chloride (4.96) > di-n-buthyl ether (3.06) > mesitylene (2.27))

[c] An analogous trend was observed for the insertion reaction:
        $[EtIrCl_2(CO)_2(AsPh_3)] + AsPh_3 \rightarrow [(COEt)IrCl_2(CO)(AsPh_3)_2]$[138]
        solvent (ε, k_2) = cyclohexanone (18.3, 4.2 x 10^{-5} s^{-1}), 1,2-dichloroethane (10.4, 15.0 x 10^{-5} s^{-1}), THF (7.7, 5.8 x 10^{-5} s^{-1}), chlorobenzene (5.6, 11.0 x 10^{-5} s^{-1})).

[d] Rh-alkyl formed after addition of CH$_3$I to $[Rh(cacsm)(CO)(PPh_3)]$ according to **Scheme 2.22** page 61.

[e] An analogous trend was observed for the insertion reaction:
        $[CpMo(CO)_3Me] + [PMePh_2] \rightarrow [CpMo(CO Me)(PMePh_2)(CO)_2]$[150] (T = 59.9(1) °C)
        (2,5-Me$_2$-THF < THF)
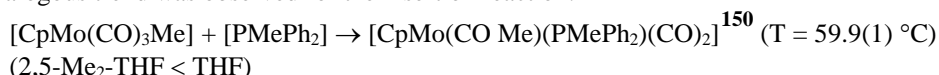
[f] E_Γ = polarity and D_n = donocity from ref [151]

A solvent-coordinated intermediate for the DMSO activated carbonyl insertion reaction of $[C_pFe(CO)_2R]$[152] according to **Scheme 2.24** was identified with NMR. This solvent-coordinated intermediate indicates a direct attack of the donor solvent at the metal centre as a mechanism for solvent participation during the carbonyl insertion reaction. The reaction of this same complex $[C_pFe(CO)_2R]$ with PPh$_3$ was also studied by Bibler *et.al.*[153] Under identical conditions in terms

[147] Butler, I.S., Basolo, F. and Pearson, R.G., *Inorg. Chem.,* **6**, 2074 (1967).

[148] Green, M, Hancock, R.I. and Wood, D.C., *J. Chem. Soc.,* **A**, 2718 (1968).

[149] Calderazzo, F. and Cotton, F.A., *Inorg. Chem.,* **1**, 30 (1962).

[150] Wax, M.J., and Bergman, R.G., *J. Amer. Chem. Soc.,* **103**, 7029 (1981).

[151] Marcus, Y., *Chem. Soc. Rev.*, 409 (1993).

[152] Nicholas, K., Raghu, S. and Rosenblum, M., *J. Organomet. Chem.,* **78**, 133 (1974).

[153] Bibler, J.P. and Wojcicki, A., *Inorg. Chem.,* **5**, 889 (1966).

of time and temperature the acyl complex was formed in the polar solvent tetrahydrofuran (THF) but not in the non-polar solvent hexane. The THF solvent thus assists in the formation of the acyl species according to the k_2-pathway of the general mechanism of **Scheme 2.21**, page 61, and occupies the vacant coordination site in the acyl complex left by the migrated methyl group.
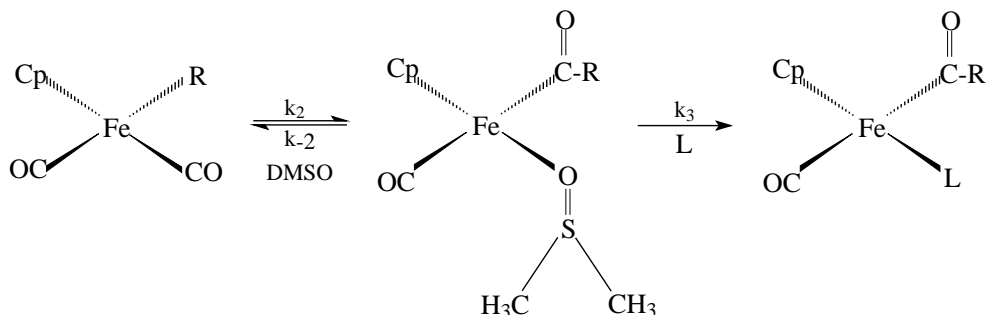
Scheme 2.24: DMSO activated carbonyl insertion reaction of [C$_p$Fe(CO)$_2$R].

The steric influence of the solvent was investigated for the CO insertion reaction of [Rh(cupf)(CO)(CH$_3$)(PPh$_3$)I] to give [Rh(cupf)(COCH$_3$)(PPh$_3$)(I)].[146] A range of THF derivatives with different steric bulkiness was used (THF, 2-Me-THF and 2,5-Me$_2$-THF) for which it was assumed that their donocity would differ but not their polarity. It was found that in spite of the higher Lewis basicity of 2,5-Me$_2$-THF (than THF) the conversion to the acyl complex still proceeds more rapidly in THF. The tendency of slowing down the methyl migration was ascribed to the larger steric demand of 2,5-Me$_2$-THF. See **Table 2.25**(c). In this case the effect of the solvent can be explained only in the context of direct attack of donor solvents at the metal centre as the alkyl migration is occurring. In other words, these migrations are "solvent catalysed".[150]

(iv)   *Effect of the entering ligand.*

The effect of the entering ligand L is intimately related to the nature of the solvent. If the solvent is nonpolar and lacks coordinating ability, then generally the insertion will proceed via an attack of L upon the alkyl compound via the k_4-pathway (**Scheme 2.21** page 61). *E.g.* the reaction [MeMn(CO)$_5$] + [C$_6$H$_{11}$NH$_2$] → [Me(CO)Mn(CO)$_4$(C$_6$H$_{11}$NH$_2$)] in hexane (see **Table 2.25** or **Table 2.26** reaction 1).

However, in a solvent that is polar and capable of coordination, competition will exist between the reaction of the intermediate with L to give the acyl product (the k_2,k_3-pathway) and the direct k_4-pathway alone.[131] If L is a sufficiently good nucleophile to react the intermediate (whether solvated or not), then the k_2 path prevails either alone (*e.g.* **Table 2.26** reactions 2 - 6) or in parallel with the k_4 path (*e.g.* **Table 2.26** reactions 7 and 8). If not, then the insertion may still proceed *via* the k_4 path (*e.g.* **Table 2.26** reactions 9 and 10).

Table 2.26: Carbonyl insertion reactions with various entering ligands L.

No.	L	k_2 / s^{-1}	k_{-3} / k_3	$k_4 / mol^{-1} dm^{+3} s^{-1}$
(a) Reaction in nonpolar solvent				
[MeMn(CO)$_5$] + [C$_6$H$_{11}$NH$_2$] $\rightarrow$ [Me(CO)Mn(CO)$_4$(C$_6$H$_{11}$NH$_2$)] (T = 25.5 °C) in hexane[143]				
1	[C$_6$H$_{11}$NH$_2$]	to small, if any	-	2.70×10^{-5}
(b) Reactions in polar medium				
[CpFe(CO)$_2$Et] + L $\rightarrow$ [CpFe(CO)L(COEt)] (T = 47.5 °C) in acetonitrile[134]				
2	PPh$_3$	1.32×10^{-4}	0.36	-
3	PMe$_2$Ph	2.22×10^{-4}	0.41	-
4	PMePh$_2$	1.78×10^{-4}	0.35	-
5	P(OMe)$_3$	1.84×10^{-4}	0.54	-
6	P(OPh)$_3$	1.35×10^{-4}	0.81	-
[CpMo(CO)$_3$Me] + L $\rightarrow$ [CpMo(CO)$_2$L(COMe)] (T = 50.7 °C) in toluene[147]				
7	P(*n*-Bu)$_3$	5.80×10^{-6}	-	6.44×10^{-5}
8	P(*n*-OBu)$_3$	5.80×10^{-6}	-	5.00×10^{-5}
9	PPh$_3$	-	-	3.22×10^{-5}
10	P(OPh)$_3$	-	-	8.33×10^{-6}
(c) Reactions with entering ligand L with varying steric demands				
[CpFe(CO)$_2$(CH$_2$Cy)] + L $\rightarrow$ [CpFe(CO)L(COCH$_2$Cy)] (T = 30°C) in DMSO[154]				
No.	L	Tolmans steric parameter θ / deg.	Tolman electronic parameter ν(CO) / cm^{-1}	$k_3 / mol^{-1} dm^{+3} s^{-1}$
11	PMe$_2$Ph	122	2065.3	$1.48(6) \times 10^{-4}$
12	PMePh$_2$	136	2067.0	$1.37(9) \times 10^{-4}$
13	PEtPh$_2$	140	2066.7	$1.12(5) \times 10^{-4}$
14	PPh$_3$	145	2068.9	$1.04(20) \times 10^{-4}$
15	P^{i}PrPh$_2$	150	2065.7	$0.79(7) \times 10^{-4}$
16	P^{t}BuPh$_2$	157	2064.7	$0.39(3) \times 10^{-4}$
17	PCy$_3$	170	2056.4	no reaction

---

[154] Cotton, J.D. and Markwell, R.D., *Inorg. Chim. Acta,* **63**, 13 (1982).

The steric demand of the incoming ligand L is illustrated for the reaction

$$[CpFe(CO)_2(CH_2Cy)] + L \rightarrow [CpFe(CO)L(COCH_2Cy)]^{154}$$
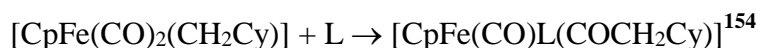
with a varying L in **Table 2.26** reactions 11 – 17. This reaction proceeded *via* the k_2,k_3-pathway of **Scheme 2.21** page 61 by setting up the pre-equilibrium

$$[CpFe(CO)_2(CH_2Cy)] + DMSO \leftrightarrow [CpFe(CO)(DMSO)(COCH_2Cy)]$$
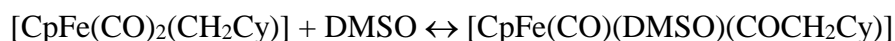
before adding the tertiary phosphine L. It is clear that, as the steric demand of the incoming phosphine increased (increase in cone angle θ), the value of k_2 decreased gradually for cone angles 120° - 130° with a more pronounced decrease in the case of the higher cone angles. The tertiary phosphine PCy_3 with a very high cone angle (170°) did no react observably. No correlation could be found between the electronic parameter ν(CO) of the complexes and their reactivity. The steric influence of the respective phosphines thus seems to be the controlling parameter in this case.

(v)   *Effect of the ancillary ligands.*

The effect of ancillary ligands on carbonyl insertion is well illustrated by the spontaneous carbonyl insertion of isomer I of $[PtCl(Ph)(CO)(PMePh_2)]$ which, in the absence of a nucleophile, produces the halide-bridged acyl complex $[Pt_2(\mu\text{-}Cl)_2(COPh)_2(PMePh_2)_2]$, IV, with which it equilibrates in solution[155] (see **Scheme 2.25**). In isomer II the migrating group Ph and CO are *trans* to one another making methyl migration impossible since a *cis* configuration is needed (see paragraph 2.2.3.2 page 55). In isomer III the migrating group Ph is *trans* to the halogen Cl that has a lower *trans* influence compared to $PMePh_2$ and thus the Pt-Ph bond is not sufficiently weakened for Ph migration to proceed (see paragraph 2.1.4.1 page 14).

---

[155] Anderson, G.K. and Cross, R.J., *J. Chem. Soc. Dalton Trans.*, 1246 (1979).
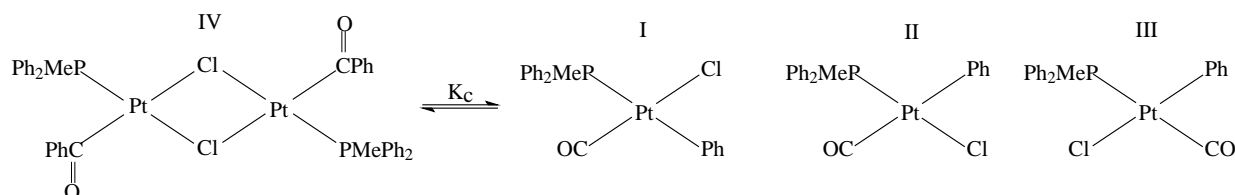
Scheme 2.25: Three geometric isomers of [PtCl(Ph)(CO)(PMePh$_2$)]. Isomer I, with PPh$_3$ *trans* to PMePh$_2$, readily undergoes carbonyl insertion to give the acyl complex [Pt$_2$(μ-Cl)$_2$(COPh)$_2$(PMePh$_2$)$_2$], IV.

As might be expected the halide-bridged acyl complex [Pt$_2$(μ-X)$_2$(COPh)$_2$(PMePh$_2$)$_2$] is favoured by the strongly bridged halides X = I > Br > Cl.[156] The effect on the equilibrium constant K$_c$ of neutral ligands L on the reaction 2[PtCl(Ph)(CO)L$_2$] $\square$ [Pt$_2$(μ-X)$_2$(COPh)$_2$L$_2$] [157] is given in **Table 2.27**. Phosphines with better electron donating power (thus a high *trans* influence) favour the formation of the halide-bridged acyl complex. The decrease in equilibrium constant K$_c$ follows the decreasing order of *trans* influence for the smaller ligands[17] (as determined by the Tolman electronic parameter ν_{CO}), but after a certain size the bulk of the ligand predominates, preventing Ph migration and overriding the electronic effect. For example PCy$_3$ has a *trans* influence similar to PEt$_3$, but the steric bulk of PCy$_3$ inhibits Ph migration almost completely. For P(*o*-Me-Ph)$_3$ no conversion of the alkyl monomer to the acyl dimer was detected. (See paragraph 2.1.3 page 10 for a discussion on the electronic and steric effect of tertiary phosphines)

Table 2.27: Equilibrium constants for the reaction 2[PtCl(Ph)(CO)L$_2$] $\square$ [Pt$_2$(μ-X)$_2$(COPh)$_2$L$_2$] in CHCl$_3$ solution[157] following the order of *trans* influence for the smaller ligands.[17]

L	K$_c$ / mol^{-1}	Tolman electronic parameter ν_{CO} / cm^{-1}	Tolman cone angle θ / deg
PEt$_3$	690	2061.7	132
PMe$_2$Ph	650	2065.3	122
PMePh$_2$	160	2067.0	136
PPh$_3$	31	2068.9	145
PCy$_3$	8.0	2056.4	170
P(*o*-Me-Ph)$_3$	≈ 0	2066.6	194
AsMePh$_2$	≈ 0	-	-
AsPh$_3$	≈ 0	-	-

The tendency that more electron rich metal centres (brought about by electron donating ligands) accelerate methyl migration was also found in the reaction

---

[156] Anderson, G.K. and Cross, R.J., *J. Chem. Soc. Dalton Trans.*, 712 (1980).

[157] Anderson, G.K. and Cross, R.J., *Acc. Chem. Res.*, **17**, 67 (1984).

$[Rh(cupf)(CO)(PX_3)(CH_3)(I)] + THF \overset{k_{-1}}{\underset{k_{+1}}{\square}} [Rh(cupf)(CO\ CH_3)(PX_3)(I)(THF)]^{146}$ (in THF).
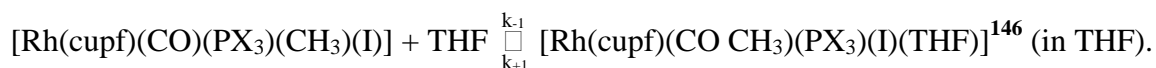
In **Table 2.28** the rate of alkyl to acyl conversion increased in the case of the isosteric tertiary phosphines (cone angle 145°) in the same order as their electron donating power: (least electron donating) p-Cl-Ph < Ph < p-MeO-Ph (most electron donating). For the more bulky phosphine PCy$_3$ the rate of acyl formation is comparable to that of PPh$_3$ in spite of the higher electron donating power of PCy$_3$, indicating again towards the deactivating steric effect that bulky ancillary ligands in a complex can have on carbonyl insertion. The bulky PCy$_3$ ligand blocks the way of entering THF molecules.[146]

Table 2.28: Steric and electronic influence of the ancillary phosphine ligand PX$_3$ on the reaction [Rh(cupf)(CO)(PX$_3$)(CH$_3$)(I)] + THF $\overset{k_{-1}}{\underset{k_{+1}}{\square}}$ [Rh(cupf)(CO CH$_3$)(PX$_3$)(I)(THF)] (in THF).[146]

PX$_3$	Tolman cone angle θ / deg	Tolmans electronic parameter ν_{CO} / cm^{-1}	K	$k_1 \times 10^4$ / s^{-1}	$k_{-1} \times 10^4$ / s^{-1}
P(p-Cl-Ph)$_3$	145	2072.8	2.44	5.19	2.13
P(Ph)$_3$	145	2068.9	1.75	7.13	4.07
P(p-MeO-Ph)$_3$	145	2066.7	0.76	8.46	11.10
P(Cy)$_3$	170	2056.4	0.33	3.23	9.77

2.2.3.5 Insertion reactions of [Rh^{III}(L,L'-BID)(CO)(CH$_3$)I(PPh$_3$)] complexes.

In this study the acyl formation from octahedral rhodium(III) alkyl complexes (formed from the oxidative addition of iodomethane to square planar rhodium(I) complexes) is considered. In this case the CO insertion reactions are of the type where no formal incoming ligand is involved for the insertion to take place and a general mechanism may be presented as in **Scheme 2.22** namely:

$$A + B \underset{k_{-1}}{\overset{k_1}{\rightleftharpoons}} C \xrightarrow{k_2} D$$

OR

$$Rh(I) + CH_3I \underset{k_{-1}}{\overset{k_1}{\rightleftharpoons}} Rh(III)\text{-alkyl} \xrightarrow{k_2} Rh(III)\text{-acyl}$$

72
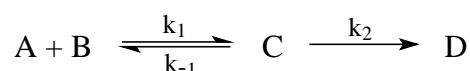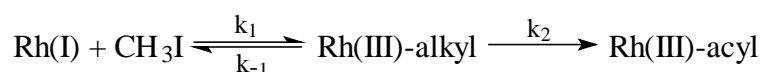
The rate of formation of the acyl and alkyl products is given by:

Equation 2.1: $\qquad k_{obs\ acyl} = \dfrac{k_2 K_1[B]}{1 + K_1[B]} = \dfrac{k_2 K_1[CH_3I]}{1 + K_1[CH_3I]}$ $\qquad$ and

Equation 2.2: $\quad k_{obs\ alkyl} = k_1[CH_3I] + k_{-1}$

with equilibrium constant $K_1 = k_1/k_{-1}$.

A summary[158] of the kinetic data for the oxidative addition of iodomethane to different [Rh(L,L'-BID)(CO)(PPh$_3$)] complexes, including the kinetic data for the formation of the corresponding Rh(III) acyl species, is given in **Table 2.29**. These results show the dramatic increase in the oxidative addition rate of the N:S type ligands compared to the O:O donor atom systems, specifically with that of the poor nucleophilic Rh(I) center in the [Rh(hfaa)(CO)(PPh$_3$)] complex. This increased reactivity is explained by the fact that these N:S ligands are capable of strongly donating electron density to the metal centre. The formation of the acyl species however, is much less dependent on the type of bidentate ligand.

Table 2.29: Summary of the kinetic data for the oxidative addition of iodomethane to different [Rh(L,L'-BID)(CO)(PPh$_3$)] (L' = bidentate ligand donor atom *trans* to PPh$_3$) in CHCl$_3$ at 25°C. Chelate = amount of atoms in the pseudo aromatic ring around the central metal, including the metal. Rate constants refer to Equation 2.1.

L,L'-BID	L	L'	chelate	K_1 /M^{-1}	k_1/M^{-1}s^{-1} (alkyl)	$t_{1/2}$*/s (alkyl)	k_2/s^{-1} (acyl)	$t_{1/2}$/s (acyl)
hfaa[7]	O	O	6	< 0.1	0.00013(1)	5300	-	-
cupf[159]	O	O	5	< 0.1	0.0050(1)	140	0.0012(1)	580
acac[7]	O	O	6	< 0.1	0.0065(4)	110	0.0016(1)	430
sacac[159]	O	S	6	< 0.1	< 0.01	< 60	-	-
hpt[51]	O	S	5	< 0.1	0.04	17	0.01	72
hacsm[158]	S	N	6	< 0.5	< 0.01	< 60	0.005	140
macsm[55]	S	N	6	4(1)	0.034(1)	20	0.0078(4)	90
macsh[158]	S	N	6	40(2)	0.56(1)	1.2	0.0072(2)	95

* $t_{1/2}$ for [MeI] = 1.0 mol dm^{-3}

[158] Steyn, G.J.J., Roodt, A. and Leipoldt, J.G., *Rhodium Ex.*, **1**, 25 (1993).

[159] Venter, J.A., Leipoldt, J.G. and van Eldik, R., *Inorg. Chem.,* **30**, 1207 (1991).

2.2.4 Ligand substitution reactions.

2.2.4.1 Definition of ligand substitution reactions.

Ligand exchange or substitution reactions on square planar complexes are usually divided into three main groups: nucleophilic substitutions, electrophilic substitutions and oxidative additions followed by reductive eliminations.[68] In this study the nucleophilic substitutions on square planar compounds of iridium and rhodium are to be considered. Due to many studies on kinetically inert complexes of platinum(II), nucleophilic substitutions at square planar complexes are one of the best understood of all inorganic reaction mechanisms.[160]

Ligand substitution reactions obey the following scheme:

$$[L_nM\text{-}X] + Y \rightarrow [L_nM\text{-}Y] + X$$
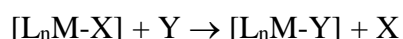
where M = metal ion and L, X and Y are any ligands. Y can also be a solvent species. In ligand substitution reactions, the metal coordination number, the oxidation level and the number of valence electrons remain unchanged.

2.2.4.2 Mechanism of ligand substitution reactions. [61]

Two limiting cases of ligand substitution reactions which can be distinguished may be defined as the dissociative and the associative mechanisms.

(i)   The dissociative mechanism resembles the S_N1 substitution in organic chemistry and proceeds as follows (X and Y may be neutral or charged ligands):

Slow step: $[L_nM - X] \xrightarrow{\quad k \quad} [L_nM] + X$

Fast step: $[L_nM] + Y \longrightarrow [L_nM - Y]$

---
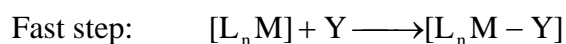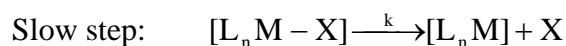
[160] Cross, R.J., *Adv. in Inorg. Chem.*, **34**, 219 (1989).

Accordingly its kinetics takes the form: rate = $k[L_nM-X]$. The entropy term, ΔS, is positive because the transitional state is less ordered than the reagents themselves. This dissociative mechanism is favoured by the presence of labile ligands L (L = THF for example). Reactions involving dissociation may proceed either with retention of stereochemistry or with racemization, depending upon the rate of trapping of the intermediate by the incoming ligand. **Scheme 2.26** illustrates the process for a octahedral complex. If the second step is very rapid, the 16-electron intermediate has no time to evolve and $[L_nM-Y]$ has the same stereochemistry as $[L_nM-X]$. However, if the second step is slow, the first-formed square pyramidal structure may rearrange to a trigonal bipyramid, which permits racemization.[61]
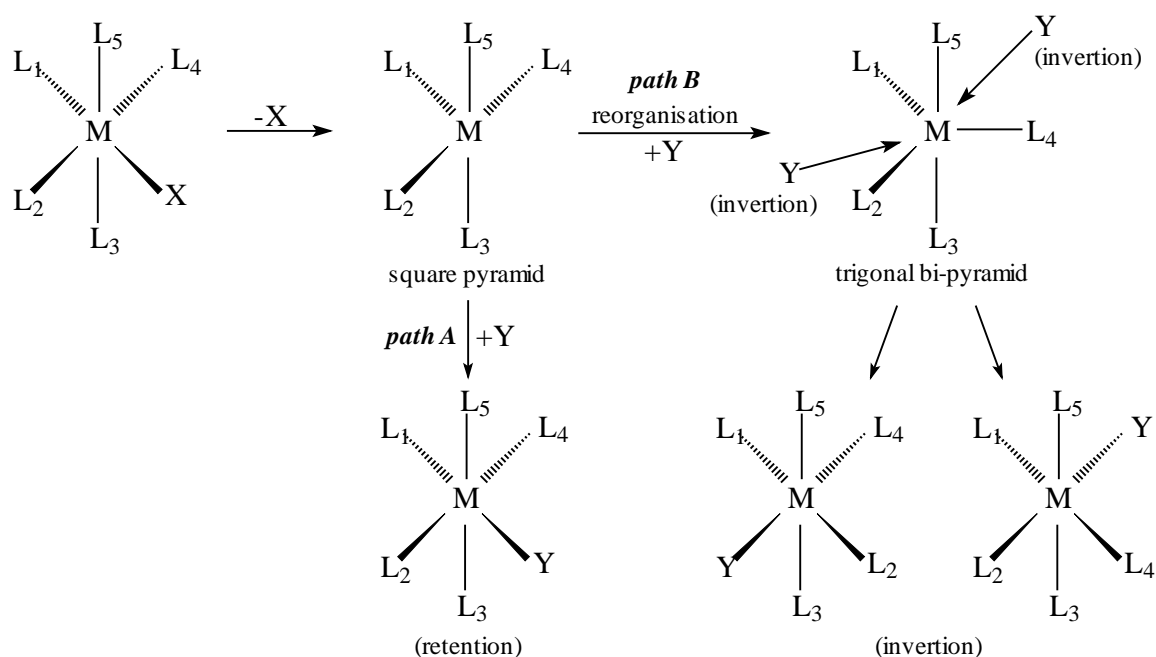
Scheme 2.26: **Schematic representation of the stereochemistry of the product of the ligand substitution reaction to an octahedral complex following a dissociative mechanism. Path A represents a fast process resulting in retaining of stereochemistry while with a slow prosess the first-formed square pyramidal structure may rearrange to a trigonal bipyramid (path B) leading to inverted stereochemistry.**

(ii)   The associative mechanism of a ligand substitution reaction obeys the following scheme:

Slow step: $[L_nMX] + Y \xrightarrow{\ k\ } [L_nMX - Y]$

Fast step: $[L_nMX - Y] \longrightarrow [L_nM - Y] + X$
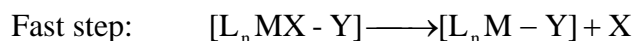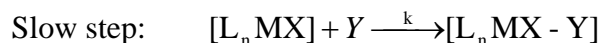
Here the kinetics takes a different form: rate = $k[L_nMX][Y] = k[complex][Y]$, resembling the S_N2 substitution in organic chemistry. The negative entropy change ΔS reflects a transitional state which is more ordered than the starting materials. This mechanism is favoured for electron-

deficient complexes (*e.g.* 16 or 17 valence electron compounds) but is not totally excluded for 18 electron compounds.[61]

There is general agreement that the vast majority of reactions on square planar complexes are associative and involve a nucleophilic attack of the entering ligand Y at the metal with the 5-co-ordinate adduct passing through the square-pyramidal and trigonal-bipyramidal stages.[68] (**Scheme 2.27**) A solvolysis step often competes with the direct replacement of X with Y in **Scheme 2.27**, leading to the rate law, **Equation 2.3**[161] where the $(k_s[\text{complex}])$-term represents the solvation pathway. (See **Scheme 2.28** for a schematic representation of **Scheme 2.27**.) For the simple rate law of **Equation 2.3** to be valid, it is necessary for the second step of the solvation pathway (in which Y replaces the coordinated solvent S) to be fast.[160]
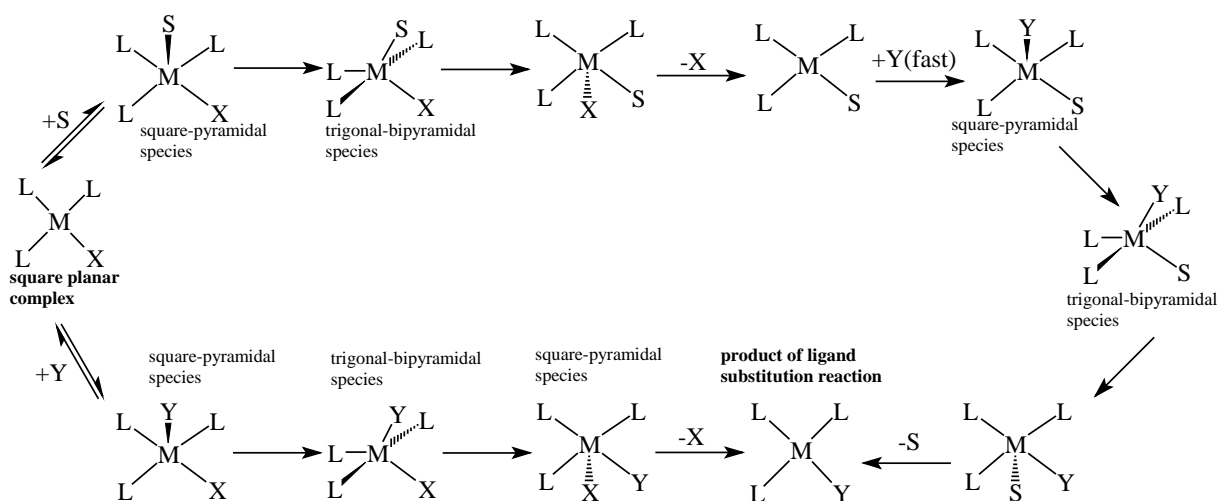
Scheme 2.27: The direct and solvent pathway of the associative mechanism of the ligand substitution reaction of square planar complexes [ML₃X]. S = solvent and Y = incoming ligand.
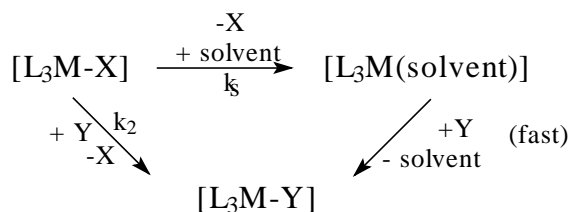
Scheme 2.28: Schematic representation of the direct and solvent pathway for the associative mechanism of a ligand substitution reaction.

[161] Wilkins, R.G., *Kinetics and Mechanism of Reactions of Transition Metal Complexes,* 2nd thoroughly revised edition, VCH, Weinheim, 1991, p.103, 232 – 242.

Equation 2.3:   Rate $= (k_s + k_2[Y])[\text{complex}]$

                          $= k_{obs}[\text{complex}]$

$k_{obs} = k_s + k_2[Y]$, where k_s is the rate constant of the solvent pathway and k_2 the rate constant of the direct pathway for the substitution of L with Y in **Scheme 2.28**.

Although the overwhelming majority of substitution studies have been stereospesific, pseudorotation could in principle accompany any ligand replacement step leading to ligand replacement without retention of configuration.[162, 163]

2.2.4.3 Factors influencing ligand substitution reactions.[161]

One of the consequences of an associative mechanism for the ligand substitution reaction of square planar complexes, is the decided importance of all the ligands – entering, leaving and remaining – on the rate of the process. This arises because all the ligands involved are present in the five-coordinated activated complex and can therefore affect its stability and the activation energy for its production. (This feature distinguishes planar from octahedral substitution.)

(i)   *Effect of the entering ligand.*

For an associative mechanism one expects that the incoming ligand would have a great influence on the reaction rate. This has been confirmed by the determination of the rate constants for the substitution of Cl by a large variety of ligands from *trans*-[Pt(py)$_2$(Cl)$_2$].[164]   **Table 2.30** summarises the rate constants of the substitution of Cl in *trans*-[Pt(py)$_2$(Cl)$_2$] with a number of nucleophiles in CH$_3$OH. The large range of reactivities is a feature of an associative mechanism and differentiates it from octahedral complexes.[161] These rate constants have been used to set up a scale of nucleophilic power for the ligand substitution in square-planar complexes, based on the

---

[162] Erickson, L.F., Ferrett, T.A. and Buhse, L.F., *Inorg. Chem.*, **22**, 1461 (1983).

[163] Cooper, M.K. and Downes, J.M., *J. Chem. Soc., Chem. Commun.,* 381 (1981).

[164] i) Belluco, U., Cattalini, L., Basolo, F., Pearson, R.G. and Turco, A., *J. Amer. Chem. Soc.*, **87**, 241 (1965),

ii) Pearson, R.G., Sobel, H. and Songstad, J., *J. Amer. Chem. Soc.*, **90**, 319 (1968)

Swain-Scott approach.[165]   The second order rate constants, k_2, for reactions in CH_3OH of nucleophiles Y with *trans*-$[Pt(py)_2(Cl)_2]$ chosen as the standard substrate according to the reaction

$$\textit{trans-}[Pt(py)_2(Cl)_2] + Y \xrightarrow{\ k_2\ } \textit{trans-}[Pt(py)_2(Cl)Y] + Cl^-$$
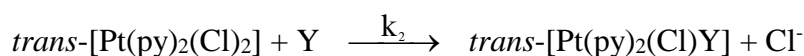
are compared with the rate constant for solvolysis k_s for the same substrate. It was found that for a variety of reactions of Pt complexes in different solvents

$$\log k_2 = sn_{Pt} + \log k_s$$

where k_2 = second order rate constant for reaction of nucleophile,

k_s = (rate constant for solvation reaction) / [solvent],

s = the nucleophile discrimination factor,

n_{Pt} = nucleophilic reactivity constant, defined as equal to $\log(k_2/k_s)$ for *trans*-$[Pt(py)_2(Cl)_2]$ in CH_3OH.

The terms s and k_s depend only on the Pt complex and not on the entering ligand. This relationship is valid in methanol and other solvents. With few exceptions the value of n_{Pt} is not dependent on the nature of the solvent.

Values of n_{Pt} are useful for correlating kinetic data for other Pt(II) complexes. Values of n_M and s for various electrophiles (metal centres M) and nucleophiles (incoming ligands) can be used to predict reaction rates. Values of n_M and s for various nucleophiles and a common electrophile (metal centre M) can be useful in the synthesis of a specific compound.

Table 2.30: Rate constants (k_2 / dm^3 mol^{-1} s^{-1}) of the reaction of *trans*-$[Pt(py)_2(Cl)_2]$ with a number of nucleophiles in CH_3OH.

Nucleo-phile	$10^3\,k_2$	n_{Pt}	pK_a[a)]	Nucleo-phile	$10^3\,k_2$	n_{Pt}	pK_a	Nucleo-phile	$10^3\,k_2$	n_{Pt}	pK_a
CH_3OH	0.00027	0.0	-1.7	**C_5H_5N**	0.55	3.19	5.23	**Ph_3Sb**	1810	6.79	-
CH_3O^-	very slow	< 2.4	15.7	**Br^-**	3.7	4.18	-7.7	**Ph_3As**	2320	6.89	-
Cl^-	0.45	3.04	-5.7	**$(CH_3)_2S$**	21.9	4.87	-5.3	**CN^-**	4000	7.14	9.3
NH_3	0.47	3.07	9.25	**I^-**	107	5.46	-10.7	**Ph_3Ph**	249000	8.93	2.73

a) pK_a values in water from ref 164.

[165] Swain, C.G. and Scott, C.B., *J. Amer. Chem. Soc.*, **75**, 141 (1953).

It is clear from the pK_a values in **Table 2.30** that there is no correlation between the pK_a values and n_{Pt} the nucleophilic reactivity constant. Nucleophilicity (a kinetic term) of the incoming ligand can therefore be used to determine the dependence of the reaction rate of square planar substitution reactions relative to the incoming ligand. Nucleophilicity is thus a kinetic term in contrast to basicity, a thermodynamic term.

Basicity of the incoming ligand (in contrast to nucleophilicity) has a rather small effect on the rate of associative square planar substitution reactions. **Table 2.31** summarises the second order rate constants k_2 for the substitution of the β-diketonato in [Rh(acac)(cod)],[166] [Ir(acac)(cod)][167] and [Rh(fca)(cod)][168] with derivatives of 1,10-phenanthroline and 2,2'-dipyridyl. No *ortho*-substituted derivatives of 1,10-phenanthroline was used, therefore the steric influence of the various derivatives of 1,10-phenanthroline should be much the same. Over a pK_a range of 3.57 to 6.31 of the derivatives of phenanthroline the reaction rate increased only from 12.4 to 29.0 dm^{+3} mol^{-1} s^{-1} in the case of the [Rh(acac)(cod)] reaction, from 1.38 to 32.3 dm^{+3} mol^{-1} s^{-1} in the case of the [Ir(acac)(cod)] reaction and from 5.46 to 17.8 dm^{+3} mol^{-1} s^{-1} in the case of the [Rh(fca)(cod)] reaction. The much faster reaction of 2,2'-dipyridyl than the reactions with the derivatives of 1,10-phenanthroline, was attributed to the fact that 2,2'-dipyridyl is much less rigid than phenanthroline (**Scheme 2.29**). A high-pressure kinetic study of the reaction between [Rh(acac)(cod)] and 1,10-phenanthroline clearly indicated an associative mechanism.[169] The large negative values of the entropy of activation ΔS^* also point to an associative mechanism for the reactions of **Table 2.31**.

(a) (b)
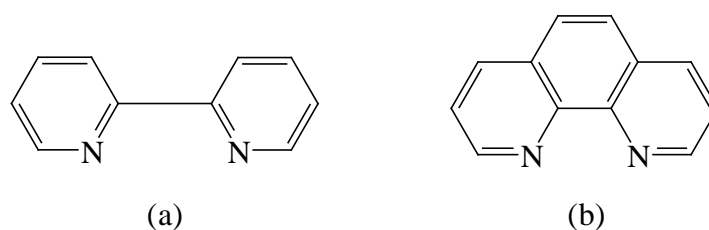
Scheme 2.29: **Schematic representation of (a) 2,2'-dipyridyl and (b) 1,10-phenanthroline.**

[166] Leipoldt, J.G., Lamprecht, G.J. and Steynberg, E.C. *J. Organomet. Chem.,* **402**, 259 (1991).

[167] Leipoldt, J.G., Basson, S.S., van Zyl, G.J. and Steyn, G.J.J., *J. Organomet. Chem.,* **418**, 241 (1991).

[168] Vosloo, T.G., *Synthesis, kinetics and structural aspects of β-diketonato complexes with a potential medical application (in Afrikaans), M.Sc. Thesis*, University of the Orange Free State, R.S.A., 1991.

[169] Leipoldt, J.G., Steynberg, E.C. and van Eldik, R., *Inorg. Chem.,* **26**, 3069 (1987)

Table 2.31: Rate constants (k_2 / dm^3 mol^{-1} s^{-1}) for the substitution of the β-diketonato in [Rh(acac)(cod)],[166] in [Ir(acac)(cod)])][167] and in [Rh(fca)(cod)][168] with derivatives of 1,10-phenanthroline and 2,2'-dipyridyl.

Incoming ligand	pK$_a$[a)]	[Rh(acac)(cod)][b)]			[Ir(acac)(cod)][c)]			[Rh(fca)(cod)][b)]		
		k_2	ΔH^*/ kJ mol^{-1}	ΔS^*/ J K^{-1} mol^{-1}	k_2	ΔH^*/ kJ mol^{-1}	ΔS^*/ J K^{-1} mol^{-1}	k_2	ΔH^*/ kJ mol^{-1}	ΔS^*/ J K^{-1} mol^{-1}
5-nitro-phenanthroline	3.57	12.4	30.8	-121	1.38	27.4	-150	5.46	25	-146
1,10-phenanthroline	4.96	29.0	32.6	-108	13.6	29.5	-125	17.8	29	-123
5,6-dimethyl-phenanthroline	5.20	19.9	38.7	-90	32.3	30.7	-113	13.7	23	-143
4,7-dimethyl-phenanthroline	5.97	18.8	36.7	-97	21.9	36.5	-97	13.2	22	-149
3,4,7,8-tetramethyl-phenanthroline	6.31	19.6	40.7	-84	22.1	28.7	-122	15.7	27	-128
2,2'-dipyridyl	4.30	124	26.8	-115	116	28.2	-109	118	31.2	-100

a)   pK$_a$ values of the conjugate acid in water from ref [170]
b)   in methanol at 25°C
c)   in acetone at 25°C

The result, that the basicity of the incoming ligand has a rather small effect on the rate of square planar substitution reaction, was also obtained for a number of substitution reactions with various amines as the entering ligand. The values of the rate constants for the reaction

$$[Pt(dipy)Cl_2] + amine \rightarrow [Pt(dipy)(amine)(Cl)]^+ + Cl^-, \qquad dipy = 2,2'\text{-dipyridyl},$$
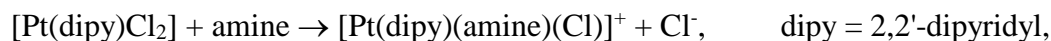
increased only from 4 X 10^{-3} to 13.4 X 10^{-3} dm^{+3} mol^{-1} s^{-1} for a pK$_a$ range of the entering amine from 1.9 to 11.12.[171] A group of amines that do not give rise to steric hindrance was chosen. The slope of the plot of log k_2 *vs.* the pK$_a$ of the entering amine was only 0.057.

Similar results were obtained for the reactions

$$[Rh(cod)(Cl)(piperidine)] + amine \rightarrow [Rh(cod)(Cl)(amine)] + piperidine^{172}$$
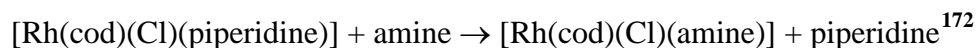
(slope of log k *vs.* the pK$_a$ = 0.17)

[170] Robb, W. and Nicholson, C.G., *S. Afr. J. Chem.*, **31**, 1 (1978).

[171] Cattalini, L., Orio, A. and Doni, A., *Inorg. Chem.,* **5**, 1517 (1966).

[172] Nicholson, C.G. and Robb, W., *Inorg. Chim. Acta,* **8**, 41 (1974).

and $[Pt(Cl)_3(DMSO)]^-$ + amine $\rightarrow$ $[Pt(Cl)_2(amine)(DMSO)]$ + Cl^- [173]

(slope of the plot of log k *vs.* the pK_a = 0.15).

(ii)   *Effect of the leaving group.*

Generally, the second order rate constant k_2 of a substitution reaction of a square planar complex increases with decreasing basicity of the leaving group and this gives rise to LFER (linear free energy relationships – the plot of log k *vs.* the pK_a of the leaving ligand – not shown). This is illustrated for the substitution reaction between $[M(\beta\text{-diketonato})(cod)]$ and 1,10-phenanthroline, with M = Rh[174] or Ir,[167] where ligands with a smaller pK_a has a much higher substitution rate (up to a difference of 10^4 for M = Rh and 10^5 for M= Ir). See **Table 2.32**.

$[Rh(\beta\text{-diketonato})(COD)]$ + 1,10-phenanthroline $\rightarrow$ $[Rh(phen)(COD)]^+$ + β-diketonato

$[Ir(\beta\text{-diketonato})(COD)]^{(a)}$ + 1,10-phenanthroline $\rightarrow$ $[Ir(\beta\text{-diketonato-}C^3)(phen)(COD)]^{(b)}$

(a) The β-diketonato is κ,κ' coordinated to Rh through the O-atoms.
(b) The β-diketonato is σ bonded to Rh through the methine carbon.

Table 2.32: Rate constants at 25°C and the activation parameters for the reaction between $[M(\beta\text{-diketonato})(cod)]$ and 1,10-phenanthroline (M = Rh[174] or Ir[167]).

β-diketonato	$pK_a^{a)}$	$[Rh(\beta\text{-diketonato})(cod)]^{b)}$			$[Ir(\beta\text{-diketonato})(cod)]^{c)}$		
		$k_2/$ dm^3 mol^{-1} s^{-1}	$\Delta H^*/$ kJ mol^{-1}	$\Delta S^*/$ J K^{-1} mol^{-1}	$k_2/$ dm^3 mol^{-1} s^{-1}	$\Delta H^*/$ kJ mol^{-1}	$\Delta S^*/$ J K^{-1} mol^{-1}
acac	8.95	29.0	32.6	-108	13.6	29.5	-125
ba	8.70	51.2	31.6	-106	85.8	31.5	-102
dbm	9.35	61.4	27.3	-119	413	26.3	-106
tfaa	6.30	1330	30.5	-83	17100	24.0	-83
tfba	6.30	2420	26.2	-93	25100	23.1	-81
hfaa	4.35	276000	23.2	-63	3000000	-	-

a) pK_a values used are those as was published in ref 174 and 167.
b)   in methanol at 25°C
c)   in acetone at 25°C

[173] Romeo, R. and Tobe, M.L., *Inorg. Chem.,* **13**, 1991 (1974).

[174] Leipoldt, J.G. and Grobler, E.C., *Transition Met. Chem.,* **11**, 110 (1986).

(iii)   *Effect of the ligands already present.*

The group *trans* to the leaving group appears to have a more pronounced influence than the two *cis* to it, on the rate of its departure. As discussed in paragraph 2.1.4.2 page 16, a coordinated ligand can be assigned an order of kinetic *trans*-effect which denotes its tendency to direct an incoming ligand in the position *trans* to itself. The greater *trans*-effect are associated with a larger rate constant for the elimination of the *trans* ligand. The relative rates of the substitution reactions of the cod or CO ligand in the complexes [M(β-diketonato)(cod)] and [M(β-diketonato)(CO)$_2$] in **Table 2.10** (page 31) give rise to the following influence of the terminal substituents CH$_3$, Ph and CF$_3$ of the various β-diketonatos on the kinetic *trans*-effect of the co-ordinating O-atoms of the β-diketonato ligands

$$(\text{smallest influence}) \; CH_3 \approx Ph < CF_3 \; (\text{largest influence})$$

The kinetic results thus revealed that an increase in the electron attracting power of one of the substituents of the β-diketonato, has an increase in the kinetic *trans*-effect. The large kinetic *trans*-effect caused by the electronegative groups can be explained by their ability to withdraw electron-density from the metal ion and thus stabilise the five co-ordinated transitional state in an associative mechanism. See also paragraph 2.1.4.4 on page 30 for a discussion on the kinetic *trans*-effect of bidentate ligands.

(iv)   *Effect of the central metal atom.*

It is usually not possible to make a comparison of the relative rate of substitution of a ligand coordinated to the three members of a given transition metal group of the periodic table. It is usually also not possible to make a comparison of the relative rate of substitution of a ligand coordinated to the three members of adjacent transition metal groups of the periodic table. The reason is that there are few complete isostructural series of square planar complexes of a given group or metals in adjacent groups. The kinetic data of the substitution reaction

$$\textit{trans-}[MCl(o\text{-tolyl})(PEt_3)_2] + \text{pyridine} \rightarrow \textit{trans-}[M(\text{pyridine})(o\text{-tolyl})(PEt_3)_2]^+ + Cl^-$$
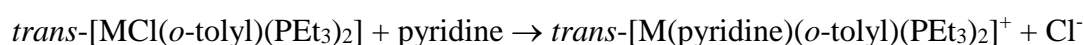
afford a unique quantitative comparison of the rates of reaction of analogous Ni(II), Pd(II) and Pt(II) compounds. The ratio of the rates is approximately 5 000 000 : 100 000 : 1 where M = Ni,

Pd and Pt respectively.[30] This result is consistent with the higher electron density of the Pt atom not favouring an associative reaction mechanism. The fact that *trans*-[NiCl(mesityl)(PEt$_3$)$_2$] reacts only 20 000 times faster with pyridine than *trans*-[PtCl(mesityl)(PEt$_3$)$_2$] is due to the fact that the mesityl group blocks the positions above and below the plane (of the square planar complex) making the smaller Ni(II) much less labile than Pt(II) to form the 5-coordinate transitional state[30] (**Scheme 2.27**, p. 76). In fact, the rate difference of 20 000 : 1 resembles those between octahedral cobalt(III) and iridium(III) complexes. For example, the relative rate of acid-hydrolysis of [M(NH$_3$)$_5$Br]$^{2+}$ complexes are about 4 000 : 1 for M = Co and Ir respectively.[30]

The results of the substitution reaction

$$[M(CN)_4]^{n-} + (CN^*)^- \rightarrow [M(CN)_3(CN^*)]^{n-} + (CN)^-$$
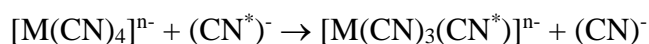
for M = Ni(II), Pd(II), Pt(II) and Au(III)[161] are consistent with the above results (k_2/dm^3 mol^{-1} s^{-1} in brackets after each complex):

(most reactive) [Ni(CN)$_4$]$^{2-}$ (> 5x10^5) > [Pd(CN)$_4$]$^{2-}$ (1.2x10^2) > [Pt(CN)$_4$]$^{2-}$ (26) (least reactive).

The results for M = Pt(II) and Au(III) permit a comparison of the relative rates of metals in the same row in adjacent groups (k_2/dm^3 mol^{-1} s^{-1} in brackets after each complex):

(most reactive) [Au(CN)$_4$]$^-$ (3.9x10^3) > [Pt(CN)$_4$]$^{2-}$ (26) (least reactive).

The above results indicate the general trend: the relative rate of substitution decreases in going from top to bottom in a given group of the transition metals as well as in going from the right to the left in a given row of the transition metals. This is the opposite of what was found in the case of the relative rate of oxidative addition to square planar metal complexes (paragraph 2.2.2.3 (i) page 40).

The results of the substitution reaction between [M(β-diketonato)(cod)] and 1,10-phenanthroline (M = Rh[174] or Ir[167] given in **Table 2.32** indicate that the rate constant k_2 for Ir(I) is comparable to and in some cases much higher than k_2 for Rh(I). This result is unexpected if compared to the general trend of the relative rate of substitution of a ligand to isostructural square planar metal

83

complexes with metal centres from the same triad as discussed above. This observation is important in terms of this study and will further be discussed in chapter 3 paragraph 3.5.4.

(v)   *Steric effect of the ligands already present.*

In contrast to the above discussion of sterical hindrance of a bulky ligand coordinated to different metal centres, the following reaction shows the influence of different bulky ligands coordinated to the same metal centre:

$$[PtCl(R)(PEt_3)_2] + py \rightarrow [Pt(py)(R)(PEt_3)_2]^+ + Cl^-$$
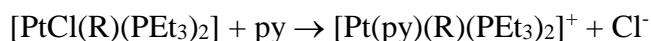
with R = phenyl, *o*-tolyl and mesityl. The relative rates of the *cis*-$[PtCl(R)(PEt_3)_2]$ isomers are 100 000 : 200 : 1 respectively, whilst for the *trans*-$[PtCl(R)(PEt_3)_2]$ isomers they are 30 : 6 : 1 respectively.[30] These results indicate:

(a) increasing steric hindrance of ligands coordinated to a metal complex, progressively retards the substitution rate of the incoming ligand, and

(b) *cis* hindrance is more effective than *trans* hindrance because the substitution rate is 10^{-5} times smaller when going from *cis*-$[PtCl(phenyl)(PEt_3)_2]$ to *cis*-$[PtCl(mesityl)(PEt_3)_2]$ in comparison to only 10^{-2} times smaller in the case of the *trans*-$[PtCl(R)(PEt_3)_2]$ isomers.

(vi)   *Effect of the solvent.*

The solvent is the reaction medium and as such, by solvating the ground and activated states, will influence the energetics of the activation process. In addition the solvent acts as a nucleophile in the reaction path represented by k_s in **Equation 2.3**.

Equation 2.3: $\text{Rate} = (k_s + k_2[Y])[\text{complex}]$

$= k_{obs}[\text{complex}]$
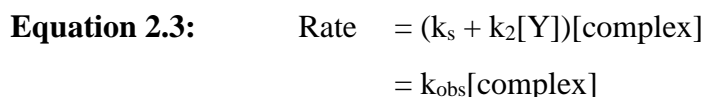
where $k_{obs} = k_s + k_2[Y]$, with k_s the rate constant for the solvent pathway and k_2 the rate constant for the direct pathway for the substitution of L with Y in **Scheme 2.28**, p. 76. A large value of k_s is observed in solvents capable of coordinating strongly to the metal so that generally the order

$(CH_3)_2SO > MeNO_2 , H_2O > ROH$

is observed.[161] In solvents that are poor coordinators such as C_6H_6 and CCl_4, the k_2 value dominates. The order of nucleophilicities does not change in different solvents.

2.3   Cyclic Voltammetry

2.3.1   Introduction

Cyclic voltammetry (CV) is one of the most versatile electroanalytical techniques for the study of electroactive species. Its versatility combined with ease of measurement has resulted in use of CV in the fields of electrochemistry, inorganic chemistry, organic chemistry and biochemistry. Organic chemists have applied the technique to the study of biosynthetic pathways and to studies of electrochemically generated free radicals. An increasing number of inorganic chemists have been using cyclic voltammograms to evaluate the effects of ligands on the oxidation/reduction potential of the central metal ion in complexes and multinuclear clusters. This type of information plays an integral part in many of the approaches directed towards solar energy conversion and in model studies of enzymatic catalysis. Knowledge of the electrochemistry of a metal complex can be useful in the selection of the proper oxidising agent to put the metal complex in an intermediate oxidation state. Electrochemical methodology has been exploited as a novel means of introducing functional groups and removing blocking agents.[175]

2.3.2   Fundamentals of electrochemistry.[176]

Cyclic voltammetry consists of cycling the potential of an electrode, which is immersed in an unstirred solution, and measuring the resulting current. The potential of this working electrode is controlled *versus* a reference electrode such as a saturated calomel electrode (SCE), a standard hydrogen electrode (SHE or NHE) or a silver/silver chloride electrode (Ag/AgCl). The controlling potential which is applied across these two electrodes can be considered an excitation signal. The excitation signal for a cyclic voltammogram is a linear potential scan with a triangular waveform as shown in **Figure 2.25**. The repetitive triangular potential excitation signal for cyclic voltammetry causes the potential of the working electrode to sweep back and

---

[175] Mabbott, G.A., *J. Chem. Ed.*, **60**, 697 (1983) and references therein.

[176] Kissinger, P.T. and Heineman, W.R., *Laboratory techniques in electroanalytical Chemistry*, Marcel Dekker, Inc., New York (1984), p. 86-93.

forth between the two designated values (the switching potentials). The potential excitation that is applied across the electrode-solution interface in order to obtain a cyclic voltammogram is illustrated by the potential-time profiles in **Figure 2.25**. The labelled segments in **Figure 2.25** can be interpreted as follows:

a   positive potential scan from +0.25 to +0.75 V,

b   direction of scan reversed at switching potential +0.75 V,

c   negative potential scan from +0.75 V to +0.25 V and

d   termination of first cycle.

Although the potential scan is frequently terminated at the end of the first cycle (point d), it can be continued for any number of cycles, hence the terminology cyclic voltammetry. The dotted line in **Figure 2.25** denotes a second cycle. The scan rate as reflected by the slope, is 0.1 V s^{-1}.
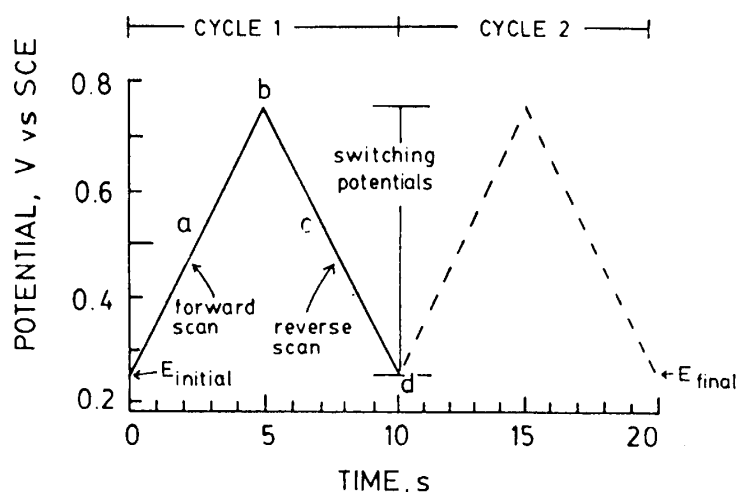
Figure 2.25:   Typical potential-time excitation signal for cyclic voltammetry.

2.3.3   A typical cyclic voltammogram.[176, 177]

A CV is obtained by measuring the current at the working electrode in an unstirred solution during a potential scan. The voltammogram is a display of current (vertical axis) *versus* potential (horizontal axis). Because the potential varies linearly with time, the horizontal axis can also be thought of as a time axis. A cyclic voltammogram that was obtained with a carbon paste

[177] Kissinger, P.T. and Heineman, W.R., *J. Chem. Ed.*, **60**, 702 (1983).

working electrode immersed in a 1.00 mmol dm^{-3} Fe^{2+} solution with H$_2$SO$_4$ as supporting electrolyte is shown in **Figure 2.26**. The potential scan profile that was applied across the electrode-solution interface to obtain this cyclic voltammogram was as depicted in **Figure 2.25**. The arrow designates the direction of the scan.
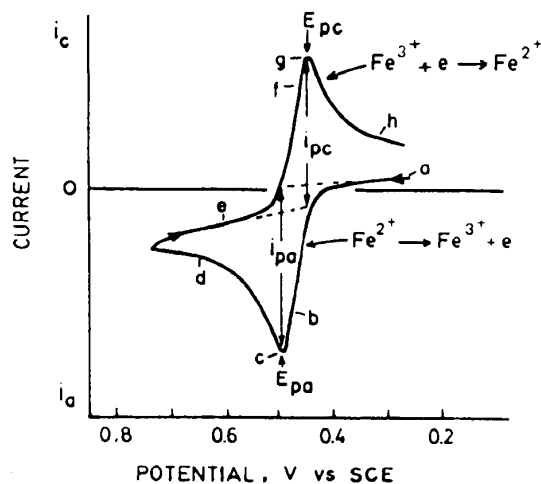
Figure 2.26: Cyclic voltammogram of a 1.00 mmol dm^{-3} Fe^{2+} solution in H$_2$SO$_4$. Scan initiated at +0.25V *versus* SCE in a positive direction at 0.1 V s^{-1}. Carbon paste working electrode.

During the scan from +0.25 V to +0.75 V, the applied potential becomes sufficiently positive at +0.4 V to cause oxidation of Fe^{2+} to occur at the electrode surface (Fe^{2+} → Fe^{3+} + e). This oxidation is accompanied by anodic current, which increases rapidly until the surface concentration of Fe^{2+} at the working electrode approaches zero as signalled by peaking of the current at point c in **Figure 2.26**. The current then decays (after c) as the solution surrounding the working electrode is depleted of Fe^{2+} due to its conversion to Fe^{3+}. The magnitude of the current is related to the slope of the concentration-distance profile for Fe^{2+} from the working electrode as described by **Equation 2.4**:

Equation 2.4:
$$i = n\text{FAD}\left(\frac{\partial C}{\partial x}\right)_{x=0} = \text{K}\left(\frac{\partial C}{\partial x}\right)_{x=0}$$

i is current (A), n is number of electrons transferred per ion (equivalents mol^{-1}), A is electrode area (cm^2), D is diffusion coefficient (cm^2 s^{-1}), C is concentration (mol cm^{-3}) and x is distance from the electrode (cm).

Simply stated, in the forward scan Fe^{3+} is electrochemically generated as indicated by the anodic current. In the reverse scan this Fe^{3+} is reduced back to Fe^{2+} as indicated by the cathodic current. Thus CV is capable of rapidly generating a new species during the forward scan and then probing its fate on the reverse scan. This is a very important aspect of this technique, because the vast majority of electrochemical reactions involve an electron transfer step which leads to a species which rapidly reacts with components of the medium *via* so-called coupled chemical reactions.

2.3.4   *Important parameters of a cyclic voltammogram.*[176, 177]

The important parameters of a cyclic voltammogram are the magnitude of the anodic peak current (i_{pa}), the cathodic peak current (i_{pc}), the anodic peak potential (E_{pa}) and the cathodic peak potential (E_{pc}). See **Figure 2.26**. One method of measuring i_{pa} and i_{pc} involves extrapolation of a baseline as shown in **Figure 2.26**. The establishment of a correct baseline is essential for the accurate measurement of peak currents but is not always easy.[175]

A redox couple in which both species rapidly exchange electrons with the working electrode is termed an electrochemically reversible couple. Such a couple can be identified from a cyclic voltammogram by measurement of the potential difference between the two peak potentials. **Equation 2.5** applies to a system that is both electrochemically and chemically reversible:

Equation 2.5:
$$\Delta E_p = E_{pa} - E_{pc} \approx \frac{0.059\,V}{n}$$

n is the number of electrons transferred, E_{pa} the anodic peak potential and E_{pc} the cathodic peak potential both in volt. This $0.059V/n$ separation of peak potentials is independent of the scan rate of a reversible couple, but slightly dependent on the switching potential and cycle number.[178] Thus, ΔE_p will have a value of 59 mV for a one-electron process such as the reduction of Fe^{3+} back to Fe^{2+}. In practice, a system with a potential difference ΔE_p up to 90 mV is often still

---

[178] Bard, A.J. and Faulkner, L.R., *Electrochemical Methods: Fundamentals and Applications*, Wiley, New York (1980), chapter 6.

considered as electrochemically and chemically reversible. Slow electron transfer at electrode surface causes the peak separation to increase.

The potential midway between the two peak potentials is the formal electrode potential $E^{0'}$ (**Equation 2.6**, corrected for the reference electrode being used) of the redox couple.

Equation 2.6:
$$E^{0'} = \frac{E_{pa} + E_{pc}}{2}$$

This $E^{0'}$ is an estimate (but not exactly the same) of the polarographic $E_{1/2}$ value (the value that was given to the potential where the current is half the value of that on the current plateau).[179]

The peak current for a reversible system is described by the Randles-Sevcik equation for the forward sweep of the first cycle:

Equation 2.7:
$$i_p = (2.69 \text{X} 10^5) n^{\frac{3}{2}} A D^{\frac{1}{2}} C \upsilon^{\frac{1}{2}}$$

i_p is the peak current , n is electron stoichiometry, A is electrode area (cm^2), D is diffusion coefficient (cm^2 s^{-1}), C is concentration and υ is the scan rate (V s^{-1}). Accordingly plots of i_{pa} and i_{pc} *versus* $\upsilon^{1/2}$ should be linear with intercepts at the origin – another characteristic of reversible systems. The values of i_{pa} and i_{pc} should be identical for a simple reversible (fast) couple. That is:

Equation 2.8:
$$\frac{i_{pa}}{i_{pc}} = 1$$

Electrochemical irreversibility is caused by a slow exchange of redox species with the working electrode. In this case **Equation 2.5**, **Equation 2.7** and **Equation 2.8** are not applicable. Theoretically electrochemical irreversibility is characterised by a separation of peak potentials that is greater than 59 mV (practically 90 mV often suffice) and dependence of ΔE_p on the scan

---

[179] Nicholson, R.S. and Shain, I., *Anal. Chem.*, **36**, 706 (1964).

rate. The term quasi-reversible is often used for a system where the electrochemical kinetics are slow, but the redox process still takes place. A complete irreversible system is one where only oxidation (or only reduction) is possible.[180] See **Figure 2.27**.
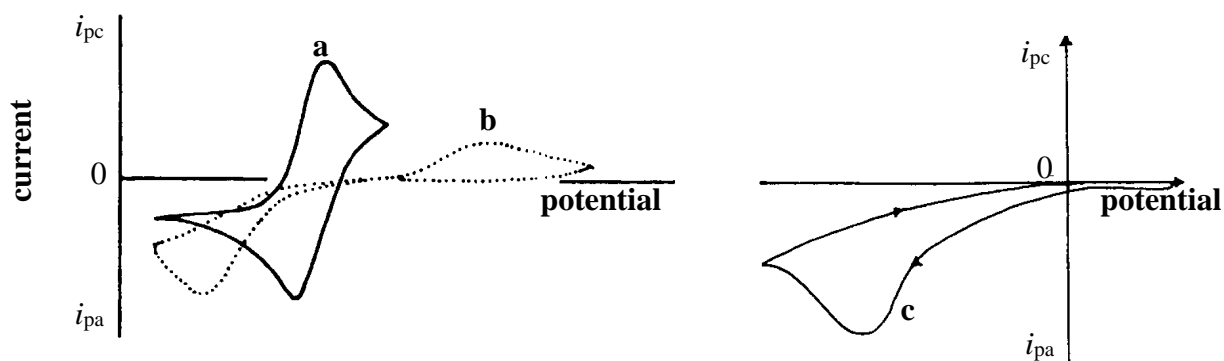
Figure 2.27: **A schematic presentation of the cyclic voltammogram expected from (a) an electrochemical reversible, (b) an electrochemical quasi-reversible and (c) an electrochemical irreversible process.**

2.3.5   Reference electrodes.

In aqueous solution the measurement of reduction potentials is facilitated by the use of reliable and universally accepted electrodes such as a saturated calomel electrode (SCE) or a standard hydrogen electrode (SHE or NHE). In many instances electrochemical measurements in water are impossible due to insolubility or instability of compounds. With a non-aqueous solvent as in this study, one may be concerned with the leakage of water from an aqueous reference electrode and a system like

$$Ag/Ag^+ \text{ (0.01 M AgNO}_3 \text{ in CH}_3\text{CN)}$$

is preferred. Since the potential of a reference electrode *versus* NHE or SCE is nearly always specified in experimental papers, inter-conversion of scales need to be established. A simple method of reporting reduction potentials in non-aqueous solvents is the use of the oxidation and reduction of ferrocene (Fc$^+$/Fc couple: $E^{0'} = 0.400$ V *vs.* NHE)[181] as an internal standard.[182, 183] In systems where the Fc$^+$/Fc couple may be inappropriate as an internal standard due to

---

[180] Christensen, P.A. and Hamnett, A., *Techniques and Mechanisms in Electrochemistry*, Blackie Academic & Professional, London (1994), p.55 – 67, 170 – 175.

[181] Koepp, H.M., Wendt, H. and Stehlow, H., *Z. Electrochem.*, **64**, 483 (1960).

[182] Gagné, R.R., Koval, C.A. and Lisensky, G.C., *Inorg. Chem.*, **19**, 2855 (1980).

[183] Gritzner, G. and Kuta, J., *Pure & Appl. Chem.*, **56**, 461 (1984).

overlapping waves, cobaltocene ($E^{0'}$ = -0.918 V *vs.* NHE),[181] or any of a variety of aromatic compounds, comprising a virtual continuum of reduction potentials, can be used. Potentials can still be related to ferrocene through a second experiment.

Figure 2.28 illustrates the use of the oxidation potential of ferrocene as an internal standard. **Figure 2.28**(a) shows the cyclic voltammogram of tris(acetylacetonato)ruthenium(III) in CH₃CN. **Figure 2.28**(b) shows the same voltammogram after adding a similar amount of ferrocene giving $E^{0'}$ for the processes in **Figure 2.28**(a) as 0.602 and –1.157 V *vs.* Fc⁺/Fc. Parts (c) and (d) of **Figure 2.28** were recorded under conditions identical with those for **Figure 2.28**(b) except that a SCE was used as reference electrode for **Figure 2.28**(c) while a copper wire was used for **Figure 2.28**(d). The values on the potential axis shifted, but the formal potentials relative to Fc⁺/Fc remain unchanged.[182]
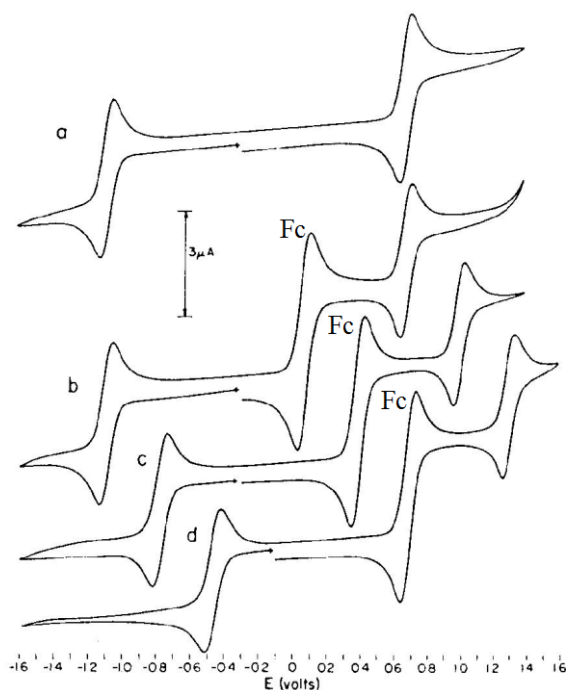
Figure 2.28: **Platinum button cyclic voltammetry at 50 mV/s of 0.005 M [Ru(acac)₃] in CH₃CN with tetrabutylammonium perchlorate (TBAP = 0.1M), (b), (c) and (d) ferrocene added. (a) and (b)** *vs.* **Ag/AgNO₃ (0.01M), (c)** *vs.* **SCE and (d)** *vs.* **Cu wire.**

The use of the Fc⁺/Fc or the bis(diphenyl)chromium(I)/bis(diphenyl)chromium(0) (BCr/BCr⁺) couple as reference for redox systems was illustrated by Gritzner[183] by measuring and reporting electrode potentials in 22 non-aqueous solvents versus these reference redox systems obtaining a nearly constant difference between the Fc⁺/Fc and the bis(diphenyl)chromium(I)/ bis(diphenyl)chromium(0) couple of 1.13 V.

2.3.6 Bulk electrolysis.

In this technique the composition of the bulk solution is altered by electrolysis *e.g.* for the electrochemical synthesis of compounds or for analytical measurement for removal or separation of solution components. Controlled potential techniques are usually the most desirable for bulk electrolysis. In controlled potential electrolysis the total amount of coulombs consumed during electrolysis is used to determine the amount of substance electrolysed. Alternatively a known amount of substance can be electrolysed to determine the number of electrons *n* transferred per molecule or ion. Determination of n is sometimes necessary to understand a cyclic voltammetry spectrum obtained for a specific compound.

During controlled potential electrolysis the analyte is completely electrolysed by applying a fixed potential to an electrode. The solution is stirred and the electrode usually has a large surface area to minimise electrolysis time. The current *i* is integrated during the course of the experiment to give the total amount of coulombs Q consumed during the experiment (see **Figure 2.29**):

Equation 2.9:
$$Q(t) = \int_0^t i(t)\partial t$$
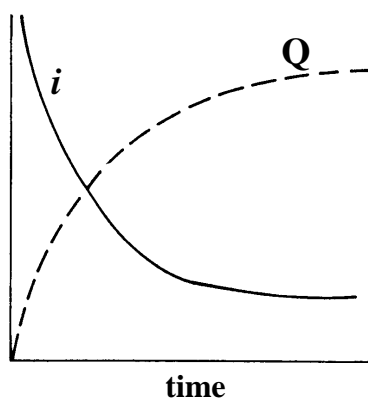
Figure 2.29: Current-time and charge-time response for controlled potential electrolysis.

When the electrolysis of the sample is completed ($i\rightarrow 0$), the total charge is used to calculate the number of electrons *n* transferred per molecule or ion for a known amount (N mol) of substance electrolysed by means of Faraday's law (**Equation 2.10**).

Equation 2.10: $Q = n\text{FN}$

Where Q = the total amount of charge consumed during the experiment / C,

      F = Faraday's number = 96485 C/eq,

      n = eq/mol *i.e.* the number of electrons transferred per molecule or ion and

      N = number of mol of substance.

2.3.7 *CV of ferrocene-containing β-diketones.*

In this study square planar Rh(I) and Ir(I)-complexes possessing a ferrocene-containing beta-diketonato ligand were used. CV's of all these complexes are presented and it is therefore logical to first look at the cyclic voltammograms of the free ferrocene-containing β-diketonatos. Cyclic voltammetry results of the five different ferrocene-containing β-diketones Hfctfa (1-ferrocenyl-4,4,4-trifluorobutane-1,3-dione or ferrocenoyltrifluoroacetone), Hfctca (1-ferrocenyl-4,4,4-trichlorobutane-1,3-dione or ferrocenoyltrichloroacetone), Hfca (1-ferrocenylbutane-1,3-dione or ferrocenoylacetone), Hbfcm (1-ferrocenyl-3-phenylpropane-1,3-dione or benzoylferrocenoylmethane) and Hdfcm (1,3-diferrocenylpropane-1,3-dione or diferrocenoylmethane) are listed in **Table 2.33** and displayed in **Figure 2.30**.[184]

Reasonable reversibility for all β-diketones were obtained with $\Delta E_p < 91$ mV for all β-diketones except Hfca ($\Delta E_p < 102$ mV), and with the peak anodic potential E_{pa} independent of the scan speed within a drift of 6 mV. All formal electrode potential $E^{0'}$ values remained constant between the scan rates of 50 and 200 mV s^{-1}. The ratio i_{pa}/ i_{pc} was in all cases close to unity, implying that the electrochemical oxidation of the iron(II) nucleus of the ferrocenyl groups is not followed by a chemically induced reduction or reaction of the iron(III) nucleus of the ferrocenium group, *e.g.* reduction by the hydroxyl group of the enol form of the β-diketone.

---

[184] du Plessis, W.C., Erasmus, J.C., Lamprecht, G.J., Conradie, J., Cameron, T.S., Aquino, M.A.S. and Swarts, J.C., *Can. J. Chem.*, **77**, 378 (1999).

Table 2.33: **Electrochemical data of 2.0 mmol dm^{-3} solutions of β-diketones of the type FcCOCH$_2$COR, measured in 0.1 mol dm^{-3} TBAPF$_6$/CH$_3$CN on a Pt electrode at 25.0(1) °C *versus* Ag/Ag$^+$. E$_{pa}$ and E$^{0'}$ (from low to high values) is reported *vs.* Fc/Fc$^+$.**

ν/mV s^{-1}	E$_{pa}$/V	ΔE$_p$ / mV	E$^{0'}$ /V	i_{pa}/μA	i_{pa}/i_{pc}	E$_{pa}$/V	ΔE$_p$ / mV	E$^{0'}$ /V	i_{pa}/μA	i_{pa}/i_{pc}
	Hdfcm - first ferrocenylgroup					Hfctca				
50	0.220	66	0.187	10.00	1.00	0.332	78	0.293	12.08	0.98
100	0.221	67	0.188	14.28	1.03	0.334	83	0.293	17.03	0.97
150	0.221	67	0.188	17.38	1.04	0.336	87	0.293	20.59	0.98
200	0.222	68	0.188	19.52	1.00	0.338	91	0.293	23.76	0.95
	Hbfcm					Hdfcm - second ferrocenylgroup				
50	0.267	73	0.230	11.58	0.97	0.333	72	0.297	12.14	1.02
100	0.271	81	0.231	16.40	1.01	0.333	73	0.297	16.67	1.04
150	0.271	82	0.231	20.37	1.01	0.334	76	0.296	17.38	1.04
200	0.273	86	0.231	23.53	1.02	0.337	79	0.298	23.33	1.04
	Hfca					Hfctfa				
50	0.279	86	0.240	12.46	0.99	0.354	74	0.317	10.53	0.96
100	0.282	92	0.236	16.86	0.99	0.352	74	0.317	14.46	0.97
150	0.286	98	0.237	20.52	1.02	0.356	77	0.317	17.56	0.98
200	0.283	102	0.237	23.60	1.03	0.357	80	0.317	20.24	0.98
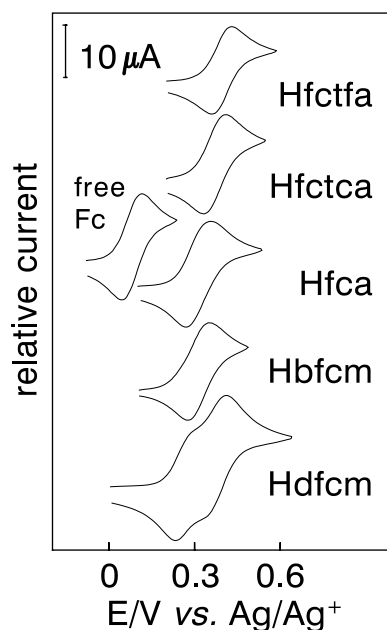
Figure 2.30: Cyclic voltammograms of 2 mmol dm^{-3} solutions of ferrocene (Fc) and β-diketones measured in 0.1 mol dm^{-3} TBAPF$_6$/CH$_3$CN at a scan rate of 50 mV s^{-1} on a Pt working electrode at 25.0(1) °C *versus* Ag/Ag$^+$.

Hdfcm showed two formal reduction potentials E$^{0'}$ = 0.188 and 0.297 V *vs.* Fc/Fc$^+$. The two formal reduction potentials were in contrast to ^{1}H NMR measurements that could not

differentiate between the two ferrocenyl groups. This observed inequality is most likely due to the improbability of both ferrocenyl groups of the same molecule, Hdfcm, coming simultaneously in reaction contact with the electrode to invoke two simultaneous one-electron transfer processes. After oxidation of only one of the ferrocenyl groups, the newly formed intermediate is the mixed valent β-diketone $FcCOCH_2COFc^+$. Good communication (*via* conjugation) between Fc and Fc^+ in $FcCOCH_2COFc^+$ leads to oxidation of the second ferrocenyl group at a higher potential than was observed for the first ferrocenyl group oxidation in Hdfcm. The result that the oxidation of a second ferrocenyl group is higher than the oxidation of the first ferrocenyl group in a diferrocenyl-containing compound, was also found for other diferrocenyl-containing compounds,[185] *e.g.* for 1-ferrocenoyl-ferrocenylprop-2-ene ($E^{0'}$ = 0.106 and 0.271V *vs.* Fc/Fc^+ in CH_3CN with 0.1 mol dm^{-3} tetrabutylammonium hexafluorophosphate as supporting electrolite),[184] biferrocene ($E^{0'}$ = -0.09 and 0.25V *vs.* Fc/Fc^+ in 1:1 CH_2Cl_2:CH_3CN with 0.1 mol dm^{-3} tetrabutylammonium hexafluorophosphate as supporting electrolite),[186] and diferrocenylacetylene ($E^{0'}$ = 0.743 and 0.610V *vs.* SCE in CH_2Cl_2 with 0.2 mol dm^{-3} *n*-Bu_4NBF_4 as supporting electrolite).[187]

The spread of the formal electrode potential $E^{0'}$ of the ferrocenyl groups of the β-diketones in **Table 2.33** is large: from 0.266V for Hdfcm to 0.395V for Hfctfa (values *versus* Ag/Ag^+). This large spread in $E^{0'}$ is the result of good communication between the ferrocenyl group and the R substituent of the β-diketones $FcCOCH_2COR$ (R = Fc, C_6H_5, CH_3, CCl_3 and CF_3) *via* the backbone of the pseudo-aromatic β-diketone core. The ferrocenyl group on the β-diketones $FcCOCH_2COR$ becomes increasingly difficult to oxidise as more electron density is withdrawn from it by the substituent R in the order:

> **(most electron donating): first ferrocenyl group of Hdfcm < C_6H_5 < CH_3**
>
> **< CCl_3 < second ferrocenyl group of Hdfcm < CF_3 (most electron withdrawing)**

This fact again implies good communication between the ferrocenyl group and the substituent R on the β-diketone $FcCOCH_2COR$ and was used to determine the group electronegativities of the R groups by measuring the formal reduction potentials $E^{0'}$ of these ferrocene-containing

---

[185] Morrison, W.H., Jr., Krogsrud, S. and Hendrickson, D.N., *Inorg. Chem.*, **12**, 1998 (1973).

[186] Brown, G.M., Meyer, T.J., Cowan, D.O., LeVanda, C., Kaufman, F., Roling, P.V. and Rausch, M.D., *Inorg. Chem.*, **14**, 506 (1975).

[187] LeVanda, C., Cowan, D.O., Leitch, C. and Bechgaard, K., *J. Am. Chem. Soc.*, **96**, 6788 (1974).

β-diketones by means of cyclic voltammetry.[184] The formal electrode potential $E^{0'}$ of these five ferrocene-containing β-diketones as well as the IR stretching frequencies of eight different methyl esters independently extrapolate to mutually consistent group electronegativities as tabulated in **Table 2.34** and displayed in **Figure 2.31**. These group electronegativities will be used in this study in comparing a variety of chemical parameters *e.g.* electrochemical results, kinetic results, pK_a values, and structural results with each other.

Table 2.34: Group electronegativities, χ_R, for the indicated R groups of the β-diketones of the type $FcCOCH_2COR$, pK_a values and formal reduction potentials $E^{0'}$ *vs.* Ag/Ag$^+$ of the β-diketones. IR carbonyl streching frequency $\nu(C=O)_R$ of esters of the type $RCOOCH_3$. Fc = ferrocenyl and Fc$^+$ = ferrocenium.

R	χ_R/Gordy scale	pK_a	$\nu(C=O)_R$/cm^{-1} [a]	$E^{0'}$/V
CF$_3$	3.01	6.53(3) [a] or 5.65[b]	1785	0.394
Cl	2.97[a]	-	1780	-
Fc$^+$	2.82	6.80	-	-
CCl$_3$	2.76	7.15(2) [a]	1768	0.370
CHCl$_2$	2.62[a]	-	1755	-
CH$_3$	2.34	10.01(2) [a]	1738	0.313
C$_6$H$_5$	2.21	10.41(2) [a]	1725	0.306
H	2.13[a]	-	1717	-
Fc	1.87	13.1(1) [a]	1700	0.265, 0.374

(a)   results from reference [188]   (b)   An estimate value from cyclic voltammetry data from reference 184.
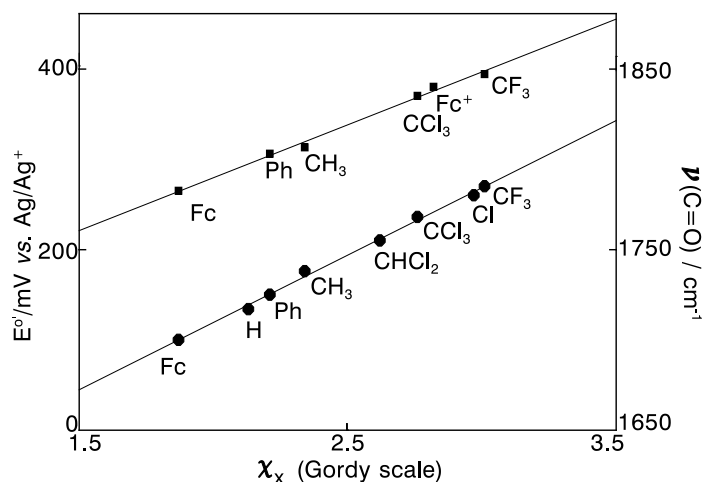
Figure 2.31: Apparent group electronegativities χ_R *vs.* the stretching frequency of the carbonyl group in methyl esters of the type $RCOOCH_3$ the (obtained by spectroscopic techniques - right axis, lower graph) or *vs.* the formal reduction potential $E^{0'}$ (obtained by electrochemical techniques namely cyclic voltammetry - left axis, upper graph). R = Fc (ferrocenyl), Ph (C$_6$H$_5$), H, CH$_3$, CHCl$_2$, Cl, Fc$^+$(ferrocenium) and CF$_3$.

---

[188] du Plessis, W.C., Vosloo, T. and Swarts, J.C., *J.C.S. Dalton Trans.*, 2507 (1998).

2.3.8 *Electrochemical oxidation of square planar rhodium and iridium complexes.*

2.3.8.1 Vaska's Ir(I) complex.

Results of the electrochemical oxidation of the well known square planar Vaska's complexes of the type [Ir(CO)XL$_2$] are presented in **Table 2.35**.[189] All the complexes underwent an irreversible one-electron oxidation. The product of the electrochemical oxidation of the [IrCl(CO)(PPh$_3$)$_2$] complex was considered as an Ir(II)-species on the basis of the number of electrons exchanged. IR and ESR (electron spin resonance) spectra results of the Ir(II)-species indicated a dimeric Ir(II) compound with a metal-metal bond. E$^{0'}$ of the [Ir(CO)X(PPh$_3$)$_2$] complexes increases in the same order as the increase in electronegativity χ_G (Gordy scale)[190] of the substituents L namely I (χ_G = 2.36) < Br (χ_G = 2.68) < Cl (χ_G = 3.00) indicating that the Ir(I) complex becomes increasingly difficult to oxidise as more electron density is withdrawn from the Ir(I) core.

Table 2.35: E$^{0'}$ and *n* (the number of electrons transferred in the electrode process) of the anodic waves corresponding to the oxidation of [Ir(CO)XL$_2$] complexes in CH$_2$Cl$_2$/0.1 mol dm^{-3} Bu$_4$NClO$_4$ on a rotating Pt electrode.[189]

X	L	*n*	E$^{0'}$/V *vs.* SCE
Cl	PPh$_3$	1.00	1.12
Br	PPh$_3$	0.95	1.10
I	PPh$_3$	0.98	1.00
Cl	PPh$_2$Et	1.08	1.08
Cl	PPhEt$_2$	1.00	1.00
Cl	PPh$_3$	1.08	0.95

2.3.8.2 Rhodium(I) oxalate complexes.

Anderson[191] investigated the electron transfer properties of the d^8 square planar monomeric Rh(I) complexes (TMA)[Rh(oxa)(CO)$_2$] (**Scheme 2.30** (a)), (TMA)[Rh(oxa)(cod)] (**Scheme 2.30** (b)),

[189] Vecernik, J., Masek, J. and Vlcek, A.A., *J.C.S. Chem. Comm.*, 737 (1975).

[190] Gordy, W., *J. Chem. Phys.,* **14**, 304 (1946).

[191] Anderson, J.E., Murphy, C.P., Real, J. and Bayón, J.C., *Inorg. Chim. Acta.*, **209**, 151 (1993).

and of the dimeric Rh(I) complex $[Rh_2(oxa)(cod)_2]$ (**Scheme 2.30** (c)) where cod = 1.5-cyclooctadiene, TMA = tetramethylammonium cation and oxa is the oxalate dianion.

(a)   (b)   (c)
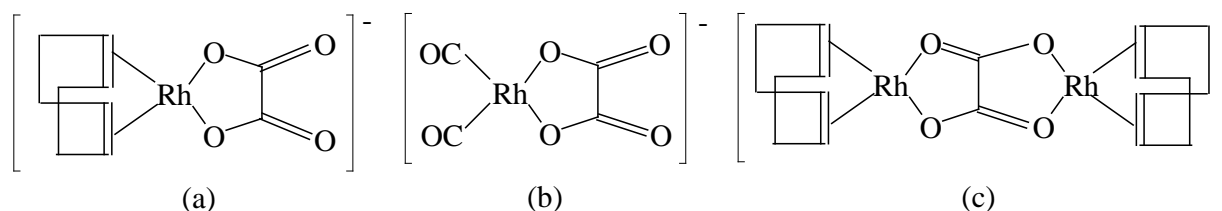
Scheme 2.30: **Square planar arrangement of (a) [Rh(oxa)(cod)]⁻, (b) [Rh(oxa)(CO)₂]⁻ and (c) [Rh₂(oxa)(cod)₂].**

The cyclic voltammograms obtained for $[Rh(oxa)(cod)]^-$ and $[Rh(oxa)(CO)_2]^-$ in THF/0.20 mol dm^{-3} tetrabutylammonium perchlorate (TBAP) at a scan rate of 100 mV s^{-1} are presented in **Figure 2.32** (a) and (c) respectively. The results of the electrochemical wave analysis of these Rh(I) complexes are presented in **Table 2.36**. The cyclic voltammograms of both (TMA)[Rh(oxa)(cod)] and (TMA)[Rh(oxa)(CO)₂] revealed the following: One oxidation peak without any indication of a reduction wave that would suggest a chemical reversible process was displayed. A very small reduction process (indicated as 1' in **Figure 2.32**(a) and (c)) was observed. Passivation of the electrode surface was observed on the second and subsequent scans in the multiple scan cyclic voltammetric data where the potential was not scanned negative of wave 1' in **Figure 2.32**(a) and (c), *e.g.* see **Figure 2.32**(b). The major difference in E$_{pa}$ with change in solvent implies participation of the solvent in the chemical reaction following the electron transfer. Thin layer experiments of the oxidation of (TMA)[Rh(oxa)(CO)₂] showed that the starting material was not regenerated by the reduction process 1' in **Figure 2.32**(c). Bulk electrolysis studies indicated two-electron oxidation process for both complexes. The location of E$_{pa}$ for (TMA)[Rh(oxa)(CO)₂] in CH₃CN was shifted 250 mV positive of the oxidation potential for the cod adduction, fully consistent with the greater π acidity of the CO ligands. The above CV data as well as results reported for oxalate compounds and IR data indicated that the oxidation of $[Rh(oxa)(cod)]^-$ and $[Rh(oxa)(CO)_2]^-$ are both best described as a two-electron process to generate a formal Rh(III) centre, followed by a chemical reaction to form a solvated Rh complex as represented by **Scheme 2.31**.
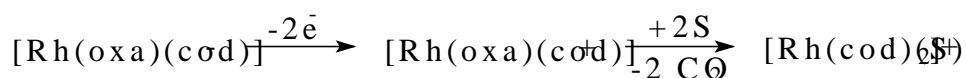
Scheme 2.31: **Schematic presentation of the electrochemical oxidation of [Rh(oxa)(cod)]⁻.**

Chemical oxidation and bulk electrolysis of the bimetallic complex [Rh$_2$(oxa)(cod)$_2$] indicated two successive two-electron steps with an equilibrium between [Rh(oxa)(cod)]$^-$, [Rh(CH$_3$CN)$_2$(cod)]$^+$, and [Rh$_2$(oxa)(cod)$_2$] which complicated the electron transfer mechanism. The first oxidation process could generate an Rh(II)-Rh(II) species or an Rh(III)-Rh(I) mixed valence species.

(a) POTENTIAL (VOLT)   **(b)** POTENTIAL (VOLT)   **(c)** POTENTIAL (VOLT)
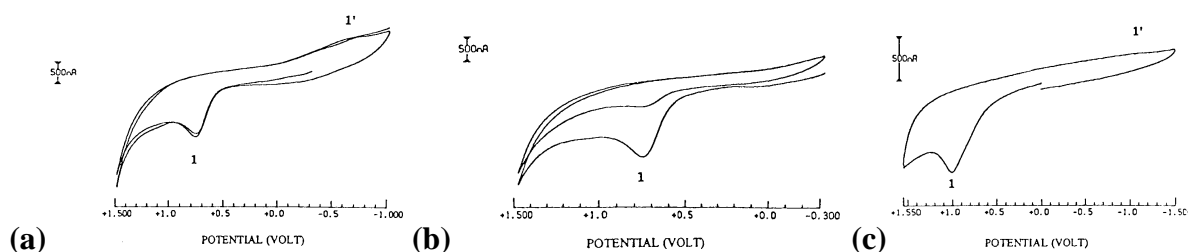
Figure 2.32: (a) Multiple scan cyclic voltammogram of a 2 mmol dm^{-3} solution of [Rh(oxa)(cod)]$^-$ in THF/0.20 mol dm^{-3} (TBAP) at a scan rate of 100 mV s^{-1}. (b) The same as (a) but with a potential range smaller on the negative side. (c) Cyclic voltammogram of a 2 mmol dm^{-3} solution of [Rh(oxa)(CO)$_2$]$^-$ in THF/0.20 mol dm^{-3} (TBAP) at a scan rate of 100 mV s^{-1}.

Table 2.36: Electrochemical results of the cyclic voltammograms of [Rh(oxa)(cod)]$^-$, [Rh(oxa)(CO)$_2$]$^-$ and [Rh$_2$(oxa)(cod)$_2$] in the solvents indicated. Scan rate of 100 mV s^{-1}, 0.20 mol dm^{-3} (TBAP) as supporting electrolyte, ferrocene added as an internal standard.

compound	solvent	n	E_{pa} vs SCE	E_{pa} vs. Fc/Fc$^+$
[Rh(oxa)(cod)]$^-$	THF	2.02(14)	0.78	0.16
	CH$_3$CN		0.58	0.09
	CH$_2$Cl$_2$		0.81	0.21
[Rh(oxa)(CO)$_2$]$^-$	THF	2.00(27)	1.09	0.36
	CH$_3$CN		0.78	0.34
	CH$_2$Cl$_2$		0.92	0.5
[Rh$_2$(oxa)(cod)$_2$]	CH$_3$CN	3.87(13)	0.75	0.36
			1.10*	0.71*

* value corresponds to the second wave of the CV of the dimeric [Rh$_2$(oxa)(cod)$_2$] complex.

2.3.8.3 Mono- and biphosphite square planar Rh(I) complexes of the general form [Rh(β-diketonato)(CO)$_n$(PR$_3$)$_{2-n}$] with n = 0 or 1 and PR$_3$ = tertiary phosphine.

(i)   *[Rh(β-diketonato)(CO)(P(OCH$_2$)$_3$CCH$_3$)]*[192] *and [Rh(β-diketonato)(P(OPh)$_3$)$_2$].*

The oxidative redox behaviour of mono- and biphosphite square planar Rh(I) complexes of the type [Rh(β-diketonato)(CO)(P(OCH$_2$)$_3$CCH$_3$)] and [Rh(β-diketonato)(P(OPh)$_3$)$_2$] for various is

---

[192] See List of Abbreviations fot the structure of P(OCH$_2$)$_3$CCH$_3$.

β-diketonatos, in CH_3CN/0.1 mol dm^{-3} tetrabutylammonium hexafluorophosphate is presented in **Table 2.37**.[193]

Table 2.37: **Electrochemical data for the [Rh(β-diketonato)(CO)(P(OCH$_2$)$_3$CCH$_3$)] and [Rh(β-diketonato)(P(OPh)$_3$)$_2$] complexes. Oxidation and reduction peaks were measured in CH$_3$CN containing 0.1 mol dm^{-3} tetrabutylammonium hexafluorophosphate as supporting electrolyte, on a glassy carbon electrode at 25.0(1) °C and at a scan rate of 100 mV s^{-1}.**[193]

β-dike-tone	pK$_a$[a]	Complex			
		[Rh(β-diketonato)(P(OPh)$_3$)$_2$]		[Rh(β-diketonato)(CO)(P(OCH$_2$)$_3$CCH$_3$)]	
		E$_{pa}$ *vs.* Fc$^+$/Fc	E$_{pc}$ *vs.* Fc$^+$/Fc	E$_{pa}$ *vs.* Fc$^+$/Fc	E$_{pc}$ *vs.* Fc$^+$/Fc
hfaa	4.35	0.881	-0.21	0.938	-0.38
tfaa	6.30	0.477	-0.45	0.482	-0.63
tfba	6.30	0.461	-0.44	0.417	-0.61
fctfa	6.56	0.312	-	-	-
ba	8.70	0.322	-0.55	0.295	-0.56
acac	8.94	0.308	-0.56	0.317	-
dbm	9.35	0.324	-0.52	0.242	-0.48
fca	10.01	0.176	-	-	-
bfcm	10.41	0.173	-	-	-
dfcm	13.10	0.124	-	-	-

(a)　　pK$_a$ values as in reference 193.

The cyclic voltammographs of CH$_3$CN solutions of the [Rh(β-diketonato)(CO)(P(OCH$_2$)$_3$CCH$_3$)] and [Rh(β-diketonato)(P(OPh)$_3$)$_2$] complexes with β-diketonato = acac, ba, tfba, dbm, tfaa and hfaa, all exhibit a single sharp anodic oxidation current peak which corresponds to the oxidation of Rh(I) according to **Equation 2.11** (confirmed by bulk electrolysis).

Equation 2.11:　　　　　　　$Rh(I) \rightarrow Rh(III) + 2e^-$

A moderate cathodic wave was observed on the reverse scan with peak seperations in excess of 700 mV in all cases. The cathodic peak currents which were observed, were related to the reduction of new chemically generated species. Examples of the representitive cyclic voltammograms of the [Rh(β-diketonato)(CO)(P(OCH$_2$)$_3$CCH$_3$)] complex (β-diketonato = dbm)

---

[193] Erasmus, J.C., *Electrochemical and chemical kinetic aspects of coordinative complexes of rhodium(I) and (III), Ph. D. Thesis*, University of the Orange Free State, R.S.A., 1997.

and of the [Rh(β-diketonato)(P(OPh)$_3$)$_2$] complex (β-diketonato = hfaa, tfaa and acac) respectively, are displayed in **Figure 2.33**.
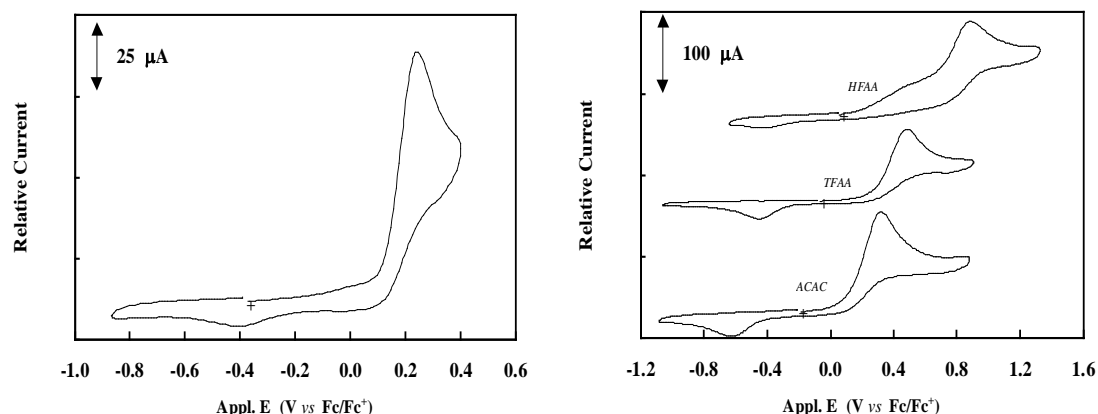
Figure 2.33: Cyclic voltammograms of (a) [Rh(β-diketonato)(CO)(P(OCH$_2$)$_3$CCH$_3$)] (β-diketonato = dbm) and of (b) [Rh(β-diketonato)(P(OPh)$_3$)$_2$] (β-diketonato = hfaa, tfaa and acac) in CH$_3$CN with 0.1 mol dm^{-3} tetrabutylammonium hexafluorophosphate as supporting electrolyte, on a glassy carbon electrode at 25.0(1) °C and at a constant sweep rate of 100 mV s^{-1}. Scan initiated in the positive direction at +.

The Rh(I) core becomes increasingly difficult to oxidise as more electron density is withdrawn from it by the substituent R and R' on the β-diketonato ligand RCOCHCOR'. Group electronegativities (χ_R) of the substituent R and R' on the β-diketone RCOCH$_2$COR' increase in the order Fc (χ_R = 1.87) < Ph (χ_R = 2.21) < CH$_3$ (χ_R = 2.34) < CF$_3$ (χ_R = 3.01)[184] which explains the progressive electron deficiency of the metal centre moving from the dfcm complex to the hfaa complex (see **Table 2.38**).

Table 2.38: Illustration of the relation between the group electronegativity (χ_R/Gordy scale) of the R group on the β-diketone RCOCH$_2$COR' and the oxidation potential E$_{pa}$ of rhodium(I) in [Rh(β-diketonato)(P(OPh)$_3$)$_2$] complexes. χ_R from reference 184 and E$_{pa}$ from reference 193.

β-dike-tonato	R'	R	χ_R of group R	E_{pa} vs. Fc$^+$/Fc	β-dike-tonato	R'	R	χ_R of group R	E_{pa} vs. Fc$^+$/Fc
fca	CH$_3$	Fc	1.87	0.176	bfcm	Ph	Fc	1.87	0.173
ba		Ph	2.21	0.322	dbm		Ph	2.21	0.324
acac		CH$_3$	2.34	0.308**	ba		CH$_3$	2.34	0.322**
tfaa		CF$_3$	3.01	0.477	tfba		CF$_3$	3.01	0.461
dfcm	Fc	Fc	1.87	0.124	fctfa	CF$_3$	Fc	1.87	0.312
bfcm		Ph	2.21	0.173	tfba		Ph	2.21	0.461
fca		CH$_3$	2.34	0.176	tfaa		CH$_3$	2.34	0.477
fctfa		CF$_3$	3.01	0.312	hfaa		CF$_3$	3.01	0.811

** unexpected order

(ii)   *Monophosphine   square   planar   Rh(I)   complexes   of   the   type*
         [Rh(β-diketonato)(CO)(PPh₃)].

Oxidation and reduction potentials of square planar rhodium(I) complexes of the type [Rh(β-diketonato)(CO)(PPh₃)] with β-diketonato = dbm, da, tfba and tfaa in CH₃CN with 0.1 mol dm^{-3} tetrabutylammonium hexafluorophosphate as supporting electrolyte, on a glassy carbon electrode at 25.0(1) °C and at a constant sweep rate of 100 mV s^{-1} are presented in **Table 2.39**.[194]

Table 2.39: Electrochemical data for complexes of the type [Rh(β-diketonato)(CO)(PPh₃)] with β-diketonato = dbm, da, tfba and tfaa measured in 0.1 mol dm^{-3} TBAPF₆/CH₃CN on a glassy carbon electrode at 25.0(1) °C and at a scan rate of 100 mV s^{-1}.[194]

β-diketonato	R	R'	χ$_{R'}$ of R' [a]	pK$_a$[b]	E$_{pa}$ *vs.* Fc⁺/Fc	E$_{pc}$ *vs.* Fc⁺/Fc
dbm	Ph	Ph	2.21	9.4	0.308	-0.76
ba	Ph	CH₃	2.34	8.7	0.336	-0.80
tfba	Ph	CF₃	3.01	6.3	0.448	-0.64
tfaa	CH₃	CF₃	3.01	6.3	0.491	-0.66

(a)   group electronegativities χ$_{R'}$ on the Gordy scale from reference 184   (b)   pK$_a$ values as in reference 194.

In agreement with the results of [Rh(β-diketonato)(CO)(P(OCH₂)₃CCH₃)] and [Rh(β-diketonato)(P(OPh)₃)₂], the electrochemical oxidation of the [Rh(β-diketonato)(CO)(PPh₃)] complexes becomes increasingly difficult to oxidise as more electron density is withdrawn from it by the substituent R and R' on the β-diketonato RCOCHCOR'. This is in agreement with the increasing order of the group electronegativities of the substituent R and R' on the β-diketone RCOCH₂COR' (from top to bottom of **Table 2.39**), namely Ph < CH₃ < CF₃.[184]

2.3.9   *CV's and correlations for this study.*

In this study CV's of square planar complexes of rhodium(I) and iridium(I) are presented. The formal reduction potential E$^{0'}$ of the ferrocenyl group of the co-ordinated β-diketonato ligand to the metal, as well as the oxidation potential of the metal have been measured. By comparing E$^{0'}$

---

[194] Lamprecht, D., *Electrochemical, kinetic and molecular mechanic aspects of rhodium(I) and rhodium(III) complexes, Ph. D. Thesis*, University of the Orange Free State, R.S.A., 1998.

of the ferrocenol group of the co-ordinated β-diketonato ligand of isostructural square planar complexes of rhodium(I) and iridium(I) with each other as well as with $E^{0'}$ of the free β-diketone, the influence of electron density of the metal centres rhodium and iridium on the formal reduction potential of the ferrocenyl group can be determined.

The influence of the ligands cod, CO, PPh$_3$ and P(OPh)$_3$ on the electron density of the metal can be determined by comparing the oxidation potential of the metal of complexes of type [Rh(β-diketonato)(CO)$_2$], [Rh(β-diketonato)(CO)(PPh$_3$)], [Rh(β-diketonato)(cod)] and [Rh(β-diketonato)(P(OPh$_3$))$_2$] (for the same β-diketonato) with each other. The electron attracting properties of the ligands should increase in the same order as the increase of the oxidation potential of the metal centre of the complex it is co-ordinated to.

The increase of the oxidation potential of the metal of complexes of type [Rh(β-diketonato)(L)(L')] for different β-diketonato ligands should (a) parallel the increase in the rate constant of substitution reactions to the metal complex, (b) be opposite to the increase in the rate constant of oxidative addition reactions to the metal complex, (c) parallel the increase in the group electronegativity (χ_R/Gordy scale) of the R group on the β-diketone RCOCH$_2$COFc and (d) be opposite to the increase of the pK$_a$ of the different β-diketones co-ordinated to the same metal complex. The same should apply to $E^{0'}$ of the ferrocenol group of the co-ordinated β-diketonato ligand to the metal of complex.

Correlation between all these parameters *viz.* the oxidation potential of the metal centre, $E^{0'}$ of the ferrocenyl group of the co-ordinated β-diketonato ligand to the metal of complex, pK$_a$ of the different β-diketones, group electronegativity (χ_R/Gordy scale) of the R group on the β-diketone RCOCH$_2$COFc and the rate constants for substitution and oxidative addition reactions for selected square planar complexes of rhodium(I) and iridium(I) will be presented in this thesis.

2.4 Synthesis of metal β-diketonato complexes.

The aim of this study was not the development of new synthetic routes. New rhodium and iridium complexes were, however, synthesised by means of known methods from new ferrocene-

containing β-diketonato ligands, the synthesis of which were recently developed in this laboratory.[188] Therefore, only a short discussion on the synthetic routes followed is relevant for this dissertation.

2.4.1 *Synthesis of β-diketones.*

A general method of synthesis of a wide variety of β-diketones is the well-known Claisen condensation[195] according to which a ketone containing an α-hydrogen atom undergoes acylation with an acid anhydride, an acid chloride, or an ester in the presence of a base, *e.g.* sodium metal, sodium ethoxide, sodium hydride, or sodium amide. An acidic reagent like boron trifluoride has also been found to be effective for acylation of a ketone to form β-diketones. The methods of synthesis of β-diketones were reviewed in 1954 by Hauser *et al.*[196] and more recently by Mushak *et. al.*[197]

The β-diketones synthesized in this study all contained a ferrocenyl group. The strong electron-donating properties of the ferrocenyl group lower the acidity of the methyl hydrogen atoms of acetylferrocene which in turn necessitates the use of strong bases *(i.e.* metal amides or alkoxides) to ensure reasonable yields. Hauser and co-workers[198] synthesized the ferrocene-containing β-diketones, Hfca[198iii)] and Hbfcm[198i)], by using potassium amide as the active base additive in liquid ammonia as solvent (**Scheme 2.32** route 1). Weinmayr[199] utilised sodium methoxide as basic initiator to prepare both Hfca and Hfctfa) in diethyl ether (**Scheme 2.32** route 2), while

---

[195] i) Vogel A.I., *Practical Organic Chemistry including Qualitative Organic Analysis,* Longman. London, 3rd edn., 1977, p. 861-865.

ii) Hauser, C.R. and Hudson, B.F. jun., in *Organic Reactions,* ed. R. Adams, Wiley, New York, 1942, vol.1, ch. 9, p. 266-302.

[196] Hauser, C.R., Swamer, F.W and Adams, J.T. in *Organic Reactions,* ed. R. Adams, Wiley, New York, 1954. vol.8, ch.3, p.59-196.

[197] Mushak, P., Glann, M.T. and Savory, J., *Fluorine Chemistry Reviews,* ed. P. Tarrant, **6**, 1973, p. 43.

[198] i) Hauser, C.R. and Lindsay. J.K., *J. Org. Chem.,* **22**, 482 (1957).

ii) Hauser, C.R. and Cain, C.E., *J. Org. Chem.,* **23**, 1142 (1958).

iii) Cain, C.F., Mashburn T.A. and Hauser, C.R., *J. Org. Chem.,* **26**, 1030 (1961).

[199] Weinmayr, V., *Naturwissenschaften*, **45**, 311 (1958).

Cullen *et. al.*[200] favoured the use of the sterically hindered base lithium diisopropylamide in the preparation of Hfca (**Scheme 2.32** route 3). In a recent paper[188] the three methods were compared and Hfctca as well as Hdfcm were also synthesized. An adaption of Cullen's lithium diisopropylamide route was found to be most convenient.
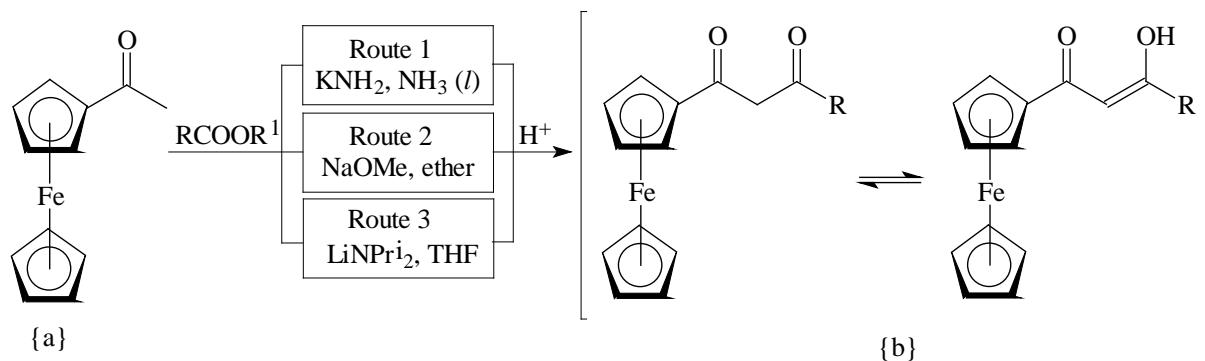
Scheme 2.32: **Claisen condensation of acetylferrocene {a} with appropriate esters (R' = ethyl or methyl) gives the β-diketones Hfctfa ({b}, R = CF₃), Hfctca ({b}, R = CCl₃), Hfca ({b}, R = CH₃), Hbfcm ({b}, R = phenyl) and Hdfcm ({b}, R = ferrocenyl). NMR studies indicated that asymmetric enolisation as shown dominates.[188] LiNPr$^i_2$ = lithium diisopropylamide.**

2.4.2 *Synthesis of metal β-diketonato complexes.*

The rhodium and iridium complexes that are important in terms of this study were all synthesized from MCl₃ (M = Rh, Ir), the desired β-diketone and the ligands cod, CO or PPh₃. **Scheme 2.33** presents a schematic presentation of the general method of synthesis of selected square planar rhodium and iridium complexes containing a β-diketonato ligand. The products obtained by substitution of the β-diketonato ligand with derivatives of 1,10-phenantroline (N-N) from the cod-complex, as well as the product from oxidative addition of CH₃I to the monocarbonyl complex, are also shown.

2.4.2.1 Mono and dicarbonyl complexes of rhodium.

Heating of [RhCl₃.3H₂O] in DMF results in the metallic dimer complex [Rh₂Cl₂(CO)₄] {c}.[201] The square planar dicarbonyl complex [Rh(β-diketonato)(CO)₂] {e} can be prepared by the

---

[200] Cullen, W.R., Rettig, S.J. and Wickenheiser, F.B., *J. Mol. Catal.,* **66**, 251 (1991).

[201] i) Varshavskii, Y.S. and Cherkasova, *Russ. J. Inorg. Chem.,* **12**, 899 (1967).

treatment of $[Rh_2Cl_2(CO)_4]$ {c} with the β-diketone in the presence of a base such as $BaCO_3$[31] or alternatively in solution in DMF.[202] [M(β-diketonato)(CO)$_2$] {e} reacts rapidly with PPh_3 with the displacement of one of the CO ligands to afford the square planar monocarbonyl complex [M(β-diketonato)(CO)(PPh$_3$)] {g} (M = Rh[31] or Ir[203]). Oxidative addition of CH_3I to the monocarbonyl complex {g} results in the alkyl [M(β-diketonato)(CH$_3$)(I)(CO)(PPh$_3$)] {h}.[7, 80] The dicarbonyl complex [M(β-diketonato)(CO)$_2$] {e} (M = Rh, Ir) can also be obtained from complex [M(β-diketonato)(cod)] {d} by substitution of the cod ligand with carbon monoxide (M = Ir or Rh).

2.4.2.2   1,5-Cyclo-octadiene complexes of rhodium and iridium.

Reduction of $[MCl_3.3H_2O]$ (M = Rh, Ir) in refluxing EtOH with 1,5-cyclo-octadiene (cod) results in the air stable dimer complex [M$_2$Cl$_2$(cod)$_2$] {b} (M = Rh,[204] Ir[205]), **Scheme 2.33**. The bridging chloride ligand can be replaced by a β-diketonato ligand to obtain the cod compound [M(β-diketonato)(cod)] {d} (M = Rh,[174, 204ii)] Ir[72, 206]). [M(β-diketonato)(cod)] {d} can also be obtained from the dicarbonyl complex [M(β-diketonato)(CO)$_2$] {e} by substitution of the CO ligands with cod (M = Rh[31]). Substitution of the β-diketonato ligand from [M(β-diketonato)(cod)] {d} with 1,10-phenanthroline (N-N) leads to four-coordinate [Rh(N-N)(cod)]$^+$ {a}[174, 168, 207] or five-coordinate[Ir(β-diketonato)(N-N)(cod)] {f}.[167 , 208

ii) Rusina, A. and Vlcek, A.A., *Nature (London),* **206**, 295 (1965).

[202] Leipoldt, J.G, Bok, L.D.C., Basson, S.S., van Vollenhoven, J.S. and Gerber, T.I.A., *Inorg. Chim. Acta.,* **25**, L63 (1977).

[203] Bonati, F. and Ugo, R., *J. Organomet. Chem.,* **11**, 341 (1968).

[204] i) Chatt, J. and Venanzi, L.M., *Nature (London),* **177**, 852 (1956).
ii) Chatt, J. and Venanzi, L.M., *J. Chem. Soc.,* **(A)**, 4735 (1957).

[205] Herde, J.L., Lambert, J.C. and Senoff, C.V., *Inorganic Synthesis,* ed. G.W. Parshall, McGraw-Hill Co., New York, **15**, 18 (1974).

[206] Basson, S.S., Leipoldt, J.G., Purcell, W. and Schoeman, J.B. *Inorg. Chim. Acta.,* **173**, 155 (1990).

[207] Du Plessis, W.C., *Synthesis, thermodynamic, electrochemical and kinetic aspects of ferrocene-containing β-diketones (in Afrikaans), M.Sc. Thesis*, University of the Orange Free State, R.S.A., 1996.

[208] Ora, L.A., Carmona, D., Esteruelas, M.A., Foces-Foces, C. and Cano, F.H., *J. Organomet. Chem.,* **258**, 357 (1983).

$[M(N-N)(cod)]^+$ {a} can also be obtained from the dimer complex $[M_2Cl_2(cod)_2]$ {b} by replacing the bridging chloride ligand by N-N (M = Rh,[209] Ir[210]).
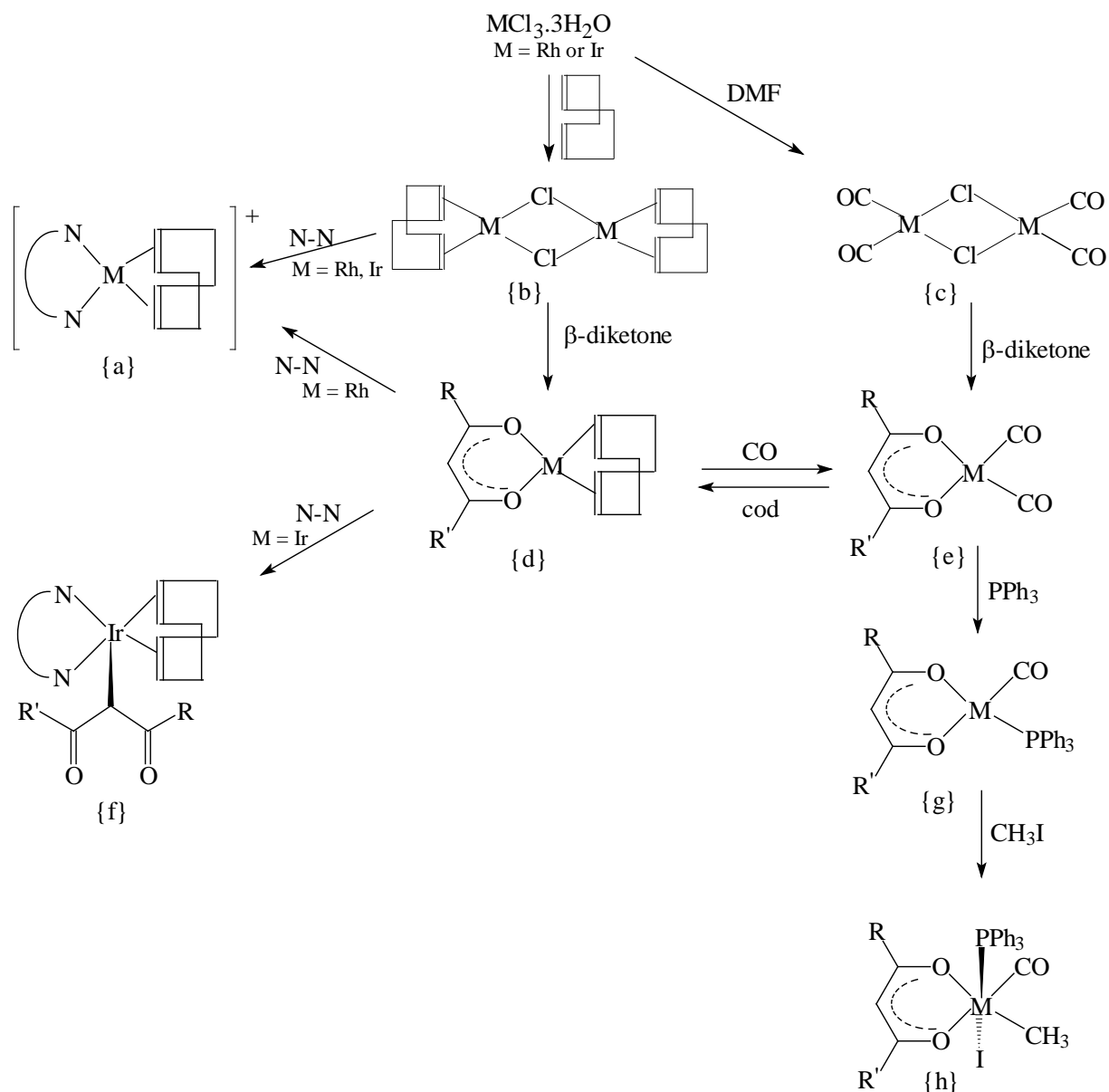
Scheme 2.33: Schematic presentation of the synthesis of selected square planar (except {f}) rhodium and iridium complexes containing a β-diketonato ligand. Products obtained by substitution of the β-diketonato ligand with derivatives of 1,10-phenantroline (N-N) from the cod-complex, as well as the product after oxidative addition of CH₃I to the monocarbonyl complex, are shown.

[209] Gillard, R.D., Harrison, K. and Mather, I.H., *J. Chem. Soc., Dalton Trans.,* 133 (1975).

[210] Mestroni, G., Camus, A. and Zassinovich, G, *J. Organomet. Chem.,* **73**, 119 (1974).

2.5 Crystal structure determination of β-diketones and metal β-diketonato complexes.

β-diketones exist in solution and in the vapour phase generally as equilibrium mixtures of keto and enol tautomers (**Scheme 2.34**). In the solid state, however, the enol form is often the sole form observed. The methine proton in the keto form and the hydroxyl proton in the enol form of the β-diketones are acidic and their removal generates 1,3-diketonato anions (**Scheme 2.34** {c}) which are the source of an extremely broad class of coordination compounds. The synthesis, structure and properties of coordination compounds of ferrocene-containing β-diketones with rhodium(I) and iridium(I) are important in terms of this study.
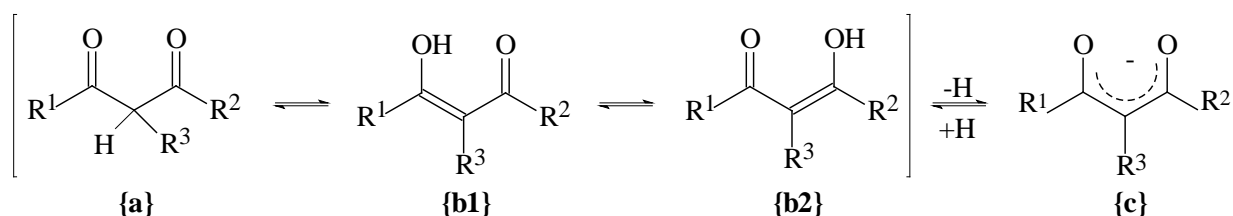
Scheme 2.34: **Schematic presentation of the keto {a} and the enol ({b1} and {b2}) tautomers of β-diketones. If H is replaced by an alkyl or any other group, enolisation is not possible any more. Substituents R^1, R^2 and R^3 are aliphatic or aromatic hydrocarbons. {c} is the 1,3-diketonato anion after removal of the acidic methine proton in the keto form or the hydroxyl proton in the enol form of the β-diketones.**

2.5.1 β-diketones.

Crystal data for selected β-diketones are summarised in **Table 2.40**. **Figure 2.34** gives the structures of the tabulated β-diketones. Most of the β-diketones isolated in the solid state, are in the enol form. There are two extreme forms of intramolecular hydrogen bonding, symmetric and asymmetric. In asymmetric enolization the ring hydrogen is bound much more tightly to one oxygen atom than to the other. Symmetric hydrogen bonds have been observed in examples having identical substituents {*e.g.* Hdbm[211] and bis(*m*-bromobenzoyl)methane (Hdbrbm)[212]} or different substituents (Hba[213]). Markedly asymmetric hydrogen bonds have been observed both for identical substituents (*e.g.* 3-hydroxy-1,3-bis(2-thienyl)prop-2-en-1-one (Hdtm)[214]; Hdbm[215]

---

[211] Etter, M.C., Jahn, D.A. and Urbañczyk-Lipkowska, Z., *Acta Cryst.*, **C43**, 260 (1987).

[212] Williams, D.E., Dumke, W.L. and Rundle, R.E., *Acta Cryst.*, **15**, 627 (1962).

[213] Jones, R.D.G., *Acta Cryst.*, **B32**, 2133 (1976).

[214] Baxter, L.A.M., Blake, A.J., Heath, G.A. and Stephenson, T.A., *Acta Cryst.*, **C46**, 508 (1990).

and Hacac[216]), and for different substituents (*e.g.* 1-(2-thienyl)-4,4,4-trifluorobutane-1,3,dione (Httfa)[217]; ω-(*p*-toluoyl)-acetopenone enol (Hten)[218]; Hfca[219] and Hbfcm[207]). The fine balance between symmetric and asymmetric hydrogen bonding is indicated by the occurrence of symmetric and asymmetric forms in two polymorphs of the same compound Hdbm.[211, 215]

In contrast to the formation of hydrogen-bonded enols (**Figure 2.34** (a) and (c)), the 3-ferrocenophane-1,3-dione (H3fco[220]) (**Figure 2.34** (b)) exists in the solid state entirely as a dione with C-C and C=O bond lengths very similar to those of the related dione 2-benzylidene-3-ferrocenophane-1,3-dione (H2b3fco[221]) where enolization is structurally impossible. The lack of enolization in H3fco results from the fact that the two cyclopentadenyl rings of the ferrocenyl are so far apart that the β-diketone backbone cannot accomodate 120° angles, thereby disallowing the enol form. For example the methine carbon has an angle of only 103.71°, approaching that of a sp^3 C-atom. A further consequence of the short length of the β-diketone backbone is ringtilt of 9.8° and bond angles of ~117° at the carbonyl carbon atoms. In 2-ethyl-1,3-diphenyl-1,3-propanedione[222] (H2edbm) the solid state structure indicates a lack of enolization associated with a markedly non-planar O=C-C-C=O fragment. The single crystal X-ray structure of 4-(ferrocenylmethyl)-2,2,6,6,-tetramethyl-3,5-heptanedione[223] (H4fcmβ) confirms that in the solid state it is indeed a non-enolized 1,3-diketone.

The crystal structure of Hacac (mp –23ºC) was determined after a drug complex crystallised from Hacac was found by means of X-ray crystal structure determination to contain one molecule of Hacac per unit in the crystal lattice. In this thesis the crystal structure of 3-ferrocenoyl-1,1,1-trifluoro-2-hydroxyprop-2-ene (Hfctfa) will be reported.

[215] i) Jones, R.D.G., *Acta Cryst.*, **B32**, 1807 (1976), ii) Williams, D.E., *Acta Cryst.*, **21**, 340 (1966), iii) Hollander, F.J., Templeton, D.H. and Zalkin, A., *Acta Cryst.*, **B29**, 1552 (1973).

[216] Camerman, A., Mastropaolo, D. and Camerman, N., *J. Am. Chem. Soc.,* **105**, 1584 (1983).

[217] Jones, R.D.G., *Acta Cryst.*, **B32**, 1224 (1976).

[218] Kato, K., *Acta Cryst.*, **B27**, 2028 (1971).

[219] Bell, W., Crayston, J.A., Glidewell, C., Mazid, M.A. and Hursthouse, B., *J. Organomet. Chem.,* **434**, 115 (1992).

[220] Gyepes, E., Glowiak, T., Toma, S. and Soldanova, J., *J. Organomet. Chem.,* **276**, 209 (1984).

[221] Gyepes, E., Glowiak, T. and Toma, S., *J. Organomet. Chem.,* **316**, 163 (1986).

[222] Mullica, D.F., Karban, J.W. and Grossie, D.A., *Acta Cryst.*, **C43**, 601 (1987).

[223] Ferguson, G., Glidewell, C. and Zakaria, C.M., *Acta Cryst.*, **C50**, 1673 (1994).

Table 2.40 (a): Selected crystallographic data for β-diketones, including the typical range of bond lengths in enolized and non-enolized 1,3-diketones. Figure 2.34 gives the structures of the tabulated β-diketones, T = triclinic, M = monoclinic, and O = orthorhombic crystal system.

β-diketone	keto or enol	C=O bond length /Å	C-O (enol) bond length /Å	C=C bond length between carbonyl groups /Å	C-C bond length between carbonyl groups /Å	O....O bond length /Å	Crystal system	Space group
Hdtm[214]	asym enol	1.286 (24)	1.308(23)	1.38(3)	1.41(3)	-	M	*Cc*
Httfa[217] (a)	asym enol	1.269(4) 1.272(4)	1.306(4) 1.310(4)	1.343(4) 1.353(3)	1.432(5) 1.417(4)	2.522(4) 2.550(4)	M	P2$_1$/*n*
Hdbm[215](b)	asym enol	1.293(4)	1.311(4)	1.391(3)	1.422(3)	2.463(4)	O	P*bca*
Hten[218]	asym enol	1.278(3)	1.316(3)	1.383(4)	1.416(4)	2.455(3)	O	P*bca*
Hacac[216]	asym enol	1.238	1.331	1.338	1.412	2.535	T	P$\bar{1}$
Hfca[219]	asym enol	1.287(6)	1.307(6)	1.373(7)	1.406(7)	2.462	O	P2$_1$2$_1$2$_1$
Hbfcm[207]	asym enol	1.284(4)	1.303(4)	1.372(4)	1.406(4)	2.464(8)	M	P2$_1$/*n*
Hhfaa[224]	asym enol	-	-	1.33(4)	1.42(3)	-	-	-
H4fcmβ[223]	keto	1.206(2) 1.206(2)	-	-	1.527(2) 1.533(2)	3.052(2)	T	P$\bar{1}$
H2edbm[222]	keto	1.221(4) 1.218(4)	-	-	1.519(4) 1.520(4)	-	M	P2$_1$/*a*
H3fco[220]	keto	1.218(4) 1.212(4)	-	-	1.528(4(1.537(4)	-	M	P2$_1$/*c*
H2b3fco[221]	keto	1.220(4) 1.216(4)	-	-	1.519(5) 1.507(5)		T	P$\bar{1}$
typical range[219]	**asym enol**	**1.269 – 1.283**	**1.306 – 1.337**	**1.343 – 1.392**	**1.403 – 1.432**	**2.46-2.55**(c)	**-**	**-**
	keto	**1.212 – 1.221**	**-**	**-**	**1.507 – 1.537**	**3.05**(c)	**-**	**-**
Hdbm[211]	sym enol	1.294(3)	1.299(3)	1.383(4)	1.387(4)	-	O	P*bac*
Hdbrbm[212]	sym enol	1.306(8)	1.306(8)	1.393(8)	1.393(8)	2.464(15)	O	P*nac*
Hba[213]	sym enol (b)	1.279(5)	1.282(4)	1.398(4)	1.409(4)	2.489(5)	M	P2$_1$/*c*

(a) Bond distances of ref 215 i). (b) Two molecules in asymmetric unit. (c) Estimated by author from above data.

Table 2.40 (b): Selected crystallographic data for the ferrocenyl group of ferrocene containing β-diketones, including the average bond lengths in 1,3-diketones.

β- diketone	keto or enol	ferrocene unsubstituted ring		ferrocene substituted ring	
		average C – C bond length /Å	average Fe – C bond length /Å	average C – C bond length /Å	average Fe – C bond length /Å
H4fcmβ	keto	1.400(5)	2.033(2)	1.416(4)	2.040(2)
H3fco	keto	-	-	1.428	2.04
H2b3fco	keto	-	-	1.420	2.03
Hfca	enol	1.396	*	1.423	*
Hbfcm	enol	1.384(23)	2.027(9)	1.412(14)	2.033(10)
typical range**	**enol / keto**	**1.38 – 1.40**	**2.03**	**1.41 – 1.43**	**2.03 – 2.04**

*Average Fe-C bond lengths Hfca equivalent, length not given. **Estimated by author from above data.

[224] Wang, S., Pang, Z., Smith, K.D.L., Hua, Y., Deslippe, C. and Wanger, M.J., *Inorg. Chem.*, **34**, 908 (1995).
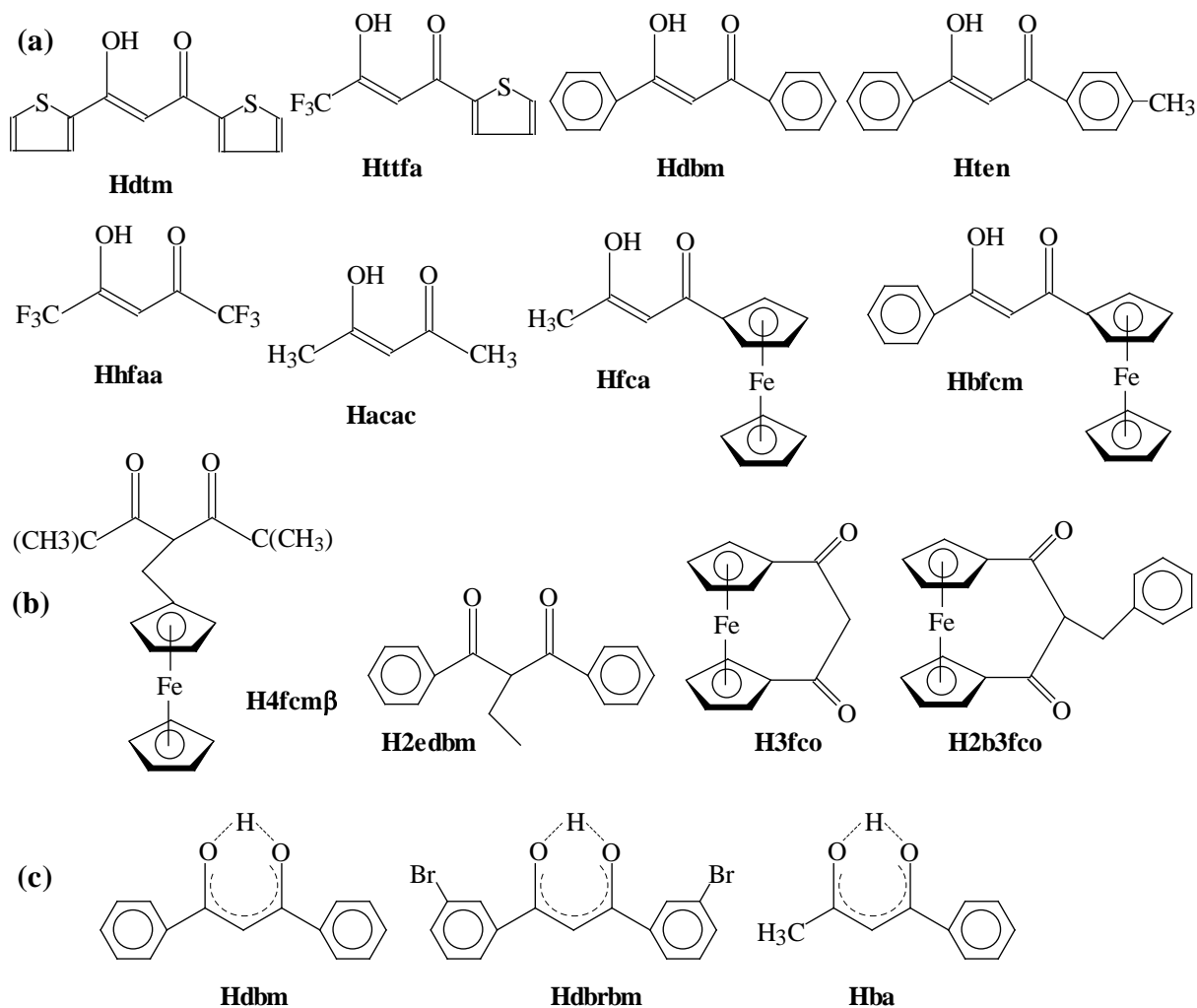
Figure 2.34: **Structures of the β-diketones: (See List of Abbreviations for those used).**
(a) enol with asymmetric hydrogen bonds *e.g.* Hdtm,[214] Httfa,[217] Hdbm,[215] Hten,[218] Hhfaa,[224] Hacac,[216]
Hfca[219] and Hbfcm[207].
(b) keto *e.g.* H4fcmβ,[223] H2edbm,[222] H3fco[220] and H2b3fco.[221]
(c) enol with symmetric hydrogen bonds *e.g.* Hdbm,[211] Hdbrbm[212] and Hba.[213]

2.5.2 *Rh(I) complexes of the type [Rh(L,L'-BID)(CO)(PPh₃)] and related Rh(III)-complexes.*

In this thesis the crystal structure of [Rh(fctfa)(CO)(PPh₃)] will be reported. **Table 2.41** presents selected crystallographic data of related rhodium(I) complexes of the type [Rh(L,L'-BID)(CO)(PPh₃)] containing L,L'-BID ligands with donor atoms (L, L') = (O, O), (N, O), (S, O) and (S, N).

111

Table 2.41: Selected crystallographic data for square planar complexes [Rh(L,L'-BID)(CO)(PPh₃)]ᵃ⁾ containing L,L'-BID ligands with L, L' donor atoms as indicated (see List of Abbreviations, T = triclinic, M = monoclinic, and O = orthorhombic crystal system).

L,L'-BID	L, L'	Ring-size	Bite angle /degree	PPh₃ *trans* (T) or *cis* (C) to Lᵇ⁾	Rh-L distance /Å	Rh-L' distance /Å	Rh-P distance /Å	Crystal system	Space group
dbm[36]	O, O	6	88.5	Symmetricalᶜ⁾	2.081(9)	2.038(10)	2.237(7)	M	Cc
acac[33]			87.9	Symmetricalᶜ⁾	2.087(4)	2.029(5)	2.244(2)	T	P$\bar{1}$
bzaa[34]			86.8	Symmetricalᶜ⁾	2.048(2)	2.01(2)	2.243(1)	T	P$\bar{1}$
tta[37]			87.5	T	2.085(7)	2.052(8)	2.245(3)	M	P2₁/*n*
tfhd[40]			87.5(4)	C	2.048(13)	2.094(9)	2.252(3)	T	P$\bar{1}$
tfdma[41]			87.5	C	2.057(6)	2.089(4)	2.239(2)	T	P$\bar{1}$
tftma[42]			88.1	C	2.061(7)	2.070(8)	2.238(3)	M	P2₁/*c*
ba[44]			88.1 / 86.2	T / C	2.079(8) / 2.018(8)	2.032(8) / 2.057(7)	2.249(3) / 2.248(3)	T	P$\bar{1}$
tfaa[40] ᵈ⁾			88.9(2)	T	2.071(6)	2.045(6)	2.231(3)	T	P$\bar{1}$
bpha[38]		5	78.4	T	2.089(3)	2.037(4)	2.232(2)	T	P$\bar{1}$
trop[35]			77.8	Symmetricalᶜ⁾	2.081(7)	2.034(7)	2.232(2)	T	P$\bar{1}$
cupf[39]			76.6	T	2.036(6)	2.024(6)	2.232(2)	-	P$\bar{1}$
salnr[46]	N, O	6	88.7	T	2.092(7)	2.027(6)	2.281(2)	O	Pbac
dmavk[47]			87.4	T	2.045(4)	2.044(3)	2.275(1)	O	Pca2₁
ox[48]		5	80.0	T	2.098(9)	2.042(5)	2.261(2)	T	P$\bar{1}$
quin[32]			78.9	T	2.162(6)	2.034(7)	2.258(2)	T	P$\bar{1}$
pic[49]			78.9	T	2.088(6)	2.066(7)	2.262(2)	T	P$\bar{1}$
sacac[50]	S, O	6	91.7	T	2.297(2)	2.023(6)	2.300(2)	T	P$\bar{1}$
dbbtu[52]			90.11(2)	T	2.307(1)	2.046(3)	2.282(1)	M	P2₁/*n*
hpt[51]		5	83.9	T	2.311(1)	2.031(2)	2.278(1)	T	P$\bar{1}$
anmetha[51] ᵉ⁾			83.4(1)	T	2.306(2)	2.029(4)	2.290(1)	T	P$\bar{1}$
cacsm[53]	S, N	6	93.5	C	2.217(14)	2.125(3)	2.268(1)	T	P$\bar{1}$
hacsm[54]			91.32(11)	T	2.307(1)	2.019(3)	2.283(1)	M	P2₁/*c*
macsm[55]			93.8	C	2.298(1)	2.087(4)	2.269(1)	M	P2₁/*n*

a) The structures of the complexes tabulated are in given in **Figure 2.9** - **Figure 2.14** and **Figure 2.16**.
b) L = oxygen atom nearest to the strongest electron attracting group of the chelate ring when L = L' = O.
c) for symmetrical ligands, L was chosen *trans* of PPh₃.
d) data for P(*p*-Cl-Ph)₃ complex.
e) data for PCy₃ complex.

The average bond lengths of the [Rh(L,L'-BID)(CO)(PPh₃)] complexes presented in **Table 2.41**, as tabulated in **Table 2.42**, indicate a tendency of:

i)   Rh-P bond lengthening from five to six-membered chelate rings,

ii)   lengthening of the Rh-donor atom bond length *cis* to P from five to six-membered chelate
        rings,

iii)   a lengthening of the Rh-donor atom bond length *trans* to P from five to six-membered
        chelate rings when the donor atoms (L, L') = (O, O) or (N, O) and

iv)   the Rh-donor atom bond length *trans* to P (2.069 – 2.311 Å) is longer than the Rh-donor
        atom bond length *cis* to P (2.031 – 2.047 Å) except for the case when the donor atoms
        (L, L') = (S, N).

It should be realized, however, that the averages given in **Table 2.42** mathematically include any
smaller effects on bond lengths that adjacent groups with different group electronegativity may
have.

Table 2.42: Average bond lengths in complexes of the type [Rh(L,L'-BID)(CO)(PPh₃)] as tabulated in Table 2.41.

Donor atoms L and L'		Rh-P bond length / Å		Rh-donor atom bond length *cis* to P/ Å		Rh-donor atom bond length *trans* to P/ Å	
		Five-membered chelate ring	Six-membered chelate ring	Five-membered chelate ring	Six-membered chelate ring	Five-membered chelate ring	Six-membered chelate ring
O	O	2.232	2.244	2.032	2.038	2.069	2.076
N	O	2.260	2.278	2.036	2.047	2.069	2.116
S	O	2.278	2.291	2.031	2.035	2.311	2.302
S	N	-	2.273	-	2.173	-	2.173
range		2.232 - 2.291 Å		2.031 – 2.047 Å [a)]		2.069 – 2.311 Å	

a)   donor atoms (L, L') = (S, N) not included in range for Rh-donor atom bond length *cis* to P.

In this thesis the crystal structure of the oxidation addition product of [Rh(fctfa)(CO)(PPh₃)] and
iodomethane, namely [Rh(fctfa)(CH₃)(I)(CO)(PPh₃)] will be also be reported. Crystallographic
data of alkyl oxidative addition products of [Rh(L,L'-BID)(CO)(PPh₃)] and iodomethane, namely
[Rh(L,L'-BID)(CH₃)(I)(CO)(PPh₃)] is given in **Table 2.43**.   **Figure 2.35** gives the structures of
the alkyl complexes. Data of acyl complexes (formed from the insertion reaction of carbonyl
after oxidative addition of iodomethane to [Rh(L,L'-BID)(CO)(PPh₃)] complexes) are given in
Table 2.44 and the structures in **Figure 2.24**, page 60. These data are given to see the influence
(if any) of the addition of iodomethane to [Rh(L,L'-BID)(CO)(PPh₃)] on the selected bond
lengths. No general trend was observed.

Table 2.43: Selected crystallographic data for octahedral Rh(III) alkyl complexes [Rh(L,L'-BID)(CH₃)(I)(CO)(PPh₃)][82, 106, 109, 110] containing L,L'-BID ligands with L, L' donor atoms as indicated (see List of Abbreviations for the different L,L'-BID; Figure 2.35 illustrates the structures of the alkyl complexes; T = triclinic, M = monoclinic, and O = orthorhombic crystal system).

L,L'-BID	L, L'	Ring-size	Bite angle /degree	PPh₃ *trans* (T) or *cis* (C) to L	Rh-L distance /(Å)	Rh-L' distance /(Å)	Rh-P distance /(Å)	addi-tion *cis or trans*	Rh-CH₃ distance /(Å)	Rh-I distance /(Å)	Space group
cupf	O, O	5	74.9(4)	T	2.175(9)	2.04(1)	2.327(4)	cis	2.08(1)	2.708(2)	P$\bar{1}$
neocupf		5	76.3(2)	T	2.128(6)	2.074(5)	2.307(2)	cis	2.092(14)	2.7111(14)	P$\bar{1}$
dmavk	N, O	6	89.5(4)	T	2.035(7)	2.042(11)	2.356(3)	trans	1.850(13)	2.8489(12)	P$\bar{1}$
ox [a)]		5	81.6(2) 80.8(2)	T	2.085(7) 2.083(7)	2.036(4) 2.037(4)	2.317(2) 2.326(2)	trans	2.104(8) 2.111(10)	2.809(1) 2.796(1)	P$\bar{1}$

a)   two [Rh(L,L'-BID)(CH₃)(I)(CO)(PPh₃)] molecules and one (CH₃)₂CO molecule in a unit
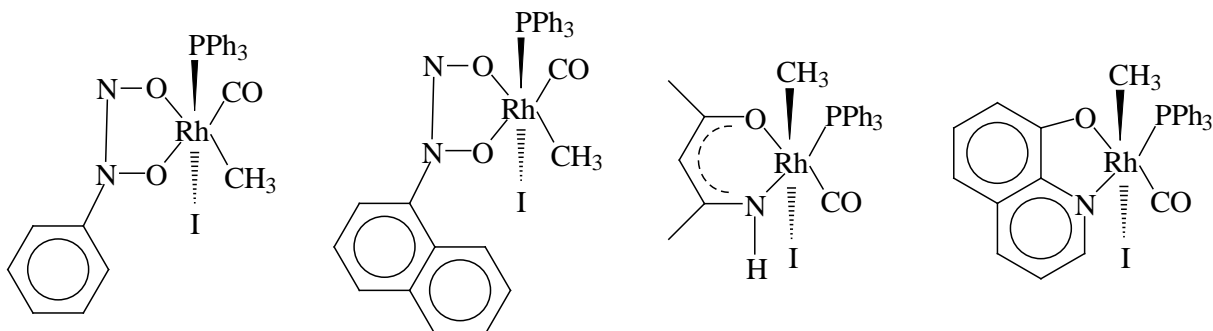
Figure 2.35: Structures of the alkyl complexes [Rh(L,L'-BID)(CH₃)(I)(CO)(PPh₃)] where L,L'-BID = cupf[82], neocupf[106], dmavk[109] and ox[110].

Table 2.44: Selected crystallographic data for square pyramidal Rh(III) acyl complexes [Rh(L,L'-BID)(COCH₃)(I)(PPh₃)][54, 128, 129, 130] containing L,L'-BID ligands with L and L', the donor atoms as indicated, and with the acyl moiety in the apical position (see Table 2.22 for the different L,L'-BID and Figure 2.24, page 60 for the structures of the acyl complexes, M = monoclinic crystal system).

L,L'-BID	L, L'	Ring-size	Bite angle /degree	PPh₃ *trans* (T) or *cis* (C) to L	Rh-L distance /(Å)	Rh-L' distance /(Å)	Rh-P distance /(Å)	Rh-C distance /(Å)	Crystal system	Space group
stcs	S, N	5	81.4(3)	T	2.284(3)	2.151(11)	2.341(3)	1.992(14)	M	P2₁/*c*
macsm		6	95.2(2)	C	2.252(2)	2.065(5)	2.321(1)	1.970(7)	M	P2₁/*c*
dmavk [a)]	N, O	6	87.4(4)	T	2.031(9)	2.054(10)	2.254(4)	1.943(14)	M	P2₁/*c*
mnt [b)]	S, S	5	88.5(1)	symme-trical[c)]	2.323(3)	2.269(3)	2.324(3)	2.006(14)	-	P2₁/*a*

a)   parameters of the major component of four slightly different molecules resulting from crystal packing effects.

b)   [Rh(L,L'-BID)(COCH₂CH₃)(I)(PPh₃)] complex

c)   for symmetrical ligands, L was chosen *trans* of PPh₃.

2.5.3 *Rh(I) complexes of the type [Rh(L,L'-BID)(D)$_n$].*

In this thesis the crystal structure of [Rh(fctfa)(CO)$_2$] complex will be presented. The substitution of only one of the carbonyl groups in [Rh(L,L'-BID)(CO)$_2$] by PPh$_3$ results in the complex [Rh(L,L'-BID)(CO)(PPh$_3$)] with the Rh-donor atom bond length *trans* to P (2.069 – 2.311 Å) longer than the Rh-donor atom bond length *cis* to P (2.031 – 2.047 Å) (see **Table 2.42** for the exception). This longer bond length is the result of the combined effect of the *trans* influence of the substituents on the L,L'-BIB and the *trans* influence of PPh$_3$. **Table 2.45** gives the crystallographic data for [Rh(L,L'-BID)(D)$_n$] complexes with symmetrical ligands D = cod (n = 1), P(OPh$_3$) (n = 2) or CO (n = 2) and the structures of the tabulated complexes are given in **Figure 2.36**. Since the ligand(s) (D)$_n$ is(are) symmetrical, the Rh-donor atom bond lengths in the [Rh(L,L'-BID)(D)$_n$] complexes was used to study the effect of the influence of the different substituents of the L,L'-BIB (*e.g.* CF$_3$, Ph, CH$_3$ and Fc) on the two donor atoms (*e.g.* O or N):

i)   The Rh-N bond length (2.098(9) Å), which is longer than the Rh-O bond length (2.051(6) Å) in the structure of [Rh(ox)(cod)] (L, L' = N, O) indicated a larger *trans* influence for the nitrogen atom than the oxygen atom. This result is in agreement with the results of the structure determination of [Rh(L,L'-BID)(CO)(PPh$_3$)] where it was shown that the carbonyl *trans* to the nitrogen atom was substituted with the PPh$_3$ ligand in the reaction of **Scheme 2.4**, page 19 (see discussion on page 27 and 28).

ii)   When the L,L'-BID is symmetrical like acac, the bonds *trans* to the L,L' group should be chemically equivalent, as was confirmed by the structure determination of the three [Rh(acac)(D)$_n$] complexes where the two Rh-O bond lengths in each complex were the same within experimental error.

iii)   The relative effects of the CF$_3$ and phenyl groups on the Rh-O bond strengths were reflected by the Rh-O bond lengths in the [Rh(tfba)(D)$_n$] complexes where the Rh-O bond length nearest to the CF$_3$ group was longer than the the Rh-O bond length nearest to the phenyl group in the [Rh(tfba)(cod)] and [Rh(tfba)(P(OPh$_3$)$_2$] complexes (the standard deviation in the [Rh(tfba)(CO)$_2$] complex were too large to draw any conclusions). The longer Rh-O bond length nearest to the CF$_3$ group confirms that the oxygen atom nearest to an electron attracting group of a chelate ring has the smallest *trans* influence (see discussion on page 22).

iv)   The structure of the [Rh(fctca)(cod)] complex indicated that fc has a larger *trans* influence than CCl₃.

v)   The crystal data of the [Rh(tfaa)(P(OPh₃)₂] complex indicated a larger *trans* influence for CF₃ than CH₃, though not exclusively within experimental error.

vi)   The crystal data of the two independent molecules [Rh(fca)(cod)] were not consistent with each other.
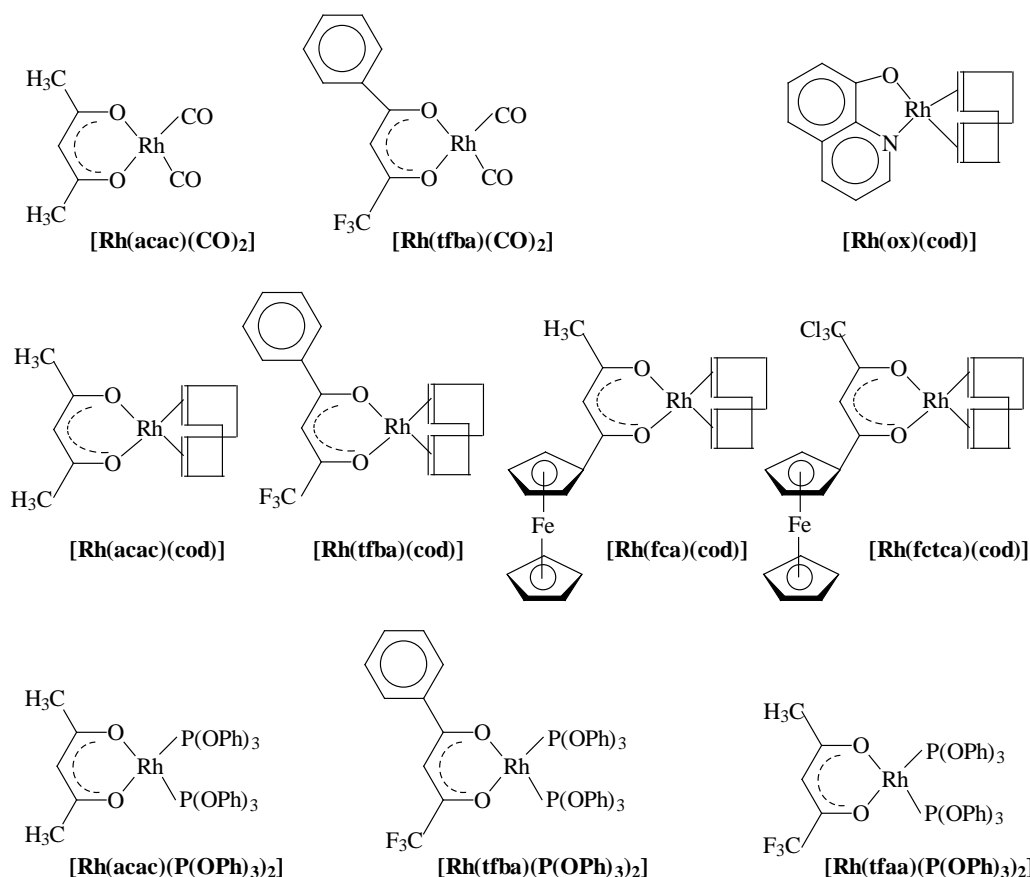
Figure 2.36: **Structures of rhodium(I) complexes of the type [Rh(L,L'-BID)(D)ₙ]:**
[Rh(L,L'-BID)(CO)₂] with L,L'-BID = acac and tfba
[Rh(L,L'-BID)(cod)] with L,L'-BID = acac, tfba, fca, fctca and ox
[Rh(L,L'-BID)(P(OPh₃))₂] with L,L'-BID = acac, tfba and tfaa.

The range of the Rh-P bond lengths in the [Rh(L,L'-BID)(P(OPh₃))₂] complexes in **Table 2.45** is 2.136 – 2.161 Å which is significantly shorter than the Rh-P bond lengths in the [Rh(L,L'-BID)(CO)(PPh₃)] complexes (average range 2.232 – 2.291 Å from **Table 2.42**). This significantly shorter Rh-P bond length in the case of the phosphite complexes is probably the result of the strong π-electron acceptor properties of the phosphite ligand,[225] resulting in a relatively stronger Rh-P bond and hence a shorter bond length.

[225] Emsley, J. and Hall, D., *The Chemistry of Phosphorous,* Harper & Row Publishers, London, (1976) p. 191.

Table 2.45: Selected crystallographic data for [Rh(L,L'-BID)(D)$_n$] complexes containing L,L'-BID ligands with donor atoms L and L' as indicated and D = cod (n = 1), P(OPh$_3$) (n = 2) or CO (n = 2) (see List of Abbreviations for L,L'-BID, Figure 2.36 for the structures of the complexes in the table, T = triclinic, M = monoclinic, and O = orthorhombic crystal system). L is more electronegative than L' or in the case of L,L'-BID = β-diketonato the oxygen atom nearest to the most electronegative group on the β-diketonato ligand (see Table 2.34 for the group electronegativities).

L,L'-BID	L, L'	Ring-size	Bite angle /degree	D	Rh-L distance /(Å)	Rh-L' distance /(Å)	Rh-D$_1$ distance /(Å)	Rh-D$_2$ distance /(Å)	Crystal system	Space group
acac[226]	O, O	6	90.8(2)	CO	2.044(4)	2.040(4)	1.831(7)	1.831(7)	T	P$\bar{1}$
tfba[202]	O, O	6	89.8		2.024(20)	2.024(16)	1.788(26)	1.815(29)	O	Pbac
acac[227]	O, O	6	89.8(2)	cod [b)]	2.054(5)	2.066(5)	2.115(7) 2.092(8)	2.101(7) 2.101(7)	M	Cc
tfba[228]	O, O	6	90.1(2)		2.066(5)	2.050(4)	2.110(9) 2.115(9)	2.126(7) 2.122(8)	M	P2$_1$/c
fca[229 a)]	O, O	6	91.3(1) 87.9(2)		2.048(3) 2.037(3)	2.039(3) 2.063(3)	2.111(4) 2.120(4) 2.118(5) 2.114(5)	2.109(4) 2.135(4) 2.123(5) 2.110(5)	T	P$\bar{1}$
fctca[207]	O, O	6	90.48(8)		2.054(2)	2.040(2)	2.095(3) 2.099(3)	2.097(3) 2.102(3)	T	P$\bar{1}$
ox[230]	N, O	5	80.9(3)		2.098(9)	2.051(6)			T	P$\bar{1}$
acac[231 a)]	O, O	6	88.8(2) 87.2(1)	P(OPh)$_3$	2.067(5) 2.081(5)	2.061(5) 2.065(5)	2.147(2) 2.142(2)	2.156(2) 2.150(2)	T	P$\bar{1}$
tfba[232]	O, O	6	88.4(2)		2.070(6)	2.067(6)	2.161(2)	2.150(2)	O	Pca2$_1$
tfaa[233 a)]	O, O	6	88.0(5) 87.9(5)		2.085(10) 2.089(13)	2.068(14) 2.084(15)	2.148(4) 2.145(6)	2.136(6) 2.138(6)	T	P$\bar{1}$

a)   Crystal data of two independent molecules.
b)   The two bond lengths provided in the Rh-D$_1$ and Rh-D$_2$ columns refer to the bond lengths from the Rh metal to each of the C-atoms in the C=C bond which the Rh metal coordinates.

[226] i) Bailey, N.A., Coates, E. and Robertson, G.B., *Chem. Commun.,* 1041 (1967).

   ii) Hug, F. and Skapski, A.C., *J. Cryst. Mol. Struct.*, **4**, 411 (1974).

[227] Tucker, P.A., Scutcher. W. and Russel, D.R., *Acta Cryst.*, **B31**, 592 (1975).

[228] Leipoldt, J.G., Basson, S.S., Lamprecht, G.J., Bok, L.D.C. and Schlebusch, J.J.J., *Inorg. Chim. Acta*, **40**, 43 (1980).

[229] Swarts, J.C., Vosloo, T.G., Leipoldt, J.G. and Lamprecht, G.J., *Acta Cryst.*, **C49**, 760 (1993).

[230] Leipoldt, J.G, and Grobler, E.C., *Inorg. Chim. Acta,* **72**, 17 (1983).

[231] Leipoldt, J.G., Lamprecht, G.J. and van Zyl, G.J., *Inorg. Chim. Acta.,* **96**, L31 (1985).

[232] Lamprecht, G.J., Leipoldt, J.G. and van Zyl, G.J., *Inorg. Chim. Acta.,* **97**, 31 (1985).

[233] van Zyl, G.J., Lamprecht, G.J. and Leipoldt, J.G., *Inorg. Chim. Acta,* **102**, L1 (1985).

3 Results and discussion.

3.1 Introduction.

In this study the synthesis, oxidative addition, substitution kinetics and cyclic voltammetry (electrochemical oxidation) of a series of new complexes of the type [Rh(β-diketonato)(CO)(PPh$_3$)] and [M(β-diketonato)(cod)] (M = Rh and Ir), are described. Manipulation of the electron density on the metal centre was achieved by changing the R group on the ferrocene-containing β-diketone, FcCOCH$_2$COR, from Fc with group electronegativity, χ_{Fc} = 1.87 on the Gordy scale, to the highly electronegative group CF$_3$ with χ_{Fc} = 3.01. The change in electron density on the central coordinating metal is reflected in parameters such as kinetic rate constants, carbonyl stretching frequencies and electrode oxidation potentials.

3.2 Synthesis and identification of compounds.

3.2.1 Synthesis of β-diketones containing a ferrocenyl group.

The β-diketones Hfctfa {3}, Hfca {4}, Hbfcm {5} and Hdfcm {6} were prepared by Claisen condensation of acetylferrocene and the appropriate ester in the presence of a base. **Scheme 3.1** illustrates the synthetic routes used for the synthesis of the ferrocene-containing β-diketones used in this study. Weinmayr's route[1] with sodium ethoxide as basic initiator was used to prepare Hfctfa {3} and Hfca {4} in yields not exceeding 52% and 35% respectively based on the initial amount of acetylferrocene used. By adapting the method of Cullen *et al.*[2] to a one-pot procedure, the LiNPr$^i_2$ route was effectively used for Hbfcm {5} (30% yield) and Hdfcm {6} (30% yield) synthesis provided that the added base was never the limiting reagent (to minimise self-aldol condensation of acetylferrocene to give side product {8} in **Scheme 3.1**) and rigorous Schlenk

---

[1] Weinmayr, V., *Naturwissenschaften*, **45**, 311 (1958).

[2] Cullen, W.R., Rettig, S.J. and Wickenheiser, F.B., *J. Mol. Catal.,* **66**, 251 (1991).

conditions were adhered to. Flash column chromatography of crude Hbfcm {5} and Hdfcm {6} was needed to separate the β-diketones {5} and {6} from {8} (1,3-diferrocenylbut-2-en-1-one or 1-ferrocenoyl-2-ferrocenylpropene). {8} is the dehydrated self-aldol condensation product of acetylferrocene. The keto-aldehyde Hfch (2-ferrocenoyl-etan-1-al or ferrocenoylacetaldehyde) {7}, prepared by the LiNPr$^i_2$ route, was provided by M.A.S. Aquino and J.C. Swarts for use in this study.
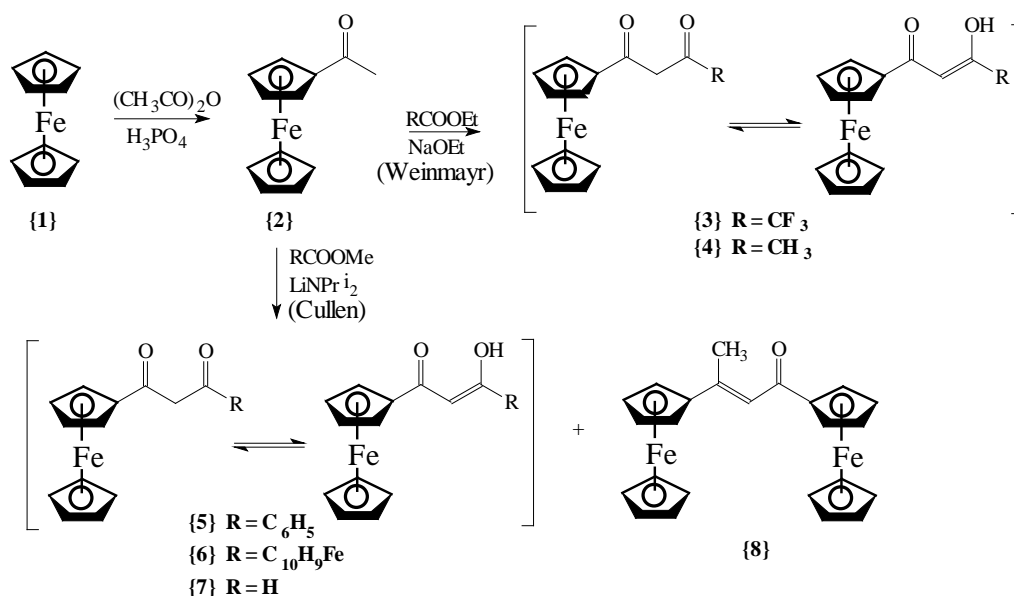
Scheme 3.1: Synthetic routes utilized during the synthesis of the ferrocene-containing β-diketones Hfctfa (R = CF$_3$) {3}, Hfca {4} (R = CH$_3$), Hbfcm {5} (R = C$_6$H$_5$), Hdfcm {6} (R = C$_{10}$H$_9$Fe) and the keto-aldehyde Hfch {7} (R = H) by Claisen condensation of acetylferrocene {2} and an appropriate ester in the presence of a base. Self-aldol condensation of acetylferrocene {2} also led to the side product {8}.

β-Diketones exist in solution and in the vapour phase[3] in equilibrium mixtures of enol and keto tautomers. Here NMR studies indicated, by comparing the relative intensities of the CH$_2$ (keto) and CH (enol) signals in solution, that the enol form dominates.[4] Regarding Hfctfa, Hfca, Hbfcm, Hdfcm and Hfch the apparent absence of more than one set of signals of the ferrocenyl substituent as well as the two observed signals of the methyl side group, the Ph group and the H group indicate that enolisation in solution is predominantly in the direction away from the aromatic ferrocenyl side group. Crystallographic data of Hfctfa presented in this study (paragraph 3.8.1), and of Hfca[5] indicate that in the solid state the enolisation also takes place in the direction away from the aromatic ferrocenyl side group. Low concentration and high

---

[3] Lowrey, A.H., D'Antonio, P.D. and Karle, J., *J. Am. Chem. Soc.,* **93**, 6399 (1971).

[4] du Plessis, W.C., Vosloo, T. and Swarts, J.C., *J.C.S. Dalton Trans.*, 2507 (1998).

[5] Bell, W., Crayston. J.A., Glidewell, C., Mazid, M.A. and Hursthouse, B., *J. Organomet. Chem.,* **434**, 115 (1992).

temperatures of the β-diketone solutions were found to favour slightly higher concentrations of the keto tautomer,[6] *i.e.* drives the equilibrium shown in **Scheme 3.1** more towards the keto side. This may account for Bell's enol:keto ratio of 17:1 for Hfca,[5] while under conditions used in this laboratory, the keto isomer of freshly isolated Hfca approached 80% (enol:keto ratio 1:4) as measured[7] by ^{1}H NMR.

3.2.2 Synthesis of ferrocene-containing β-diketonato complexes of rhodium(I) and rhodium(III).

3.2.2.1   Rhodium(I) complexes of the type [Rh(β-diketonato)(cod)].

[Rh(β-diketonato)(cod)] complexes {10} – {15}, were obtained in good yields up to 77% as red solids by treating β-diketones with [Rh$_2$Cl$_2$(cod)$_2$] {9} at room temperature as illustrated in **Scheme 3.2**.[8] The yellow dimer {9} was obtained by standard methods[9] in yields up to 58%.
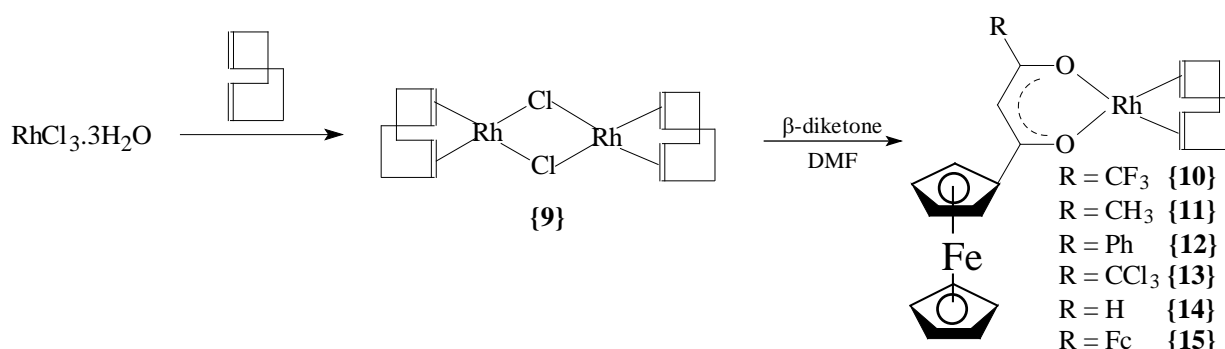
Scheme 3.2: **Reaction scheme for the complexation of ferrocene-containing β-diketones with [Rh₂Cl₂(cod)₂] {9} at room temperature to obtain [Rh(fctfa)(cod)] {10}, [Rh(fca)(cod)] {11}, [Rh(bfcm)(cod)] {12}, [Rh(fctca)(cod)] {13}, [Rh(fch)(cod)] {14} and [Rh(dfcm)(cod)] {15}.**

---

[6] Yogev, A. and Mazur, Y., *J. Org. Chem.,* **32**, 2162 (1967).

[7] Swarts, J.C. and Davis, W.L., unpublished results.

[8] The [Rh(fctca)(cod)] and [Rh(bfcm)(cod)] complexes were provided by J.C. Swarts and W.C. (Ina) du Plessis for use in this study.   The [Rh(fch)(cod)] complex, with Hfch the keto-aldehyde 2-ferrocenoyl-etan-1-al, was provided by J.C. Swarts and M.A.S. Aquino for use in this study.

[9] Chatt, J. and Venanzi, L.M., *J. Chem. Soc.,* **(A)**, 4735 (1957).

3.2.2.2   Rhodium(I) complexes of the type [Rh(β-diketonato)(CO)$_2$].

The new, red, [Rh(β-diketonato)(CO)$_2$] complexes with β-diketonato = fctfa, fca, bfcm and dbm, synthesized during this study, were obtained by two different reaction pathways (**Scheme 3.3**) in yields up to 70%. The dimer [Rh$_2$Cl$_2$(CO)$_4$] {16} used in route 1, was a convenient starting material for the synthesis of all the [Rh(β-diketonato)(CO)$_2$] complexes except for [Rh(dfcm)(CO)$_2$] {20}. [Rh$_2$Cl$_2$(CO)$_4$] {16} was obtained *in situ* by refluxing RhCl$_3$.3H$_2$O in DMF for *ca.* 1 hour until a light yellow refluxing mixture was observed. [Rh(dfcm)(CO)$_2$] could only be obtained impure in trace amounts *via* this route. [Rh(dfcm)(CO)$_2$] {20} was obtained in a 77% yield, by treating a [Rh(dfcm)(cod)] {15} in acetone solution with CO(g), at a pressure 10 mm Hg above atmospheric pressure for *ca.* 30 minutes to force the equilibrium {[Rh(dfcm)(cod)] + CO □ [Rh(dfcm)(CO)$_2$] + cod} to the right. [Rh(dfcm)(CO)$_2$] {20} was precipitated from the reaction mixture to prevent the cod in the solution to react again with {20}, the desired product. The yellow, ferrocene-free complexes with β-diketonato = dbm, tfhd, tfdma, tftma, ba and tfba were obtained by route 1 following published procedures[10] (reaction scheme not shown).
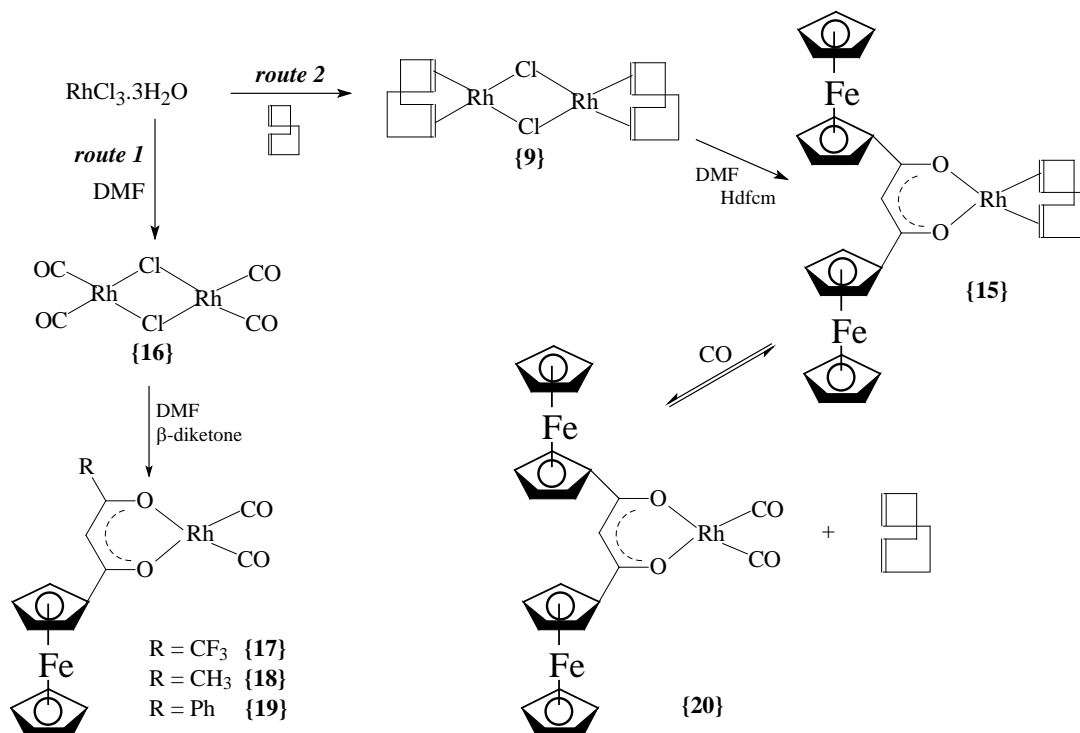
Scheme 3.3: Synthetic routes for the synthesis of the [Rh(β-diketonato)(CO)$_2$] complexes {17} - {20} from RhCl$_3$.3H$_2$O. [Rh(dfcm)(CO)$_2$] {20} could only be obtained pure in high yields following route 2.

---

10 (i) Bonati, F. and Wilkinson, G., *J. Chem. Soc.,* 3156 (1964)

(ii) Leipoldt, J.G., Basson, S.S., and Nel, J.T., *Inorg. Chim. Acta,* **74**, 85 (1983),

3.2.2.3   Rhodium(I) complexes of the type [Rh(β-diketonato)(CO)(PPh₃)].

The new deep-red [Rh(β-diketonato)(CO)(PPh₃)] complexes with β-diketonato = fctfa, fca, bfcm and dfcm were obtained by adding an equivalent amount of PPh₃ (**Scheme 3.4**), dissolved in hexane, to a [Rh(β-diketonato)(CO)₂] *n*-hexane solution.   The reaction is immediate with precipitation of the product [Rh(β-diketonato)(CO)(PPh₃)].   Yields of up to 92% were obtained. The yellow, ferrocene-free complexes with β-diketonato = dbm, tfhd, tfdma, tftma, ba and tfba were obtained as described before.[10]
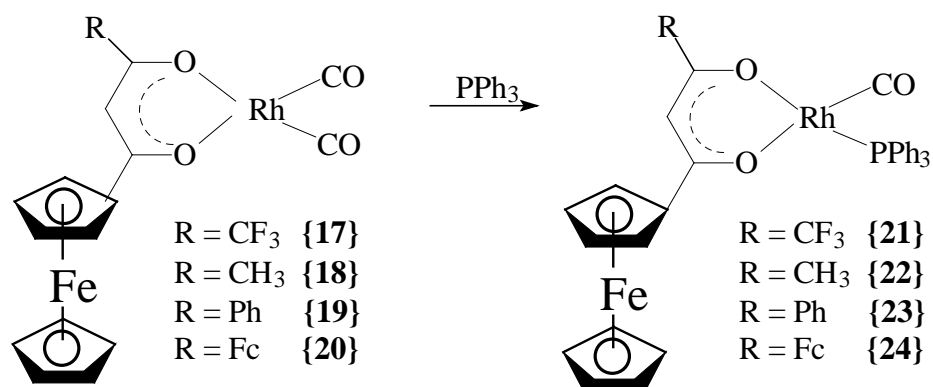
Scheme 3.4: Synthesis of the [Rh(β-diketonato)(CO)(PPh₃)] complexes {21} - {24} from the corresponding [Rh(β-diketonato)(CO)₂] complexes {17} – {20}.

¹H-NMR spectra showed that for each of the [Rh(β-diketonato)(CO)(PPh₃)] complexes with β-diketonato = fctfa, fca, bfcm, tfhd, tfdma, tftma, ba and tfba, two isomers exist in solution.   It was found that the ratio of the isomers is independent of concentration in the concentration range 0.020 – 0.0028 mol dm⁻³, but solvent dependant (see page 128).   The ¹H-NMR spectra of [Rh(fctfa)(CO)(PPh₃)] {21} and [Rh(fca)(CO)(PPh₃)] {22} in **Figure 3.1** page 124 clearly distinguish between the two isomers of {21} and {22} as shown in **Scheme 3.5**. The difference between the two isomers manifested especially in the large difference in the position, δ_H in ppm, of the signals of the protons of the ferrocenyl group of the β-diketonato ligand, *eg* for {22} (**Figure 3.1** (b)):

δ_H(300 MHz, CDCl₃) **ISOMER 1**:   1.71 (3H, s, CH₃), 4.19 (5H, s, C₅H₅), 4.37 (2H, t, C₅H₄), 4.79 (2H, t, C₅H₄), 5.73 (1H, s, CH) and 7.38 – 7.78 (15H, m, aromatic).

δ_H(300 MHz, CDCl₃) **ISOMER 2**: 2.19 (3H, s, CH₃), 3.91 (5H, s, C₅H₅), 4.08 (2H, t, C₅H₄), 4.15 (2H, t, C₅H₄), 5.78 (1H, s, CH) and 7.38 – 7.78 (15H, m, aromatic).

The equilibrium constant K_c = [isomer 1]/[isomer 2] = 0.22/1.00 of the [Rh(fca)(CO)(PPh$_3$)] isomers, is calculated from the peak integrals of the methine proton of the β-diketonato ligand fca. Other combinations of peak integration, utilizing for instance the ferrocenyl fragment peak integrals, could equally have been valid, *e.g.* 0.46/2.15 = 0.21 or 0.49/2.12 = 0.23 or 1.11/5.03 = 0.22. The two isomers are the isomer with PPh$_3$ *trans* to the oxygen nearest to the more electron donating ferrocenyl group of the chelate ring, the expected isomer due to electronic considerations labelled as isomer 2, and the isomer with PPh$_3$ *cis* to the oxygen nearest to the ferrocenyl group (isomer 1) as defined in **Scheme 3.5** page 124. The isomer of which the ^{1}H NMR peak positions of the protons of the ferrocenyl group are more downfield than those of the other isomer, is labelled isomer 1 (see **Figure 3.1**). The structural assigment of isomers 1 and 2 in **Scheme 3.5** was done utilizing the following arguments. It is known that electron withdrawing groups such as acetyl in acetylferrocene move the position of the protons of the substituted cyclopentadiene ring downfield in a similar way as was found for isomer 1.[11] Alternatively, electron donating substituents such as ethyl in ethylferrocene move these protons more to an upfield position.[12] Utilizing this observation, the influence of PPh$_3$ and CO on the carbonyl group next to the ferrocenyl group in isomers 1 and 2 (**Scheme 3.5**) can now be evaluated. In the case of isomer 2, the PPh$_3$ group donates electron density *via* the σ bond to rhodium and accordingly to the oxygen *trans* to PPh$_3$ and nearest to the ferrocenyl group. This results in a relatively higher electron density on the ferrocenyl group of isomer 2 than on the ferrocenyl group of isomer 1, similar to that found for ethylferrocene as compared to acetylferrocene. Therefore, the higher electron density on the protons of the ferrocenyl group of isomer 2 manifest in ^{1}H NMR peak positions of the protons of the ferrocenyl group which are more upfield than those of isomer 1.

In contrast to the two isomers found in solution for {21}, {22} and {23}, the ^{1}H-NMR spectra of the [Rh(dfcm)(CO)(PPh$_3$)] {24} (**Figure 3.2**) and [Rh(dbm)(CO)(PPh$_3$)] complexes indicated only one isomer in solution. Only one isomer is expected for *e.g.* {24}, because the β-diketonato ligand, dfcm, is symmetrical and the two isomers are identical. A summary of values for K_c can be found in **Table 3.1** page 126.

---

[11] Bublitz, D.E. and Rinehart, K.L., *Organic Reactions,* **17**, 76 (1969).

[12] Swarts, P.J., Immelman, M., Lamprecht, G.J., Greyling, S.E. and Swarts, J.C., *S.Afr.J.Chem.,* **50**, 208 (1997).
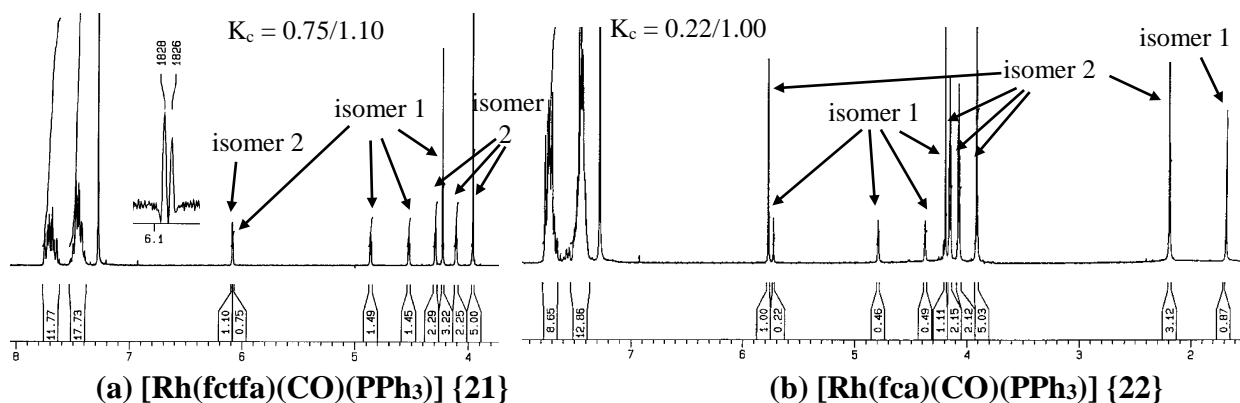
Figure 3.1: ¹H-NMR spectra in CDCl₃ indicate two isomers (see Scheme 3.5) for complexes of the type [Rh(β-diketonato)(CO)(PPh₃)] with an unsymmetrical β-diketonato ligand.
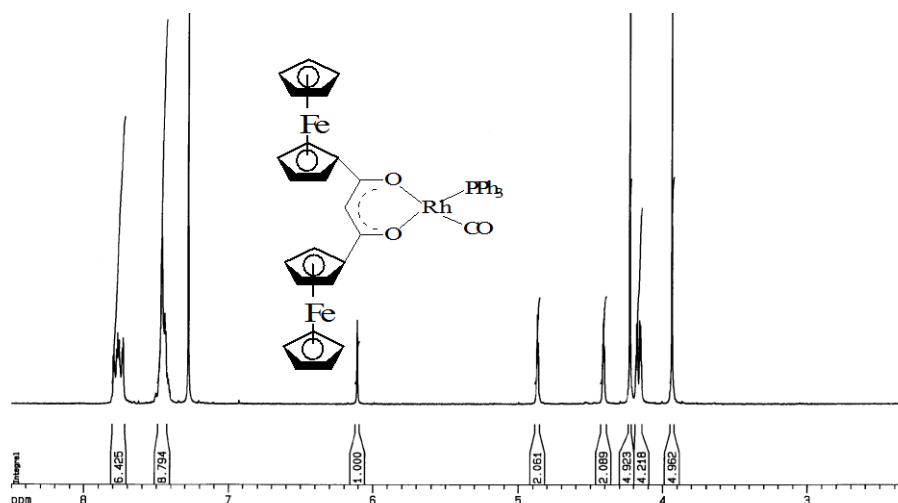
Figure 3.2: The ¹H-NMR spectrum in CDCl₃of [Rh(dfcm)(CO)(PPh₃)] {24} indicates only one isomer for complexes of the type [Rh(β-diketonato)(CO)(PPh₃)] with a symmetrical β-diketonato ligand.
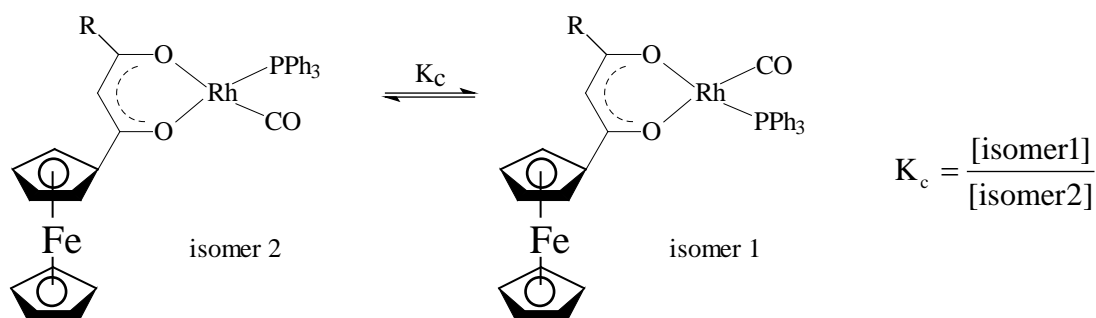
Scheme 3.5: The equilibrium between the two isomers of the complexes [Rh(β-diketonato)(CO)(PPh₃)] with the ferrocene-containing β-diketones Hfctfa, Hfca and Hbfcm. Electronic considerations utilizing group electronegativities, predict that isomer 2 should be dominant. This was found to be true in solution, but a crystal structure of isomer 1 was solved in this study.

^{31}P NMR spectra of [Rh(fctfa)(CO)(PPh$_3$)] {21} and [Rh(fca)(CO)(PPh$_3$)] {22} are presented in **Figure 3.3**. ^{31}P NMR spectra distinguish between the two isomers of the [Rh(fca)(CO)(PPh$_3$)] complex {22} (two doublets, δ^{31}P = 47.53 and 49.05 ppm, overlapping partially), but the doublets overlap exactly for the [Rh(fctfa)(CO)(PPh$_3$)] complex at 48.04 ppm, which is not the case for the ^{1}H NMR signals. The only other compound in which ^{31}P NMR signals for different isomers overlapped exactly, was [Rh(tftma)(CO)(PPh$_3$)].

The ^{31}P NMR spectrum of [Rh(dfcm)(CO)(PPh$_3$)] {24}, **Figure 3.4** (a), indicates only one isomer of {24}. This is again expected since dfcm is a symmetrical β-diketonato ligand. Complexes of other symmetrical β-diketonatos, notably acac and dbm (**Figure 3.4** (b), **Table 3.1**) also showed only one isomer. **Table 3.1** gives the δ^1H, δ^{31}P and $^1J(^{31}$P-^{103}Rh) for the complexes synthesized and related complexes.
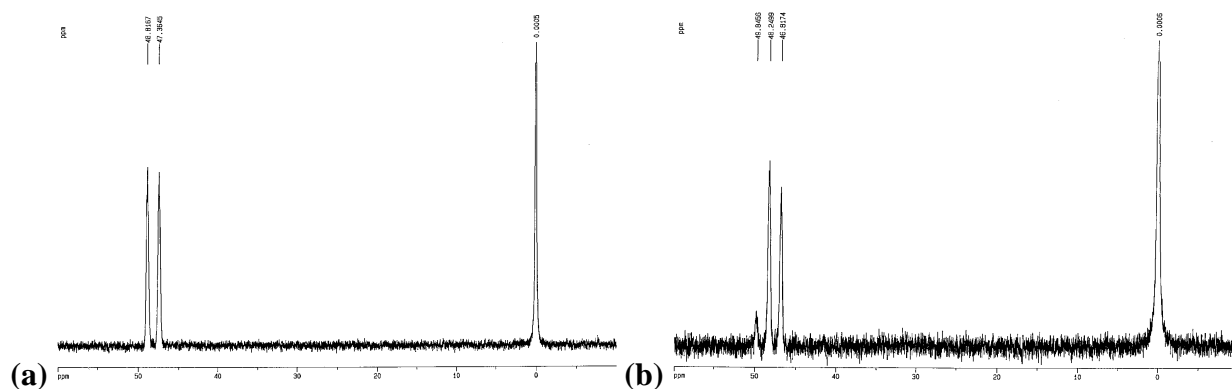
Figure 3.3: ^{31}P NMR spectra referenced to SiMe$_4$ at 0 ppm, of (a) [Rh(fctfa)(CO)(PPh$_3$)] {21} and (b) [Rh(fca)(CO)(PPh$_3$)] {22}. Two isomers are distinguished for {22}, but doublets overlap exactly for {21}.
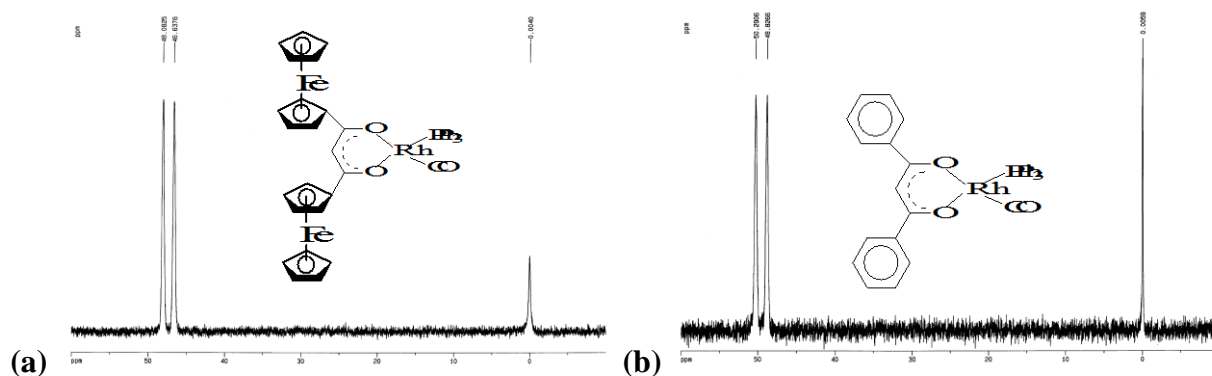
Figure 3.4: ^{31}P NMR spectra of (a) [Rh(dfcm)(CO)(PPh$_3$)] {24} and (b) [Rh(dbm)(CO)(PPh$_3$)].

Table 3.1: ^{31}P and ^{1}H NMR spectral parameters, υ(C=O) and the ratio of the isomers (as illustrated in Scheme 3.5) in solution of CDCl$_3$, for selected [Rh(β-diketonato)(CO)(PPh$_3$)] complexes and the rhodium(III) complex [Rh(fctfa)(CO)(CH$_3$)(I)(PPh$_3$)].

β-dike-tonato	iso-mer no.	δ^{31}P /ppm	$^1J(^{31}$P-^{103}Rh) /Hz	δ^1H /ppm	Ratio isomers	K$_c$	υ(CO)/cm^{-1} KBr	CDCl$_3$
fctfa	1	48.04	176.4	6.045, 4.83, 4.50, 4.20	40%	0.68	1986	1990
	2	48.04	176.4	6.045, 4.27, 4.09, 3.94	60%			
tftma	1	47.85	172.9	7.3-8, 6.04, 0.70	42%	0.72	1992	1988
	2	47.85	172.9	7.3-8, 6.04, 1.26	58%			
fca	1	49.05	193.9	5.73, 4.80, 4.38, 4.195, 1.70	18%	0.22	1980	1983
	2	47.53	174.0	5.78, 4.16, 4.08, 3.90, 2.21	82%			
tfdma	1	47.75	178.0	7.3-8, 5.88, 2.30, 0.60	50%	1.00	1984	1988
	2	48.72	175.7	7.3-8, 5.89, 2.71, 1.20	50%			
tfhd	1	49.14	177.2	7.3-8, 5.85, 2.05, 0.56	40%	0.67	1966	1988
	2	47.86	174.8	7.3-8, 5.89, 2.50, 1.20	60%			
ba	1	49.28	175.8	7-8, 6.08, 1.53	32%	0.47	1980	1982
	2	49.37	174.8	7-8, 6.13, 2.23	68%			
tfaa[13]	1	49.57	177.7	*	*	*	1983	1988
	2	47.72	176.9					
tfba	1	49.94	175.8	7 – 8, 6.57	50%	1.00	1983	1991
	2	48.06	177.0		50%			
dfcm	-	47.36	175.6	7.40 – 7.82, 6.11, 4.87, 4.41, 4.23, 4.18, 4.16, 3.94	-	-	1977	1982
acac[13]	-	48.84	175.7	*	-	-	1983[14]	1984[14]
dbm	-	49.56	177.9	7.1-8.1, 6.85	-	-	1979	1988
Rh(III) fctfa	1	29.33	116.5	5.30, 4.76, 4.47, 4.39, 4.31, 4.31, 1.78	-	-	2056	2064

* ^{31}P NMRspectral parameters from ref 13, other parameters not given.

The variation of the K$_c$ with temperature for the equilibrium shown in **Scheme 3.5** may be mathematically quantified by

$$\ln K_{c2} = \ln K_{c1} - \frac{\Delta_r H}{R}\left(\frac{1}{T_2} - \frac{1}{T_1}\right)$$

with K$_{c2}$ and K$_{c1}$ the equilibrium constants at temperatures T$_1$ and T$_1$, R = 8.314 JK^{-1}mol^{-1} and Δ_rH the reaction enthalpy as defined elsewhere.[15,16] The above equation also implies that a graph of lnKc *vs.* 1/T should be linear,[16] with slope -Δ_rH/R. **Figure 3.6** illustrates this linearity for [Rh(fctfa)(CO)(PPh$_3$)] and [Rh(bfcm)(CO)(PPh$_3$)]. [Rh(dfcm)(CO)(PPh$_3$)] could not be

[13] Steyn, G.J.J., Roodt, A., Poletaeva, I. and Varshavsky, Y.S., *J. Organomet. Chem.,* **536**, 197 (1997).

[14] Otto, S., Roodt, A., Erasmus, J.C. and Swarts, J.C., *Polyhedron*, **17**, 2447 (1998).

[15] Maron, S.H. and Lando, J.B., *Fundamentals of Physical Chemistry,* Macmillan Publishing Co. Inc., New York, 1974, p 376 – 383.

[16] Atkins, P.W., *Physical Chemistry*, fifth edition, Oxford University Press, Oxford, 1994, p. 141 – 154, 288.

subjected to this treatment because it has no different isomers, since dfcm is a symmetrical β-dikonate ligand. K_c and Δ_rH values from these graphs are summarized in **Table 3.2**. The thermodynamic quantities "Gibbs free energy", Δ_rG, and reaction entropy, Δ_rS, may be calculated from the equations $\Delta_rG = RT\ln K_c$ and $\Delta_rG = \Delta_rH - T\Delta_rS$.[17] Results at 298K are summarized in **Table 3.2**.
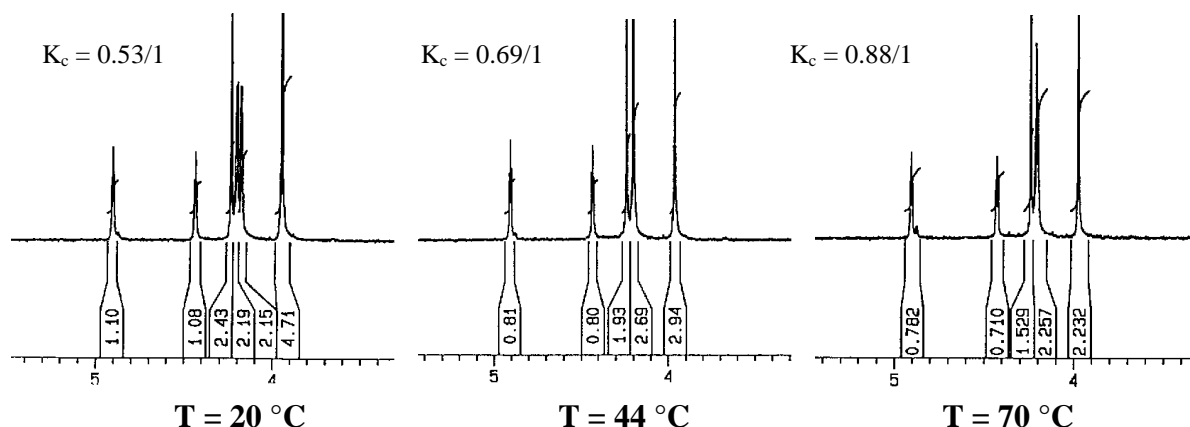
Figure 3.5: *Fragments* of ¹H NMR spectra of [Rh(bfcm)(CO)(PPh₃)] in CDCl₃ at different temperatures. The ¹H NMR peak positions of the protons of the ferrocenyl groups of isomer 1 and isomer 2 can clearly be distinguished from each other and are therefore convenient in calculating an average value K_c = [isomer 1]/[isomer 2] at the different T.
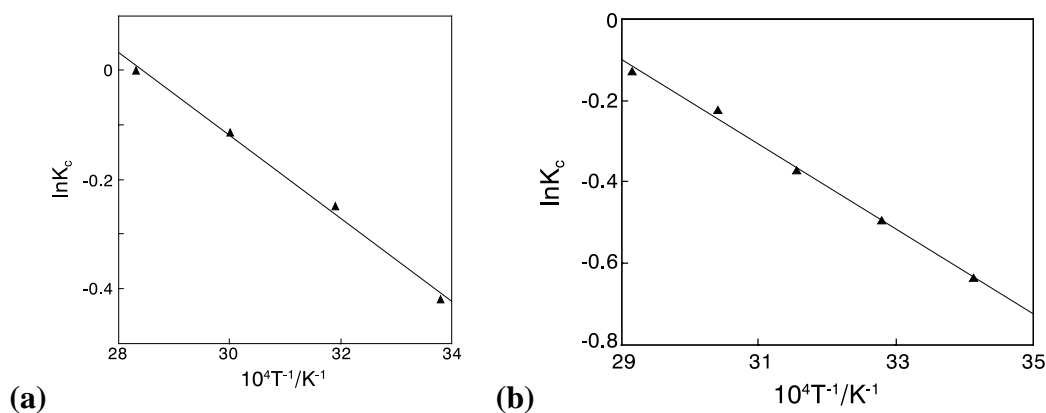
Figure 3.6: Temperature dependence of K_c for the equilibrium position between the two isomers of the (a) [Rh(fctfa)(CO)(PPh₃)] and (b) [Rh(bfcm)(CO)(PPh₃)] complex. Slope of graph = $-\Delta_rH/R$.

Table 3.2: The average equilibrium constant K_c at 298K for the equilibrium shown in Scheme 3.5 and the thermodynamic data at 298 K relevant to this equilibrium for [Rh(β-diketonato)(CO)(PPh₃)] complexes with β-diketonato = fctfa, fca and bfcm.

complex	K_c(298K)	Δ_rH / kJ mol⁻¹	Δ_rG / kJ mol⁻¹	Δ_rS / J mol⁻¹K⁻¹
[Rh(fctfa)(CO)(PPh₃)]	0.68	6.2(3)	0.97(4)	17.6(6)
[Rh(fca)(CO)(PPh₃)]	0.22	7.6(3)	3.0(1)	15(1)
[Rh(bfcm)(CO)(PPh₃)]	0.56	8.6(3)	1.4(3)	24(2)

---

17 Atkins, P.W., *Physical Chemistry*, fifth edition, Oxford University Press, Oxford, 1994, p. 141, 154, 276 and 289.

^{1}H NMR determination of K_c for [Rh(fctfa)(CO)(PPh$_3$)] in different solvents revealed that the equilibrium constant, K_c for the reaction shown in **Scheme 3.5** page 124, is solvent dependent. **Figure 3.7** displays the NMR spectra in different solvents of the signals of the protons of the ferrocenyl group of fctfa coordinated to [Rh(fctfa)(CO)(PPh$_3$)]. The results in **Table 3.3** and **Figure 3.8** illustrate that the ratio of the isomers in a solvent is linear dependent on the solvent polarity. The observed relationship is imperical and must, at least in part, be a consequence of improved solvation by solvent molecules of higher solvent polarity. However, further research is required to completely explain the observed tendency. The only exception to the observed trend was the non-polar solvent cyclohexane.

(a)   **(b)**   **(c)**   **(d)**   **(e)**   **(f)**
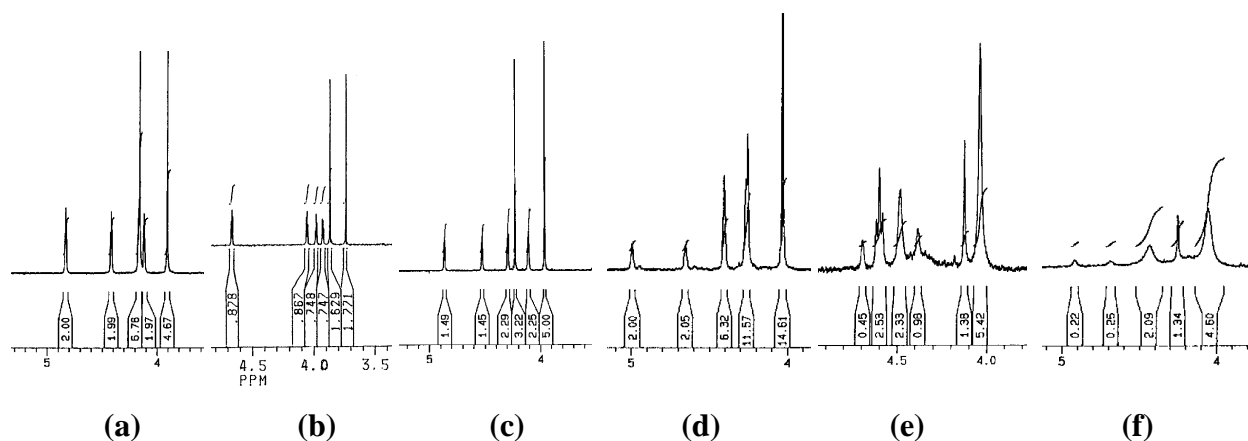
Figure 3.7: **Fragments of ^{1}H NMR spectra of [Rh(fctfa)(CO)(PPh$_3$)] in different solvents at 298 K, illustrating the solvent dependence of the equilibrium position of the two isomers of the [Rh(fctfa)(CO)(PPh$_3$)] complex:**

(a) cyclohexane (K_c = 1), (b) benzene (K_c = 0.88), (c) chloroform (K_c = 0.68), (d) acetone (K_c = 0.33), (e) DMSO (K_c = 0.2) and (f) acetonitrile (K_c = 0.1).

Table 3.3: The average equilibrium constant K_c(298K) for the equilibrium position of the isomers of the [Rh(fctfa)(CO)(PPh$_3$)] complex in different solvents.

solvent	formula solvent	polarity	K_c(298K)
cyclohexane	C$_6$D$_{12}$	0.04	1
benzene	C$_6$D$_6$	0.32	0.88
chloroform	CDCl$_3$	0.40	0.68
acetone	(CD$_3$)$_2$CO	0.56	0.33
DMSO	(CD$_3$)$_2$SO	0.62	0.2
acetonitrile	CD$_3$CN	0.65	0.1
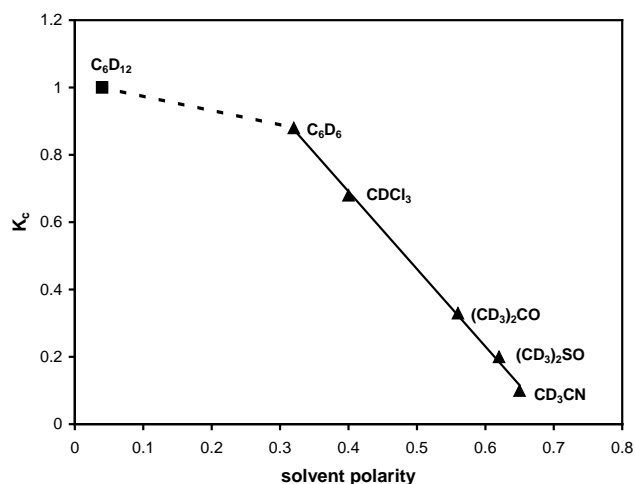
Figure 3.8: Linear dependence of the equilibrium constant K_c at 298K for the equilibrium between the isomers of the [Rh(fctfa)(CO)(PPh3)] complex in different solvents as a function of solvent polarity. Only the non-polar and non-coordinating solvent cyclohexane does not fit the linear trend.

3.2.2.4 Rhodium(III) complex.

The oxidative addition product [Rh(fctfa)(CO)(CH3)(I)(PPh3)] {25} was obtained from the reaction between [Rh(fctfa)(CO)(PPh3)] {21} and an excess of MeI dissolved in hexane. **Figure 3.25** page 158, presents the ^{1}H NMR spectrum of {25}. The structure of {25} will be discussed in paragraph 3.8.4 page 275.
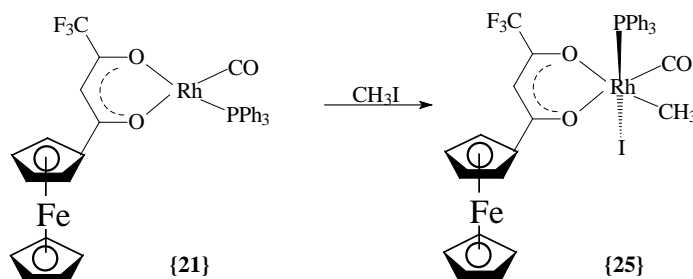
Scheme 3.6: Oxidative addition of MeI to [Rh(fctfa)(CO)(PPh3)], {21}, leads to the rhodium(III) complex [Rh(fctfa)(CO)(CH3)(I)(PPh3)], {25}.

3.2.2.5 Infrared spectra of mono and di-carbonyl rhodium complexes.

The mono and di-carbonyl products formed during the synthetic routes as described in the previous paragraphs, give different infrared stretching frequency for the CO moieties for each one. For example, the spectrum of [Rh(fctfa)(CO)$_2$] supported on KBr, gives two distinctive separate peaks at 2008 and 2074 cm^{-1}, **Figure 3.9**(a). Upon substitution of one of the carbonyl ligands with a tertiary phosphine PPh3, monocarbonyl(phosphine)rhodium(I) compounds are

obtained. These compounds show only one carbonyl peak as is the case for [Rh(fctfa)(CO)(PPh$_3$)] with ν(CO) = 1986 cm^{-1}, **Figure 3.9**(b). The lower CO wavenumber observed for monocarbonyl(phosphine)rhodium(I) compounds is in agreement with the higher electron density on the rhodium centre due to electron donation of PPh$_3$ through the σ bond to the rhodium nucleus.

The product of the reaction of the monocarbonyl(phosphine)rhodium(I) species with iodomethane yields a Rh(III) complex which gives a spectrum such as in **Figure 3.9**(c). The rhodium(III) nucleus is more electron deficient than the rhodium(I) nucleus and this manifests in a single peak at a higher wavenumber than that observed for the CO peak in monocarbonyl(phosphine)rhodium(I) complexes. For [Rh(fctfa)(CO)(CH$_3$)(I)(PPh$_3$)] the IR stretching CO wavenumber is 2056 cm^{-1}.

By noting from the de Broglie equation, $\Delta E = hc/\lambda$, that shorter wavelengths (*i.e.* longer wavenumber in cm^{-1}) represent stronger C-O bond energies in CO and therefore weaker Rh-C bonds, it follows that the Rh(III)-C bond (ν = 2056 cm^{-1} in [Rh(fctfa)(CO)(CH$_3$)(I)(PPh$_3$)]) is weaker than Rh(I)-C bonds (ν = 1986 cm^{-1} in [Rh(fctfa)(CO)(PPh$_3$)]). It is interesting to note, using the above criteria, that both of the Rh(I)-C bonds in dicarbonyl complexes such as [Rh(β-diketonato)(CO)$_2$)] is weaker than the Rh(I)-C bond in the corresponding [Rh(β-diketonato)(CO)(PPh$_3$)]) complex. From the observed long wavenumbers for CO signals in [Rh(β-diketonato)(CO)$_2$)] complexes, it may also be deduced that the rhodium(I) nucleus in these dicarbonylrhodium(I) complexes should be oxidized with more difficulty than the rhodium(I) nucleus in monocarbonyl(phosphine)rhodium(I) complexes. This intuitive expectation was shown to be correct in cyclic voltammetry studies discussed in paragraph 3.6.9.1 page 247. A summary of the CO positions in the IR spectra of ferrocene-containing β-diketonato mono and dicarbonylrhodium(I) complexes is given in **Table 3.4**.

Table 3.4: Carbonyl stretching frequencies of selected rhodium(I) complexes.

β-diketonato ligand	ν(CO)/cm^{-1}	
	[Rh(β-diketonato)(CO)$_2$]	[Rh(β-diketonato)(CO)(PPh$_3$)]
fctfa	2074, 2008	1986
fca	2068, 2014	1980
bfcm	2074, 1998	1977
dfcm	2074, 2008	1977
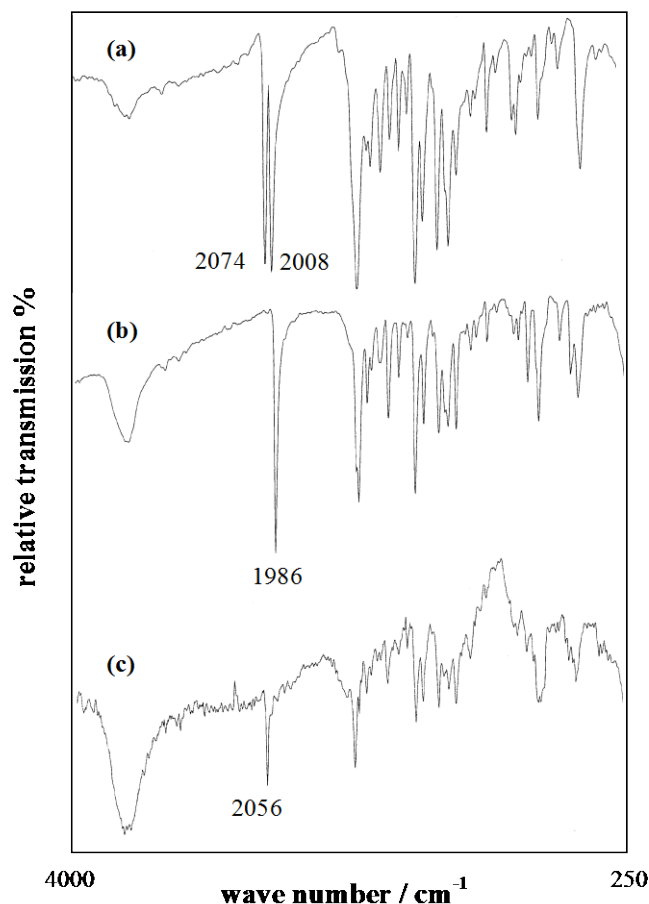
Figure 3.9: The infrared spectra for the complexes (a) [Rh(fctfa)(CO)$_2$] {17}, (b) [Rh(fctfa)(CO)(PPh$_3$)] {21} and (c) [Rh(fctfa)(CO)(CH$_3$)(I)(PPh$_3$)] {25} in KBr-pellets.

3.2.3 Synthesis β-diketonato complexes of iridium(I) and iridium(III).

3.2.3.1 Iridium(I) complexes of the type [Ir(β-diketonato)(cod)].

The [Ir(β-diketonato)(cod)] complexes {27} – {34} were obtained by treating the β-diketones with commercially available [Ir$_2$Cl$_2$(cod)$_2$] {26} at room temperature as illustrated in **Scheme 3.7**. It is important to note that the ferrocene-containing [Ir(β-diketonato)(cod)] reaction products have to be precipitated from the reaction mixture without delay, within 30 seconds of mixing solutions, in order to prevent conversion of the desired product to a new complex, tentatively assigned to be [Ir^{III}Cl$_2$(β-diketonato)(cod)].

For a β-diketone with a pK$_a$ > 7, *e.g.* Hfca and Hbfcm, NaHCO$_3$ was added in a stoichiometric amount to the β-diketone mixture to generate the β-diketonato anion which is the actual

131

complexing ligand. An excess of 10% [Ir$_2$Cl$_2$(cod)$_2$] was found to be beneficial for all syntheses, but especially for β-diketones with a higher pK$_a$ (*eg* Hbfcm). It was found that the reaction product isolated after 30 s for Hbfcm, still contained 19% unreacted β-diketone while the reaction product isolated after 30 s for Hfctfa contained no unreacted β-diketone. It was therefore concluded that β-diketones with higher pK$_a$'s were found to reacted more slowly than β-diketones with lower pK$_a$'s. A summary of β-diketones pK$_a$'s may be found in paragraph 3.3 page 137. The incorporation of the ferrocene moiety into the iridium complexes {32} – {34} resulted in the compounds having a reddish colour whereas the ferrocene free complexes {27} – {31} were yellow in colour.
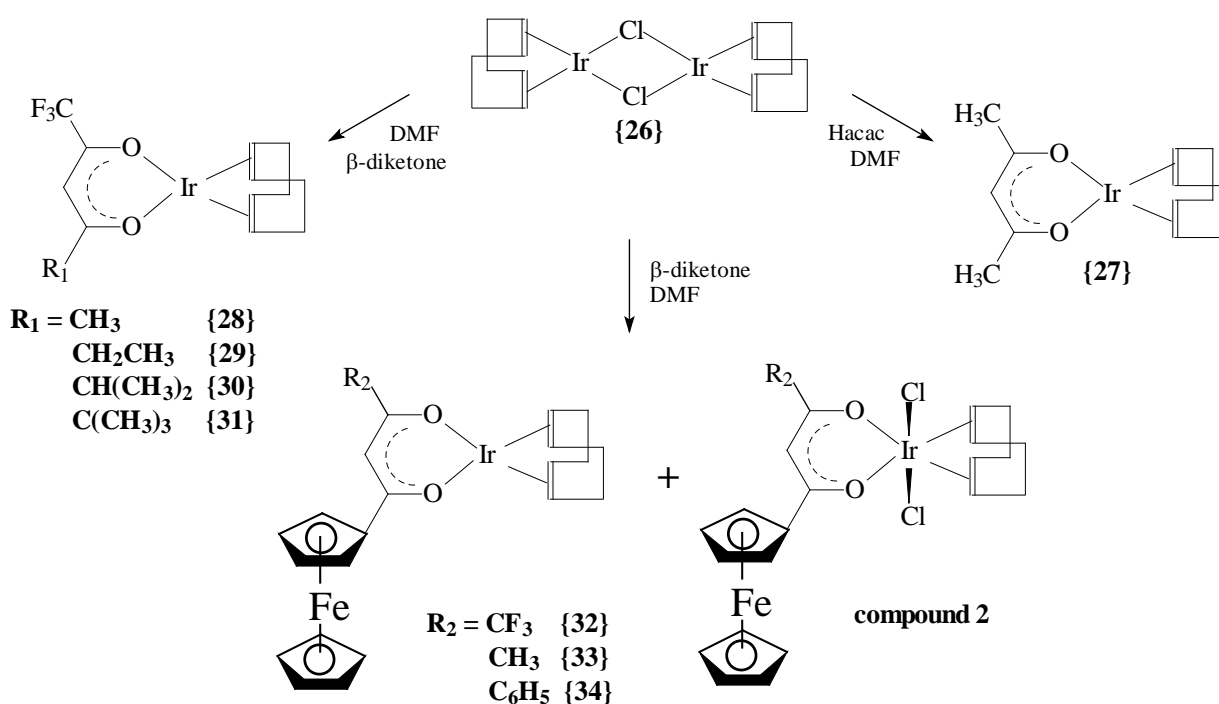
Scheme 3.7: Synthesis of [Ir(acac)(cod)] {27} (92% yield), [Ir(tfaa)(cod)] {28} (74% yield), [Ir(tfhd)(cod)] {29} (77% yield), [Ir(tfdma)(cod)] {30} (68% yield), [Ir(tftma)(cod)] {31} (59% yield), [Ir(fctfa)(cod)] {32} (92% yield), [Ir(fca)(cod)] {33} (83% yield) and [Ir(bfcm)(cod)] {34} (66% yield).

Upon synthesizing [Ir(β-diketonato)(cod)] complexes, it was noted that two very similar products were isolated from the reaction mixture. One compound, the desired [Ir(β-diketonato)(cod)] complexes, was active towards β-diketonato substitution reactions with, for example, phenanthroline. The other compound, provisionally labelled compound 2, was inert towards β-diketonato substitution reactions with phenanthroline. **Figure 3.10** highlights the ^{1}H NMR differences between the two compounds for β-diketonato = fctfa. Compound 2 is indicated with *. At δ = 5.98 ppm (insert in **Figure 3.10**) the active β-diketone methine proton, associated with

the substitution kinetically active complex, is demonstrated to be slightly to the right of the β-diketone methine proton of the kinetically inactive complex for the compound with β-diketonato = tfdma. The DMF signals shown in **Figure 3.10** are remnants from the reaction solvent and were found very difficult to remove completely within a short enough time scale to prevent excess decomposition of the active [Ir(β-diketonato)(cod)] complex. The ferrocene-containing complexes, *i.e.* those with β-diketonato = fctfa, fca and bfcm, were found to decompose about 15% per day, whereas non-ferrocene-containing compounds showed no decomposition after a period of 2 years. To date the ferrocene-containing complexes could not be successfully recrystallized. Purification by flash chromatography on kieselgel (eluent ether-hexane 2:3 by volume) resulted in decomposition of the desired kinetically active product. It also became fixated halfway down the column. By using a short column and high pressure, a small amount (±4%) of [Ir(bfcm)(cod)] could be isolated. This purified product, like the ferrocene-free complexes, was stable for lengthy periods (at least 3 months).
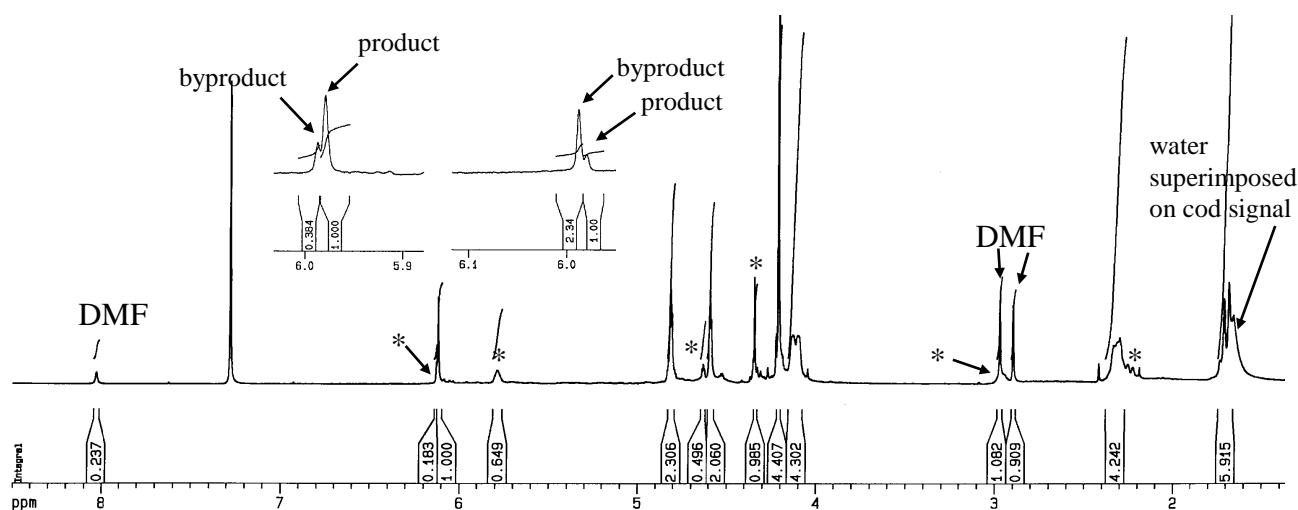
Figure 3.10: **^{1}H NMR spectrum containing a mixture of the substitution active complex [Ir(fctfa)(cod)] and the unknown substitution-inactive byproduct (compound 2 in text and marked with *) obtained during the course of the synthesis. The insert demonstrates the difference between β-diketone methine proton of both complexes for the compound [Ir(tfdma)(cod)]. Insert top left gives the signals of the products isolated from the reaction mixture after 20 min and the insert top right of the products isolated after 90 min. The spectra indicate that the longer the reaction time during [Ir(β-diketonato)(cod)] synthesis, the more of the unknown byproduct formed.**

To minimize the formation of the kinetically inactive compound 2 during the synthesis of complexes possessing a ferrocenyl group, the reactants had to be dissolved prior to mixing and the reaction had to be terminated by precipitation with ice/water from the solvent, DMF, within 30 seconds of mixing. Initially a great uncertainty surrounded the identity of the unknown

compound 2. Provisional information includes the following: the NMR spectrum of the purified compound 2 (**Figure 3.11**), clearly indicates a 1:1 ration for the ligands cod and fctfa. The cod peak at $\delta \approx 5.8$ ppm is very much more downfield than the equivalent signal for kinetically active [Ir$^{\text{I}}$(fctfa)(cod)]. This indicates that the ligands of compound 2 are more electron deficient than in the kinetically active compound. Similar downfield movements are observed for most of the NMR peaks (see **Figure 3.10**). This downfield shift of NMR signal positions indicate that compound 2 might be an iridium(III) complex. An electrochemical investigation (cyclic voltammetry, see paragraph 3.6.6 and 3.6.7, page 233) confirmed this suspicion. While [Ir$^{\text{I}}$(fctfa)(cod)] could be oxidize to an iridium(II) species at 0.325 mV, complex 2 showed no such oxidation peaks (see **Figure 3.79** page 239).
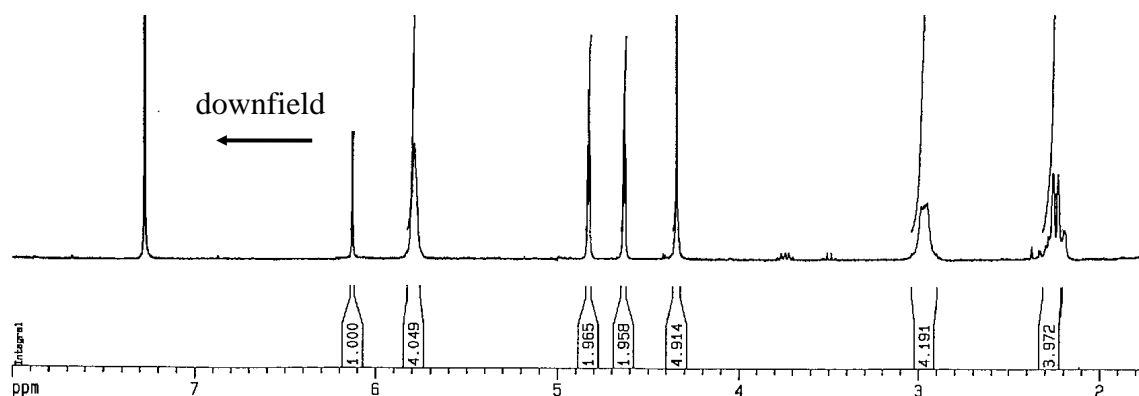
Figure 3.11: ^{1}H NMR spectrum of the isolated Ir(III) complex [Ir(Cl)$_2$(fctfa)(cod)] which is the "kinetically inactive" product labelled compound 2 and marked with * in Figure 3.10.

Most known iridium(III) complexes are octahedral.[18] As the starting material during the synthetic reaction includes [Ir$_2$(Cl)$_2$(cod)$_4$], it follows that there should be free Cl$^-$ ions in the reaction mixture, creating the suspicion that compound 2 may be [Ir(Cl)$_2$(fctfa)(cod)] which has a molecular mass of 694.39. A mass spectrum of compound 2 was drawn and is shown in **Figure 3.12**, top. A dominant peak at molecular mass 694 is clearly visible. Note that the peaks above a molecular mass of 700 are enlarged 10 times. **Figure 3.12**, bottom, shows the mass spectrum of the kinetically active complex [Ir(fctfa)(cod)]. A dominant peak at 623 is clearly visible which corresponds to the molecular mass of this compound. Although elemental analysis of compound 2 did not fall within acceptable (*i.e.* within 0.4%) limits for all elements, the discrepancy was not so large that it really cast serious doubt on the identity of compound 2. A summary of the elemental analysis is given in **Table 3.5** page 135.

---

[18] Wilkinson, G.,*Comprehensive Coordination Chemistry*, Pergamon Press, New York, 1987, vol 4., p. 1124.
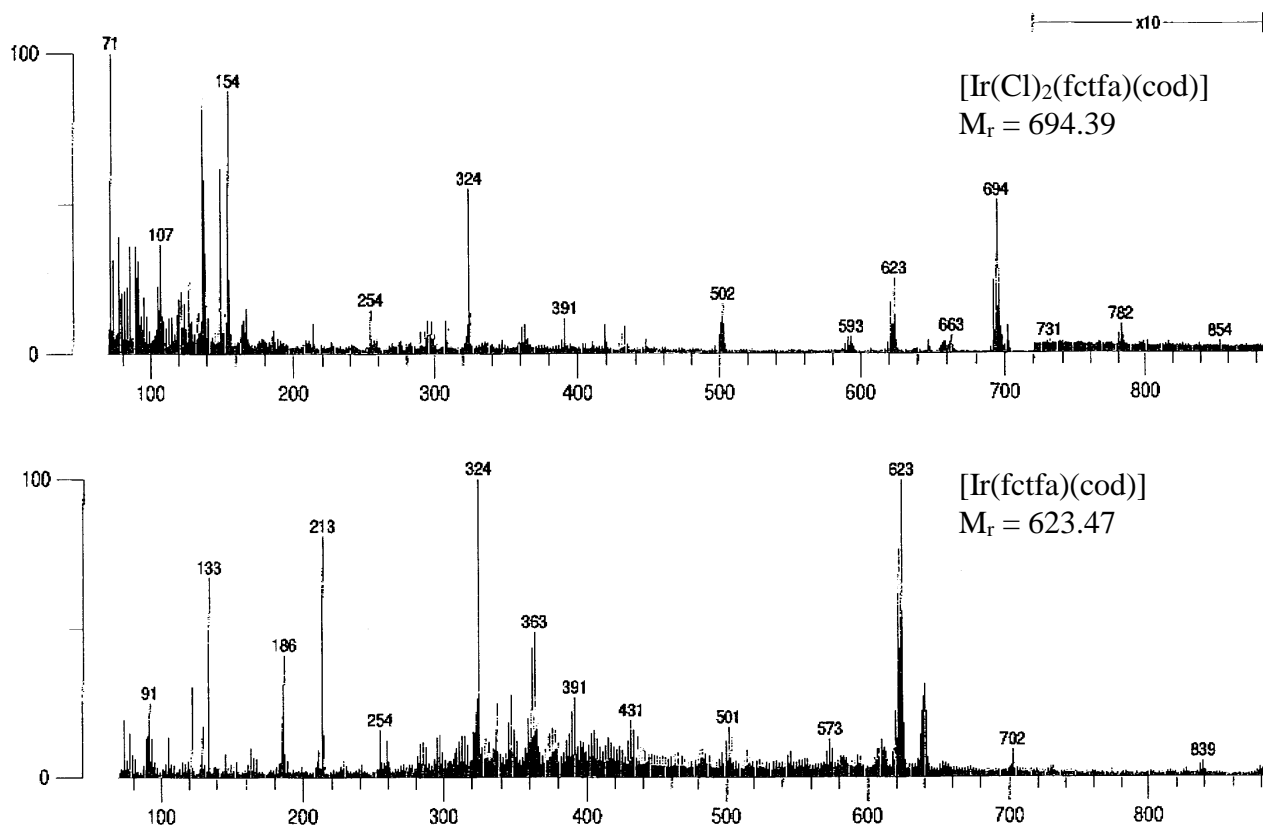
Figure 3.12: Mass spectra of [Ir(fctfa)(cod)] (bottom) and [Ir(Cl)₂(fctfa)(cod)] (above).

Table 3.5: Results of the microanalysis of [Ir(fctfa)(cod)] and [Ir(Cl)₂(fctfa)(cod)].

complex	formula		%C	%H	%Ir	%F	%Cl
[Ir(fctfa)(cod)] **M$_r$ = 623.47**	C$_{22}$H$_{22}$F$_3$ FeO$_2$Ir	calculated	42.38	3.56	30.83	9.14	-
		found	39.78	3.53	30.96	7.08	-
[IrCl$_2$(fctfa)(cod)] **M$_r$ = 694.39**	C$_{22}$H$_{22}$F$_3$ FeO$_2$IrCl$_2$	calculated	38.05	3.19	27.7	8.21	10.2
		found	39.92	3.60	24.8	6.89	10.7

It is therefore concluded, upon evaluating the described evidence in the previous paragraphs, that the most probable identity of compound 2 is the iridium(III) complex [IrCl₂(fctfa)(cod)]. Unfortunately, to date it was not possible to obtain suitable crystals of this compound for X-ray crystallography to prove its structure beyond doubt.   The synthesis of all other ferrocene-containing iridium(I) complexes, [Ir^I(β-diketonato)(cod)], was also accompanied by the formation of the corresponding byproduct, [Ir^{III}Cl₂(β-diketonato)(cod)]. A proposed structure of these compounds is presented in **Figure 3.13**. The iridium(III) compounds were isolated from the reaction mixture by allowing it to react with [Ir₂Cl₂(cod)₂] {26} according to **Scheme 3.7**, page 132, for at least an hour.

135
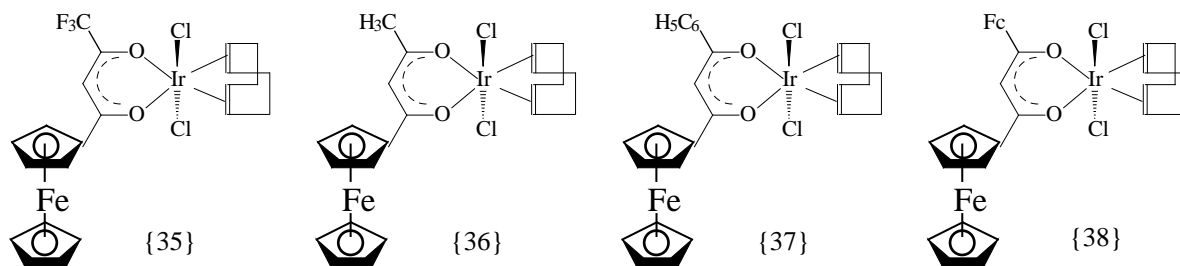
Figure 3.13: Structure of [Ir(III)(Cl)₂(fctfa)(cod)] {35}, [Ir(III)(Cl)₂(βfca)(cod)] {36}, [Ir(III)(Cl)₂(bfcm)(cod)] {37} and [Ir(III)(Cl)₂(dfcm)(cod)] {38}.

Finally another comment can be made regarding the observed downfield shift of the ^{1}H NMR peaks of [Ir^{III}(Cl)₂(fctfa)(cod)] as compared to [Ir^I(fctfa)(cod)]. During the course of this study it became necessary to synthesize [Ir^{III}(CH₃)(I)(β-diketonato)(cod)] according to **Scheme 3.8**. This provided an ideal opportunity to compare ^{1}H NMR signal positions of other iridium(III) complexes with those obtained for [Ir^{III}(Cl)₂(β-diketonato)(cod)]. A summary of the peak positions of the cod ligand is given in **Table 3.6**. It is noticeable how the trend of more downfield ^{1}H NMR peak positions for iridium(III) complexes as compared to the positions of iridium(I) complexes is consistent for all examples. It is also noticeable that the [Ir^{III}(Cl)₂(β-diketonato)(cod)] peaks are more downfield than those of [Ir^{III}(CH₃)(I)(β-diketonato)(cod)]. This observation is consistent with electron density arguments. The group electronegativity of the methyl, iodo and chloro groups is 2.34[19], 2.47 and 3.03[20] respectively. It follows, therefore, that the iridium(III) cores of the chlorine-containing complexes are more electron deficient than the iridium(III) cores of the MeI-containing complexes. The consequence of this is a cod fragment in the chloride complex which is more electron deficient than the cod fragments in the MeI-containing iridium(III) complexes. The expectation, therefore, would be that the ^{1}H NMR cod signals of [Ir^{III}(Cl)₂(β-diketonato)(cod)] should be more downfield than the the ^{1}H NMR cod signals of [Ir^{III}(CH₃)(I)(β-diketonato)(cod)] complexes. This was found to be the case, for which results are summarized in **Table 3.6**.

---

[19] du Plessis, W.C., Erasmus, J.C., Lamprecht, G.J., Conradie, J., Cameron, T.S., Aquino, M.A.S. and Swarts, J.C., *Can. J. Chem.*, **77**, 378 (1999).

[20] Wells, P.R., *Prog. Phys. Org. Chem.,* **6**, 111 (1968).
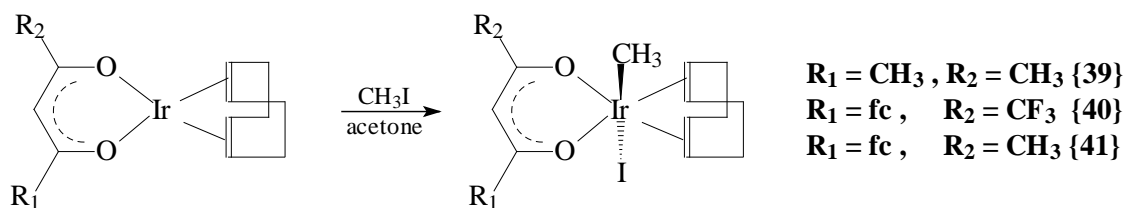
Scheme 3.8: Reaction scheme for the synthesis of [Ir(III)(CH$_3$)(I)(β-diketonato)(cod)] complexes, β-diketonato = acac (yield 39%), fctfa (yield 22%) and fca (yield = 33%).

Table 3.6: ^{1}H NMR positions (δ-values in ppm referenced to Me$_4$Si) of the protons of the cod ligand in iridium(I) and iridium(III) complexes. The cod ^{1}H NMR positions of the protons iridium(III) complexes are shifted downfield to a higher Lamor frequency compared to those found for iridium(I) complexes.

complex	signal	[Ir(I)(β-diketonato)(cod)]	[Ir(III)(CH$_3$)(I)(β-diketonato)(cod)]	[Ir(III)Cl$_2$(β-diketonato)(cod)]
acac	cod olefinic protons	3.99	4.21, 5.21	5.71
	half of cod aliphatic protons	2.27	2.62, 3.11	2.92
	other half of cod aliphatic protons	1.64	2.01, 2.19	2.27
fctfa	cod olefinic protons	4.12	4.28, 5.33	5.79
	half of cod aliphatic protons	2.32	2.66, 3.17	2.97
	other half of cod aliphatic protons	1.70	1.95, 2.22	2.24
fca	cod olefinic protons	4.00	4.21, 5.25	5.72
	half of cod aliphatic protons	2.32	2.63, 3.16	2.96
	other half of cod aliphatic protons	1.67	1.96, 2.23	2.26

3.3   pK$_a$ determinations.

3.3.1 Introduction.

The pK$_a$ of the β-diketones Htfhd and Htftma and the keto-aldehyde Hfch were determined in 10 % acetonitrile/water mixture, $\mu = 0.100$ mol dm^{-3} (NaClO$_4$) at 21.0(1) ^{0}C by measuring the UV absorbance/pH data with titration from high to low pH and a least squares fit[21] of the absorbance/pH data using **Equation 3.1**.

---

[21] MINSQ, Least squares parameter Estimation, Version 3.12, MicroMath, 1990.

Equation 3.1:
$$A_T = \frac{A_{HA}10^{-pH} + A_A 10^{-pK_a}}{10^{-pH} + 10^{-pK_a}}$$

A_T = total absorbance, A_{HA} the absorbance of the β-diketone in the protonated form and A_A the absorbance of the β-diketone in the deprotonated (basic) form. 'Apparent' pK_a values were determined in this study, since no attempt in this study was made to distinguish between the experimentally obtained 'apparent' pK_a values and the separate pK_a values for the enol and keto tautomers. The term pK_a will be used for the determined 'apparent' pK_a values.

3.3.2   The pK_a of Hfch, Htfhd and Htftmaa.

The UV/visible spectra of the protonated (acidic form) and deprotonated (basic form) of β-diketones Htfhd and Htftma and the keto-aldehyde Hfch are shown in **Figure 3.14** with the peak absorption coefficients in **Table 3.7**. This table also gives the concentration of the β-diketones and the keto-aldehyde during the pK_a determination as well as the pK_a as determined from the data in **Figure 3.15**.

Table 3.7: pK_a values and molar extinction coeffisients ε at $λ_{max}$ of the β-diketones Htfhd and Htftma and the keto-aldehyde Hfch in 10% acetonitrile /water mixture.

β-diketone / keto-aldehyde	pK_a	$λ_{max}$ (deprotonated) / nm [ε / dm³ mol⁻¹ cm⁻¹]		$λ_{exp}$	c / mol dm⁻³
Htfhd	6.64(1)	305	[15730]	320	1.78×10^{-4}
Hfch	7.04(1)	327	[15380]	330	1.17×10^{-4}
Htftma	7.13(1)	307	[19150]	320	1.53×10^{-4}

(a)   (b)   (c)
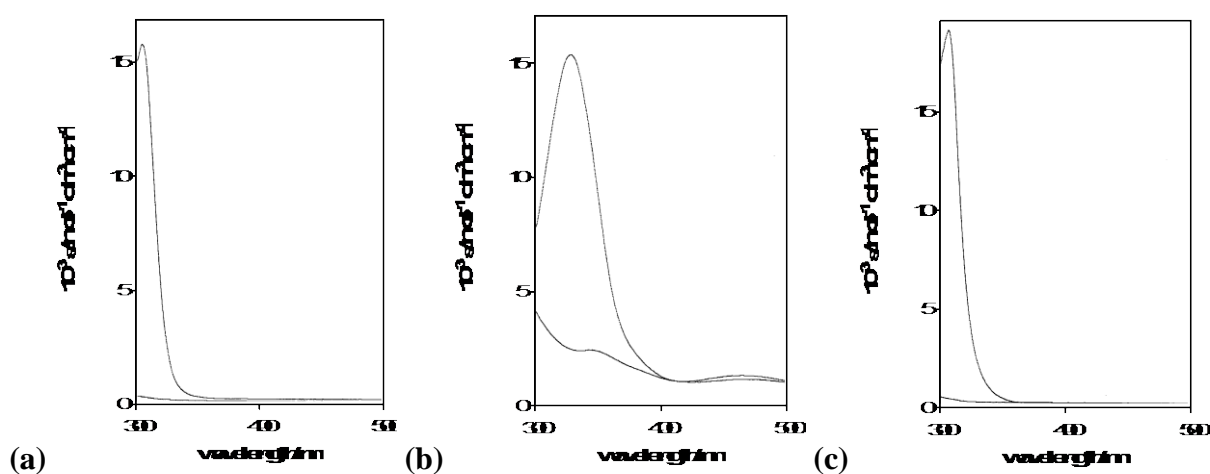
Figure 3.14: UV/visible spectra of the protonated (below) and deprotonated (basic form , line above) of (a) β-diketone Htfhd, (b) keto-aldehyde Hfch and (c) β-diketone Htftma in 10 % acetonitrile/water mixture, μ = 0.100 mol dm⁻³ (NaClO₄) at 21.0(1) ⁰C.

The newly determined pK_a values fits in the series of increasing pK_a values of β-diketones[35, 22, 59, 58] as follows (pK_a values in brackets after each β-diketone):

(*strongest acid*) **Hhfaa (4.71) < Htfba (6.3) = Htfaa (6.3) < Hfctfa (6.56) < Htfhd (6.64) < Htfdma (6.80) < Hfch (7.04) < Hfctca (7.13) = Htftma (7.13) < Hba (8.70) < Hacac (8.95) < Hdbm (9.35) < Hfca (10.01) < Hbfcm (10.41) < Hdfcm (13.1)** (*strongest base*)

(a)   (b)   (c)
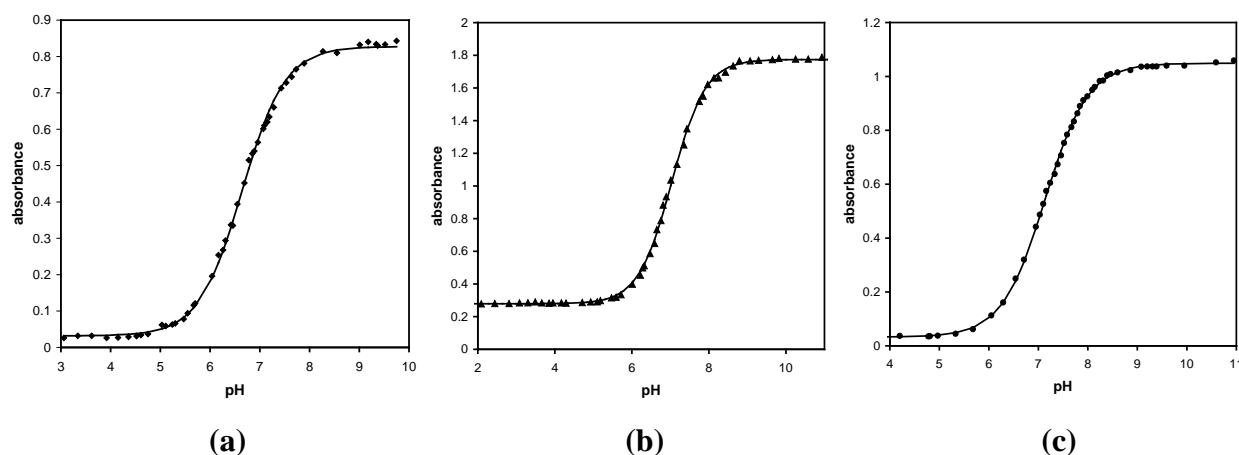
Figure 3.15: **Effect of pH on absorbance for (a) Htfhd at 320 nm, (b) Hfch at 330 nm and (c) Htftma at 320 nm in 10 % acetonitrile/water mixture, μ = 0.100 mol dm^{-3} (NaClO$_4$) at 21.0(1) ^{0}C. The solid line presents the least square fit of Equation 3.1.**

3.4   Oxidative addition and insertion reactions.

3.4.1   *Introduction.*

In previous studies of oxidative addition of iodomethane to complexes of the type [Rh(β-diketonato)(CO)(PPh$_3$)] and related complexes, a variety of mechanisms was proposed, depending on the type of rhodium complex studied. These mechanisms include

(a)   Rh(I) + CH$_3$I □ Rh(III)-alkyl1 → Rh(III)-acyl1   Steyn[23, 24] *et.al.*

(b)   Rh(I) + CH$_3$I □ Rh(III)-alkyl1 □ Rh(III)-acyl1   Leipoldt[25] *et.al.*

---
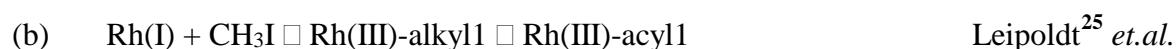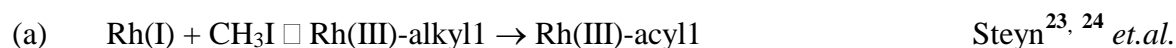
[22] Basson, S.S., Leipoldt, J.G., and Nel, J.T., *Inorg. Chim. Acta,* **84**, 167 (1984).

[23] Steyn, G.J.J., Roodt, A. and Leipoldt, J.G., *Inorg. Chem.,* **31**, 3477 (1992).

[24] Steyn, G.J.J., Roodt, A. and Leipoldt, J.G., *Rhodium Ex.*, **1**, 25 (1993).

(c)   Rh(I) + CH$_3$I $\square$ Rh(III)-alkyl1 $\rightarrow$ Rh(III)-acyl1 $\rightarrow$ Rh(III)-alkyl2   Smit.[26]

(d)   Rh(I) + CH$_3$I $\square$ Rh(III)-alkyl1 $\square$ Rh(III)-acyl1 $\square$ Rh(III)-alkyl2   Basson[22, 27] *et.al.*

The simplest case, Rh(I) + CH$_3$I $\rightarrow$ Rh(III)-alkyl1, has not yet been described. All reported studies to date showed that initial oxidative addition is followed by CO insertion. It is doubtful if a [Rh(β-diketonato)(CO)(PPh$_3$)] complex will be found that can undergo oxidative addition, but not carbonyl insertion because if a ligand is taylored to be so bulky that it sterically prevent CO insertion, it will probably also *not* allow oxidative addition to take place. This study also describes the oxidative addition of iodomethane to complexes of the type [Rh(β-diketonato)(CO)(PPh$_3$)] with the ferrocene-containing β-diketonato ligands fctfa, fca, bfcm and dfcm. For all four complexes a similar reaction sequence was observed. The full reaction scheme can be divided in three sets of reactions:

Reaction scheme 3.1:

$$\text{Rh(I)}+ \text{CH}_3\text{I} \underset{k_{-1}}{\overset{k_1}{\rightleftharpoons}} \left\{ [\text{Rh(III)-alkyl1}] \overset{K_2=k_2/k_{-2}}{\rightleftharpoons} [\text{Rh(III)-acyl1}] \right\} \underset{k_{-3}}{\overset{k_3}{\rightleftharpoons}} [\text{Rh(III)-alkyl2}] \underset{k_{-4}}{\overset{k_4}{\rightleftharpoons}} [\text{Rh(III)-acyl2}]$$

First set of reactions

Second set of reactions

Third set of reactions
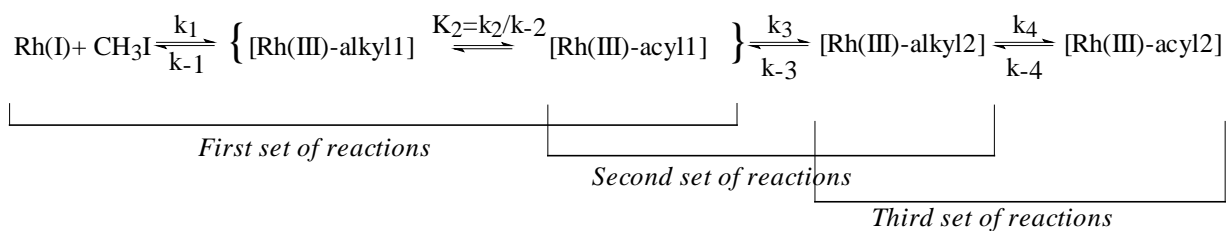
Close inspection of reaction schemes (a) – (d) above, reveals that they are all only special cases of the general **Reaction scheme 3.1**. Scheme (a) is obtained if k$_{-2}$ = k$_3$ = k$_4$ = 0. Scheme (b) is obtained if k$_3$ = k$_4$ = 0. Scheme (c) is obtained if k$_{-2}$ = k$_{-3}$ = k$_4$ = 0 and scheme (d) is obtained if k$_4$ = 0.

The equilibrium [Rh(III)-alkyl1 $\square$ Rh(III)-acyl1] has been suggested by Basson[27] *et. al.* and Leipoldt[25] *et. al.*, but the value of k$_{-2}$ was small and it was a slow equilibrium. Unique evidence has been found in this study that both k$_2$ and k$_{-2}$ can be of sufficient size to allow detection of the equilibrium constant K$_2$ and to present it as a fast equilibrium. The k$_4$ step was previously

---

[25] Leipoldt, J.G., Basson, S.S. and Botha, L.J., *Inorg. Chim. Acta,* **168**, 215 (1990).

[26] Smit. D.M.C., *Synthesis and kinetic study of rhodium(I) complexes containing organic tripod ligands (in Afrikaans), Ph. D. Thesis,* University of the Orange Free State, R.S.A., 1995.

[27] Basson, S.S., Leipoldt, J.G., Roodt, A., Venter, J.A. and van der Walt. T.J., *Inorg. Chim. Acta,* **35**, 119 (1986).

observed by Smith,[26] but no attempt was made to characterize it. This study presents the first opportunity to determine rate constants for this step even though the actual structure of Rh(III)-acyl2 complexes remains uncertain to date.

NMR measurements showed that each of the general species Rh(I), Rh(III)-alkyl1, Rh(III)-alkyl2, Rh(III)-acyl1 and Rh(III)-acyl2 complexes in the general **Reaction scheme 3.1** above is not a single entity, but is a mixture of isomers originating both from unsymmetric β-diketonato ligand and from the stereochemistry originating from MeI addition. Regarding isomers originating from the β-diketonato ligand fctfa, fca and bfcm, two isomers were observed by NMR (par. 3.2.2.3). These two isomers correspond to

1) the isomer with PPh$_3$ *trans* to the oxygen closest to ferrocenyl group, and
2) the isomer with PPh$_3$ *cis* to the oxygen closest to ferrocenyl group.

Since dfcm is a symmetric β-diketonato ligand, [Rh(dfcm)(CO)(PPh$_3$)], {24}, as well as the Rh(III)-alkyl and acyl oxidative addition products of {24}, only show one major isomer in solution that originates from this β-diketonato ligand.

In the following paragraphs, the experimental results that implied the above reaction sequence are systematically presented.

3.4.2   The Beer Lambert Law.

A linear relationship (not shown) between UV absorbance, A, and concentration, c, for the complexes [Rh(β-diketonato)(CO)(PPh$_3$)] with the ferrocene-containing β-diketonato ligands fctfa, fca, bfcm and dfcm, confirms the validity of the Beer Lambert law (A = εcl with l = path length = 1 cm) for each one of these complexes. The extinction coefficient, ε, for each complex is given in **Table 3.8**. The error of all the data is presented according to crystallographic conventions. For example k$_{obs}$ = 0.0446(1) s^{-1} implies k$_{obs}$ = (0.0446 ± 0.0001) s^{-1}. All the [Rh(β-diketonato)(CO)(PPh$_3$)] complexes were tested for stability in the various solvents by means of overlay IR and UV spectra for at least 24 hours.

Table 3.8: Molar extinction coefficients ε at the indicated wavelength λ for the complexes [Rh(β-diketonato)(CO)(PPh₃)] with the ferrocene-containing β-diketones Hfctfa, Hfca, Hbfcm and Hdfcm. Values in round brackets represent the error in the last digits.

Complex	solvent	λ/nm [ε/dm³ mol⁻¹ cm⁻¹]	Complex	solvent	λ/nm [ε/dm³ mol⁻¹ cm⁻¹]
[Rh(fctfa)(CO)(PPh₃)]	chloroform	498[2060(10)]	[Rh(bfcm)(CO)(PPh₃)]	chloroform	500[1520(10)]
	acetone	530[1860(5)]	[Rh(dfcm)(CO)(PPh₃)]	chloroform	379[12500(200)]
[Rh(fca)(CO)(PPh₃)]	chloroform	493[880(6)]			473[3780(20)]

3.4.3   The oxidative addition reaction between iodomethane and [Rh(fctfa)(CO)(PPh₃)].

The kinetic rate constants for the oxidative addition reaction between iodomethane and [Rh(fctfa)(CO)(PPh₃)] were determined by IR, UV/visible and NMR spectroscopy under pseudo first-order conditions. Rate constants, obtained by each of these techniques, were consistent (**Table 3.14** page 166). Rate constants were calculated utilizing a suitable fitting program[21] which fitted kinetic data to the first-order equation[28] $[A]_t = [A]_0\ e^{(-k_{obs}\ t)}$ ($[A]_t$ = absorbance of selected species at time t.

3.4.3.1   The infrared monitored reaction between CH₃I and [Rh(fctfa)(CO)(PPh₃)].

(i)   The infrared monitored reaction between CH₃I and [Rh(fctfa)(CO)(PPh₃)] in chloroform as solvent.

The reaction sequence of the reaction between [Rh(fctfa)(CO)(PPh₃)] and iodomethane in chloroform in the range 1690 – 2140 cm⁻¹ as monitored by infrared spectroscopy, T = 25 ºC, is illustrated in **Figure 3.16** page 145. **Figure 3.16**(a) shows that the rate of disappearance of the Rh(I)-carbonyl complex (signal at 1990 cm⁻¹, k_{obs} = 0.011(1) s⁻¹) basically corresponds to the formation of the Rh(III)-alkyl1 species (k_{obs} = 0.011(6) s⁻¹, peak at 2082 cm⁻¹) and the formation of the Rh(III)-acyl1 complex at 1729 cm⁻¹ (k_{obs} = 0.011(1) s⁻¹). The half-life of this reaction, under the indicated CH₃I concentration and temperature conditions is 63 s. Since it is highly unlikely that the Rh(III)-acyl1 species can be formed from an undetected, Rh(III)-alkyl1 species different from the detected Rh(III)-alkyl1 species at *exactly* the same rate, this result is indicative of a *fast* equilibrium between the Rh(III)-alkyl1 and Rh(III)-acyl1 species. The same conclusion could be drawn using ¹H NMR data and will be discusssed in paragraph 3.4.3.3 page 155. The latter process was labelled the *first set* of reactions that can be presented by the reaction:

Reaction scheme 3.2: *First set* **of reactions:**

$$[Rh^I(\beta\text{-diketonate})(CO)(PPh_3)] + CH_3I \underset{k_{-1}}{\overset{k_1}{\rightleftharpoons}} \left[Rh(III)\text{-alkyl1} \underset{k_{-2}}{\overset{k_2}{\rightleftharpoons}} Rh(III)\text{-acyl1} \right]$$
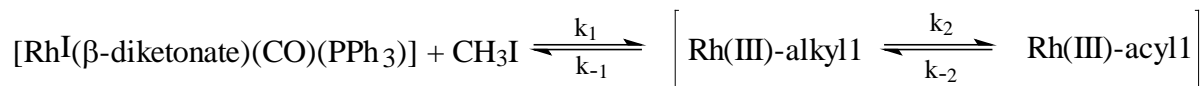
where $K_2 = k_2/k_{-2}$ represents the equilibrium constant between the Rh(III)-alkyl1 and Rh(III)-acyl1 species. The k_{-1} step above was only detected in CHCl$_3$ solutions as described below.

The CH$_3$I concentration dependence of k_{obs} of this reaction sequence in chloroform as monitored on IR is illustrated graphically in **Figure 3.17** page 146. Upon realizing that [MeI] $\gg$ [Rh(fctfa)(CO)(PPh$_3$)], it follows that these graphs satisfy the following equation[28]

Equation 3.2: $\qquad k_{obs} = k_1[CH_3I] + k_{-1}$

with the average value for k_1 = slope = 0.0062(3) dm^3 mol^{-1} s^{-1} and k_{-1} = intercept = 0.0005(2) s^{-1}. Individual k_1 and k_{-1} values are given in **Table 3.9** page 147.

A *second*, much slower ($t_{1/2} \approx 1.1$ hours ≈ 4000 s) *set* of reactions as observed on the IR is illustrated in **Figure 3.16**(b) where the Rh(III)-acyl1 species at 1729 cm^{-1} and the Rh(III)-alkyl1 species at 2082 cm^{-1} disappears at the same rate ($k_{obs} = 0.00017(1)$ s^{-1}) as the formation of the Rh(III)-alkyl2 species ($k_{obs} = 0.00017(3)$ s^{-1}) at 2064 cm^{-1}. By comparing rate constants, the *second set* of reactions is $0.011/0.00017 \approx 65$ times slower than the *first set* of reactions. Further evidence that there exists a *fast* equilibrium between the Rh(III)-alkyl1 and Rh(III)-acyl1 species are found from the observation that the Rh(III)-alkyl1 species at 2082 cm^{-1} disappears at the same rate as the Rh(III)-acyl1 species at 1729 cm^{-1}. Since the *second set* of reactions is very much slower than the *first set* of reactions, it was treated in isolation. Data from the interface at the boundary between set one and set two were, however, disregarded. This second reaction was found to be independent of [CH$_3$I]. The kinetic data of the second reaction are consistent with:

Reaction scheme 3.3: *Second set* **of reactions:**

$$\left[Rh(III)\text{-alkyl1} \overset{K_2}{\rightleftharpoons} Rh(III)\text{-acyl1} \right] \overset{k_3}{\longrightarrow} Rh(III)\text{-alkyl2}$$

---
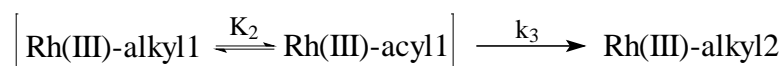
[28] Espenson, J.H., *Chemical Kinetics and Reaction Mechanisms,* Second Ed., McGraw-Hill, New York, p.15, 49.

The *second set* of reactions was followed by a very slow ($t_{1/2} \approx 40$ hours) *third reaction*. This third reaction, illustrated in **Figure 3.16**(c) includes the slow first-order disappearance of the Rh(III)-alkyl2 species ($k_{obs} = 0.0000049(5)$ s^{-1}) at 2064 cm^{-1} and the appearance, at the same rate, of a new Rh(III)-acyl2 species at 1714 cm^{-1} ($k_{obs} = 0.0000044(2)$ s^{-1}). These two rates are within experimental error identical (average = 0.0000047 s^{-1}). Both are independent of [CH$_3$I]. The long half-life of the third reaction implied that it could not be followed with great accuracy, as solvent evaporation became difficult to control. The kinetic data of the third reaction are consistent with:

Reaction scheme 3.4: *Third set* **of reactions:**

$$Rh(III)\text{-alkyl2} \xrightarrow{k_4} Rh(III)\text{-acyl2}$$
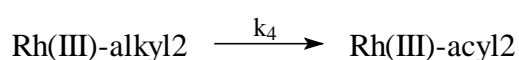
The overall reaction sequence for this oxidative addition reaction may therefore be represented as

$$[Rh^I(fctfa)(CO)(PPh_3)] + CH_3I \underset{k_{-1}}{\overset{k_1}{\rightleftharpoons}} \left\{ [Rh^{III}(fctfa)(CO)(PPh_3)(CH_3)(I)]^1 \underset{k_{-2}}{\overset{k_2}{\rightleftharpoons}} [Rh^{III}(fctfa)(CO)(PPh_3)(COCH_3)(I)]^1 \right\} \xrightarrow{k_3}$$

$$[Rh^{III}(fctfa)(CO)(PPh_3)(CH_3)(I)]^2 \xrightarrow{k_4} [Rh^{III}(fctfa)(CO)(PPh_3)(COCH_3)(I)]^2$$
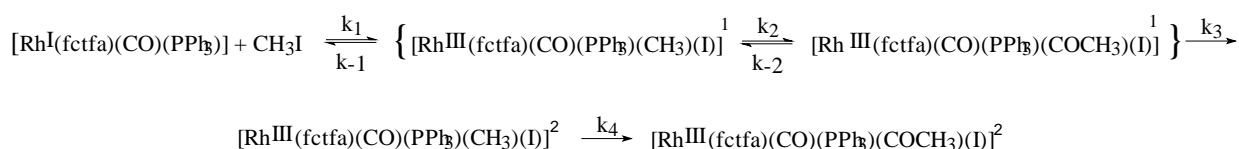
where the exponents "1" and "2" refer to alkyl1, acyl1, alkyl2 or acyl2. A more general way of writing the above mechanism, is

Reaction scheme 3.5:

$$[Rh^I(\beta\text{-diketonate})(CO)(PPh_3)] + CH_3I \underset{k_{-1}}{\overset{k_1}{\rightleftharpoons}} \left\{ [Rh(III)alkyl1] \underset{k_{-2}}{\overset{k_2}{\rightleftharpoons}} [Rh(III)acyl1] \right\} \underset{k_{-3}}{\overset{k_3}{\rightarrow}} [Rh(III)alkyl2] \underset{k_{-4}}{\overset{k_4}{\rightarrow}} [Rh(III)acyl2]$$
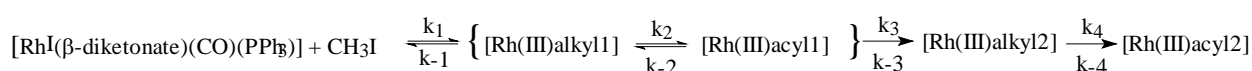
It was also possible, because of the long half-life, to crystallize the Rh(III)-alkyl2 species from the reaction mixture before the formation of the Rh(III)-acyl2 species. Paragraph 3.8.3 page 269 describes the crystal structure of the [Rh(III)(fctfa)(CO)(CH$_3$)(I)(PPh$_3$)]-alkyl2 species.

The reaction rates for the infrared monitoring of the oxidative addition reaction between CH$_3$I and [Rh(fctfa)(CO)(PPh$_3$)] in chloroform at 25 °C, as obtained from different concentrations of CH$_3$I (0.3 – 1.7 mol dm^{-3}, **Figure 3.17**), are summarized in **Table 3.9** page 147. **Table 3.28** page 188 summarizes the infrared monitoring of the oxidative addition reaction between CH$_3$I and [Rh(β-diketonato)(CO)(PPh$_3$)] complexes in chloroform at 25 °C for β-diketonato fctfa, fca, bfcm and dfcm.
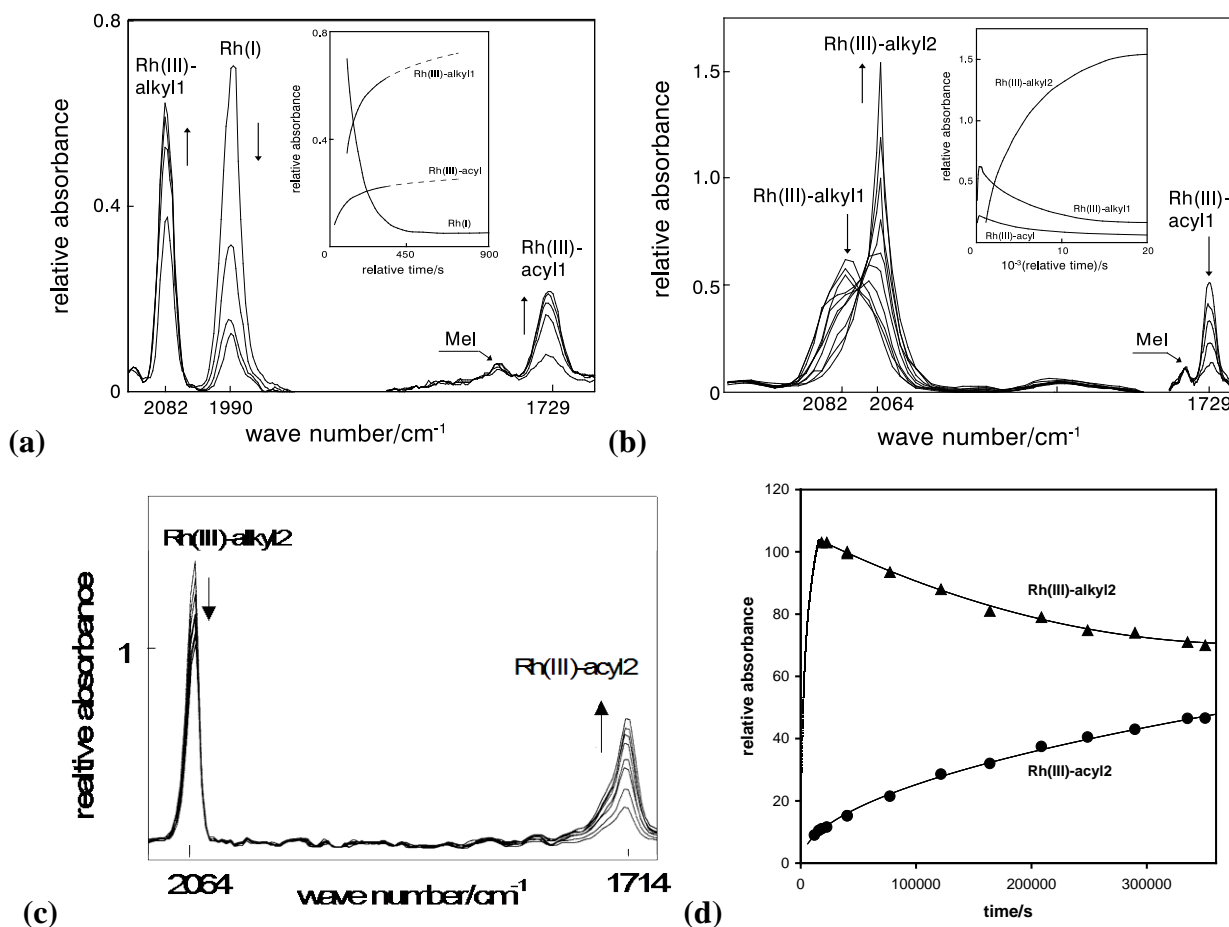
Figure 3.16: Illustration of the infrared monitoring of the oxidative addition reaction between CH₃I and [Rh(fctfa)(CO)(PPh₃)] in chloroform. T = 25 °C, [Rh(fctfa)(CO)(PPh₃)] = 0.01 mol dm⁻³, [MeI] = 1.673 mol dm⁻³, inserts give the absorbance *vs.* time data of the indicated species:

(a) The *first set* of reactions indicating disappearance of Rh(I) at 1990 cm⁻¹ and the simultaneous appearance of Rh(III)-alkyl1 at 2082 cm⁻¹ and Rh(III)-acyl1 at 1729 cm⁻¹. The illustrated spectra were recorded at time t = 0 (Rh(III)-acyl1 only), 74, 149, 224 and 299 s.

(b) The *second set* of reactions illustrating the simultaneous disappearance of Rh(III)-alkyl1 and Rh(III)-acyl1 and the formation of a Rh(III)-alkyl2 species at 2064 cm⁻¹. The illustrated spectra were recorded at t = 554, 734, 1094, 1919, 2819, 3719, 4905, 7605, 10305 and 20205 s for the Rh(III)-alkyl1 and Rh(III)-alkyl2 peaks, and at t = 554, 1919, 3719, 7605 and 20205 s for the Rh(III)-acyl1 peak.

(c) The *third set* of reactions illustrating the simultaneous disappearance Rh(III)-alkyl2 and the formation of a new Rh(III)-acyl2 species at 1714 cm⁻¹. The illustrated spectra were recorded at t = 40408, 77290, 121558, 163948, 208646, 248726, 289746 and 335308 s. (d) gives the absorbance *vs.* time data of (c).
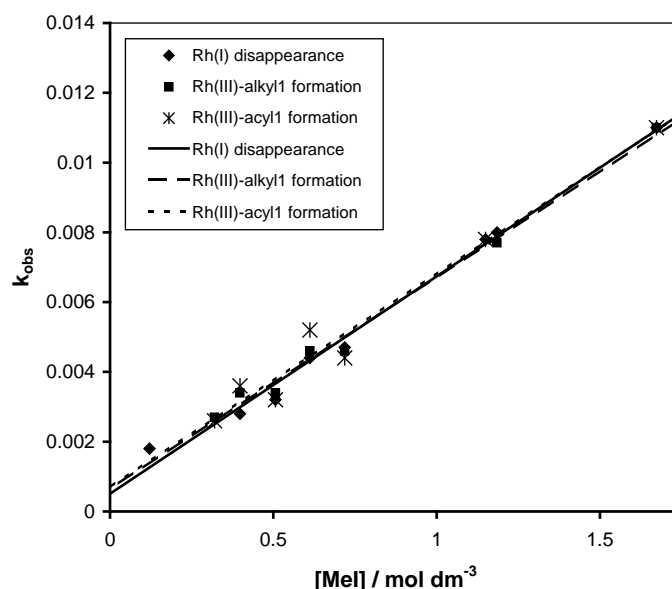
Figure 3.17: k_{obs} of the oxidative addition reaction between CH₃I and [Rh(fctfa)(CO)(PPh₃)] in chloroform at various concentrations CH₃I as monitored on an infrared spectrophotometer (T = 25 ºC). **For all practical purposes Rh(I) disappearance, Rh(III)-alkyl1 formation and Rh(III)-acyl1 formation had the same dependence on [MeI].**

(ii)   The infrared monitored reaction between CH₃I and [Rh(fctfa)(CO)(PPh₃)] in acetone as solvent.

The observed reaction sequence of [Rh(fctfa)(CO)(PPh₃)] with iodomethane in acetone (T = 25 ºC) in the range 1960 – 2100 cm⁻¹ as monitored by infrared was basically the same as observed in chloroform, except that the formation of the Rh(III)-acyl complexes could not be followed on the IR due to the strong absorbance of acetone in this region of the IR (1650 – 1800 cm⁻¹).

The *first set* of reactions observed (IR spectra not shown) was the disappearance of the Rh(I)-carbonyl complex, signal at 1987 cm⁻¹ with k_{obs} = 0.00411(7) s⁻¹ that basically corresponds to the formation of the Rh(III)-alkyl1 species (k_{obs} = 0.0042(1) s⁻¹, observed at 2082 cm⁻¹). The [CH₃I] dependence of k_{obs} in the case of the *first set* of reactions in acetone is illustrated graphically in **Figure 3.18**. Unlike what was observed in CHCl₃ (**Figure 3.17**), in acetone this graph passes through the origin. This means that in acetone the reverse, k_{-1}, step is too small to be detected compared to k_1. The same **Reaction scheme 3.2** as on page 143, therefore still applies, with the exception that $k_1 \gg k_{-1} \approx 0$. Second-order rate constants are summarized in **Table 3.9**.

The *second* observed reaction was the formation of the Rh(III)-alkyl2 species (k_{obs} = 0.00016(2) s⁻¹) at 2059 cm⁻¹. Disappearance of the precursor acyl1-species could not be observed in acetone

due to interference of the acetone carbonyl bond. However, the disappearance of the Rh(III)-alkyl1 species at 2082 cm^{-1} took place within experimental error at the same rate, k_{obs} = 0.00020(4) s^{-1} as the formation of the Rh(III)-alkyl2 species. These results, obtained in acetone, are consistent with **Reaction scheme 3.3** on page 143.

(a)   **(b)**
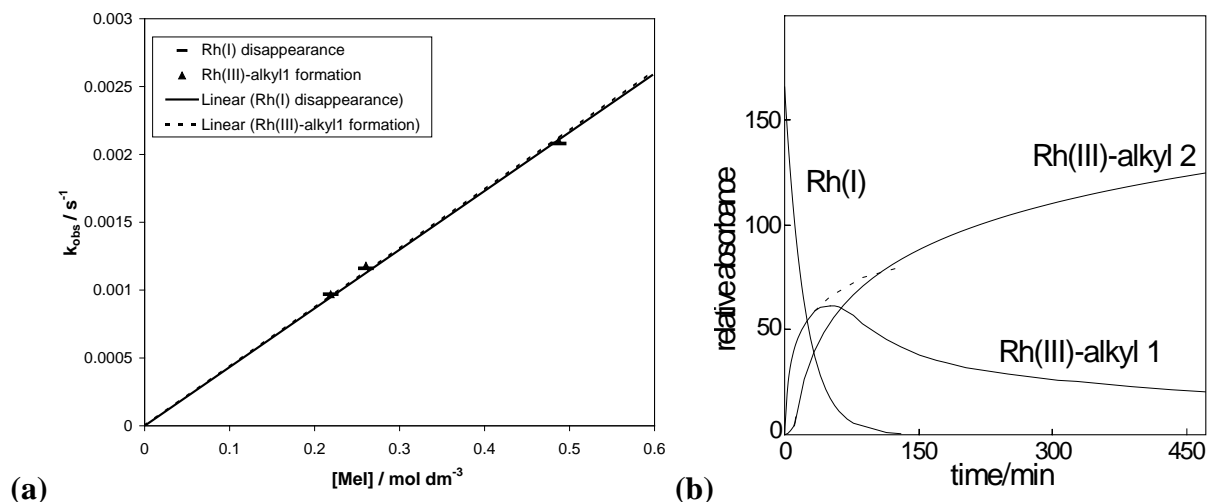
Figure 3.18: (a) k_{obs} for the *first set* of reactions as a function of CH$_3$I concentration for the oxidative addition reaction between CH$_3$I and [Rh(fctfa)(CO)(PPh$_3$)] in acetone$^{\#}$ as monitored on the infrared spectrophotometer. T = 25 ^{o}C, [Rh(fctfa)(CO)(PPh$_3$)] = 0.002 mol dm^{-3}. (b) Absorbance *vs.* time data of the oxidative addition reaction between CH$_3$I and [Rh(fctfa)(CO)(PPh$_3$)] in acetone with [CH$_3$I] = 0.260 mol dm^{-3}. $^{\#}$ k_{obs} in acetone as obtained from IR measurements, is in accordance with the kinetic rate constant as obtained from UV/visible measurements over the concentration range 0.16 mol dm^{-3} < [MeI] < 2.8 mol dm^{-3}, see **Figure 3.23**.

Table 3.9: Kinetic rate constants for the oxidative addition of MeI to [Rh(fctfa)(PPh$_3$)(CO)] in chloroform and acetone at 25.0(1) ^{o}C, IR monitored. The species that were monitored to obtain the individual rate constants are indicated in the headings.

First set of reactions					
Solvent	**Rh(I) disappearance**		**Rh(III)-alkyl1 formation**		**Rh(III)-acyl1 formation**	
	k_1/dm^{3}mol^{-1}s^{-1}	k_{-1}/s^{-1}	k_1/dm^{3}mol^{-1}s^{-1}	k_{-1}/s^{-1}	k_1/dm^{3}mol^{-1}s^{-1}	k_{-1}/s^{-1}
chloroform	0.0062(3)	0.0005(2)	0.0061(3)	0.0006(2)	0.0061(5)	0.0007(4)
acetone	0.00411(7)	0	0.0042(1)	0		*
Second set of reactions (k_3/s^{-1})					
	Rh(III)-alkyl1 disappearance		**Rh(III)-acyl1 disappearance**		**Rh(III)-alkyl2 formation**	
chloroform	0.00017(1)		0.00017(1)		0.00017(3)	
acetone	0.00020(4)		*		0.00016(2)	
Third set of reactions (k_4/s^{-1})					
	Rh(III)-alkyl2 disappearance		**Rh(III)-acyl2 formation**			
chloroform	0.0000049(5)		0.0000044(2)			
acetone	0.0000026(5)		*			

* It is not possible to follow the formation of Rh(III)-acyl species in acetone on IR due to the strong absorbance of acetone in the same region as the Rh(III)-acyl species on the IR.

The *third set* of reactions includes the slow disappearance of the Rh(III)-alkyl2 species (k_{obs} = 0.0000026(5) s^{-1}) at 2059 cm^{-1} and the assumed appearance of a new Rh(III)-acyl2 species. Again this new assumed Rh(III)-acyl2 species could not be observed in acetone on the IR, due to overlapping of the solvent carbonyl peak. The reaction rates for the infrared monitoring of the oxidative addition reaction between CH$_3$I and [Rh(fctfa)(CO)(PPh$_3$)] in acetone at 25 °C are summarized in **Table 3.9** page 147.

(iii)   Consecutive reaction treatment.

In essence, upon recognizing that CH$_3$I was in large excess, the general reaction scheme in acetone is one of consecutive reactions without any equilibriums, namely:

Reaction scheme 3.6: $\quad\quad A \xrightarrow{k_{1obs}} B \xrightarrow{k_3} C \xrightarrow{k_4} D$
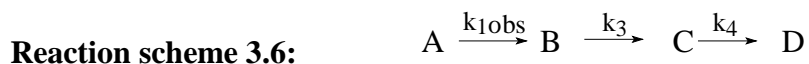
with A = [Rh^I(fctfa)(CO)(PPh$_3$)], B = [Rh(III)-alkyl1 $\square$ Rh(III)-acyl1], C = Rh(III)-alkyl2 and D = Rh(III)-acyl2. By ignoring D, the concentration of A at time t is described by:[29]

Equation 3.3: $\quad\quad [A]_t = [A]_0 \exp(-k_{1obs}t)$

the concentration of B at time t by:[29]

Equation 3.4: $\quad\quad [B]_t = \dfrac{k_{1obs}[A]_0}{k_3 - k_{1obs}}\left[\exp(-k_{1obs}t) - \exp(-k_3t)\right]$

and the concentration of C at time t by[29]

Equation 3.5: $\quad\quad [C]_t = [A]_0\left\{1 - \dfrac{1}{k_3 - k_{1obs}}\left[k_3 \exp(-k_{1obs}t) - k_{1obs} \exp(-k_3t)\right]\right\}$

Equation 3.3 was already fitted to the absorbance *vs.* time data of the Rh(I) disappearance (graph on page 147) and results in k_{1obs} = 0.0012(1) s^{-1} for [CH$_3$I] = 0.2604 mol dm^{-3}, or k_1 = 0.0046(4) dm^3 mol^{-1} s^{-1}. (The value given in **Table 3.9**, 0.00411(7) s^{-1} was the average of all determined k_1 values as per **Figure 3.18**). Upon performing a least squares fit of the available absorbance *vs.* time data of the Rh(III)-alkyl1 peak for the reaction in acetone to **Equation 3.4**, **Figure 3.19** (a),

the rate constants were determined as $k_{1obs} = 0.0012(1)$ s^{-1} and $k_3 = 0.00010(1)$ dm^3 mol^{-1} s^{-1}. The value of k_{1obs} corresponds very close with that obtained by using the previous treatment, *i.e.* by looking at each reaction set in isolation. The value of k_3 was slightly (37%) smaller than the expected value of $0.00016(2)$ s^{-1}. However, fitting **Equation 3.5** to the available data, absorbance *vs.* time data of the Rh(III)-alkyl2 peak (see **Figure 3.19** (b)), resulted in $k_{1obs} = 0.0022(6)$ s^{-1} ($k_1 \approx 0.0084$ dm^3 mol^{-1} s^{-1}), while $k_3 = 0.00018(1)$ s^{-1}. This value of k_3 corresponds well to that previously obtained, by treating data sets as separate, isolated, quantities. With this fitting k_1 was larger (83%) than expected. Bearing in mind the difficulty of obtaining large amounts of data points with an infrared spectrophotometer, the observed deviations between k_1 and k_3 obtained from **Equation 3.4** and **Equation 3.5** are not regarded as significant, but rather the consequence of fitting to little data to complicated equations. The results obtained by both the consecutive reaction treatment and as individual data sets are, therefore, regarded as mutually consistent and confirm the proposed mechanism.

(a)   **(b)**
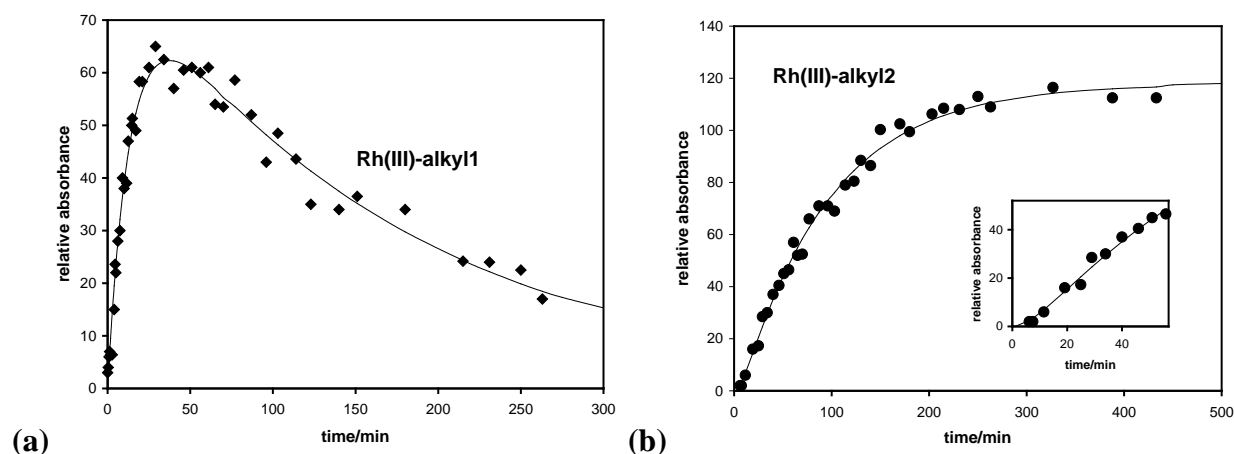
Figure 3.19:   Absorbance *vs.* time data of the IR monitoring of the reaction between CH_3I and $[Rh(fctfa)(CO)(PPh_3)]$ in acetone. T = 25°C, $[CH_3I] = 0.2604$ mol dm^{-3} and $[Rh(fctfa)(CO)(PPh_3)] = 0.002$ mol dm^{-3}.   In (a), the solid line indicates the consecutive reaction fitting according to Equation 3.4 for the absorbance of the Rh(III)-alkyl1 species. A data fit to Equation 3.5 for the absorbance of the Rh(III)-alkyl2 species is shown in (b).   The insert in (b) represents an enlargement of the initial stages of Rh(III)-alkyl2 formation.

By ignoring A in **Reaction scheme 3.6** (page 148) and applying the consecutive reaction kinetic **Equation 3.4** to intermediate C for the compound series B, C and D, values of k_3 and k_4 were found to be $0.00016(1)$ and $0.0000055(3)$ s^{-1}. The value for k_3 corresponded well to the above described determined values. The value for k_4 is larger than the value obtained from the treatment of data in isolation, namely $k_4 = 0.0000026(5)$ s^{-1}, but kinetically they are

---

[29] Espenson, J.H., *Chemical Kinetics and Reaction Mechanisms,* Second Ed., McGraw-Hill, New York, p.70 – 75.

indistinguishable. **Equation 3.5** could not be fitted to formation data of D, from the reaction in acetone as solvent, due to interference of the acetone carbonyl peak in the region of Rh(III)-acyl2 detection.

When the consecutive reaction treatment of data were applied to reactions performed in chloroform, the mathematical model broke down as shown by the poor fit in **Figure 3.20**. The breakdown of the model is attributed to the detected equilibrium step k_{-1} in the mechanism

$$A \underset{k_{-1}}{\overset{k_1}{\rightleftharpoons}} B \xrightarrow{k_3} C$$
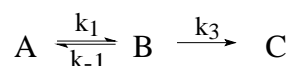
The full treatment of such monophasic reversible reactions is quite complex[30], and can thus best be handled by treating the data sets as separate, isolated quantities. In the rest of this study, oxidative addition rate constants were obtained by treating data sets as separate, isolated quantities. This could be done on the grounds of the above discussion and the fact that the rate constants of the different steps differ more than tenfold. The obtained rate constants indicated that half-lives for the first step in the reaction sequence never were larger than 385 s, but at high MeI concentrations the half-life was as short as 63 s. In contrast the half-lives of the second and third MeI independent steps were ~ 4000 s and 40 hours (144000 s) respectively.
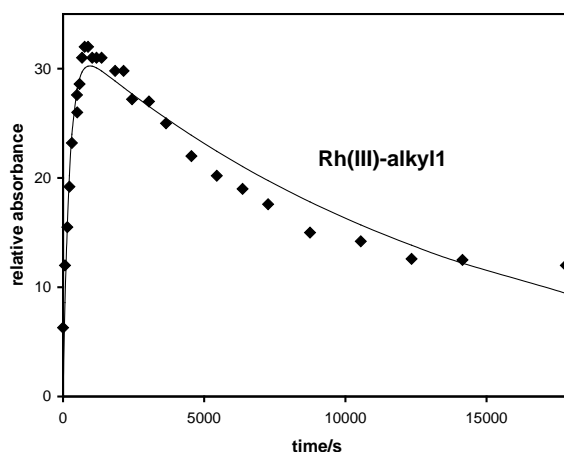
Figure 3.20: Absorbance *vs.* time data of the IR monitoring of the reaction between CH_3I and $[Rh(fctfa)(CO)(PPh_3)]$ in chloroform. $T = 25°C$, $[CH_3I] = 0.4077$ mol dm^{-3} and $[Rh(fctfa)(CO)(PPh_3)] = 0.007$ mol dm^{-3}. The solid line indicates the consecutive reaction fitting according to Equation 3.4 for the absorbance of the Rh(III)-alkyl1 species. The fit is very poor because of the observable equilibrium in the reaction sequence.

---

[30] Wilkins, R.G., *Kinetics and Mechanism of Reactions of Transition Metal Complexes,* 2nd thoroughly revised edition, VCH, Weinheim, 1991, p. 15.

3.4.3.2 The UV/visible monitored reaction between CH₃I and [Rh(fctfa)(CO)(PPh₃)] in various solvents.

The reaction between CH$_3$I and [Rh(fctfa)(CO)(PPh$_3$)] was also monitored on an UV/visible spectrophotometer and all three reaction steps could be identified. The reaction rate constant obtained for the first step corresponded to the rate constant for the disappearance of the Rh(I) monocarbonyl species as observed by IR. The rate constant for the second and third steps also corresponded to the rate constant for the *second* and *third sets* of reactions as observed on the IR spectrophotometer. The second step is the formation of the Rh(III)-alkyl2 species and the third step is the formation of the final reaction product, the Rh(III)-acyl2 species [Rh(fctfa)(COCH$_3$)(I)(PPh$_3$)]^2.

In chloroform, all three reaction steps could be followed at 530 nm on the UV/visible spectrophotometer. The second reaction could *also* be followed at 375 nm giving rate constants in agreement with those obtained at 530nm. **Figure 3.21** illustrates the absorbance *vs.* time data for the first and second reaction, obtained for selected oxidative addition reactions of CH$_3$I to [Rh(fctfa)(CO)(PPh$_3$)]. Rate constants for the third reaction (measured at 25°C, see **Table 3.10** page 155, not illustrated) were obtained at 530, 500 and 400 nm.

(a)   **(b)**
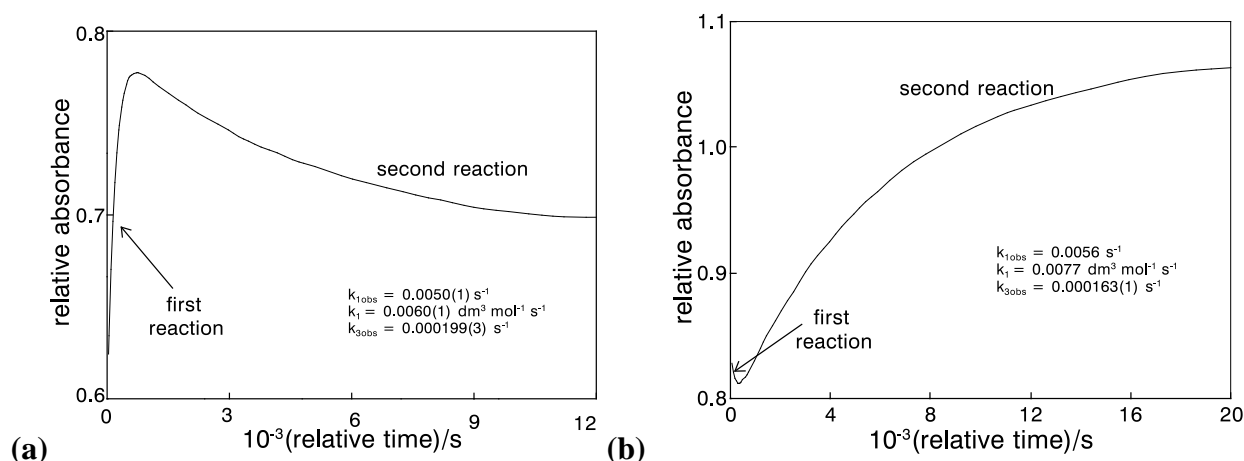
Figure 3.21: Absorbance *vs.* time data for the UV/visible monitored oxidative addition reaction of CH₃I to [Rh(fctfa)(CO)(PPh₃)] in chloroform at (a) 530 nm, [Rh(fctfa)(CO)(PPh₃)] = 0.0002 mol dm⁻³, [MeI] = 0.7282 mol dm⁻³ and (b) 375 nm, [Rh(fctfa)(CO)(PPh₃)] = 0.0003 mol dm⁻³, [MeI] = 0.8365 mol dm⁻³ (T = 25 ºC). The value of k₁ = 0.0077 dm³ mol⁻¹ s⁻¹ at 375 nm is inaccurate because the change in absorbance is small.

The temperature and MeI concentration dependence of the oxidative addition reaction between CH$_3$I and [Rh(fctfa)(CO)(PPh$_3$)] as monitored on the UV/visible spectrophotometer in chloroform at 530 nm for the first reaction and at 530 and 375 nm for the second reaction are

151

given in **Figure 3.22**. Data obtained at 530 nm in acetone (first reaction only) are given in **Figure 3.23**.

The standard enthalpy and entropy of activation, ΔH* and ΔS*, for the different reaction steps were determined from least-squares fits[21] of the reaction rate constants *vs.* temperature data according to the Eyring relationship[31] **Equation 3.6**. **Equation 3.6** may also be written in the linear form as in **Equation 3.7**.

Equation 3.6:
$$k = \frac{k_B T}{h} \exp(-\frac{\Delta H *}{RT}) \exp(\frac{\Delta S *}{R})$$

Equation 3.7:
$$\ln \frac{k}{T} = -\frac{\Delta H *}{RT} + \frac{\Delta S *}{R} + \ln \frac{k_B}{h}$$

k_B is Boltzmann's constant, h Planck's constant and R the gas constant. A plot of $\ln(k/T)$ *vs.* T^{-1} is linear with a slope of $-\Delta H*/R$ and an intercept of $\{\ln(k_B/h) + \Delta S*/R\} = \{23.760 + \Delta S*/R\}$. This linear relationship is illustrated in inserts in the relevant temperature *vs.* concentration graphs, *e.g.* **Figure 3.22**. The standard free energy of activation ΔG* may be calculated from the equation $\Delta G* = \Delta H* - T\Delta S*$.[32] The activation parameters at 298K are summarized in **Table 3.10** page 155.

(a)   **(b)**
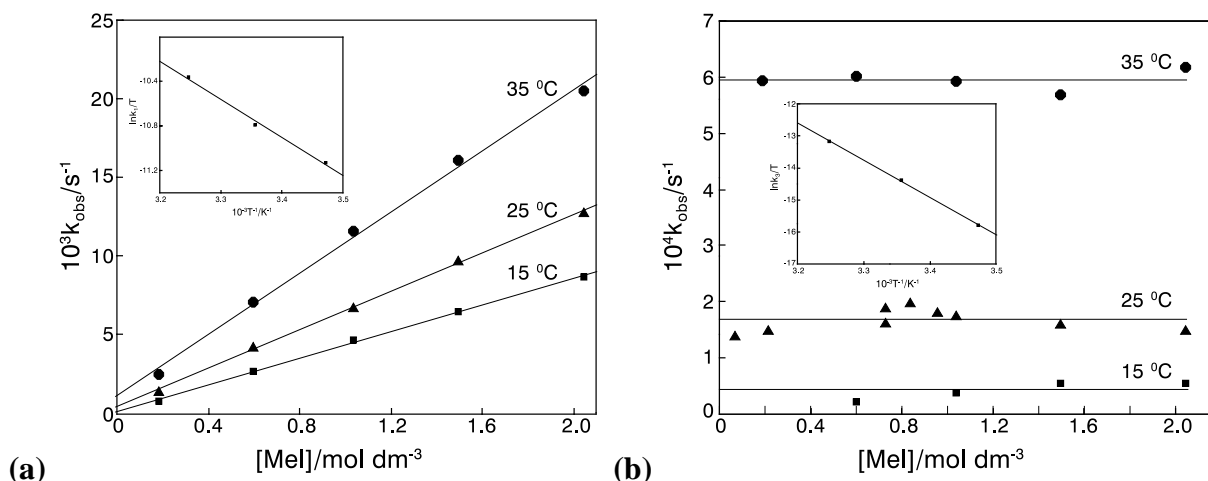
Figure 3.22: **Temperature and MeI concentration dependence for the oxidative addition of CH₃I to [Rh(fctfa)(CO)(PPh₃)] as monitored on the UV/VIS spectrophotometer in chloroform (a) at 530 nm for the first reaction {Rh(I) + MeI ☐ [Rh(III)-alkyl1 ☐ Rh(III)-acyl1]} and (b) at 530 and 375 nm for the second reaction {[Rh(III)-alkyl1 ☐ Rh(III)-acyl1] → Rh(III)-alkyl2}.**

[31] Espenson, J.H., *Chemical Kinetics and Reaction Mechanisms,* Second Ed., McGraw-Hill, New York, p. 156.

[32] Atkins, P.W., *Physical Chemistry*, fifth edition, Oxford University Press, Oxford, 1994, p. 939 – 950.
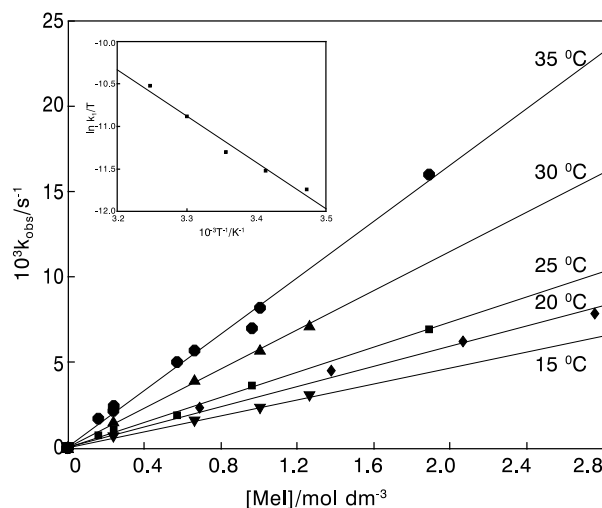
Figure 3.23: Temperature and MeI concentration dependence for the *first set* of reactions for the oxidative addition of CH$_3$I to [Rh(fctfa)(CO)(PPh$_3$)] as monitored on the UV/VIS spectrophotometer in acetone at 530 nm.

(a)   **(b)**
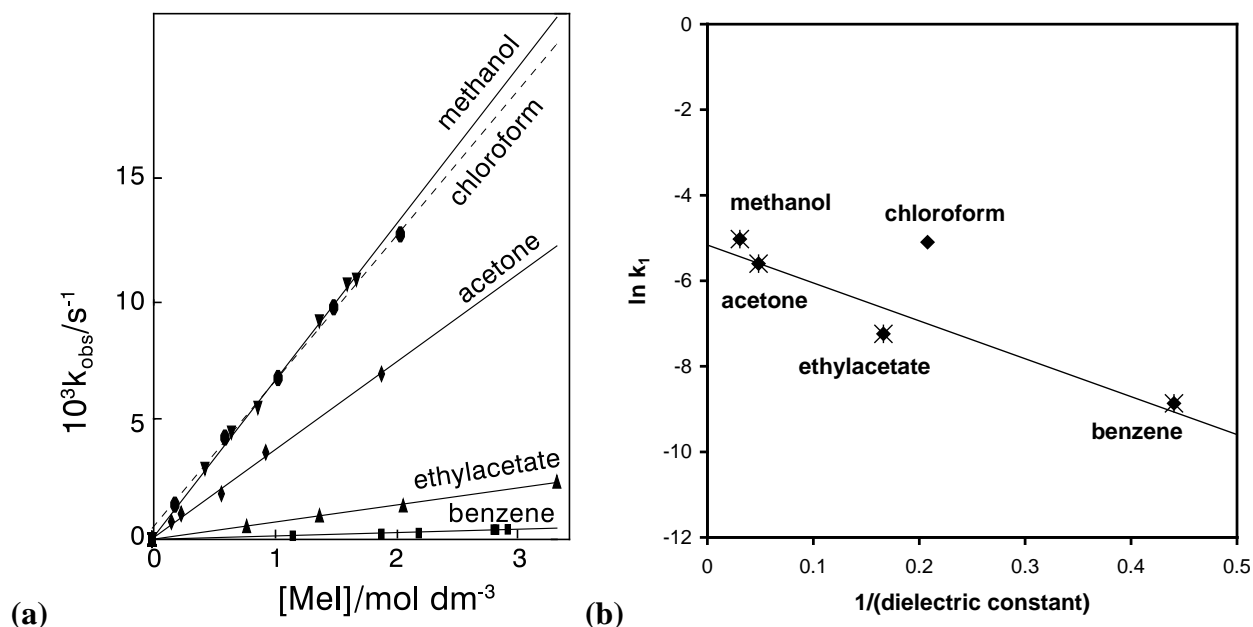
Figure 3.24: **(a)** Solvent and MeI concentration dependence of the *first reaction set* {[Rh(fctfa)(CO)(PPh$_3$)] + CH$_3$I □ [Rh(III)-alkyl1 □ Rh(III)-acyl1]} as monitored on the UV/visible spectrophotometer at T = 25 °C. **(b)** Relationship between the second-order rate constant, k$_1$, and the dielectric constant of the solvent used during the UV monitoring of the oxidative addition of CH$_3$I to [Rh(fctfa)(CO)(PPh$_3$)], *first reaction set*, at 25°C. Chloroform does not fit the trend.

The MeI concentration dependence of oxidative addition reaction between CH$_3$I and [Rh(fctfa)(CO)(PPh$_3$)] in the solvents methanol, chloroform, acetone, ethylacetate and benzene (first reaction only) is given in **Figure 3.24** (a). It is interesting to note that only chloroform as solvent shows an observable k$_{-1}$ step. Kinetic rate constants for the oxidative addition of MeI to [Rh(β-diketonato)(PPh$_3$)(CO)] in various solvents are summarized in **Table 3.10** page 155. With the exception of chloroform as solvent, the increase in the rate of the first step of oxidative

153

addition in the different solvents follows the same pattern as the increase in the dielectric constant, $\varepsilon_{25°C}$. Data are presented as "solvent ($\varepsilon_{25°C}$, $k_1/dm^3mol^{-1}s^{-1}$)" and is arranged from smallest to largest rate constant.

(Smallest rate constant) benzene (**2.27**, 0.000141) < ethyl acetate (**6.02**, 0.000716)

< < acetone (**20.7**, 0.00370) < chloroform (**4.81**,* 0.00611)

< methanol (**32.6**, 0.00658) (largest rate constant) (* exception)

The solvent can be regarded as an "inert" medium or it can act as a nucleophile and an active participant in the reaction. The dielectric constant of the solvent is the most important parameter with regard to the description of the solvent as an "inert" medium. Consider the following equation: $A+B \; \square \; (A,B)^* \rightarrow AB$. If the transitional state, $(A,B)^*$ is polar, more polar solvents will stabilize its formation and consequently lead to an increase in the reaction rate. The dielectric effect can be semi-quantitatively evaluated for ion-ion or ion-dipolar reactant mixtures, where electrostatic considerations dominate. For a reaction between two ions of charge Z_A and Z_B, the rate constant, at zero ionic strength, is given by:[33]

Equation 3.8: $\qquad \ln k = \ln k_0 - \dfrac{e^2}{2\varepsilon kT}\left[\dfrac{(Z_A + Z_B)^2}{r^*} - \dfrac{Z_A^2}{r_A} - \dfrac{Z_B^2}{r_B}\right]$

k_0 is the hypothetical rate constant in a medium of infinite dielectric constant, ε is the dielectric constant, r_A, r_B, and r^* are the radii of the reactant ions A and B and the activated complex respectively. During a reaction between an ion Z_A and a polar molecule (that is $Z_B = 0$), **Equation 3.8** becomes **Equation 3.9**.

Equation 3.9: $\qquad\qquad \ln k = \ln k_0 - \dfrac{Z_A^2 e^2}{2\varepsilon kT}\left[\dfrac{1}{r_A} - \dfrac{1}{r^*}\right]$

A plot of lnk *versus* ε^{-1} should therefore be linear. **Figure 3.24** (b) displays this relationship between the second-order rate constant of the *first reaction set* obtained in the various solvents during the oxidative addition, and ε. It was found that with the exception of chloroform, more polar solvents (*i.e.* those with higher dielectric constants) led to a larger second-order rate constant for oxidative addition. The non zero intercept obtained for the rate constant k_{obs} *vs.* [MeI] in chloroform (**Figure 3.22** and **Figure 3.24**), indicated in chloroform a reverse step, k_{-1}, that was not the case for the other solvents. A probable reason for this observation is that $CHCl_3$,

like CH_3I, may itself participate in oxidative addition reactions. This would imply that the CH_3I oxidative addition transition state prior to the formation of the reaction product may be involved in exchange reactions with $CHCl_3$ and account for the observed k_{-1} step. The "apparent" mechanistic difference probably implies that **Equation 3.9** does not hold good for the reaction in chloroform to the same extent as it does for other solvents.

Table 3.10: Selected temperature dependent kinetic rate constants and activation parameters for the oxidative addition of MeI to [Rh(fctfa)(PPh₃)(CO)], as monitored on the UV/visible spectrophotometer, in various solvents. k_1, k_3 and k_4 are the rate constant associated with the first, second and third stages of this oxidative addition reaction.

Solvent	$\varepsilon_{25°C}$	T / °C	k_1/ dm³mol⁻¹s⁻¹	$\Delta H^*(k_1)$ / kJ mol⁻¹	$\Delta S^*(k_1)$ / J mol⁻¹K⁻¹	k_3/s⁻¹	$\Delta H^*(k_3)$ / kJ mol⁻¹	$\Delta S^*(k_3)$ / J mol⁻¹K⁻¹	k_4/s⁻¹
methanol	32.6	25.0(1)	0.00658(3)	-	-	-	-	-	-
chloroform	4.81#	15.0(1)	0.00424(9)*	29(3)	-188(9)	0.00004(1)	93(1)	-5(3)	-
		25.0(1)	0.00611(1)*			0.00017(2)			4.4(1)x10⁻⁶
		35.0(1)	0.00973(4)*			0.00059(2)			-
acetone	20.7	15.0(1)	0.0023(1)	50(4)	124(4)	-	-	-	-
		20.0(1)	0.0029(1)			-	-	-	-
		25.0(1)	0.00370(4)			-	-	-	-
		30.0(1)	0.0057(1)			-	-	-	-
		35.0(1)	0.0083(4)			-	-	-	-
ethylacetate	6.02	25.0(1)	0.000716(4)	-	-	-	-	-	-
benzene	2.27	25.0(1)	0.000141(2)	-	-	-	-	-	-

* k_{-1} = 0.0001(1), 0.0005(1) and 0.0011(4) s⁻¹ at 15, 25 and 35 °C respectively.   # ε at 20 °C

3.4.3.3 The ¹H and ³¹P NMR monitored reaction between CH₃I and [Rh(fctfa)(CO)(PPh₃)].

(i) *Introduction.*

The reaction between CH_3I and [Rh(fctfa)(CO)(PPh₃)] was monitored by ¹H NMR. In the *first set* of reactions, the two major Rh(I) isomers {referred to as Rh(I)A and Rh(I)B, the choice of the labels are arbitrary and has no significance} reacted with CH_3I to form at least two isomers of the Rh(III)-alkyl1 product {referred to as Rh(III)-alkyl 1A and Rh(III)-alkyl 1B} which underwent a CO insertion reaction to form at least two isomers of the Rh(III)-acyl1 product {referred to as Rh(III)-acyl 1A and Rh(III)-acyl 1B} (the *first set* of reactions – see reaction scheme below). As before, Rh(III)-alkyl1 and Rh(III)-acyl1 formed at the same rate, indicating

---

33 Wilkins, R.G., *Kinetics and Mechanism of Reactions of Transition Metal Complexes,* 2ⁿᵈ thoroughly revised edition, VCH, Weinheim, 1991, chapter 2.

again that these two products are in equilibrium with each other. During the *second set* of reactions, the acyl ligand of the two isomers of the Rh(III)-acyl1 product underwent decarbonylation to form two isomers of the Rh(III)-alkyl2 complex {referred to as Rh(III)-alkyl 2A and Rh(III)-alkyl 2B}. As before, Rh(III)-alkyl1 and Rh(III)-acyl1 disappeared at the same rate, indicating again that these two products are in equilibrium with each other. It was not practical to follow the *third set* of reactions to the end by ^{1}H NMR, due to the slowness of the reaction ($t_{1/2} \approx 40$ h). By carefully comparing the positions and integrals of the different signals, the spectral parameters of the different isomers could be identified as given in **Table 3.11** page 157. The reaction sequence observed by NMR was therefore completely consistent with that implicated by IR and UV studies. The new feature introduced by the NMR study is the existence of more than one isomer for each intermediate. **Reaction scheme 3.5** on page 144 can, therefore, be rewritten to include the different *prominent* isomers as follows:

Reaction scheme 3.7: (*First set* of reactions*)*

$$\{Rh(I)A \rightleftharpoons Rh(I)B\} + CH_3I \underset{k_{-1}}{\overset{k_1}{\rightleftharpoons}}$$

$$\left[\{Rh(III)\text{-alkyl1A} \rightleftharpoons Rh(III)\text{-alkyl1B}\} \underset{k_{-2}}{\overset{k_2}{\rightleftharpoons}} \{Rh(III)\text{-acyl1A} \rightleftharpoons Rh(III)\text{-acyl1B}\} \right]$$
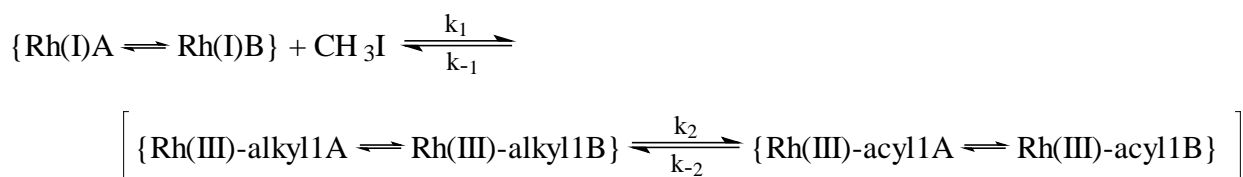
Reaction scheme 3.8: *Second set* of reactions

$$\left[\{Rh(III)\text{-alkyl1A} \rightleftharpoons Rh(III)\text{-alkyl1B}\} \underset{k_{-2}}{\overset{k_2}{\rightleftharpoons}} \{Rh(III)\text{-acyl1A} \rightleftharpoons Rh(III)\text{-acyl1B}\} \right]$$

$$\overset{k_3}{\longrightarrow} \quad \{Rh(III)\text{-alkyl2A} \rightleftharpoons Rh(III)\text{-alkyl 2B}\}$$
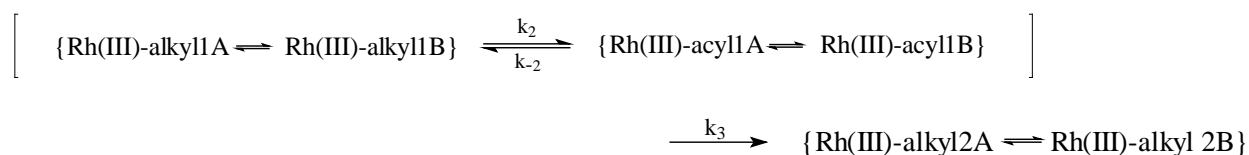
Reaction scheme 3.9: *Third set* of reactions

$$\{Rh(III)\text{-alkyl2A} \rightleftharpoons Rh(III)\text{-alkyl 2B}\} \overset{k_4}{\longrightarrow} \{Rh(III)\text{-acyl 2A} \rightleftharpoons Rh(III)\text{-acyl 2B}\}$$
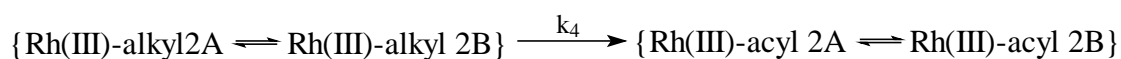
The A and B isomers of each species (*e.g.* acyl 1A and acyl 1B) exist in a fast equilibrium with each other, because

(i)   the observed rate constant for the disappearace or formation of an A and a B isomer (of the same species) was found to be the same within experimental error (**Table 3.12** page 159) and

(ii)   the ratio Rh(I)A/Rh(I)B = 60/40 is not the same as the ratio Rh(III)-alkyl1A/Rh(III)-alkyl1B = 28/72 or the ratio Rh(III)-acyl1A/Rh(III)-acyl1B = 50/50 (**Table 3.11**). If the

reaction was (Rh(I)A + MeI □ {Rh(III)-alkyl1A □ Rh(III)-acyl1A}) for the A isomers and separately (Rh(I)B + MeI □ {Rh(III)-alkyl1B □ Rh(III)-acyl1B}) for the B isomers, and if no equilibrium between isomers A and B existed, the ratio A:B of these isomers would have been the same throughout the reaction.

The ^{31}P NMR spectral parameters of the ^{31}P NMR monitored oxidative addition reaction of 0.021 mol dm^{-3} [Rh(fctfa)(CO)(PPh$_3$)] with 0.500 mol dm^{-3} CH$_3$I in CDCl$_3$ are also given in **Table 3.11**. The same reaction sequence and reaction products were observed on ^{1}H and on ^{31}P NMR. The observed ratio of isomer A to isomer B in each case was also the same.

Table 3.11: ^{1}H and ^{31}P NMR spectral parameters of the different isomeric forms of [Rh(fctfa)(CO)(PPh$_3$)] and the Rh(III) complexes formed during the oxidative addition reaction of MeI to [Rh(fctfa)(CO)(PPh$_3$)]. K_c = [RhB-species]/[RhA-species].

compound	K_c	^{31}P NMR			^{1}H NMR					
		δ^{31}P /ppm	^{1}J(^{31}P-^{103}Rh) /Hz	Ratio isomers on ^{31}P NMR	Ratio isomers on ^{1}H NMR	δ^1H methine proton β-diketone ligand/ppm	δ^1H CH$_3$-group from MeI/ppm	δ^1H ferrocene-group β-diketone ligand /ppm		
								5H	2H	2H
Rh(I)A	0.68	48.04	176.4	-	60%	6.045	-	3.94	4.09	4.27
Rh(I)B		48.04	176.4	-	40%	6.045	-	4.20	4.50	4.83
Rh(III)-alkyl 1A	2.57	33.23	125	28%	28%	6.055	1.47	4.29	4.73	*
Rh(III)-alkyl 1B		32.80	124	72%	72%	6.055	1.42	4.34	*	*
Rh(III)-acyl 1A	1.00	38.38	155	50%	50%	6.08	3.05	4.17	*	*
Rh(III)-acyl 1B		37.57	155	50%	50%	6.08	2.98	3.94	*	*
Rh(III)-alkyl 2A	4.56	27.09	115.2	19%	18%	5.45	2.15	4.23	*	*
Rh(III)-alkyl 2B		29.33	116.5	81%	82%	5.30	1.78	4.31 4.39	4.31	4.47 4.76
Rh(III)-acyl 2A	-	-	-	-	-	-	2.99	-	-	-
Rh(III)-acyl 2B		-	-	-	-	-	3.01	-	-	-

* Peaks could not uniquely be identified due to exessive overlapping.

The Rh(III)-alkyl 2B isomer could be isolated in solid form and its structure could be determined by X-ray crystallography, see paragraph 3.8.3. The ^{1}H and ^{31}P NMR spectrum of the crystalline isolated Rh(III)-alkyl 2B isomer were identical to the spectrum as observed during the monitoring of the *second set* of reactions during the oxidative addition reaction of [Rh(fctfa)(CO)(PPh$_3$)] with MeI in CDCl$_3$ solutions. An important observation was that upon dissolving the solid crystalline Rh(III)-alkyl 2B isomer in CDCl$_3$ isomerization to the Rh(III)-alkyl 2A isomer sets in (**Figure 3.25** and **Figure 3.26** (a)). After 4 days of the Rh(III)-alkyl 2B isomer in solution in CDCl$_3$ traces of Rh(I), Rh(III)-alkyl1 and Rh(III) acyl1 were observed on ^{31}P NMR (**Figure 3.26** (b)), indicating mutual communication between the different species (no

excess of MeI in this case to force the reaction in one direction). This means that **Reaction scheme 3.5**, page 144, also has a k_{-3} and k_{-4} step, but when an excess of MeI is added to the starting Rh(I) complex, the k_{-3} and k_{-4} steps are simply not observed. The full reaction sequence for the oxidative addition of MeI to [Rh(fctfa)(CO)(PPh$_3$)] is therefore not **Reaction scheme 3.5**, but rather

Reaction scheme 3.10:

$$[\text{Rh}^{\text{I}}(\beta\text{-diketonate})(\text{CO})(\text{PPh}_3)] + \text{CH}_3\text{I} \underset{k_{-1}}{\overset{k_1}{\rightleftharpoons}} \left\{ [\text{Rh(III)alkyl1}] \underset{k_{-2}}{\overset{k_2}{\rightleftharpoons}} [\text{Rh(III)acyl1}] \right\} \underset{k_{-3}}{\overset{k_3}{\rightleftharpoons}} [\text{Rh(III)alkyl2}] \underset{k_{-4}}{\overset{k_4}{\rightleftharpoons}} [\text{Rh(III)acyl2}]$$
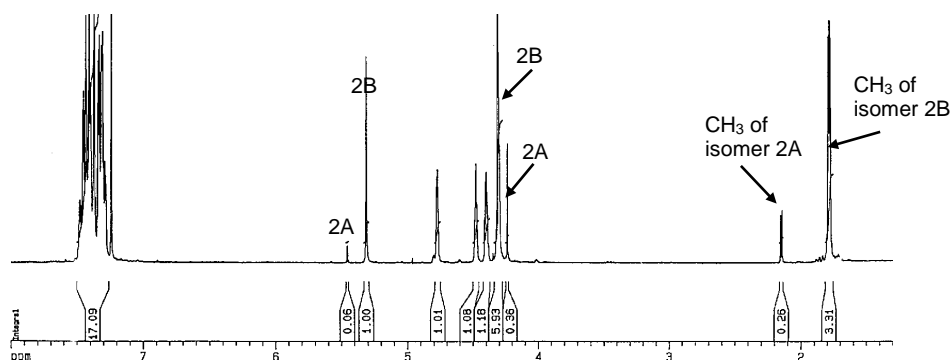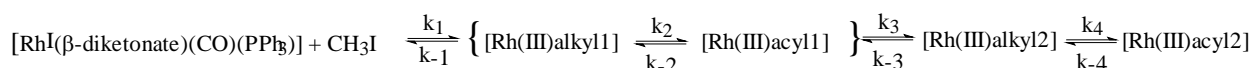
Figure 3.25: ^{1}H NMR spectrum of the previously isolated crystalline Rh(III)-alkyl 2B isomer on which a X-ray structure determination was performed. Upon dissolving the pure solid crystalline Rh(III)-alkyl 2B isomer in CDCl$_3$, slow isomerization to the Rh(III)-alkyl 2A isomer immediately sets in. At the time of the NMR, the equilibrium position of Rh(III)-alkyl 2B : Rh(III)-alkyl 2A = 82:18 has not yet been reached.
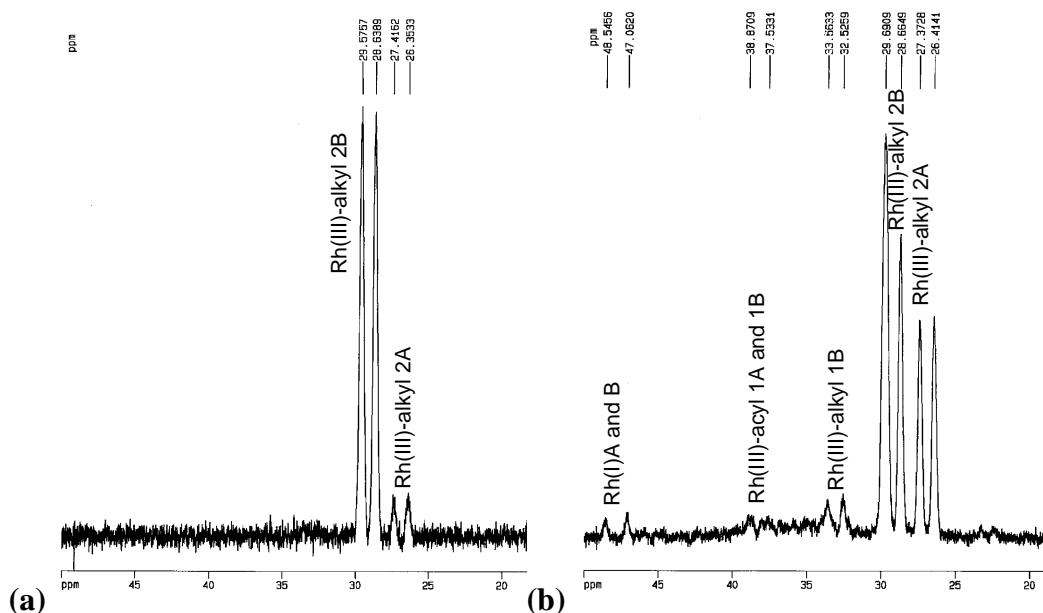
Figure 3.26: ^{31}P NMR spectrum of the isolated crystalline Rh(III)-alkyl 2B isomer (a) 30 min and (b) 4 days after dissolved in CDCl$_3$. Spectrum (a) indicates that upon dissolving the solid crystalline Rh(III)-alkyl 2B isomer in CDCl$_3$ isomerization to the Rh(III)-alkyl 2A isomer sets in. Spectrum (b) showed traces of Rh(I), Rh(III)-alkyl1 and Rh(III) acyl1, indicating that equilibrium between the different species in CDCl$_3$ solution exists if an excess of MeI does not drive the reaction completely to the Rh(III)-alkyl2 or acyl2 end of the mechanism.

(ii)   Kinetics.

The reaction of [Rh(fctfa)(CO)(PPh$_3$)] with CH$_3$I was investigated by ^{1}H NMR spectroscopy in CDCl$_3$ at 25°C with [Rh(fctfa)(CO)(PPh$_3$)] = 0.0183 mol dm^{-3} and [CH$_3$I] = 0.3674 mol dm^{-3}. 0.05% *p*-xylene (per volume CDCl$_3$) was added as internal marker because some of the aromatic peaks of the Rh(III) reaction products overlapped with the CDCl$_3$ peak. By following the change in concentration (proportional to the integration units) of the different reaction species, as identified in **Table 3.11** page 157, with time, the observed reaction rate could be determined. Examples of NMR fragments, illustrating the formation and decrease of identified signals, are given in **Figure 3.27** and **Figure 3.29**. Representative examples of the iu (integration units) *vs.* time graphs for specified signals are given in **Figure 3.28** and a summary of the kinetic rate constants that could be determined for the reaction of [Rh(fctfa)(CO)(PPh$_3$)] with CH$_3$I by ^{1}H NMR spectroscopy, is given in **Table 3.12**.

Table 3.12: Kinetic rate constants of the oxidative addition of MeI to [Rh(fctfa)(PPh$_3$)(CO)], as monitored on ^{1}H NMR in CDCl$_3$ at T = 25°C: (a) for the *first set* of reactions and (b) for the *second and third set* of reactions (on the next page). [Rh(fctfa)(CO)(PPh$_3$)] = 0.0183 mol dm^{-3} and [CH$_3$I] = 0.3674 mol dm^{-3}. Rate constants for proton signals that could not uniquely be identified or kinetically followed are not reported.

reaction	compound	identification	amount H	δ^1H / ppm	k_{obs} / s^{-1}	k_1 / dm^3 mol^{-1}s^{-1}
first	**Rh(I)A** **disappearance**	ferrocene-group of β-diketone ligand	5	3.94	0.0021(1)	-
			2	4.09	0.0016(1)	-
		average second-order rate constant Rh(I)A			0.0019(4)*	0.005(1)
	Rh(I)B **disappearance**	ferrocene-group of β-diketone ligand	5	4.20	0.0019(1)	-
			2	4.83	0.0017(1)	-
		average second-order rate constant Rh(I)B			0.0018(1)	0.0049(3)
		average second-order rate constant for the disappearance of Rh(I)			0.0019(1)	0.005(1)
	Rh(III)-alkyl 1A **appearance**	CH$_3$-group from MeI	3	1.47	0.0033(9)	-
		ferrocene-group of β-diketone ligand	5	4.29	0.0019(3)	-
			2	4.73	0.0022(1)	-
		average second-order rate constant Rh(III)-alkyl 1A			0.0025(7)	0.007(2)
	Rh(III)-alkyl 1B **appearance**	CH$_3$-group from MeI	3	1.42	0.0024(5)	-
		ferrocene-group of β-diketone ligand	5	4.34	0.0021(4)	-
		average second-order rate constant Rh(III)-alkyl 1B			0.0023(2)	0.0063(5)
		average second-order rate constant for the appearance of Rh(III)-alkyl1			0.0024(1)	0.007(1)
	Rh(III)-acyl 1A **appearance**	CH$_3$-group from MeI	3	3.05	0.0023(4)	-
		ferrocene-group of β-diketone ligand	5	4.17	0.0025(4)	-
		methine proton β-diketone ligand	1	6.08	0.0029(6)	-
		average second-order rate constant Rh(III)-acyl1A			0.0026(3)	0.0070(9)
	Rh(III)-acyl 1B **appearance**	CH$_3$-group from MeI	3	2.98	0.0023(3)	-
		ferrocene-group of β-diketone ligand	5	3.94	0.0024(4)	-

		methine proton β-diketone ligand	1	6.08	0.0029(6)	-
		average second-order rate constant Rh(III)-acyl1B			0.0025(3)	0.0068(8)
	average second-order rate constant for the appearance of Rh(III)-acyl1				0.0026(1)	0.007(1)
	average second-order rate constant for the first reaction				**0.0023(4)**	**0.006(1)**

Table 3.12 (b): *second and third set* **of reactions.**

reaction	compound	identification	amount H	δ^1H / ppm	k_{obs} / s^{-1}
second	**Rh(III)-alkyl 1A** **disappearance**	CH_3-group from MeI	3	1.47	0.00013(2)
		ferrocene-group of β-diketone ligand	2	4.73	0.00011(1)
		methine proton β-diketone ligand	1	6.055	0.00012(1)
		average $k_{3\ alkyl\ 2A}$ / s^{-1}			0.00012(1)
	Rh(III)-alkyl 1B **disappearance**	CH_3-group from MeI	3	1.42	0.00012(2)
		ferrocene-group of β-diketone ligand	5	4.34	0.00010(1)
		methine proton β-diketone ligand	1	6.055	0.00012(1)
		average $k_{2\ alkyl\ 1B}$ / s^{-1}			0.00011(1)
	Rh(III)-acyl 1A **disappearance**	CH_3-group from MeI	3	3.05	0.00013(3)
		ferrocene-group of β-diketone ligand	5	4.17	0.00012(2)
		methine proton β-diketone ligand	1	6.08	0.00011(1)
		average $k_{3\ acyl\ 1A}$ / s^{-1}			0.00012(1)
	Rh(III)-acyl 1B **disappearance**	CH_3-group from MeI	3	2.98	0.00012(2)
		ferrocene-group of β-diketone ligand	5	3.94	0.00011(1)
		methine proton β-diketone ligand	1	6.08	0.00011(1)
		average $k_{3\ acyl\ 1B}$ / s^{-1}			0.00011(1)
	Rh(III)-alkyl 2A **appearance**	methine proton β-diketone ligand	1	5.45	0.00011(3)
		average $k_{3\ alkyl\ 2A}$ / s^{-1}			0.00011(3)
	Rh(III)-alkyl 2B **appearance**	CH_3-group from MeI	3	1.78	0.00014(1)
		ferrocene-group of β-diketone ligand	5+1	4.31	0.00011(1)
			1	4.39	0.00010(2)
			1	4.47	0.00011(3)
			1	4.76	0.00010(2)
		methine proton β-diketone ligand	1	5.30	0.00011(1)
		average $k_{3alkyl\ 2B}$ / s^{-1}			0.00011(1)
		average rate constant for the second reaction: k_3 / s^{-1}			**0.00011(1)**
third	**Rh(III)-alkyl 2B** **disappearance**	ferrocene-group of β-diketone ligand	5+1	4.31	0.0000012(4)
			1	4.39	0.000005(5)
			1	4.47	0.0000060(8)
			1	4.76	0.0000059(6)
		methine proton β-diketone ligand	1	5.30	0.0000047(6)
		average k_4 / s^{-1}			0.000005(2)
		average rate constant for the third reaction: k_4 / s^{-1}			**0.000005(2)**

NOTE: Due to the overlapping of the signals of the protons of the ferrocene-group of the β-diketone ligand of the different species, the kinetics of the 2H signals of the ferrocene-group could in general not be followed.

* The standard deviation σ from the average value $\overline{X} = \sum_{i=1}^{n} \frac{X_i}{n}$ for a range of n measured values x_i, is obtained

by: $\sigma = \sqrt{\dfrac{\sum_{i=1}^{n}(x_i - \overline{x})^2}{n-1}}$

(a)

(b)
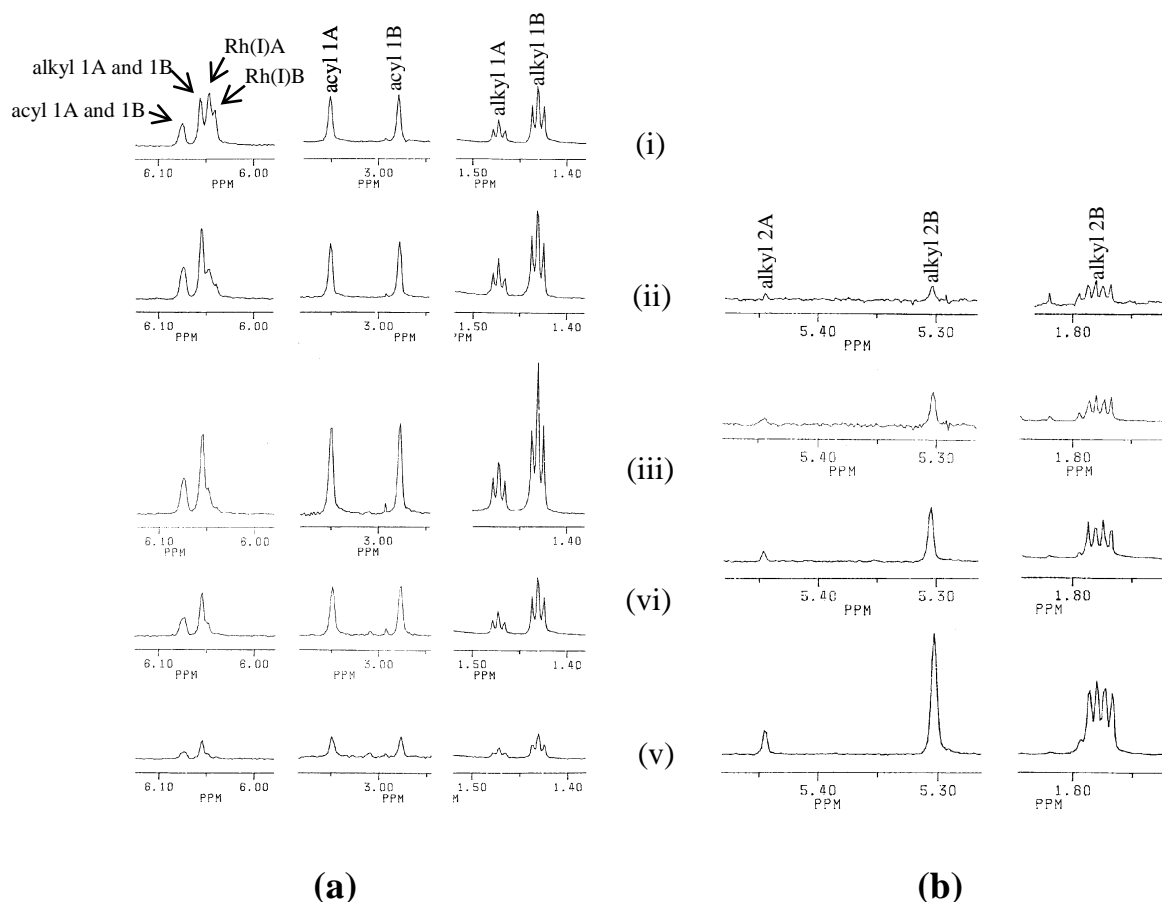
Figure 3.27: Fragments of the ^{1}H NMR spectra in CDCl$_3$ illustrating the reaction sequence during the oxidative addition and the following carbonyl insertion and deinsertion reactions of 0.0183 mol dm^{-3} [Rh(fctfa)(CO)(PPh$_3$)] reacting with 0.3674 mol dm^{-3} CH$_3$I in CDCl$_3$ (T = 25°C) at time (i) t = 380 s, (ii) t = 938 s, (iii) t = 1658 s, (iv) t = 4965 s and (v) t = 26760 s.

(a). The spectra in (a) illustrate the decrease in the signal of the methine proton of the β-diketone ligand of the Rh(I)A and Rh(I)B isomers at 6.045 ppm with the simultaneous formation {(a)(i) to (iii)} and decrease {(a)(iii) to (v)} of the signals of the methine proton of the β-diketone ligand of the alkyl 1A and 1B, as well as the acyl 1A and 1B isomers at 6.04 – 6.08 ppm as indicated in (a)(i). The reaction sequence is also illustrated by the CH$_3$-group of the acyl 1A and 1B isomers at *ca* 3ppm and the alkyl 1A and 1B isomers at *ca* 1.45 ppm.

Note the multiplet of the CH$_3$ group of the Rh(III)-alkyl1 and Rh(III)-alkyl2 isomers is due to coupling with Rh (spin ½) and P (spin ½).

(b). The spectra in (b) illustrate the increase in the signals of the methine proton of the β-diketone ligand of the alkyl 2A and 2B at 5.45 and 5.30 ppm respectively, as well as the increase in the signals of the CH$_3$-group of the alkyl 2B isomer at 1.78 ppm. (Alkyl 2A at 2.15 ppm not shown.)

162
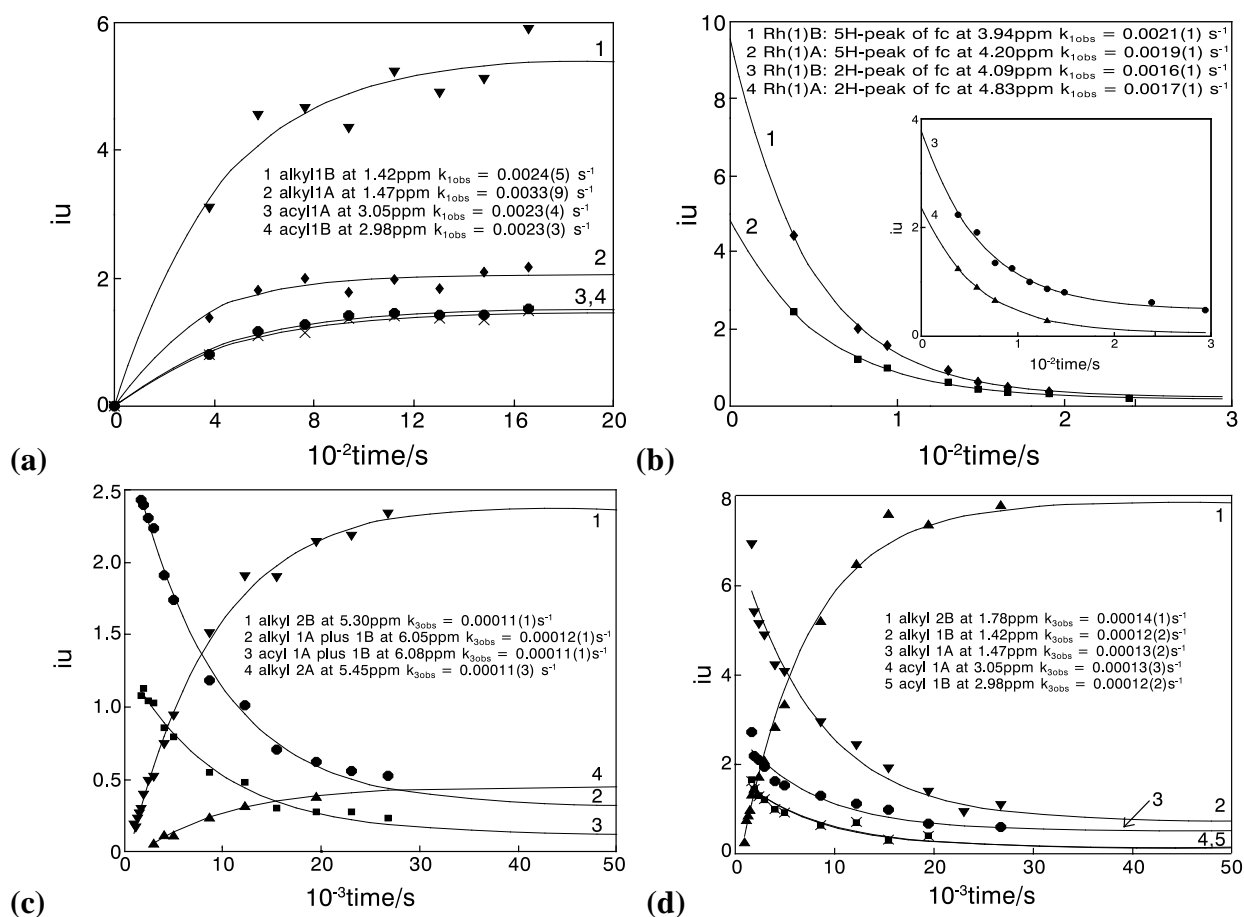
Figure 3.28: Representative examples of the iu (integration units) *vs.* time graphs for specified signals of the oxidative addition of 0.3674 mol dm^{-3} MeI to 0.0183 mol dm^{-3} [Rh(fctfa)(PPh$_3$)(CO)] in CDCl$_3$ as monitored on ^{1}H NMR at T = 25°C. **(a) and (b)** illustrate the reaction sequence of the *first set* of reactions with (a) the signal of the CH$_3$-group and (b) signals of the ferrocene-group of β-diketone ligand of the species as indicated. **(c) and (d)** illustrate the reaction sequence of the *second set* of reactions with (c) the signal of the methine peak of the coordinated β-diketone ligand and (d) the signal of the CH$_3$-group (from oxidatively added MeI) of the species as indicated.
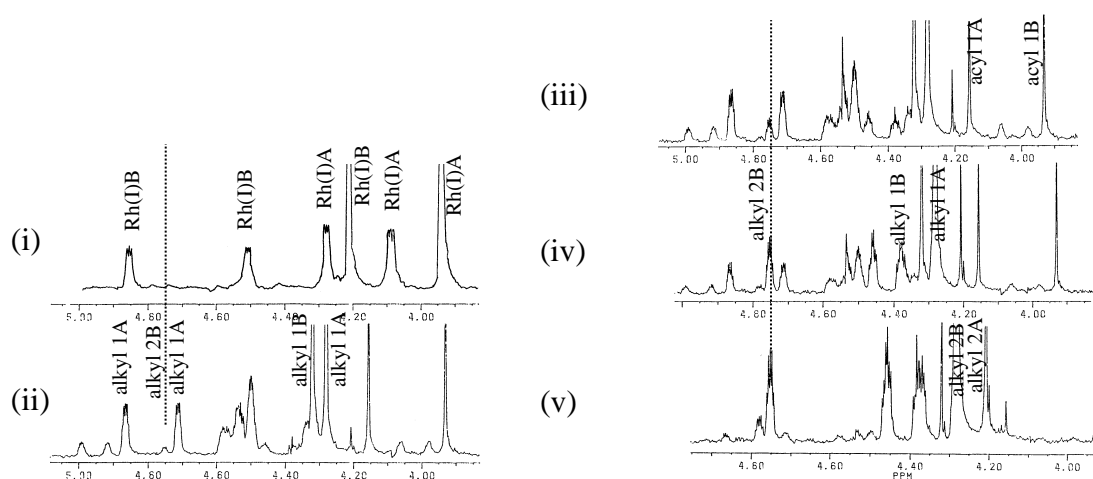
Figure 3.29: ^{1}H NMR spectra in CDCl$_3$ of the signals of the protons of the ferrocene ligand of fctfa coordinated to [Rh(fctfa)(CO)(PPh$_3$)] illustrating the reaction sequence during the oxidative addition and the following carbonyl insertion and deinsertion reactions of 0.02122 mol dm^{-3} [Rh(fctfa)(CO)(PPh$_3$)] reacting with 1.610 mol dm^{-3} CH$_3$I in CDCl$_3$ (T = 25 °C) at relative time (i) t = 0 s, (ii) t = 1155 s, (iii) t = 2800 s, (iv) t = 9790 s and (v) t = 89360 s.

163

The oxidative addition of MeI (0.500 mol dm^{-3}) to [Rh(fctfa)(PPh$_3$)(CO)] (0.021 mol dm^{-3}) was monitored on ^{31}P NMR in CDCl$_3$ at T = 25°C for 19 h. The main aim of this experiment was to identify the reaction products and not to do an accurate kinetic run, because only eight spectra could be taken during the reaction period. Selected ^{31}P NMR spectra, illustrating the reaction sequence, are given in **Figure 3.31**. **Figure 3.30** illustrates the integration units *vs.* time data for the specified signals of the oxidative addition reaction up to 25000 s. The reaction rate for the signals as summarized in **Table 3.13** could be determined. It was not practical to follow the reaction long enough to observe the acyl 2A and 2B products because t$_{1/2}$ of the third reaction was ≈ 43 h.

Table 3.13: Kinetic rate constants of the oxidative addition of 0.500 mol dm^{-3} MeI to 0.021 mol dm^{-3} [Rh(fctfa)(PPh$_3$)(CO)], as monitored on ^{31}P NMR in CDCl$_3$ at T = 25°C.

reaction	signal	δ^{31}P / ppm	k$_{obs}$ / s^{-1}
first	Rh(I)A + (I)B disappearance	48.04	0.0026(5)
	Rh(III)-alkyl 1B appearance	33.23	0.0031(5)
	Rh(III)-alkyl 1A appearance	32.80	-
	Rh(III)-acyl 1A appearance	38.38	0.0028(5)
	Rh(III)-acyl 1B appearance	37.57	0.0028(5)
	average second-order rate constant of the *first set* of reactions k$_1$ / dm^3 mol^{-1}s^{-1}		**0.005(1)**
second	Rh(III)-alkyl 2A appearance	27.09	0.00008(1)
	Rh(III)-alkyl 2B appearance	29.33	0.00014(1)
	Rh(III)-alkyl 1B disappearance	33.23	0.00012(2)
	Rh(III)-acyl 1A disappearance	38.38	0.00012(4)
	Rh(III)-acyl 1B disappearance	37.57	0.00012(4)
	*average k$_3$ / s^{-1}		**0.00012(2)**

* k$_{3obs}$ / s^{-1} for acyl signals inaccurate and not used in calculation of average k$_{3obs}$ / s$^-$
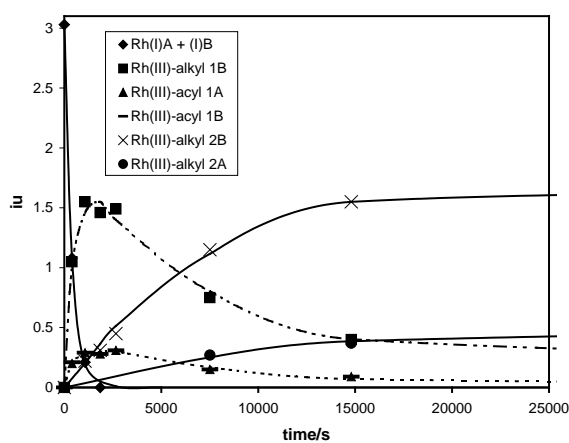
Figure 3.30: Integration units (iu) *vs.* time data for the specified signals of the oxidative addition of 0.500 mol dm^{-3} MeI to 0.021 mol dm^{-3} [Rh(fctfa)(PPh$_3$)(CO)] as monitored on ^{31}P NMR in CDCl$_3$ at T = 25°C.

164

first reactions

second reaction
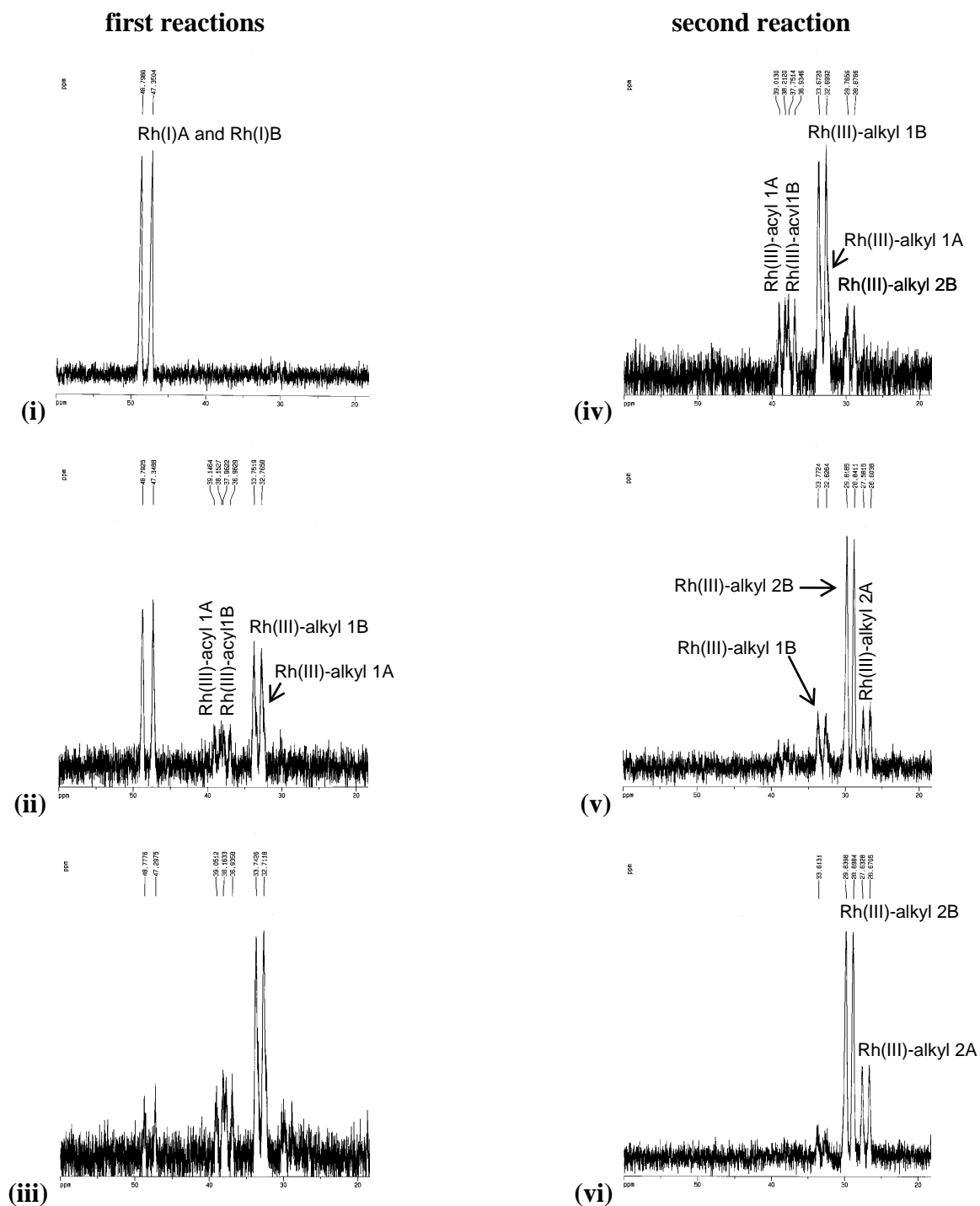
Figure 3.31: Selected ^{31}P NMR spectra illustrating the reaction sequence of the oxidative addition of 0.500 mol dm^{-3} MeI to 0.021 mol dm^{-3} [Rh(fctfa)(PPh$_3$)(CO)] in CDCl$_3$ at T = 25°C at time (i) t = 0, (ii) t = 398 s, (iii) t = 1070 s (towards the end of the *first set* of reactions) (vi) at t = 1849 s, (v) t = 14800 s and (vi) t = 69520 s (near the end of the second reaction).

3.4.3.4 Correlation of the kinetic rate constants of the reaction between CH₃I and [Rh(fctfa)(CO)(PPh₃)] as obtained by various spectroscopic methods.

A reasonable correlation has been obtained for the kinetic rate constants of the oxidative addition and the following carbonylation and decarbonylation reactions between CH₃I and [Rh(fctfa)(CO)(PPh₃)] as determined from data obtained by various spectroscopic methods (**Table 3.14**).

Table 3.14: The kinetic rate constants of the oxidative addition reaction between CH₃I and [Rh(fctfa)(CO)(PPh₃)] as obtained by various spectroscopic methods in chloroform at 25°C. k_1, k_3 and k_4 **are the rate constants associated with the *first, second and third stages* of the reaction of MeI to [Rh(fctfa)(CO)(PPh₃)].**

Method	k_1/dm^{3}mol^{-1}s^{-1}	k_{-1}/s^{-1}	k_3/s^{-1}	k_4/s^{-1}
IR	0.0061(2)	0.0006(2)	0.00017(1)	0.0000047(4)
UV/visible	0.00611(1)	0.0005(1)	0.00017(2)	0.0000044(1)
^{1}H NMR	0.006(1)	**	0.00011(1)	0.000005(2)
^{31}P NMR	0.005(1)	**	0.00012(2)	**

** not determined

3.4.4 *The reaction between iodomethane and [Rh(fca)(CO)(PPh₃)]*

3.4.4.1 The infrared monitored reaction between CH₃I and [Rh(fca)(CO)(PPh₃)].

The reaction sequence of the reaction between [Rh(fca)(CO)(PPh₃)] and iodomethane, with chloroform as reaction medium, in the range 1690 – 2140 cm^{-1} as monitored by infrared spectroscopy, T = 25 ºC, is illustrated in **Figure 3.32** page 168.   **Figure 3.32**(a) shows the disappearance of the Rh(I)-carbonyl complex (signal at 1983 cm^{-1}, in CHCl₃ containing 0.0517 mol dm^{-3} CH₃I; k_{obs} = 0.00382(5) s^{-1}) with the simultaneous formation of the Rh(III)-alkyl1 species (k_{obs} = 0.0056(2) s^{-1}, peak at 2077 cm^{-1}) followed by the formation of the Rh(III)-acyl1 complex at 1719 cm^{-1} at a slower rate (k_{obs} = 0.0018(2) s^{-1}). Utilizing the results of **Figure 3.33**, page 169, graphical extrapolation to [CH₃I] = 1.673 mol dm^{-3} gives k_{obs} for Rh(I) disappearance ±0.11 s^{-1} with a halflive of ±6 s. This implies that Rh(I) undergoes oxidative addition in the [Rh(fca)(CO)(PPh₃)] complex approximately ten times faster than in the [Rh(fctfa)(CO)(PPh₃)] complex (k_{obs} = 0.011 s^{-1}) under the corresponding concentration conditions described on page

142. Probably the most valid explanation for the 46% discrepancy between k_{obs} for Rh(I) disappearance and k_{obs} for Rh(III)-alkyl1 appearance, may be found in the lack of enough data points to determine the rate constants more accurately. Similar drifts (or errors) were observed during the treatment of data using consecutive kinetics, as described on page 148. The CH_3I concentration dependence of k_{obs} for the case of the *first set* of reactions in chloroform is illustrated graphically in **Figure 3.33** page 168. Unlike what was observed for the oxidative addition of MeI to [Rh(fctfa)(CO)(PPh₃)] in chloroform (in paragraph 3.4.3.1 page 142), this graph for the [Rh(fca)(CO)(PPh₃)] complex, passes through the origin, indicating $k_{-1} \approx 0$. The observed rate of formation of Rh(III)-acyl1 was also ±47% of the rate of Rh(I) disappearance. While a lack of sufficient data points may also be the reason for this discrepancy, the observed slower rate of Rh(III)-acyl1 appearance is considered to be real and not a mathematical artifact. This would imply that the equilibrium involving the k_2 and k_{-2} steps in **Reaction scheme 3.2**, page 143,

$$[Rh^I(\beta\text{-diketonate})(CO)(PPh_3)] + CH_3I \underset{k_{-1}\sim 0}{\xrightarrow{k_1}} \left[Rh(III)\text{-alkyl1} \underset{k_{-2}}{\overset{\overset{\textit{slow equilibrium}}{k_2}}{\rightleftharpoons}} Rh(III)\text{-acyl1} \right]$$
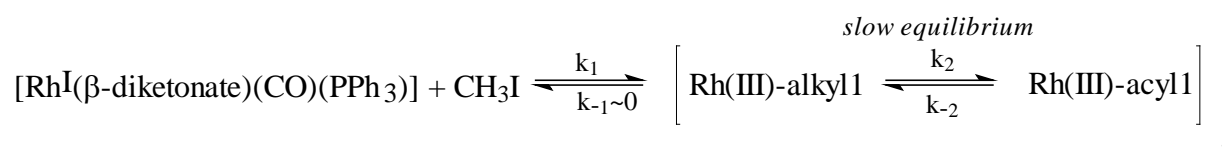
is to slow to be maintained during the oxidative addition of CH_3I to [Rh(fca)(CO)(PPh₃)]. This is in contrast to what was found for the corresponding oxidative addition steps for the [Rh(fctfa)(CO)(PPh₃)] complex. It should be noted that Rh(III)-alkyl1 formation is at least ten times faster ($k_{obs} = 0.066 - 0.100$ mol dm⁻³ s⁻¹) in the [Rh(fca)(CO)(PPh₃)] compared to the [Rh(fctfa)(CO)(PPh₃)] complex ($k_{obs} = 0.006$ mol dm⁻³ s⁻¹) which puts the observation that the k_2/k_{-2} equilibrium is to slow to be maintained during the *first set* of reactions in the [Rh(fca)(CO)(PPh₃)] complex in perspective. A similar slow equilibrium was found for the [Rh(bfcm)(CO)(PPh₃)] and [Rh(dfcm)(CO)(PPh₃)] complexes and will be described later (paragraphs 3.4.5.1 and 3.4.6.1). The observed data relating to reaction step one are given in **Table 3.15** page 169.

The *second*, much slower ($t_{1/2} \approx 4$ h), *set* of reactions as observed on the IR is illustrated in **Figure 3.32** (b). Here the Rh(III)-alkyl1 species at 2077 and the Rh(III)-acyl1 species at 1719 cm⁻¹ started to disappear at the same rate ($k_{obs} = 0.000044(2)$ s⁻¹ and $0.00005(1)$ s⁻¹) with the simultaneous formation of the Rh(III)-alkyl2 species, also at the same rate, ($k_{obs} = 0.000071(4)$ s⁻¹) at 2059 cm⁻¹. This observation, that the Rh(III)-alkyl1 species disappears at the same rate as the Rh(III)-acyl1 species, supplies further evidence that there exists an equilibrium between these

two species. Note that although the *first set* of reactions is approximately ten times faster in the [Rh(fca)(CO)(PPh₃)] complex compared to the [Rh(fctfa)(CO)(PPh₃)] complex, the *second set* of reactions is almost two times slower (**Table 3.29** page 187). Since the *second set* of reactions is much slower than the *first set* of reactions, the data of the *second set* of reactions for determining the rate constant, could be treated in isolation. The kinetic data of the second reaction are consistent with **Reaction scheme 3.3** page 144.

$$\left[\text{Rh(III)-alkyl1} \; \underset{K_2}{\overset{}{\rightleftharpoons}} \; \text{Rh(III)-acyl1} \right] \; \xrightarrow{k_3} \; \text{Rh(III)-alkyl2}$$
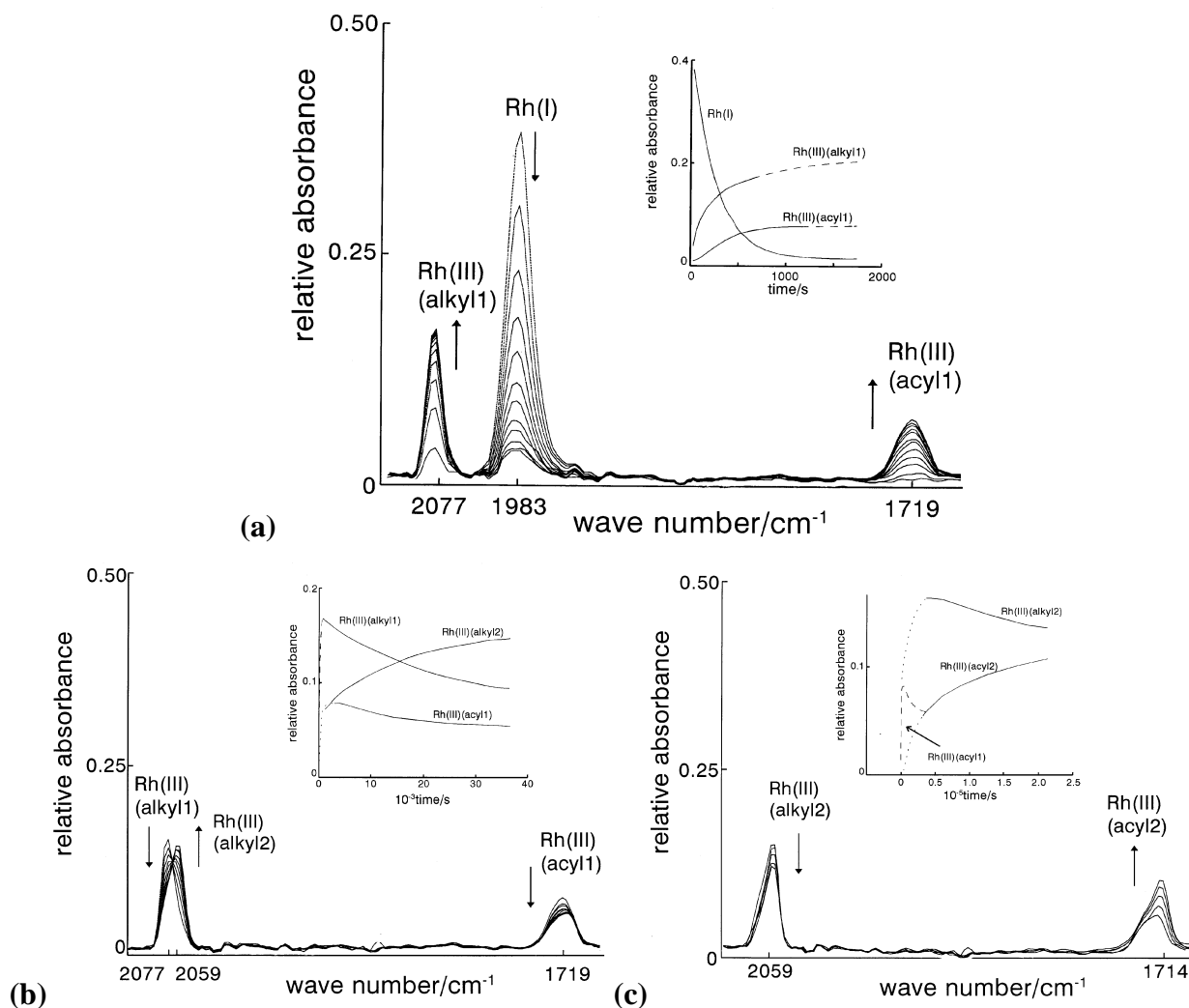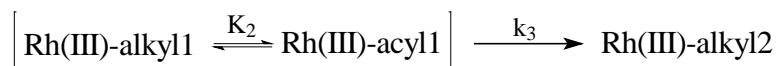
Figure 3.32: Infrared monitoring of the oxidative addition reaction between CH₃I (0.0517 mol dm⁻³) and [Rh(fca)(CO)(PPh₃)] (0.0068 mol dm⁻³) in chloroform (T = 25 ⁰C). The inserts give the absorbance *vs.* time data of the indicated species.

(a) The *first set* of reactions illustrated at time t = 28, 96, 164, 231, 300, 370, 439, 509, 578, 653, 722 and 790 s.

(b) The *second set* of reactions illustrated at t = 3874, 7200, 11033, 14434, 18223, 22295, 25895, 29476 and 34061 s.

(c) The *third set* of reactions illustrated at t = 36631, 85980, 125548, 169423 and 213231 s.

The *third*, very slow (t$_{1/2}$ ≈ 48 h), *set* of reactions illustrated in **Figure 3.32** (c) includes the slow disappearance of the Rh(III)-alkyl2 species (k$_{obs}$ = 0.000005(2) s^{-1}) at 2059 cm^{-1} and the appearance at the same rate of a new Rh(III)-acyl2 species at 1714 cm^{-1} (k$_{obs}$ = 0.000003(1) s^{-1}). The long half-life of this reaction implied that it could not be followed with great accuracy due to, for example, evaporation problems of the solvent. The kinetic data of the third reaction are consistent with **Reaction scheme 3.4** page 144.
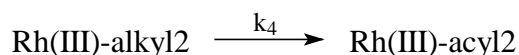
$$\text{Rh(III)-alkyl2} \xrightarrow{\ k_4\ } \text{Rh(III)-acyl2}$$

The reaction rates for the infrared monitored oxidative addition reaction between CH$_3$I and [Rh(fca)(CO)(PPh$_3$)] in chloroform at 25 °C (as well as the following carbonyl insertion and decarbonylation reactions), as obtained from *different* concentrations CH$_3$I (0.05 – 0.35 mol dm^{-3}), are summarized in **Table 3.15**. The overall reaction sequence for the oxidative addition reaction of MeI to [Rh(fca)(CO)(PPh$_3$)] is consistent with **Reaction scheme 3.5** (page 144) proposed for the oxidative addition of [Rh(fctfa)(CO)(PPh$_3$)]. The only difference is that the k$_{-1}$ step in the *first reaction set* is non observable and that the equilibrium involving the k$_2$ and k$_{-2}$ steps are slow in comparison with [Rh(fctfa)(CO)(PPh$_3$)].
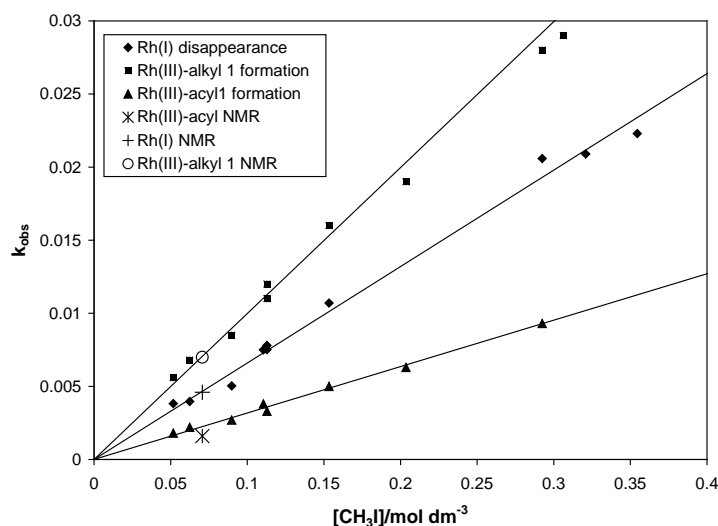
Figure 3.33: k$_{obs}$ for the *first set* of reactions as a function of CH$_3$I concentration for the oxidative addition reaction between CH$_3$I and [Rh(fca)(CO)(PPh$_3$)] in chloroform as monitored on the infrared spectrophotometer (T = 25 °C). The second-order rate constant for disappearance of the Rh(I)-carbonyl complex (k$_1$ = 0.066(2) dm^3 mol^{-1} s^{-1}) and the formation of the Rh(III)-alkyl1 species (k$_1$ = 0.100(3) dm^3 mol^{-1} s^{-1}) are followed by the formation of the Rh(III)-acyl1 complex at a slower rate (k$_1$ = 0.032(1) dm^3 mol^{-1} s^{-1}). The observed rate constant for the different species as observed on ^{1}H NMR at [MeI] = 0.0707 mol dm^{-3} are also shown (paragraph 3.4.4.3 page 171, Table 3.18).

Table 3.15: Kinetic rate constants for the oxidative addition of MeI to [Rh(fca)(PPh₃)(CO)] in chloroform at 25.0(1) °C (IR monitored). The species that were monitored to obtain the individual rate constants are indicated in the headings.

First set of reactions			
Complex	**Rh(I) disappearance**	**Rh(III)-alkyl1 formation**	**Rh(III)-acyl1 formation***
	k_1/dm³mol⁻¹s⁻¹	k_1/dm³mol⁻¹s⁻¹	k_1'/dm³mol⁻¹s⁻¹
[Rh(fca)(PPh₃)(CO)]	0.066(2)	0.100(3)	0.032(1)
Second set of reactions (k_3/s⁻¹)			
	Rh(III)-alkyl1 disappearance	**Rh(III)-acyl1 disappearance**	**Rh(III)-alkyl2 formation**
[Rh(fca)(PPh₃)(CO)]	0.00010(1)	0.00009(1)	0.00008(1)
Third set of reactions (k_4/s⁻¹)			
	Rh(III)-alkyl2 disappearance	**Rh(III)-acyl2 formation**	
[Rh(fca)(PPh₃)(CO)]	0.000007(5)**	0.000002(1)**	

* k_1' relating to the formation of Rh(III)-acyl1 was not labelled k_1 since the equilibrium K_2 is not fast enough to be maintained completely during the disappearance of Rh(I). It was not labelled k_2 because the rate constant does not distinguish between the relative concentrations of Rh(I), Rh(III)-alkyl1 and Rh(III)-acyl1 while the equilibrium is set up.

** Inaccurate because of the slowness of the reaction ($t_{1/2} \approx 48$ hours).

3.4.4.2   The UV monitored reaction between CH₃I and [Rh(fca)(CO)(PPh₃)].

The oxidative addition reaction between CH₃I and [Rh(fca)(CO)(PPh₃)] in chloroform monitored on UV/visible spectrophotometer also indicated three separate reaction steps which are in accordance with the IR results. All three reactions could be followed at 493 nm. The second reaction, however, underwent a small change in absorbance at 493 nm (due to the influence of the third reaction) as opposed to the large change in absorbance at 410 nm. The method of biphasic kinetics[34] was used to calculate the rate constant for the second reaction at 493 nm, giving $k_3 = 0.00008(1)$ s⁻¹, which is consistent with the value $k_3 = 0.000087(1)$ s⁻¹ determined at 410 nm. k_3 at 410 nm was determined by treating the data for the second reaction in isolation. Reliable k_3 values could be determined at 410 nm, because of the large change in absorbance for the second reaction at this wavelength, the small change in absorbance for the third reaction and because the first step is more than 70 times slower than the rate of the second reaction steps.

Figure 3.34 (b) illustrates the method of biphasic kinetics to obtain the rate constant of the first reaction, k_{1obs}, at 410 nm. The linear portion of the plot $\ln(A_t-A1)$ *vs.* time of **Figure 3.34** (b) gives rate constants for the second stage (k_3). The intercept x and slope k_3 allowed the modified plot of $\ln(A1-A_t+x\exp(-k_3t))$ *vs.* time, t, to be carried out (insert in **Figure 3.34** (b)), the slope

yielding rate constant k_{1obs} for the first stage (A_t = absorbance at time t, A1 = absorbance at t = ∞). k_{1obs} determined this way, resulted in 0.0066(1) s^{-1}, which is similar to the value of 0.00615(1) s^{-1} determined for k_{1obs} at 493 nm, by treating the kinetic data at 493 nm in isolation. The small change in absorbance of the second reaction at 493 nm makes this wavelength particularly suitable to determine reliable k_{1obs} values. The method of biphasic kinetics is suitable for two consecutive reactions where the change in absorbance of the second reaction influences the absorbance of the first reaction, with the rate constant of the first reaction at least four times the rate constant of the second reaction.

Temperature and MeI concentration dependence of the oxidative addition reaction between CH$_3$I and [Rh(fca)(CO)(PPh$_3$)], as well as the following carbonyl insertion and decarbonylation reactions, as monitored on the UV/VIS spectrophotometer in chloroform, are given in **Figure 3.35** and summarized in **Table 3.16**.

(a)   **(b)**
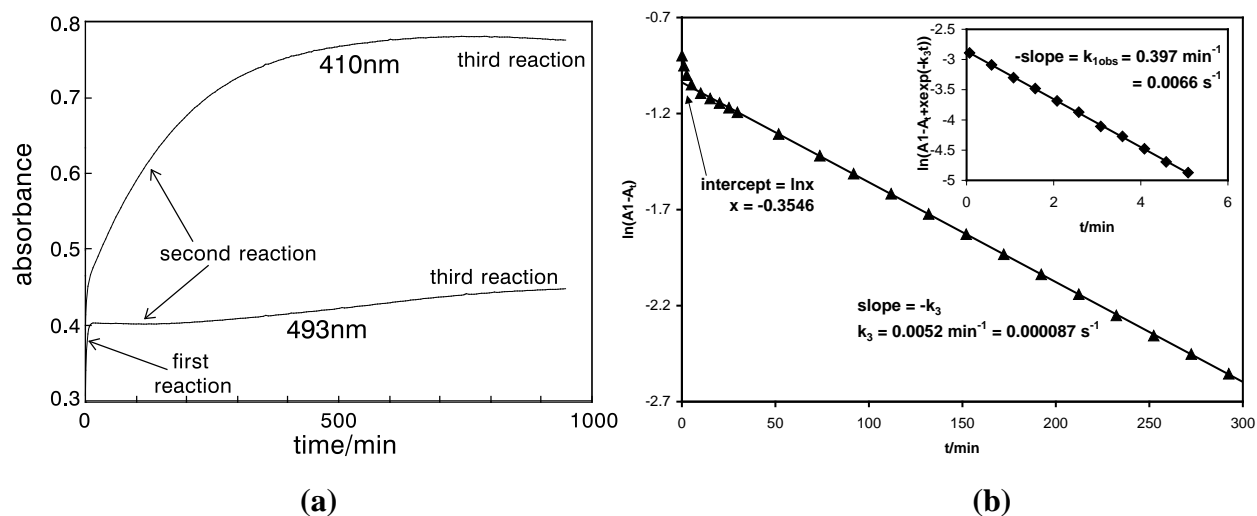
Figure 3.34: **(a) Absorbance *vs*. time data of the UV monitoring of the reaction between 0.0004 mol dm^{-3} [Rh(fca)(CO)(PPh$_3$)] and 0.0942 mol dm^{-3} MeI at 493 and 410 nm. By treating the kinetic data of the different reaction steps in isolation, the following rate constants were obtained: k_{1obs} (493 nm) = 0.00615(1) s^{-1}, k_3 (410 nm) = 0.000087(1) s^{-1}, k_4 (493 nm) = 0.0000073(8) s^{-1}. (b) Illustration of the method of biphasic kinetics at 410 nm. Kinetic plots from absorbance readings illustrating the first two phases of the reaction at 410 nm. The rate constant k_3 (410 nm) = 0.000087(1) s^{-1} was obtained from the slope of the linear portion of the lower graph. Using the y-axis intercept (lnx) and k_3, the top plot in the insert gives k_{1obs} (410 nm biphasic) = 0.0066(1) s^{-1}, which is similar to k_{1obs} (493 nm) = 0.00615(1) s^{-1}.**

---

[34] Swarts, J.C. and Sykes, A.G., *Anti-Cancer Drug Design*, **9**, 41 (1994).
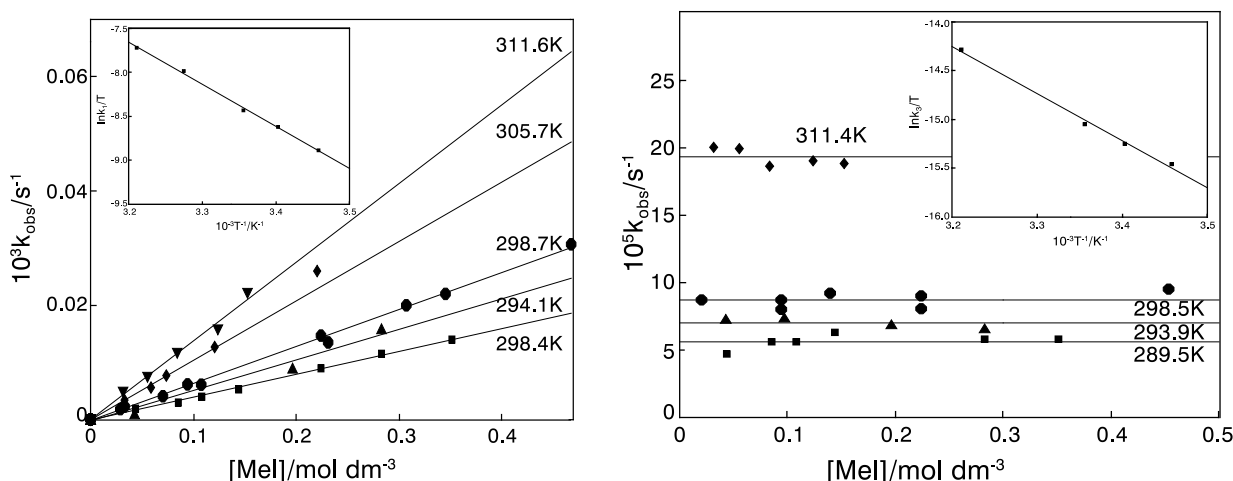
Figure 3.35: Temperature and MeI concentration dependence of the oxidative addition reaction of CH_3I to $[Rh(fca)(CO)(PPh_3)]$ as monitored on the UV/VIS spectrophotometer in chloroform (a) at 493 nm for the first reaction and (b) at 410 nm for the second reaction $\{[Rh(III)\text{-}alkyl1 \square Rh(III)\text{-}acyl1] \rightarrow Rh(III)\text{-}alkyl2\}$. Data of k_2 at 25.5° were also obtained at 493nm.

Table 3.16: Selected temperature dependent kinetic rate constants and activation parameters for the oxidative addition of MeI to $[Rh(fca)(PPh_3)(CO)]$, as monitored on the UV/visible spectrophotometer in chloroform and acetone. Data for all the reactions were obtained at 493 nm. The second reaction was also monitored at 410 nm and the third reaction was also followed at 525 nm.

Solvent	ε^*	T / °C	k_1/ $dm^3mol^{-1}s^{-1}$	$\Delta H^*(k_1)$ / $kJ\ mol^{-1}$	$\Delta S^*(k_1)$ /$J\ mol^{-1}$ K^{-1}	k_3/s^{-1}	$\Delta H^*(k_3)$ / $kJ\ mol^{-1}$	$\Delta S^*(k_3)$ /$J\ mol^{-1}$ K^{-1}	k_4/s^{-1}
chloroform	4.81	16.2	0.040(1)	40(2)	-133(5)	0.000056(4)	41.7(2)	-183(7)	-
		20.9	0.053(4)			0.000070(1)			-
		25.5	0.065(1)			0.000087(2)			0.0000077(5)
		32.5	0.104(2)			-			-
		38.4	0.138(4)			0.000193(2)			-
acetone	20.7	25.0	0.0455(6)	-	-	0.000050(5)	-	-	-

* dielectric constant.

3.4.4.3 The ^1H and ^{31}P NMR monitored reaction between CH_3I and $[Rh(fca)(CO)(PPh_3)]$.

The reactions between CH_3I and $[Rh(fca)(CO)(PPh_3)]$ were monitored by ^1H and ^{31}P NMR. As in the case of the ^1H NMR monitored oxidative addition of CH_3I to $[Rh(fctfa)(CO)(PPh_3)]$, the two $[Rh^I(fca)(CO)(PPh_3)]$ isomers {referred to as Rh(I)A and Rh(I)B, the choice of the labels is arbitrary and has no significance} reacted with CH_3I to form at least two isomers of the Rh(III)-alkyl1 product {referred to as Rh(III)-alkyl 1A and Rh(IIII)-alkyl 1B} which underwent a CO insertion reaction to form two isomers of the Rh(III)-acyl1 product {referred to as Rh(III)-acyl 1A and Rh(IIII)-acyl 1B}. As observed on IR and UV, the Rh(III)-acyl1 isomers formed at a

slower rate than the Rh(III)-alkyl1 isomers. This also pionts towards a slow equilibrium for the k_2 and k_{-2} steps . This *first set of reactions* is fully consistent with IR and UV results and can also be described by **Reaction scheme 3.7** page 156. The *second and third sets* of reactions observed on NMR, are also fully consistent with IR and UV results. The only difference is that at least two isomers were observed on ^{1}H NMR for each reaction species, similar to what was observed for oxidative addition of CH_3I to $[Rh(fctfa)(CO)(PPh_3)]$. The *second and third sets* of reactions observed on NMR can, therefore, also be described by **Reaction scheme 3.8** and **Reaction scheme 3.9** page 156. It was possible to follow the third reaction on ^{1}H NMR long enough to determine rate constants for the formation of the acyl2 species. Selected ^{1}H NMR spectra of the formation and disappearance of the signals of the CH_3-acyl group are illustrated in **Figure 3.36**.

The main aim of the ^{31}P NMR experiment was to identify the reaction products (see **Figure 3.37**) and not to do an accurate kinetic run. The rate constants, as obtained from kinetic runs on the NMR, are given in **Table 3.18** and **Table 3.19**, and compare reasonably well with rate constants as obtained by IR and UV/visible studies as summarized in **Table 3.20** page 176. The A and B isomers of each species (*e.g.* acyl 1A and acyl 1B) were found to exist in a fast equilibrium with each other for the same reasons as described on page 156. The ^{1}H and ^{31}P spectral parameters of the different isomers that could be identified are given in **Table 3.17**.

Table 3.17: ^{1}H and ^{31}P NMR spectral parameters of the different isomeric forms of [Rh(fca)(CO)(PPh₃)] and the Rh(III) complexes formed during the oxidative addition reaction of [Rh(fca)(CO)(PPh₃)] with MeI. K_c = [RhB-species]/[RhA-species].

compound	K_c	^{31}P NMR δ^{31}P /ppm	^{1}J(PRh) /Hz	Ratio isomers on ^{31}P NMR	^{1}H NMR Ratio isomers on ^{1}H NMR	δ^1H methine proton β-diketone ligand /ppm	δ^1H CH₃ group β-diketone ligand /ppm	δ^1H CH₃ group from MeI /ppm	δ^1H ferrocene-group β-diketone ligand /ppm 5H	2H	2H
Rh(I)A	0.22	47.53	174.0	80%	82%	5.78	2.21	-	3.90	4.08	4.16
Rh(I)B		49.05	193.9	20%	18%	5.73	1.70	-	4.195	4.38	4.80
Rh(III)-alkyl 1A	0.52	30.10	125	69%	66%	5.83	*	1.495	4.27	*	*
Rh(III)-alkyl 1B		33.31	120	31%	34%	5.83	*	1.42	4.33	*	*
Rh(III)-acyl 1A	2.13	38.17	180	31%	32%	5.72	1.73	3.09	4.17	*	*
Rh(III)-acyl 1B		36.82	160	69%	68%	5.77	2.05	2.99	3.90	*	*
Rh(III)-alkyl 2A	0.82	28.34	128	-	55%	5.19	*	*	4.32	*	*
Rh(III)-alkyl 2B		#	#	-	45%	5.19	*	1.65	4.21	*	*
Rh(III)-acyl 2A	1.50	#	#	-	40%	*	*	3.03	4.02	*	*
Rh(III)-acyl 2B		#	#	-	60%	*	*	3.00		*	*

* positions could not be uniquely identified due to overlapping of proton signals of the ferrocene ligand with each other, or overlapping with the signal of free MeI. **#** peaks not observed because reaction could not be followed long enough on ^{31}P NMR.
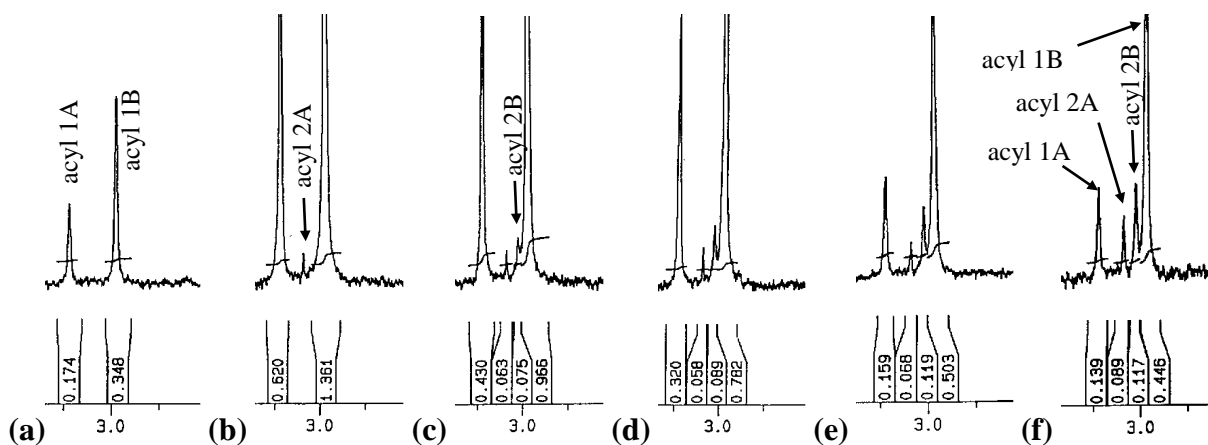
Figure 3.36: The CH₃ ¹H NMR peak in CDCl₃ illustrates the reaction sequence of the different *acyl species* during the oxidative addition and the following carbonyl insertion and deinsertion reactions of 0.01918 mol dm⁻³ [Rh(fca)(CO)(PPh₃)] reacting with 0.2034 mol dm⁻³ CH₃I in CDCl₃ (T = 25°C) at time (a) t = 96.5 s, (b) t = 1512.5 s, (c) t = 13824 s, (d) t = 26254 s (e) t = 100054 s and (f) t = 187549 s.

Table 3.18: Kinetic rate constants of the oxidative addition of MeI to [Rh(fca)(PPh₃)(CO)], as monitored on ¹H NMR in CDCl₃ at T = 25°C.(a) for the *first set* of reactions and (b) for the *second and third set* of reactions. [Rh(fca)(CO)(PPh₃)] = 0.01918 mol dm⁻³ when [CH₃I] = 0.2034 mol dm⁻³ and 0.01208 mol dm⁻³ when [CH₃I] = 0.0707 mol dm⁻³.   (a): *First set* of reactions.

reaction	compound	identification	amount H	δ^1H / ppm	k_{obs} / s⁻¹ for [MeI]/mol dm⁻³ 0.0707	k_{obs} / s⁻¹ for [MeI]/mol dm⁻³ 0.2034
first	**Rh(I)A disappearance**	ferrocene-group of β-diketone ligand	5	3.90	0.0043(2)	0.014#
			2	4.08	0.0045(3)	0.011#
			2	4.16	0.0042(1)	0.011#
		methine proton β-diketone ligand	1	5.78	0.0046(1)	-
		average k₁obs Rh(I)A / s⁻¹			0.0044(2)	0.012(2)
		k₁ Rh(I)A / dm³ mol⁻¹s⁻¹			0.0062(3)	0.059(9)
	Rh(I)B disappearance	CH₃-group of β-diketone ligand	3	1.70	0.0046(1)	0.011#
		ferrocene-group of β-diketone ligand	5	4.19	0.0052(2)	0.013#
			2	4.80	0.0045(5)	0.010#
		average k₁obs Rh(I)B / s⁻¹			0.0048(4)	0.011(2)
		k₁ Rh(I)B / dm³ mol⁻¹s⁻¹			0.068(6)	0.056(5)
		average rate constant for Rh(I) disappearance k₁ / dm³ mol⁻¹s⁻¹			**0.061(3)**	
	Rh(III)-alkyl 1A appearance	CH₃-group from MeI	3	1.495	0.0083(6)	0.015(4)
		ferrocene-group of β-diketone ligand	5	4.27	0.0069(4)	0.022(7)
		methine proton β-diketone ligand	1	5.83	0.0043(4)	0.012(2)
		average k_obs alkyl 1A / s⁻¹			0.007(2)	0.016(5)
	Rh(III)-alkyl 1B appearance	CH₃-group from MeI	3	1.42	0.0054(4)	0.012(4)
		ferrocene-group of β-diketone ligand	5	4.33	0.0084(7)	0.018(6)
		average k_obs alkyl 1B / s⁻¹			0.007(2)	0.015(4)
	Rh(III)-acyl 1A appearance	CH₃-group of β-diketone ligand	3	1.73	0.0014(1)	0.0029(4)
		CH₃-group from MeI	3	3.09	0.0015(1)	0.0028(2)
		ferrocene-group of β-diketone ligand	5	4.17	0.0014(1)	0.0026(6)
		methine proton β-diketone ligand	1	5.72	0.0014(2)	0.0022(4)
		average k_obs acyl 1A / s⁻¹			0.0014(1)	0.0026(4)
	Rh(III)-acyl 1B appearance	CH₃-group from MeI	3	2.99	0.0016(1)	0.0021(2)
		ferrocene-group of β-diketone ligand	5	3.90	0.0017(2)	0.0033(2)
		average k_obs acyl 1B / s⁻¹			0.0016(1)	0.0027(8)

Table 3.18 (b): *Second and third set* **of reactions.**

reaction	compound	identification	amount H	δ^1H / ppm	k_{obs} / s^{-1} for 0.2034 mol dm^{-3} MeI
second	**Rh(III)-alkyl 1A disappearance**	CH$_3$-group from MeI	3	1.495	0.000039(3)
		ferrocene-group of β-diketone ligand	5	4.27	0.000036(7)
		methine proton β-diketone ligand	1	5.83	0.000037(4)
		average k$_{3obs\ alkyl\ 1A}$ / s^{-1}			0.000037(1)
	Rh(III)-alkyl 1B disappearance	CH$_3$-group from MeI	3	1.42	0.000032(3)
		ferrocene-group of β-diketone ligand	5	4.33	0.00005(1)
		average k$_{3obs\ alkyl\ 1B}$ / s^{-1}			0.00004(1)
	Rh(III)-acyl 1A disappearance	CH$_3$-group of β-diketone ligand	3	1.73	0.000060(7)
		CH$_3$-group from MeI	3	3.09	0.000039(3)
		ferrocene-group of β-diketone ligand	5	4.17	0.000040(7)
		methine proton β-diketone ligand	1	5.72	0.000034(7)
		average k$_{3obs\ acyl\ 1A}$ / s^{-1}			0.00004(1)
	Rh(III)-acyl 1B disappearance	CH$_3$-group from MeI	3	2.99	0.000034(4)
		ferrocene-group of β-diketone ligand	5	3.90	0.000039(2)
		methine proton β-diketone ligand	1	5.77	0.000040(1)
		average k$_{3obs\ acyl\ 1B}$ / s^{-1}			0.000038(3)
	Rh(III)-alkyl 2A appearance	ferrocene-group of β-diketone ligand	5	4.32	0.000061(5)
		methine proton β-diketone ligand	1	5.19	0.000055(2)
		average k$_{3obs\ alkyl\ 2A}$ / s^{-1}			0.000058(4)
	Rh(III)-alkyl 2B appearance	CH$_3$-group from MeI	3	1.65	0.000064(6)
		ferrocene-group of β-diketone ligand	5	4.21	0.000050(3)
		methine proton β-diketone ligand	1	5.19	0.000055(2)
		average k$_{3obs\ alkyl\ 2B}$ / s^{-1}			0.000056(6)
		average rate constant for second reaction k$_3$			**0.00005(1)**
third	**Rh(III)-alkyl 2A disappearance**	ferrocene-group of β-diketone ligand	5	4.32	0.000001(2)*
		average k$_{4obs\ alkyl\ 2A}$ / s^{-1}			-
	Rh(III)-alkyl 2B disappearance	CH$_3$-group from MeI	3	1.65	0.000001(4)*
		ferrocene-group of β-diketone ligand	5	4.21	0.0000012(8)*
		methine proton β-diketone ligand	1	5.19	0.0000050(1)
		average k$_{4obs\ alkyl\ 2B}$ / s^{-1}			0.0000050(1)
	Rh(III)-acyl 2A appearance	CH$_3$-group of β-diketone ligand	3	5.98	0.000006(1)
		CH$_3$-group from MeI	3	3.03	0.0000043(9)
		ferrocene-group of β-diketone ligand	5	4.02	0.000005(1)
		average k$_{4obs\ acyl\ 2A}$ / s^{-1}			0.000005(1)
	Rh(III)-acyl 2B appearance	CH$_3$-group of β-diketone ligand	3	5.90	0.000008(1)
		CH$_3$-group from MeI	3	3.00	0.000008(1)
		average k$_{4obs\ acyl\ 2B}$ / s^{-1}			0.000008(1)
		average rate constant for third reaction average k$_4$			**0.000006(2)**

NOTE: Due to the overlapping of the signals of the ferrocene-group of the β-diketone ligand of the different species, the kinetics of the 2H signals of the ferrocene-group was not followed. Most of the signals of the CH$_3$-group of β-diketone ligand of the different alkyl species overlapped with the signal of free MeI and the kinetics of these signals could therefore also not be followed.

* Values too inaccurate to use for average

No standard deviation, because k$_{obs}$ was obtained from only three data points.
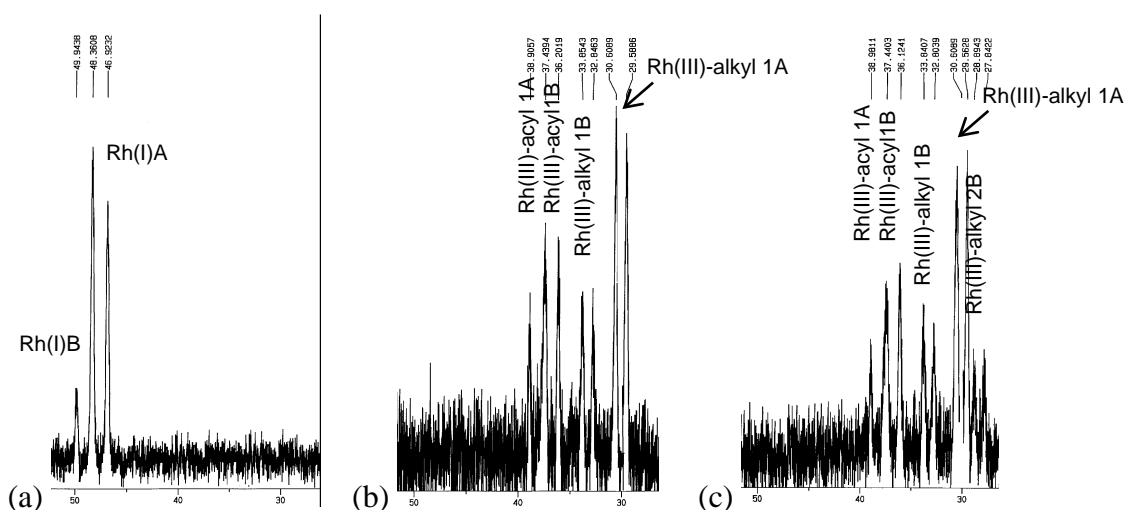
Figure 3.37: Selected ^{31}P NMR spectra illustrating the reaction sequence of the oxidative addition of 0.500 mol dm^{-3} MeI to 0.018 mol dm^{-3} [Rh(fca)(PPh$_3$)(CO)] in CDCl$_3$ at T = 25°C at time (a) t = 0, (b) t = 1753 s (towards the end of the first reactions) and (c) t = 7925 s (during the second reaction).

Table 3.19: Kinetic rate constants of the oxidative addition of 0.500 mol dm^{-3} MeI to 0.018 mol dm^{-3} [Rh(fca)(PPh$_3$)(CO)], as monitored on ^{31}P NMR in CDCl$_3$ at T = 25°C.

reaction	signal	$\delta^{31}P$ / ppm	k_{obs} / s^{-1}
first	Rh(III)-acyl 1A appearance	38.17	0.0023(1)
	Rh(III)-acyl 1B appearance	36.82	0.0023(9)
	average k$_{2obs}$ / s^{-1}		0.0023(9)
second	Rh(III)-alkyl 1A disappearance	30.10	0.00015(6)*
	Rh(III)-alkyl 1B disappearance	33.31	0.00008
	Rh(III)-acyl 1A disappearance	38.17	0.00007(5)
	Rh(III)-acyl 1B disappearance	36.82	0.00009(6)
	average k$_{3obs}$ / s^{-1}		0.00008(1)

* Not used for average

3.4.4.4 Correlation of the kinetic constants of the reaction between CH$_3$I and [Rh(fca)(CO)(PPh$_3$)] as obtained by various spectroscopic methods.

The same reaction sequence as well as a reasonable correlation for the rate constants have been obtained for the oxidative addition and the following carbonylation and decarbonylation reactions between CH$_3$I and [Rh(fca)(CO)(PPh$_3$)], as determined from data obtained by the various spectroscopic methods (**Table 3.20**).

Table 3.20: **The kinetic rate constants of the oxidative addition reaction between CH₃I and [Rh(fca)(CO)(PPh₃)] as obtained by the various spectroscopic methods in chloroform at 25 °C.**

Method	k_1/dm³mol⁻¹s⁻¹	k_3/s⁻¹	k_4/s⁻¹
IR	0.066(2)	0.00009(1)	0.000005(4)
UV/visible	0.065(1)	0.000087(5)	0.0000077(5)
¹H NMR	0.061(5)	0.00005(1)	0.000006(2)
³¹P NMR	##	0.00008(1)	*

to fast to determine on ³¹P NMR   * not determined

3.4.5 *The reaction between iodomethane and [Rh(bfcm)(CO)(PPh₃)]*

The reactions between CH₃I and [Rh(bfcm)(CO)(PPh₃)] were monitored by IR and UV/visible. The same reaction sequence (three *sets* of reactions) as described for the reaction between CH₃I and [Rh(fctfa)(CO)(PPh₃)] in paragraph 3.4.3.3, page 155 - 156, was observed. The rate constants as obtained from kinetic runs on the IR and UV/visible spectrophotometers are summarized in **Table 3.23** page 179.

3.4.5.1   The infrared monitored reaction between CH₃I and [Rh(bfcm)(CO)(PPh₃)].

The reaction rates for the infrared monitored oxidative addition reaction between CH₃I and [Rh(bfcm)(CO)(PPh₃)] in chloroform as reaction medium at 25 °C, as obtained from different CH₃I concentrations, are illustrated graphically in **Figure 3.38** for the *first set* of reactions. A wider range of CH₃I consentrations was used in the UV study, see **Figure 3.39**. The pseudo-first-order rate constant for disappearance of the Rh(I)-carbonyl complex (signal at 1982 cm⁻¹, k_1 = 0.066(3) dm³ mol⁻¹ s⁻¹; approximately the same rate as for the [Rh(fca)(CO)(PPh₃)] complex) is kinetically not significantly different from the formation of the Rh(III)-alkyl1 species (peak at 2073 cm⁻¹, k_1 = 0.130(3) dm³ mol⁻¹ s⁻¹), which is followed by the formation of the Rh(III)-acyl1 complex at 1714 cm⁻¹ at a slower rate (k_1' = 0.030(2) dm³ mol⁻¹ s⁻¹). The observed rate of formation of the Rh(III)-alkyl1 complex was found to be a little higher and the observed rate of formation of the Rh(III)-acyl1 complex was found to be a little lower than the disappearance of the Rh(I)-complex for the same reasons as adequately described on pages 165 - 166. This *first set* of reactions, as well as the *second and third reaction sets*, are consistent with **Reaction**

scheme 3.5 page 144, as was found for the oxidative addition of MeI to the [Rh(fctfa)(CO)(PPh$_3$)] and [Rh(fca)(CO)(PPh$_3$)] complexes. The k$_{-1}$ step in the *first set of reactions* is absent for the [Rh(bfcm)(CO)(PPh$_3$)] complex and the equilibrium involving the k$_2$ and k$_{-2}$ steps is slow in comparison with the k$_1$ step, similar as was found for the [Rh(fca)(CO)(PPh$_3$)] complex. Rate constants as obtained from different CH$_3$I concentrations (0.03 – 1.5 mol dm^{-3}) are summarized in **Table 3.21** for all three *sets* of reactions observed.
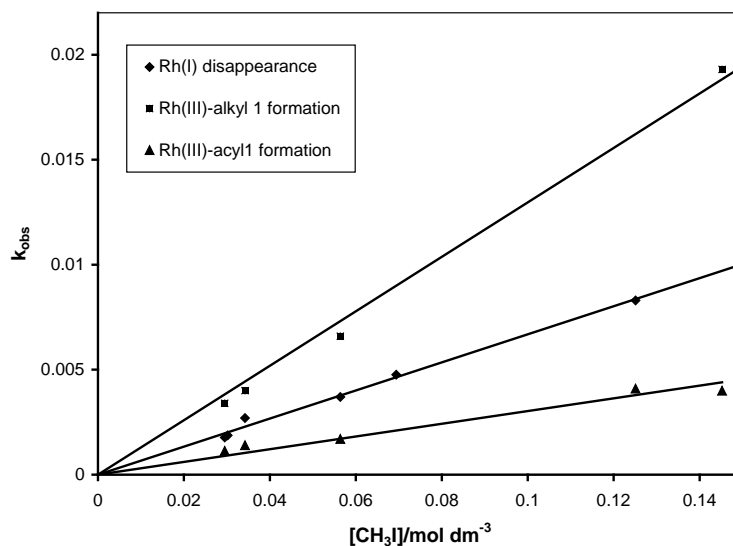
Figure 3.38: k$_{obs}$ of the oxidative addition reaction between CH$_3$I and [Rh(bfcm)(CO)(PPh$_3$)] in chloroform at various concentrations [CH$_3$I] as monitored on the infrared spectrophotometer (T = 25 °C).

Table 3.21: Kinetic rate constants for the oxidative addition of MeI to [Rh(bfcm)(PPh$_3$)(CO)] in chloroform at 25.0(1) °C (IR monitored). The species that were monitored to obtain the individual rate constants are indicated in the headings.

First set of reactions			
Complex	**Rh(I) disappearance**	**Rh(III)-alkyl1 formation**	**Rh(III)-acyl1 formation***
	k$_1$/dm^{3}mol^{-1}s^{-1}	**k$_1$/dm^{3}mol^{-1}s^{-1}**	**k$_1$'/dm^{3}mol^{-1}s^{-1}**
[Rh(bfcm)(PPh$_3$)(CO)]	0.066(3)	0.130(3)	0.030(2)
Second set of reactions (k$_3$/s^{-1})			
	Rh(III)-alkyl1 disappearance	**Rh(III)-acyl1 disappearance**	**Rh(III)-alkyl2 formation**
[Rh(bfcm)(PPh$_3$)(CO)]	0.00010(1)	0.00013(6)	0.00012(4)
Third set of reactions (k$_4$/s^{-1})			
	Rh(III)-alkyl2 disappearance	**Rh(III)-acyl2 formation**	
[Rh(bfcm)(PPh$_3$)(CO)]	0.000006(1)	0.000005(2)	

* See footnote **Table 3.15** page 169.

3.4.5.2 The UV monitored reaction between CH$_3$I and [Rh(bfcm)(CO)(PPh$_3$)].

UV/visible monitoring of the oxidative addition reaction between CH$_3$I and [Rh(bfcm)(CO)(PPh$_3$)] in chloroform indicated three separate reaction steps in accordance with the IR results. All three reactions could be followed at 380 nm. The oxidative addition rate constants were obtained by treating the data sets as separate, isolated quantities. This could successfully be done because there was more than a tenfold difference in reaction rates for the different reaction steps. The dependence of the oxidative addition reaction between CH$_3$I and [Rh(bfcm)(CO)(PPh$_3$)] (as well as the following carbonyl insertion and decarbonylation reactions), on temperature and MeI concentration, as monitored on the UV/VIS spectrophotometer in chloroform is illustrated in **Figure 3.39**. Results are summarized in **Table 3.22**.

Table 3.22: Temperature dependent kinetic rate constants and activation parameters for the oxidative addition of MeI to [Rh(bfcm)(PPh$_3$)(CO)] in chloroform.

Solvent	ε	T / °C	k_1/ dm^3 mol^{-1}s^{-1}	$\Delta H^*(k_1)$ / kJ mol^{-1}	$\Delta S^*(k_1)$ / J mol^{-1}K^{-1}	k_3/s^{-1}	$\Delta H^*(k_3)$ / kJ mol^{-1}	$\Delta S^*(k_3)$ / J mol^{-1}K^{-1}	k_4/s^{-1}
chloroform	4.81	13.7(1)	0.041(1)	45(1)	-116(4)	-	-	-	-
		16.4(1)	0.047(2)			-	-	-	-
		25.0(1)	0.077(2)			0.00012(1)	48(4)	-160(10)	4.8(9)x10^{-6}
		31.1(1)	0.188(4)			0.000196(3)			-
		39.9(1)	0.20(1)			0.000329(5)			-
acetone	20.7	25.0(1)	0.0409(3)	-	-	-	-	-	-

(a)　**(b)**

Figure 3.39: Temperature and MeI concentration dependence of the oxidative addition reaction between CH$_3$I and [Rh(bfcm)(CO)(PPh$_3$)] as monitored on the UV/VIS spectrophotometer in chloroform at 380 nm for (a) the first reaction and (b) the second reaction {[Rh(III)-alkyl1 ⎯ Rh(III)-acyl1] → Rh(III)-alkyl2}.

3.4.5.3 Correlation of the kinetic constants of the reaction between CH₃I and [Rh(bfcm)(CO)(PPh₃)] as obtained by the various spectroscopic methods.

The same reaction sequence and reasonable correlation for the rate constants have been obtained for the oxidative addition and the following carbonylation and decarbonylation reactions between CH$_3$I and [Rh(bfcm)(CO)(PPh$_3$)], as determined from data obtained by the various spectroscopic methods (**Table 3.23**).

Table 3.23: The kinetic rate constants of the oxidative addition reaction between CH$_3$I and [Rh(bfcm)(CO)(PPh$_3$)] as obtained by the various spectroscopic methods in chloroform at 25 °C. k_1, k_3 and k_4 are the rate constant associated with the first, second and third stages of the oxidative addition reaction.

Method	k_1/dm^{3}mol^{-1}s^{-1}	k_3/s^{-1}	k_4/s^{-1}
IR	0.066(3)	0.00012(1)	0.000005(2)
UV/visible	0.077(2)	0.00012(1)	0.0000048(9)

3.4.6 The reaction between iodomethane and [Rh(dfcm)(CO)(PPh₃)].

The reactions between CH$_3$I and [Rh(dfcm)(CO)(PPh$_3$)] were monitored by IR, UV/visible and ^{1}H NMR. The same reaction sequence as in **Reaction scheme 3.5** page 144, described for the reaction between CH$_3$I and [Rh(fctfa)(CO)(PPh$_3$)], was observed by each spectrophotometric method. Reasonable correlation of the rate constants for the oxidative addition, the following carbonylation and decarbonylation reactions between CH$_3$I and [Rh(dfcm)(CO)(PPh$_3$)], as determined from data obtained by the various spectroscopic methods, has been obtained (**Table 3.27** page 186).

3.4.6.1 The infrared monitored reaction between CH₃I and [Rh(dfcm)(CO)(PPh₃)].

Three *sets* of reactions in the infrared monitored reaction between CH$_3$I and [Rh(dfcm)(CO)(PPh$_3$)], as illustrated in **Figure 3.40**, were also observed. The reaction rates obtained in the infrared monitoring of the oxidative addition reaction between CH$_3$I and [Rh(bfcm)(CO)(PPh$_3$)] in chloroform at 25 °C, as obtained from different CH$_3$I concentrations (0.03 – 0.3 mol dm^{-3}), are illustrated in **Figure 3.41** and summarized in **Table 3.24** page 182.
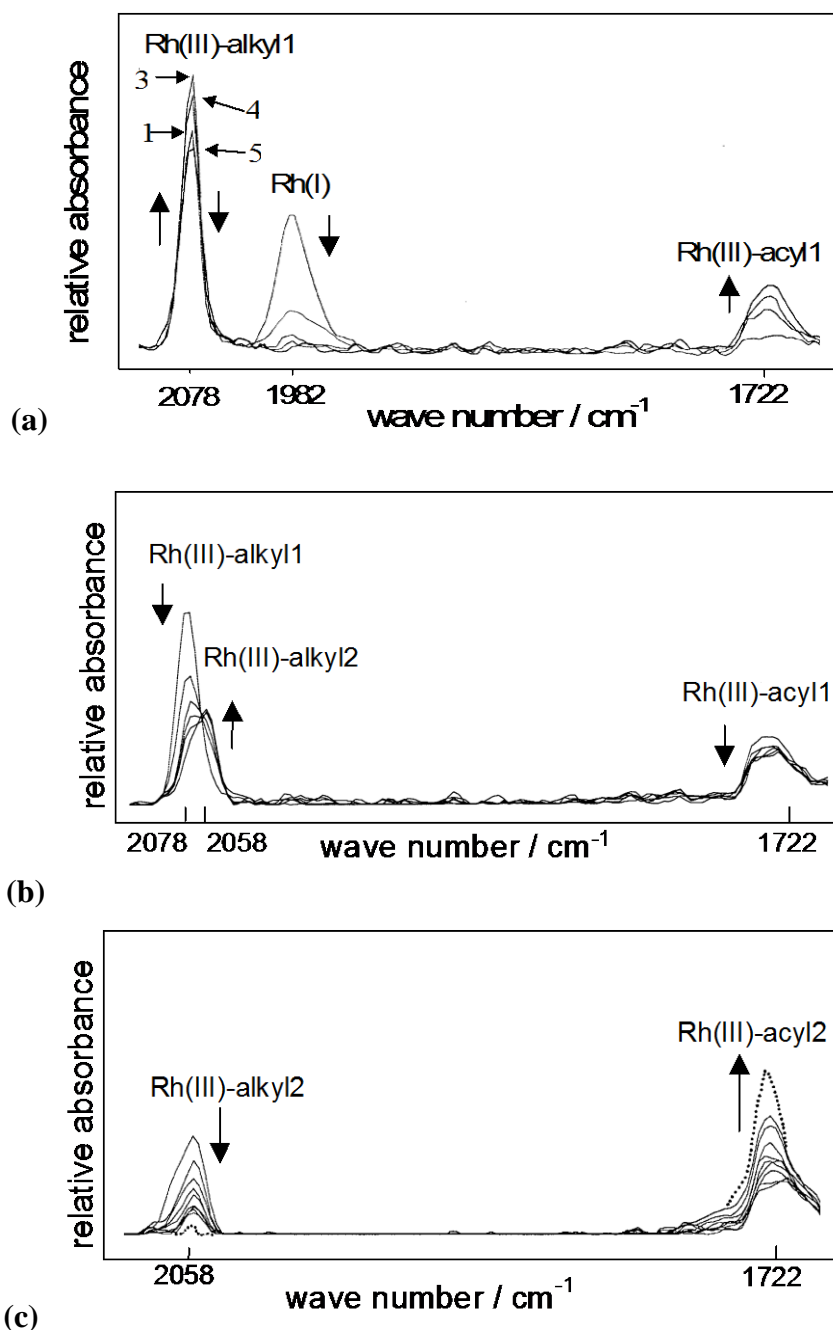
Figure 3.40: Infrared monitoring of the oxidative addition reaction between CH$_3$I and [Rh(dfcm)(CO)(PPh$_3$)] in chloroform. [MeI] = 0.2957 mol dm^{-3}, [Rh(dfcm)(CO)(PPh$_3$)] = 0.009 mol dm^{-3}.

(a) The *first set* of reactions at t = 23 (scan 1), 53 (scan 2 - Rh(I) only), 90 (scan 3), 160 (scan 4) and 720 s (scan 5).

(b) Selected scans for the *second set* of reactions at t = 960, 4560, 7500, 11100, 14700 and 20400 s.

(c) Selected scans for the *third set* of reactions at t = 21960, 71100, 106200, 161700, 201300, 253200, 331200, 419400 and 504000 s.   ············ = spectrum after 15 days.

It is clear from the *first set* of reactions in **Figure 3.40** (a) that the pseudo-first-order rate constant for disappearance of the Rh(I)-carbonyl complex (signal at 1982 cm^{-1}, k$_{1obs}$ = 0.046 s^{-1}) basically corresponds to the simultaneous formation of the Rh(III)-alkyl1 species at 2078 cm^{-1} (k$_{1obs}$ = 0.075 s^{-1}) followed by the formation of the Rh(III)-acyl1 complex at 1722 cm^{-1} at a slower rate

($k_{1'obs\ acyl}$ = 0.011(1) s^{-1}). Utilizing the results of **Figure 3.41**, graphical extrapolation of the CH$_3$I concentration to 1.673 mol dm^{-3} results in k_{1obs} for Rh(I) disappearance as 0.259 s^{-1} and $t_{1/2}$ = 2.7 s; slightly faster than the reaction of the [Rh(fca)(CO)(PPh$_3$)] complex. The observed rate of formation of the Rh(III)-alkyl1 complex was found to be a little higher and the observed rate of formation of the Rh(III)-acyl1 complex was found to be a little lower than the disappearance of the Rh(I)-complex for reasons adequately described on pages 165 - 166. Kinetic data for the three different species involved in step 1 were also collected on ^{1}H NMR (**Table 3.26** page 185). There the values of the rate constants for the Rh(I) disappearance and the Rh(III)-alkyl1 formation were in agreement with each other which further emphasizes that the IR obtained values for k_1 are in fact the same. Deductions leading to the nature of the equilibrium {Rh(III)-alkyl1 ▢ Rh(III)-acyl1} can be made from **Figure 3.40**. The equilibrium is too slow to be maintained during the disappearance of Rh(I). Rh(III)-alkyl1 is first formed during oxidative addition of MeI to Rh(I) and after its formation, it rearranges by carbonyl insertion, at a slightly slower rate, to yield Rh(III)-acyl1. Once Rh(I) is depleted, the equilibrium position between Rh(III)-alkyl1 and Rh(III)-acyl1, is quickly reached and it was found that Rh(III)-alkyl1 ($k_{3\ alkyl1}$ = 0.00014(3) s^{-1}) and Rh(III)-acyl1 ($k_{3\ acyl1}$ = 0.00018(6) s^{-1}) disappear at the same rate to form Rh(III)-alkyl2. Therefore it is concluded that the equilibrium between Rh(III)-alkyl1 and Rh(III)-acyl1 is fast enough to be maintained as Rh(III)-acyl1 converts to Rh(III)-alkyl2. The rate for Rh(III)-alkyl2 formation is $k_{3\ alkyl2}$ = 0.00014(3) s^{-1}. The Rh(III)-acyl1 and the Rh(III)-acyl2 species were both observed at the same wavenumber, 1722 cm^{-1}. NMR measurements, paragraph 3.4.6.3, indicated towards different Rh(III)-acyl1 and Rh(III)-acyl2 species.
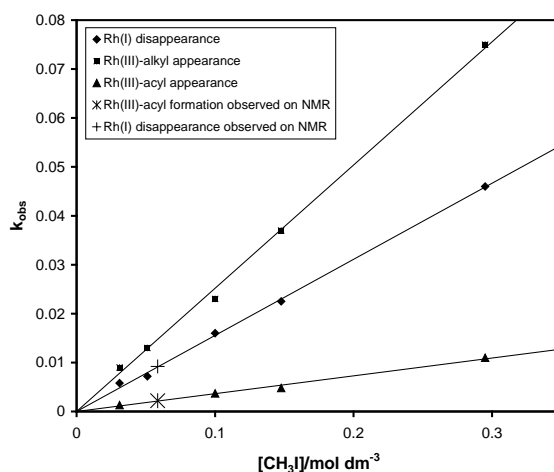
Figure 3.41: k_{obs} for the *first set* of reactions as function of CH$_3$I concentration for the oxidative addition reaction between CH$_3$I and [Rh(dfcm)(CO)(PPh$_3$)] in chloroform at 25 ºC, as monitored on IR. T indicates the rate constant of the acyl formation and + the rate constant of theRh(I) disappearance as observed on ^{1}H NMR.

Table 3.24: Kinetic rate constants for the oxidative addition of MeI to [Rh(dfcm)(PPh₃)(CO)] in chloroform at 25.0(1) ºC, IR monitored. The species that were monitored to obtain the individual rate constants are indicated in the headings.

First set of reactions			
Complex	Rh(I) disappearance	Rh(III)-alkyl1 formation	Rh(III)-acyl1 formation*
	k_1/dm³mol⁻¹s⁻¹	k_1/dm³mol⁻¹s⁻¹	k_1'/dm³mol⁻¹s⁻¹
[Rh(dfcm)(PPh₃)(CO)]	0.155(4)	0.252(4)	0.037(2)
Second set of reactions (k_3/s⁻¹)			
	Rh(III)-alkyl1 disappearance	Rh(III)-acyl1 disappearance	Rh(III)-alkyl2 formation
[Rh(dfcm)(PPh₃)(CO)]	0.00014(3)	0.00015(5)	0.00014(3)
Third set of reactions (k_4/s⁻¹)			
	Rh(III)-alkyl2 disappearance	Rh(III)-acyl2 formation	
[Rh(dfcm)(PPh₃)(CO)]	0.000012(1)	0.000010(4)	

* See footnote **Table 3.15** page 169.

3.4.6.2 The UV monitored reaction between CH₃I and [Rh(dfcm)(CO)(PPh₃)].

The UV/visible monitored oxidative addition reaction between CH₃I and [Rh(bfcm)(CO)(PPh₃)] in chloroform as reaction medium, indicated three separate reaction steps in accordance with the IR results. All three reactions could be followed at 525 nm. Rate constants determined from data obtained at 380 nm for the second and third reactions, as well as at 570 nm for the third reaction, were in agreement with the rate constants determined at 525 nm. The dependence of the oxidative addition reaction between CH₃I and [Rh(dfcm)(CO)(PPh₃)] (as well as the following carbonyl insertion and decarbonylation reactions), on temperature and MeI concentration, as monitored on the UV/VIS spectrophotometer in chloroform is given in **Figure 3.42** and summarized in **Table 3.25**.

Table 3.25: Temperature dependent kinetic rate constants and activation parameters for the oxidative addition of MeI to [Rh(dfcm)(PPh₃)(CO)] in chloroform.

Solvent	ε	T / ºC	k_1 / dm³mol⁻¹s⁻¹	$\Delta H^*(k_1)$ / kJ mol⁻¹	$\Delta S^*(k_1)$ / J mol⁻¹K⁻¹	k_3/s⁻¹	$\Delta H^*(k_3)$ / kJ mol⁻¹	$\Delta S^*(k_3)$ / J mol⁻¹K⁻¹	k_4/s⁻¹
chloroform	4.81	15.0(1)	0.0976(1)			-	-	-	-
		25.0(1)	0.157(2)	33.6(7)	-147(2)	0.00013(1)	48.1(3)	-150(10)	1.8(2)x10⁻⁵
		35.0(1)	0.252(4)			0.00024(1)			-
		40.0(1)	0.3201(5)			0.00034(1)			-

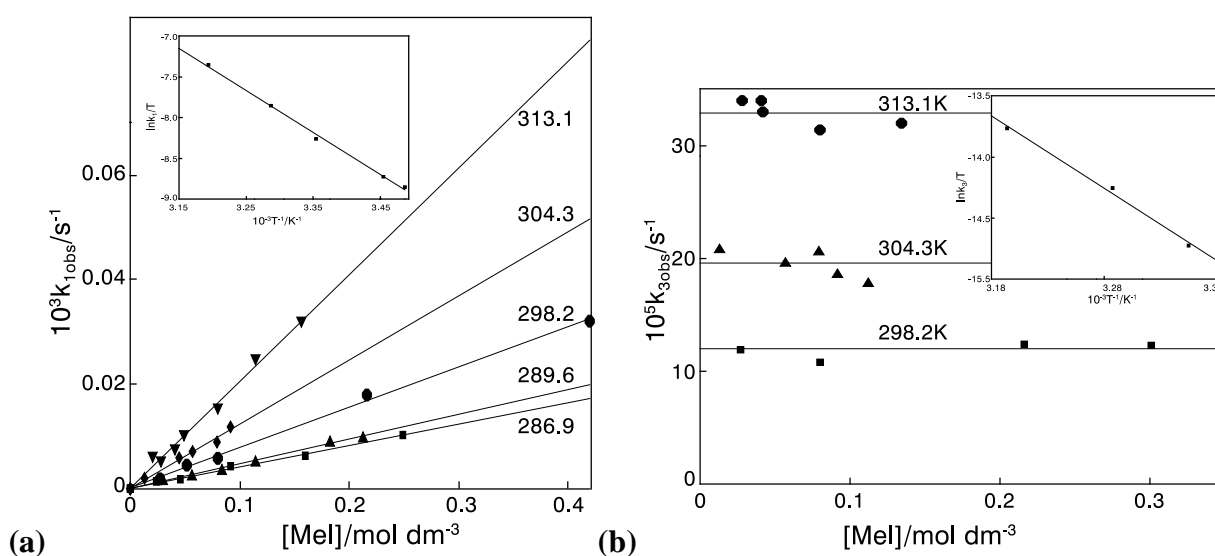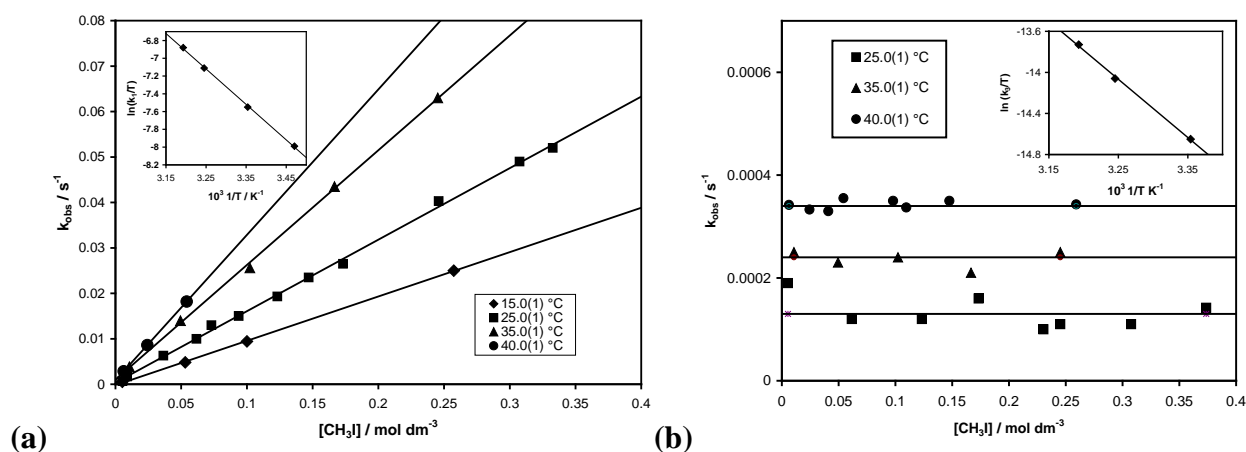**Figure 3.42:** Temperature and MeI concentration dependence of the oxidative addition reaction between CH$_3$I and [Rh(dfcm)(CO)(PPh$_3$)] as monitored on the UV/VIS spectrophotometer in chloroform (a) at 525 nm for the first reaction and (b) at 525 and 380 nm for the second reaction {[Rh(III)-alkyl1 □ Rh(III)-acyl1] → Rh(III)-alkyl2}.

3.4.6.3 The ^{1}H NMR monitored reaction between CH$_3$I and [Rh(dfcm)(CO)(PPh$_3$)].

The *first set* of reactions between 0.0585 mol dm^{-3} CH$_3$I and 0.0072 mol dm^{-3} [Rh(dfcm)(CO)(PPh$_3$)] was monitored by ^{1}H NMR. By carefully comparing the positions and integrals of the different signals, the spectral parameters of the different isomers could be identified as illustrated in **Figure 3.43**. The same reaction sequence as observed on IR and UV/visible, was observed on NMR. This reaction process is consistent with **Reaction scheme 3.2** page 143, which holds also for the oxidative addition of MeI to [Rh(fctfa)(CO)(PPh$_3$)], [Rh(fca)(CO)(PPh$_3$)] and [Rh(bfcm)(CO)(PPh$_3$)]. In the case of the oxidative addition of MeI to [Rh(dfcm)(CO)(PPh$_3$)], however, the *only* Rh(I) "isomer" reacted with MeI to form only *one* main Rh(III)-alkyl1 and *one* main Rh(III)-acyl1 species during the *first set* of reactions. The second and third reactions were not followed on ^{1}H NMR, but from spectra taken after 1 and 2 days, it was clear that only *one* main Rh(III)-alkyl2 "isomer" and only *one* main Rh(III)-acyl2 "isomer" formed with ^{1}H NMR signals at the positions indicated in **Table 3.26** and illustrated in **Figure 3.43** (c). The rate constants obtained from a kinetic run on the NMR are given in **Table 3.26** and compare reasonably well with the rate constants obtained from IR and UV measurements. Rate constants obtained from all three spectrophotometric methods are summarized in **Table 3.27** page 186.

(a)

(b)

(c)
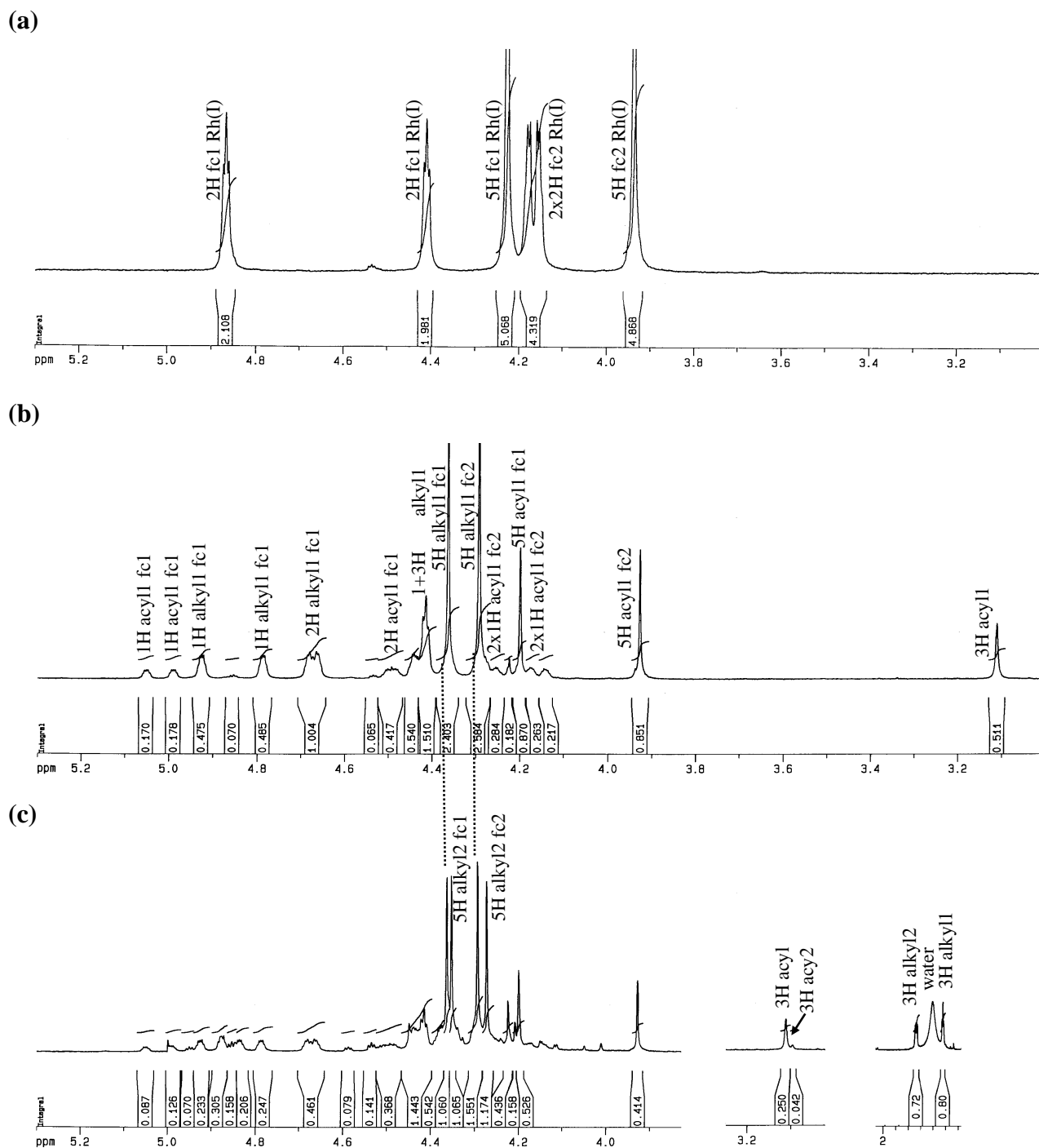
Figure 3.43: Portions of a ^{1}H NMR spectra in CDCl$_3$ showing the protons of the ferrocenyl groups fc1 and fc2 of dfcm in (a) [Rh(dfcm)(CO)(PPh$_3$)] and (b) 887 s after the oxidative addition of 0.0072 mol dm^{-3} [Rh(dfcm)(CO)(PPh$_3$)] with 0.0585 mol dm^{-3} CH$_3$I in CDCl$_3$ (T = 25 °C) was initiated. The signal at 3.11 ppm = δ^{1}H of the CH$_3$-group of the acyl1 reaction product. (c) ^{1}H NMR spectra of the reaction mixture after 1 day, illustrating selective ^{1}H NMR positions of the alkyl2 and acyl2 reaction products.

Table 3.26: Kinetic rate constants for the oxidative addition of 0.05848 mol dm^{-3} MeI to 0.0072 mol dm^{-3} [Rh(dfcm)(PPh$_3$)(CO)], as monitored on ^{1}H NMR in CDCl$_3$ at T = 25 °C. The *second* (carbonyl deinsertion) and *third set* of reactions (carbonyl insertion) were not studied kinetically on ^{1}H NMR.

compound	identification	amount H	δ^1H / ppm	k_{obs} / s^{-1}
Rh(I)	methine proton β-diketone ligand	1	6.10	0.0097(7)
	ferrocene-group I of β-diketone ligand	5	4.23	0.0087(3)
		2	4.41	-
		2	4.87	0.0086(4)
	ferrocene-group II of β-diketone ligand	5	3.93	0.0099(3)
		2	4.17	0.0108(6)*
		2	4.18	0.0103(7)*
	average **k$_{1obs}$ / s^{-1}**			0.0092(7)
	k$_{1\ Rh(I)}$ / dm^3 mol^{-1}s^{-1}			0.16(1)
Rh(III)-alkyl 1	methine proton β-diketone ligand	1	6.15	0.007
	ferrocene-group I of β-diketone ligand	5	4.37	0.0085
		1	4.92	0.011(1)
		1	4.79	0.011(1)
		2	4.68	0.0106(9)
	ferrocene-group II of β-diketone ligand	5	4.29	0.0095(4)
		1	4.41 – 4.45	0.010(1)
		3		-
	CH$_3$-group	3	1.50	0.013(2)
	average **k$_{obs\ alkyl1}$ / s^{-1}**			0.010(2)
	k$_{alkyl\ 1}$ / dm^3 mol^{-1}s^{-1}			0.17(3)
Rh(III)-acyl 1	methine proton β-diketone ligand	1	6.14	0.0023(4)
	ferrocene-group I of β-diketone ligand	5	4.22	0.0022(2)
		1	5.05	0.0020(2)
		1	4.99	0.0021(2)
		2	4.49	0.0023(1)
	ferrocene-group II of β-diketone ligand	5	3.92	0.0021(2)
		1	4.14	0.0026(2)
		1	4.17	0.0026(2)
		2	4.24 – 4.30	-
	CH$_3$-group	3	3.11	0.0018(2)
	average **k$_{obs\ acyl\ 1}$ / s^{-1}**			0.0022(3)
Rh(III)-alkyl 2[#]	CH$_3$-group	3	1.74	-
	ferrocene-group I of β-diketone ligand	5	4.27	-
	ferrocene-group II of β-diketone ligand	5	4.36	-
Rh(III)-acyl 2[#]	CH$_3$-group	3	3.09	-

* Values not used for the average because of too high value for k$_{obs}$ due to the overlapping of peaks with those of the ferrocene-group II of β-diketone ligand of Rh(III)-acyl1.

[#] The other δ^1H positions of Rh(III)-alkyl 2 and Rh(III)-acyl were not identified because the the second and third reactions were not followed.

3.4.6.4 Correlation of the kinetic constants of the reaction between CH₃I and [Rh(dfcm)(CO)(PPh₃)] as obtained by the various spectroscopic methods.

The reactions between CH₃I and [Rh(dfcm)(CO)(PPh₃)] as monitored by IR, UV/visible and ^{1}H NMR followed the same reaction sequence as described for the reaction between CH₃I and [Rh(fctfa)(CO)(PPh₃)] in paragraph 3.4.3.3 page 155. Reasonable correlation for the rate constants for the three individual steps has been obtained (**Table 3.27**).

Table 3.27: Kinetic rate constants of the oxidative addition reaction between CH₃I and [Rh(dfcm)(CO)(PPh₃)] as obtained by the various spectroscopic methods in CHCl₃ at 25 °C. k_1, k_3 and k_4 are the rate constant associated with the first, second and third stages of the reaction of MeI to [Rh(dfcm)(CO)(PPh₃)].

Method	k_1/dm³mol⁻¹s⁻¹	k_3/s⁻¹	k_4/s⁻¹
IR	0.155(4)	0.00014(3)	0.000010(3)
UV/visible	0.157(2)	0.00013(1)	0.000018(2)
^{1}H NMR	0.16(1)	-	-

3.4.7 Correlation of the reaction between iodomethane and [Rh(β-diketonato)(CO)(PPh₃)] complexes with one another and with other related complexes.

The IR and UV/visible results for the oxidative addition of MeI to the four complexes [Rh(β-diketonato)(PPh₃)(CO)], where β-diketonato = fctfa, fca, bfcm and dfcm, are summarized in **Table 3.28** and **Table 3.29** respectively. The large negative ΔS* values for the oxidative addition step (k_1 step, **Table 3.29**) for all four complexes [Rh(β-diketonato)(PPh₃)(CO)] indicate an associative activation in terms of a possible three center transition state, especially in view of the fact that Rh(III)-acyl1 product is formed from the Rh(III)-alkyl1 product of oxidative addition. For the Rh(III)-acyl1 species to form, a *cis* configuration of -CH₃ and -CO relative to one another is preferable in the Rh(III)-alkyl species, and such a coordination mode is most probable from the collapse of a three centre transition state. As was pointed out in chapter 2, however, one should take great caution in deducing a transition state from reaction products, especially from a secondary product such as the Rh(III)-acyl1 species which was formed from the Rh(III)-alkyl1 species , since the latter could have undergone isomerization to form the favourable *cis*-CO-Rh-CH₃ configuration required for CO insertion. The very small ΔS* for the k_3 step in the [Rh(fctfa)(CO)(PPh₃)] complex (**Table 3.29**) is surprising and no suitable explanation for this observation can at this stage be provided.

Table 3.28: **Kinetic rate constants for the oxidative addition of MeI to [Rh(β-diketonato)(PPh₃)(CO)] in chloroform at 25.0(1)ºC (IR monitored) for β-diketonato = fctfa, fca, bfcm and dfcm. The species that were monitored to obtain the individual rate constants are indicated in the headings.**

First set of reactions			
Complex	**Rh(I) disappearance**	**Rh(III)-alkyl1 formation**	**Rh(III)-acyl1 formation**
	$k_1/dm^3mol^{-1}s^{-1}$	$k_1/dm^3mol^{-1}s^{-1}$	$k_1'/dm^3mol^{-1}s^{-1}$
[Rh(fctfa)(PPh₃)(CO)]	0.0062(3); k_{-1}/s^{-1} = 0.0005(2)	0.0061(3); k_{-1}/s^{-1} = 0.0006(2)	0.0061(5); k_{-1}/s^{-1} = 0.0007(4)
[Rh(fca)(PPh₃)(CO)]	0.066(2)	0.100(3)	0.032(1)
[Rh(bfcm)(PPh₃)(CO)]	0.066(3)	0.130(3)	0.030(2)
[Rh(dfcm)(PPh₃)(CO)]	0.155(4)	0.252(4)	0.037(2)

Second set of reactions (k_3/s^{-1})						
	Rh(III)-alkyl1 disappearance	**Rh(III)-acyl1 disappearance**	**Rh(III)-alkyl2 formation**			
[Rh(fctfa)(PPh₃)(CO)]	0.00017(1)	0.00017(1)	0.00017(3)			
[Rh(fca)(PPh₃)(CO)]	0.00010(1)	0.00009(1)	0.00008(1)			
[Rh(bfcm)(PPh₃)(CO)]	0.00010(1)	0.00013(6)	0.00012(4)			
[Rh(dfcm)(PPh₃)(CO)]	0.00014(3)	0.00015(5)	0.00014(3)			

Third set of reactions (k_4/s^{-1})			ν_{CO} (CHCl₃)/cm⁻¹				
	Rh(III)-alkyl2 disappearance	**Rh(III)-acyl2 formation**	Rh^I	Rh^III-alkyl1	Rh^III-acyl1	Rh^III-alkyl2	Rh^III-acyl2
[Rh(fctfa)(PPh₃)(CO)]	0.0000049(5)	0.0000044(2)	1990	2082	1729	2064	1714
[Rh(fca)(PPh₃)(CO)]	0.000007(5)	0.000002(1)	1983	2077	1719	2059	1714
[Rh(bfcm)(PPh₃)(CO)]	0.000006(1)	0.000005(2)	1982	2073	1714	2065	1714
[Rh(dfcm)(PPh₃)(CO)]	0.000012(1)	0.000010(4)	1982	2078	1722	2058	1722

Table 3.29: Kinetic rate constants at 25.0(1) ºC and activation parameters for the first step during oxidative addition of MeI to [Rh(β-diketonato)(PPh₃)(CO)] in chloroform (UV/visible monitored) for β-diketonato = fctfa, fca, bfcm and dfcm. k_1, k_3 and k_4 are the rate constant associated with the first, second and third stages of the oxidative addition reaction.

β-diketone	$k_1/dm^3mol^{-1}s^{-1}$	$\Delta H^*(k_1)/$ kJ mol⁻¹	$\Delta S^*(k_1)/$ J mol⁻¹K⁻¹	$\Delta G^*(k_1)/$ kJ mol⁻¹	$10^4 k_3/s^{-1}$	$\Delta H^*(k_3)/$ kJ mol⁻¹	$\Delta S^*(k_3)/$ J mol⁻¹K⁻¹	$\Delta G^*(k_3)/$ kJ mol⁻¹	$10^6 k_4/s^{-1}$
fctfa	0.00611(1)*	29(3)	-188(9)	85(3)	1.7(2)	93(1)	-5(3)	94(2)	4.4(1)
fca	0.065(1)	40(2)	-133(5)	80(3)	0.87(5)	41.7(2)	-183(7)	96(3)	7.7(5)
bfcm	0.077(2)	45(1)	-116(4)	80(2)	1.2(1)	48(4)	-160(10)	96(6)	4.8(9)
dfcm	0.157(2)	33.6(7)	-147(2)	77(2)	1.3(1)	48.1(3)	-160(10)	96(3)	18(2)

* k_{-1}=0.0005(1) s⁻¹

The influence of the different substituents R bonded to the ferrocene-containing β-diketones FcCOCH₂COR coordinated to the [Rh(β-diketonato)(PPh₃)(CO)] complexes, on the rate of oxidative addition, is illustrated in **Table 3.30**. It is obvious that the reaction rate increases as R is replaced by more electron donating groups from top to bottom in **Table 3.30**. The group

electronegativities χ_R[35] are used here as a measurement of the electron donating power of the R substituents. The increasing electron donating power of the substituent R on the ferrocene-containing β-diketones increases the electron density on the metal, rendering it a better nucleophile and thereby increasing the oxidative addition rates. The results in **Table 3.30** illustrate that the pK_a[35] of β-diketone and ν_{CO} of the [Rh(β-diketonato)(PPh$_3$)(CO)] complex can also give an indication of the electron density on the metal centre. For pK_a's, faster rates are associated with higher pK_a's. The carbonyl stretching frequency is less sensitive, but lower wave numbers are associated with faster rates of oxidative addition.

The relationship between k_1 of the oxidative addition reaction of MeI to the [Rh(β-diketonato)(PPh$_3$)(CO)] complexes of this study, together with k_1 of the oxidative addition reaction of related [Rh(L,L'-BID)(CO)(PPh$_3$)] complexes[36, 37, 25, 22, 27, 38, 39] *and* the pK_a of the protonated L,L'-BID or β-diketonato, is illustrated in **Figure 3.44**. A linear relationship was observed. An exponential relationships, similar to the dotted line in **Figure 3.44**, were obtained for the second-order rate constant k_2 for the substitution reaction between [M(β-diketonato)(cod)] and 1,10-phenanthroline, see **Figure 3.48** page 196 for M = Rh and **Figure 3.55** page 204 for M = Ir.

Table 3.30: **The influence of the different substituents R bonded to the ferrocene-containing β-diketones FcCOCH$_2$COR coordinated to the [Rh(β-diketonato)(PPh$_3$)(CO)] complexes, on the electron density of the metal centre as measured by the group electronegativity χ_R, the pK_a of β-diketone, ν_{CO} of the rhodium complex and rate of oxidative addition of MeI to the rhodium(I) complex.**

complex	R	χ_R	pK$_a$ of β-diketone	ν_{CO} (KBr)/cm^{-1}	k$_1$/dm^{3}mol^{-1}s^{-1}
[Rh(fctfa)(PPh$_3$)(CO)]	CF$_3$	3.01	6.56	1986	0.00611(1)
[Rh(fca)(PPh$_3$)(CO)]	CH$_3$	2.34	10.01	1980	0.065(1)
[Rh(bfcm)(PPh$_3$)(CO)]	C$_6$C$_5$	2.21	10.41	1977	0.077(2)
[Rh(dfcm)(PPh$_3$)(CO)]	Fc	1.87	13.10	1977	0.157(2)

[35] du Plessis, W.C., Vosloo, T. and Swarts, J.C., *J.C.S. Dalton Trans.*, 2507 (1998).

[36] Basson, S.S., Leipoldt, J.G., Roodt, A. and Venter, J.A., *Inorg. Chim. Acta,* **128**, 31 (1987).

[37] Lamprecht, D., *Electrochemical, kinetic and molecular mechanic aspects of rhodium(I) and rhodium(III) complexes, Ph. D. Thesis*, University of the Orange Free State, R.S.A., 1998.

[38] Preston, H., *"Specific isomer formation and oxidative addition behavior of rhodium(I)thiolato complexes"*, *Ph.D. Thesis*, University of the Orange Free State, R.S.A., 1993.

[39] Steyn, G.J.J., *"Mechanistic study of Nitrogen/Sulphur Donor Atom Bidentate Ligand Influence on the Iodomethane Oxidative Addition to Carbonylphosphinerhodium(I) Complexes"*, *Ph.D. Thesis*, University of the Orange Free State, R.S.A., 1994.
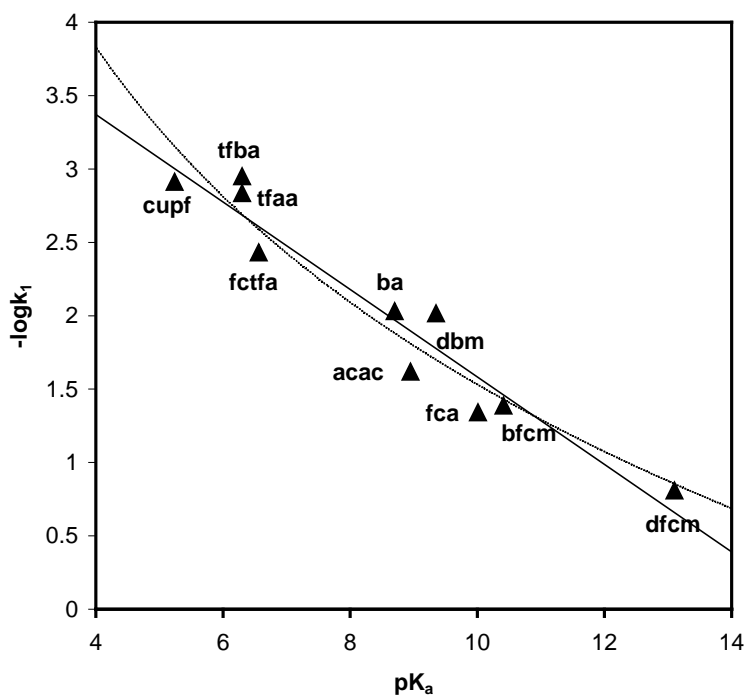
Figure 3.44: **Linear relationship (solid line) between $\log k_1$ of the oxidative addition reaction of [Rh(L,L'-BID)(CO)(PPh₃)] complexes with MeI, at 25 °C, in acetone and the pK_a of the protonated L,L'-BID. Rate constant k_1 for L,L'-BID = acac was measured in 1,2-dichloroethane and dfcm in chloroform; a smaller value is expected in acetone. The exponential curve, ……. , resembles the similar relationship in substitution kinetics as shown in Figure 3.48 more closely.**

The effect of structural changes on the activation free energy $\Delta G^* = \Delta H^* - T\Delta S^*$ of a reaction goes with changes in the activation enthalpy (ΔH^*) and activation entropy (ΔS^*) of the reaction and is a function of temperature.[40] The correlation of activation enthalpy with activation entropy for a specific range of reactions should have the following isokinetic relationship: $\Delta H^* = T\Delta S^* + \Delta G^*$. A graph of ΔH^* *vs.* ΔS^* will therefore have an intercept ΔG^* and a slope the isokinetic temperature, T. The isokinetic temperature is that temperature at which all the reactions represented on the line occur at the same rate.[33] **Figure 3.45** gives the isokinetic relationship of the oxidative addition of iodomethane to [Rh(L,L'-BID)(CO)(PPh₃)] complexes (k_1 step for all related complexes, see **Table 3.31**) and also of the decarbonylation (k_3 step) for complexes of this study. The small deviation from the line indicates that a common mechanism is oparative for those of **Figure 3.45** and similar metal complexes.[41]

[40] Espenson, J.H., *Chemical Kinetics and Reaction Mechanisms,* Second Ed., McGraw-Hill, New York, p. 164, 165.

[41] van Eldik, R., Palmer, D.A., Kelm, H. and Harris, G.M., *Inorg. Chem.,* **19**, 3679 (1980).

Table 3.31: **Summary of the kinetic data for the oxidative addition of iodomethane to different [Rh(L,L'-BID)(CO)(PPh$_3$)] (= bidentate ligand donor atom *trans* to PPh$_3$) in CHCl$_3$ at 25°C. n = amount of atoms in chelate, including the central metal.**

L,L'-BID	L	L'	n	K_1/M^{-1}	$k_1/M^{-1}s^{-1}$ (alkyl)	$\Delta H^*(k_1)/$ kJ mol^{-1}	$\Delta S^*(k_1)/$ J mol^{-1}K^{-1}	$\Delta G^*(k_1)/$ kJ mol^{-1}	$k_1'/M^{-1}s^{-1}$ (acyl)	k_2/s^{-1} (acyl)
cupf[42]	O	O	5	< 0.1	0.0050(1)	33(3)	-180(9)	87(5)	-	0.0012(1)
fctfa	O	O	6	-	0.0066(1)	29(3)	-188(9)	85(3)	0.0067(3)	-
sacac[42]	O	S	6	< 0.1	0.0108	37(2)	-160(6)	85(3)	-	-
hacsm[24]	S	N	6	< 0.5	< 0.01	42(4)	-150(10)	88(7)	-	0.005
macsm[23]	S	N	6	4(1)	0.034(1)	23(3)	-200(10)	83(6)	-	0.0078(4)
hpt[38]	O	S	5	< 0.1	0.021(1)	-	-	-	-	0.01
fca	O	O	6	-	0.068(5)	40(2)	-133(5)	80(3)	0.032(1)	-
bfcm	O	O	6	-	0.130(3)	45(1)	-116(4)	80(2)	0.030(2)	-
dfcm	O	O	6	-	0.22(1)	33.6(7)	-147(2)	77(2)	0.037(2)	-
macsh[24]	S	N	6	40(2)	0.56(1)	26(4)	-166(3)	75(5)	-	0.0072(2)
cacsm[39]	S	N	6	-	0.0559(6)	39(7)	-140(20)	80(10)	-	0.005(1)
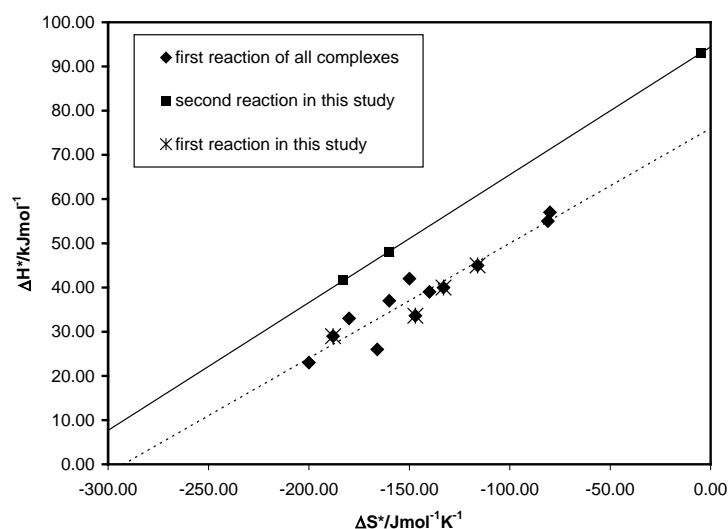
Figure 3.45: The isokinetic relationship of the oxidative addition of iodomethane to [Rh(L,L'-BID)(CO)(PPh$_3$)] complexes. Data are form Table 3.29 (top graph, *second set* of reactions) and Table 3.31 (bottom graph, *first set* of reactions). The isokinetic temperature for the *first set* of reactions is 260 K and for the *second set* of reactions it is 290K.

3.4.8 Mechanistic implications and conclusions.

A complete general reaction scheme for the oxidative addition of iodomethane to complexes of the type [Rh(β-diketonato)(PPh$_3$)(CO)] could be determined. The mechanism was deduced for

---

[42] Venter, J.A., Leipoldt, J.G. and van Eldik, R., *Inorg. Chem.,* **30**, 2207 (1991).

complexes with ferrocene-containing β-diketonato = fctfa, fca, bfcm and dfcm, but all other previous studies on this type of complexes illustrate just special cases of the general mechanism developed in this study.

From the presented NMR results in this study, it is clear that different isomers of the same species react at the same rate and are in fast equilibrium with each other. IR and NMR results indicated that the Rh(III)-alkyl1 and Rh(III)-acyl1 species are in a fast equilibrium with each other for [Rh(fctfa)(PPh$_3$)(CO)]. The other β-diketonato complexes show a slower equilibrium between the Rh(III)-alkyl1 and Rh(III)-acyl1. For all complexes studied the slower equilibrium between the Rh(III)-alkyl1 and Rh(III)-acyl1 was fast enough to be maintained during the slow conversion of Rh(III)-acyl1 to Rh(III)-alkyl2. The final proposed reaction mechanism for the oxidative addition of iodomethane to [Rh(β-diketonato)(PPh$_3$)(CO)] of ferrocene-containing β-diketonato = fctfa, fca, bfcm and dfcm is as given in **Scheme 3.9**. The rate constants k$_{-1}$, k$_{-3}$ and k$_{-4}$ in all cases were too small to be detected, except for k$_{-1}$ = 0.0005 s^{-1} for the [Rh(fctfa)(PPh$_3$)(CO)] reaction in chloroform. It was not possible to determine k$_2$ or k$_{-2}$ separately in this study as no clearcut saturation kinetics, even as 1.673 mol dm^{-3} could be observed. The rate constants in **Scheme 3.9** that could be determined, are summarized in **Table 3.32**.

$$\begin{bmatrix} \text{Rh(I)A} \\ \updownarrow \text{K}_{\text{C1}} \\ \text{Rh(I)B} \end{bmatrix} + \text{CH}_3\text{I} \;\underset{\text{k}_{-1}}{\overset{\text{k}_1}{\rightleftharpoons}}\; \left\{ \begin{bmatrix} \text{Rh(III)-alkyl1A} \\ \updownarrow \text{K}_{\text{C2}} \\ \text{Rh(III)-alkyl 1B} \end{bmatrix} \;\underset{\text{k}_{-2}}{\overset{\text{k}_2, \text{K}_2}{\rightleftharpoons}}\; \begin{bmatrix} \text{Rh(III)-acyl1A} \\ \updownarrow \text{K}_{\text{C3}} \\ \text{Rh(III)-acyl1B} \end{bmatrix} \right\}$$

$$\underset{\text{k}_{-3}}{\overset{\text{k}_3}{\rightleftharpoons}} \begin{bmatrix} \text{Rh(III)-alkyl2A} \\ \updownarrow \text{K}_{\text{C4}} \\ \text{Rh(III)-alkyl 2B} \end{bmatrix} \;\underset{\text{k}_{-4}}{\overset{\text{k}_4}{\rightleftharpoons}}\; \begin{bmatrix} \text{Rh(III)-acyl 2A} \\ \updownarrow \text{K}_{\text{C5}} \\ \text{Rh(III)-acyl 2B} \end{bmatrix}$$
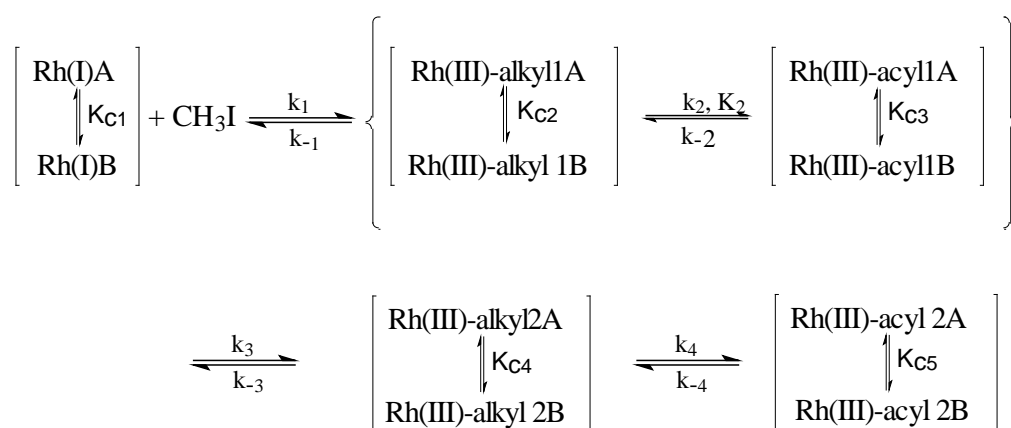
Scheme 3.9: **A complete general reaction mechanism for the oxidative addition of iodomethane to [Rh(β-diketonato)(PPh$_3$)(CO)] complexes. Rate and equilibrium constants are summarized in Table 3.32.**

This study is the first to *observe* the k$_{-2}$ step, although it was proposed for the oxidative addition of iodomethane to [Rh(acac)(PPh$_3$)(CO)][27], [Rh(sacac)(PPh$_3$)(CO)][25] and [Rh(ox)(PPh$_3$)(CO)][43].

---

[43] Van Aswegen, K.G., *Kinetic and structural aspects of the oxidative addition reactions of rhodium(I) complexes with iodomethane (in Afrikaans), M.Sc. Thesis,* University of the Orange Free State, R.S.A., 1990.

This study was also a first to determine the actual rate of conversion from Rh(III)-alkyl2 to Rh(III)-acyl2. Observation of the third step, *i.e.* the k_4 step, was only observed once before in the study of [Rh(TrisO₃)(PPh₃)(CO)][26] with HTrisO₃ = tris(diphenylphosphinoyl)methane. Formation of a Rh(III)-alkyl2 species on IR, the *second* reaction *set*, was observed in only two previous studies, namely the oxidative addition of iodomethane to [Rh(acac)(PPh₃)(CO)][27] and [Rh(TrisO₃)(PPh₃)(CO)].[26]

Table 3.32: Rate and equilibrium constants appropiate to Scheme 3.9 for the oxidative addition of iodomethane to [Rh(β-diketonato)(PPh₃)(CO)] with β-diketonato = fctfa, fca, bfcm and dfcm at 25°C in chloroform. Experimentally $k_{-1} = k_{-3} = k_{-4} \approx 0$, except for the [Rh(fctfa)(PPh₃)(CO)] complex in chloroform , where $k_{-1} = 0.0005$ s^{-1}. K_{ci} = [RhB-species]/[RhA-species] with i = 1, 2, …. 5 were determined from NMR data.

β-diketone	k_1/dm³mol⁻¹s⁻¹	$10^4 k_3$/s⁻¹	$10^6 k_4$/s⁻¹	K_{c1}	K_{c2}	K_{c3}	K_{c4}	K_{c5}
fctfa	0.00611(1)	1.7(2)	4.4(1)	0.68	2.57	1.00	4.56	*
fca	0.065(1)	0.87(5)	7.7(5)	0.22	0.52	2.13	0.82	1.50
bfcm	0.077(2)	1.2(1)	4.8(9)	0.56	*	*	*	*
dfcm#	0.157(2)	1.3(1)	18(2)	-	-	-	-	-

* not determined   # only one isomer

3.5   Substitution reactions.

3.5.1 *Substitution of [Rh(fch)(cod)] {14} with 1,10-phenanthroline.*

In this section of this thesis the substitution of the ferrocene-containing keto-aldehyde fch from the rhodium complex [Rh(fch)(cod)] with 1,10-phenanthroline is reported. It is observed that phenanthroline reacts with [Rh(fch)(cod)] with the replacement of fch as illustrated in **Scheme 3.10**.
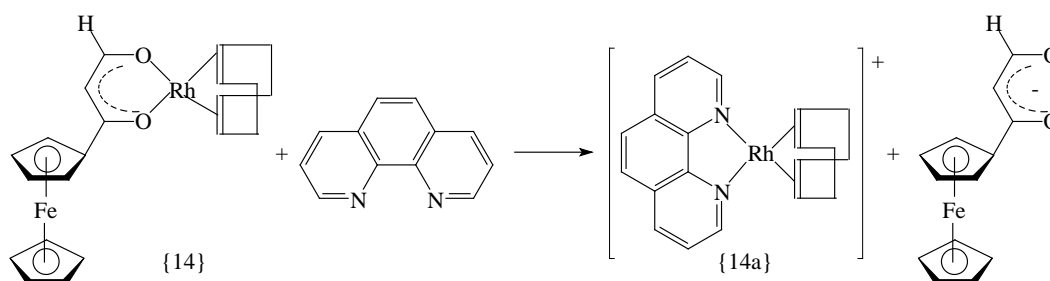
Scheme 3.10: Substitution of the ferrocene-containing keto-aldehyde fch from the square planer rhodium complex [Rh(fch)(cod)] with 1,10-phenanthroline to give [Rh(phen)(cod)]⁺.

The product of the reaction between [Rh(fch)(cod)] and phenanthroline was isolated as the

perchlorate salt, by adding a concentrated solution of NaClO₄ to the reaction mixture of equivalent amounts of [Rh(fch)(cod)] and phenanthroline in acetone. The resulting orange precipitate was removed by filtration. The infrared and visible spectra of the product confirmed that the product obtained corresponded to the product obtained from the reaction between [Rh₂Cl₂(cod)₂] and phenanthroline, *viz.* [Rh(phen) (cod)]⁺, {14a}. The UV spectra of [Rh(fch)(cod)] and the product of substitution of [Rh(fch)(cod)] and phenanthroline *viz.* [Rh(phen)(cod)]⁺ in methanol at 25°C are given in **Figure 3.46** (a). The linear relationship between the absorbance and concentration of [Rh(fch)(cod)] in **Figure 3.46** (b) confirms the validity of the Beer Lambert law for the [Rh(fch)(cod)] complex.
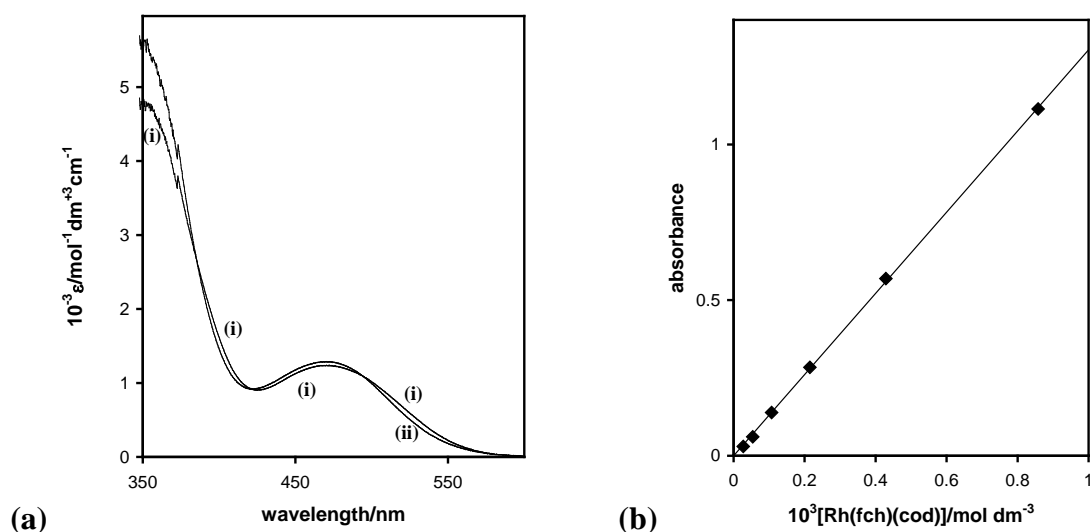
Figure 3.46: (a) UV spectra of (i) [Rh(fch)(cod)] {14} and (ii) [Rh(phen)(cod)]⁺ in methanol at 25°C. (b) Graph of absorbance *vs* concentration of [Rh(fch)(cod)] {14} at 470 nm confirming the validity of the Beer Lambert law, A = εcl, for the [Rh(fch)(cod)] complex. ε(470 nm) = 1300(10) dm⁻³ mol⁻¹ cm⁻¹; ε(525 nm) = 661(6) dm⁻³ mol⁻¹ cm⁻¹.

The reaction rate constants were obtained by following the formation of [Rh(phen)(cod)]⁺ at 525 nm. An excess of 6 to 70 fold phenanthroline was used for all experiments in order to achieve pseudo-first-order reaction conditions. Linear first-order plots were obtained for at least two half-lives. The pseudo-first-order rate constants were determined for various phenanthroline concentrations in MeOH at three different temperatures (15.4, 25.0 and 35.0 ⁰C). The effect of the phenanthroline concentration on the pseudo-first-order rate constants of the reaction with [Rh(fch)(cod)] is shown in **Figure 3.47** (a). The Eyring curve (see **Equation 3.7** page 152) of ln(k₂/T) *versus* 1/T of the substitution reaction of [Rh(fch)(cod)] with 1,10-phenanthroline in methanol is given in **Figure 3.47** (b). The values of the second-order rate constants at the various temperatures and the activation parameters are given in **Table 3.33**. The large negative values of ΔS* suggest an associative mechanism and are of the same order and magnitude as

194

found for the substitution reactions of [Rh(β-diketonato)(cod)] complexes with 1,10-phenanthroline as summarized in **Table 3.37** page 208. High pressure studies of the acac and tfaa complexes also suggested an associative mechanism.[44]
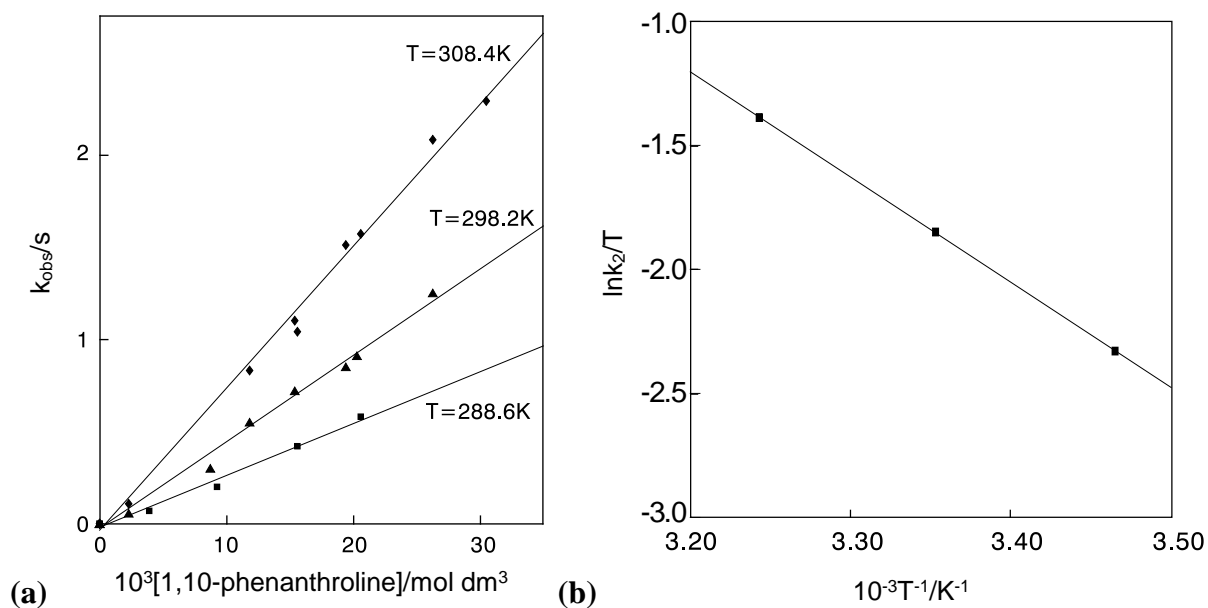
Figure 3.47: **(a)** **Plot of k_{obs}** *versus* **[phen] at various temperatures and (b) the Eyring curve of $\ln(k_2/T)$** *versus* **1/T for the substitution reaction of 0.0004 mol dm^{-3} [Rh(fch)(cod)] {14} with 1,10-phenanthroline.**

Table 3.33: **Values of the second-order rate constants k_2 at the various temperatures and the activation parameters of the reaction of [Rh(fch)(cod)] {14} with 1,10-phenanthroline in methanol.**

complex	T / ^{0}C	k_2/dm^3 mol^{-1} s^{-1}	ΔH^*/kJ mol^{-1}	ΔS^*/J mol^{-1} K^{-1}	ΔG^*/kJ mol^{-1}
[Rh(fch)(cod)]	15.4 25.0 35.0	28.1(9) 47(1) 77(2)	35(2)	-94.7(1)	63

Scheme 3.11 gives a schematic presentation of the associative mechanism of the substitution reaction of [Rh(fch)(cod)] {14} with 1,10-phenanthroline. The rate determining step, k_2, involves the formation of a five-coordinate species {14b}, followed by breakage of one of the two oxygen-Rh bonds of fch coordinated to the rhodium nucleus. A stronger bond is expected for the Rh-O bond nearer to the ferrocenyl-group than the Rh-O nearer to H because of the higher group electronegativity of H (2.13) than that of fc (1.87). It is thus to be expected that the weaker Rh-O bond nearer to H will break first with the simultaneous formation of a bond between Rh and the still un-coordinated N of 1,10-phenanthroline, to form the five-coordinated transitional state {14c}, which quickly reacts to form the product of the substitution reaction

---

[44] Leipoldt, J.G., Steynberg, E.C. and van Eldik, R., *Inorg. Chem.,* **26**, 3068 (1987).

[Rh(phen)(cod)]$^+$. The final fast step involves dissosiation of {14c} to generate free fch$^-$ and the substitution product [Rh(phen)(cod)]$^+$, {14a}.
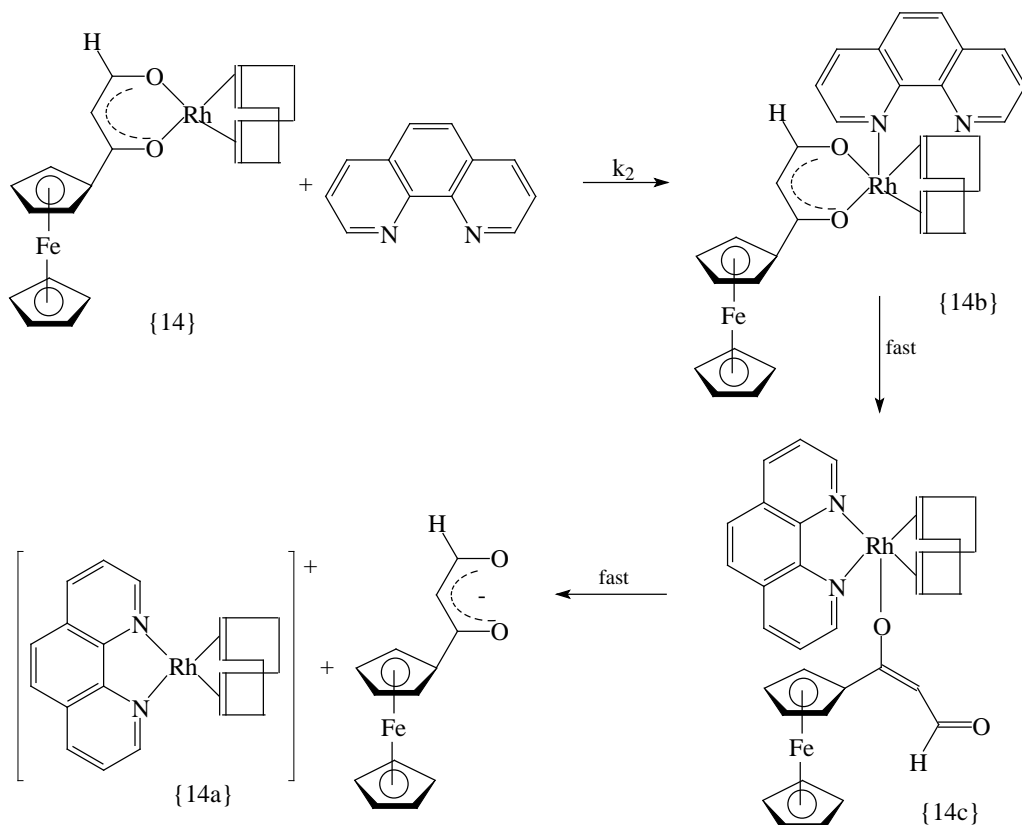
Scheme 3.11: Schematic presentation of the associative mechanism of the substitution reaction of **[Rh(fch)(cod)] {14} with 1,10-phenanthroline.**

As discussed in chapter 2, square-planar substitution reactions with incoming ligand Y obey the general rate law:

Equation 3.10: Rate = $(k_s + k_2[Y])$ [complex] = k_{obs} [complex]

The second-order rate constant k_2 refers to the bimolecular attack of Y on the complex (in **Scheme 3.11** phen on {14}). The first-order rate constant k_s refers to the bimolecular attack of the solvent, in this case methanol, on the complex {14}. For the reaction studied, the plot of k_{obs} *vs.* phen concentration passes through the origin, suggesting $k_s \ll k_2$ for methanol as solvent. The observed zero intercept is to be expected because the displacement rate of the bidentate keto-aldehyde ligand by a monodentate solvent would be much slower or even approach zero, compared to keto-aldehyde displacement by the bidentate ligand phen. For the substitution reaction between [Rh(fch)(cod)] and phenanthroline the general rate law presented in **Equation**

3.10 simplifies to:

$$-\frac{d[Rh(fch)(cod)]}{dt} \quad = \quad k_2[phen][Rh(fch)(cod)] \quad \text{because } k_s \sim 0$$

$$= \quad k_{obs}[Rh(fch)(cod)] \qquad \text{with } k_{obs} = k_2[phen]$$

3.5.2 *Correlation of the reaction between the [Rh(fch)(cod)] complex and 1,10-phenanthroline with substitution reactions of other related rhodium complexes.*

The effect of the pK_a values of the various β-diketones and Hfch on the reaction rate is shown in the free energy relationship **Figure 3.48** (data in **Table 3.37** page 208). **Figure 3.48** reveals that the rate of substitution kinetics of complexes possessing more basic β-diketonate or fch as ligand is more independent of the pK_a of the β-diketone or Hfch than those complexes possessing β-diketonate ligands with lower pK_a. From **Table 3.37** page 208, the following reactivity order of the [Rh(β-diketonato)(cod)] or [Rh(fch)(cod)] complexes for the rate constants of the substitution reaction of [Rh(β-diketonato)(cod)] or [Rh(fch)(cod)] with 1,10-phenanthroline can be given (this order does not exactly parallel the rate - pK_a relationship in **Figure 3.48**):

(fastest substitution) hfaa > tfba > fctca > tfaa > fctfa > dbm > ba> fch > bfcm >acac >fca > dfcm
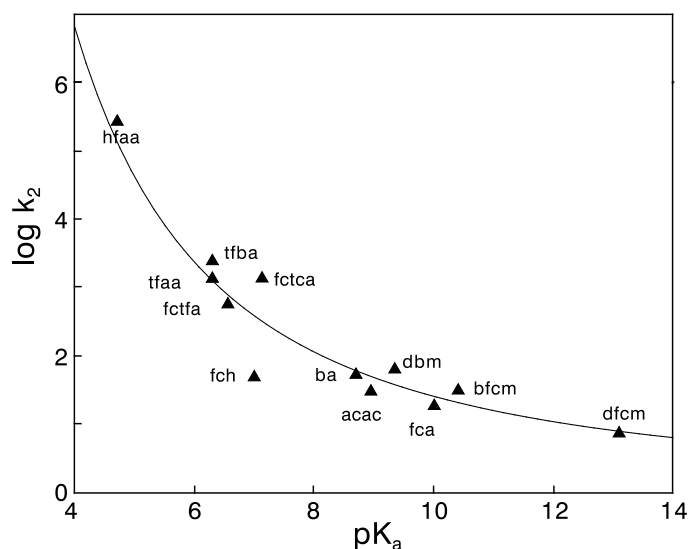
Figure 3.48: The relationship between pK_a values of various β-diketones as well as the *β-keto-aldehyde* Hfch and second-order rate constant k_2 for the substitution reaction between [Rh(β-diketonato)(cod)] or [Rh(fch)(cod)] and 1,10-phenanthroline in methanol at 25 °C. Numerical data are provided in data in Table 3.37 page 208.

3.5.3   Substitution reactions of [Ir(β-diketonato)(cod)] complexes with 1,10-phenanthroline.

In this section the kinetics of the reaction between [Ir(β-diketonato)(cod)] complexes and 1,10-phenanthroline in acetone medium is reported for β-diketonato = tftma, tfdma, tfhd, fctfa, fca and bfcm.   The objective was to compare the mechanism of these reactions with that of the corresponding rhodium complexes, as well as with the reaction of 1,10-phenanthroline (phen) with related previously investigated [Ir(β-diketonato)(cod)] complexes.   Two separate aspects, steric influence and electronic effects, were investigated.   The choice of the series of β-diketonatos $(CF_3COCHCOR)^-$ = tfhd, tfdma and tftma was to investigate the steric influence (if any) of the substituent R as it increased in size from CH_2CH_3 to $CH(CH_3)_2$ to $C(CH_3)_3$ on the substitution rate of the β-diketonato ligand from the [Ir(β-diketonato)(cod)] complexes with phen.   In contrast to the steric influence, the series of β-diketonatos $(FcCOCHCOR')^-$ = fctfa, fca and bfcm with substituents R' = CF_3, CH_3 and C_6H_5 has different electronic properties (χ_{CF3}[19] = 3.01, pK_a = 6.56; χ_{CH3} = 2.34, pK_a = 10.01; χ_{Ph} = 2.21, pK_a 10.41).

Two iridium complexes were obtained during the attempted synthesis of [Ir(β-diketonato)(cod)] complexes (paragraph 3.2.3 page 131).   Only the complex isolated within 30 s underwent the substitution prosesses described in this section of this thesis.   The compound isolated after longer periods of synthesis was completely inert towards substitution kinetics with 1,10-phenanthroline.

In contrast to the reactions of the rhodium complexes [Rh(β-diketonato)(cod)] with 1,10-phenanthroline (**Equation 3.11**), it was found that [Ir(acac)(cod)] reacts with 1,10-phenanthroline to give the five-coordinated carbon-bonded β-diketonato complex [Ir(acac-C^3)(phen)(cod)][45] according to **Equation 3.12**. ^{1}H NMR of the reaction between the [Ir(β-diketonato)(cod)] complexes and 1,10-phenanthroline confirmed that the reaction product contained a cod ligand (three 4H signals), a phen ligand (four 2H signals) as well as the β-diketone ligand (signals not corresponding to those of the free β-diketone).   Representative examples are given in **Table 3.34**.   The reactions of the [Ir(β-diketonato)(cod)] complexes and 1,10-phenanthroline are thus expected to be represented by **Equation 3.12**.

---

[45] Oro, L.A., Carmona, D., Esteruelas, M.A., Foces-Foces, C. and Cano, F.H., *J. Organomet. Chem.,* **258**, 357 (1983).

Equation 3.11: [Rh(β-diketonato)(cod)] + phen → [Rh(phen)(cod)]$^+$ + (β-diketonato)$^-$

Equation 3.12: [Ir(β-diketonato)(cod)] + phen → [Ir(β-diketonato-C^3)(phen)(cod)][46]
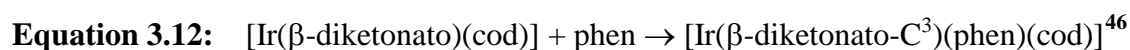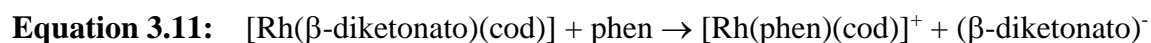
Table 3.34: ^{1}H NMR (δ-values in ppm referenced to Me$_4$Si) of the free β-diketone, [Ir(I)(β-diketonato)(cod)] and [Ir(III)(β-diketonato-C^3)(cod)(phen)] for β-diketone = Hfctfa and Htfdma.

β-diketonato	signal	β-diketone (enol)	[Ir(I)(β-diketonato)(cod)]	[Ir(III)(β-diketonato-C^3)(cod)(phen)]
fctfa	3 x 4H cod protons	-	1.70, 2.32, 4.12	2.00, 2.45, 4.42
	4 x 2H phen protons	-	-	8.10, 8.46, 8.80
	β-diketone Fc group	4.20, 4.65, 4.85	4.22, 4.59, 4.82	4.10, 4.61, 4.61
	β-diketone methine proton	6.07	6.12	5.77
tfdma	3 x 4H cod protons	-	1.69, 2.29, 4.14	2.08, 2.49, 4.60
	1 x 4H, 2 x 2H phen protons	-	-	8.18, 8.64, 8.87
	β-diketone CH(CH3)$_2$ group	1.22, 2.65	1.14, 2.65	1.05, 3.25
	β-diketone methine proton	5.96	5.98	5.23

The reaction between the [Ir(β-diketonato)(cod)] complexes and 1,10-phenanthroline is still considered as a substitution reaction, although the β-diketone is not actually substituted from the [Ir(β-diketonato)(cod)] complexes as in the case of the corresponding rhodium complexes. The reason for this interpretation is because the β-diketone changed its mode of coordination from κO,κO' to C^3. In [Ir(β-diketonato)(cod)] complexes both metal-oxygen bonds are broken and two new metal-nitrogen bonds are formed when phen comes in. This could not have happened if the β-diketonato ligand was not formally substituted.

Table 3.35: Molar extinction coefficient ε of [Ir(β-diketonato)(cod)] complexes at 25.0(1)°C in acetone. The concentration, c, of the iridium complex and the wavelength at which the reaction between [Ir(β-diketonato)(cod)] and phen has been followed, are also given.

Complex	λ_{max}/nm [ε/dm^3 mol^{-1} cm^{-1}]	λ_{exp}/nm	c_{exp} of [Ir(β-diketonato)(cod)] /mol dm^{-3}
[Ir(fca)(COD)]	360[4750(40)]	600	0.0004
[Ir(bfcm)(COD)]	490[2950(20)]	560	0.0002
[Ir(fctfa)(COD)]	384 [3900(20)]	515	0.0002
[Ir(tfhd)(COD)]	380 [1400(8)]	560	0.0005 or 0.0001 at low [phen]
[Ir(tfdma)(COD)]	380 [1670(20)]	560	0.0005 or 0.0001 at low [phen]
[Ir(tftma)(COD)]	380 [1561(7)]	560	0.0009 or 0.0001 at low [phen]

---

[46] The β-diketonato is κ,κ' coordinated to Rh through the O-atoms in [Ir(β-diketonato)(cod)], but in [Ir(β-diketonato-C^3)(phen)(cod)] the β-diketone is σ bonded to Rh through the methine carbon (labelled C^3 for acac).

A linear relationship between the absorbance and concentration of all the [Ir(β-diketonato)(cod)] complexes confirms the validity of the Beer Lambert law for these complexes. Molar extinction coefficients, ε, at the wavelengths indicated, are summarized in **Table 3.35**.

The reactions between the [Ir(β-diketonato)(cod)] complexes and 1,10-phenanthroline have been followed in acetone medium on a stopped-flow spectrophotometer at the wavelengths as indicated in **Table 3.35**. The concentration of the [Ir(β-diketonato)(cod)] complexes was as tabulated in **Table 3.35**. For the reactions with low [phen], the concentration in the case of the [Ir(β-diketonato)(cod)] complexes with β-diketone = tftma, tfdma and tfhd was lowered to 0.0001 mol dm^{-1} to assure pseudo-first-order conditions. In these cases, kinetic measurements under pseudo-first-order conditions for different concentrations of the [Ir(β-diketonato)(cod)] complex, for a constant [phen], confirmed that the concentration [Ir(β-diketonato)(cod)] did not influence the value of the observed kinetic rate constant. The effect of the concentration of 1,10-phenanthroline on the pseudo-first-order rate constants at different temperatures and the Eyring curve (**Equation 3.7** page 152) for the substitution reaction between [Ir(β-diketonato)(cod)] and 1,10-phenanthroline in acetone medium for the β-diketones = tftma, tfdma, tfhd, fctfa, fca and bfcm are illustrated in **Figure 3.49** to **Figure 3.54** respectively. The values of the second-order rate constants at the various temperatures and the activation parameters for all the complexes studied, are summarized in **Table 3.36** page 203.
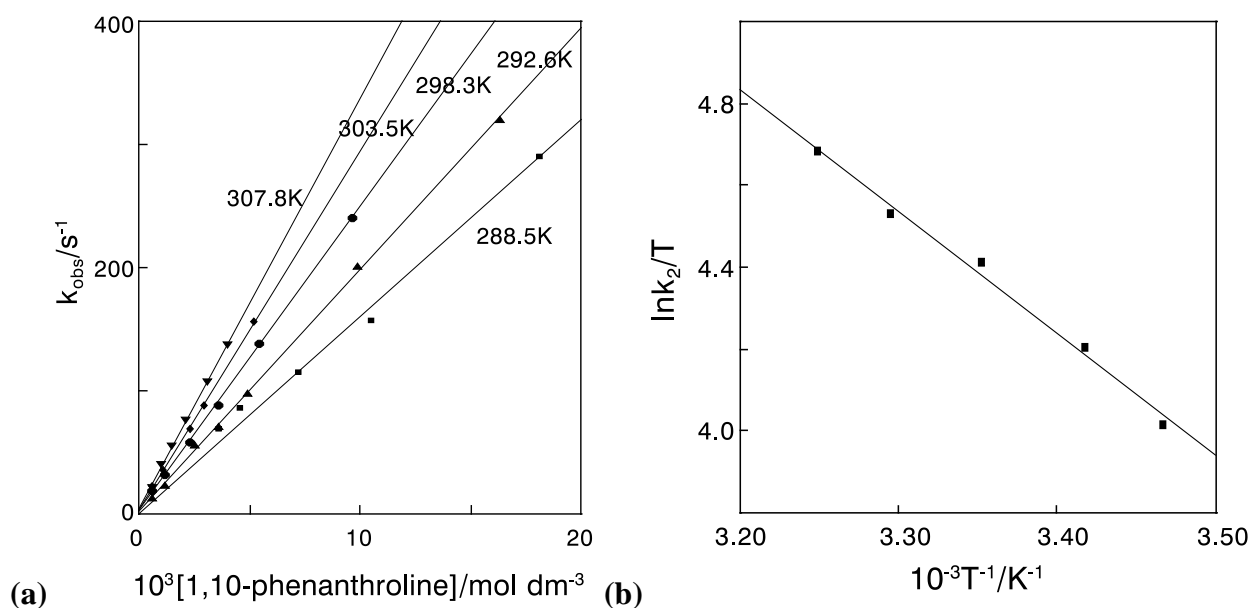
Figure 3.49: (a) Plot of k_{obs} *versus* [phen] at various temperatures and (b) the Eyring curve of ln(k_2/T) *versus* 1/T for the substitution reaction of [Ir(tftma)(cod)] with 1,10-phenanthroline. [Ir(tftma)(cod)] = 0.0001 - 0.0009 mol dm^{-3}, but see Table 3.35 and discussion on page 199.

(a)

(b)
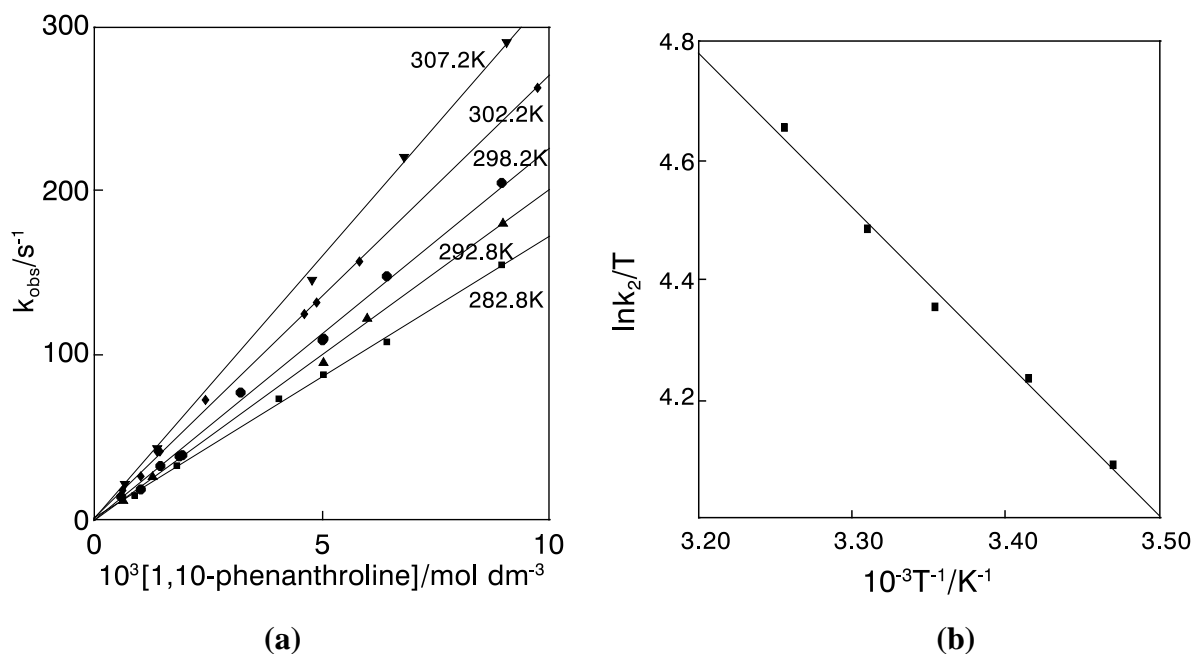
Figure 3.50: (a) Plot of k_{obs} *versus* [phen] at various temperatures and (b) the Eyring curve of $\ln(k_2/T)$ *versus* $1/T$ for the substitution reaction of [Ir(tfdma)(cod)] with 1,10-phenanthroline. [Ir(tfdma)(cod)] = 0.0001 - 0.0005 mol dm^{-3}, but see Table 3.35 and discussion on page 199.

(a)

(b)
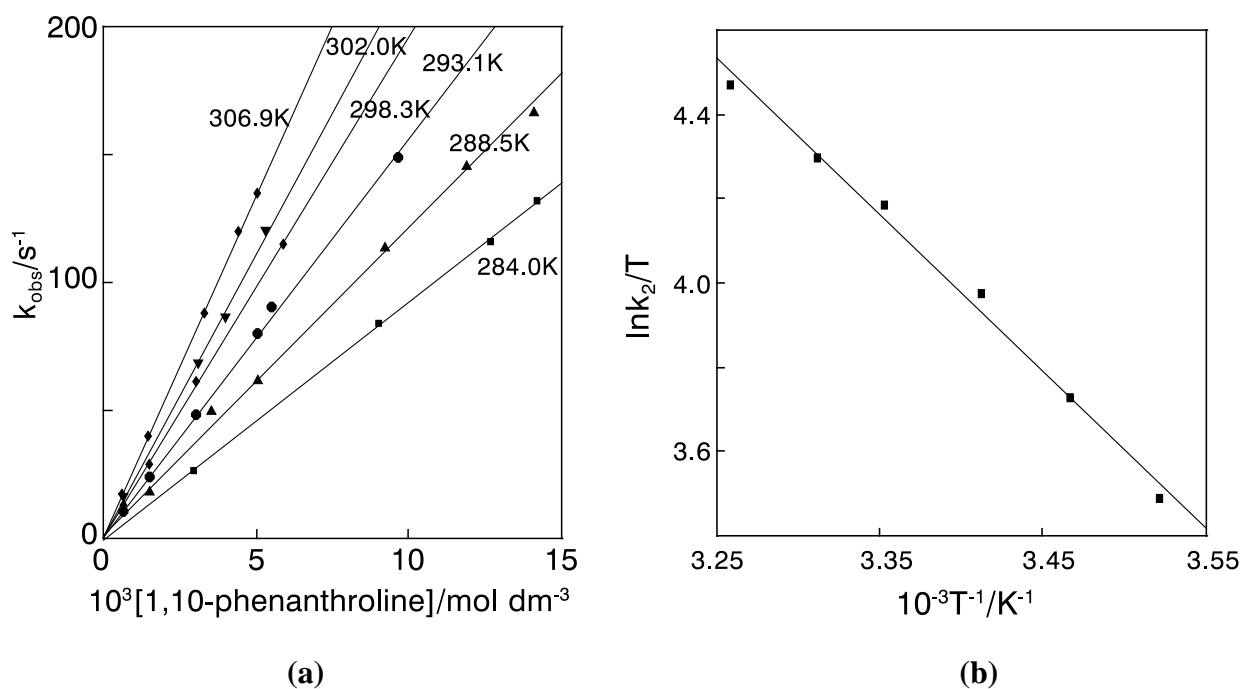
Figure 3.51: (a) Plot of k_{obs} *versus* [phen] at various temperatures and (b) the Eyring curve of $\ln(k_2/T)$ *versus* $1/T$ for the substitution reaction of [Ir(tfhd)(cod)] with 1,10-phenanthroline. [Ir(tfhd)(cod)] = 0.0001 - 0.0005 mol dm^{-3}, but see Table 3.35 and discussion on page 199.
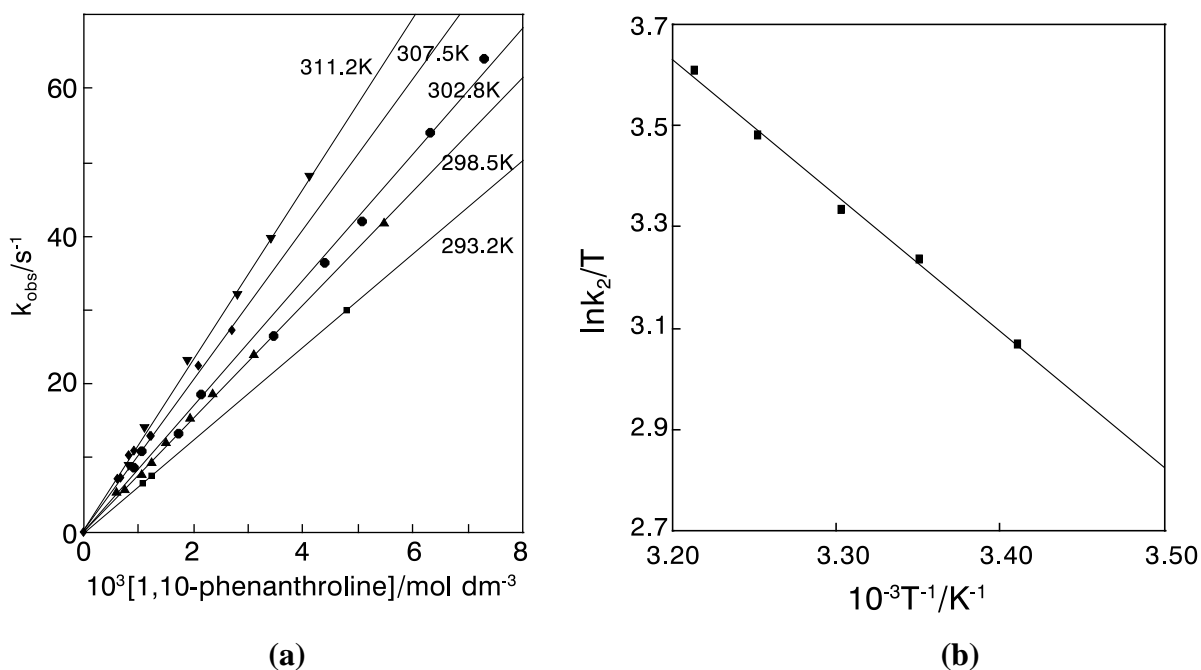
Figure 3.52: (a) Plot of k_{obs} *versus* [phen] at various temperatures and (b) the Eyring curve of $\ln(k_2/T)$ *versus* 1/T for the substitution reaction of [Ir(fctfa)(cod)] with 1,10-phenanthroline. [Ir(fctfa)(cod)] = 0.0002 mol dm^{-3}.
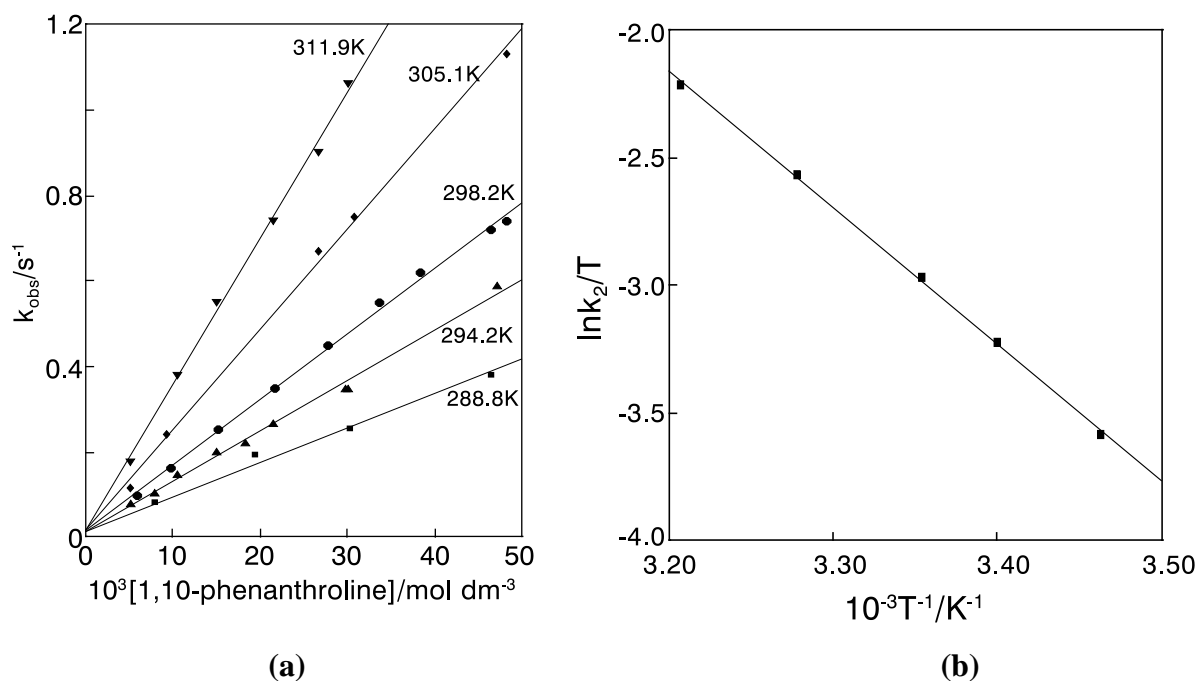
Figure 3.53: (a) Plot of k_{obs} *versus* [phen] at various temperatures and (b) the Eyring curve of $\ln(k_2/T)$ *versus* 1/T for the substitution reaction of [Ir(fca)(cod)] with 1,10-phenanthroline. [Ir(fca)(cod)] = 0.0004 mol dm^{-3}.
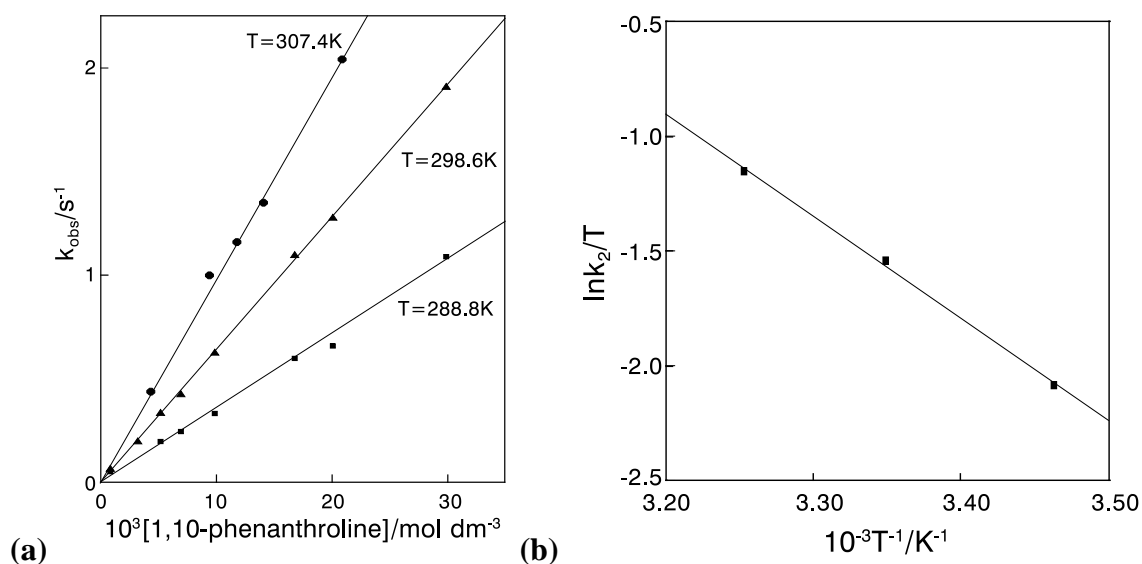
Figure 3.54: **(a)** **Plot of k$_{obs}$** *versus* **[phen] at various temperatures and (b) the Eyring curve of ln(k$_2$/T)** *versus* **1/T for the substitution reaction of [Ir(bfcm)(cod)] with 1,10-phenanthroline. [Ir(bfcm)(cod)] = 0.0002 mol dm^{-3}.**

Kinetic results discussed in chapter 2 paragraph 2.2.4.3 (iii) revealed that a decrease in the electron attracting power (as can be measured by decreasing group electronegativity χ_R, or by decreasing pK$_a$) of one of the substituents R or R' of the β-diketone (R'COCH$_2$COR), causes a decrease in the kinetic *trans*-effect, resulting in a smaller rate constant for the substitution of the *trans* ligand. In this study the β-diketonato ligand itself was displaced and not the ligand *trans* of a specific β-diketonato ligand. In considering the series of β-diketonates (FcCOCHCOR)$^-$ = fctfa, fca and bfcm with substituents R = CF$_3$, CH$_3$ and C$_6$H$_5$, the second-order rate constant of substitution (in dm^3 mol^{-1} s^{-1}) of the β-diketonato ligand from the [Ir(β-diketonato)(cod)] with phen followed the same sequence as the discussed substitution of the ligand *trans* to it (chapter 2). The sequence, with substitution rate constants (**Table 3.36**), group electronegativity and β-diketone pK$_a$ is given below.

(fastest substitution) fctfa (7600, χ_{CF3}[19] = 3.01, pK$_a$ = 6.56)

> bfcm (63.9, χ_{Ph} = 2.21, pK$_a$ = 10.41) ≈ fca (15.3, χ_{CH3} = 2.34, pK$_a$ = 10.01)
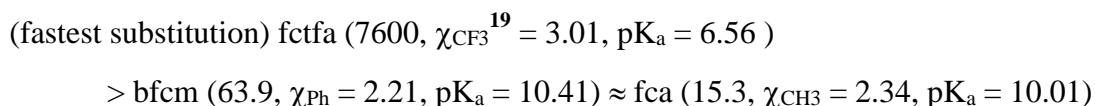
Results discussed in chapter 2 paragraph 2.2.4.3. (v) indicated that an increasing steric hindrance of ligands coordinated to a metal complex, progressively retards the substitution rate of a incoming ligand. In considering the results of **Table 3.36** of the series of β-diketonatos (CF$_3$COCHCOR)$^-$ = tfaa,[47] tfhd, tfdma and tftma {with R = CH$_3$, CH$_2$CH$_3$, CH(CH$_3$)$_2$ and

---

[47] see **Table 3.37** page 208 for substitution rate of the reaction of [Ir(tfaa)(cod)] with phen

$C(CH_3)_3$ which systematically increases in bulk} coordinated to the [Ir(β-diketonato)(cod)] complex, the sequence of the corresponding second-order rate constant of β-diketonato substitution in dm^3 mol^{-1} s^{-1}, from the [Ir(β-diketonato)(cod)] with phen is :

17100 (R = CH_3, pK_a = 6.30), 19600 (R = CH_2CH_3, pK_a = 6.64),

23200 (R = $CH(CH_3)_2$, pK_a = 6.8) and 24600 (R = $C(CH_3)_3$, pK_a = 7.13)

For all practical purposes, therefore, these rate constants are the same which indicates that bulkiness of the R substituent on β-diketonato leaving ligand (R is three atoms away from the iridium core) has no effect on the rate of substitution by an incoming ligand, in this case phen.

Table 3.36: Values of the second-order rate constants k_2 at the various temperatures and the activation parameters of the reaction of the [Ir(β-diketonato)(cod)] complexes (β-diketone = tftma, tfdma, tfhd, fctfa, fca and bfcm) with 1,10-phenanthroline in acetone.

complex	T/°C	k_2/dm^3 mol^{-1} s^{-1}	$\Delta H^{0*}/kJ$ mol^{-1}	$\Delta S^{0*}/J$ mol^{-1} K^{-1}	$\Delta G^{0*}/kJ$ mol^{-1}
[Ir(fca)(cod)] **Hfca (pK$_a$ = 10.01):** **FcCOCH$_2$COCH$_3$**	15.6 21.0 25.0 31.9 38.7	8.0(5) 11.7(2) 15.3(3) 23.4(7) 34(1)	43.3(8)	-77(3)	66(2)
[Ir(bfcm)(cod)] **Hbfcm (pK$_a$ = 10.41):** **FcCOCH$_2$COC$_6$H$_5$**	15.6 25.4 34.2	35.9(8) 63.9(5) 97(2)	36(2)	-90(6)	63(4)
[Ir(fctfa)(cod)] **Hfctfa (pK$_a$ = 6.56):** **FcCOCH$_2$COCF$_3$**	20.0 25.3 29.6 34.3 38.0	6310(1) 7600(100) 8500(300) 10000(300) 11500(300)	24(1)	-92(4)	51(3)
[Ir(tfhd)(cod)] **Htfhd (pK$_a$ = 6.64):** **CF$_3$COCH$_2$COCH$_2$CH$_3$**	10.8 15.3 19.9 25.1 28.8 33.7	9300(100) 11700(300) 15600(300) 19600(300) 22200(800) 26800(300)	31(2)	-60(5)	49(3)
[Ir(tfdma)(cod)] **Htfdma (pK$_a$ = 6.8):** **CF$_3$COCH$_2$COCH(CH$_3$)$_2$**	15.0 19.6 25.0 29.0 34.0	17200(400) 20200(500) 23200(100) 26800(100) 32300(600)	22(1)	-89(4)	49(2)
[Ir(tftma)(cod)] **Htftma (pK$_a$ = 7.13):** **CF$_3$COCH$_2$COC(CH$_3$)$_3$**	15.3 19.4 25.1 30.3 34.6	16000(1000) 19600(200) 24600(300) 29100(500) 33300(700)	25(1)	-79(4)	49(2)

Table 3.37 page 208 gives the rate constants and activation parameters for the reaction between [Ir(β-diketonato)(cod)] and 1,10-phenanthroline for the complexes studied, as well as related, previously studied, iridium complexes. The following reactivity order in terms of substitution kinetics, utilizing rate constants, for β-diketonato substitution with phen from [Ir(β-diketonato)(cod)] complexes can be deduced:

(fastest substitution) hfaa > tfba > tftma > tfdma > tfhd > tfaa > fctfa

> dbm > ba > bfcm > fca > acac.

This order does not exactly parallel the order of decreasing pK_a for the β-diketone as is illustrated in **Figure 3.55**. It is noticeable that the effect of terminal substituents on the β-diketone in the reactivity of the [Ir(β-diketonato)(cod)] complexes towards substitution and rebinding of the β-diketonato ligand to form C^3-bonded β-diketonato complexes, is comparable to that observed for the reaction of the corresponding rhodium(I) complexes with phenanthroline (paragraph 3.5.2 page 196).   The relationship of log k_2 *versus* the pK_a of the β-diketone for the [Ir(β-diketonato)(cod)] complexes (**Figure 3.55**) is similar to the corresponding relationship of the [Rh(β-diketonato)(cod)] complexes (**Figure 3.48** page 196).   This suggests that the rate determining step of the formation of the five-coordinated C^3-bonded β-diketonato complexes of iridium(I) and the rate determining step for the complete removal by substitution of the β-diketonato ligand from rhodium(I) complexes are probably the same and should correspond to the formation of the 5-coordinate intermediate 32b in **Scheme 3.12**. All other steps are fast and could not be separately characterized.

Figure 3.55: **The relationship between the pK_a of various β-diketones and the second-order rate constant, k_2, for the substitution reaction between [Ir(β-diketonato)(cod)] and 1,10-phenanthroline in acetone at 25 °C.**

The large negative values of ΔS^* (**Table 3.36**) of the [Ir(β-diketonato)(cod)] complexes of this study suggest an associative mechanism and are of the same order and magnitude as found for the substitution reactions of related, previously studied, [Ir(β-diketonato)(cod)] complexes with 1,10-phenanthroline as summarized in **Table 3.37** page 208. The observed large negative entropy values of the [M(β-diketonato)(cod)] complexes of this study and for previously investigated [M(β-diketonato)(cod)] (M = Rh, Ir) complexes, *as well as* the negative values of the volume of activation for [Rh(β-diketonato)(cod)][44] complexes, suggest an associative substitution mechanism for both rhodium(I) and iridium(I) complexes. The reaction mechanism for the substitution the reaction between [Ir(β-diketonato)(cod)] and 1,10-phenanthroline may thus be presented as in **Scheme 3.12**.
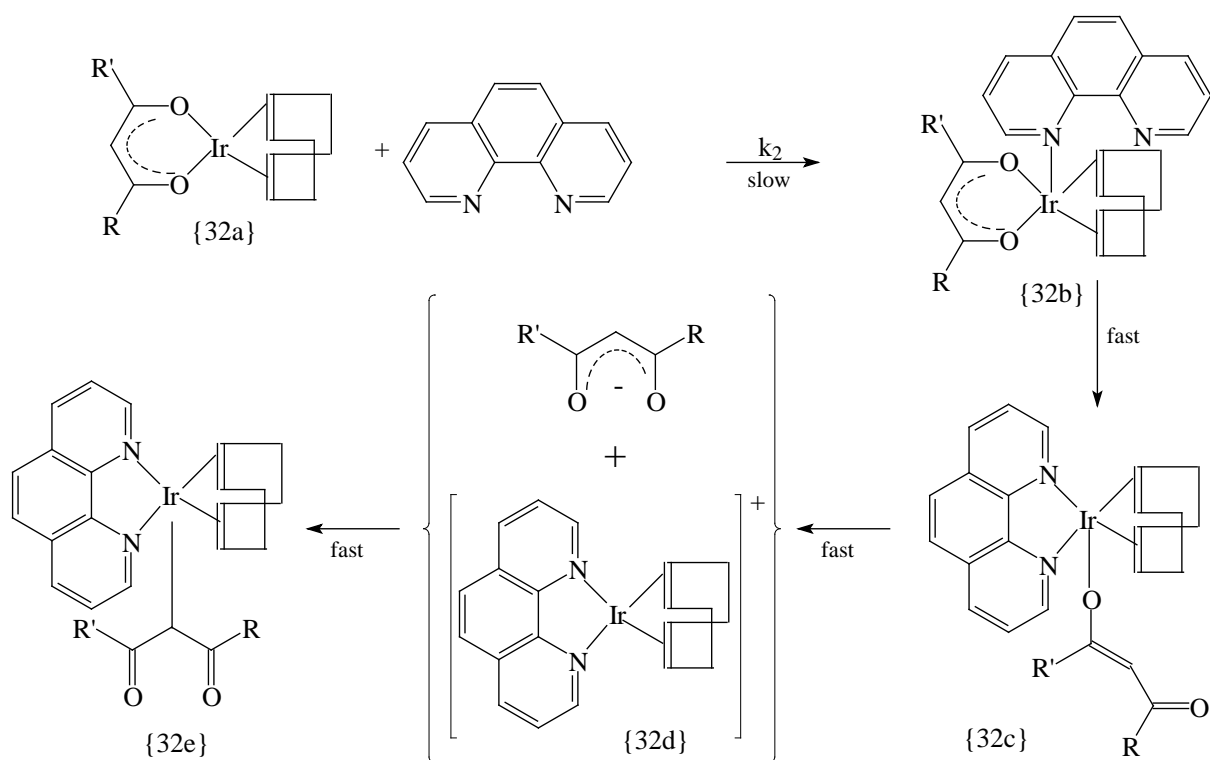
Scheme 3.12: Schematic presentation of the associative mechanism of the substitution reaction between [Ir(β-diketonato)(cod)] and 1,10-phenanthroline. R' and R are the substituents on the β-diketonate ligand (R'COCHCOR)⁻. It is expected that the Ir-O bond nearer to the more electronegative substituent (R = CF₃, Ph or CH₃ in this study) will break first (chapter 2 paragraph 2.1.4.3).

The reaction between the different [Ir(β-diketonato)(cod)] complexes and the incoming ligand 1,10-phenanthroline is represented by:

Equation 3.12:   [Ir(β-diketonato)(cod)] + phen $\rightarrow$ [Ir(β-diketonato-C^3)(phen)(cod)]
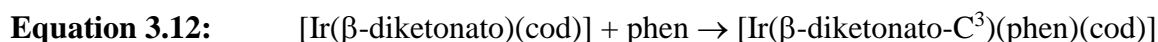
Since all the plots of k_{obs} *vs.* [phen] pass through the origin, the rate law for the reaction can be simplified in the following way:

Rate = $(k_s + k_2[phen])$ [Ir(β-diketonato)(cod)]

  = $k_2[phen]$ [Ir(β-diketonato)(cod)]   because $k_s = 0$ in **Equation 3.10** page 195

  = k_{obs} [Ir(β-diketonato)(cod)]   with $k_{obs} = k_2[phen]$

The second-order rate constant k_2 refers to the bimolecular attack of phen on the iridium complex while k_s represents the first-order rate constant involving solvent based reactions. The observed zero intercept is to be expected because the displacement the bidentate β-diketonato by a monodentate solvent would be very slow compared to the actual substitution reactions studied in this project.

3.5.4 Comparison of the substitution parameters of different [M(β-diketonato)(cod)] complexes with 1,10-phenanthroline where M = Rh and Ir.

Substitution rate constants at 25°C and activation parameters for the reaction between different Rh(I) and Ir(I) complexes of the type [M(β-diketonato)(cod)] or [Rh(fch)(cod)] and 1,10-phenanthroline are summarized in **Table 3.37**. The second-order rate constants given in **Table 3.37** indicate that the rate of substitution for Rh and Ir complexes is fairly similar if β-diketonato ligands have a $pK_a > 7$. However, if the β-diketonato pK_a is smaller than 7, the iridium complexes react approximately one order of magnitude faster than the Rh complexes. The higher rate of substitution for the iridium complexes than for the rhodium complexes is in contrast to what was expected in going from top to bottom in a given periodic table group of transition metals as discussed in chapter 2 paragraph 2.2.4.3 (iv) in going from Ni to Pd to Pt. The higher k_2 for iridium complexes is probably due to the fact that the bulky cod ligand blocks the axial position above and below the plane of the square planer complexes [M(β-diketonato)(cod)] more effectively for [Rh(β-diketonato)(cod)] than for the [Ir(β-diketonato)(cod)] complexes since the Ir atomic radius (1.36Å) is larger than the Rh atomic radius (1.34Å). Ionic radii of Ir are also slightly larger for Ir compared to Rh.[48] The bulky cod ligands will therefore hinder the approach of the bulky 1,10-phenanthroline and thus retard the rate of displacement (k_2 step in

---

[48] Cotton, F.A., Wilkinson, G., Murillo, C.A. and Bochmann, M., *Advanced Inorganic Chemistry*, John Wiley, New York, 1999, p. 1301 - 1304.

Scheme 3.11, page 195, and **Scheme 3.12** page 205), making the [Rh(β-diketonato)(cod)] complex less able to form or accomodate the 5-coordinate transitional state (with the bulky 1,10-phenanthroline) than the [Ir(β-diketonato)(cod)] complex. This exception is supported by the fact that the final substitution product for Ir complexes is actually 5-coordinate while for the Rh complexes it is 4-coordinate.[45] The determined structures of the [Rh(β-diketonato)(cod)][49, 50, 51, 55] and [Ir(β-diketonato)(cod)][52] complexes explain why the cod ligand can prevent the approach of the incoming phen ligand (**Figure 3.56**). Cod coordinate facially with π bonds, not σ bonds, to the Rh and Ir metallic core. This means the C=C coordination fragment of cod is perpendicular to the square planer coordinating geometry around the Rh and Ir centres. By necessity, the square planar coordinating plane around the metal centres passes approximately through the middle of the C=C double bond. This means a fragment of cod, approximate equal in size, is above and below the square planar coordinating plane around the metal nucleus. It is thus to be expected that the reactivity of these complexes would be sensitive to the steric effect between the entering ligand and the complex itself because on both sides of the square planar coordinating plane, cod fragments sterically hinder the approach of the incoming ligand to the vacant axial positions. The crystal structure of the [Ir(acac)(cod)(CH$_3$)(I)][53] also illustrates this blocking steric effect of the cod ligands in the [Ir(acac)(cod)] molecule; the H$_3$C-Ir-I bond angle (156.6(7)°) deviates significantly from the expected 180°, with both carbon and iodine atoms displaced towards the acac ring atom plane away from the cod ligand. It is not exactly certain why Ir and Rh β-diketonato complexes undergo β-diketonato substitution at approximately the same rate if the β-diketonato $pK_a > 7$. What is certain in these cases is that the electron donating properties of these basic β-diketonatos enlarge the relative electron density around the metal core more than the β-diketonatos with low pK_a's possesing electron withdrawing properties. This may have the effect that the rate determining k_2 step in **Scheme 3.11**, page 195, and **Scheme 3.12**, page 205, which involves the formation of a bond between an already electron rich metallic core and an electron rich (*i.e.* basic) phen ligand, becomes so slow, that the bottle-neck effect the cod ligand has in fast reactions, becomes irrelevant in slow reaction rates.

---

[49] Tucker, P.A., Scutcher. W. and Russel, D.R., *Acta Cryst.*, **B31**, 592 (1975).

[50] Swarts. J.C., Vosloo, T.G., Leipoldt, J.G. and Lamprecht, G.J., *Acta Cryst.*, **C49**, 760 (1993).

[51] Leipoldt, J.G., Basson, S.S., Lamprecht, G.J., Bok, L.D.C. and Schlebusch, J.J.J., *Inorg. Chim. Acta*, **40**, 43 (1980).

[52] Tucker, P.A., *Acta Cryst.*, **B37**, 1113 (1981).

[53] Basson, S.S., Leipoldt, J.G., Purcell, W. and Schoeman, J.B., *Acta Cryst.*, **C45**, 2000 (1989).
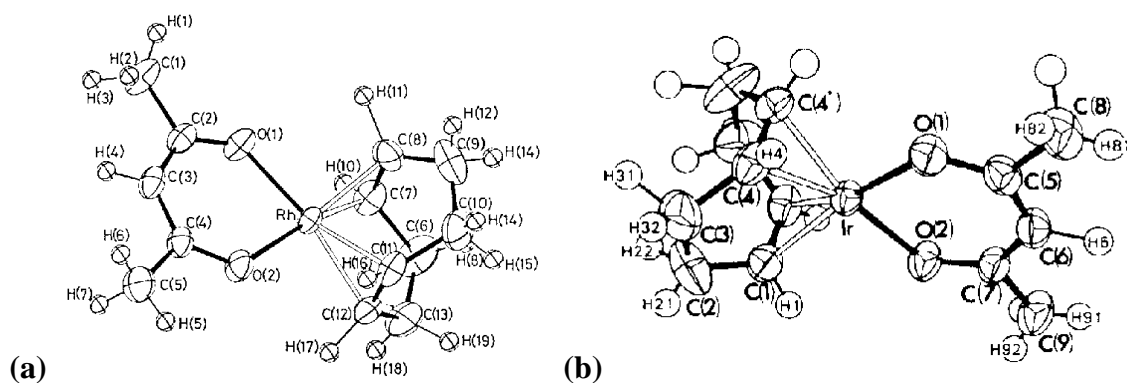
Figure 3.56: Structure of (a) [Rh(acac)(cod)][49] and (b) [Ir(acac)(cod)][52]. The C=C double bonds C(7)-C(8), C(11)-C(12), C(1)-C(1') and C(4)-C(4') are almost perpendicular to the square planar coordination plane.

Table 3.37: Rate constants at 25°C and activation parameters for the reaction between [M(β-diketonato)(cod)] or [M(fch)(cod)] and 1,10-phenanthroline (M = Rh[54, 55, 56], Ir[57]).

β-dike-tonato ligand	pK$_a$[(a)]	[Rh(β-diketonato)(cod)][(b)]				[Ir(β-diketonato)(cod)][(c)]			
		k_2/ dm^3 mol^{-1}s^{-1}	ΔH^*/ kJ mol^{-1}	ΔS^*/ J K^{-1} mol^{-1}	ΔG^*/ kJ mol^{-1}	k_2/ dm^3 mol^{-1} s^{-1}	ΔH^*/ kJ mol^{-1}	ΔS^*/ J K^{-1} mol^{-1}	ΔG^*/ kJ mol^{-1}
dfcm	≈13.1(1)	7.0(2)	19(5)	-162(17)	67(10)	-	-	-	-
bfcm	10.41(2)	30(3)	30.7(3)	-113(1)	64(2)	63.9(5)[(d)]	36(2)	-90(6)	63(4)
fca	10.01(1)	17.8(2)	29(4)	-123(14)	65(8)	15.3(3)[(d)]	43.3(8)	-77(3)	66(2)
dbm	9.35	61.4	27.3	-119	62	413	26.3	-106	58
acac	8.95	29.0	32.6	-108	64	13.6	29.5	-125	67
ba	8.70	51.2	31.6	-106	63	85.8	31.5	-102	62
fctca	7.13(2)	1375(10)	31(2)	-81(5)	55(1)	-	-	-	-
tftma	7.13(1)[(d)]	-	-	-	-	24600(300)[(d)]	25(1)	-79(4)	49(2)
fch[(e)]	7.04(1)[(d)]	47(1)[(d)]	35(2)	-94.7(1)	63	-	-	-	-
tfdma	6.8	-	-	-	-	23200(100)[(d)]	22(1)	-89(4)	49(2)
tfhd	6.64(1)[(d)]	-	-	-	-	19600(300)[(d)]	31(2)	-60(5)	49(3)
fctfa	6.56(3)	558(10)	25.3(4)	-107(1)	57.2(1)	7600(100)[(d)]	24(1)	-92(4)	51(3)
tfaa	6.30	1330	30.5	-83	55	17100	24.0	-83	49
tfba	6.30	2420	26.2	-93	53	25100	23.1	-81	47
hfaa	4.71(1)	276000	23.2	-63	41	3000000	-	-	-

(a) pK$_a$ values from ref **58** , 35 (ferrocene-containing β-diketones), 22 (Htfdma), **59** (Hhfaa) and current study (Hfch, Htftma, Htfhd). (b) In methanol at 25°C. (c) In acetone at 25°C. (d) This study. (e) Hfch is a keto-aldehyde.

54 Leipoldt, J.G. and Grobler, E.C., *Transition Met. Chem.,* **11**, 110 (1986).

55 Du Plessis, W.C., *Synthesis, thermodynamic, electrochemical and kinetic aspects of ferrocene-containing β-diketones (in Afrikaans), M.Sc. Thesis*, University of the Orange Free State, R.S.A., 1996.

56 Vosloo, T.G., *Synthesis, kinetics and structural aspects of β-diketonato complexes with a potential medical application (in Afrikaans), M.Sc. Thesis*, University of the Orange Free State, R.S.A., 1991.

57 Leipoldt, J.G., Basson, S.S., van Zyl, G.J. and Steyn, G.J.J., *J. Organomet. Chem.,* **418**, 241 (1991).

58 Stary, J., *The Solvent Extraction of Metal Chelates*, MacMillan Company, New York (1964), p. 196 – 202.

59 Ellinger, M., Duschner, H. and Starke, K., *J. Inorg. Nucl. Chem.*, **40**, 1063 (1978).

3.6   Cyclic voltammetry.

The formal reduction potential ($E^{0'}$ values *vs.* Ag/Ag$^+$) of the ferrocenyl group of Hfch and of the ferrocenyl group of the β-diketonato ligands in several rhodium and iridium complexes is reported in this part of this study. Peak anodic oxidation potentials, E_{pa}, of the metals rhodium and iridium are also reported. Correlation between $E^{0'}$ or E_{pa} and several parameters such as pK_a, kinetic rate constants and group electronegativity are also reported. All values are measured *vs.* Ag/Ag$^+$ in the presence of ferrocene as an internal standard. $E^{0'}$(Fc/Fc$^+$) = 0.077 V *vs.* Ag/Ag$^+$;[19] 0.400V *vs.* NHE[60].

3.6.1   *Cyclic voltammetry of Hfch and correlation to ferrocene-containing β-diketones.*

First, the formal reduction potential of 2-ferrocenoyletan-1-al (Hfch = FcCOCH$_2$COH) {7} was determined and compared to $E^{0'}$ of ferrocene-containing β-diketones of the type FcCOCH$_2$COR with R = CF$_3$, CCl$_3$, CH$_3$, C$_6$H$_5$ and Fc.

Cyclic voltammetry results for Hfch are shown in **Figure 3.57** (a) and are summarized in **Table 3.38**. The difference in peak anodic (E_{pa}) and peak cathodic potential (E_{pc}), ΔE_p, for Hfch, indicate reasonable electrochemical reversibility. Electrochemical reversibility of a one-electron process at 25 ^{0}C is characterized by ΔE_p = 59 mV and is independent of scan speed. The largest E_{pa} drift detected was 5 mV when the scan rate was increased from 50 to 200 mV s^{-1}, but this did not influence $E^{0'}$. The $E^{0'}$ values remained constant between scan rates of 50 and 200 mV s^{-1}**.** The ratio i_{pa} / i_{pc} (i_{pa} and i_{pc} are the peak anodic and cathodic currents) was in all cases close to unity. This implies that the electrochemical oxidation of the iron(II) nucleus of the ferrocenyl groups is not followed by a chemically induced reduction[61] of the Fe(III) nucleus of the ferrocenium group by the hydroxyl group of the enol form of Hfch, a reaction that has been observed in other ferrocenyl/hydroxyl systems.[62] The peak current, i_p, for the first cycle of a electrochemical reversible system[63] is described by the Randles-Sevcik equation.

[60] Koepp, H.M., Wendt, H. and Stehlow, H., *Z. Electrochem.*, **64**, 483 (1960).

[61] Kissinger, P.T. and Heineman, W.R., *J. Chem. Ed.*, **60**, 702 (1983).

[62] (i) Swarts, J.C., Neuse, E.W. and Lamprecht, G.J., *J. Inorg. Organomet. Polym.*, **4**, 143 (1994).

Equation 3.13: $$i_p = (2.69X10^5)n^{\frac{3}{2}}AD^{\frac{1}{2}}C\upsilon^{\frac{1}{2}}$$

with n the amount of electrons transferred, one for the ferrocenyl group, A the electrode area in cm^2, D the diffusion coefficient in $cm^2\ s^{-1}$, C the concentration and υ the scan rate in $V\ s^{-1}$. The predicted linear relationships between i_p and $\upsilon^{1/2}$ were found and are illustrated in **Figure 3.57** (b).

(a)   **(b)**
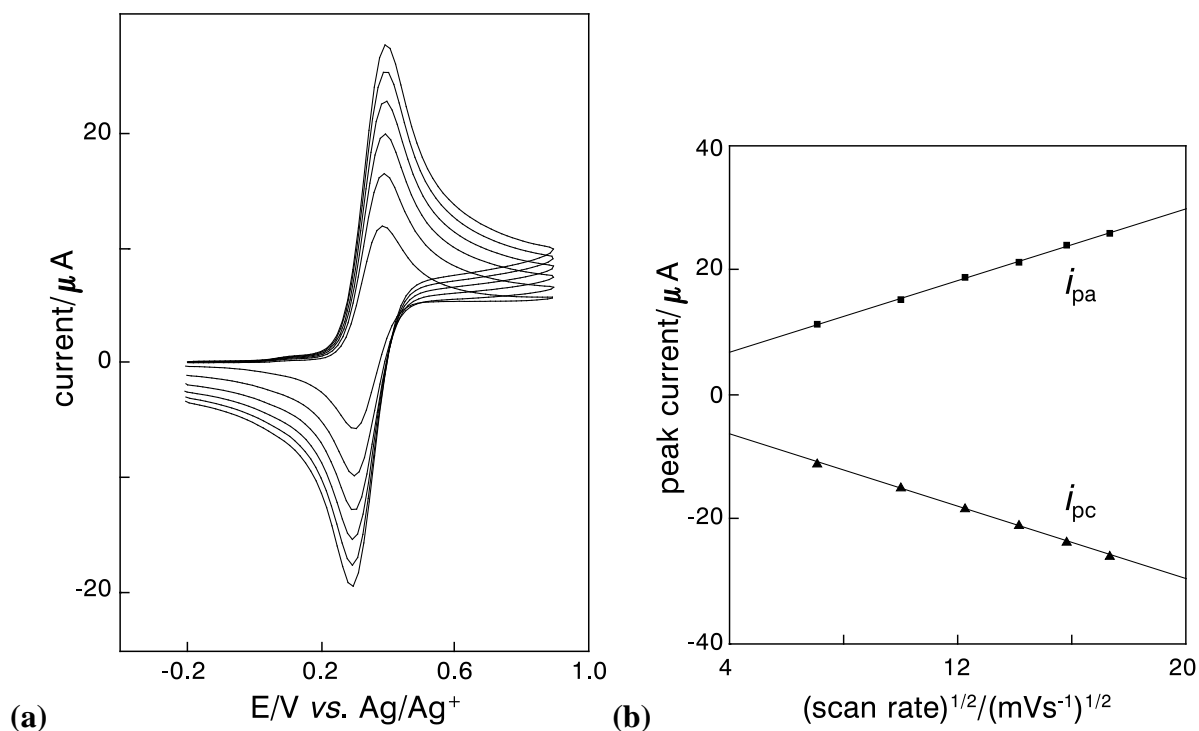
Figure 3.57: **(a).** **Cyclic voltammograms of a 2 mmol dm^{-3} solution of Hfch measured in 0.1 mol dm^{-3} TBAPF$_6$/CH$_3$CN at scan rates of 50, 100, 150, 200, 250 and 300 mV s^{-1} on a Pt working electrode at 25.0(1) °C *versus* Ag/Ag$^+$. (b) Anodic and cathodic peak currents *and* (scan rate)$^{1/2}$ has a linear relationship which illustrates the validity of the Randles-Sevcik equation for Hfch. Graph slopes = ±1.45(3) μA (mVs^{-1})$^{-1/2}$.**

The cyclic voltammetric response of Hfch, together with the CV's of ferrocene and the five ferrocene-containing β-diketones of the type FcCOCH$_2$COR with R = CF$_3$, CCl$_3$, CH$_3$, C$_6$H$_5$ and Fc[19] are illustrated in **Figure 3.58** (a). As reported previously, ferrocene itself under identical conditions showed reversible behaviour (ΔE_p = 62 mV, i_{pa} / i_{pc} = 1.00 at a scan rate of 50 mV s^{-1} with E$^{0'}$ = 0.077 mV *versus* Ag/Ag$^+$ reference electrode). The same electrochemical results were obtained when ferrocene was added as internal standard to the Hfch solution as illustrated in **Figure 3.58** (b).

(ii) Swarts, J.C., *Macromolecular Drug carriers for biomedical Applications, Ph.D. Thesis*, University of the Witwatersrand, (1991) p. 221 – 224.

[63] Mabbott, G.A., *J. Chem. Ed.*, **60**, 697 (1983).

Table 3.38: Electrochemical data of the keto-aldehyde Hfch measured in 0.1 mol dm^{-3} TBAPF$_6$/CH$_3$CN on a Pt electrode at 25.0(1) °C versus Ag/Ag$^+$, [Hfch] = 2.0 mmol dm^{-1}.

v/mV s^{-1}	E$_{pa}$/V	ΔE$_p$ / mV	E$^{0'}$ /V vs. Ag/Ag$^+$	E$^{0'}$ /V vs. Fc/Fc$^+$	i_{pa}/μA	i_{pa} / i_{pc}
50	0.384	82	0.342	0.265	11.26	1.02
100	0.388	88	0.344	0.267	15.21	1.02
150	0.388	89	0.344	0.267	18.79	1.03
200	0.389	94	0.342	0.265	21.18	1.02

(a)   **(b)**
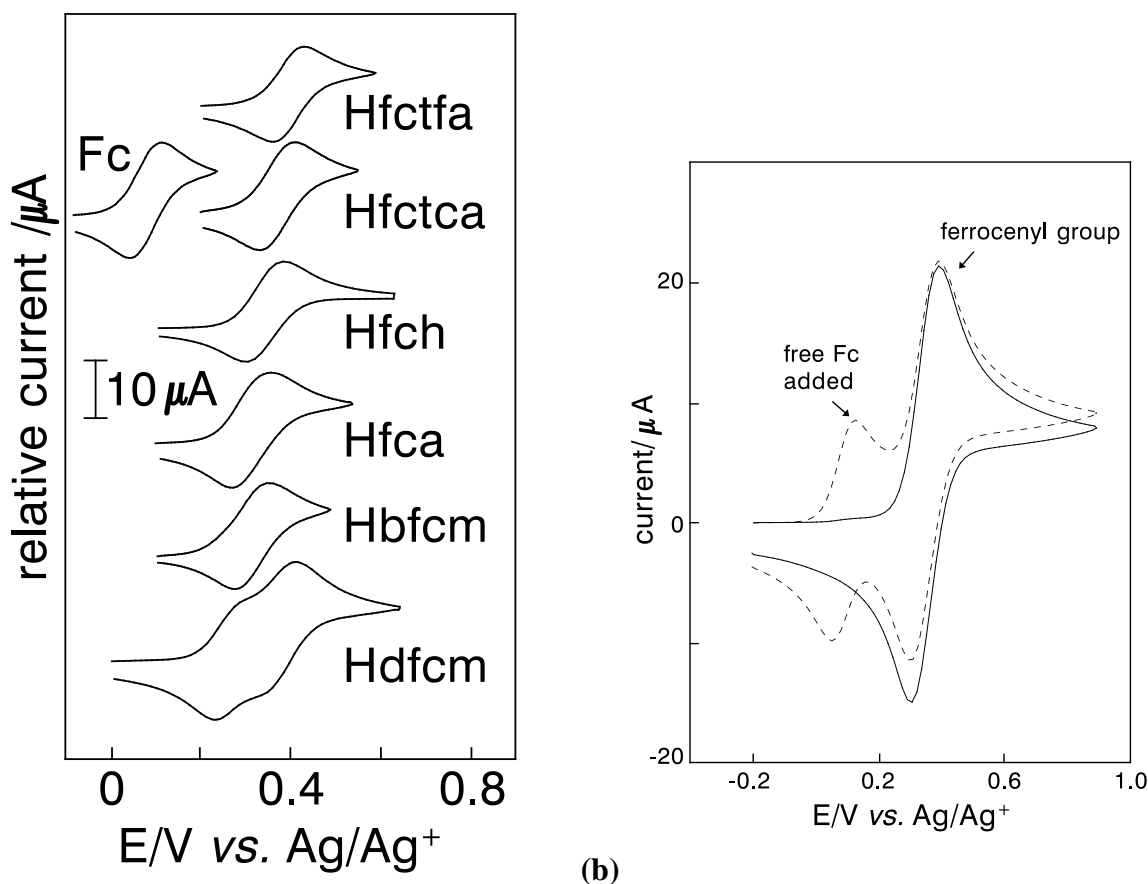
Figure 3.58: **(a) Cyclic voltammograms of 2 mmol dm^{-3} solutions of ferrocene (Fc), Hfch and ferrocene-containing β-diketones measured in 0.1 mol dm^{-3} TBAPF$_6$/CH$_3$CN at a scan rate of 50 mV s^{-1} on a Pt working electrode at 25.0(1) °C versus Ag/Ag$^+$. (b) CV of a 2.7 mmol dm^{-3} solution Hfch at a scan rate of 100 mV s^{-1} with ferrocene added as an internal standard. E$^{0'}$(Fc) = 0.077 mV and ΔE$_p$(Fc) = 69.6 mV.**

The summary of the chemical and electrochemical data of the various FcCOCH$_2$COR in **Table 3.39** indicates that the ferrocenyl group on FcCOCH$_2$COR becomes increasingly difficult to oxidize as more electron density is withdrawn from it by the substituent R in the order:

(least electron withdrawing) Fc < C$_6$H$_5$ < CH$_3$ < H < CCl$_3$

< Fc$^+$ < CF$_3$ (most electron withdrawing).

Fc^+ is the abbreviation for the oxidized ferrocenyl ion, *i.e.* ferrocenium. This fact implies good communication between the ferrocenyl group and the substituent R on $FcCOCH_2COR$ and allows for the determination of group electronegativities of the R-groups by measuring the reduction potentials $E^{0'}$ of the ferrocenyl group on $FcCOCH_2COR$. In a previous study, group electronegativity, χ_H, of 2.13 (Gordy scale) was allocated to the bonded hydrogen group on the grounds of the value of the carbonyl stretching frequency of molecules of the type XCOY, X,Y = H, Cl, Br.[64] With the formal reduction potential of Hfch now known ($E^{0'}$ = 344 mV), it was found that the value χ_H = 2.13 did not fit the linear relationship between $E^{0'}$ and χ_R for $FcCOCH_2COR$ with R = Fc, C_6H_5, CH_3, CCl_3 and CF_3 as illustrated in **Figure 3.59** (a). To fit the linear $E^{0'}$ - χ_R relationship, the group electronegativity of the H group must be χ_H = 2.55. The group electronegativity value χ_H = 2.55 (Gordy scale) is the same value that was allocated to H from calculations using the IR stretching frequencies (bond vibrations), ν_{PO}, of $R^1R^2R^3PO$. R^1, R^2 and R^3 are the groups for which group electronegativities were determined.[20] The fact that R = H is an 'atomic' group, probably explains why the "group electronegativity" value of 2.13 for H as obtained by utilizing the carbonyl stretching frequency of the ketone HCOX, is less accurate. Canonical forms[64] of the type
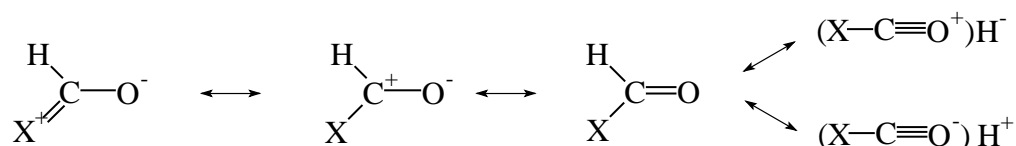
will result in the measured CO frequency not being representative of a true carbonyl stretching frequency and it must, therefore, translate into an incorrect χ_H value.

The dependence of the reduction potentials $E^{0'}$ on the pK_a of $FcCOCH_2COR$ is displayed in **Figure 3.59** (b). Hfch and Hfctfa do not fit on the linear line. The deviation in the case of Hfctfa[35] was explained by reversible hydroxylation as shown in **Scheme 3.13** (a), similar to that observed for Hhfaa[59] **Scheme 3.13** (b). Further research is required to explain this observed deviation in the case of Hfch, but reversible hydroxylation as shown in **Scheme 3.13**, may be relevant.

---

[64] Kagarise, R.E., *J. Am. Chem. Soc.,* **77**, 1377 (1955).

(a)   **(b)**
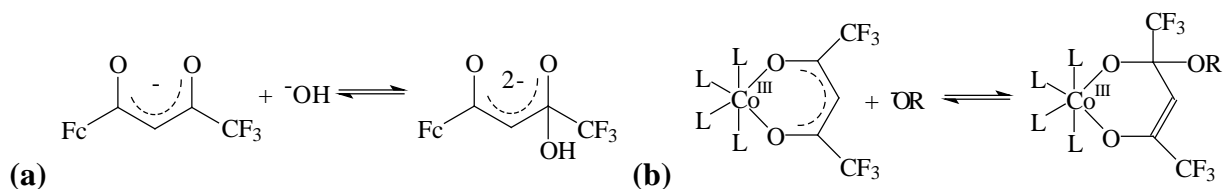
Scheme 3.13: **(a)** Reversible hydroxylation of the basic form of Hfctfa. **(b)** Reversible hydroxylation (R=H)[65] and methoxylation (R=Me)[66] for hfaa complexes of cobalt(III). L = ammonia or an amine.

Table 3.39: Group electronegativities, χ_R, for the indicated R groups, observed β-diketone pK_a values, $\nu(C=O)_R$ of esters of the type $RCOOCH_3$ and formal reduction potentials $E^{0'}$ vs. Ag/Ag⁺ of the ferrocenyl group, Fc, in $FcCOCH_2COR$.

R	χ_R/Gordy scale [c]	pK_a [a]	$\nu(C=O)_R$/cm⁻¹ [a]	$E^{0'}$/V [c]
CF₃	3.01	6.53(3)	1785	0.394
CCl₃	2.76	7.15(2)	1768	0.370
CH₃	2.34	10.01(2)	1738	0.313
C₆H₅	2.21	10.41(2)	1725	0.306
H	2.55 [b]	7.04(1) [b]	1717	0.344 [b]
Fc	1.87	13.1(1)	1700	0.265, 0.374

(a) results from reference 35   (b) results from this study   (c) results from reference 19 and 35.

(a)   **(b)**
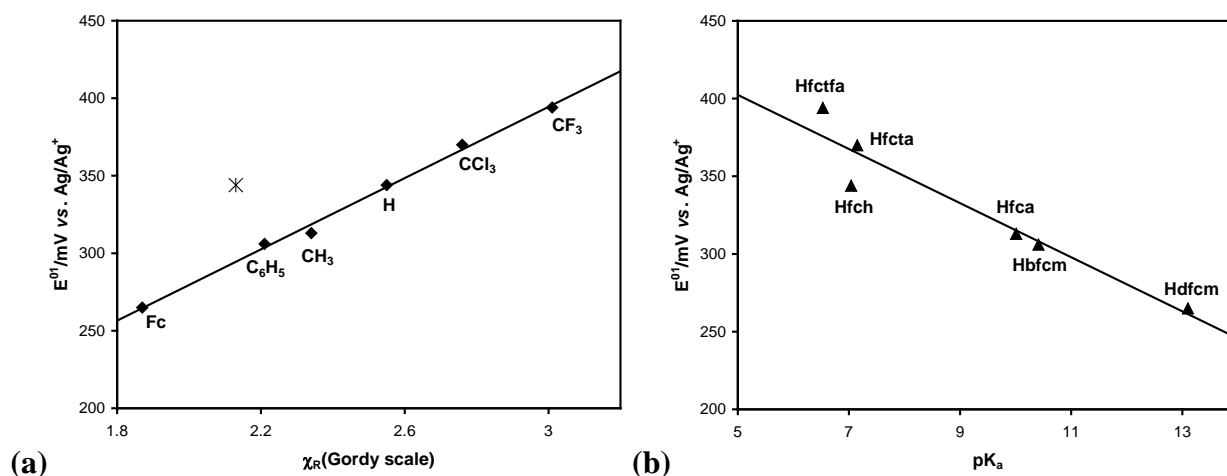
Figure 3.59: **(a)** Linear relationship between formal reduction potential, $E^{0'}$, and group electronegativity, χ_R, of $FcCOCH_2COR$ with R = Fc, C₆H₅, CH₃, CCl₃, CF₃ and H. The point marked T indicates that $\chi_H = 2.13$ obtained from IR studies on HCOOMe is incorrect. The group electronegativity of H should be $\chi_H = 2.55$. **(b)** The relationship between the formal reduction potentials, $E^{0'}$, of the ferrocenyl group and the pK_a of $FcCOCH_2COR$.

[65] Aygen, S., Paulus, E.F., Kitamura, Y. and van Eldik, R., *Inorg. Chem.*, **26**, 769 (1987).

[66] Purcell, W., Leipoldt, J.G. and Kitamura, Y., *Inorg. Chim. Acta,* **177**, 151 (1990).

3.6.2 Cyclic voltammetry of [Rh(fch)(cod)] and [Rh(β-diketonato)(cod)] complexes.

The CV of [Rh(fca)(cod)] displayed in **Figure 3.61** (a) page 216 represents the general trend observed for all [Rh(FcCOCHCOR)(cod)] complexes as displayed in **Figure 3.61** (b). The electrochemical data of these [Rh(FcCOCHCOR)(cod)] complexes are summarized in **Table 3.41** page 217. The cyclic voltammograms of the [Rh(FcCOCHCOR)(cod)] complexes ($R = CF_3$, CCl_3, H, C_6H_5, CH_3 and Fc) all exhibit an electrochemically irreversible anodic oxidation peak which corresponds to the oxidation of rhodium(I) according to **Equation 3.14** as well as an electrochemically reversible Fc^+/Fc couple according to **Equation 3.15**. The peak anodic current i_{pa} of the ferrocenyl group was determined as described in the next paragraph. The ratio $i_{pa}/i_{pc} \approx 1$ and $\Delta E_p < 80$ mV at scan rates 50 mV s^{-1} for the CV of the ferrocenyl group for all the [Rh(FcCOCHCOR)(cod)] complexes (**Table 3.41** page 217, except for $R = CCl_3$ with $\Delta E_p = 92$ mV), indicate a one-electron transfer for the Fc ligand (**Equation 3.15**). The bulk electrolysis (paragraph 3.6.8 page 243) confirmed that 3 electrons were transferred during the oxidation of the [Rh(FcCOCHCOR)(cod)] complexes. Two electrons were required by the Rh^{3+}/Rh^{1+} couple while one electron was needed for the Fc^+/Fc couple. A two-electron process to generate a Rh(III) centre was also found for the CV of [Rh(oxa)(cod)][67] as described in chapter 2, paragraph 2.3.8.2.

Equation 3.14: $Rh(I) \rightarrow Rh(III) + 2e^-$

Equation 3.15: $Fc^+ + e^- \square Fc$

The anodic peak current $i_{pa}(Fc)$ of the ferrocenyl group (peak 2 in **Figure 3.60**) of the [Rh(FcCOCHCOR)(cod)] complexes could not be measured directly from the CV of [Rh(FcCOCHCOR)(cod)] due to the overlapping of the oxidation peak of the ferrocenyl group with the oxidation peak of rhodium(I) (peak 1 in **Figure 3.60**). The following reasoning was applied to obtain it. The oxidation decay current of the ferrocenyl group and of rhodium(I) are both proportional to the diffusion rate of the [Rh(FcCOCHCOR)(cod)] complex. Since both Rh and Fc are part of the same complex, this diffusion rate should be the same even though Rh(I) oxidation represents a two electron and Fc a one electron process (because the molecule does not split in half to allow different diffusion rates for the Rh and Fc fragments). The decaying current of Rh(I) oxidation can therefore be reconstructed by multiplying the decaying current of Fc

[67] Anderson, J.E., Murphy, C.P., Real, J. and Bayón, J.C., *Inorg. Chim. Acta.*, **209**, 151 (1993).

oxidation from the basis line AC with the ratio i_{pa}(Rh)/i_{pc}(Fc) to allow for the two electron flow during Rh(I) oxidation as compared to the one electron flow during Fc oxidation. The artificially obtained line is shown as **-----** in **Figure 3.60**. This line may then be translatorily shifted without distortion to coincide exactly with the E_{pa} value of the rhodium(I) oxidation peak (peak 1 in **Figure 3.60**) and is indicated by **……** in **Figure 3.60**. The anodic peak current i_{pa}(Fc) of the ferrocenyl group can then be measured as the perpendicular current between peak 2 and the newly obtained anodic decay current for Rh(I) oxidation, as indicated in **Figure 3.60**. Irreversibility of the Rh^{3+}/Rh^{1+} redox process is not important as only the oxidation current was considered in this construction. Unpublished studies in this laboratory of Rh(I) oxidation of similar non-ferrocene-containing Rh(I) complexes (chapter 2 paragraph 2.3.8.3) showed that the newly formed Rh(III) complex is stable enough not to decompose during the time scale of an oxidative sweep till the reversal potential is reached.
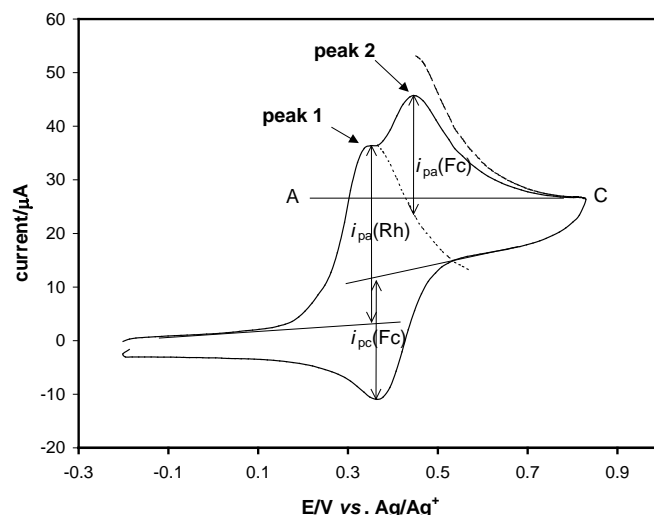
Figure 3.60: **Construction of the decay current of Rh(I) oxidation may be achieved by multiplying the decaying current of Fc oxidation (peak 2) with the ratio i_{pa}(Rh)/i_{pc}(Fc). The artificially obtained line is shown as ----- . This line is then translatorily shifted without distortion to coincide exactly with the E_{pa} value of the rhodium(I) oxidation peak (peak 1) and is indicated by ……. The anodic peak current i_{pa}(Fc) of the ferrocenyl group can then be measured as the current between peak 2 and the newly obtained anodic decay current for Rh(I) oxidation.**

Klingler and Kochi[68] have demonstrated that, under conditions where follow-up chemical reactions are much faster than the reverse electron transfer (as is the case here with the oxidation of Rh(I)), the anodic peak potential becomes independent of these follow-up chemical reactions since the forward electron transfer is the rate-determining step. The anodic peak potential E_{pa} may then be expressed in terms of the electrode potential $E^{0'}$, the transfer coefficient β and the electron transfer rate constants $k(E^{0'})$ and $k(E_{pa})$ at the peak potential and the electrode potential

---

[68] Klinger, R.J. and Kochi, J.K., *J. Am. Chem. Soc.,* **102**, 4790 (1980).

respectively: $E_{pa} = E^{0'} + [nRT/\beta F]ln[k(E_{pa})/k(E^0_{ox})],$

$k(E_{pa})$ is a function of the sweep rate ν according to $k(E_{pa}) = 2.18[D\beta nF\nu/RT]^{1/2}$. The other symbols are standard and were defined on page 210. According to Klinger, if D, which is proportional to $i_{pa}/(C\nu^{1/2})$, is constant for a series of metal complexes, and β and $k(E^{0'})$ are constant, the peak oxidation potential E_{pa} may be linearly related to $E^{0'}$ with a slope of unity at constant sweep rate, $E_{pa} = E^{0'} + constant.$

Under such conditions, the anodic peak potential E_{pa} may replace $E^{0'}$ as the thermodynamically defined electrode potential in determining relative relationships. The ratio $i_{pa}/(C\nu^{1/2})$ for the oxidation of rhodium of the [Rh(FcCOCHCOR)(cod)] complexes as given in **Table 3.40**, are constant within the experimental error. The rhodium (or iridium) anodic peak potential E_{pa} will therefore be used in this thesis for determining relationships between E_{pa} and various other physical quantities including substitution kinetic rate constants, k_2.
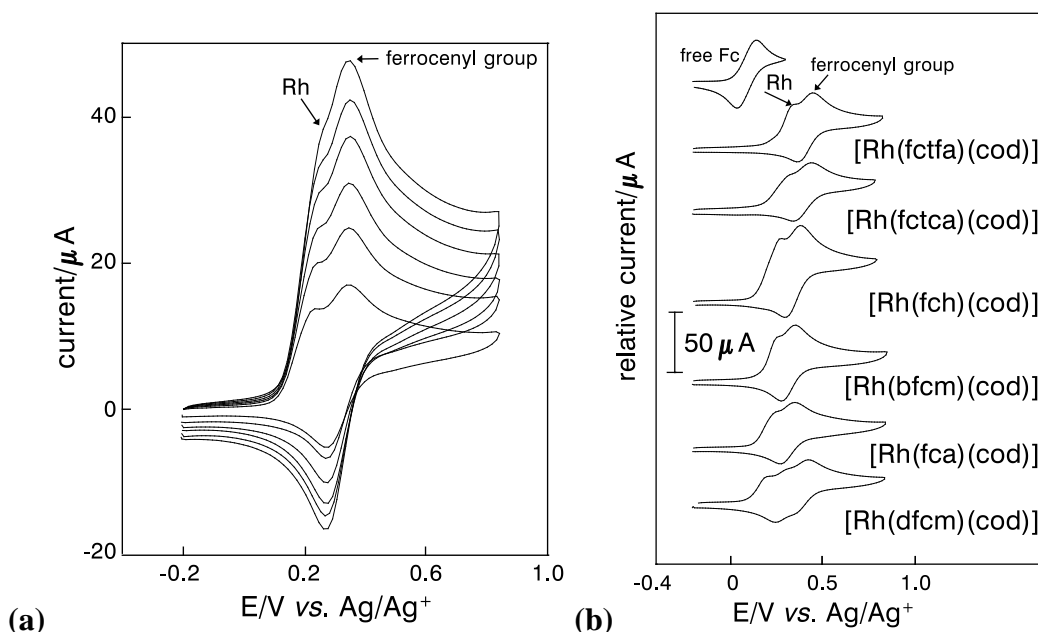
Figure 3.61: (a) Cyclic voltammograms of a 1 mmol dm⁻³ solution of [Rh(fca)(cod)] measured in 0.1 mol dm⁻³ TBAPF₆/CH₃CN at scan rates of 25 - 150 mV s⁻¹ (25 mV increments) on a glassy carbon working electrode at 25.0(1) °C *versus* Ag/Ag⁺. (b) Cyclic voltammograms of different [Rh(FcCOCHCOR)(cod)] complexes measured at a scan rate of 100 mV s⁻¹ under the same conditions as in (a) with R = CF₃, CCl₃, H, C₆H₅, CH₃ and Fc. Concentrations of the complexes indicated in **Table 3.41**.

Table 3.40: The ratio $i_{pa}/(C\nu^{1/2})$ proportional to the diffusion coefficient D for the electrochemical oxidation of rhodium in various [Rh(FcCOCHCOR)(cod)] complexes.

R group	CF₃	CCl₃	H	C₆H₅	CH₃	Fc	average
$i_{pa}/(C\nu^{1/2})$	3.20(4)	3.34(4)	3.28(3)	3.34(3)	3.16(4)	3.1(2)	3.2(1)

Table 3.41: **Electrochemical data and conditions for complexes of the type [Rh(FcCOCHCOR)(cod)] measured in 0.1 mol dm^{-3} TBAPF$_6$/CH$_3$CN on a glassy carbon electrode at 25.0(1) °C versus Ag/Ag$^+$. The concentration of the complexes is indicated within the table.**

v/m V_s^{-1}	rhodium		ferrocenyl group					rhodium		ferrocenyl group				
	E_{pa} /V	i_{pa} /μA	E_{pa} /V	ΔE_p /mV	$E^{0'}$ /V	$-i_{pc}$/ μA	i_{pa}/i_{pc}	E_{pa} /V	i_{pa} /μA	E_{pa} /V	ΔE_p /mV	$E^{0'}$ /V	$-i_{pc}$/ μA	i_{pa}/i_{pc}
	[Rh(fctfa)(cod)] - 1.0 mmol dm^{-3}							[Rh(fca)(cod)] - 1.0 mmol dm^{-3}						
50	0.332	22.8	0.445	77	0.406	17.1	0.98	0.247	19.1	0.345	71	0.309	12.3	0.98
100	0.346	33.2	0.446	80	0.406	23.9	1.02	0.254	28.6	0.347	76	0.309	16.9	1.02
150	0.358	39.3	0.449	88	0.405	28.3	1.01	0.264	35.6	0.347	78	0.309	21.1	1.00
200	0.358	45.5	0.449	91	0.404	31.9	1.04	0.269	41.8	0.347	81	0.307	25.3	0.99
	[Rh(fctca)(cod)] - 0.8 mmol dm^{-3}							[Rh(dfcm)(cod)] - 0.8 mmol dm^{-3} first ferrocenyl group						
50	0.321	18.5	0.432	92	0.386	14.8	0.98	0.200	12.1	0.310	64	0.278	*	*
100	0.333	25.9	0.437	95	0.389	19.2	0.98	0.212	19.9	0.315	71	0.280	*	*
150	0.341	31.9	0.429	98	0.390	23.0	0.98	0.219	25.6	0.317	76	0.279	*	*
200	0.345	37.2	0.438	100	0.388	25.9	1.00	0.222	30.6	0.320	81	0.280	*	*
	[Rh(fch)(cod)] - 1.7 mmol dm^{-3}							[Rh(dfcm)(cod)] - 0.8 mmol dm^{-3} second ferrocenyl group						
50	0.263	31.5	0.380	79	0.341	22.0	0.98	-	-	0.420	81	0.380	10.4	*
100	0.273	49.3	0.380	83	0.338	33.4	0.97	-	-	0.423	88	0.379	17.7	*
150	0.281	61.8	0.384	91	0.338	40.1	0.97	-	-	0.424	92	0.378	22.2	*
200	0.294	73.1	0.387	97	0.338	46.8	0.99	-	-	0.425	95	0.377	25.4	*
	[Rh(bfcm)(cod)] - 1.0 mmol dm^{-3}							* not accurately determinable						
50	0.249	24.3	0.348	67	0.314	17.6	0.98							
100	0.261	33.9	0.350	74	0.314	24.7	0.97							
150	0.266	41.9	0.354	79	0.314	30.6	0.98							
200	0.274	47.6	0.356	85	0.314	35.5	0.98							

Rhodium(III) reduction.

The main focus area of this thesis was to investigate, by means of cyclic voltammetry, the electrochemical behaviour of the ferrocenyl fragment of the ligand coordinated to rhodium. The results indicated that Rh(I) is oxidised at potentials not too far from the potential range in which the ferrocenyl fragment is active. Therefore a great deal of attention is also given to the interpretation of the results of Rh(I) oxidation. The electrochemically generated Rh(III) complex is reduced in the potential range ((-0.4) – (-0.9)) V. While it is not the objective to interpret and explain the position, size and shape of the observed Rh(III) reduction waves, at least one example of Rh(III) reduction is shown for the sake of completeness. **Figure 3.62** presents selected CV's of the [Rh(fca)(cod)] and [Rh(fch)(cod)] complexes over a wide potential window. There is no Rh(III) present in the analyte solution and it can only be generated electrochemically by the oxidation of Rh(I). During the negative scans, indicated with dashed lines, there was no Rh(III) to be reduced back to Rh(I), but there was Rh(I) in the analyte solution to be oxidized. The small reduction peak at *ca.* –0.44 V *vs.* Ag/Ag$^+$, obtained from a positive scan (solid line) is, therefore,

coupled to the oxidation peak for Rh(I) as indicated.
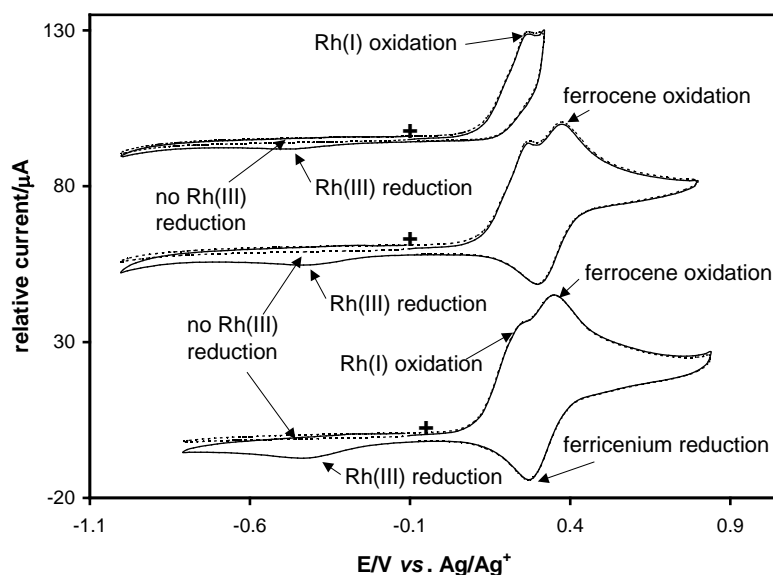
Figure 3.62: Cyclic voltammogram of 1.2 mmol dm^{-3} [Rh(fca)(cod)] (bottom) and 1.1 mmol dm^{-3} [Rh(fch)(cod)] (middle and top) measured in 0.1 mol dm^{-3} TBAPF$_6$/CH$_3$CN at a scan rate of 100 mV s^{-1} on a glassy carbon working electrode at 25.0(1) °C *versus* Ag/Ag$^+$. Scans initiated at + in the positive scan direction for the solid lines and in the negative scan direction for the dashed lines.

The chemical and electrochemical data in **Table 3.42** were used to set up a linear free energy relationship between the substitution kinetic parameter k_2 and the thermodynamic quantity E_{pa} of Rh in [Rh(FcCOCHCOR)(cod)] (**Figure 3.63** (b)). Substitution rate constants, k_2, are for the reaction between various [Rh(FcCOCHCOR)(cod)] complexes and 1,10-phenanthroline in methanol at 25.0(1) °C. A definite relation was found between $\log k_2$ and $E_{pa}(Rh^I)$. The fastest substitution was observed in complexes where Rh^I showed the most positive oxidation potentials.

Table 3.42: Electrochemical data and substitution kinetic data for [Rh(FcCOCHCOR)(cod)] complexes. R = CF$_3$, CCl$_3$, H, C$_6$H$_5$, CH$_3$ and Fc. Oxidation peak potentials were measured in 0.1 mol dm^{-3} TBAFP$_6$/CH$_3$CN on a glassy carbon electrode at 25.0(1) °C at a constant sweep rate of 100 mV s^{-1} and are reported *vs.* Ag/Ag$^+$. Substitution rate constants k_2 are for the reaction between various [Rh(FcCOCHCOR)(cod)] complexes and 1,10-phenanthroline in methanol at 25.0(1) °C. pK$_a$ values are for the free uncoordinated β-diketones.

complex	R	χ_R/Gordy scale [a]	E_{pa}(Rh) [d] / V	$E^{0'}$(Fc) [d] / V	pK$_a$ [b]	k_2 [c] /mol^{-1} dm^3 s^{-1}	log k_2
[Rh(dfcm)(cod)]	Fc	1.87	0.212	0.280, 0.379	13.1(1)	7.0(2)	1.946
[Rh(fca)(cod)]	CH$_3$	2.34	0.254	0.309	10.01(1)	17.8(2)	2.879
[Rh(bfcm)(cod)]	C$_6$H$_5$	2.21	0.261	0.314	10.41(2)	30(3)	3.401
[Rh(fch)(cod)]	H	2.55 [d]	0.273	0.338	7.04(1) [d]	47 [d]	3.85
[Rh(fctca)(cod)]	CCl$_3$	2.97	0.333	0.389	7.13(2)	1375(10)	7.226
[Rh(fctfa)(cod)]	CF$_3$	3.01	0.346	0.406	6.56(3)	588(10)	6.324

(a) results from reference 19   (b) results from reference 35
(c) results from reference 54, 55 and 56   (d) results from this study

The relationship between $E^{0'}$ of the ferrocenyl group in [Rh(FcCOCHCOR)(cod)] and the pK_a of the free uncoordinated FcCOCH$_2$COR shown in **Figure 3.63** (a), indicates, as in the case of the free Hfch (paragraph 3.6.1), that the pK_a of Hfch alone, does not give a proper indication of the group electronegativity of Hfch.

(a)   **(b)**
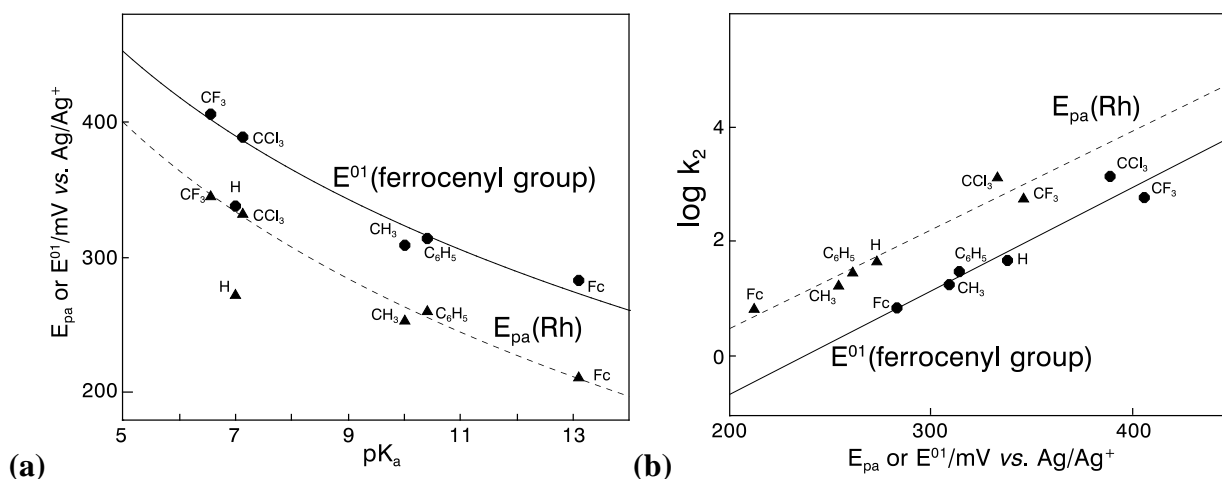
Figure 3.63: (a) The relationship between $E^{0'}$ of the ferrocenyl group or E_{pa} of Rh in [Rh(FcCOCHCOR)(cod)] and the pK_a of the free uncoordinated FcCOCH$_2$COR. R is indicated on the graph. R = H was not fitted in both relationships. (b) Linear dependence of the log of the second-order rate constant of the substitution of the (FcCOCHCOR)$^-$ ligand with phen from [Rh(FcCOCHCOR)(cod)], logk_2, and $E^{0'}$ of the ferrocenyl group or E_{pa} of Rh in [Rh(FcCOCHCOR)(cod)].

The fairly linear trend between E_{pa}(Rh) and group electronegativities in **Figure 3.64**, indicates the Rh(I) core becomes increasingly difficult to oxidize (*i.e.* larger E_{pa}-values) as the R groups of the coordinating β-diketonato ligands, (FcCOCHCOR)$^-$, becomes more electronegative. Group electronegativities (in brackets) of the substituents R increase in the order Fc(1.87) < C$_6$H$_5$(2.21) ≈ CH$_3$(2.34) < H(2.55) < CCl$_3$(2.97) < CF$_3$(3.01),[19] which explains the progressive electron deficiency of the metal centre towards moving from the [Rh(FcCOCHCOFc)(cod)] to the [Rh(FcCOCHCOCF$_3$)(cod)] complex. The linear line through E_{pa} is almost parallel to the linear line through $E^{0'}$ indicating good communication (*via* conjugation) between the R and the Fc group on the (FcCOCHCOR)$^-$ ligand as well as between R and the Rh(I)-core of the complexes. $E^{0'}$ of the ferrocenyl group in [Rh(FcCOCHCOR)(cod)] and $E^{0'}$ of the ferrocenyl group in FcCOCH$_2$COR are for all practical purposes equal. The linear lines through $E^{0'}$(free β-diketone) and $E^{0'}$(Rh complex) in **Figure 3.64** are parallel and 3 mV apart. The almost identical values of $E^{0'}$ indicate that rhodium(I) and cod have little influence on the electron density of the ferrocenyl group.
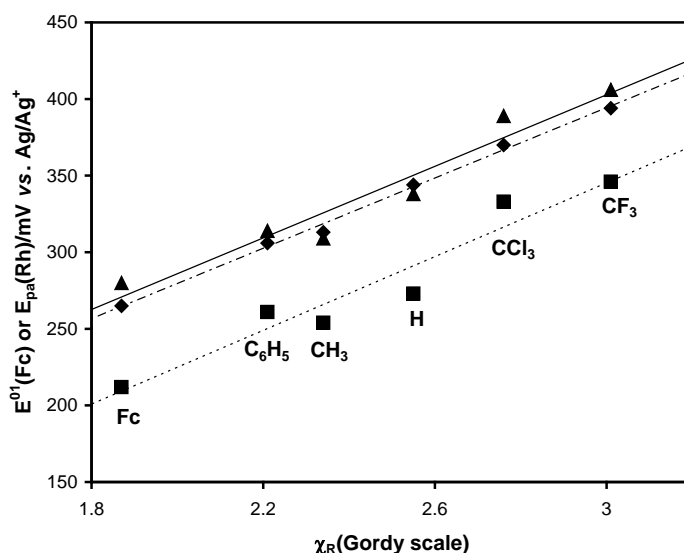
Figure 3.64: Relationships between

(a) $E^{0'}$ of the ferrocenyl group of the free FcCOCH$_2$COR (. _ . _ . _ . _ . _ . and υ) and χ_R,

(b) $E^{0'}$ of the ferrocenyl group in [Rh(FcCOCHCOR)(cod)] (_____ and σ) and χ_R and

(c) the anodic oxidation potential E_{pa} of rhodium in [Rh(FcCOCHCOR)(cod)] (………… and ■) and χ_R,

with χ_R the group electronegativity and R = Fc, C$_6$H$_5$, CH$_3$, CCl$_3$, CF$_3$ and H.

3.6.3 Cyclic voltammetry of [Rh(β-diketonato)(CO)(PPh$_3$)] complexes.

The CV of [Rh(dfcm)(CO)(PPh$_3$)] (**Figure 3.65** (a)) is very similar to the corresponding CV of [Rh(dfcm)(cod)] (**Figure 3.61** (b) page 216), namely it exhibits an electrochemically irreversible anodic oxidation peak which corresponds to the oxidation of rhodium(I) to rhodium(III), as well as two electrochemically reversible Fc$^+$/Fc couples which correspond to the one-electron redox process of each of the two ferrocenyl groups of the dfcm ligand coordinated to [Rh(dfcm)(CO)(PPh$_3$)]. Reasonable reversibility with ΔE_p < 90 mV (**Table 3.43** page 224) for the redox couples of the two ferrocenyl groups was obtained for scan rates up to 250 mV s^{-1}. The previously determined electrochemically irreversible two-electron oxidation of the [Rh(dbm)(CO)(PPh$_3$)], [Rh(ba)(CO)(PPh$_3$)], [Rh(tfba)(CO)(PPh$_3$)] and [Rh(tfaa)(CO)(PPh$_3$)][37] complexes with no ferrocene-containing β-diketonato ligands coordinated to it, confirms that the electrochemically irreversible anodic oxidation peak of [Rh(dfcm)(CO)(PPh$_3$)] (**Figure 3.65** (a)) corresponds to the oxidation of rhodium(I) to rhodium(III).

The CV of [Rh(fctfa)(CO)(PPh$_3$)] (**Figure 3.66** (a) page 223) on the other hand, exhibits two electrochemically irreversible anodic oxidation peaks, as well as the electrochemically reversible couple which corresponds to the oxidation of the ferrocenyl group of the fctfa ligand coordinated

221

to [Rh(fctfa)(CO)(PPh₃)].   These two electrochemically irreversible anodic oxidation peaks are interpreted to correspond to the oxidation of rhodium(I) to rhodium(III) of the two isomers of [Rh^I(fctfa)(CO)(PPh₃)] as described in paragraph 3.2.2.3 page 122.   The ^1H NMR of [Rh(fctfa)(CO)(PPh₃)] clearly distinguishes between the two isomers of [Rh(fctfa)(CO)(PPh₃)] in solution (**Figure 3.66** (b).) The large value $\Delta E_p > 108$ mV for the oxidation of the ferrocenyl group is most probably due to the fact that the oxidation and reduction peaks of the ferrocenyl group of the two isomers of [Rh(fctfa)(CO)(PPh₃)] are near to each other, but not exactly overlapping, resulting in broad peak potential signals.   A distinction between the two different E_{pa} values for the electrochemical oxidation of the two isomers of [Rh(fctfa)(CO)(PPh₃)] was possible, because the time-scale between the oxidation of the two isomers (*ca.* 3 s) is faster than the time-scale of the equilibrium between the two isomers.
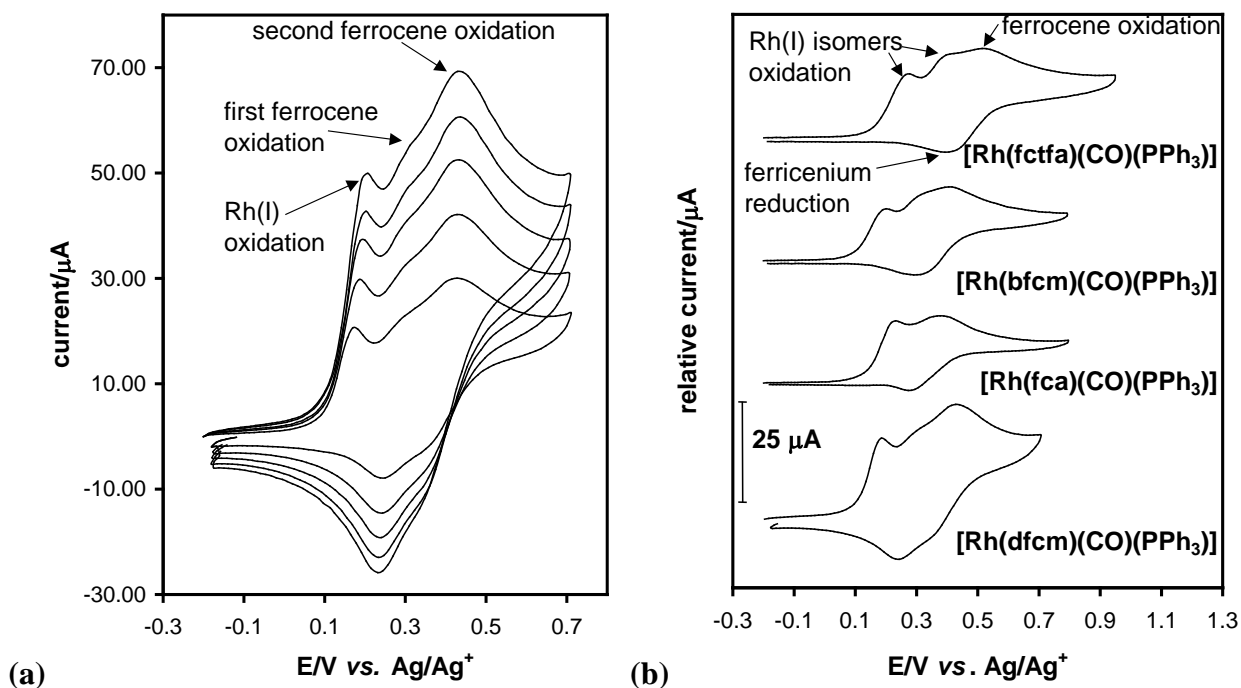
Figure 3.65: : (a) Cyclic voltammograms of 1 mmol dm^{-3} solution of [Rh(dfcm)(CO)(PPh₃)] measured in 0.1 mol dm^{-3} TBAPF₆/CH₃CN at scan rates of 50 - 250 mV s^{-1} (50 mV increments) on a glassy carbon working electrode at 25.0(1) °C.   (b) Cyclic voltammograms of 0.67 mmol dm^{-3} solutions of different [Rh(β-diketonato)(CO)(PPh₃)] complexes measured at scan rate 100 mV s^{-1} under the same conditions as (a).

The observation of two electrochemically irreversible anodic oxidation peaks, corresponding to the oxidation of rhodium(I) of the two isomers of the [Rh(β-diketonato)(CO)(PPh₃)] complex, and an electrochemically reversible Fc$^+$/Fc couple, which corresponds to the redox process of the ferrocenyl group of the β-diketonato ligand coordinated to [Rh(β-diketonato)(CO)(PPh₃)] with large $\Delta E_p > 100$ mV, was also observed for the ferrocene-containing β-diketonato complexes [Rh(fca)(CO)(PPh₃)]   and   [Rh(bfcm)(CO)(PPh₃)].   The   [Rh(fca)(CO)(PPh₃)]   and

[Rh(bfcm)(CO)(PPh₃)] complexes, as in the case of the [Rh(fctfa)(CO)(PPh₃)] complex, also showed two isomers in solution, which is in contrast to the [Rh(dfcm)(CO)(PPh₃)] complex which showed only one isomer in solution, **Figure 3.2** page 124. The reduction peaks (-0.78 and –0.37 V *v.s.* Ag/Ag⁺) of the two [Rh(fca)(CO)(PPh₃)] isomers, are illustrated in **Figure 3.67**. The fact that no cathodic activity prevails when the sweep is initiated in the negative direction, **Figure 3.67** top, confirms that the reduction peaks observed are coupled to the oxidation of the two Rh(I) isomers. The fact that no reduction peak at –0.37 V is observed when the scan direction in **Figure 3.67** (bottom CV indicated by -----) is reversed at 0.27 V, just after the oxidation of the first Rh(I) isomer, confirms that the reduction peak at –0.37 V is coupled to the oxidation peak of the second Rh(I) isomer. In the case of the second Rh(I) isomer, its oxidation peak largely overlaps the Fc/Fc⁺ couple as observed at the broad oxidation peak at 0.34 – 0.42 V. The values of the peak anodic currents, i_{pa}, of the first isomer of the [Rh(fca)(CO)(PPh₃)], [Rh(bfcm)(CO)(PPh₃)] and [Rh(fctfa)(CO)(PPh₃)] complexes in **Figure 3.65** (b) differ, due to the fact that K_c of the isomers of these complexes in solutions of 0.1 mol dm⁻³ TBAPF₆/CH₃CN differs (paragraph 3.2.2.3 page 122). These i_{pa} values are also less than the peak anodic current of the one isomer of [Rh(dfcm)(CO)(PPh₃)]. The value of the reduction peaks, i_{pc}, of ferrocenium, however, is the same, 9 μA, for all four complexes in **Figure 3.65** (b).

The observed results of **Figure 3.65** may also be consistent with a second interpretation. *Eg.* in the [Rh(fctfa)(CO)(PPh₃)] complex, the first and second oxidation waves for Rh(I) may not correspond to Rh(I) → Rh(III) oxidation for the different isomers. The first wave may correspond to Rh(I) → Rh(II) oxidation and the second to Rh(II) → Rh(III) oxidation. However, since rhodium(II) complexes are known to be labile, except in the case where Rh(II) dimers are coordinated to acetate ligands, the author is of the opinion that, although the oxidation Rh(I) → Rh(III) in successive *observable* steps is not impossible, it is rather unlikely. Further more, if Rh(I) → Rh(II) oxidation corresponds to the first observed oxidation peak and Rh(II) → Rh(III) corresponds to the second, one would expect that the peak currents, i_{pa}, for Rh(I) → Rh(II) oxidation should for all complexes be the same. Since, according to the discussion in the previous paragraph and by inspection of **Figure 3.65** (b), it is found not to be the case, with the present state of knowledge, the author favours the isomer explanation.

(a)

(b)
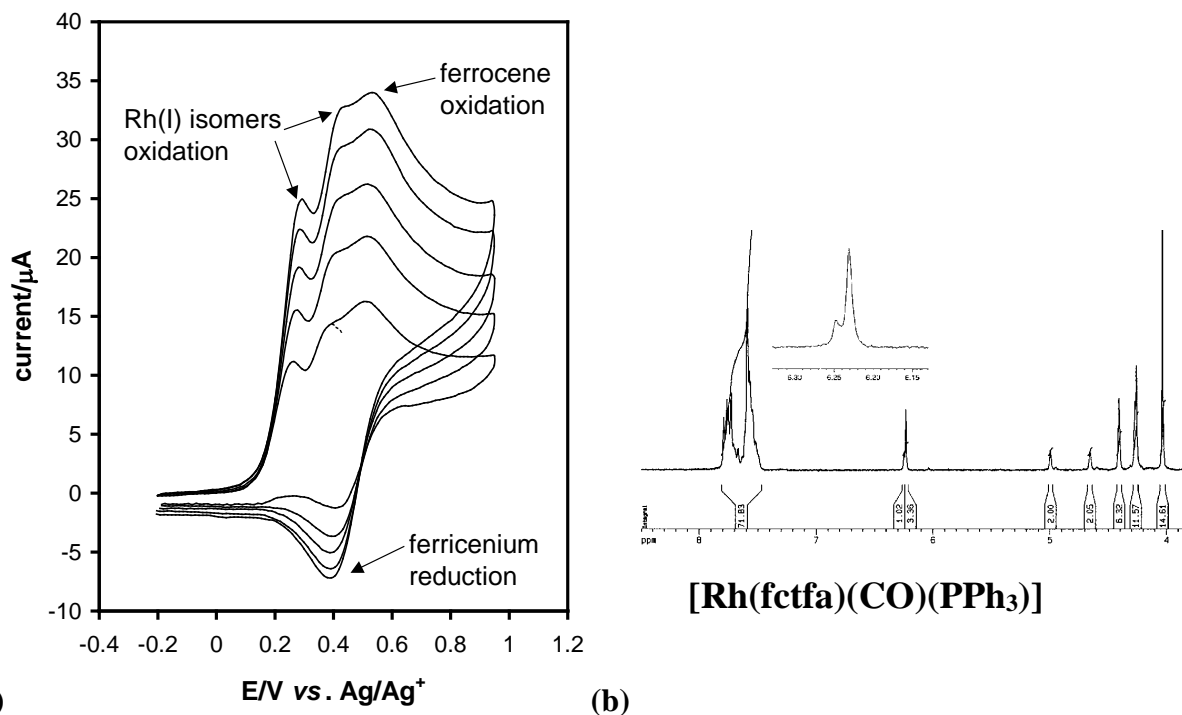
[Rh(fctfa)(CO)(PPh₃)]

Figure 3.66: (a) Cyclic voltammograms of 0.67 mmol dm^{-3} [Rh(fctfa)(CO)(PPh$_3$)] measured in 0.1 mol dm^{-3} TBAPF$_6$/CH$_3$CN at scan rates of 50, 100, 150, 200 and 250 (largest i_{pa}) mV s^{-1} on a glassy carbon working electrode at 25.0(1) °C *versus* Ag/Ag **(b)** The ^{1}H NMR of [Rh(fctfa)(CO)(PPh$_3$)] clearly distinguishes between the two isomers of [Rh(fctfa)(CO)(PPh$_3$)] in solution of acetone-d$_6$.
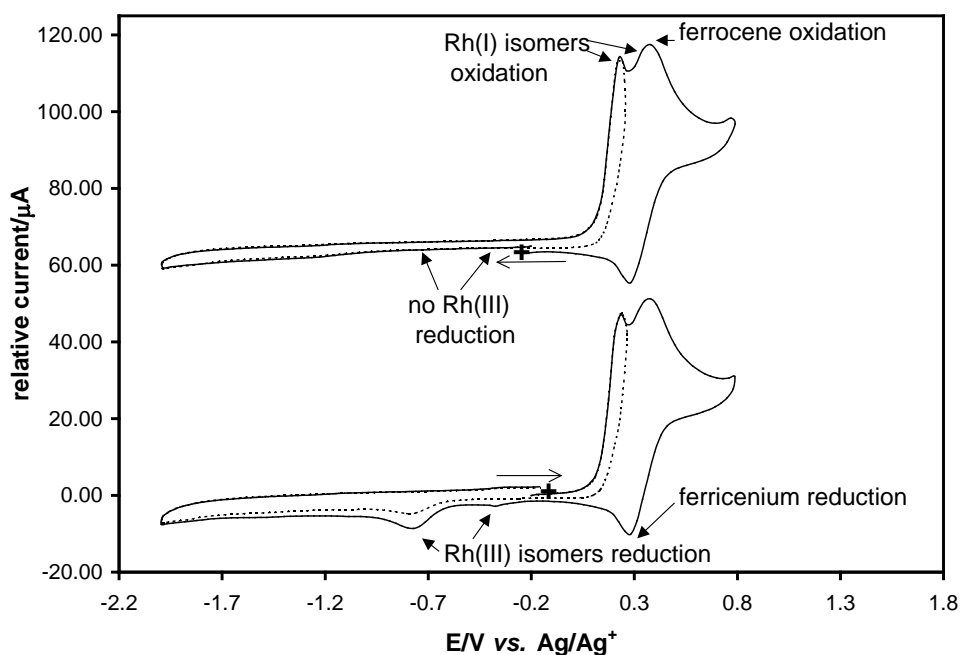
Figure 3.67: Cyclic voltammogram of 2 mmol dm^{-3} [Rh(fca)(CO)(PPh$_3$)] measured in 0.1 mol dm^{-3} TBAPF$_6$/CH$_3$CN at a scan rate of 100 mV s^{-1} on a glassy carbon working electrode at 25.0(1) °. Scans initiated at + in the directions indicated.

224

Table 3.43: Electrochemical data for complexes of the type [Rh(β-diketonato)(CO)(PPh₃)] measured in 0.1 mol dm⁻³ TBAPF₆/CH₃CN on a glassy carbon electrode at 25.0(1) °C *versus* Ag/Ag⁺. The concentration of the complexes was 0.67 mmol dm⁻³.

ν /mVs⁻¹	rhodium		ferrocenyl group			rhodium	ferrocenyl group		
	E_{pa}/V isomer 1	E_{pa}/V isomer 2	E_{pa} /V	ΔE_p /mV	$E^{0'}$ /V	E_{pa}/V isomer 1	E_{pa} /V	ΔE_p /mV	$E^{0'}$ /V
[Rh(fctfa)(CO)(PPh₃)]						**[Rh(dfcm)(CO)(PPh₃)] first ferrocenylgroup**			
50	0.264	0.393	0.510	108	0.459	0.172	0.314	72	0.278
100	0.273	0.404	0.518	122	0.457	0.185	0.314	74	0.277
150	0.283	0.418	0.518	122	0.457	0.193	0.317	79	0.278
200	0.283	0.429	0.526	135	0.459	0.202	0.319	85	0.277
250	0.288	0.434	0.526	135	0.459	0.204	0.321	87	0.278
[Rh(bfcm)(CO)(PPh₃)]						**[Rh(dfcm)(CO)(PPh₃)] second ferrocenylgroup**			
50	0.191	-	0.402	100	0.349	-	0.427	77	0.389
100	0.200	*ca.* 0.35	0.408	117	0.350	-	0.429	81	0.389
150	0.207	-	0.408	117	0.350	-	0.431	85	0.389
200	0.212	-	0.411	124	0.349	-	0.433	89	0.388
250	0.219	-	0.413	129	0.349	-	0.433	89	0.389
[Rh(fca)(CO)(PPh₃)]									
50	0.217	-	0.378	102.4	0.327				
100	0.231	*ca.* 0.33	0.378	102.4	0.327				
150	0.241	-	0.378	102.4	0.327				
200	0.245	-	0.378	102.4	0.327				

The chemical and electrochemical data in **Table 3.44** for [Rh(β-diketonato)(CO)(PPh₃)] complexes were used to set up a linear free energy relationship between the kinetic parameter k_1 and the thermodynamic quantity E_{pa} of Rh in [Rh(β-diketonato)(CO)(PPh₃)] (**Figure 3.68** (b)). k_1 = the chemical oxidative addition rate constant for the first step of the oxidative addition reaction between various [Rh(β-diketonato)(CO)(PPh₃)] complexes and iodomethane in acetone at 25.0(1) °C. The fairly linear trend indicates the Rh(I) core becomes increasingly difficult to oxidize (*i.e.* larger E_{pa}-values) as the R groups of the coordinating β-diketonato ligands, become more electronegative. Electron density is withdrawn from the Rh(I) by the substituents R = CF₃, C₆H₅, CH₃ and Fc on the β-diketone backbone. Group electronegativities (in brackets) of the substituents R increase in the order Fc(1.87) < C₆H₅(2.21) ≈ CH₃(2.34) < CF₃(3.01), which explains the progressive electron deficiency of the metal centre in moving from the [Rh(dfcm)(CO)(PPh₃)] to the [Rh(hfaa)(CO)(PPh₃)] complex.

The free energy relationship between the pK$_a$ of the free β-diketones coordinated to the [Rh(β-diketonato)(CO)(PPh₃)] complexes and E_{pa} of Rh in [Rh(β-diketonato)(CO)(PPh₃)] is displayed in **Figure 3.68** (a).

Table 3.44: Electrochemical and chemical oxidation data of the [Rh(β-diketonato)(CO)(PPh₃)] complexes. Oxidation peak potentials were measured in 0.1 mol dm⁻³ TBAFP₆/CH₃CN on a glassy carbon electrode at 25.0(1) °C at a constant sweep rate of 100 mV s⁻¹ and are reported *vs.* Ag/Ag⁺. Chemical oxidative addition rate constants k_1 are for the first step of the oxidative addition reaction between various [Rh(β-diketonato(CO)(PPh₃)] complexes and iodomethane in acetone at 25.0(1) °C. pK_a of the free β-diketone is also given.

complex	E_{pa}(Rh) / V	$E^{0'}$(Fc) / V	pK_a [d]	k_1/ mol⁻¹ dm³ s⁻¹	log k_1
[Rh(dfcm)(CO)(PPh₃)] [a]	0.185	0.277; 0.389	13.1(1)	0.155 [e]	0.00270
[Rh(fca)(CO)(PPh₃)] [a]	0.231	0.378	10.01(1)	0.0455(6)	0.000794
[Rh(bfcm)(CO)(PPh₃)] [a]	0.200	0.208	10.41(2)	0.0409(3)	0.000714
[Rh(fctfa)(CO)(PPh₃)] [a]	0.273; 0.404	0.457	6.56(3)	0.00370(4)	0.000065
[Rh(dbm)(CO)(PPh₃)] [b]	0.397	-	9.35	0.00961	0.000168
[Rh(ba)(CO)(PPh₃)] [b]	0.425	-	8.7	0.00930	0.000162
[Rh(tfba)(CO)(PPh₃)] [b]	0.537	-	6.3	0.00112	0.000020
[Rh(tfaa)(CO)(PPh₃)] [b]	0.580	-	6.3	0.00146	0.000025
[Rh(hfaa)(CO)(PPh₃)] [c]	0.65	-	4.71(1)		

(a) results from this study (b) results from reference 37 (c) preliminary value
(d) pK_a from reference 35, 58 and 59 (e) value in chloroform, a smaller value is expected in acetone.

(a)   **(b)**
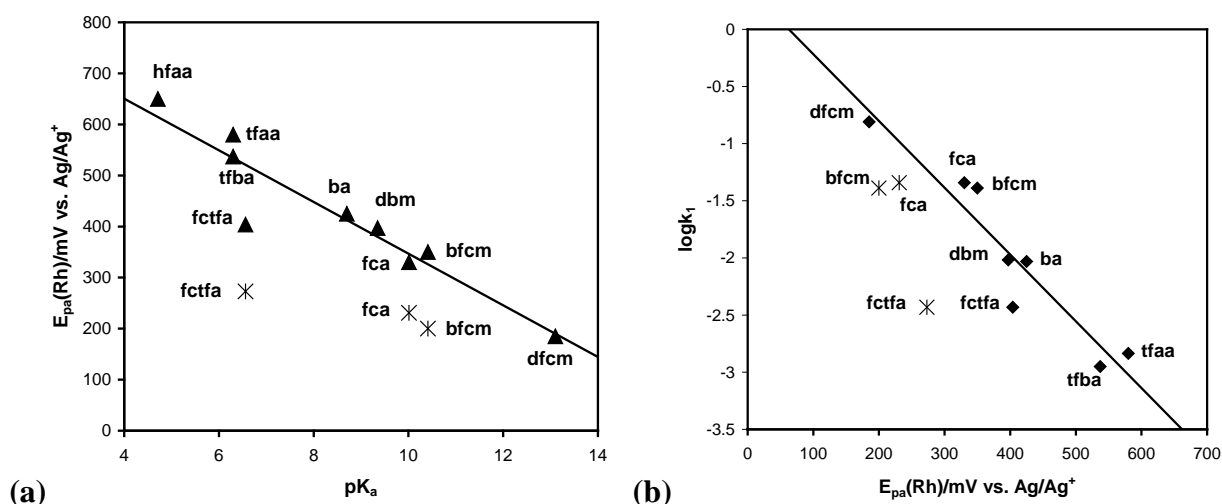
Figure 3.68: (a) The relationship between E_{pa} of Rh in [Rh(β-diketonato)(CO)(PPh₃)] complexes and the pK_a of the free β-diketones. (b) Linear dependence of the kinetic parameter k_1 {the rate constant of the oxidative addition reaction of iodomethane and [Rh(β-diketonato)(CO)(PPh₃)]} and E_{pa} of Rh in [Rh(β-diketonato)(CO)(PPh₃)] measured at a scan rate of 100 mV s⁻¹ under the same conditions as (a). R, R' = CF₃, C₆H₅, CH₃ or Fc. Pionts marked with Σ refer to the first Rh(I) oxidation peak and were not used in the linear fits.

Figure 3.69 illustrates that $E^{0'}$ of the ferrocenyl group in [Rh(FcCOCHCOR)(CO)(PPh₃)] is higher than $E^{0'}$ of the ferrocenyl group in the free β-diketone FcCOCH₂COR, indicating that it is more difficult to oxidize the ferrocenyl group of the (FcCOCHCOR)⁻ ligand bonded to an already oxidized Rh(III) complex (before ferrocene oxidation take place the Rh(I) nucleus is always *in situ* oxidized to Rh(III)), than to oxidize the ferrocenyl in the free β-diketone FcCOCH₂COR.
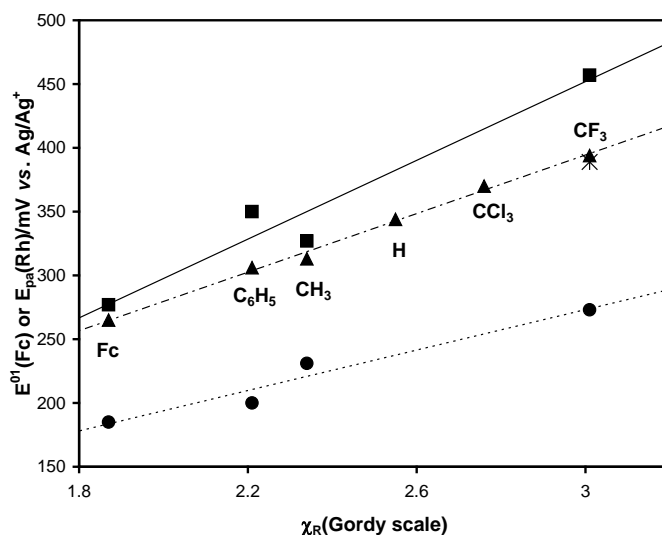
Figure 3.69: Relationships between
(a) $E^{0'}$ of the ferrocenyl group of the free β-diketone or Hfch (. _ . _ . _ . _ . _ . and σ) and χ_R,
(b) $E^{0'}$ of the ferrocenyl group in [Rh(FcCOCHCOR)(CO)(PPh₃)]} (_____ and ■) and χ_R,
(c) E_{pa} of rhodium in [Rh(FcCOCHCOR)(CO)(PPh₃)] (………. and ●) and χ_R and
(d) E_{pa} of rhodium, second isomer, of [Rh(FcCOCHCOCF₃)(CO)(PPh₃)] (Σ)and χ_R,
with χ_R the group electronegativity and R = Fc, C₆H₅, CH₃, CCl₃, CF₃ and H.

3.6.4 Cyclic voltammetry of the rhodium(III) complex [Rh(fctfa)(CH₃)(I)(CO)(PPh₃)].

The CV of the Rh(III) complex [Rh(fctfa)(CH₃)(I)(CO)(PPh₃)] (**Figure 3.70**) exhibits, as was expected, no oxidation of Rh(I) to Rh(III). Only a single electrochemically reversible Fc⁺/Fc couple of the ferrocenyl group of [Rh(fctfa)(CH₃)(I)(CO)(PPh₃)], with $\Delta E_p < 90$ mV for scan rates up to 200 mV s⁻¹, (**Table 3.45**) were observed. The formal reduction potential of the ferrocenyl group in this Rh(III) complex, $E^{0'} = 0.307(6)$ V, is less than $E^{0'}$ for the ferrocenyl group of all known rhodium(I) complexes with fctfa coordinated to it (**Table 3.57** page 247) and 150 mV less positive than $E^{0'} = 0.457$ V for [Rh(fctfa)(CO)(PPh₃)]. $E^{0'} = 0.307(6)$ V for [Rh(fctfa)(CH₃)(I)(CO)(PPh₃)] is in the same order as $E^{0'} = 0.304$ V for the rhodium(III) complex [Rh(fctfa)(CH₃)(I)(P(OPh)₃)₂].[69] $E^{0'} = 0.304$ V for the latter rhodium(III) complex is also more than 150 mV less positive than $E^{0'} = 0.468$ V of the corresponding rhodium(I) complex [Rh(fctfa)(P(OPh)₃)₂] as summarized in **Table 3.57** page 247. The methyl and iodide ligands in the rhodium(III) complexes, donate electron density *via* σ bonds to the rhodium(III). However, it is not possible for a Rh(III) nucleus to be more electron-rich than a Rh(I) nucleus. The answer to

---

[69] Erasmus, J.J.C., *Synthesis and the kinetic, thermodynamic and electrochemical aspects of ferrocene-containing metal complexes with a potential medical application (in Afrikaans), M. Sc. Thesis,* University of the Orange Free State, R.S.A., 1994.

this apparent anomaly is probably locked up in the observation that in all ferrocene-containing Rh(I) complexes investigated except for the [Rh(β-diketonato)(CO)$_2$] complexes (paragraph 3.6.5), the Rh(I) nucleus was first oxidised to Rh(III) before the ferrocenyl group became involved in a redox process with the working electrode. As a result, the sited Fc$^+$/Fc couples for the Rh(I) complexes does *not* really belong to a Rh(I) complex, but rather to an unknown *in situ* formed Rh(III) complex. The remaining two ligands that will coordinate to this *in situ* formed, probably octahedral Rh(III) complex, apart from CO, PPh$_3$ and fctfa, is unknown. It can only be electrolyte anions (PF$_6^-$) or, more likely, solvent molecules (CH$_3$CN). In both cases the electron donating properties would not match that of Me and I in [Rh(fctfa)(CH$_3$)(I)(CO)(PPh$_3$)]. It is therefore expected that the ferrocenyl group of [Rh(fctfa)(CH$_3$)(I)(CO)(PPh$_3$)] should have lower formal reduction potentials than the *in situ* formed complexes just described. However, to be 150 mV more negative appears to be a very extensive shift towards easier oxidation. It was shown that by changing R in FcCOCH$_2$COR from CH$_3$ (χ_{CH3} = 3.01) to Fc (χ_{Fc} = 1.87), the formal reduction potential of the ferrocenyl group was lowered 126 mV from 406 to 280 mV. On this base, the two unknown ligands of the *in situ* formed Rh(III) complex must have excessively poor electron donating properties compared to CH$_3$ and I. Solvent CH$_3$CN coordination would probably best satisfy this criteria. It should be noted that Ir(I) and Ir(III) complexes described in paragraph 3.6.6 and 3.6.7, showed the same general trend as Rh(I) and Rh(III).
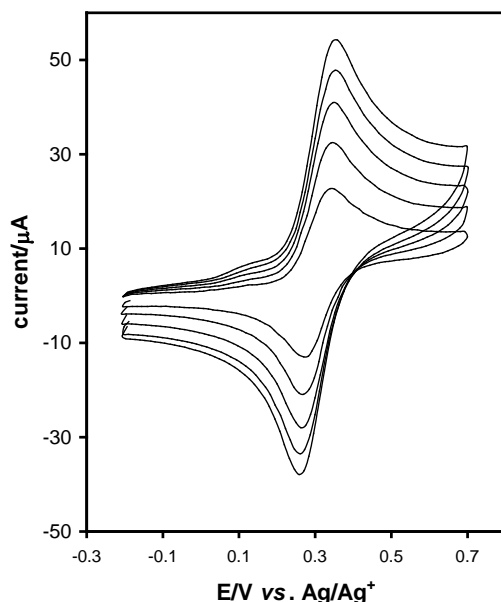
Figure 3.70: Cyclic voltammograms of a 1.5 mmol dm^{-3} solution of [Rh(fctfa)(CH$_3$)(I)(CO)(PPh$_3$)] measured in 0.1 mol dm^{-3} TBAPF$_6$/CH$_3$CN at scan rates of 50 - 250 mV s^{-1} (50 mV increments) on a glassy carbon working electrode at 25.0(1) °C *versus* Ag/Ag$^+$. The CV exhibits a single electrochemically reversible couple which corresponds to the formal reduction potential of the ferrocenyl group of the fctfa ligand coordinated to [Rh(fctfa)(CH$_3$)(I)(CO)(PPh$_3$)].

Table 3.45: Electrochemical data for the oxidation and reduction of the ferrocenyl group of the rhodium(III) complex [Rh(fctfa)(CH₃)(I)(CO)(PPh₃)] measured in 0.1 mol dm⁻³ TBAPF₆/CH₃CN on a glassy carbon electrode at 25.0(1) °C versus Ag/Ag⁺. The concentration of the complex was 1.5 mmol dm⁻³.

ν/mVs⁻¹	E_{pa}/V	ΔE_p/mV	$E^{0\prime}$/V	i_{pa}/μA	i_{pa}/i_{pc}
50	0.345	74	0.308	18.2	1.02
100	0.346	79	0.307	25.8	1.02
150	0.350	84	0.308	32.4	1.02
200	0.352	90	0.307	36.4	1.03
250	0.354	94	0.307	40.8	1.03

3.6.5   Cyclic voltammetry of [Rh(β-diketonato)(CO)₂] complexes.

The CV of the [Rh(β-diketonato)(CO)₂] complexes with β-diketonato = fca and bfcm (**Figure 3.71**) all exhibits a single electrochemically reversible couple which corresponds to the formal reduction potential of the ferrocenyl group of the β-diketone ligand coordinated to [Rh(β-diketonato)(CO)₂] with $\Delta E_p < 100$ mV for scan rates up to 200 mV s⁻¹. The complex possessing dfcm shows two ferrocenyl formal reduction potentials because of the presence of two ferrocenyl moieties. The ratio $i_{pa}/i_{pc} \sim 1$ (**Table 3.46**) as expected for the Fc⁺/Fc couple.

(a)   **(b)**
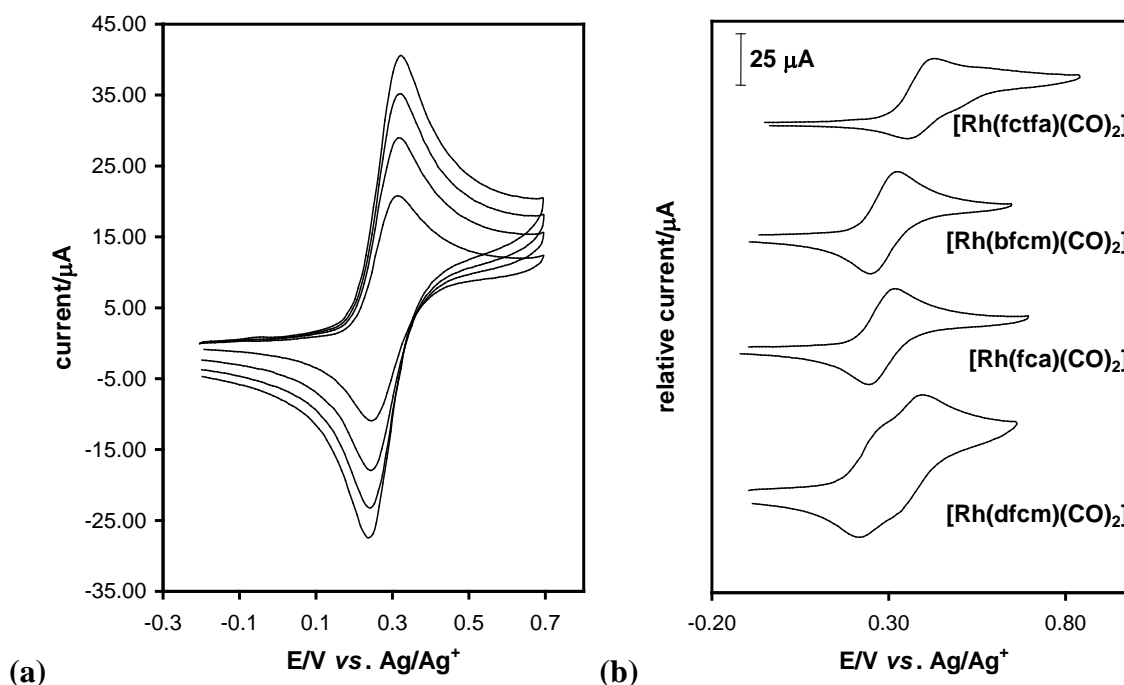
Figure 3.71: (a) Cyclic voltammograms of 1 mmol dm⁻³ solution of [Rh(fca)(CO)₂] measured in 0.1 mol dm⁻³ TBAPF₆/CH₃CN at scan rates of 50 – 200 mV s⁻¹ (50 mV increments) on a glassy carbon working electrode at 25.0(1) °C.   (b) Cyclic voltammograms of different [Rh(β-diketonato)(CO)₂] complexes at a scan rate 100 mV s⁻¹ measured under the same conditions as (a). Both graphs show only the waves related to the Fc/Fc⁺ couple. Rh(I) oxidation occurs at much higher potentials, see **Figure 3.74** and **Table 3.47**.

The CV of the [Rh(fctfa)(CO)₂] complex, however, exhibits two electrochemically reversible couples of which the first (peak 1 in **Figure 3.72** (a)) corresponds to the oxidation of the ferrocenyl group of the fctfa ligand coordinated to [Rh(fctfa)(CO)₂] with $\Delta E_p < 85$ mV for scan rates up to 200 mV s⁻¹. The ¹H NMR spectrum of the [Rh(fctfa)(CO)₂] complex in CDCl₃ showed one set of proton signals corresponding to the signals of the protons of the ferrocenyl group and the methine proton of the fctfa ligand coordinated to [Rh(fctfa)(CO)₂]. One set was expected for the [Rh(fctfa)(CO)₂] complex, because only one isomer is possible for this dicarbonyl complex. However, in CD₃CN solution, two sets of signals were observed, see **Figure 3.72** (b). Since the ¹H NMR spectrum in CDCl₃ confirmed the purity of [Rh(fctfa)(CO)₂], the second species in CD₃CN must be solvent coordinated. The second peak of the CV of [Rh(fctfa)(CO)₂] in 0.1 mol dm⁻³ TBAPF₆/**CH₃CN** (peak 2 in **Figure 3.72** (a)), therefore, corresponds to the five-coordinate [Rh(fctfa)(CO)₂(CH₃CN)] complex. The tendency to solvent coordination was not clearly identified for complexes not possessing a highly electron withdrawing CF₃ group.
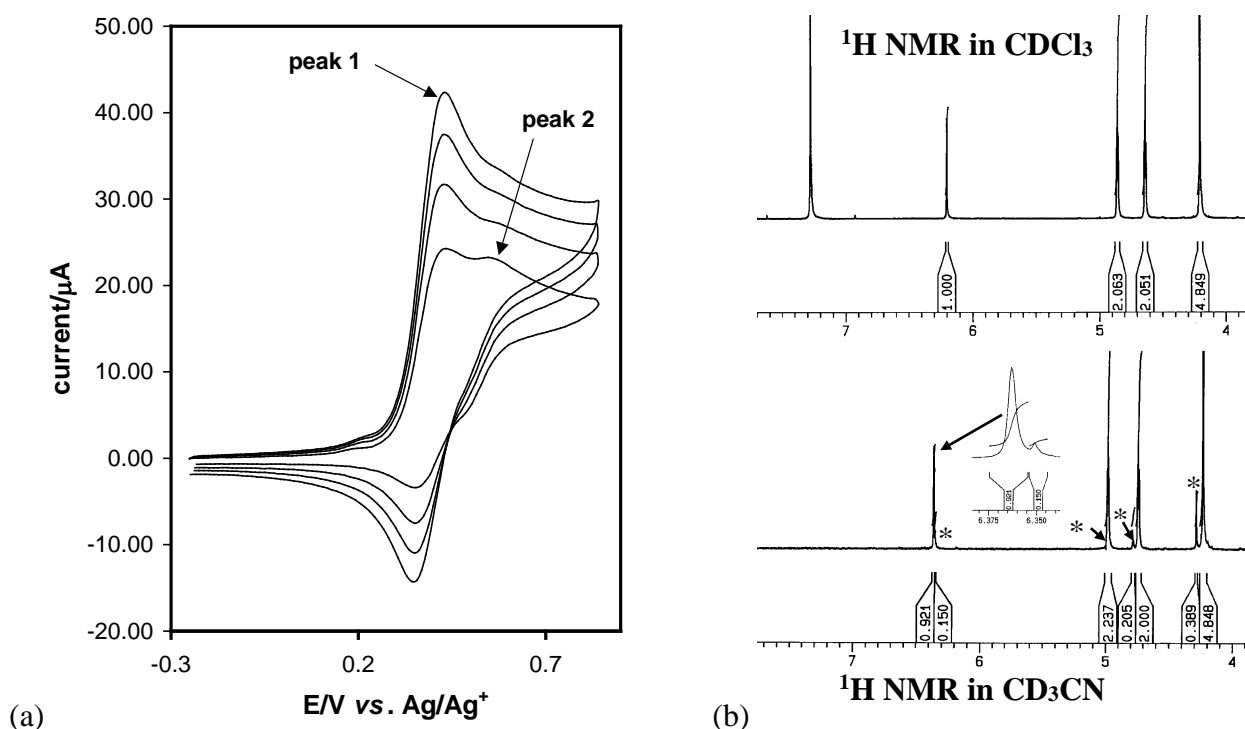
Figure 3.72: (a) **Cyclic voltammograms of 1 mmol dm⁻³ solution of [Rh(fctfa)(CO)₂] measured in 0.1 mol dm⁻³ TBAPF₆/CH₃CN at scan rates of 50 – 200 mV s⁻¹ (50 mV increments) on a glassy carbon working electrode at 25.0(1) °C. Peak 1 represents the signal corresponding to the Fc⁺/Fc couple in four-coordinate [Rh(fctfa)(CO)₂].Peak 2 represents the signal corresponding to the Fc⁺/Fc couple in five-coordinate [Rh(fctfa)(CO)₂(CH₃CN)]. (b) ¹H NMR of [Rh(fctfa)(CO)₂] in CDCl₃ and CD₃CN. The spectrum in CD₃CN shows a second solvent-coordinated species of [Rh(fctfa)(CO)₂] in solution of CD₃CN, _viz._ the five-coordinate [Rh(fctfa)(CO)₂(CD₃CN)] complex, signals marked with *.**

Table 3.46: Electrochemical data for complexes of the type [Rh(β-diketonato)(CO)$_2$] measured in 0.1 mol dm^{-3} TBAPF$_6$/CH$_3$CN on a glassy carbon electrode at 25.0(1) °C versus Ag/Ag$^+$. The concentration of the complexes was 1.0(1) mmol dm^{-3}.

ν/mVs^{-1}	E$_{pa}$/V	ΔE$_p$/mV	E$^{0'}$/V	i_{pa}/μA	i_{pa}/i_{pc}	E$_{pa}$/V	ΔE$_p$/mV	E$^{0'}$/V	i_{pa}/μA	i_{pa}/i_{pc}
	[Rh(fctfa)(CO)$_2$]					[Rh(dfcm)(CO)$_2$] – first ferrocenylgroup				
50	0.434	85	0.392	21.9	*	0.284	60	0.254	*	*
100	0.432	79	0.392	28.0	*	0.300	82	0.259	*	*
150	0.430	81	0.390	32.8	*	0.302	90	0.257	*	*
200	0.429	82	0.388	36.7	*	0.309	105	0.257	*	*
	[Rh(bfcm)(CO)$_2$]					[Rh(dfcm)(CO)$_2$] – second ferrocenylgroup				
50	0.322	72	0.286	20.3	1.16	0.401	92	0.355	*	*
100	0.326	78	0.287	28.6	1.13	0.396	90	0.353	*	*
150	0.330	82	0.289	35.6	1.16	0.396	95	0.350	*	*
200	0.332	90	0.287	40.9	1.16	0.399	100	0.349	*	*
	[Rh(fca)(CO)$_2$]					* not accurately determinable				
50	0.311	68	0.277	18.8	1.08					
100	0.316	73	0.280	26.3	1.09					
150	0.318	76	0.279	31.7	1.08					
200	0.321	82	0.280	36.1	1.07					

In **Figure 3.73** the CV's of [Rh(fca)(CO)$_2$] are displayed over a larger potential window. The Rh(I) oxidation peak is observed at 0.931 V and the Rh(III) reduction peak at –0.833 V, independent of the scan rate up to 250 mV s^{-1}. The [Rh(dfcm)(CO)$_2$] complex showed the highest Rh(I) oxidation potentail at 1.109 V *vs.* Ag/Ag$^+$ (**Figure 3.74**). Although this is an unexpected result, it is easily explained. Before the Rh(I)-core is oxidized, the two ferrocenyl groups (χ_{Fc} = 1.87) of the dfcm ligand are oxidized to a ferricenium group with χ_{Fc+} = 2.82.[19] The ferricenium group almost equals the electron withdrawing properties of the CF$_3$ group with χ_{CF3} = 3.01. Since [Rh(dfcm)(CO)$_2$] has two ferricenium groups attached to it before the Rh(I) core is oxidized to Rh(III), the oxidation potential of 1.109 V is put into perspective. The E$_{pa}$(Rh) for the [Rh(β-diketonato)(CO)$_2$] complexes is 546 – 899 mV higher than E$_{pa}$(Rh) for the corresponding [Rh(β-diketonato)(cod)] complexes. A 250 mV more positive peak anodic potential was obtained for the oxidation of rhodium(I) to rhodium(III) in the [Rh(oxa)(CO)$_2$] complex compared to the peak rhodium anodic potential for [Rh(oxa)(cod)], also in CH$_3$CN as solvent.[67] **Figure 3.74** (b) illustrates the much larger drift in the Rh(I) oxidation potentials compared to that observed for E$^{0'}$ for the Fc/Fc$^+$ couple when changing R from Fc to CF$_3$ in complexes of the type [Rh(FcCOCHCOR)(CO)$_2$]. The peak anodic potential *vs.* Fc/Fc$^+$ for the [Rh(β-diketonato)(CO)$_2$] and [Rh(β-diketonato)(cod)] complexes is given in **Table 3.47** page 231 and the rhodium(I) oxalate complexes are described in chapter 2 paragraph 2.3.8.2.[67] The CV of the non-ferrocene containing [Rh(tfba)(CO)$_2$] complex also exhibits an

electrochemically irreversible anodic Rh(I) oxidation peak in the region 0.8 – 1.12V, see **Figure 3.75**.

Bulk electrolysis of the [Rh(β-diketonato)(CO)$_2$] complexes (paragraph 3.6.8 page 243) at potentials positive of the Rh(I) oxidation peak counted for 3 electrons, confirming the one and two-electron oxidation of the Fc$^+$/Fc and Rh^{3+}/Rh^{1+} couples respectively. The similar i_{pa} values for the Fc$^+$/Fc couples of 1.2 mmol dm^{-3} solution of free ferrocene and 1.2 mmol dm^{-3} solution of [Rh(fca)(CO)$_2$] in **Figure 3.73** (a) also indicate that the reversible couple at 280 mV represents a one-electron oxidation process.

The ΔE_p(Rh) > 1 V for all the [Rh(β-diketonato)(CO)$_2$] complexes of this study, indicates a definite irreversable system for the Rh^{3+}/Rh^{1+} couple. The smallest ΔE_p(Rh) observed was ~1V for the [Rh(fctfa)(CO)$_2$] complex and the largest ~2V for the [Rh(bfcm)(CO)$_2$] complex. This is in accordance with ΔE_p(Rh) ~2V for the [Rh(oxa)(CO)$_2$] complex in THF as solvent.[67]
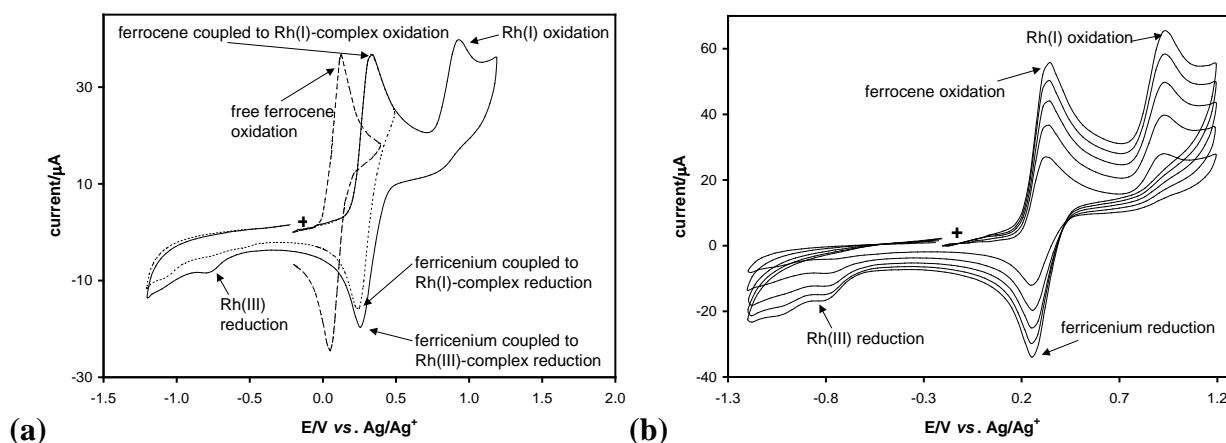
Figure 3.73: Cyclic voltammograms of 1.2 mmol dm^{-3} solution of [Rh(fca)(CO)$_2$] measured in 0.1 mol dm^{-3} TBAPF$_6$/CH$_3$CN at scan rates of (a) 100 mV s^{-1} and (b) 50, 100, 150, 200 and 250 mV s^{-1} on a glassy carbon working electrode at 25.0(1) °C. In (a) a scan of 1.2 mmol dm^{-3} solution of free ferrocene is superimposed. Scans initiated in the positive direction at +.

Table 3.47: Comparison of the peak anodic potential E$_{pa}$ /V (*vs.* Fc/Fc$^+$) of Rh(I) oxidation in CH$_3$CN at a scan rate 100 mV s^{-1} of the oxidation of rhodium(I) to rhodium(III) in [Rh(L,L'-BID)(CO)$_2$] and [Rh(L,L'-BID)(cod)] complexes with the L,L'-BIB ligand as indicated. The supporting electrolyte was 0.20 mol dm^{-3} TBAP in the case of the oxa complex and 0.1 mol dm^{-3} TBAPF$_6$ in the case of the other ligands.

complex	L,L'-BID ligands				
	dfcm	fca	bfcm	oxa[70]	fctfa
[Rh(L,L'-BID)(CO)$_2$] E$_{pa}$ /V (*vs.* Fc/Fc$^+$)	1.032	0.854	0.728	0.34	0.911
[Rh(L,L'-BID)(cod)] E$_{pa}$ /V (*vs.* Fc/Fc$^+$)	0.133	0.175	0.182	0.09	0.267
E$_{pa}$(dicarbonyl complex) - E$_{pa}$(cod complex) / mV	899	679	546	250	644
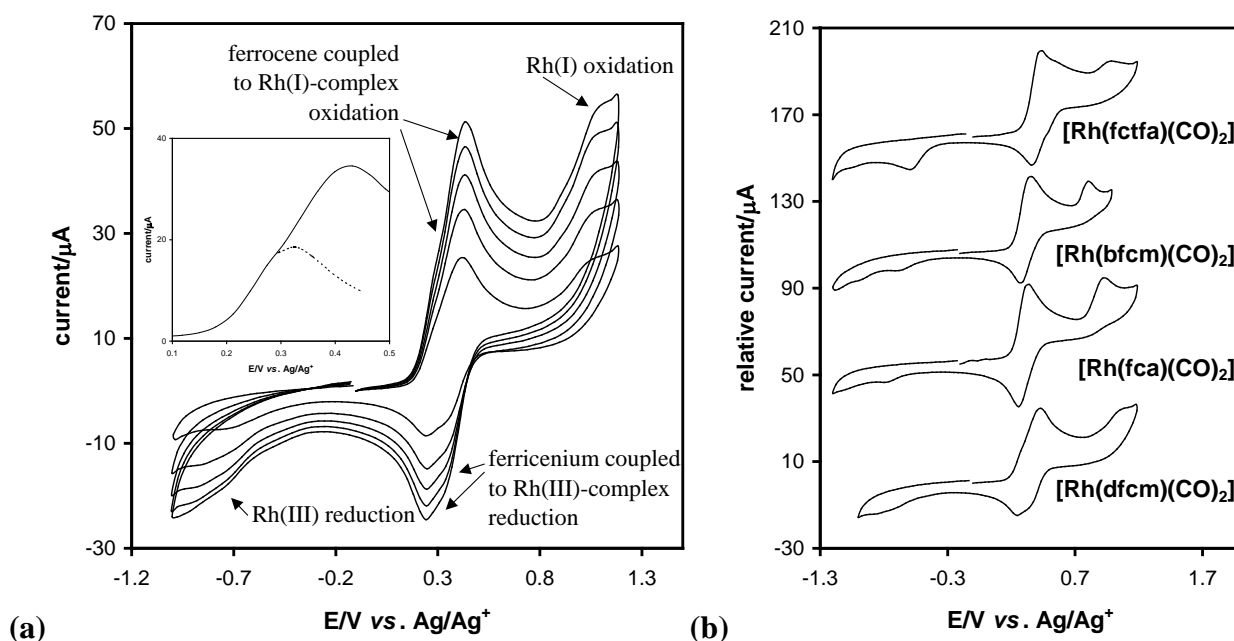
Figure 3.74: (a) Cyclic voltammograms of 0.5 mmol dm^{-3} solution of [Rh(dfcm)(CO)$_2$] measured in 0.1 mol dm^{-3} TBAPF$_6$/CH$_3$CN at scan rates of 50 – 250 mV s^{-1} (50 mV increments) on a glassy carbon working electrode at 25.0(1) °C. Insert indicates an enlargement of the ferrocene coupled to Rh(I)-complex oxidation for the 100 mV s^{-1} scan. (b) Cyclic voltammograms of 1.2 mmol dm^{-3} solutions of different [Rh(β-diketonato)(CO)$_2$] complexes ([Rh(dfcm)(CO)$_2$] = 0.5 mmol dm^{-3}) at a scan rate 100 mV s^{-1} measured under the same conditions as (a).
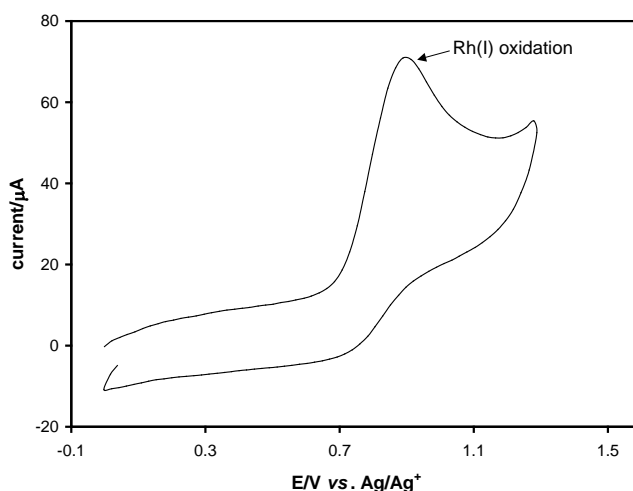
Figure 3.75: CV of the non-ferrocene containing [Rh(tfba)(CO)$_2$] complex with an electrochemically irreversible anodic Rh(I) oxidation peak at 0.92 V.

3.6.6   Cyclic voltammetry of [Ir(β-diketonato)(cod)] complexes.

The cyclic voltammograms of the ferrocene-containing [Ir(β-diketonato)(cod)] complexes (β-diketonato = fctfa, fca and bfcm) as displayed in **Figure 3.76** (b), all exhibit an electrochemially irreversible anodic oxidation peak which corresponds to the oxidation of iridium as well as an

233

irreversible electrochemical Fc^+/Fc couple ($\Delta E_{max} = 162$ mV) which corresponds to the oxidation of ferrocene according to **Equation 3.15**. The peak anodic current i_{pa} of the ferrocenyl group was determined as described in paragraph 3.6.2 page 214. For all the complexes $\Delta E_p > 118$ mV for the CV of the ferrocenyl group and the ratio i_{pa}/i_{pc} constant for a specific complex, but unequal to unity except in the case of the [Ir(fca)(cod)] complex (**Table 3.48**). Bulk electrolysis (paragraph 3.6.8 page 243) indicated that only 2 electrons were transferred during the oxidation of the [Ir(fctfa)(cod)] complex. One electron is needed for the Fc^+/Fc couple while the other corresponds to the oxidation of Ir(I) to Ir(II) according to **Equation 3.16**. The oxidation of iridium(I) to iridium(II) was also found to be a one-electron transfer process, as measured by bulk electrolysis, for the non-ferrocene-containing β-diketonato complex [Ir(acac)(cod)]. Electrochemical oxidation of the square planer Vaska's complexes [Ir(CO)XL$_2$] (X = Cl, Br and I; L = PPh$_3$, PPh$_2$Et and PPhEt$_2$) as discussed in chapter 2 paragraph 2.3.8.1, also resulted in an irreversible one-electron oxidation process for each complex.[70] The CV's of ferrocene and non-ferrocene-containing β-diketonato [Ir(β-diketonato)(cod)] complexes with β-diketonato =fctfa, fca, bfcm, tftma, tfdma, tfhd, tfaa and acac, are displayed in **Figure 3.76**. The E_{pa} for the Ir^{2+}/Ir^{1+} couple of each complex is given in **Table 3.49** page 236.

Equation 3.15: $\qquad\qquad$ $Fc^+ + e^- \ \square\ Fc$

Equation 3.16: $\qquad\qquad$ $Ir(I) \rightarrow Ir(II) + e^-$
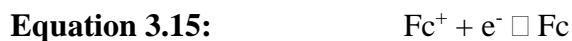
Kissinger[61] illustrated that the ratio i_{pa}/i_{pc} can significantly be influenced by chemical reactions coupled to the electrode process. Electrochemical oxidation leads to an oxidized species that may rapidly react with other species present in the solvent *e.g.* unoxidized species or components of the medium, the so-called coupled chemical reactions. The large ΔE_p values and $i_{pa}/i_{pc} \neq 1$ of the CV's of the ferrocenyl group of the ferrocene-containing [Ir(β-diketonato)(cod)] complexes, indicate electrochemical irreversibility and the possibility of coupled chemical reactions. The possibility of the oxidized iridium(II) species forming iridium(II) dimers, will be discussed in paragraph 3.6.8 page 243.

---

[70] Vecernik, J., Masek, J. and Vlcek, A.A., *J.C.S. Chem. Comm.*, 737 (1975).

Table 3.48: Electrochemical data for complexes of the type [Ir(β-diketonato)(cod)] measured in 0.1 mol dm^{-3} TBAPF$_6$/CH$_3$CN on a glassy carbon electrode at 25.0(1) °C versus Ag/Ag$^+$ and scan rates 50 - 200 mV s^{-1}. The concentration of the complexes was 3.0(1) mmol dm^{-3}, β-diketonato = fctfa, fca and bfcm.

	iridium		ferrocenyl group				
ν/mVs^{-1}	E_{pa}/V	i_{pa}/μA	E_{pa}/V	ΔE_p/mV	$E^{0'}$/V	i_{pa}/μA	i_{pa}/i_{pc}
[Ir(fctfa)(cod)] - 3.0(1) mmol dm^{-3}							
50	0.311	43	0.464	129	0.400	30	0.74
100	0.325	66	0.466	133	0.400	42	0.74
150	0.335	84	0.469	139	0.400	50	0.74
200	0.345	98	0.469	141	0.400	58	0.74
[Ir(bfcm)(cod)] - 3.0(1) mmol dm^{-3}							
50	0.233	42	0.381	118	0.325	42	0.80
100	0.245	62	0.388	129	0.324	57	0.78
150	0.260	81	0.394	139	0.325	68	0.79
200	0.267	92	0.397	149	0.325	77	0.80
[Ir(fca)(cod)] - 3.0(1) mmol dm^{-3}							
75	0.237	68	0.397	144	0.325	39	1.01
100	0.243	80	0.397	144	0.325	44	1.00
150	0.253	98	0.301	154	0.324	54	1.02
200	0.259	117	0.405	162	0.324	62	1.00

(a)   **(b)**
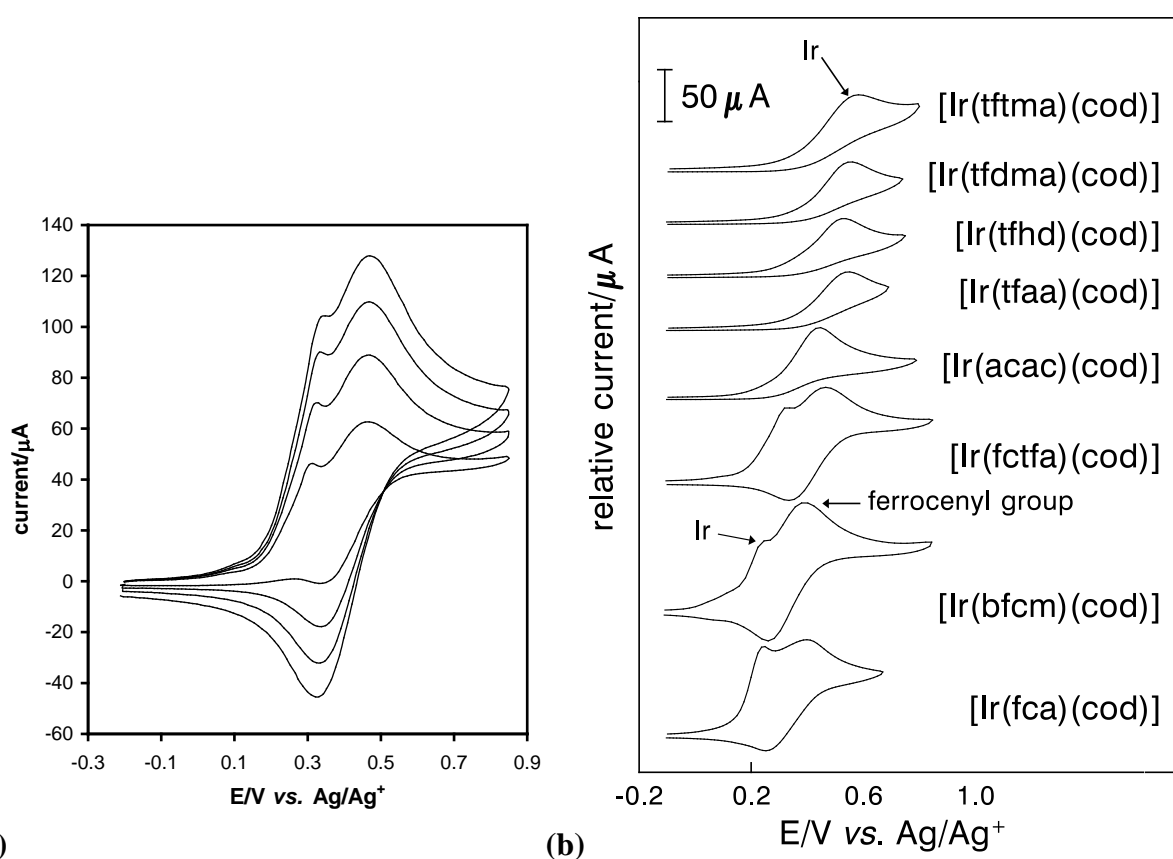
Figure 3.76: (a) Cyclic voltammograms of 3 mmol dm^{-3} solution of [Ir(fctfa)(cod)] measured in 0.1 mol dm^{-3} TBAPF$_6$/CH$_3$CN at scan rates of 50 - 200 mV s^{-1} on a glassy carbon working electrode at 25.0(1) °C. (b) Cyclic voltammograms of 3 mmol dm^{-3} solution of ferrocene and non-ferrocene-containing β-diketonato [Ir(β-diketonato)(cod)] complexes measured at a scan rate of 100 mV s^{-1} under the same conditions as (a).

The chemical and electrochemical data in **Table 3.49** were used to try and establish a linear free energy relationship between the substitution kinetic parameter k_2 and the thermodynamic quantity E_{pa} of Ir in [Ir(β-diketonato)(cod)] (**Figure 3.77** (b)). Substitution rate constants, k_2, are for the reaction between various [Ir(β-diketonato)(cod)] complexes and 1,10-phenanthroline in acetone at 25 °C. No clear-cut relationship could be formulated, however, the results indicate that the fastest substitution was observed in complexes where Ir(I) showed more positive oxidation potentials.

The relationship between E_{pa} of Ir in [Ir(β-diketonato)(cod)] and the pK_a of the free uncoordinated β-diketones in the [Ir(β-diketonato)(cod)] complexes is illustrated in **Figure 3.77** (a). No clear general trend could be observed, which is in contrast to the corresponding relationship for the [Rh(β-diketonato)(cod)] complexes in **Figure 3.63** page 219. In the case of the [Rh(β-diketonato)(cod)] complexes, however, the E_{pa}(Rh) of only *ferrocene-containing* [Rh(β-diketonato)(cod)] complexes were determined.

(a)   **(b)**
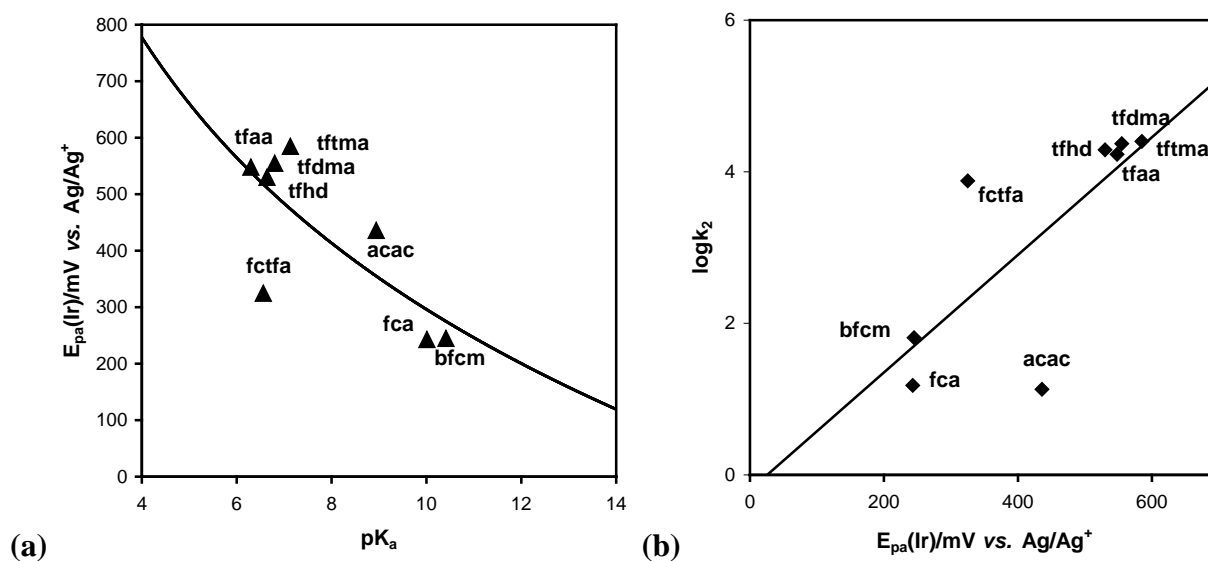
Figure 3.77: (a) Relationship between the pK_a of free uncoordinated β-diketones and E_{pa} *versus* Ag/Ag$^+$ of Ir in [Ir(β-diketonato)(cod)], measured in 0.1 mol dm^{-3} TBAPF$_6$/CH$_3$CN at a scan rate of 100 mV s^{-1} on a glassy carbon working electrode at 25.0(1) °C. (b) Relationship between log of the second-order rate constant of the substitution of the β-diketonato ligand with phen from [Ir(β-diketonato)(cod)], logk_2, and E_{pa} of Ir in [Ir(β-diketonato)(cod)] measured at scan rate 100 mV s^{-1} under the same conditions as (a).

Relationships between $E^{0'}$(Fc) or E_{pa}(Ir) in ferrocene-containing iridium-β-diketonate complexes *and* the group electronegativity χ_R or the R group bonded to the ferrocene-containing β-diketonate ligand (FcCOCHCOR)$^-$, are illustrated in **Figure 3.78**. **Figure 3.78** illustrates that $E^{0'}$ of the ferrocenyl group in [Ir(β-diketonato)(cod)] and $E^{0'}$ of the ferrocenyl group in the free β-

diketone $FcCOCH_2COR$ do not differ more than 19 mV. The almost similar values of $E^{0'}$ indicates that Ir(I) and cod have little influence on the electron density of the ferrocenyl group.

The anodic oxidation potential E_{pa} of iridium in [Ir(β-diketonato)(cod)] is 75 – 82 mV lower than the reduction potential $E^{0'}$ of the ferrocenyl group of the β-diketonate ligand in [Ir(β-diketonato)(cod)], see **Table 3.50**. Upon considering the [Rh(β-diketonato)(cod)] complexes, the rhodium centre becomes oxidized 53 – 68 mV more negatively than the ferrocene moiety in the β-diketonate ligand. The Rh(I) nucleous, however, is oxidized at slightly more positive potentials (~20 mV) than its iridium counterpart. This indicates that Ir(I) may be slightly more nucleophilic than Rh(I) because Ir(I) must have a larger electron density if it is easier to oxidize than Rh(I). This is consistent with the fact that complexes of the third row of transition elements (*eg.* iridium) show higher rate constants for oxidative addition than isostrutural complexes of the second row (*eg.* rhodium)) {chapter 2 paragraph 2.2.2.3 (i)}.

Table 3.49: **Electrochemical data and substitution kinetic data for [Ir(β-diketonato)(cod)] complexes. Oxidation peak potentials were measured in 0.1 mol dm^{-3} TBAFP$_6$/CH$_3$CN on a glassy carbon electrode at 25.0(1) °C at a constant sweep rate of 100 mV s^{-1} and are reported *vs*. Ag/Ag$^+$. Substitution rate constants, k$_2$, are for the reaction between various [Ir(β-diketonato)(cod)] complexes and 1,10-phenanthroline in acetone at 25.0(1) °C. pK$_a$ values are for the free uncoordinated β-diketones.**

complex	pK$_a$ (β-diketone)*	E_{pa}(Ir)/V vs Ag/Ag$^+$	k$_2$/mol^{-1} dm^3 s^{-1}	log k$_2$
[Ir(bfcm)(cod)]	10.41(2)	0.245	63.9(5)	1.81
[Ir(fca)(cod)]	10.01(1)	0.243	15.3(3)	1.18
[Ir(acac)(cod)]	8.94	0.436	13.6$^{\#}$	1.13
[Ir(fctfa)(cod)]	6.56(3)	0.325	7600(100)	3.88
[Ir(tfaa)(cod)]	6.30	0.548	17100$^{\#}$	4.23
[Ir(tfhd)(cod)]	6.64(1)	0.530	19600(300)	4.29
[Ir(tfdma)(cod)]	6.80	0.555	23200(400)	4.37
[Ir(tftma)(cod)]	7.13(1)	0.585	24600(300)	4.40

* pK$_a$ from ref. 35, 22, 58, 59 and this study paragraph 3.3. $^{\#}$ k$_2$ from ref. 57.

Table 3.50: **Formal reduction potential, $E^{0'}$, of the ferrocenyl group of the β-diketone in [M(β-diketonato)(cod)] and the anodic oxidation potential, E_{pa}, of the metal in [M(β-diketonato)(cod)], with M = Rh or Ir. $E^{0'}$ and E_{pa} are given *versus* Fc/Fc$^+$.**

complex	($E^{0'}$ or E_{pa})/V of complex with β-diketonato ligand				
	fctfa	bfcm	fca	dfcm first ferrocenyl group	dfcm second ferrocenyl group
$E^{0'}$(Fc) [Ir(β-diketonato)(cod)]	0.317	0.241	0.242	-	-
E_{pa} (Ir) [Ir(β-diketonato)(cod)]	0.242	0.162	0.160	-	-
{$E^{0'}$(Fc) - E_{pa}(Ir)} [Ir(β-diketonato)(cod)]	0.075	0.079	0.082	-	-
$E^{0'}$(Fc) [Rh(β-diketonato)(cod)]	0.329	0.237	0.232	0.203	0.302
E_{pa} (Rh) [Rh(β-diketonato)(cod)]	0.269	0.184	0.177	0.135	-
{$E^{0'}$(Fc) - E_{pa}(Rh)} [Rh(β-diketonato)(cod)]	0.060	0.053	0.055	0.068	-
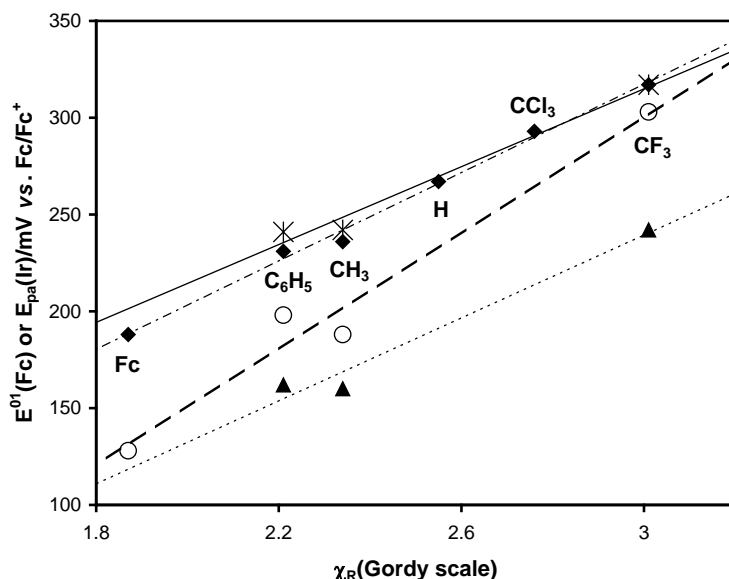
Figure 3.78: Relationships between
(a) $E^{0'}$ of the ferrocenyl group of the free β-diketone (. _. _ . _ . _ . and υ.) and χ_R,
(b) $E^{0'}$ of the ferrocenyl group in [Ir(β-diketonato)(cod)]} (_____ and Σ) and χ_R,
(c) E_{pa} of iridium in [Ir(β-diketonato)(cod)] (……….. and σ) and χ_R and
(d) $E^{0'}$ of the ferrocenyl group [Ir(III)Cl₂(β-diketonato)(cod)]} (_ _ _ _ _ _ _ and μ) and χ_R,
with χ_R the group electronegativity and R = Fc, C₆H₅, CH₃, CCl₃, CF₃ and H. Ferrocene was used as internal standard, $E^{0'}$ = 0.083 mV *versus* Ag/Ag⁺. Data of Figure 3.78 summarized in Table 3.55 page 243.

3.6.7 Cyclic voltammetry of [IrCl₂(β-diketonato)(cod)] complexes.

The cyclic voltammograms of the oxidation of the ferrocenyl group of iridium(III) complexes [IrCl₂(β-diketonato)(cod)] with β-diketonato = fctfa, fca. bfcm and dfcm are displayed in **Figure 3.79** (a). The CV's of the [IrCl₂(β-diketonato)(cod)] with β-diketonato = fctfa, fca and bfcm were measured in 0.1 mol dm⁻³ TBAPF₆/CH₃CN. The CV of [IrCl₂(dfcm)(cod)] were measured in 0.1 mol dm⁻³ TBAPF₆/CH₂Cl₂, due to the poor solibility of this complex in CH₃CN. Ferrocene was added as internal standard in order to compare the electrochemical parameters of these complexes with each other. Paragraph 2.3.5 chapter 2 discusses the use of ferrocene as an internal standard.

Figure 3.79 (b) (data in **Table 3.52** page 240) illustrates that the $E^{0'}$ of the [IrCl₂(fctfa)(cod)] complex *vs.* Fc/Fc⁺ is 0.302V, irrespective of the solvent. In the **solvent CH₃CN**, the $E^{0'}$ of the ferrocenyl group of the β-diketonato ligand coordinated to [IrCl₂(fctfa)(cod)] is 0.385 V *vs.* Ag/Ag⁺ and the $E^{0'}$ of free ferrocene added as internal standard, is 0.083 V *vs.* Ag/Ag⁺. $E^{0'}$ of the ferrocenyl group of the β-diketonato ligand coordinated to [IrCl₂(fctfa)(cod)] in the solvent

CH$_3$CN is, therefore, {(0.385 – 0.083) = **0.302**} **V** *vs.* **Fc/Fc$^+$**. In the **solvent CH$_2$Cl$_2$,** the E$^{0'}$ of the ferrocenyl group of the β-diketonato ligand coordinated to [IrCl$_2$(fctfa)(cod)] is 0.492 V *vs.* Ag/Ag$^+$ and the E$^{0'}$ of free ferrocene added as internal standard, is 0.189 V *vs.* Ag/Ag$^+$. Accordingly, E$^{0'}$ of the ferrocenyl group of the β-diketonato ligand coordinated to [IrCl$_2$(fctfa)(cod)] in the solvent CH$_2$Cl$_2$ is, therefore, {(0.492 – 0.189) = **0.303**} **V** *vs.* **Fc/Fc$^+$**.
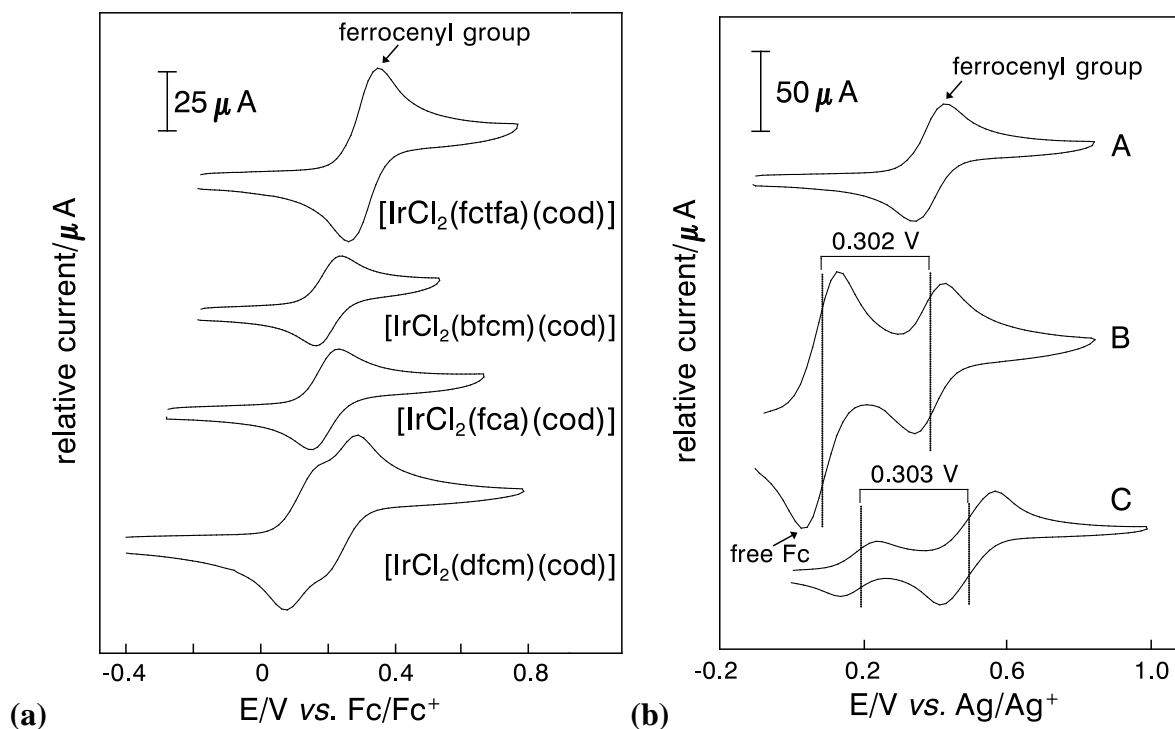
Figure 3.79: **(a) Cyclic voltammograms of the oxidation of the ferrocenyl group of iridium(III) complexes of the type [IrCl$_2$(β-diketonato)(cod)] measured in 0.1 mol dm^{-3} TBAPF$_6$/solvent on a glassy carbon electrode at 25.0(1) °C at scan rate 100 mV s^{-1}. (b) Cyclic voltammogram of the oxidation of the ferrocenyl group of [IrCl$_2$(fctfa)(cod)]. Scan A and B in 0.1 mol dm^{-3} TBAPF$_6$/CH$_3$CN and C in 0.1 mol dm^{-3} TBAPF$_6$/CH$_2$Cl$_2$, B and C with ferrocene added. CV's were measured on a glassy carbon electrode at 25.0(1) °C. The solvent did not influence the formal reduction potentail E$^{0'}$ of [IrCl$_2$(fctfa)(cod)] = 0.303 V when expressed *vs.* Fc/Fc$^+$. E$^{0'}$ of [IrCl$_2$(fctfa)(cod)] *vs.* Fc/Fc$^+$ is indicated as the distance in V between E$^{0'}$ of the ferrocenyl group of [IrCl$_2$(fctfa)(cod)] and E$^{0'}$ of free ferrocene added. E$^{0'}$ of ferrocene as internal standard 83 mV *vs.* Ag/Ag$^+$. (E$^{0'}$ *vs.* Ag/Ag$^+$ is indicated by ……. in (b).)**

Table 3.51 gives the electrochemical data of the [IrCl$_2$(β-diketonato)(cod)] complexes in the different solvents *vs.* Ag/Ag$^+$ and **Table 3.52** the same data *vs.* Fc/Fc$^+$. E$^{0'}$ of free ferrocene as internal standard in solutions of iridium complexes, was 83 mV *vs.* Ag/Ag$^+$, which was a little higher than was measured for ferrocene as internal standard in solutions of rhodium complexes *viz.* 77 mV.

The CV of the iridium(III) complexes of the type [IrCl$_2$(β-diketonato)(cod)] exhibit, as was expected a single electrochemically reversible couple which corresponds to the oxidation of the

ferrocenyl group of the β-diketonato ligand coordinated to [IrCl$_2$(β-diketonato)(cod)]. No iridium oxidation or reduction peak was observed. The ferrocenyl wave showed $\Delta E_p < 91$ mV and $i_{pa}/i_{pc} \approx 1.1$ for scan rates up to 200 mV s^{-1} when using CH$_3$CN as solvent. (**Table 3.51**). The ratio i_{pa}/i_{pc} for [IrCl$_2$(dfcm)(cod)] and [IrCl$_2$(fctfa)(cod)] in CH$_2$Cl$_2$ as solvent, was unity within experimental error (peak currents for [IrCl$_2$(dfcm)(cod)] were measured as described in **Figure 3.80** page 240). The ratio $i_{pa}/i_{pc} \approx 1.1$ for [IrCl$_2$(β-diketonato)(cod)] complexes in CH$_3$CN as solvent, is most probably due to the poor solubility of these complexes in CH$_3$CN. Larger ΔE_p values in CH$_2$Cl$_2$ than in CH$_3$CN probably are because of less efficient heterogeneous electron transfer kinetics from the complexes in solution to the electrode because of the lower polarity of CH$_2$Cl$_2$. The ratio $i_{pa}/i_{pc} \sim 1$ and $\Delta E_p < 91$ mV in CH$_3$CN indicates towards a one-electron transfer process in the ferrocenyl group of the β-diketonato ligand coordinated to [IrCl$_2$(β-diketonato)(cod)] according to **Equation 3.15**.

Equation 3.15:   Fc$^+$ + e$^-$ ⇌ Fc

Table 3.51: Electrochemical data for the oxidation of the ferrocenyl group of iridium(III) complexes of the type [IrCl$_2$(β-diketonato)(cod)] measured in the indicated solvent containing 0.1 mol dm^{-3} TBAPF$_6$ on a glassy carbon electrode at 25.0(1) °C versus Ag/Ag$^+$. The concentration of the complexes was as indicated.

ν / mVs^{-1}	E_{pa}/V	ΔE_p/mV	$E^{0'}$/V	i_{pa}/μA	i_{pa}/i_{pc}	E_{pa}/V	ΔE_p/mV	$E^{0'}$/V	i_{pa}/μA	i_{pa}/i_{pc}
	[IrCl$_2$(dfcm)(cod)] – first ferrocenyl group 1.5(1) mmol dm^{-3} in CH$_2$Cl$_2$					[IrCl$_2$(dfcm)(cod)] – second ferrocenyl group 1.5(1) mmol dm^{-3} in CH$_2$Cl$_2$				
25	0.384	98	0.335	15.3	1.00	0.482	84	0.440	14.7	0.98
50	0.384	100	0.334	20.7	1.05	0.483	87	0.440	19.8	1.00
75	0.387	103	0.336	24.1	1.02	0.487	92	0.441	23.9	1.00
100	0.392	111	0.337	28.8	1.02	0.493	103	0.442	27.8	0.99
	[IrCl$_2$(fca)(cod)] – 1.0(1) mmol dm^{-3} in CH$_3$CN					[IrCl$_2$(bfcm)(cod)] – 1.0(1) mmol dm^{-3} in CH$_3$CN				
50	0.307	76	0.269	16.6	1.09	0.315	71	0.280	14.1	1.15
100	0.309	78	0.270	22.7	1.09	0.318	74	0.281	19.6	1.15
150	0.313	85	0.271	27.6	1.11	0.322	81	0.281	24.0	1.15
200	0.315	91	0.270	32.3	1.11	0.322	83	0.280	27.7	1.16
	[IrCl$_2$(fctfa)(cod)] – 2.0(1) mmol dm^{-3} in CH$_3$CN					[IrCl$_2$(fctfa)(cod)] – 1.0(1) mmol dm^{-3} in CH$_2$Cl$_2$				
50	0.424	76	0.386	31.4	1.18	0.552	128	0.488	28.3	1.00
100	0.428	87	0.385	43.2	1.13	0.567	150	0.492	39.2	1.05
150	0.433	87	0.387	52.8	1.11	0.579	173	0.492	52.8	1.05
200	0.430	91	0.385	59.8	1.12	0.579	174	0.492	59.6	1.04

Table 3.52: Electrochemical data of the oxidation of the ferrocenyl group of iridium(III) complexes of the type [IrCl$_2$(β-diketonato)(cod)] measured in 0.1 mol dm^{-3} TBAPF$_6$ on a glassy carbon electrode at 25.0(1) °C versus Fc/Fc$^+$. The concentration of the complexes and solvent used were as indicated in the table below.

ν/mVs^{-1}	E$^{0'}$/V	ν/mVs^{-1}	E$^{0'}$/V	ν/mVs^{-1}	E$^{0'}$/V
[IrCl$_2$(dfcm)(cod)] - first ferrocenylgroup 1.5(1) mmol dm^{-3} in CH$_2$Cl$_2$		**[IrCl$_2$(fca)(cod)] 1.0(1) mmol dm^{-3} in CH$_3$CN**		**[IrCl$_2$(fctfa)(cod)] 2.0(1) mmol dm^{-3} in CH$_3$CN**	
25	0.146	50	0.186	50	0.303
50	0.145	100	0.187	100	0.302
75	0.147	150	0.188	150	0.304
100	0.148	200	0.187	200	0.302
[IrCl$_2$(dfcm)(cod)] - second ferrocenylgroup 1.5(1) mmol dm^{-3} in CH$_2$Cl$_2$		**[IrCl$_2$(bfcm)(cod)] 1.0(1) mmol dm^{-3} in CH$_3$CN**		**[IrCl$_2$(fctfa)(cod)] 1.0(1) mmol dm^{-3} in CH$_2$Cl$_2$**	
25	0.251	50	0.197	50	0.299
50	0.251	100	0.198	100	0.303
75	0.252	150	0.198	150	0.303
100	0.253	200	0.197	200	0.303
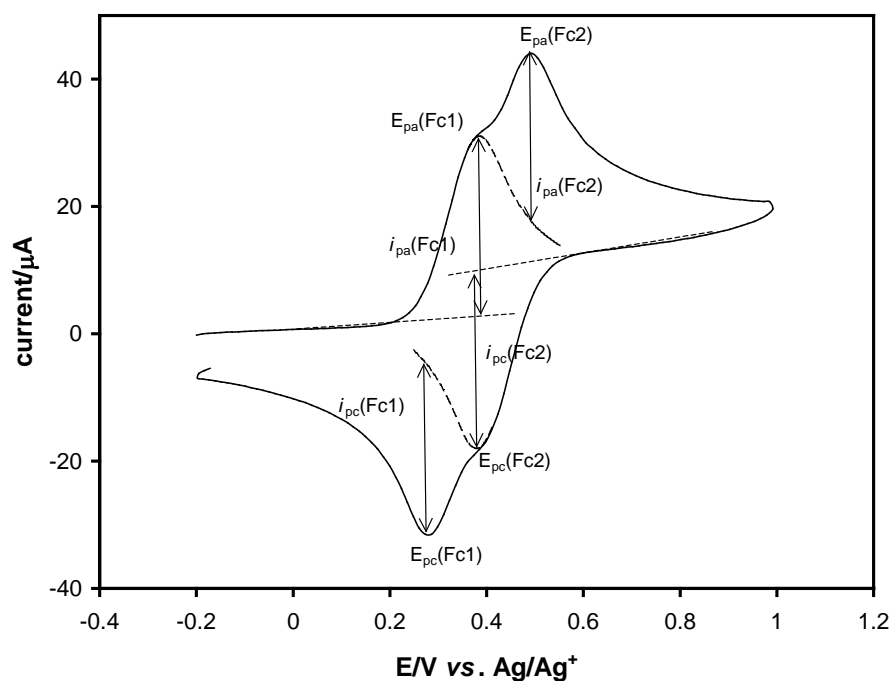
Figure 3.80: CV of [IrCl$_2$(dfcm)(cod)] in 0.1 mol dm^{-3} TBAPF$_6$/CH$_2$Cl$_2$ measured on a glassy carbon electrode at a scan rate 100 mV s^{-1} and 25.0(1) °C versus Ag/Ag$^+$. Since both ferrocenyl groups are part of the same complex, their decaying currents should be the same. The decaying current of the first ferrocenyl group Fc1 oxidation is therefore constructed by translatorily shifting, without distortion, the decaying current of the second ferrocenyl group, Fc2, oxidation, to coincide exactly with the E$_{pa}$(Fc1) value of the Fc1 oxidation peak. The anodic peak current i_{pa}(Fc2) of the second ferrocenyl group can then be measured as indicated. The same construction holds for the reduction of Fc2 by translatorily shifting, without distortion, the decaying current of the Fc1 reduction, to coincide exactly with the E$_{pc}$(Fc2) value of the Fc2 reduction peak. Note that the decaying current of Fc2 oxidation is the same (just in the opposite direction) as the decaying current of Fc1 reduction for this electrochemically reversible process.

241

The possibility that the [IrCl$_2$(β-diketonato)(cod)] complexes are dimers is excluded, because the CV of a [IrCl$_2$(β-diketonato)(cod)] complex showed only one Fc to Fc$^+$ oxidation peak. Two oxidation peaks for the ferrocenyl group would be expected if the [IrCl$_2$(β-diketonato)(cod)] complexes were dimers, as was found for the following two dimer complexes. (i) The [Ir$_2$Cl$_2$(cod)$_2$] dimer complex contains the two iridium(I) moieties. They are oxidized at different positions, E$_{pa}$ = 0.55 and 0.91 V in 0.1 mol dm^{-3} TBAPF$_6$/CH$_3$CN on a glassy carbon electrode at 25.0(1) °C *versus* Ag/Ag$^+$ (**Figure 3.81**). (ii) Diferrocenyl-containing compounds show two different formal reduction potentials.[71, 72, 73] For example, for the free β-diketone Hdfcm, the formal reduction potential of the two ferrocenyl groups is E$^{0'}$ = 0.188 and 0.297 V *vs.* Fc/Fc$^+$ respectively.[19]
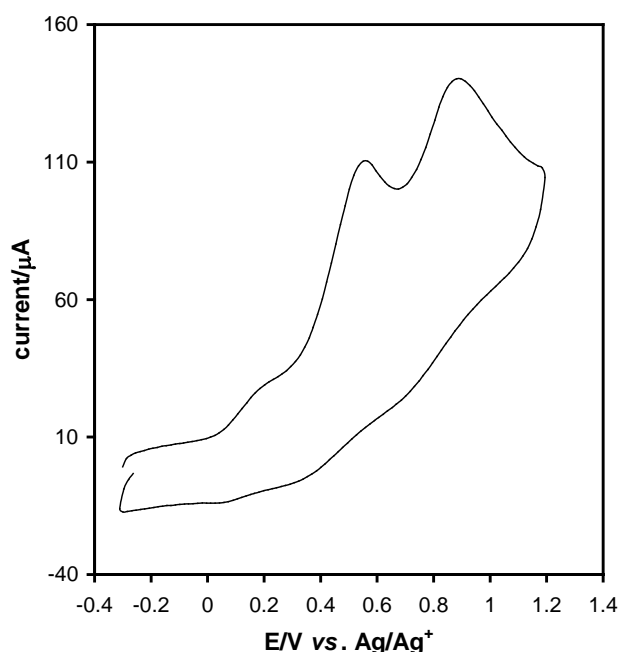
Figure 3.81: CV of the [Ir$_2$Cl$_2$(cod)$_2$] complex at scan rate 100 mV s^{-1}. The two iridium(I) moieties in the complex are oxidized at different positions E$_{pa}$ = 0.55 and 0.91 V in 0.1 mol dm^{-3} TBAPF$_6$/CH$_3$CN on a glassy carbon electrode at 25.0(1) °C.

The linear free energy relationship between E$^{0'}$ of the ferrocenyl group in [IrCl$_2$(β-diketonato)(cod)] and pK$_a$ of the free uncoordinated β-diketone is displayed in **Figure 3.82** with the data summarized in **Table 3.53**.

[71] Morrison, W.H., Jr., Krogsrud, S. and Hendrickson, D.N., *Inorg. Chem.*, **12**, 1998 (1973).

[72] Brown, G.M., Meyer, T.J., Cowan, D.O., LeVanda, C., Kaufman, F., Roling, P.V. and Rausch, M.D., *Inorg. Chem.*, **14**, 506 (1975).

[73] LeVanda, C., Cowan, D.O., Leitch, C. and Bechgaard, K., *J. Am. Chem. Soc.*, **96**, 6788 (1974).

Table 3.53: : pK$_a$ of the free uncoordinated β-diketone and E$^{0'}$ values *vs.* Fc/Fc$^+$ of the ferrocenyl group in [IrCl$_2$(β-diketonato)(cod)] at scan rate 100 mV s^{-1} and 25.0(1) °C.

complex	pK$_a$ (β-diketone)	E$^{0'}$/V vs Fc/Fc$^+$
[IrCl$_2$(dfcm)(cod)]	13.1(1)	0.148; 0.253
[IrCl$_2$(fca)(cod)]	10.01(1)	0.187
[IrCl$_2$(bfcm)(cod)]	10.41(2)	0.198
[IrCl$_2$(fctfa)(cod)]	6.56(3)	0.302
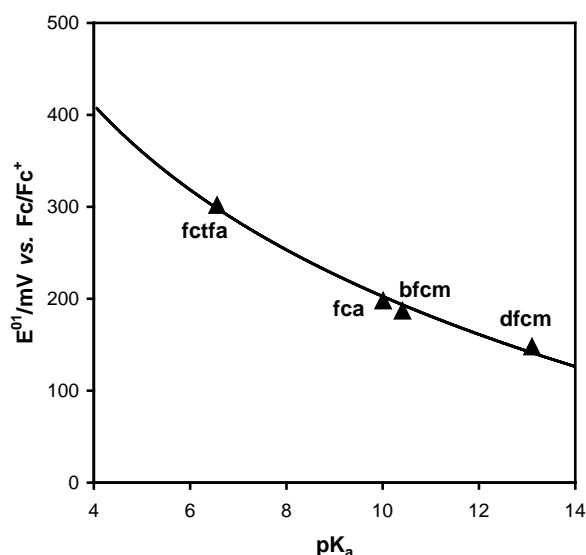
Figure 3.82: Relationship between E$^{0'}$ at 25°C of the ferrocenyl group in [IrCl$_2$(β-diketonato)(cod)] and the pK$_a$ of the free uncoordinated β-diketone.

The formal reduction potential E$^{0'}$ of the ferrocenyl group of the β-diketonato ligand coordinated to the [Ir(III)Cl$_2$(β-diketonato)(cod)] complexes is 14 – 55 mV less positive than E$^{0'}$ of the ferrocenyl group of the β-diketonato ligand coordinated to the corresponding iridium(I) complexes (**Table 3.54**). The Rh(I) and Rh(III) complexes described in paragraphs 3.6.3 and 3.6.4, showed the same general trend as Ir(I) and Ir(III). As was described in paragraph 3.6.4, it is possible that the ferrocenyl group of the β-diketonato ligand coordinated to Ir(III) nucleus of [Ir(III)Cl$_2$(β-diketonato)(cod)] is more easily oxidized than the ferrocenyl group of the β-diketonato ligand coordinated to the unknown *in situ* formed Ir(III) nucleus of the oxidized [Ir(I)(β-diketonato)(cod)] complex. The two unknown ligands coordinating to the *in situ* formed Ir(III) complex that results from the [Ir(β-diketonato)(cod)] oxidation, must have stronger electron withdrawing properties than the two chloride ligands of [Ir(III)Cl$_2$(β-diketonato)(cod)]. Further research is required to completely clarify this matter. **Table 3.55** gives a summary of the E$^{0'}$ values of the ferrocenyl group of the free β-diketone, [Ir(β-diketonato)(cod)] and [IrCl$_2$(β-diketonato)(cod)].

Table 3.54: Comparison of the electrochemical data for the iridium(I) complexes of the type [Ir(β-diketonato)(cod)] with iridium(III) complexes of the type [IrCl$_2$(β-diketonato)(cod)] at 25.0(1) °C vs. Ag/Ag$^+$.

ν/mVs^{-1}	[Ir(I)(β-diketonato)(cod)]				[Ir(III)Cl$_2$(β-diketonato)(cod)]		
	E$_{pa}$(Ir)/V	E$_{pa}$(Fc group)/V	ΔE$_p$/mV	E$^{0'}$/V	E$_{pa}$(Fc group)/V	ΔE$_p$/mV	E$^{0'}$/V
β-diketonato = bfcm							
50	0.233	0.381	118	0.325	0.315	71	0.280
100	0.245	0.388	129	0.324	0.318	74	0.281
150	0.260	0.394	139	0.325	0.322	81	0.281
200	0.267	0.397	149	0.325	0.322	83	0.280
β-diketonato = fca							
100	0.243	0.397	144	0.325	0.309	78	0.270
150	0.253	0.401	154	0.324	0.313	85	0.271
200	0.259	0.405	162	0.324	0.315	91	0.270
β-diketonato = fctfa							
50	0.311	0.464	129	0.400	0.424	76	0.386
100	0.325	0.466	133	0.400	0.428	87	0.385
150	0.335	0.469	139	0.400	0.433	87	0.387

Table 3.55: Comparison of E$^{0'}$ values of the ferrocenyl group of the free β-diketone, E$^{0'}$ of the ferrocenyl group of the β-diketonato ligands coordinated to different iridium complexes and E$_{pa}$ of iridium at 25.0(1) °C and scan rate 100 mV s^{-1} *versus* Fc/Fc$^+$. Ferrocene was used as internal standard, E$^{0'}$(Free Fc) = 0.083(6) mV *versus* Ag/Ag$^+$.

complex	(E$^{0'}$ or E$_{pa}$)/V of the complexes with β-diketonato ligands				
	fctfa	bfcm	fca	dfcm first ferrocenyl group	dfcm second ferrocenyl group
E$_{pa}$ (Ir) [Ir(β-diketonato)(cod)]	0.242	0.162	0.160	-	-
E$^{0'}$(Fc) [Ir(III)Cl$_2$(β-diketonato)(cod)]	0.302	0.198	0.187	0.148	0.253
E$^{0'}$(Fc) free β-diketone	0.317	0.231	0.236	0.188	0.297
E$^{0'}$(Fc) [Ir(β-diketonato)(cod)]	0.317	0.241	0.242	-	-

3.6.8 Bulk electrolysis.

Bulk electrolysis was performed on a selection of complexes representing all the different types of complexes that CV's were taken from. Only the oxidation step of each couple was subjected to bulk electrolysis. Examples of the current-time and charge-time data obtained are displayed in **Figure 3.83** with the results summarized in **Table 3.56**. The rhodium and iridium complexes revealed different electrochemical behaviour. Ferrocene-containing β-diketonato complexes of rhodium(I) exhibit the following electrochemical behaviour with a three electron transfer process (see results obtained in **Table 3.56**):

Equation 3.14: $\qquad$ Rh(I) $\rightarrow$ Rh(III) + 2e$^-$

Equation 3.15: $\qquad$ Fc$^+$ + e$^-$ $\square$ Fc

In contrast, results in **Table 3.56** indicated that ferrocene-containing β-diketonato complexes of iridium(I) exhibit a two-electron transfer process:

Equation 3.16: $\qquad$ Ir(I) $\rightarrow$ Ir(II) + e$^-$

Equation 3.15: $\qquad$ Fc$^+$ + e$^-$ $\square$ Fc

Electrochemical oxidation of the non-ferrocene-containing β-diketonato complex [Ir(acac)(cod)] was also found to be a one-electron transfer process, *i.e.* as shown in **Equation 3.16**. The square planer Vaska's complexes [Ir(CO)XL$_2$] (X = Cl, Br and I; L = PPh$_3$, PPh$_2$Et and PPhEt$_2$) as discussed in chapter 2 paragraph 2.3.8.1, also underwent one-electron oxidations.[70]
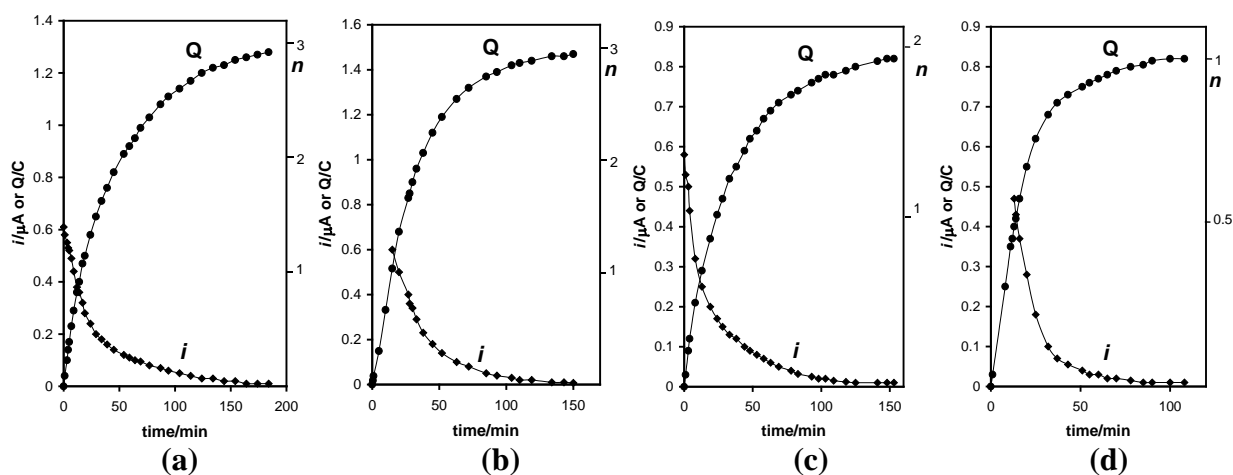
Figure 3.83: Current-time and charge-time response for (a) [Rh(fctfa)(CO)(PPh$_3$)], (b) [Rh(fctfa)(CO)$_2$], (c) [Ir(fctfa)(cod)] and (d) [Ir(acac)(cod)]. Righthand axes indicate *n* = electrons transferred per molecule.

Table 3.56: Results from bulk electrolysis. Electrolysis was performed on N mol of the indicated complexes in 0.1 mol dm^{-3} TBAPF$_6$/CH$_3$CN at 25.0(1) °C at the plateau potential of the anodic voltammetric wave E$_{exp}$, using a carbon plate working electrode. Q = the total charge collected and *n* = electrons transferred per molecule.

complex	mass/mg	N/mol	E$_{exp}$/V	Q	Q/NF	*n*
[Rh(fctfa)(cod)]	1.7	3.18 x 10^{-6}	0.83	0.91	2.96	3
[Rh(fctfa)(CO)(PPh$_3$)]	3.2	4.47 x 10^{-6}	1.0	1.28	2.97	3
[Rh(fctfa)(CO)$_2$]	2.5	5.19 x 10^{-6}	0.8	1.46	2.94	3
[Rh(fca)(CO)$_2$]	2.7	6.3 x 10^{-6}	1.10	1.78	2.92	3
[Ir(fctfa)(cod)]	2.8	4.49 x 10^{-6}	1.20	0.82	1.89	2
[Ir(acac)(cod)]	3.4	8.51 x 10^{-6}	0.80	0.82	1.00	1

Other researchers in this laboratory have found that with the addition of a complexing ligand to bulk electrolysis solutions, certain rhodium(I) complexes led to a better quantitative electron transfer.[37] This was not necessary for any of the complexes of this study, as a clean 3:1, 2:1 or 1:1 electron transfer ratio was observed. However, it does not exclude the possibility that the addition of an coordinating ligand to bulk electrolysis iridium solutions may lead to a 3:1 electron transfer ratio rather than the 2:1 electron transfer ratio in case of the [Ir(β-diketonato)(cod)] complexes. This possibility will be pursued in a forthcoming study.

Monomeric Ir(II) complexes such as [Ir^{II}(C$_6$Cl$_5$)$_2$(cod)] are known,[74] and because of the reasoning on page 241, the author suspects that the electrochemically generated Ir(II) complexes of this study may have a similar structure. However, the possibility exists that the [Ir(β-diketonato)(cod)] complexes form dimers when they are oxidized to the iridium(II) oxidation state, because many complexes of iridium(II) have a dimeric structure.[75] Towards this end the following evidence may be sited. Two possible configurations of the di-iridium complex [(Ph$_3$P)$_2$(CO)$_2$Br$_2$Ir$_2$(C$_{10}$H$_4$S$_4$)] are possible, *viz.* the five-coordinated 16-electron Ir(III) structure (a) in **Figure 3.84**, or the six-coordinated 18-electron Ir(II) structure (b) in **Figure 3.84**. An X-ray crystal structure study reveals that the dimeric Ir(II) structure (b) was adopted.[76] **Figure 3.85** displays more examples of structures of stable dimeric iridium(II) complexes.[76, 77, 78, 79]

(a) (b)
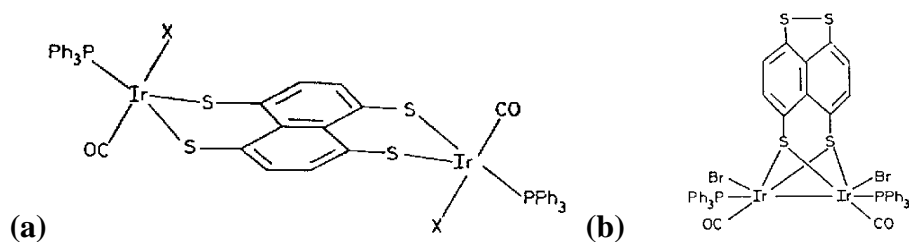
[74] Cotton, F.A., Wilkinson, G., Murillo, C.A. and Bochmann, M., *Advanced Inorganic Chemistry*, John Wiley, New York,1999, p. 1056.

[75] Wilkinson, G.,*Comprehensive Coordination Chemistry*, Pergamon Press, New York, 1987, vol 4., p. 1120.

[76] Teo, B.K. and Snyder-Robinson, P.A., *J.C.S. Chem. Comm.,* 255 (1979).

[77] Bonnet, J.J., Thorez, A., Maisonnat, A., Galy, J. and Poilblanc, R., *J Am.Chem. Soc.*, **101**, 5940 (1979).

[78] Bonnet, J.J., Kalck, P. and Poilblanc, R., *Angew. Chem. Int. Ed. Engl.,* **19**, 551 (1980).

[79] Rasmussen, P.G., Anderson, J.E., Bailey, O.H. and Tamres, M., *J. Am. Chem. Soc.,* **107**, 279 (1985).

Figure 3.84: Two possible configurations of the complex [(Ph₃P)₂(CO)₂Br₂Ir₂(C₁₀H₄S₄)]: (a) The sterically more favourable [(Ph₃P)(CO)BrIrS₂C₁₀H₄S₄IrBr(CO)(PPh₃)] Ir(III)-Ir(III) dimer and (b) the electronically more favourable [(Ph₃P)₂(CO)₂Br₂Ir₂S₂C₁₀H₄S₂] Ir(II)-Ir(II) dimer. X-ray structure analysis confirmed the Ir(II)-Ir(II) dimer stucture (b).[76]

(a)　　　　　　　　　　　　　　　　(b)

(c)　　　　　　　　　　　　　　　　(d)
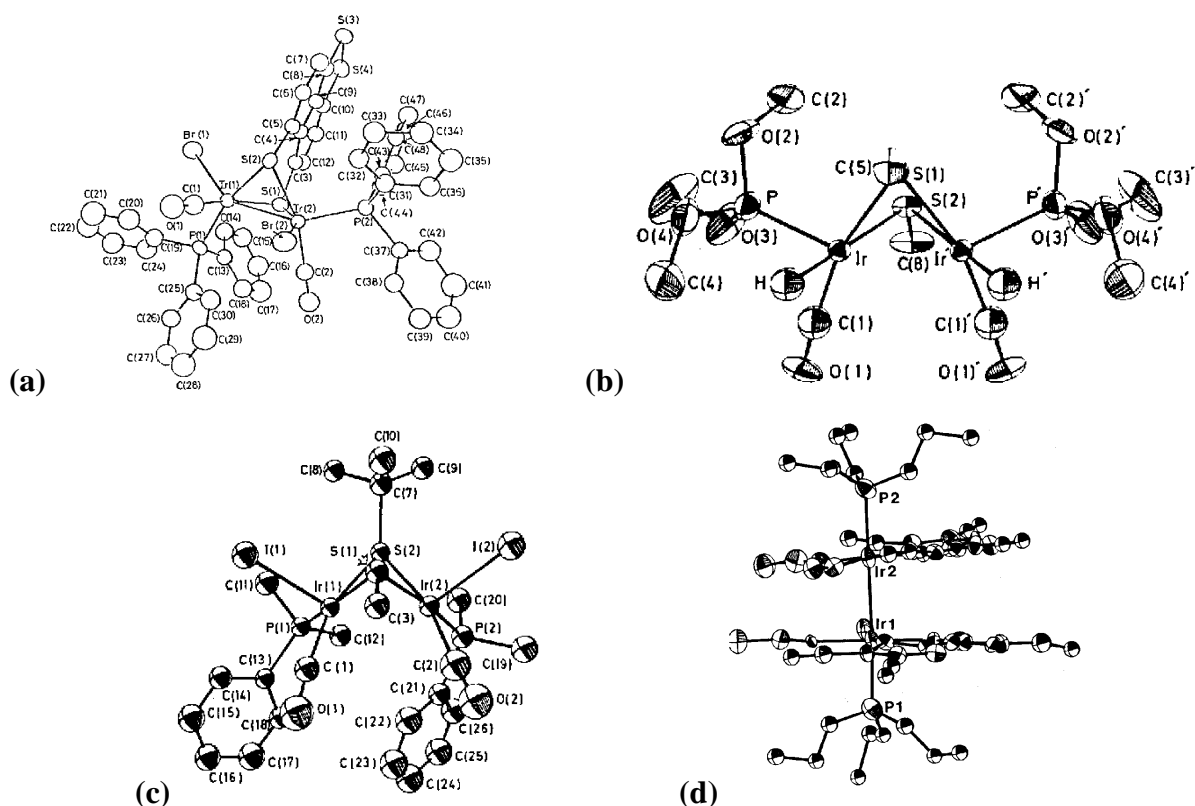
Figure 3.85: Structures of stable dimeric iridium(II) complexes:

(a) [(Ph₃P)₂(CO)₂Br₂Ir₂S₂C₁₀H₄S₂][76]　　(b) [Ir(H)(μ-S*t*-Bu)(CO)(P(OMe)₃)]₂[77]

(c) [Ir₂(μ-S*t*-Bu)₂(CO)₂(PMe₂Ph)₂I₂][78]

(d) [Ir₂(Tcbiim)₂(CO)₂(CH₃CN)₂(P(OEt)₃)(CH₃CN)],[79] H₂Tcbiim = tertacyanobiimidazole.

3.6.9 Correlation of the formal reduction/oxidation potentials of different rhodium(I), rhodium(III) and iridium(I) complexes.

3.6.9.1 β-diketone, [Rh(β-diketonato)(CO)₂], [Rh(β-diketonato)(CO)(PPh₃)], [Rh(β-diketonato)(CO)(PPh₃)(CH₃)I] and related ferrocene-containing β-diketonato rhodium complexes.

The formal reduction potential, $E^{0'}$, of the ferrocenyl group of the free β-diketone and $E^{0'}$ of the ferrocenyl group of the β-diketonato ligands coordinated to different rhodium complexes are

given in **Table 3.57** for comparison purposes. The anodic oxidation potential of Rh, $E_{pa}(Rh)$ in the different rhodium complexes discussed in this study, is illustrated in **Figure 3.86** for comparison purposes.

Table 3.57: Comparison of $E^{0'}/V$ of the ferrocenyl group of the free β-diketone and $E^{0'}/V$ of the ferrocenyl group of the β-diketonato ligands coordinated to different rhodium complexes 25.0(1) °C versus Ag/Ag$^+$.

complex	$E^{0'}/V$ of complexes with β-diketonato ligands				
	fctfa	bfcm	fca	dfcm first ferrocenyl group	dfcm second ferrocenyl group
[Rh^{III}(β-diketonato)(CH$_3$)(I)(P(OPh)$_3$)$_2$][69]	0.304	-	-	-	-
[Rh^{III}(β-diketonato)(CH$_3$)(I)(CO)(PPh$_3$)]	0.307	-	-	-	-
[Rh^I(β-diketonato)(CO)$_2$]	0.392	0.287	0.280	0.259	0.353
free β-diketone	0.394	0.308	0.313	0.265	0.374
[Rh^I(β-diketonato)(cod)]	0.406	0.314	0.309	0.280	0.379
[Rh^I(β-diketonato)(CO)(PPh$_3$)]	0.457	0.350	0.327	0.277	0.389
[Rh^I(β-diketonato)(P(OPh)$_3$)$_2$][69]	0.468	-	0.325	0.345	0.438
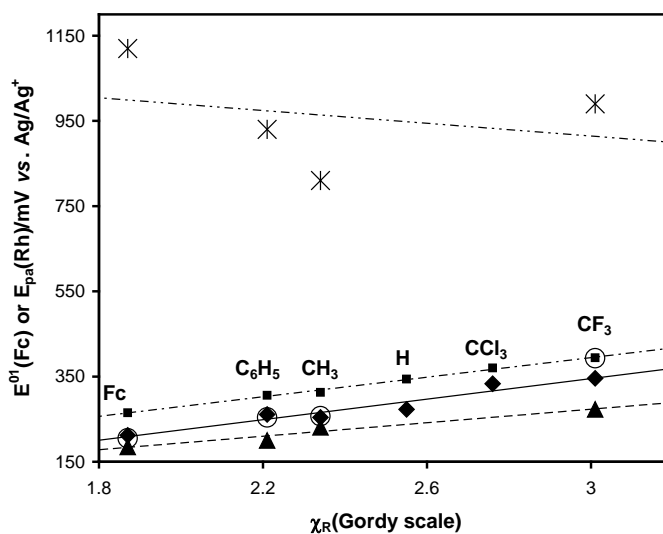
Figure 3.86: Relationships between (from top to bottom)
(a) $E^{0'}$ of the ferrocenyl group of the free β-diketone or Hfch} (. _ . _ . _ . _ . _ . and ■) and χ$_R$,
(b) E_{pa} of rhodium in [Rh(FcCOCHCOR)(CO)$_2$], (.. _ .. _ _ _ .. _ .. _ .. and. Σ) and χ$_R$,
(c) E_{pa} of rhodium in [Rh(FcCOCHCOR)(cod)] (_____ and υ) and χ$_R$,
(d) E_{pa} of rhodium in [Rh(FcCOCHCOR)(CO)(PPh$_3$)] (- - - - - -- - - - and σ) and χ$_R$, and
(e) E_{pa} of rhodium in [Rh(β-diketonato)(P(OPh)$_3$)$_2$] (pionts indicated as O) and χ$_R$,
with χ$_R$ the group electronegativity and R = Fc, C$_6$H$_5$, CH$_3$, CCl$_3$, CF$_3$ and H.

3.6.9.2 [Rh(β-diketonato)(cod)] and [Ir(β-diketonato)(cod)].

Figure 3.87 illustrates that E_{pa} for the oxidation of iridium(I) to iridium(II) in [Ir(fctfa)(cod)] is 21 mV lower than the oxidation of rhodium(I) to rhodium(III) in the isostructural [Rh(β-diketonato)(cod)] complexes, but the oxidation of the ferrocenyl group in the [M(β-diketonato)(cod)] complexes, M = Rh or Ir, is approximately the same (see **Table 3.58** for the exact values for the diferent complexes). The last mentioned observation is unexpected, because the oxidation of the ferrocenyl group takes place when the metal centre is in different oxidation states, Ir(II) or Rh(III).

(a) **(b)**
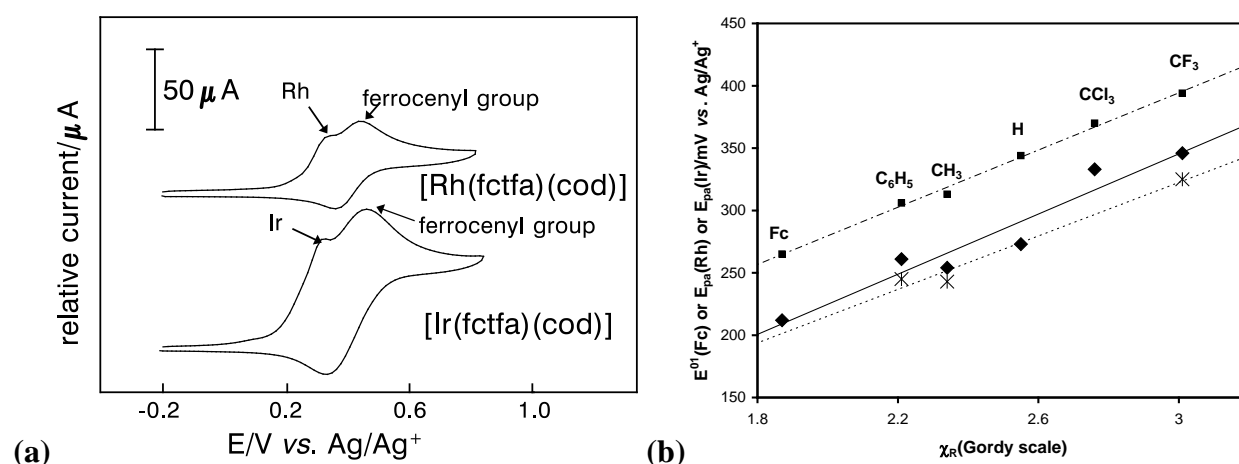
Figure 3.87: **(a)** **CV of [M(fctfa)(cod)] measured in 0.1 mol dm⁻³ TBAPF₆/CH₃CN at a scan rate of 100 mV s⁻¹ on a glassy carbon electrode at 25.0(1) °C versus Ag/Ag⁺.   M = Rh and Ir.   The concentration of the iridium complex is 3 mmol dm⁻³ and of the rhodium complex 1 mmol dm⁻³.**
(b) Relationships between (from top to bottom)
(i) $E^{0'}$ of the ferrocenyl group of the free β-diketone or Hfch (. _ . _ . _ . _ . _ . and ■) and χ_R,,
(ii) E_{pa} of rhodium in [Rh(FcCOCHCOR)(cod)] (_____ and σ) and χ_R, and
(iii) E_{pa} of iridium in [Ir(FcCOCHCOR)(cod)] } (.............. and Σ) and χ_R,
with χ_R the group electronegativity and R = Fc, C₆H₅, CH₃, CCl₃, CF₃ and H.

Table 3.58:   Comparison of the electrochemical data of complexes of the type [M(β-diketonato)(cod)] measured in 0.1 mol dm⁻³ TBAPF₆/CH₃CN at a scan rate of 100 mV s⁻¹ on a glassy carbon electrode at 25.0(1) °C versus Ag/Ag⁺. M = Rh and Ir.

complex	E_{pa}/V (Rh or Ir)	$E^{0'}$/V (ferrocenyl group)	ΔE_p/mV (ferrocenyl group)	i_{pa}/i_{pc} (ferrocenyl group)
[Rh(fctfa)(cod)]	0.346	0.406	80	1.02
[Ir(fctfa)(cod)]	0.325	0.400	133	0.74
[Rh(bfcm)(cod)]	0.261	0.314	74	0.98
[Ir(bfcm)(cod)]	0.245	0.324	129	0.78
[Rh(fca)(cod)]	0.254	0.309	76	1.02
[Ir(fca)(cod)]	0.243	0.325	144	1.00

The slightly more positive oxidation potentials for rhodium complexes compared to the isostructural iridium complexes are consistent with

(i) the fact that complexes of the third row of transition elements (*eg.* iridium) showed higher rate constants for oxidative addition than isostructural complexes of the second row (*eg.* rhodium) {chapter 2 paragraph 2.2.2.3 (i)} and

(ii) the greater stability of higher oxidation states for $5d$ transition elements compared with those of the $4d$ series.[80]

Not much information about the electrochemical behaviour of $4d/5d$ pairs of structural analogues is available, but the cuboidal $[Mo_4Te_4(CN)_{12}]^{6-}$ complex shows much higher oxidation potentials than the isostructural $[W_4Te_4(CN)_{12}]^{6-}$ complex.[80] $[W_4Te_4(CN)_{12}]^{6-}$ displays a negative shift of 254 mV for the 4+/5+ couple and 366 mV for the 5+/6+ couple compared to the $[Mo_4Te_4(CN)_{12}]^{6-}$ analogue. In the case of the tri-nuclear acetato-briged $[M_3(\mu_3\text{-}O)(\mu\text{-}OAc)_6(py)_3]^+$ complexes (M = Rh, Ir; py = pyridine) the Rh complex undergoes reversibly one-electron oxidation at a 640 mV higher potential than its Ir analogue.[81]

Higher oxidation potentials for rhodium than for iridium in the bimetallic complexes $[NBu_4][M_2(dcbmi)(cod)_2]$ and $[NBu_4][M_2(dcbmi)(CO)_4]$ (H_3dcbmi = 2-methylimidazole-4,5-dicarboxylic acid) were observed for the the two-electron oxidation process M(I)-M(I) to M(II)-M(II).[82] The $[NBu_4][Rh_2(dcbmi)(cod)_2]$ complex in CH_3CN showed a 280 mV higher oxidation potential than the corresponding iridium complex. The $[NBu_4][Rh_2(dcbmi)(CO)_4]$ complex in CH_3CN showed a 610 mV higher oxidation potential than the corresponding iridium complex. From the structure of the dcbmi complex in **Figure 3.88** (a) it is clear that conjugation to the metal is less favourable compared to the $[M(\beta\text{-diketonato})(cod)]$ complexes of this study. The conjugation in the $[M(\beta\text{-diketonato})(cod)]$ complexes is controlled by the group electronegativities of the groups on the β-diketone coordinated to the $[M(\beta\text{-diketonato})(cod)]$ complex as can be seen in the relationships between group electonegativities, kinetic rate constants and peak anodic oxidation potential of M. Also, the dcbmi complexes have a netto negative charge, while the β-diketonato complexes in this study are neutral. Better communication between the groups on the β-diketonato ligand and M as well as the charge

---

[80] Fedin, V.P., Kalinina, I.V., Samsonenko, D.G., Mironov, Y.V., Sokolov, M.N., Elsegood, M.R.J., Clegg, W. and Sykes, A.G., *Inorg. Chem.*, **38**, 1956 (1999).

[81] Tahahashi, K., Umakoshi, K., Kikuchi, A., Sasaki, Y., Tominaga, M. and Taniguchi, I.Z*., Naturforsch,* **50b**, 551 (1995).

[82] Anderson, J.E., Gregory, T.P., Net, G. and Bayón, J.C., *J. Chem. Soc. Dalton Trans.,* 487 (1992).

difference must contribute to the smaller difference in the anodic oxidation potential between Ir and Rh for the [M(β-diketonato)(cod)] complexes compared to the cited dcbmi complexes.

Although, a one-electron oxidation is observed for the the [Ir(β-diketonato)(cod)] complexes and a two-electron process for the the [Rh(β-diketonato)(cod)] complexes, it is interesting to note that there is a linear correlation between the oxidation potential of the Ir(I)-Ir(II) couple and the oxidation potential of the Rh(I)-Rh(III) couple: $E_{pa}(Ir)/E_{pa}(Rh) = 0.91(4)$ for the [M(β-diketonato)(cod)] complexes in this study (**Figure 3.89**). This indicates that the same factors determine the oxidation potentials for the complexes of the two metals.

(a) M = Rh^I or Ir^I **(b)**
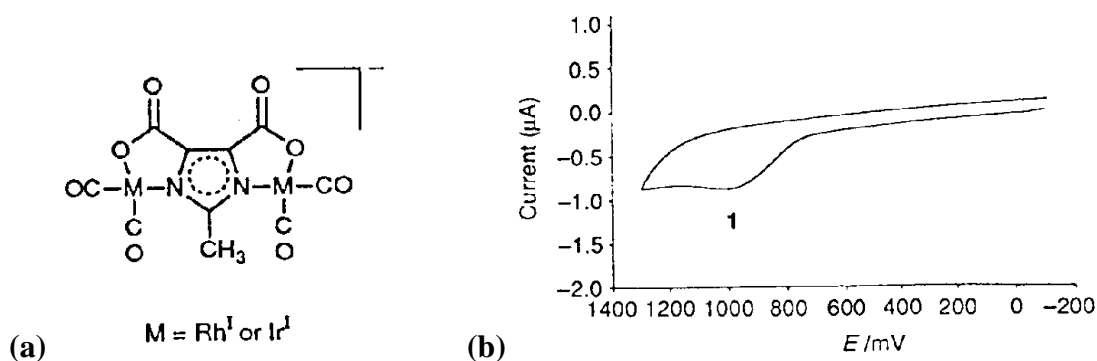
Figure 3.88: (a) Structure of [M$_2$(dcbmi)(CO)$_2$]$^-$. (b) Cyclic voltammogram of a 7.80 x 10^4 mol dm^{-3} solution of [NBu$_4$][Rh$_2$(dcbmi)(CO)$_4$] in 0.20 mol dm^{-3} NBu$_4$ClO$_4$/CH$_2$Cl$_2$ at a scan rate of 100 mV s^{-1} *vs.* SCE. E$_{pa}$ = 0.94 V, E$^{0'}$ for ferrocene = 0.36 V.[82]
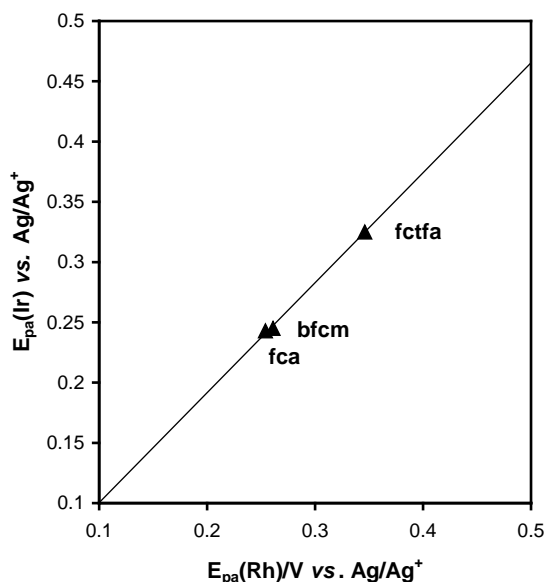
Figure 3.89: The relationship between E$_{pa}$(Ir), the oxidation potential of the Ir(I)-Ir(II) couple and E$_{pa}$(Rh) the oxidation potential of the Rh(I)-Rh(III) couple for the [M(β-diketonato)(cod)] complexes with β-diketonato = fctfa, fca and bfcm. Slope = 0.91(4).

3.7 Group electronegativity, rate constants, carbonyl stretching frequencies, pK$_a$ and oxidation potentials.

For all the complexes of the type [M(R$_1$COCHCOR$_2$)(X)] with M = Rh or Ir, X = (CO)$_2$, (CO)(PPh$_3$), (cod) or (P(OPh$_3$)$_2$) it is clear that the group electronegativity of the R groups on the β-diketonato ligand directly influences the electron density on the metal centre. Since the change in electron density on the metal is reflected by parameters such as the kinetic rate constants, carbonyl stretching frequencies, pK$_a$ and formal reduction potentials, a relationship between these parameters and group electronegativities of R$_1$ and R$_2$ should exist. **Table 3.59** gives a summary of the parameters that will be used to determine these relationships. Paragraphs 3.7.1 to 3.7.4 will illustrate that the sum of the group electronegativities of R$_1$ and R$_2$ of the β-diketonato ligand (R$_1$COCHCOR$_2$)$^-$ coordinated to [M(R$_1$COCHCOR$_2$)(X)], gives a good indication of the electron density (nucleophilicity) on the metal M = rhodium or iridium.

Table 3.59: Kinetic rate constants, carbonyl stretching frequencies and E$_{pa}$ values of the indicated rhodium and iridium complexes, as well as pK$_a$ and group electronegativities of the R substituent of the free uncoordinated the β-diketone.

| β-diketonato ligand (R$_1$COCHCOR$_2$)$^-$ | | | | | [Rh(R$_1$COCHCOR$_2$)(CO)(PPh$_3$)] [a] | | | [Rh(R$_1$COCHCOR$_2$)(cod)] [b] | | [Ir(R$_1$COCHCOR$_2$)(cod)] [c] | | [Rh(R$_1$COCHCOR$_2$)(POPh$_3$)$_2$] [d] | |
abre-via-tion	R$_1$	R$_2$	(χ_{R1} + χ_{R2})/ (Gordy scale) [e]	pK$_a$ [f]	v(C=O)/ cm^{-1}	E$_{pa}$(Rh)/ mV vs. Ag/Ag$^+$	k$_1$/ mol^{-1} dm^{3}s^{-1}	E$_{pa}$(Rh)/ mV vs. Ag/Ag$^+$	k$_2$/ mol^{-1} dm^{3}s^{-1}	E$_{pa}$(Ir)/ mV vs. Ag/Ag$^+$	k$_2$/ mol^{-1} dm^{3}s^{-1}	E$_{pa}$(Rh)/ mV vs. Fc/Fc$^+$	k$_1$/ mol^{-1} dm^{3}s^{-1}
dfcm	Fc	Fc	3.74	13.1	1977	185	0.155 [h]	212	7	-	-	124	0.177
bfcm	Fc	C$_6$H$_5$	4.08	10.41	1977	200, 350[i]	0.0409	261	30	245	63.9	173	-
fca	Fc	CH$_3$	4.21	10.01	1980	231, 330[i]	0.0455	254	17.8	243	15.3	176	0.151
fch	Fc	H	4.22	7.04	-	-	-	273	47	-	-	-	-
dbm	C$_6$H$_5$	C$_6$H$_5$	4.42	9.35	1979	397	0.00961	-	61.4	-	413	324	0.0149
ba	C$_6$H$_5$	CH$_3$	4.55	8.70	1980	425	0.00930	-	51.2	-	85.8	322	0.0342
fctca	Fc	CCl$_3$	4.63	7.13	-	-	-	333	1375	-	-	-	-
acac	CH$_3$	CH$_3$	4.68	8.95	-	-	0.024 [g]	-	29	436	13.6	308	0.096
fctfa	Fc	CF$_3$	4.88	6.56	1986	273, 404[i]	0.0037	346	558	325	7600	312	0.0155
tfba	C$_6$H$_5$	CF$_3$	5.22	6.30	1983	537	0.00112	-	2420	-	25100	461	0.00263
tfaa	CF$_3$	CH$_3$	5.35	6.30	1983	580	0.00146	-	1330	548	17100	477	0.0056
hfaa	CF$_3$	CF$_3$	6.02	4.71	-	650	-	-	276000	-	3000000	881	0.00024

(a) v(C=O) this study and ref 14 see **Table 3.1** page 126, E$_{pa}$(Rh) and k$_1$ this study and ref 37 see **Table 3.44** page 225.
(b) E$_{pa}$(Rh) this study, k$_1$ this study and ref 54, 55 and 56 see **Table 3.37** page 208.
(c) E$_{pa}$(Ir) this study, k$_1$ this study and ref 57 see **Table 3.37** page 208.

(d) E_{pa}(Rh) from ref 84, k_1 from ref [83] and [84].
(e) group electronegativities of this study and ref 19 see **Table 3.39** page 213.
(f) pK_a from ref. 35, 58, 59 and this study paragraph 3.3.
(g) value in 1,2-dichloroethane, a slightly smaller value is expected in acetone.
(h) value in chloroform, a smaller value is expected in acetone.
(i) two E_{pa} values correspond to oxidation of the two isomers of [Rh(R_1COCHCOR$_2$)(CO)(PPh$_3$)]

3.7.1   Group electronegativities and rate constants.

Since the metal atoms Rh or Ir acts as a nucleophile when it undergoes oxidative addition (chapter 2 paragraph 2.2.2.2), it is to be expected that anything that affects the nucleophilicity (or basicity) of the metal, will influence the rate of oxidative addition reactions. Any influence of a ligand bonded to the metal, that will increase the electron density on the metal centre, will lead to an increased rate of oxidative addition, assuming all other influences, factors and parameters remain constant. **Figure 3.90** illustrates that the sum of the group electronegativities of R_1 and R_2 of the β-diketonato ligand (R_1COCHCOR$_2$)⁻ coordinated to [Rh(β-diketonato)(CO)(PPh$_3$)] and [Rh(β-diketonato)(POPh$_3$)$_2$] is linearly dependant on $\log k_1$. k_1 is the rate constant for the oxidative addition of iodomethane to these rhodium complexes. It is therefore concluded that the sum of the group electronegativities R_1 and R_2 of the β-diketonato ligand (R_1COCHCOR$_2$)⁻ coordinated to [Rh(β-diketonato)(CO)(PPh$_3$)] or [Rh(β-diketonato)(POPh$_3$)$_2$] gives a good indication of the electron density (nucleophilicity) of rhodium in each complex.

Increased electron density on the metal centre, however, leads to a decrease in the rate of β-diketone substitution with phen (chapter 2 paragraph 2.2.4.3) in [M(β-diketonato)(cod)] with M = Rh or Ir, as is illustrated in **Figure 3.91**. The linear relationship between $\log k_2$, the second-order substitution rate constant, and ($\chi_{R1} + \chi_{R2}$) is clear. As with oxidative addition, ($\chi_{R1} + \chi_{R2}$) gives a good indication of the electron density (nucleophilicity) on rhodium or iridium in each complex.

[83] van Zyl, G.J., Lamprecht, G.J., Leipoldt, J.G. and Swaddle, T.W., *Inorg. Chim. Acta.,* **143**, 223 (1988).

[84] Erasmus, J.J.C., *Electrochemical and chemical kinetic aspects of coordinative complexes of rhodium(I) and (III), Ph. D. Thesis*, University of the Orange Free State, R.S.A., 1997.

(a) **(b)**
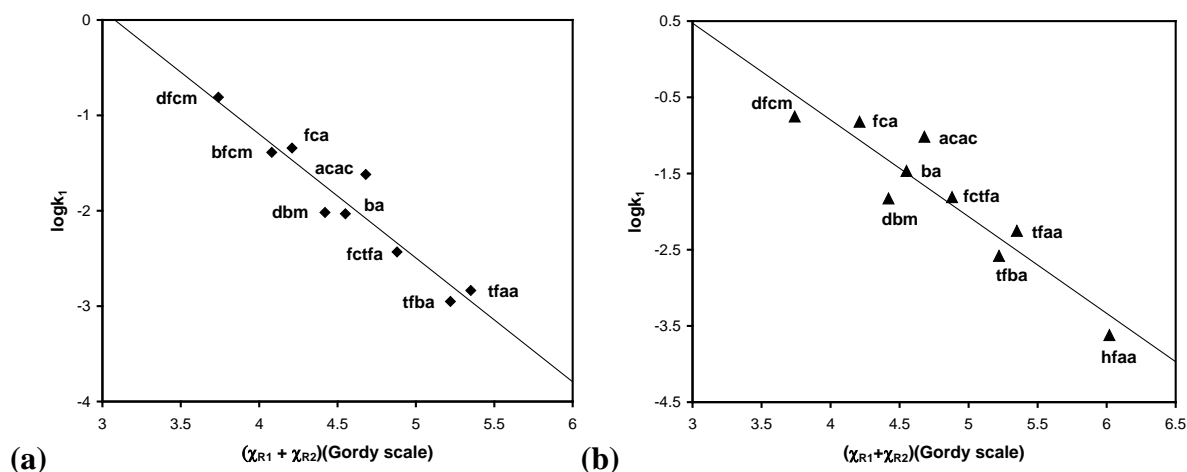
Figure 3.90: Relationship between $\log k_1$, the second-order rate constant for the first step of oxidative addition of iodomethane to (a) $[Rh(R_1COCHCOR_2)(CO)(PPh_3)]$ and (b) $[Rh(R_1COCHCOR_2)(POPh_3)_2]$ and the sum of the group electronegativities of R_1 and R_2, $(\chi_{R1} + \chi_{R2})$, of the β-diketonato ligand $(R_1COCHCOR_2)^-$ coordinated to the rhodium complexes. The β-diketonato ligands are as indicated.

(a) **(b)**
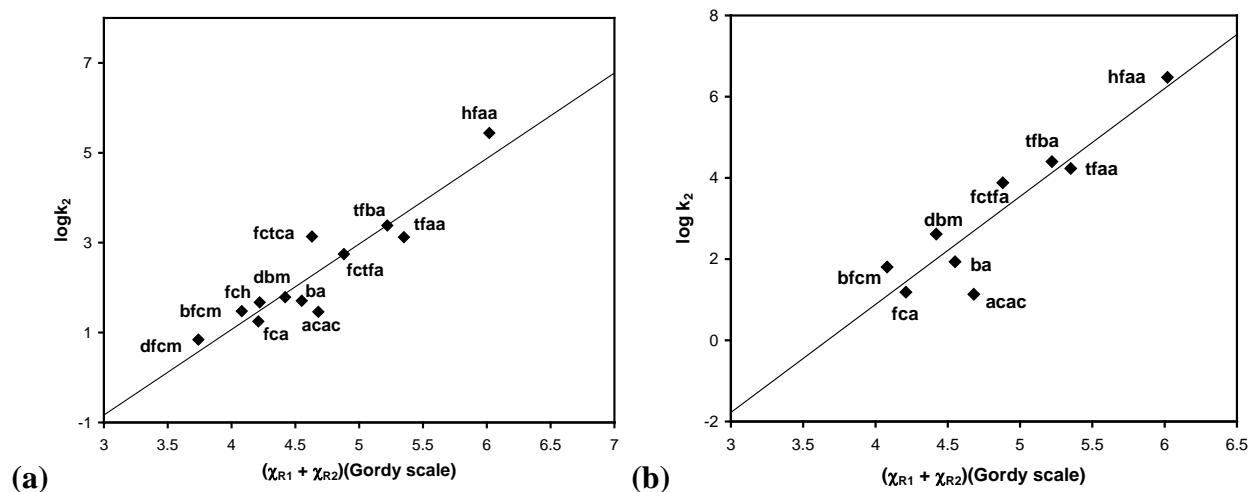
Figure 3.91: Relationship between k_2, the second-order rate constant of the substitution of the β-diketonato ligand with 1,10-phenentroline in (a) $[Rh(β\text{-diketonato})(cod)]$ and (b) $[Ir(β\text{-diketonato})(cod)]$ and the sum of the group electronegativities of R_1 and R_2 $(\chi_{R1} + \chi_{R2})$ of the β-diketonato ligand $(R_1COCHCOR_2)^-$ coordinated to the metal complexes. The β-diketonato ligands are as indicated.

3.7.2 Group electronegativities and oxidation potentials.

The higher the oxidation potential of the metal in $[Rh(β\text{-diketonato})(CO)(PPh_3)]$ or $[M(β\text{-diketonato})(cod)]$ (M = Rh and Ir) complexes, the lower electron density is expected on M. Groups R_1 and R_2 on the β-diketonato ligand $(R_1COCHCOR_2)^-$ coordinated to a metal complex with high group electronegativities are expected to withdraw more electron density from the

metal centre. The metal M should then be relatively more electron-deficient and consequently a high oxidation potential, E_{pa}, of M is expected. **Figure 3.92** illustrates that larger values of (χ_{R1} + χ_{R2}) of the β-diketonato ligand (R$_1$COCHCOR$_2$)$^-$ coordinated to the metal complexes lead to more positive oxidation potentials, E_{pa}, of M, for M = Rh or Ir. Again, (χ_{R1} + χ_{R2}) of the β-diketonato ligand (R$_1$COCHCOR$_2$)$^-$ coordinated to [M(β-diketonato)(cod)] gives a good indication of the electron density (nucleophilicity) on rhodium or iridium.
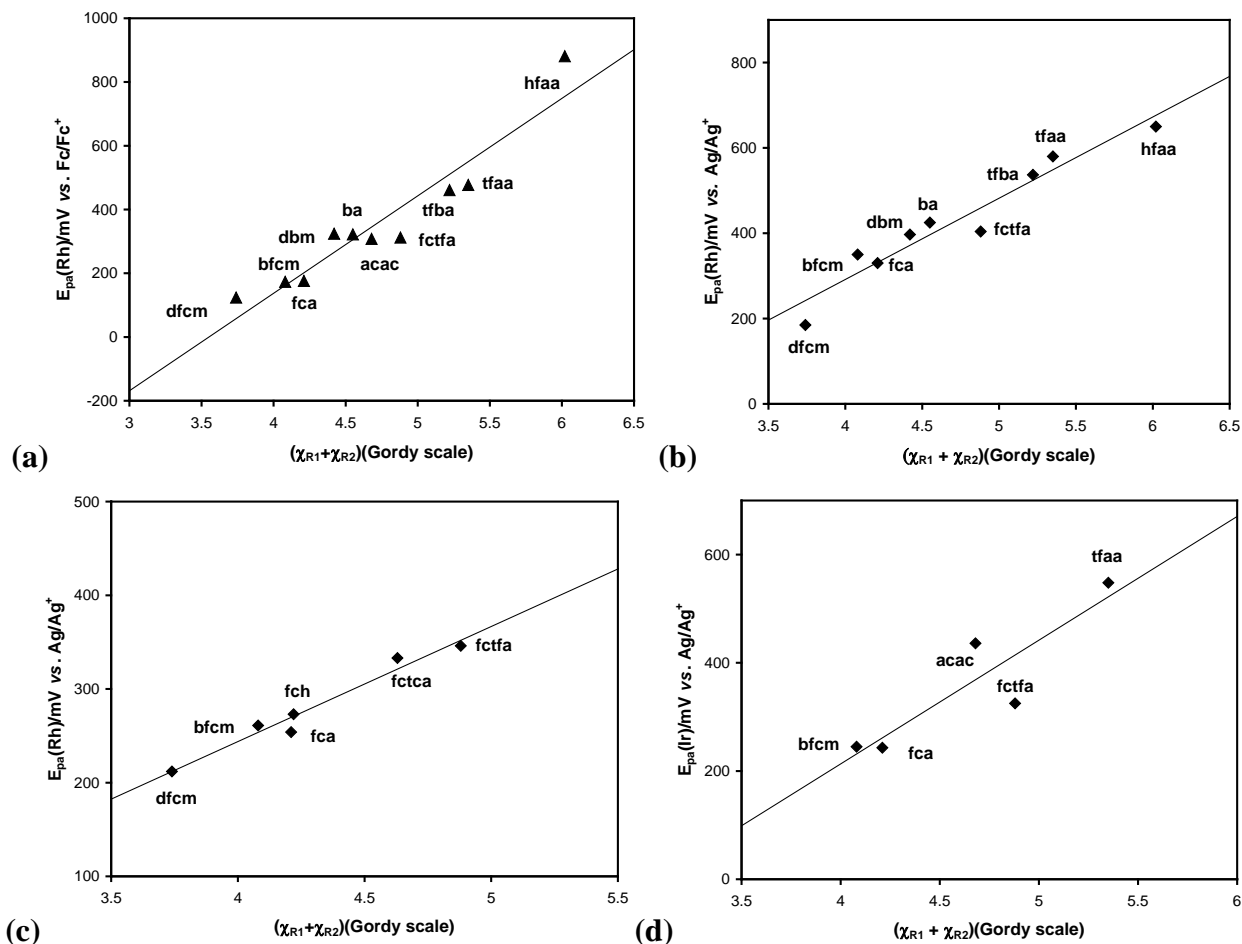
Figure 3.92: Relationship between the oxidation potential E_{pa} of Rh or Ir in
(a) [Rh(R$_1$COCHCOR$_2$)(POPh$_3$)$_2$]
(b) [Rh(R$_1$COCHCOR$_2$)(CO)(PPh$_3$)] (only E_{pa}(Rh) of second isomers of ferrocene-containing complexes),
(c) [Rh(R$_1$COCHCOR$_2$)(cod)] and
(d) [Ir(R$_1$COCHCOR$_2$)(cod)]
and the sum of the group electronegativities of R$_1$ and R$_2$ (χ_{R1} + χ_{R2}) of the β-diketonato ligand
(R$_1$COCHCOR$_2$)$^-$ coordinated to the metal complexes. The β-diketonato ligands are as indicated.

3.7.3 Group electronegativities and carbonyl stretching frequencies.

Increased electron density on a metal centre, results in lower CO infrared frequencies (chapter 2 paragraph 2.1.2). **Figure 3.93** illustrates, as was expected, that in complexes of the type

[Rh(R$_1$COCHCOR$_2$)(CO)(PPh$_3$)] the infrared CO stretching frequency ν_{CO} increases as R$_1$ and R$_2$ are replaced by more electron withdrawing groups, *i.e.* groups with a high group electronegativity. Since the sum of the group electronegativities of R$_1$ and R$_2$ of the β-diketonato ligand (R$_1$COCHCOR$_2$)$^-$ coordinated to [Rh(R$_1$COCHCOR$_2$)(CO)(PPh$_3$)], varies linearly with ν_{CO}, it also gives a good indication of the electron density (nucleophilicity) on rhodium.
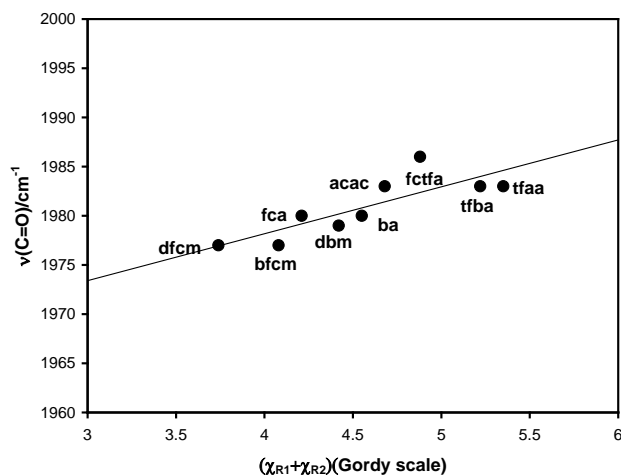
Figure 3.93: Relationship between the carbonyl stretching frequency ν(C=O) of [Rh(R$_1$COCHCOR$_2$)(CO)(PPh$_3$)] and the sum of the group electronegativities of R$_1$ and R$_2$ ($\chi_{R1} + \chi_{R2}$) of the β-diketonato ligand (R$_1$COCHCOR$_2$)$^-$ coordinated to [Rh(R$_1$COCHCOR$_2$)(CO)(PPh$_3$)]. The β-diketonato ligands are as indicated.

3.7.4   Group electronegativities and pK$_a$ of the β-diketones.

Figure 3.94 presents the relationship between the pK$_a$ of a β-diketone [R$_1$COCH$_2$COR$_2$] and sum of the group electronegativities ($\chi_{R1} + \chi_{R2}$) of the groups R$_1$ and R$_2$ on the β-diketone. Groups with a high group electronegativity (highly electron withdrawing) on the β-diketone backbone making it more acidic with a resulting decrease in the pK$_a$ of the β-diketone. Hhfaa with two CF$_3$ groups (χ_{CF3} = 3.01), is the most acidic β-diketone with pK$_a$ of 4.71. In contrast, on the other end of the scale, the pK$_a$ of Hdfcm with two Fc groups (χ_{Fc} = 1.87), is 13.1. The effect of the electronegativity of each group is additive (although not linear) in determining the acidity (or basicity) of the β-diketone.

256
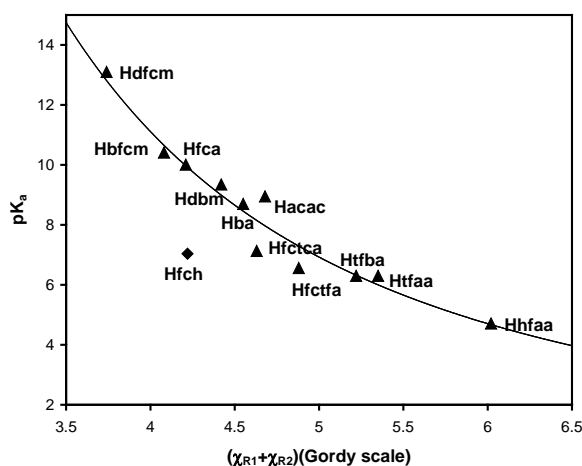
Figure 3.94: Relationship between the pK_a and the sum of the group electronegativities ($\chi_{R1} + \chi_{R2}$) of the groups R_1 and R_2 on the β-diketone [$R_1COCH_2COR_2$]. The β-diketones are as indicated. The keto aldehyde **Hfch** does not fit the obtained trend.

3.8   Structure determinations.

3.8.1   The crystal structure data of Hfctfa (3-ferrocenoyl-1,1,1-trifluoro-2-hydroxyprop-2-ene).

A perspective view of Hfctfa showing atom labelling is presented in **Figure 3.95**. Crystal data of Hfctfa are summarized in **Table 3.60**, bond lengths and angles can be found in **Table 3.61** and **Table 3.62** respectively. The locations of H10 and H11 were estimated from a difference Fourier synthesis, see **Figure 3.96** page 260.
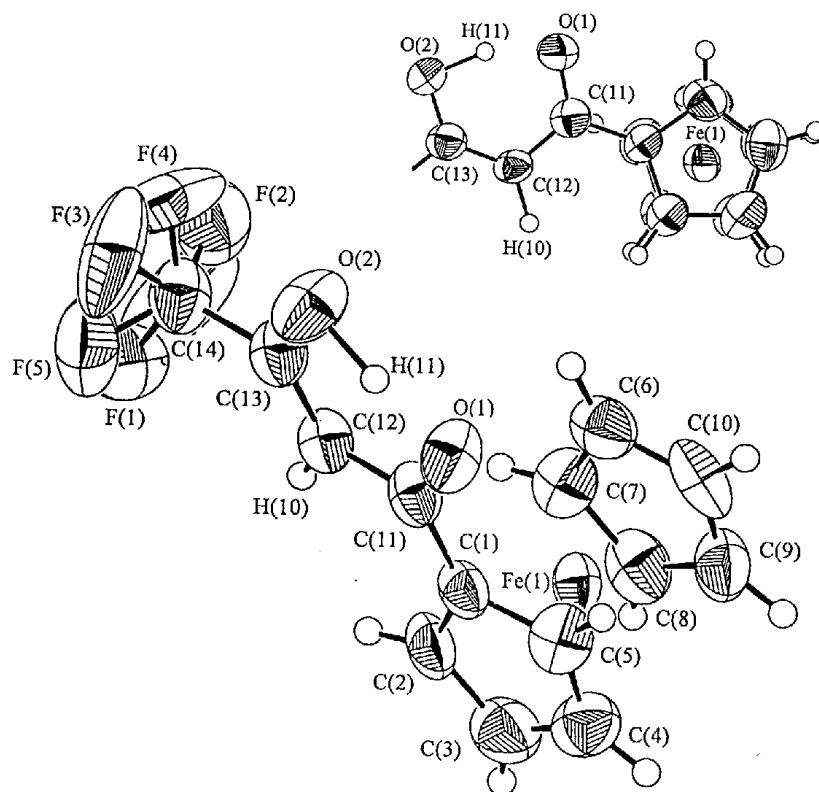
Figure 3.95: A perspective view of FcTFA showing atom labelling. The view from above down the C_5 ferrocenyl axis (top right) highlights the eclipsed conformation of the ferrocenyl group and the assymetric enolisation of the molecule.

In contrast to what was found in [Rh(fctfa)(CO)(PPh$_3$)], the trifluoromethyl group in free Hfctfa is disordered. The bond length C12-C13 [1.345(6) Å] is notably shorter than that of C11-C12 [1.432(6) Å], indicating that Hfctfa, like Hfca[5] and Hbfcm[55], enolised asymmetrically in a direction away from the ferrocenyl group. C11-C12-C13 [120.0(4)°] is within experimental error the theoretical value of 120°. as expected for sp^2 hybridization. The O1-O2 distance of 2.549(6) Å provides further support for the enolic structure of Hfctfa. β-Diketones in the keto form have O-O distances of *ca.* 3.05Å[85] (chapter 2 paragraph 2.5.1). From the difference map, H11 is shown to be approximately 0.33 Å further away from O1 than from O2 with H11-O2 *ca.* 1.15 Å. The cyclopentadienyl rings of the ferrocenyl group deviated only 2.17(1)° (**Figure 3.95**) from an eclipsed conformation although the energy barrier to cyclopentadienyl rotation[86] in ferrocene (which includes conversion from the eclipsed to the staggered conformation) is very small (4 $\pm$ 1 kJ mol^{-1}).

---

[85] Ferguson, G., Glidewell, C. and Zakaria, C.M., *Acta Cryst.*, **C50**, 1673 (1994).

[86] Haaland, A. and Nilsson, J., *J. Chem. Soc. Chem. Commun.*, **88** (1968).

Table 3.60: Crystal data and structure refinement for Hfctfa.

Empirical formula	$C_{14} H_{11} F_3 Fe O_2$	Cu Kα wavelength; μ	1.54178 Å; 97.12 cm^{-1}
Formula weight	324.08	F(000)	656
Temperature	296(1) K	Scan type; $2\theta_{max}$	ω-2θ ; 130°
Crystal size mm^3	0.40x0.14x0.10	Scan width	(1.37 + 0.35 tanθ)^o
Crystal system	Monoclinic	Scan rate (in ω)	16.0^o/min (up to 6 scans)
Space group	P2$_1$/n(No. 14)	Take-off Angle	6°
Unit cell dimensions	a = 5.991(1) Å	Refl. Collected	2275
	b = 10.235(2) Å	Unique refl.	2056 [R(int) = 0.044]
	c = 21.076(1) Å	Refinement method	Full-matrix least squares on F
	β = 90.84(1) ^{o}	Data[$I>3\sigma(I)$]; parameters	949 ; 208
Volume	1292.3(3) Å^3	Goodness-of-fit on F	1.36
Density (calculated)	1.666 g/cm^3	Final R indices [$I>3\sigma(I)$] [a]	R = 0.029, R$_w$ = 0.030
Z	4	Largest diff. peak / hole	0.20/-0.19 e Å^{-3}

(a) $R = \sum \left\| F_0 \right| - \left| F_c \right\| / \sum \left| F_0 \right| = 0.029$ and $R_w = \left[\sum w \left(\left| F_0 \right| - \left| F_c \right| \right)^2 / \sum w F_0^2 \right]^{0.5} = 0.030$.

Table 3.61: **Bond lengths [Å] for Hfctfa. The standard deviation of the last decimal is given in brackets.**

Fe(1)-C(1)	2.020(4)	Fe(1)-C(2)	2.019(4)	C(3)-C(4)	1.398(7)	O(1)-H(11)	1.48
Fe(1)-C(3)	2.048(5)	Fe(1)-C(4)	2.049(5)	C(6)-C(7)	1.395(7)	C(2)-H(1)	0.95
Fe(1)-C(5)	2.048(5)	Fe(1)-C(6)	2.041(5)	C(7)-C(8)	1.395(7)	C(4)-H(3)	0.95
Fe(1)-C(7)	2.033(5)	Fe(1)-C(8)	2.037(4)	C(9)-C(10)	1.395(7)	C(6)-H(5)	0.95
Fe(1)-C(9)	2.032(5)	Fe(1)-C(10)	2.028(5)	C(12)-C(13)	1.345(6)	C(8)-H(7)	0.95
F(1)-C(14)	1.306(7)	F(2)-C(14)	1.336(8)	C(4)-C(5)	1.405(7)	C(10)-H(9)	0.95
F(3)-C(14)	1.267(7)	F(4)-C(14)	1.27(1)	C(6)-C(10)	1.418(7)	O(2)-H(11)	1.15
F(5)-C(14)	1.35(1)	F(6)-C(14)	1.177(8)	C(8)-C(9)	1.399(7)	C(3)-H(2)	0.95
O(1)-C(11)	1.277(5)	O(2)-C(13)	1.297(5)	C(11)-C(12)	1.432(6)	C(5)-H(4)	0.95
C(1)-C(2)	1.420(6)	C(1)-C(5)	1.436(6)	C(13)-C(14)	1.515(7)	C(7)-H(6)	0.95
C(1)-C(11)	1.448(6)	C(2)-C(3)	1.410(7)	C(12)-H(10)	1.00	C(9)-H(8)	0.95

Table 3.62: Bond angles [deg] for Hfctfa. The standard deviation of the last decimal is given in brackets.

C(7)-Fe(1)-C(9)	67.9(2)	C(1)-C(5)-C(4)	107.6(4)	Fe(1)-C(6)-C(7)	69.7(3)
C(8)-Fe(1)-C(9)	40.2(2)	Fe(1)-C(6)-C(10)	69.1(3)	C(7)-C(6)-C(10)	107.5(4)
C(9)-Fe(1)-C(10)	40.2(2)	Fe(1)-C(7)-C(6)	70.3(3)	Fe(1)-C(7)-C(8)	70.1(3)
Fe(1)-C(1)-C(5)	70.4(2)	C(6)-C(7)-C(8)	108.1(4)	Fe(1)-C(8)-C(7)	69.8(3)
C(2)-C(1)-C(5)	107.3(4)	Fe(1)-C(8)-C(9)	69.7(3)	C(7)-C(8)-C(9)	108.7(5)
C(5)-C(1)-C(11)	125.3(4)	Fe(1)-C(9)-C(8)	70.1(3)	Fe(1)-C(9)-C(10)	69.7(3)
Fe(1)-C(2)-C(3)	70.9(3)	C(8)-C(9)-C(10)	107.6(5)	Fe(1)-C(10)-C(6)	70.1(3)
Fe(1)-C(3)-C(2)	68.6(3)	Fe(1)-C(10)-C(9)	70.1(3)	C(6)-C(10)-C(9)	108.1(4)
C(2)-C(3)-C(4)	108.8(5)	O(1)-C(11)-C(1)	119.0(4)	C(1)-C(11)-C(12)	120.0(4)
Fe(1)-C(4)-C(5)	69.9(3)	C(1)-C(11)-C(12)	121.0(4)	C(11)-C(12)-C(13)	120.0(4)
Fe(1)-C(5)-C(1)	68.3(2)	O(2)-C(13)-C(12)	126.3(4)	O(2)-C(13)-C(14)	112.3(4)
C(7)-Fe(1)-C(10)	67.9(2)	C(12)-C(13)-C(14)	121.4(4)	F(1)-C(14)-C(13)	110.6(5)
C(8)-Fe(1)-C(10)	67.4(2)	F(2)-C(14)-C(13)	112.4(5)	F(3)-C(14)-C(13)	114.8(5)
Fe(1)-C(1)-C(2)	69.4(2)	F(4)-C(14)-C(13)	112.4(6)	F(5)-C(14)-C(13)	108.0(6)
Fe(1)-C(1)-C(11)	122.0(3)	F(6)-C(14)-C(13)	115.5(6)	Fe(1)-C(4)-C(3)	70.0(3)

C(2)-C(1)-C(11)	107.8(4)	C(1)-C(2)-C(3)	107.8(4)	C(3)-C(4)-C(5)	108.6(5)
Fe(1)-C(2)-C(1)	69.4(2)	Fe(1)-C(3)-C(4)	70.1(3)	Fe(1)-C(5)-C(4)	70.0(3)
C(1)-Fe(1)-C(2)	41.2(2)	C(1)-Fe(1)-C(3)	68.4(2)	C(4)-Fe(1)-C(9)	107.0(2)
C(1)-Fe(1)-C(4)	68.6(2)	C(1)-Fe(1)-C(5)	41.3(2)	C(5)-Fe(1)-C(6)	124.7(2)
C(1)-Fe(1)-C(6)	109.4(2)	C(1)-Fe(1)-C(7)	122.9(2)	C(5)-Fe(1)-C(8)	159.0(2)
C(1)-Fe(1)-C(8)	157.6(2)	C(1)-Fe(1)-C(9)	161.3(2)	C(5)-Fe(1)-C(10)	109.2(2)
C(1)-Fe(1)-C(10)	125.6(2)	C(2)-Fe(1)-C(3)	40.5(2)	C(6)-Fe(1)-C(8)	67.2(2)
C(2)-Fe(1)-C(4)	68.2(2)	C(2)-Fe(1)-C(5)	68.9(2)	C(6)-Fe(1)-C(10)	40.8(2)
C(2)-Fe(1)-C(6)	124.7(2)	C(2)-Fe(1)-C(7)	107.4(2)	C(4)-Fe(1)-C(10)	122.5(2)
C(2)-Fe(1)-C(8)	121.0(2)	C(2)-Fe(1)-C(9)	155.8(2)	C(5)-Fe(1)-C(7)	159.9(2)
C(2)-Fe(1)-C(10)	162.2(2)	C(3)-Fe(1)-C(4)	39.9(2)	C(5)-Fe(1)-C(9)	123.7(2)
C(3)-Fe(1)-C(5)	67.5(2)	C(3)-Fe(1)-C(6)	160.2(2)	C(6)-Fe(1)-C(7)	40.1(2)
C(3)-Fe(1)-C(7)	123.4(2)	C(3)-Fe(1)-C(8)	106.9(2)	C(6)-Fe(1)-C(9)	68.0(2)
C(3)-Fe(1)-C(9)	120.7(2)	C(3)-Fe(1)-C(10)	156.5(2)	C(7)-Fe(1)-C(8)	40.1(2)
C(4)-Fe(1)-C(5)	40.1(2)	C(4)-Fe(1)-C(6)	159.3(2)	-	-
C(4)-Fe(1)-C(7)	158.6(2)	C(4)-Fe(1)-C(8)	122.8(2)	-	-
C(11)-C(1)-H(11)	99.8	O(1)-H(11)-O(2)	150.2	C(9)-C(8)-H(7)	125.6
Fe(1)-C(2)-H(1)	125.7	C(13)-O(2)-H(11)	98.0	C(8)-C(9)-H(8)	126.1
C(3)-C(2)-H(1)	126.6	C(1)-C(2)-H(1)	125.6	Fe(1)-C(10)-H(9)	125.8
C(2)-C(3)-H(2)	125.3	Fe(1)-C(3)-H(2)	126.6	C(9)-C(10)-H(9)	126.0
Fe(1)-C(4)-H(3)	126.9	C(4)-C(3)-H(2)	125.9	C(13)-C(12)-H(10)	124.1
C(5)-C(4)-H(3)	126.3	C(3)-C(4)-H(3)	125.0	C(7)-C(8)-H(7)	125.7
C(1)-C(5)-H(4)	126.2	Fe(1)-C(5)-H(4)	126.2	Fe(1)-C(9)-H(8)	124.4
Fe(1)-C(6)-H(5)	126.6	C(4)-C(5)-H(4)	126.2	C(10)-C(9)-H(8)	126.3
C(10)-C(6)-H(5)	126.5	C(7)-C(6)-H(5)	126.0	C(6)-C(10)-H(9)	125.9
C(6)-C(7)-H(6)	125.8	Fe(1)-C(7)-H(6)	125.1	C(11)-C(12)-H(10)	115.8
Fe(1)-C(8)-H(7)	126.2	C(8)-C(7)-H(6)	126.1	-	-

It was established spectroscopically that uncoordinated Hfctfa enolizes, in solution, in a direction away from the ferrocenyl group on the grounds of the apparent absence of more than one set of signals for the ferrocenyl substituent, as well as the two observed signals for the methyl side group.[35] The structural details that may be used to explain the spectroscopically observed direction of asymmetrical enolization, are however, centred on the longer bond length C13-C14 [1.515(7) Å] as compared to C11-C1 [1.448(6) Å] and the dihedral angle of 7.84° between the pseudo-aromatic system forming plane 1 defined by atoms O1-C11-C12-C13-O2 (**Figure 3.95**) and the planar cyclopentadienyl ring of the aromatic ferrocenyl moiety bound to it. These two structural details emphazise effective conjugation of the ferrocenyl group into the pseudo-aromatic system of plane 1. This conjugation can take place in at least two ways, as demonstrated with the formation of canonical forms **III** and **IV** of the two theoretically possible enol forms **I** and **II** of Hfctfa (**Scheme 3.14**).
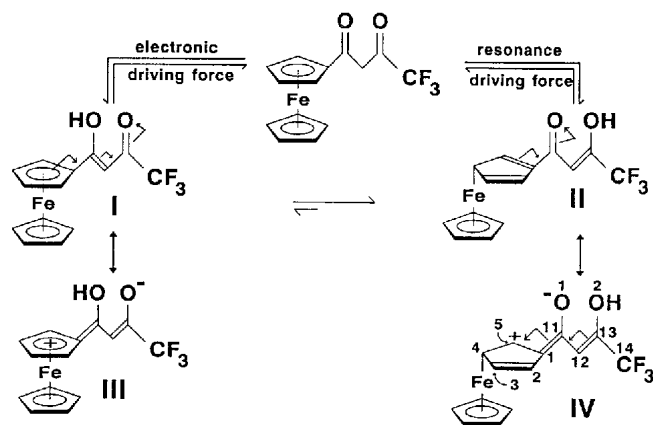
Scheme 3.14: Electronic considerations in terms of electronegativity, χ, favour I as the enol form of FcTFA. However, structure II was shown by crystallography and NMR to be dominant. A dihedral angle of 7.84° between the aromatic ferrocenyl group and the pseudo-aromatic β-diketone core implies that energy-lowering canonical forms such as IV make a noticeable contribution to the overall existence of Hfctfa. For the sake of clarity the ferrocenyl group in II and IV is shown in just one canonical form but in both cases the iron atom can be bound to any of the five cyclopentadienyl carbon atoms as indicated in I. Likewise, the positive charge of IV is also not confined to the single position shown, but rather oscillates between C(2) and C(5) (it cannot be on C(1); atom numbers are indicated next to individual atoms) to give rise to four different canonical forms as indicated in III. $\chi_{trifluoromethyl} = 3.01$, $\chi_{ferrocenyl} = 1.87$.

Either the enol isomer **I** can convert to one of its canonical forms, **III,** or isomer **II** will convert to the canonical form **IV**. Both these conversions will lower the energy of the system. To decide which of these energy-lowering processes is favoured, the bond lengths O1-C11 [1.277(5) Å] and O2-C13 [1.297(5) Å] plays a pivitol role. Typical C=O bond lengths are 1.23(1) Å[87] (in the case of β-diketones, see for example reference 85), whereas β-diketone C-O (enol) bond lengths are in the region of 1.3 – 1.4 Å.[5] For Hfctfa, C13-O2 [1.297(5) Å] (enol) is perfectly normal, but C11-O2 [1.277(5) Å] does not remotely resemble typical C=O bond lengths. In fact, this bond is so long that it approaches typical single, enol, C-O, bond lengths, a situation that can only arise if the canonical form **IV** makes a large contribution to the overall structure of Hfctfa. The conclusion is therefore as before,[35] that despite the large difference in group electronegativities of the ferrocenyl and the trifluoromethyl groups, resonance driving forces always will carry priority over electronic driving forces to determine which enol form of a β-diketone possessing aromatic side groups is favoured. Zwitterionic canonical structures resembling **IV** are key intermediates in the enolization process of ferrocenyl- and phenyl-containing β-diketones. It should be noted that, although the canonical forms indicated in **Scheme 3.14** explain the ^{1}H NMR[35] and crystallographically observed dominance of isomer **II** over **I**, they do by no means imply that other canonical forms and relationships do not also exist.

---

[87] Weast, R.C., *Handbook of Chemistry and Physics,* 63th edition, The Chemical Rubber Co., Ohio, p. F180-181.
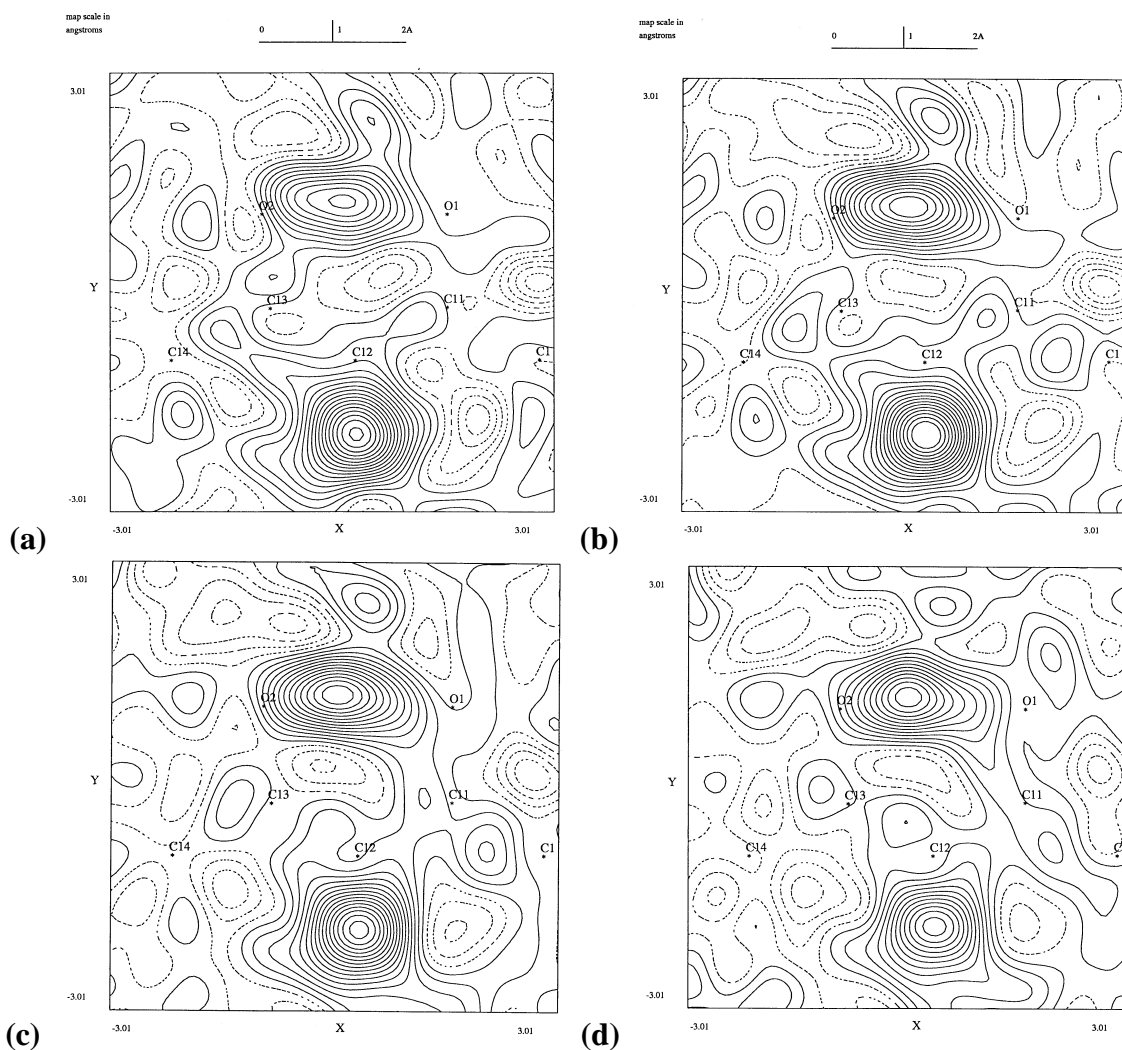
Figure 3.96: Difference Fourier synthesis in estimating the positions of H(10) and H(11). Plane defined by the three atoms O(1), O(2) and C(12), contour interval 0.03 e/Å³, origin translation along x = 1.00 Å, origin translation along y = 1.00 Å, map rotation = 0°. Perpendicular offset (a) 0.20, (b) 0.00, (c) –0.20 and (d) –0.40.

In assigning typical bond lengths for β-diketone enol C=O double bonds, it is therefore important to distinguish between β-diketones containing an aromatic group (*e.g.* phenyl or ferrocenyl) and β-diketones void of aromatic groups (*e.g.* Hacac). Considering the crystal data of the various β-diketones presented in chapter 2 paragraph 2.5.1, table 2.40 (a), page 110, as well as the data of Hfctfa, it is now possible to assign a typical range of bond lengths for β-diketones containing an aromatic group and another range for β-diketones without aromatic substituents as in **Table 3.63**.

Table 3.63: The *range of typical* bond lengths in enolized and non-enolized β-diketones. The β-diketones used to obtain the ranges of bond lengths are specified in the footnote with structures as displayed in figure 2.34, page 111.

β-diketone	C=O bond length /Å	C-O (enol) bond length /Å	C=C bond length between carbonyl groups /Å	C-C bond length between carbonyl groups /Å	O….O bond length /Å
keto	1.206 – 1.221	-	-	1.507 – 1.537	*ca.* 3.05
asymmetrical enol containing an aromatic group	1.269 – 1.287	1.297 – 1.316	1.343 – 1.391	1.406 – 1.432	2.46-2.55
asymmetrical enol without an aromatic group	1.24	1.33	1.33 – 1.34	1.41 – 1.42	2.5
symmetrical enol	1.28 – 1.31		1.38 - 1.41		*ca.* 2.5

Keto: H3fco[88], H2b3fco[89], H2edbm[90], H4fcmβ.[91] **Symmetrical enol:** Hdbm,[92] Hdbrbm,[93] Hba.[94]

Asymmetrical enol containing an aromatic group: Hdtm,[95] Hdbm,[96] Httfa,[97] Hten,[98] Hfca[99] and Hbfcm.[55]

Asymmetrical enol without an aromatic group: Hhfaa,[100] Hacac.[101]

[88] Gyepes, E., Glowiak, T., Toma, S. and Soldanova, J., *J. Organomet. Chem.,* **276**, 209 (1984).

[89] Gyepes, E., Glowiak, T. and Toma, S., *J. Organomet. Chem.,* **316**, 163 (1986).

[90] Mullica, D.F., Karban, J.W. and Grossie, D.A., *Acta Cryst.*, **C43**, 601 (1987).

[91] Ferguson, G., Glidewell, C. and Zakaria, C.M., *Acta Cryst.*, **C50**, 1673 (1994).

[92] Etter, M.C., Jahn, D.A. and Urbañczyk-Lipkowska, Z., *Acta Cryst.*, **C43**, 260 (1987).

[93] Williams, D.E., Dumke, W.L. and Rundle, R.E., *Acta Cryst.*, **15**, 627 (1962).

[94] Jones, R.D.G., *Acta Cryst.*, **B32**, 2133 (1976).

[95] Baxter, L.A.M., Blake, A.J., Heath, G.A. and Stephenson, T.A., *Acta Cryst.*, **C46**, 508 (1990).

[96] i) Jones, R.D.G., *Acta Cryst.*, **B32**, 1807 (1976), ii) Williams, D.E., *Acta Cryst.*, **21**, 340 (1966), iii) Hollander, F.J., Templeton, D.H. and Zalkin, A., *Acta Cryst.*, **B29**, 1552 (1973).

[97] Jones, R.D.G., *Acta Cryst.*, **B32**, 1224 (1976).

[98] Kato, K., *Acta Cryst.*, **B27**, 2028 (1971).

[99] Bell, W., Crayston, J.A., Glidewell, C., Mazid, M.A. and Hursthouse, B., *J. Organomet. Chem.,* **434**, 115 (1992).

[100] Wang, S., Pang, Z., Smith, K.D.L., Hua, Y., Deslippe, C. and Wanger, M.J., *Inorg. Chem.*, **34**, 908 (1995).

[101] Camerman, A., Mastropaolo, D. and Camerman, N., *J. Am. Chem. Soc.,* **105**, 1584 (1983).

3.8.2 *The crystal structure data of [Rh(fctfc)(CO)₂].*

A perspective view of [Rh(fctfa)(CO)$_2$] showing atom labelling is presented in **Figure 3.97**. Crystal data of Hfctfa are summarized in **Table 3.64**, selected bond lengths and angles can be found in **Table 3.65** and **Table 3.66** respectively. The molecular packing of the [Rh(fctfa)(CO)$_2$] crystal is illustrated in **Figure 3.98** page 266. As was found in Hfctfa and [Rh(fctfa)(CO)(PPh$_3$)(CH$_3$)(I)], the trifluoromethyl group is disordered. Both a rotational disorder and a translational displacement disorder were observed.
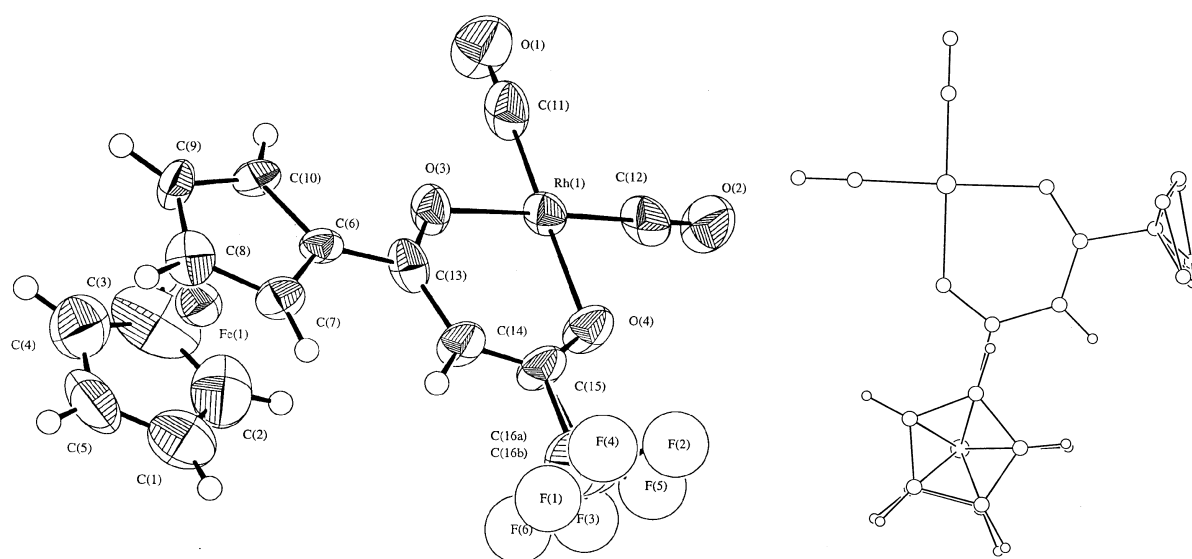
Figure 3.97: A perspective view of [Rh(fctfa)(CO)₂] showing atom labelling. The view right highlights the disorderded trifluoromethyl group and the square planar geometry around the Rh nucleus.

The rhodium atom has a square planar coordination with the Rh-C(11) and Rh-C(12) distances 1.83(2) Å and 1.84(1) Å. The angles C(11)-Rh-C(12) and O(3)-Rh-O(4) are 89.1(6)° and 90.2(3)° respectively. The Rh-O and Rh-C bond lengths are within the experimental error, the same as in [Rh(acac)(CO)$_2$][102] and [Rh(tfba)(CO)$_2$][103] (**Table 3.68** page 266), except for the Rh-O(3) (**Figure 3.97**) distance, 2.054(8) Å. Bond Rh-O(3) is 0.032 Å longer than Rh-O(4) because of the stronger electron donating property of the ferrocenyl group (χ_{Fc} = 1.87), compared to that of the CF$_3$ group (χ_{CF3} = 3.01) on the β-diketonato ligand fctfa. One would, therefore,

---

[102] Hug, F. and Skapski, A.C., *J. Cryst. Mol. Struct.*, **4**, 411 (1974).

also expect an electronic influence of the CF_3 group on the Rh-C(11) [1.83(2) Å] bond, *trans* to O(4) nearest to CF_3, and of the ferrocenyl group on the Rh-C(12) [1.84(1) Å] bond. The Rh-C(11) bond length 1.84(1) Å and the Rh-C(12) bond length 1.83(2) Å, were, however, too inaccurate to interpret small differences in bond lengths. The error in the Rh-C bonds is 0.02 Å while in the more accurate Rh-O bonds it was 0.008 Å. These inaccurate Rh-C bond lengths are most probably due to the large thermal vibrations of the small CO ligands relative to the more rigid and large β-diketonato ligand fctfa. In the latter case the electronic effect of the substituents on the β-diketonato ligand was observed in the Rh-O(3) and Rh-O(4) bond lengths. On the grounds of the similar, inaccurate, Rh-C bond lengths, it is therefore not possible to forecast which carbonyl group will be replaced by PPh_3 in the substitution reaction

$$[Rh(\beta\text{-diketonato})(CO)_2] + PPh_3 \rightarrow [Rh(\beta\text{-diketonato})(CO)(PPh_3)] + CO$$
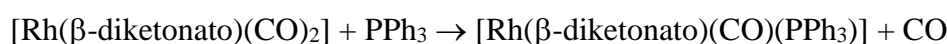
Table 3.64: Crystal data and structure refinement for [Rh(fctfa)(CO)₂].

Empirical formula	$C_{16}H_{10}F_3FeO_4Rh$	Mo Kα wavelength; μ	0.71069 Å; 18.79 cm⁻¹
Formula weight	482.00	F(000)	1888.00
Temperature	296(1) K	Scan type; $2\theta_{max}$	ω-2θ ; 60°
Crystal size mm³	0.10x0.18x0.22	Scan width	(0.63 + 0.35 tanθ)°
Crystal system	Monoclinic	Scan rate (in ω)	16.0°/min (up to 6 scans)
Space group	C2/c(#15)	Take-off Angle	6°
Unit cell dimensions	a = 13.266(3) Å	Refl. Collected	5291
	b = 19.553(3) Å	Unique refl.	5091 [R(int) = 0.084]
	c = 13.278(3) Å	Refinement method	Full-matrix least squares on F
	β = 100.92(2) °	Data[$I>3\sigma(I)$]; parameters	1411 ; 204
Volume	3382(1) Å³	Goodness-of-fit on F	1.86
Density (calculated)	1.893 g/cm³	Final R indices [$I>3\sigma(I)$] [a]	R = 0.0549, R_w = 0.0622
Z	8	Largest diff. peak / hole	1.01/-0.95 e Å⁻³

(a) $R = \sum \left\| F_0 \right| - \left| F_c \right\| / \sum \left| F_0 \right| = 0.0549$ and $R_w = \left[\sum w \left(\left| F_0 \right| - \left| F_c \right| \right)^2 / \sum w F_0^2 \right]^{0.5} = 0.0622$.

The bond angles in the Rh(I) coordination polyhedron, 89.1(6)°, 90.2(3)°, 89.8(5)° and 90.8(5)°, are very close to the ideal 90° geometry as expected for dsp^2 hybridization. In contrast, much larger deviations from the expected 120° were found in the sp^2 hibridized C atoms of the β-diketonato skeleton. The C(13)-C(14)-C(15) and O(3)-C(13)-C(14) bond angles, both 124(1)°, are distorted by 4° and bond angle O(4)-C(15)-C(14) [131(1)°] deviates by 11° from the expected

103 Leipoldt, J.G, Bok, L.D.C., Basson, S.S., van Vollenhoven, J.S. and Gerber, T.I.A., *Inorg. Chim. Acta.,* **25**, L63 (1977).

120° for sp^2 hibridized C atoms. The C(13)-O(3) and C(15)-O(4) bonds in the β-diketonato skeleton of the [Rh(β-diketonato)(CO)$_2$] complex and the C(11)-O(1) and C(13)-O(2) bonds in the free β-diketone, Hfctfa, were, however, very similar: 1.26(1) Å *vs.* 1.277(5) Å and 1.28(1) Å *vs.* 1.297(5) Å, respectively.

Table 3.65: Bond lengths [Å] for [Rh(fctfa)(CO)$_2$]. The standard deviation of the last decimal is given in brackets.

Rh(1)-O(3)	2.054(8)	C(6)-C(13)	1.47(2)	C(6)-C(7)	1.43(2)	C(10)-H(9)	0.95
Rh(1)-C(11)	1.83(2)	C(14)-C(15)	1.36(2)	C(8)-C(9)	1.43(2)	C(14)-H(10)	0.95
Rh(1)-O(4)	2.022(8)	C(13)-C(14)	1.41(2)	C(9)-C(10)	1.39(2)	C(1)-H(1)	0.95
Rh(1)-C(12)	1.84(1)	C(1)-C(5)	1.40(2)	C(6)-C(10)	1.40(1)	C(2)-H(2)	0.95
O(1)-C(11)	1.14(1)	C(2)-C(3)	1.42(3)	C(7)-C(8)	1.43(2)	C(3)-H(3)	0.95
O(3)-C(13)	1.26(1)	C(3)-C(4)	1.39(3)	C(7)-H(6)	0.95	C(4)-H(4)	0.95
O(2)-C(12)	1.12(1)	C(4)-C(5)	1.39(2)	C(8)-H(7)	0.95	C(5)-H(5)	0.95
O(4)-C(15)	1.28(1)	C(1)-C(2)	1.43(3)	C(9)-H(8)	0.95	-	-

Table 3.66: Bond angles [deg] for [Rh(fctfa)(CO)$_2$]. The standard deviation of the last decimal is given in brackets.

O(3)-Rh(1)-O(4)	90.2(3)	O(3)-Rh(1)-C(11)	90.8(5)	C(8)-C(9)-C(10)	107(1)
O(3)-Rh(l)-C(12)	177.4(5)	O(4)-Rh(1)-C(11)	178.3(5)	C(10)-C(9)-H(8)	126.3
O(4)-Rh(1)-C(12)	89.8(5)	C(11)-Rh(1)-C(12)	89.1(6)	C(6)-C(10)-H(9)	125.0
Rh(1)-O(3)-C(13)	127.3(9)	Rh(1)-C(4)-C(15)	122.7(8)	Rh(1)-C(11)-O(1)	179(1)
C(2)-O(1)-C(5)	107(2)	C(2)-C(1)-H(1)	126.6	C(3)-C(13)-C(6)	115(1)
C(5)-C(1)-H(1)	126.7	C(1)-C(2)-C(3)	108(2)	C(6)-C(13)-C(14)	120(1)
C(1)-C(2)-H(2)	126.3	C(3)-C(2)-H(2)	126.0	C(13)-C(14)-H(10)	117.7
C(2)-C(3)-C(4)	107(2)	C(2)-C(3)-H(3)	126.5	O(4)-C(15)-C(14)	131(1)
C(4)-C(3)-H(3)	126.0	C(3)-C(4)-C(5)	109(2)	C(8)-C(9)-H(8)	126.4
C(3)-C(4)-H(4)	125.9	C(5)-C(4)-H(4)	125.5	C(6)-C(10)-C(9)	110(1)
C(1)-C(5)-C(4)	109(2)	C(1)-C(5)-H(5)	125.1	C(9)-C(10)-H(9)	124.9
C(4)-C(5)-H(5)	125.7	C(7)-C(6)-C(10)	107(1)	Rh(1)-C(12)-O(2)	178(1)
C(7)-C(6)-C(13)	127(1)	C(10)-C(6)-C(13)	125(1)	O(3)-C(13)-C(14)	124(1)
C(6)-C(7)-C(8)	107(1)	C(6)-C(7)-H(6)	126.4	C(13)-C(14)-C(15)	124(1)
C(8)-C(7)-H(6)	126.4	C(7)-C(8)-C(9)	108(1)	C(15)-C(14)-H(10)	117.9
C(7)-C(8)-H(7)	126.1	C(9)-C(8)-H(7)	125.9	-	-

The free β-diketonato ligand was obviously asymmetrically enolized in the direction away from the ferrocenyl group by virtue of the bond lengths C(11)-C(12), 1.432(6) Å, and C(12)-C(13), 1.345(6) Å. In contrast, bond lengths C(13)-C(14) = 1.41(2) Å and C(14)-C(15) = 1.36(2) Å in the pseudo aromatic core of [Rh(fctfa)(CO)$_2$], do not give a clear indication to asymmetric enolate Rh-coordination.

266

Table 3.67: Least squares planes for [Rh(fctfa)(CO)₂]. The standard deviation of the last decimal is given in brackets.

Plane number 1		Plane number 2		Plane number 3	
Atoms defining plane	Distance/Å	Atoms defining plane	Distance/Å	Atoms defining plane	Distance/Å
C(1)	0.02(2)	C(6)	0.01(1)	C(13)	0.0
C(2)	-0.00(2)	C(7)	-0.01(1)	C(14)	0.0
C(3)	-0.01(2)	C(8)	0.01(1)	C(15)	0.0
C(4)	0.03(2)	C(9)	-0.00(1)	-	-
C(5)	-0.03(2)	C(10)	-0.00(1)	-	-
Additional Atoms		**Additional Atoms**		**Additional Atoms**	
C(6)	3.344	C(1)	-3.265	C(6)	0.003
C(7)	3.275	C(2)	-3.340	C(7)	-0.019
C(8)	3.253	C(3)	-3.336	C(8)	0.123
C(9)	3.263	C(4)	-3.238	C(9)	0.276
C(10)	3.319	C(5)	-3.271	C(10)	0.198
-	-	C(13)	-0.118	-	-
-	-	C(14)	-0.301	-	-
-	-	C(15)	-0.428	-	-
Summary				**Dihedral angles between planes (°)**	
plane	mean deviation	χ^2		plane	1	1
1	0.0188	6.7		2	2.34	2.34
2	0.0073	2.3		3	7.18	172.41
3	0.0000	0.0		-	-	-

An obvious feature of the [Rh(fctfa)(CO)₂] complex was the inaccuracy of many bond lengths, *e.g.* C(14)-C(15) = 1.36(2) Å; C(11)-O(1) = 1.14(1) Å; Rh-C(11) = 1.83(2) Å and C(3)-C(4) = 1.39(3) Å. Errors in the free β-diketone ligand and in the [Rh(fctfa)(CO)(PPh₃)] complex are at least one order of magnitude smaller. The only two other crystallographically characterized [Rh(β-diketonato)(CO)₂] complexes, [Rh(acac)(CO)₂] and [Rh(tfba)(CO)₂], showed similar large errors, see **Table 3.68**. The conclusion is drawn that these large errors are an inherent property of all [Rh(β-diketonato)(CO)₂] complexes and probably explains why [Rh(β-diketonato)(CO)₂] crystal structures are virtually unavailable. In contrast an abundance of [Rh(β-diketonato)(CO)(PPh₃)] complexes have been characterized crystallography (chapter 2 paragraph 2.5.2 and 2.5.3). The exact cause for the observed large errors in the [Rh(β-diketonato)(CO)₂] complexes is not clearly understood, but probably may be traced at least partially to the lightness and minuteness of the CO ligand (M_r = 28) as compared to the rather heavy β-diketonato ligand (*e.g.* M_r(fctfa) = 323)

The Rh….Rh distance is 3.346(2) Å. This distance is incompatible with metal-metal bonding. A

stereoscopic view of the packing of [Rh(fctfa)(CO)$_2$] molecules is shown in **Figure 3.98**.

The C-C bond lengths of the cyclopentadienyl ring (mean 1.41 Å) is similar to the C-C bond lengths for an aromatic C-C bond, 1.395(3)Å.[87] The cyclopentadienyl rings are almost planar with a dihedral angle of 2.34° and for all practical purposes are in the eclipsed (D$_{5h}$ symmetry) arrangement, see **Table 3.67**, plane 1 and 2, and **Figure 3.97**. The dihedral angle between the pseudo-aromatic system forming plane 3, defined by atoms C13-C14-C15, and the planar cyclopentadienyl ring of the aromatic ferrocenyl moiety bound to it (plane 2), is 7.18°.
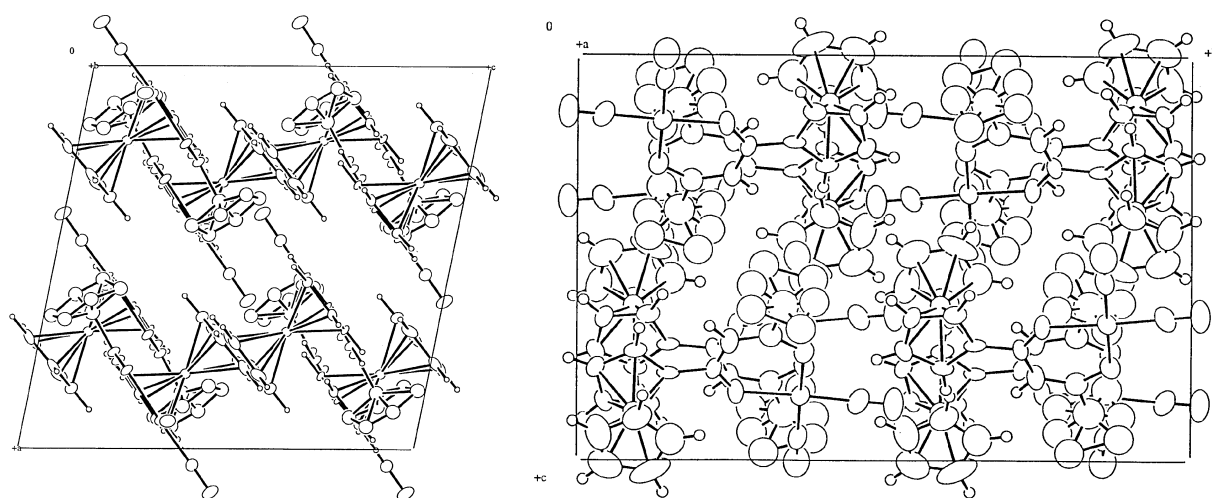
Figure 3.98: View of the packing of [Rh(fctfa)(CO)$_2$] molecules.

Table 3.68: Selected crystallographic data for [Rh(β-diketonato)(CO)$_2$] complexes containing β-diketonato ligands. O' is the β-diketonato oxygen atom nearest to the most electronegative group on the β-diketonato ligand. C' is the carbon atom of the carbonylgroup *trans* of O'. T = triclinic, M = monoclinic, and O = orthorhombic crystal system.

β-diketonato ligand	Bite angle (O-Rh-O') /degree	Angle (C-Rh-C') /degree	Rh-O distance /(Å)	Rh-O' distance /(Å)	Rh-C distance /(Å)	Rh-C' distance /(Å)	Crystal system	Space group
acac[104]	90	85	2.06	2.05	1.75	1.76	T	P$\bar{1}$
acac[102]	90.8(2)	88.9(3)	2.044(4)	2.040(4)	1.831(7)	1.831(7)	T	P$\bar{1}$
tfba[103]	89.8(7)	87.0(11)	2.024(16)	2.024(20)	1.788(26)	1.815(29)	O	Pbac
fctfa	90.2	89.1(6)	2.054(8)	2.022(8)	1.84(1)	1.83(2)	M	C2/c

[104] Bailey, N.A., Coates, E. and Robertson, G.B., *Chem. Commun.,* 1041 (1967).

3.8.3 The crystal structure data of [Rh(fctfa)(CO)(PPh₃)] (carbonyl(ferrocenoyltrifluoroacetonato-κO,κO)-triphenylphosphinerhodium(I)).

The numbering system of the atoms in the molecule is shown in **Figure 3.99**. The crystal data of [Rh(fctfa)(CO)(PPh₃)] are summarized in **Table 3.69**. The bond lengths and bond angles with their standard deviations are given in **Table 3.70** and **Table 3.71** respectively.
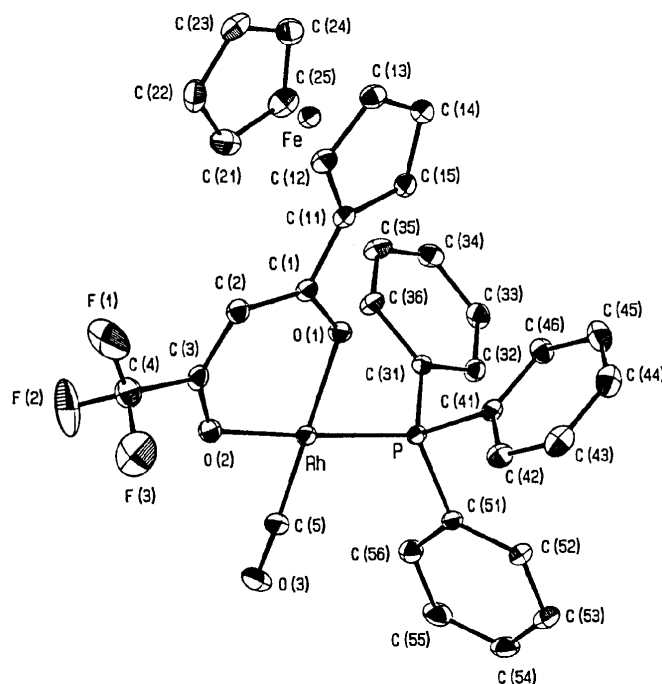
Figure 3.99: A perspective view of [Rh(fctfa)(CO)(PPh₃)]showing atom labelling.

The calculation of the best plane through the atoms Rh, O(2), O(3), P and C(5), plane 1 **Table 3.72**, page 272, showed that the coordination polyhedron is planar within experimental error. The various ligand-rhodium-ligand bond angles deviate significantly from the expected 90° for a dsp^2 hybridization: P-Rh-O(1) = 85.9(1)°, P-Rh-C(5) = 92.7(1)°, O(1)-Rh-O(2) = 88.6(1)° and C(5)-Rh-O(2) = 92.9(2)°, see **Table 3.71**.

The average C-C bond distance (1.382Å) in the planer phenyl rings is in agreement with the normal value (1.394 Å) for the aromatic C-C bond.[105] All the bond angles in the phenyl rings are 120° within the experimental error, *e.g.* C(32)-C(33)-C(34) = 119.8(4)°. The phosphorous atom

displays a distorted tetrahedral geometry and is surrounded by the rhodium atom and three carbon atoms of the phenyl rings bound to it. The bond angles around P differ at the most 12° from 109°28', the angle for a regular tetrahedron. The mean P-C distance is 1.824 Å, and compares well with that observed in [Rh(trop)(CO)(PPh₃)],[106] 1.826 Å, [Rh(bpha)(CO)(PPh₃)],[107] 1.831 Å, and [Rh(tta)(CO)(PPh₃)],[108] 1.827 Å. The Rh-P bond distance, 2.232(1) Å, is in the same order as found for [Rh(L,L'-BID)(CO)(PPh₃)] complexes with L = L' = O as described in chapter 2 paragraph 2.5.2.

Table 3.69: Crystal data and structure refinement for [Rh(fctfa)(CO)(PPh₃)].

Empirical formula	$C_{33}H_{25}F_3FeO_3RhP$	Z	2
Formula weight	716.28	Mo Kα wavelength; μ	0.71073 Å; 1.961 mm⁻¹
Temperature	298 K	F(000)	720
Crystal size mm³	0.25x0.15x0.30	Scan type; $2\theta_{max}$	ω-2θ ; 60°
Crystal system	Triclinic	Scan width	$(0.43 + 0.34 \tan\theta)°$
Space group	P$\bar{1}$	Scan rate (in ω)	5.49°/min
Unit cell dimensions	a = 10.439(2) Å	$2\theta_{min}$	6°
	b = 12.605(1) Å	Refl. Collected	8569
	c = 13.307(1) Å	Unique refl.	7733 [R(int) = 0.045]
	α = 107.77(1)	Refinement method	Full-matrix least squares on F
	β = 100.45(1) °	Data[$I>3\sigma(I)$]; parameters	6083 ; 380
	γ = 107.76(1)	Final R indices [$I>3\sigma(I)$] (a)	R = 0.045, R$_w$ = 0.044
Volume	1513.5(4) Å³	Largest diff. peak / hole	0.66/-0.41 e Å⁻³
Density (calculated)	1.52 g/cm³	-	-

The Rh-C(5)-O(3) chain is approximately linear, 178.1(4)°, with the C(5)-O(3) bond distance 1.147(5) Å, which compares well with that found in [Rh(acac)(CO)(PPh₃)],[109] 1.153(11) Å, [Rh(trop)(CO)(PPh₃)],[106] 1.151(15) Å, [Rh(bzaa)(CO)(PPh₃)],[110] 1.142(4) Å, and [Rh(tta)(CO)(PPh₃)],[108] 1.153(16) Å. The Rh-C(5) bond length of 1.801(5) Å, could be determined more accurately than the Rh-C bond lengths in [Rh(fctfa)(CO)₂], 1.83(2) Å and

[105] Sutin, L.E., *Tables of Interatomic Distances and configuration in Molecules and Ions, Supplement 1956 – 1959,* The Chemical Society, London, p. S16s.

[106] Leipoldt, J.G., Bok, L.D.C., Basson, S.S. and Meyer, H., *Inorg. Chim. Acta,* **42**, 105 (1980).

[107] Leipoldt, J.G. and Grobler, E.C., *Inorg. Chim. Acta,* **60** 141 (1982).

[108] Leipoldt, J.G., Bok, L.D.C., van Vollenhoven, J.S. and Pieterse, A.I., *J. Inorg. Nucl. Chem.,* **40**, 61 (1978).

[109] Leipoldt, J.G., Basson, S.S., Bok, L.D.C. and Gerber, T.I.A., *Inorg. Chim. Acta.,* **26**, L35 (1978).

[110] Roodt, A., Leipoldt J.G., Swarts, J.C. and Steyn, G.J.J., *Acta Cryst.,* **C48**, 547 (1992).

1.84(1) Å. Due to the large errors in the Rh-C bond lengths in the [Rh(fctfa)(CO)$_2$] complex, it is not possible to make any meaningful comparisons between the Rh-C bond lengths of the [Rh(fctfa)(CO)$_2$] and [Rh(fctfa)(CO)(PPh$_3$)] complexes.

Table 3.70: Interatomic bond lengths [Å] for [Rh(fctfa)(CO)(PPh$_3$)]. The standard deviation of the last decimal is given in brackets.

Rh-P	2.232(1)	Rh-O(1)	2.048(3)	C(3)-C(2)	1.368(6)	C(3)-C(4)	1.515(6)
Rh-O(2)	2.070(3)	Rh-C(5)	1.801(5)	C(32)-C(33)	1.390(6)	C(36)-C(35)	1.388(6)
Fe-C(15)	2.041(4)	Fe-C(12)	2.027(4)	C(12)-C(11)	1.432(6)	C(12)-C(13)	1.415(6)
Fe-C(11)	2.023(4)	Fe-C(14)	2.052(5)	C(41)-C(42)	1.393(6)	C(41)-C(46)	1.390(6)
Fe-C(13)	2.054(5)	Fe-C(23)	2.039(5)	C(56)-C(55)	1.391(7)	C(53)-C(54)	1.368(7)
Fe-C(22)	2.026(5)	Fe-C(25)	2.021(5)	C(53)-C(52)	1.381(6)	C(33)-C(34)	1.371(6)
Fe-C(24)	2.038(5)	Fe-C(21)	2.020(5)	C(43)-C(42)	1.390(7)	C(43)-C(44)	1.372(8)
P-C(51)	1.831(4)	P-C(31)	1.818(4)	C(14)-C(13)	1.415(6)	C(54)-C(55)	1.379(7)
P-C(41)	1.823(4)	O(1)-C(1)	1.266(5)	C(46)-C(45)	1.389(7)	C(44)-C(45)	1.369(8)
O(2)-C(3)	1.264(5)	C(51)-C(56)	1.377(6)	C(34)-C(35)	1.370(7)	F(3)-C(4)	1.280(7)
C(51)-C(52)	1.385(5)	C(1)-C(11)	1.467(6)	C(23)-C(22)	1.400(8)	C(23)-C(24)	1.393(8)
C(1)-C(2)	1.413(5)	C(31)-C(32)	1.391(5)	C(22)-C(21)	1.413(8)	F(2)-C(4)	1.295(8)
C(31)-C(36)	1.394(5)	C(5)-O(3)	1.147(5)	F(1)-C(4)	1.273(7)	C(25)-C(24)	1.388(8)
C(15)-C(11)	1.425(6)	C(15)-C(14)	1.419(6)	C(25)-C(21)	1.385(8)	-	-

As was found for the the [Rh(fctfa)(CO)$_2$] complex, the *dsp*^{2} hybridization around the Rh(I) nucleus is closer to ideal, with angles almost 90°, than the *sp*^{2} hybridization of the β-diketonato skeleton where large deviations from the expected 120° were found. These last mentioned angles deviate by 4°- 10° from the standard 120° expected for *sp*^{2} hibridization with the C(1)-C(2)-C(3) bond angle = 124.3(4)°, bond angle O(2)-C(3)-C(2) = 130.3(4)° and bond angle O(1)-C(1)-C(2) = 124.3(4)°. In the case of Hfctfa, the corresponding bond angles all approached 120° very closely.

The trifluoromethyl group in [Rh(fctfa)(CO)(PPh$_3$)] is not disordered, contrary to what was found for the free β-diketone Hfctfa, the [Rh(fctfa)(CO)$_2$] and [Rh(fctfa)(CO)(PPh$_3$)(CH$_3$)(I)] (paragraph 3.8.4) complexes.

The Rh-O(2) bond, nearest to the electronegative CF$_3$ group [2.070(2) Å] is 0.022 Å longer than the Rh-O(1) bond [2.048(3) Å] nearest to the ferrocenyl group. The Rh-O(2) bond is also 0.048 Å longer than the corresponding bond, Rh-O(4), in the [Rh(fctfa)(CO)$_2$] complex. The Rh-O(1) bond, 2.048(3) Å, nearest to the ferrocenyl group in the [Rh(fctfa)(CO)(PPh)$_3$] complex, however, is similar to the corresponding bond, Rh-O(3), 2.054(8) Å, in the [Rh(fctfa)(CO)$_2$]

complex. The lengthening in the Rh-O(2) bond in the [Rh(fctfa)(CO)(PPh₃)] complex may thus be attributed to the relative *trans* influence of the triphenylphosphine ligand.

Table 3.71: Bond angles [deg] for [Rh(fctfa)(CO)(PPh₃)]. The standard deviation of the last decimal is given in brackets.

P-Rh-O(1)	85.9(1)	C(42)-C(41)-C(46)	119.4(4)	C(14)-Fe-C(21)	153.0(3)
O(1)-Rh-O(2)	88.6(1)	C(54)-C(53)-C(52)	119.7(5)	C(23)-Fe-C(21)	67.9(2)
O(1)-Rh-C(5)	177.2(2)	C(42)-C(43)-C(44)	119.9(5)	C(25)-Fe-C(21)	40.1(2)
C(15)-Fe-C(12)	69.0(2)	C(1)-C(2)-C(3)	124.3(4)	Rh-P-C(51)	120.9(1)
C(12)-Fe-C(11)	41.4(2)	Fe-C(14)-C(13)	69.9(3)	C(51)-P-C(31)	103.1(2)
C(12)-Fe-C(14)	68.3(2)	C(53)-C(54)-C(55)	119.9(4)	C(51)-P-C(41)	103.7(2)
C(15)-Fe-C(13)	68.3(2)	C(43)-C(44)-C(45)	120.2(5)	Rh-O(1)-C(1)	128.5(3)
C(11)-Fe-C(13)	68.8(2)	Fe-C(13)-C(14)	69.8(3)	P-C(51)-C(56)	119.0(3)
C(15)-Fe-C(23)	162.9(2)	C(51)-C(52)-C(53)	121.3(4)	C(56)-C(51)-C(52)	118.5(4)
C(11)-Fe-C(23)	155.3(2)	C(36)-C(35)-C(34)	120.6(4)	O(1)-C(1)-C(2)	124.3(4)
C(13)-Fe-C(23)	109.1(2)	Fe-C(23)-C(22)	69.4(3)	P-C(31)-C(32)	121.9(3)
C(12)-Fe-C(22)	108.9(2)	C(22)-C(23)-C(24)	107.9(5)	C(32)-C(31)-C(36)	118.7(4)
C(14)-Fe-C(22)	164.3(2)	Fe-C(22)-C(21)	69.3(3)	Fe-C(15)-C(11)	68.8(2)
C(23)-Fe-C(22)	40.3(2)	Fe-C(25)-C(24)	70.7(3)	C(11)-C(15)-C(14)	107.9(4)
C(12)-Fe-C(25)	164.3(2)	C(24)-C(25)-C(21)	108.5(5)	O(2)-C(3)-C(4)	112.4(4)
C(14)-Fe-C(25)	119.0(2)	C(3)-C(4)-F(3)	112.0(5)	C(31)-C(32)-C(33)	120.6(4)
C(23)-Fe-C(25)	67.5(2)	F(3)-C(4)-F(2)	103.1(6)	Fe-C(12)-C(11)	69.2(2)
C(15)-Fe-C(24)	125.6(2)	F(3)-C(4)-F(1)	105.1(6)	C(11)-C(12)-C(13)	108.1(4)
C(11)-Fe-C(24)	162.8(2)	Fe-C(24)-C(23)	70.0(3)	Fe-C(11)-C(15)	70.1(2)
C(13)-Fe-C(24)	120.2(2)	C(23)-C(24)-C(25)	108.4(5)	Fe-C(11)-C(12)	69.4(2)
C(22)-Fe-C(24)	67.5(2)	Fe-C(21)-C(25)	70.0(3)	C(15)-C(11)-C(12)	107.5(4)
C(15)-Fe-C(21)	118.9(2)	P-Rh-O(2)	172.7(1)	P-C(41)-C(46)	123.0(3)
C(11)-Fe-C(21)	107.6(2)	P-Rh-C(5)	92.7(1)	C(51)-C(56)-C(55)	120.4(5)
C(13)-Fe-C(21)	165.4(3)	O(2)-Rh-C(5)	92.9(2)	C(32)-C(33)-C(34)	119.8(4)
C(22)-Fe-C(21)	40.9(2)	C(15)-Fe-C(11)	41.1(2)	C(41)-C(42)-C(43)	120.2(5)
C(24)-Fe-C(21)	67.3(2)	C(15)-Fe-C(14)	40.6(2)	Fe-C(14)-C(15)	69.3(2)
Rh-P-C(31)	114.9(1)	C(11)-Fe-C(14)	68.7(2)	C(15)-C(14)-C(13)	108.4(4)
Rh-P-C(41)	107.3(1)	C(12)-Fe-C(13)	40.6(2)	C(41)-C(46)-C(45)	119.4(5)
C(31)-P-C(41)	105.5(2)	C(14)-Fe-C(13)	40.3(2)	Fe-C(13)-C(12)	68.7(3)
Rh-O(2)-C(3)	123.7(3)	C(12)-Fe-C(23)	120.8(2)	C(12)-C(13)-C(14)	108.1(4)
P-C(51)-C(52)	122.4(3)	C(14)-Fe-C(23)	126.6(2)	C(33)-C(34)-C(35)	120.3(4)
O(1)-C(1)-C(11)	116.0(3)	C(15)-Fe-C(22)	154.4(2)	C(46)-C(45)-C(44)	120.9(5)
C(11)-C(1)-C(2)	119.7(4)	C(11)-Fe-C(22)	120.3(2)	Fe-C(23)-C(24)	70.0(3)
P-C(31)-C(36)	119.3(3)	C(13)-Fe-C(22)	127.7(2)	Fe-C(22)-C(23)	70.3(3)
Rh-C(5)-O(3)	178.1(4)	C(15)-Fe-C(25)	106.9(2)	C(23)-C(22)-C(21)	107.4(5)
Fe-C(15)-C(14)	70.2(2)	C(11)-Fe-C(25)	125.7(2)	Fe-C(25)-C(21)	69.9(3)
O(2)-C(3)-C(2)	130.3(4)	C(13)-Fe-C(25)	153.4(2)	C(56)-C(55)-C(54)	120.1(5)
C(2)-C(3)-C(4)	117.3(5)	C(22)-Fe-C(25)	67.9(2)	C(3)-C(4)-F(2)	112.8(5)
C(31)-C(36)-C(35)	119.9(4)	C(12)-Fe-C(24)	154.5(2)	C(3)-C(4)-F(1)	116.3(5)
Fe-C(12)-C(13)	70.8(3)	C(14)-Fe-C(24)	107.9(2)	F(2)-C(4)-F(1)	106.5(6)
Fe-C(11)-C(1)	122.5(3)	C(23)-Fe-C(24)	39.9(2)	Fe-C(24)-C(25)	69.4(3)
C(1)-C(11)-C(15)	124.4(4)	C(25)-Fe-C(24)	40.0(2)	Fe-C(21)-C(22)	69.8(3)
C(1)-C(11)-C(12)	128.0(4)	C(12)-Fe-C(21)	127.6(2)	C(22)-C(21)-C(25)	107.8(5)
P-C(41)-C(42)	117.7(3)	-	-	-	-

Based on electronic considerations as described in paragraph 2.1.4.3 page 19, one would expect that the O(3) in the[Rh(fctfa)(CO)$_2$] complex, the oxygen atom nearest to the ferrocenyl group, will have the largest *trans* influence. On the grounds of electronic considerations, it is thus expected that the CO group *trans* to O(3) in the [Rh(fctfa)(CO)$_2$] would be displaced by PPh$_3$ in the substitution reaction

$$[Rh(fctfa)(CO)_2] + PPh_3 \rightarrow [Rh(fctfa)(CO)(PPh_3)] + CO$$
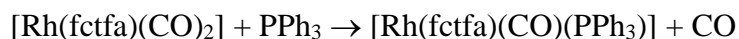
The crystal structure determination of [Rh(fctfa)(CO)(PPh)$_3$], however, showed that the carbonyl group *trans* to the oxygen atom nearest to the more electronegative CF$_3$-group was substituted with PPh$_3$. Dominance of the steric hindrance of the ferrocenyl group over the electronic influence, may be the reason for this unexpected substitution (chapter 2, paragraph 2.1.4.3). However, the similar Rh-C bond lengths in the structure of the [Rh(fctfa)(CO)$_2$] complex, 1.82(2) and 1.84(1) Å, showed no obviously weaker bonded carbonyl group. Therefore, there should not be a preferred CO group that should be substituted with PPh$_3$. Since both the *cis* and *trans* isomers of [Rh(fctfa)(CO)(PPh)$_3$] were observed on ^{1}H NMR (paragraph 3.2.2.3, **Figure 3.1** page 124), it is more probable that the lower crystallization energy of the obtained crystal, determined which isomer crystallized from solution, and not electronic considerations as predicted by the polarization theory of Grinberg.[111]

The C(3)-O(2) and C(1)-O(1) bonds in the β-diketonato skeleton of the [Rh(β-diketonato)(CO)(PPh$_3$)] complex are very similar, 1.264(5) Å and 1.266(5) Å respectively. The C(3)-O(2) bond, nearer to CF$_3$, however, is smaller than the corresponding bond length in the free β-diketone, Hfctfa, 1.264(5) Å *vs.* 1.297(5) Å. The C(1)-O(1) bond is in the same order as the corresponding bond length in Hfctfa, 1.266(5) Å *vs.* 1.277(5) Å.

The free β-diketone was obviously asymmetrically enolized in the direction away from the ferrocenyl group by virtue of the bond lengths C(11)-C(12), 1.432(6) Å, and C(12)-C(13), 1.345(6) Å. The bond lengths C(1)-C(2) = 1.413(5) Å and C(2)-C(3) = 1.368(6) Å in the pseudo aromatic core of [Rh(fctfa)(CO)(PPh$_3$)], also give an indication of an asymmetric enolate Rh-coordination. However, since C(1)-O(1) and C(3)-O(2) are equal in length, it is concluded that [Rh(fctfa)(CO)(PPh$_3$)] is largely a symmetrical structure with deviations in *e.g.* Rh-O bond lengths, which are the result of electronic factors from the CF$_3$ and Fc groups and also of the relative *trans* influence of the CO and PPh$_3$ groups.

---

[111] Grinberg, A.A., *Acta Physiochim.,* USSR, **3**, 573 (1935).

The cyclopentadienyl rings are within experimental error, planar (planes 4 and 5 in **Table 3.72**) and almost parallel [dihedral angle 1.8(9)°] while the average angle of deviation from a fully eclipsed configuration is 8.7°. The cyclopentadienyl ring which is bonded to the β-diketonato chelate ring, is however, not co-planar with the chelate ring - it makes an angle of 12.1(5)° with plane 6 defined by atoms O(1), O(2), C(1), C(2), C(3), Rh, P and C(5), the plane through the chelate ring and the coordination polyhedron (**Table 3.72**).

Table 3.72: Least squares planes for [Rh(fctfa)(CO)(PPh₃)]. The standard deviation of the last decimal is given in brackets.

Plane number 1		Plane number 2		Plane number 3	
Atoms defining plane	**Distance/Å**	**Atoms defining plane**	**Distance/Å**	**Atoms defining plane**	**Distance/Å**
Rh	0.021(59)	P	-0.057(65)	O(1)	-0.042(32)
P	-0.062(59)	C(5)	0.079(66)	C(1)	0.016(32)
C(5)	-0.074(60)	O(1)	0.49(65)	C(2)	0.018(32)
O(1)	0.044(59)	O(2)	-0.071(65)	C(3)	0.011(32)
O(2)	-0.077(59)	**Plane number 6**		C(4)	-0.043(32)
Plane number 4		**Atoms defining plane**	**Distance/Å**	O(2)	0.040(32)
Atoms defining plane	**Distance/Å**	O(1)	0.062(67)	**Plane number 5**	
C(11)	-0.000(6)	O(2)	-0.003(67)	**Atoms defining plane**	**Distance/Å**
C(12)	0.002(6)	C(1)	0.049(67)	C(21)	0.003(7)
C(13)	-0.004(6)	C(2)	-0.045(67)	C(22)	-0.001(8)
C(14)	0.003(6)	C(3)	-0.081(67)	C(23)	-0.001(7)
C(15)	-0.002(6)	Rh	0.037(67)	C(24)	0.003(7)
-	-	P	-0.107(67)	C(25)	-0.003(7)
-	-	C(5)	0.088(67)	-	-
Dihedral angles between planes (°)		**Dihedral angles between planes (°)**		**Dihedral angles between planes (°)**	
plane	**plane**	**angle**	**plane**	**plane**	**angle**	**plane**	**plane**	**angle**
1	2	0.0(2)	2	3	5.7(4)	3	5	8.4(8)
1	3	5.7(4)	2	4	13.7(5)	3	6	4.1(4)
1	4	13.7(5)	2	5	13.5(6)	4	5	1.8(9)
1	5	13.5(6)	2	6	1.6(2)	4	6	12.1(5)
1	6	1.6(2)	3	4	8.2(7)	5	6	12.0(6)
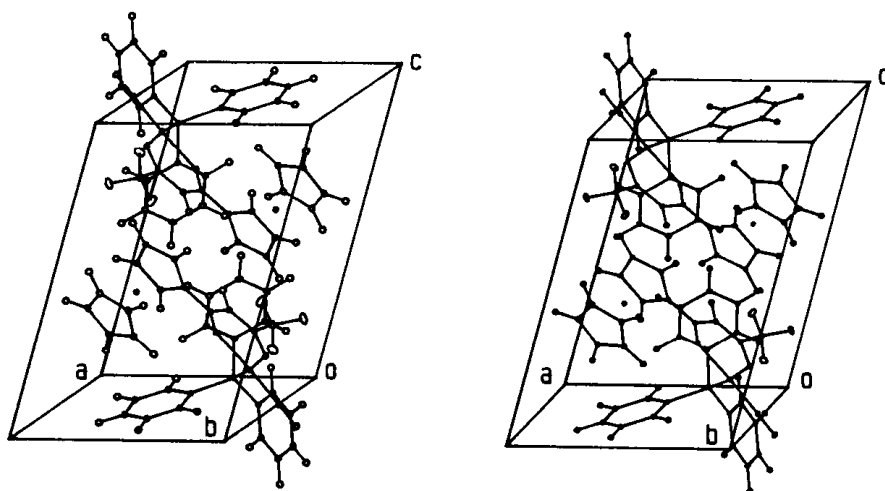
Figure 3.100: Stereoview of [Rh(fctfa)(CO)(PPh₃)] showing the packing of the unit cell.

274

3.8.4 *The crystal structure data of [Rh(fctfa)(CO)(PPh₃)(CH₃)I].*

The numbering system of the atoms in the molecule is shown in **Figure 3.101**. The crystal data of [Rh(fctfa)(CO)(PPh$_3$)(CH$_3$)I] are summarized in **Table 3.73**. The bond lengths and bond angles with their standard deviations are given in **Table 3.74** and **Table 3.75** respectively.
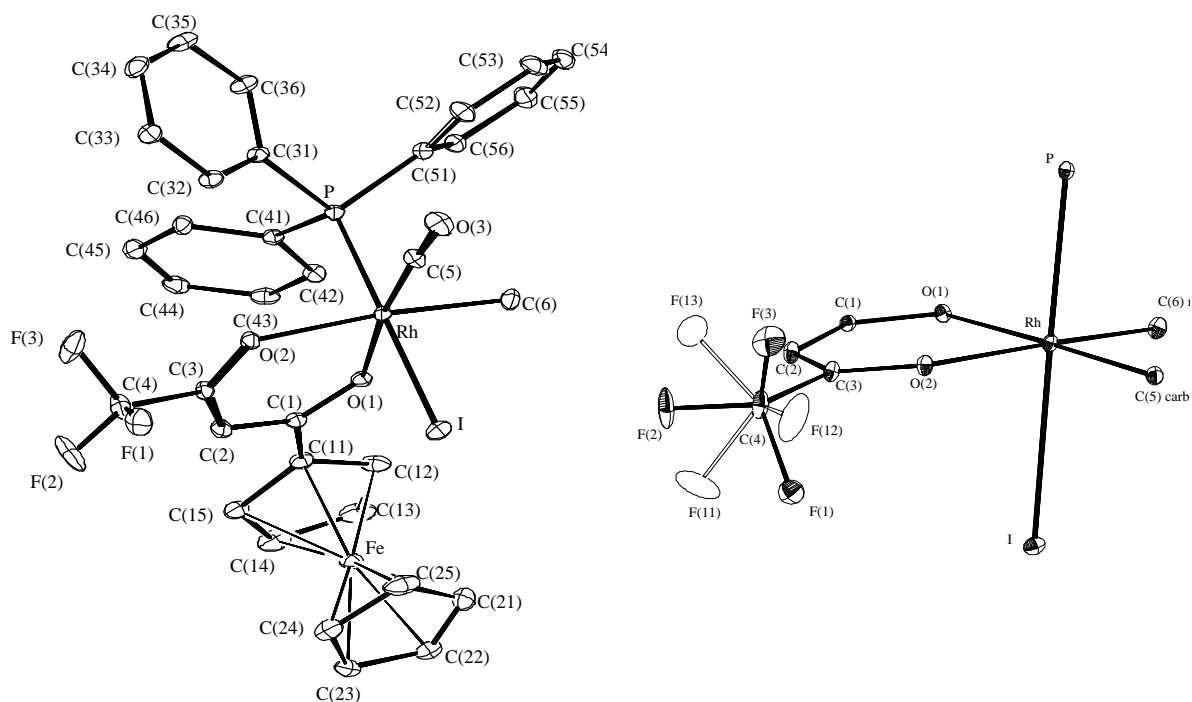
Figure 3.101: A perspective view of [Rh(fctfa)(CO)(PPh₃)(CH₃)I] showing atom labelling.

Table 3.73: Crystal data and structure refinement for [Rh(fctfa)(CO)(PPh₃)(CH₃)I].

Empirical formula	C$_{34}$H$_{28}$F$_3$FeO$_3$RhPI	Mo Kα wavelength; μ	0.71073 Å; 1.961 mm^{-1}
Formula weight	858.2219	F(000)	1688.0
Temperature	293(2) K	Scan type; $2\theta_{max}$	ω-2θ ; 50º
Crystal size mm^3	0.075x0.150x0.650	Scan width	(0.43 + 0.34 tanθ)º
Crystal system	Monoclinic	Scan rate (in ω)	5.49º/min
Space group	P2$_1$/c	$2\theta_{min}$	6º
Unit cell dimensions	$a = 10.769(2)$ Å	Refl. Collected	4717
	$b = 15.153(3)$ Å	Unique refl.	4420 [R(int) = 0.0588]
	$c = 20.413(5)$ Å	Refinement method	Full-matrix least squares on F
	$\beta = 94.31(2)$ º	Data[$I>2\sigma(I)$]; parameters	4414 ; 429
Volume	3221(1) Å^3	Goodness-of-fit on F	1.045
Density (calculated)	1.716 g/cm^3	Final R indices [$I>2\sigma(I)$] [a]	R = 0.0588, R$_w$ = 0.1692
Z	4	Largest diff. peak / hole	1.841/-1.087 e Å^{-3}

An obvious feature of [Rh(fctfa)(CO)(PPh₃)(CH₃)I] and other known Rh(III) alkyl complexes of the form [Rh(L,L'-BID)(CO)(PPh₃)(CH₃)I],[36, 112, 113, 114] is that in all these complexes the iodo ligand, I, is bonded in the axial position of the octaheder, above or below the equatorial array formed by L, L', CO and CH₃ or PPh₃. The carbonyl group, CO, was in all the complexes in the equatorial plane of the octaheder. Chapter 2 figure 2.35 displays the structures of the Rh(III) alkyl complexes.

The equatorial plane formed by O(2), O(3), C(6) and C(5), plane 2 in **Table 3.76** page 278, is approximately planar. The various ligand-rhodium-ligand bond angles, C(5)-Rh-C(6) = 88.4(4)°, C(5)-Rh-O(2) = 97.2(3)°, O(2)-Rh-O(1) = 88.03(19)° and O(1)-Rh-C(6) = 86.2(3)°, deviate 2 – 7° from 90°, see **Table 3.75**. The I ligand is 2.656(4) Å in the axial position above, and the P atom 2.378(4) Å in the axial position below plane 2.

The average C-C bond distance (1.375Å) in the phenyl rings is within experimental error (max 0.016 Å) near the normal value (1.394 Å) for the aromatic C-C bond.[105] All the bond angles in the phenyl rings are close to 120°. The phosphorous atom is approximately tetrahedrally surrounded by the rhodium atom and three carbon atoms of the phenyl rings. The bond angles around P differ no more than 7° from 109°28', the angle for a regular tetrahedron. The mean P-C distance is 1.822 Å, and almost the same as in [Rh(fctfa)(CO)(PPh₃)], 1.824 Å. The Rh-P bond distance, 2.320(2) Å, is much longer than the Rh-P bond distance for [Rh(fctfa)(CO)(PPh₃)], 2.232(1) Å, indicating a change in oxidation state from Rh(I) to Rh(III), results in a weaker Rh-P bond. The Rh-P bond distance in this [Rh(fctfa)(CO)(PPh₃)(CH₃)I] complex is also longer than the range of Rh-P bond distances, 2.231 – 2.300 Å, for the different [Rh^I(L,L'-BID)(CO)(PPh₃)] complexes as tabulated in table 2.41, chapter 2. The Rh-P bond distance in the [Rh(fctfa)(CO)(PPh₃)(CH₃)I] complex is, however, in the same order as was found for other Rh(III) alkyl complexes, *e.g.* [Rh(cupf)(CO)(PPh₃)(CH₃)I],[36] 2.327(4) Å, [Rh(neocupf)(CO)(PPh₃)(CH₃)I],[112] 2.307(2) Å and [Rh(ox)(CO)(PPh₃)(CH₃)I],[113] 2.321(2) Å (average of two molecules found in one unit cell), see chapter 2, table 2.43, page 114.

---

[112] Basson, S.S., Venter, J.A. and Roodt, A., *Manuscript in preparation.*

[113] van Aswegen, K.G., Leipoldt, J.G., Potgieter, I.M., Lamprecht, G.J., Roodt, A. and van Zyl, G.J., *Trans. Met. Chem.,* **16**, 369 (1991).

[114] Damoense, L.J., Roodt, A., Purcell, W., Galding, M.R. and Varshavsky, Y.S. *Manuscript in preparation.*

Table 3.74: Bond lengths [Å] for [Rh(fctfa)(CO)(PPh₃)(CH₃)I]. The standard deviation of the last decimal is given in brackets.

Rh-C(5)	1.834(9)	P-C(31)	1.818(7)	C(1)-C(11)	1.474(9)	C(31)-C(32)	1.382(11)
Rh-O(1)	2.076(5)	P-C(51)	1.823(7)	C(2)-C(3)	1.377(11)	C(32)-C(33)	1.383(12)
Rh-C(6)	2.078(8)	P-C(41)	1.824(8)	C(3)-C(4)	1.518(12)	C(33)-C(34)	1.358(14)
Rh-O(2)	2.159(5)	F(1)-F(12)	1.15(16)	C(4)-F(12)	1.09(4)	C(34)-C(35)	1.370(14)
Rh-P	2.320(2)	F(1)-C(4)	1.323(17)	C(4)-F(13)	1.31(4)	C(35)-C(36)	1.403(12)
Rh-I	2.716(1)	F(1)-F(11)	1.46(7)	C(4)-F(11)	1.34(4)	C(41)-C(46)	1.366(11)
Fe-C(21)	1.992(11)	F(2)-F(11)	1.08(5)	C(11)-C(12)	1.416(13)	C(41)-C(42)	1.392(12)
Fe-C(25)	2.020(11)	F(2)-F(13)	1.13(5)	C(11)-C(15)	1.449(12)	C(42)-C(43)	1.403(13)
Fe-C(12)	2.024(9)	F(2)-C(4)	1.261(15)	C(12)-C(13)	1.402(14)	C(43)-C(44)	1.349(15)
Fe-C(11)	2.024(7)	F(3)-F(12)	0.94(15)	C(13)-C(14)	1.388(18)	C(44)-C(45)	1.349(14)
Fe-C(13)	2.029(12)	F(3)-C(4)	1.33(2)	C(14)-C(15)	1.410(15)	C(45)-C(46)	1.385(12)
Fe-C(14)	2.029(10)	F(3)-F(13)	1.39(8)	C(21)-C(22)	1.378(17)	C(51)-C(56)	1.396(11)
Fe-C(24)	2.032(11)	O(1)-C(1)	1.264(8)	C(21)-C(25)	1.447(19)	C(51)-C(52)	1.401(12)
Fe-C(23)	2.036(9)	O(2)-C(3)	1.277(9)	C(22)-C(23)	1.346(15)	C(52)-C(53)	1.382(12)
Fe-C(15)	2.039(9)	O(3)-C(5)	1.118(10)	C(23)-C(24)	1.408(15)	C(53)-C(54)	1.335(15)
Fe-C(22)	2.043(10)	C(1)-C(2)	1.404(11)	C(24)-C(25)	1.408(18)	C(54)-C(55)	1.372(16)
-	-	–	–	C(31)-C(36)	1.376(10)	C(55)-C(56)	1.383(13)

The Rh-I bond axis is slightly but significantly inclined by 3.59(14)° towards O(2) and the Rh-P bond is almost perpendicular to Rh-C(5) and Rh-C(6) and declined by more than 2° degrees away from O(1) and O(2). This resulted in a 2.25(05)° deviation from linearity for the I-Rh-P bond axis. A deviation from linearity (3.4°) for the Rh-I bond axis was also found for the [Rh(cupf)(CO)(PPh₃)(CH₃)I][36] complex.

The Rh-C(5)-O(3) chain is approximately linear, 175.6(8)°, with the C(5)-O(3) bond distance 1.118(10) Å, which is smaller than the C(5)-O(3) bond distance of 1.147(5) Å in [Rh(fctfa)(CO)(PPh₃)]. The Rh-C(5) bond length of 1.834(9) Å is larger than the corresponding bond length, 1.801(5) Å, in [Rh(fctfa)(CO)(PPh₃)]. In accordance with what was found for the Rh-P bond, changing of the oxidation of the Rh core from one to three resulted in longer Rh-C bond lengths. Due to the large errors in the Rh-C bond lengths in the [Rh(fctfa)(CO)₂] complex, it is not possible to make any comparison between the Rh-C bond lengths of the [Rh(fctfa)(CO)₂] and [Rh(fctfa)(CO)(PPh₃)(CH₃)I] complexes.

The Rh-O(1) bond, 2.076(5), is 0.083 Å shorter than the Rh-O(2) bond. Both Rh-O(1) and Rh-O(2) bonds in [Rh(fctfa)(CO)(PPh₃)(CH₃)I] are longer than the Rh-O(1) and Rh-O(2) bonds in [Rh(fctfa)(CO)(PPh₃)], 2.076(5) Å *v.s.* 2.048(3) Å and 2.159(5) Å *v.s.* 2.070(3) Å, respectively. The Rh-O(1) bond in both complexes is *trans* to the CO group, but Rh-O(2) is *trans* to the PPh₃ group in [Rh(fctfa)(CO)(PPh₃)] and *trans* to the CH₃ group in [Rh(fctfa)(CO)(PPh₃)(CH₃)I].

Table 3.75: Bond angles [deg] for [Rh(fctfa)(CO)(PPh₃)(CH₃)I]. The standard deviation of the last decimal is given in brackets.

C(5)-Rh-O(1)	173.8(3)	C(24)-Fe-C(22)	67.0(5)	C(14)-C(13)-C(12)	108.2(10)
C(5)-Rh-C(6)	88.4(4)	C(23)-Fe-C(22)	38.5(4)	C(14)-C(13)-Fe	70.0(7)
O(1)-Rh-C(6)	86.2(3)	C(15)-Fe-C(22)	150.1(4)	C(12)-C(13)-Fe	69.6(6)
C(5)-Rh-O(2)	97.2(3)	C(31)-P-C(51)	104.2(3)	C(13)-C(14)-C(15)	109.6(9)
O(1)-Rh-O(2)	88.03(19)	C(31)-P-C(41)	109.0(4)	C(13)-C(14)-Fe	70.0(7)
C(6)-Rh-O(2)	173.4(3)	C(51)-P-C(41)	102.6(4)	C(15)-C(14)-Fe	70.1(5)
C(5)-Rh-P	90.7(3)	C(31)-P-Rh	111.0(2)	C(14)-C(15)-C(11)	106.6(10)
O(1)-Rh-P	92.37(15)	C(51)-P-Rh	115.3(3)	C(14)-C(15)-Fe	69.3(6)
C(6)-Rh-P	90.6(3)	C(41)-P-Rh	113.9(3)	C(11)-C(15)-Fe	68.6(5)
O(2)-Rh-P	92.84(15)	F(12)-F(1)-C(4)	52(2)	C(22)-C(21)-C(25)	108.6(11)
C(5)-Rh-I	87.3(3)	F(12)-F(1)-F(11)	101(3)	C(22)-C(21)-Fe	72.0(7)
O(1)-Rh-I	89.73(14)	C(4)-F(1)-F(11)	57.3(15)	C(25)-C(21)-Fe	69.9(6)
C(6)-Rh-I	90.3(3)	F(11)-F(2)-F(13)	134(4)	C(23)-C(22)-C(21)	108.9(11)
O(2)-Rh-I	86.41(14)	F(11)-F(2)-C(4)	69(3)	C(23)-C(22)-Fe	70.4(6)
P-Rh-I	177.75(5)	F(13)-F(2)-C(4)	66(3)	C(21)-C(22)-Fe	68.1(6)
C(21)-Fe-C(25)	42.3(6)	F(12)-F(3)-C(4)	54(4)	C(22)-C(23)-C(24)	109.5(11)
C(21)-Fe-C(12)	108.3(5)	F(12)-F(3)-F(13)	107(5)	C(22)-C(23)-Fe	71.0(6)
C(25)-Fe-C(12)	118.8(5)	C(4)-F(3)-F(13)	57.4(17)	C(24)-C(23)-Fe	69.6(6)
C(21)-Fe-C(11)	129.2(5)	C(1)-O(1)-Rh	127.3(4)	C(25)-C(24)-C(23)	108.1(11)
C(25)-Fe-C(11)	108.0(4)	C(3)-O(2)-Rh	122.3(5)	C(25)-C(24)-Fe	69.2(7)
C(12)-Fe-C(11)	40.9(4)	O(1)-C(1)-C(2)	126.6(6)	C(23)-C(24)-Fe	69.9(6)
C(21)-Fe-C(13)	117.0(6)	O(1)-C(1)-C(11)	114.2(7)	C(24)-C(25)-C(21)	104.9(10)
C(25)-Fe-C(13)	152.1(7)	C(2)-C(1)-C(11)	119.2(7)	C(24)-C(25)-Fe	70.1(6)
C(12)-Fe-C(13)	40.5(4)	C(3)-C(2)-C(1)	125.4(7)	C(21)-C(25)-Fe	67.8(7)
C(11)-Fe-C(13)	68.8(4)	O(2)-C(3)-C(2)	129.4(7)	C(36)-C(31)-C(32)	118.7(7)
C(21)-Fe-C(14)	149.5(6)	O(2)-C(3)-C(4)	111.4(7)	C(36)-C(31)-P	120.1(6)
C(25)-Fe-C(14)	166.8(7)	C(2)-C(3)-C(4)	119.2(7)	C(32)-C(31)-P	120.9(6)
C(12)-Fe-C(14)	67.8(5)	F(12)-C(4)-F(2)	127.7(18)	C(33)-C(32)-C(31)	121.4(9)
C(11)-Fe-C(14)	68.9(4)	F(12)-C(4)-F(13)	105(6)	C(34)-C(33)-C(32)	119.7(9)
C(13)-Fe-C(14)	40.0(5)	F(2)-C(4)-F(13)	52(3)	C(33)-C(34)-C(35)	120.3(8)
C(21)-Fe-C(24)	68.4(5)	F(12)-C(4)-F(1)	56(8)	C(34)-C(35)-C(36)	120.3(8)
C(25)-Fe-C(24)	40.7(5)	F(2)-C(4)-F(1)	110.9(16)	C(31)-C(36)-C(35)	119.6(8)
C(12)-Fe-C(24)	153.5(4)	F(13)-C(4)-F(1)	142(2)	C(46)-C(41)-C(42)	118.8(8)
C(11)-Fe-C(24)	119.5(4)	F(12)-C(4)-F(3)	45(8)	C(46)-C(41)-P	124.6(6)
C(13)-Fe-C(24)	165.3(5)	F(2)-C(4)-F(3)	107.6(15)	C(42)-C(41)-P	116.6(7)
C(14)-Fe-C(24)	128.8(6)	F(13)-C(4)-F(3)	64(3)	C(41)-C(42)-C(43)	120.0(9)
C(21)-Fe-C(23)	66.8(5)	F(1)-C(4)-F(3)	99.4(14)	C(44)-C(43)-C(42)	119.6(9)
C(25)-Fe-C(23)	68.4(5)	F(12)-C(4)-F(11)	113(7)	C(45)-C(44)-C(43)	120.5(10)
C(12)-Fe-C(23)	164.3(4)	F(2)-C(4)-F(11)	49(3)	C(44)-C(45)-C(46)	121.3(10)
C(11)-Fe-C(23)	153.5(4)	F(13)-C(4)-F(11)	100(3)	C(41)-C(46)-C(45)	119.9(8)
C(13)-Fe-C(23)	127.0(4)	F(1)-C(4)-F(11)	67(3)	C(56)-C(51)-C(52)	119.2(7)
C(14)-Fe-C(23)	108.4(5)	F(3)-C(4)-F(11)	135(2)	C(56)-C(51)-P	118.9(7)
C(24)-Fe-C(23)	40.5(4)	F(12)-C(4)-C(3)	117(2)	C(52)-C(51)-P	121.9(6)
C(21)-Fe-C(15)	168.9(5)	F(2)-C(4)-C(3)	115.0(10)	C(53)-C(52)-C(51)	119.2(9)
C(25)-Fe-C(15)	128.7(5)	F(13)-C(4)-C(3)	106(2)	C(54)-C(53)-C(52)	121.4(10)
C(12)-Fe-C(15)	68.9(4)	F(1)-C(4)-C(3)	111.3(9)	C(53)-C(54)-C(55)	120.3(9)
C(11)-Fe-C(15)	41.8(3)	F(3)-C(4)-C(3)	111.5(13)	C(54)-C(55)-C(56)	121.0(10)
C(13)-Fe-C(15)	68.4(5)	F(11)-C(4)-C(3)	114(2)	C(55)-C(56)-C(51)	118.9(10)
C(14)-Fe-C(15)	40.6(4)	O(3)-C(5)-Rh	175.6(8)	F(2)-F(11)-C(4)	61.6(19)
C(24)-Fe-C(15)	108.9(5)	C(12)-C(11)-C(15)	106.8(7)	F(2)-F(11)-F(1)	113(4)
C(23)-Fe-C(15)	118.8(4)	C(12)-C(11)-C(1)	127.0(8)	C(4)-F(11)-F(1)	56(3)
C(21)-Fe-C(22)	39.9(5)	C(12)-C(11)-Fe	69.5(5)	F(3)-F(12)-F(1)	151(5)
C(25)-Fe-C(22)	68.8(5)	C(15)-C(11)-Fe	69.6(4)	F(3)-F(12)-C(4)	82(6)
C(12)-Fe-C(22)	128.3(5)	C(1)-C(11)-Fe	121.8(5)	F(1)-F(12)-C(4)	73(7)
C(11)-Fe-C(22)	166.8(4)	C(13)-C(12)-C(11)	108.8(10)	F(2)-F(13)-C(4)	62(2)
C(13)-Fe-C(22)	107.6(5)	C(13)-C(12)-Fe	69.9(6)	F(2)-F(13)-F(3)	112(5)
C(14)-Fe-C(22)	117.2(5)	C(11)-C(12)-Fe	69.5(5)	C(4)-F(13)-F(3)	59(3)

The Rh-I distance of 2.716(1) Å, being slightly longer than the range 2.60 – 2.69 Å reported for complexes having a ligand with a small *trans* influence opposite the Rh-I bond,[115, 116] is however still shorter than Rh-I bonds with CH_3 *trans* to the iodine atom. Examples of Rh-I bonds with CH_3 *trans* to it, are $[Rh(dmavk)(CO)(PPh_3)(CH_3)I]$,[114] 2.849(1) Å, $[Rh(ox)(CO)(PPh_3)(CH_3)I]$,[113] 2.803(1) Å, and $[Rh^{III}(CH_3)\{C_2(DO)(DOBF_2)\}]$,[115] (*trans* methyliodo[difluoro[3,3'-(trimethylenedinitrilo)bis(2-pentanone oximato)]borate]rhodium(III)), 2.813(1) Å. The present Rh-I distance thus implies that PPh_3 has a smaller *trans* influence than an alkyl group.

As was the case for $[Rh(fctfa)(CO)_2]$ and $[Rh(fctfa)(CO)(PPh_3)]$, large deviations of the expected 120° for sp^2 hybridization in the β-diketonato skeleton were found. The bond angles are distorted by 5°- 9° from the standard 120° with the C(1)-C(2)-C(3) bond angle = 125.4(7)°, bond angle O(2)-C(3)-C(2) = 129.4(7)° and bond angle O(1)-C(1)-C(2) = 126.6(6)°. In the case of Hfctfa, the corresponding bond angles were all 120° within experimental error.

The C(3)-O(2) and C(1)-O(1) bonds in the β-diketonato skeleton of the $[Rh(β\text{-diketonato})(CO)(PPh_3)(CH_3)(I)]$ complex are similar, 1.277(9) Å and 1.264(8) Å respectively. Both bonds are smaller than the corresponding bonds in the free Hfctfa. The C(3)-O(2) bond, nearer to CF_3, however, is in the same order as the corresponding bond length in $[Rh(fctfa)(CO)(PPh_3)]$, 1.277(9) Å *vs.* 1.264(5) Å. The C(1)-O(1) bond is also in the same order as the corresponding bond length in $[Rh(fctfa)(CO)(PPh_3)]$, 1.264(8) Å *vs.* 1.266(5) Å.

The free β-diketonato ligand was obviously asymmetrically enolized in the direction away from the ferrocenyl group by virtue of the bond lengths C(11)-C(12), 1.432(6) Å, and C(12)-C(13), 1.345(6) Å. In contrast, the bond lengths C(1)-C(2) = 1.404(11) Å and C(2)-C(3) = 1.377(11) Å in the pseudo aromatic core of $[Rh(fctfa)(CO)(PPh_3)(CH_3)(I)]$, do not give an indication of asymmetric enolate Rh-coordination.

---

[115] Collman, J.P., Christian, P.A., Current, S., Denisevich, P., Halbert, T.R., Schmittou, E.R. and Hodgson, K.O., *Inorg. Chem.,* **15**, 223 (1976).

[116] Basson, S.S., Leipoldt, J.G., Potgieter, I.M., Roodt, A. and van der Waldt, T.J., *Inorg. Chim. Acta,* **119**, L9 (1986).

Table 3.76: Least squares planes for [Rh(fctfa)(CO)(PPh₃)(CH₃)I]. The standard deviation of the last decimal is given in brackets.

Plane number 1		Plane number 2		Plane number 3	
Atoms defining plane	**Distance/Å**	**Atoms defining plane**	**Distance/Å**	**Atoms defining plane**	**Distance/Å**
Rh	-0.0466(29)	C(5)	-0.0045(36)	Rh	0.0660(28)
C(5)	0.0085(36)	C(6)	0.0047(38)	O(1)	-0.0471(39)
C(6)	0.0161(40)	O(1)	-0.0044(36)	O(2)	-0.0752(42)
O(1)	0.0059(36)	O(2)	0.0041(34)	C(1)	-0.0140(52)
O(2)	0.0161(36)	**Additional Atoms**		C(2)	0.0471(61)
Additional Atoms		P	-2.3777(42)	C(3)	0.0232(57)
P	-2.3660(36)	I	2.6558(38)	**Additional Atoms**	
I	2.6675(30)	-	-	P	-2.2290(40)
Plane number 4		**Plane number 5**		I	2.7560(26)
Atoms defining plane	**Distance/Å**	**Atoms defining plane**	**Distance/Å**	**Dihedral angles between planes (°)**		
C(11)	0.0045(54)	C(21)	-0.0086(71)	**plane**	**plane**	**angle**
C(12)	-0.0044(63)	C(22)	0.0109(75)	1	2	0.04(22)
C(13)	0.0026(72)	C(23)	-0.0086(71)	1	3	6.97(23)
C(14)	0.0003(71)	C(24)	0.0030(67)	2	3	6.99(23)
C(15)	-0.0030(59)	C(25)	0.0033(67)	3	4	3.11(45)
Additional Atom		**Additional Atom**		4	5	1.37(62)
Fe	1.6347(43)	Fe	-1.6381(48)	-	-	-

The cyclopentadienyl rings are within experimental error, planar (planes 4 and 5 in **Table 3.76**) and almost parallel [dihedral angle 1.37(62)°] while the average angle of deviation from a fully eclipsed configuration is 12.9°, see illustration in **Figure 3.102** (c). The cyclopentadienyl ring which is bonded to the β-diketonato chelate ring, is almost co-planar with the chelate ring - it forms an angles 3.11(45)° with plane 3 defined by atoms O(1), O(2), C(1), C(2), C(3) and Rh, the plane through the chelate ring (**Table 3.76**).

The trifluoromethyl group in [Rh(fctfa)(CO)(PPh₃)(CH₃)(I)] is disordered, similar to what was found for the free β-diketone Hfctfa, and [Rh(fctfa)(CO)₂] (paragraphs 3.8.1 and 3.8.2). **Figure 3.102** (b) and (c) illustrate the intermolecular interaction between F and either a hydrogen on a ferrocenyl group, or a hydrogen on a phenyl ring from *another* molecule, F(3)-H(53) = 2.661 Å, F(3)-H(12) = 2.669 Å, F(12)-H(53) = 2.652 Å, F(12)-H(13) = 2.667 Å, F(13)-H(36) = 2.606 Å. These intermolecular interactions link one molecule to another in the unit cell. However, intramolecular interaction, prevents free rotation of the CF₃ group. Two preferred CF₃ orientations are observed and is the cause for the disorder. The first involves a strong interaction between F(2) and H(2), the hydrogen bonded to C(2), as well as a weak interaction between both F(1) and F(3) with O(2). The contact distances are F(2)-H(2) = 2.362 Å, F(1)-O(2) = 2.702 Å and F(3)-O(2) = 2.718 Å respectively. These intermolecular interactions lead to one of the two

observed CF$_3$ orientations. The other CF$_3$ orientation, involving F(12), F(11) and F(13), is the result of a strong interaction between F(12) and O(2) and a weak interaction of both F(11) and F(13) with H(2). The intramolecular contact distances are F(12)-O(2) = 2.485 Å, F(11)-H(2) = 2.727 Å and F(13)-H(2) = 2.624 Å respectively.

(a)

(b)

(c)
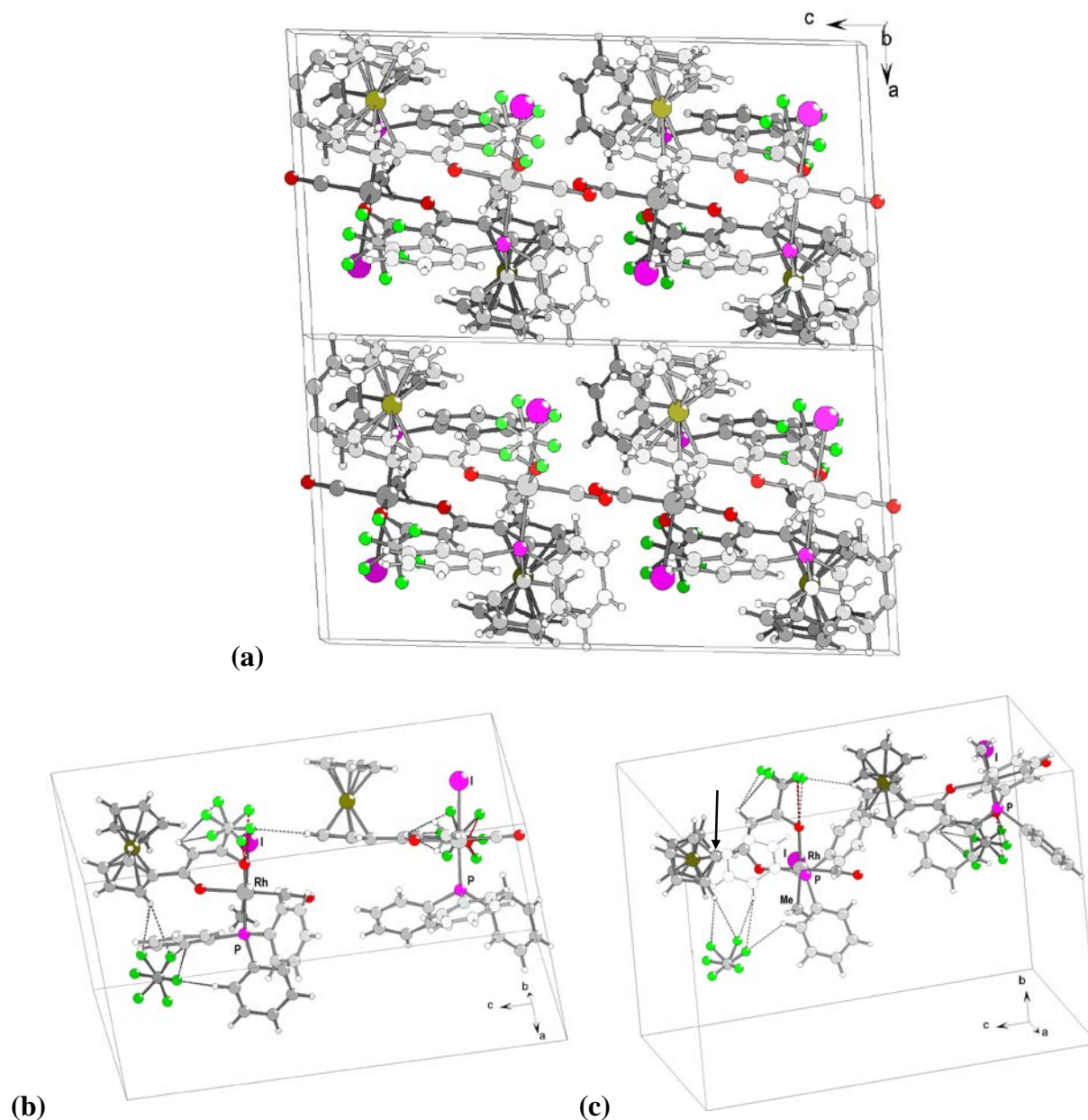
Figure 3.102: **Packing of [Rh(fctfa)(CO)(PPh$_3$)(CH$_3$)(I)] viewed from different observation points: View (a) at the top illustrates the molecular packing in two unit cells. Views (b) illustrate the intermolecular interaction between the F atoms and the H atom of either a ferrocenyl group or a phenyl group. View(c) illustrates intramolecular interactions between F atoms and either the H(2) bonded to C(2) of the β-diketonato or to the O(2) atom of the β-diketonato closest to the CF$_3$ group. Also illustrated is the 12.9° deviation from the eclipse cyclopentadienyl formation in the ferrocenyl fragment of [Rh(fctfa)(CO)(PPh$_3$)(CH$_3$)(I)] down the C(11)-C(25) axis (see arrow).**

3.8.5   *^{13}C and ^{31}P study of [Rh(L,L'-BID)(CO)(PPh$_3$)] complexes.*

A solution containing the isomeric [Rh(L,L'-BID)(CO)(PPh$_3$)] complexes as discussed in paragraph 3.2.2.3 page 122, exhibits:

(i) two ^{13}C NMR doublets of doublets with similar values of $\delta^{13}C$, $^1J(^{13}C$-$^{103}Rh)$ and $^2J(^{13}C$-$^{31}P)$, corresponding to signals of C of the carbonyl group of the two main isomers[13] (see **Appendix B**) and

(ii) two ^{31}P NMR doublets with similar values of $\delta^{31}P$ and $^1J(^{31}P$-$^{103}Rh)$, corresponding to the signals of P of the PPh$_3$ group of the two main isomers. The region around δ 185 ppm on the ^{31}P NMR corresponds to carbonyl groups bound to rhodium.[117]

^{13}C and ^{31}P NMR data together with Rh-C (of carbonyl group) and Rh-P (of PPh$_3$ group) bond distances for a range of [Rh(L,L'-BID)(CO)(PPh$_3$)] complexes are summarized in **Table 3.77** and **Table 3.79** respectively. The correlation between ^{31}P NMR parameters and Rh-P bond distances is illustrated in **Figure 3.103**. ^{13}C NMR data for Hfctfa, [Rh(fctfa)(CO)$_2$] and the two main isomers of [Rh(fctfa)(CO)(PPh$_3$)], are given in **Table 3.78**. ^{31}P and ^{13}C NMR spectra are given in **Appendix B**.

In paragraph 2.1.4.3, chapter 2, it was shown that the Rh-P bond distance in square planar complexes of the type [Rh(L,L'-BID)(CO)(PPh$_3$)] is a good indicator of the relative *trans* influence of the donor atoms in the bidentate ligand (L,L'-BID), as summarized in table 2.9 page 28, with the general trend:

Rh-P bond length *trans* to O atoms < Rh-P bond length *trans* to N atoms < Rh-P bond length *trans* to S atoms.

The data in **Table 3.77** indicate that the Rh-C bond distance in square planar complexes of the type [Rh(L,L'-BID)(CO)(PPh$_3$)], follows the *same trend* as the Rh-P bonds, namely,

Rh-C bond length *trans* to O atoms < Rh-C bond length *trans* to N atoms < Rh-C bond length *trans* to S atoms.

---

[117] Bresler, L.S., Buzina, N.A., Varshavsky, Yu.S., Kiseleva, N.V. and Cherkasova, T.G., *J. Organomet. Chem.*, **171**, 229 (1979).

Table 3.77: ^{13}C NMR parameters[13] and Rh-C bond lengths[a] for square planar complexes [Rh(L,L'-BID)(CO)(PPh$_3$)][a].

L,L'-BID ligand	Rh-C bond *trans*	Rh-C distance /Å	δ^{13}C/ppm	$^1J(^{13}$C-^{103}Rh)/Hz	$^2J(^{13}$C-^{31}P)/Hz
ba	O	1.739(14)	-	-	-
		1.768(14)	-	-	-
tftma	O	1.765(14)	-	-	-
cupf	O	1.78(1)	189.90, 189.75[b]	76.7, 76.0	25.4, 25.5
tta	O	1.780(12)	188.12, 188.27[b]	77.8, 78.5	24.6, 24.4
dbbtu	O	1.781(6)	-	-	-
tfdma	O	1.781(9)	-	-	-
dmavk	O	1.784(5)	191.20, 190.30[b]	73.8, 66.9	21.9, 22.8
ox	O	1.786(9)	190.70	72.3	22.6
quin	O	1.787(13)	-	-	-
anmetha [c]	O	1.787(6)	193.16	69.7	20.8
salnr	O	1.791(1)	-	-	-
tfhd	O	1.796(17)	-	-	-
trop	O	1.797(12)	189.85	75.5	25.3
tfaa [d]	O	1.800(11)	188.24, 188.18[b]	77.6, 77.4	24.6, 24.8
hpt	O	1.800(3)	192.50	70.8	20.9
bzaa	O	1.801(4)	-	-	-
fctfa[e]	O	1.801(5)	189.00, 189.07[b]	79.3, 79.3	24.1, 24.1
acac	O	1.801(8)	189.10	75.7	24.8
pic	O	1.802(11)	189.84	75.3	22.5
sacac	O	1.808(11)	190.83	73.6	21.1
bpha	O	1.809(6)	-	-	-
dbm	O	1.812(13)	-	-	-
hacsm	N	1.823(4)	192.22	63.8	20.5
cacsm	S	1.829(5)	190.02	72.1	21.8
macsm	S	1.836(5)	-	-	-

a) The structures of the complexes tabulated are in given in chapter 2. See table 2.41, page 112 for references to bond lengths.   b) Two isomers.   c) Data for PCy$_3$ complex.   d) Data for P(*p*-Cl-Ph)$_3$ complex. e) Results from this study.

Table 3.78: ^{13}C NMR data for Hfctfa, [Rh(fctfa)(CO)$_2$] and the two main isomers of [Rh(fctfa)(CO)(PPh$_3$)]. s = singlet, q = quartet, (d,d) = doublet of doublets.

compound	signal (type)					
	C nearest to Fc (s)	C nearest to CF$_3$ (q)		C of carbonyl group(s) (d, d)		
	δ^{13}C /ppm	δ^{13}C /ppm	$^1J(^{13}$C-^{19}F) /Hz	δ^{13}C /ppm	$^1J(^{13}$C-^{103}Rh) /Hz	$^2J(^{13}$C-^{31}P) /Hz
Hfctfa	195.00	171.74	35.8	-		
[Rh(fctfa)(CO)$_2$]	192.67	165.82	32.6	183.16, 183.16	74.0, 74.0	16.6, 16.6
[Rh(fctfa)(CO)(PPh$_3$)] (two isomers)	191.72 190.34	167.43 164.95	31.8	189.00 189.07	79.3 79.3	24.1 24.1

^{13}C and ^{31}P NMR studies[118, 119] of [Rh(RCOCHCNR')(CO)(PPh$_3$)] complexes, R, R' = CH$_3$, C$_6$H$_5$, CF$_3$ and C(CH$_3$)$_3$, showed that the values of $^1J(^{13}$C-^{103}Rh) and $^1J(^{31}$P-^{103}Rh), are larger when the CO group (for ^{13}C spectra) or the PPh$_3$ ligand (for ^{31}P spectra) is *trans* to the weakly

---

[118] Cherkasova, T.G., Osetrova, L.V. and Varshavsky, Yu.S., *Rhodium Ex.*, **1**, 8 (1993).

[119] Galding, M.R., Cherkasova, T.G., Osetrova, L.V. and Varshavsky, Yu.S., *Rhodium Ex.*, **1**, 14 (1993).

donating O-atom, and they are smaller when the ligands are in the *trans*-position to the stronger donor N-atom,

$$^1J(^{31}P\text{-}^{103}Rh)\ (P\text{-}trans\text{-}O) > {}^1J(^{31}P\text{-}^{103}Rh)\ (P\text{-}trans\text{-}N)$$

$$^1J(^{13}C\text{-}^{103}Rh)\ (CO\text{-}trans\text{-}O) > {}^1J(^{13}C\text{-}^{103}Rh)\ (CO\text{-}trans\text{-}N).$$

For example, for the two isomers of [Rh(dmavk)(CO)(PPh₃)] it was found that $^1J(^{31}P\text{-}^{103}Rh)$ = 149.7 Hz (P *trans* to N) is smaller than the $^1J(^{31}P\text{-}^{103}Rh)$ value of 172.0 Hz (P *trans* to O).

Table 3.79: ³¹P NMR parameters and Rh-P bond lengths for square planar complexes [Rh(L,L'-BID)(CO)(PPh₃)] and related rhodium(III) complexes. L,L'-BID = six-membered chelate ring containing donor atoms L and L'.

no.	L,L'-BID	Rh-P bond *trans*	Rh-P distance/(Å)	δ³¹P/ppm	$^1J(^{31}P\text{-}^{103}Rh)$/Hz
1	fctfa*	O, O	2.232(1), -	48.04, 48.04	176.4, 176.4
2	dbm	O	2.237(7)[120]	49.56	177.9
3	tftma	O, O	2.238(3),[121] -	47.85, 47.85	172.9, 172.9
4	tfdma	O, O	2.239(2),[10(ii)] -	48.72, 47.75	175.7, 178.0
5	bzaa	O	2.243(1)[110]	49.44	175.0
6	acac	O	2.244(2)[109]	48.84	175.7
7	tta	O, O	2.245(3),[108] -	47.84, 47.78	177.7, 176.7
8	ba	O, O	2.248(3), 2.249(3)[122]	49.28, 49.37	175.8, 174.8
9	tfhd	O, O	2.252(3),[123] -	49.14, 47.86	177.2, 174.8
10	dmavk (acyl)	-	2.260(4)[124]	-	153
11	cacsm	N	2.268(1)[13, 39]	45.2	144.6
12	dmavk	N, O	2.275(1),[125] -	41.45, 54.91	149.7, 172.0
13	hacsm	S	2.283(1)[13]	42.70	148.9
14	sacac	S	2.300(2)[126]	35.36	144.5
15	fctfa (alkyl)*	-	2.319(3)	28.34	116
16	dmavk (alkyl)	-	2.356(3)[127]	-	107

³¹P NMR parameters from this study, except for L,L'-BID = acac, tta, cacsm, dmavk, hacsm and sacac which is from reference 13, dmavk (alkyl and acyl) from reference 127.   * This study.

[120] Lamprecht, D., Lamprecht, G.J., Botha, J.M., Umakoshi, K. and Sasaki, Y., *Acta Cryst.,* **C53**, 1403 (1997).

[121] Steynberg, E.C., Lamprecht, G.J. and Leipoldt, J.G., *Inorg. Chim. Acta,* **133**, 33 (1987).

[122] Purcell. W., Basson, S.S., Leipoldt, J.G., Roodt, A. and Preston, H. *Inorg. Chim. Acta,* **234**, 153 (1995).

[123] Leipoldt, J.G., Basson, S.S., and Potgieter, J.H., *Inorg. Chim. Acta,* **117**, L3 (1986).

[124] Damoense, L.J., Purcell, W., and Roodt, A., *Rhodium Ex.,* **14**, 4 (1995).

[125] Damoense, L.J., Purcell, W., Roodt, A. and Leipoldt, J.G., *Rhodium Ex.,* **5**, 10 (1994).

[126] Botha, L.J., Basson, S.S. and Leipoldt, *Inorg. Chim. Acta,* **126**, 25 (1987).

[127] Damoense, L.J., Roodt, A., Purcell, W., Galding, M.R. and Varshavsky, Y.S. *Manuscript in preparation.*

The data of **Table 3.79** clearly indicate that longer Rh-P bonds result in smaller $^1J(^{31}\text{P-}^{103}\text{Rh})$ values. **Figure 3.103** illustrates the linear relationship between $^1J(^{31}\text{P-}^{103}\text{Rh})$ and Rh-P bond distances for six-membered chelate rings. The linear relationship between $\delta^{31}\text{P}$, in ppm, and Rh-P bond lengths is also illustrated. The graphs imply that approximate Rh-P bond lengths can be calculated utilizing the equations

$$\text{d(Rh-P)} = -0.0014(1) \times {}^1J(^{31}\text{P-}^{103}\text{Rh}) + 2.49(2) = -0.0039(4) \times \delta^{31}\text{P} + 2.44(2).$$

These two equations are applicable for Rh-P bond lengths, d(Rh-P), between 2.23 Å and 2.36 Å.

The data in **Table 3.79** also indicate that coupling constants $^1J(^{31}\text{P-}^{103}\text{Rh})$ in complexes with PPh$_3$ *trans* to a N or a S atom are very similar, but smaller than coupling constants in complexes with PPh$_3$ *trans* to an O atom,

$$^1J(^{31}\text{P-}^{103}\text{Rh})\ (P\text{-}trans\text{-}O) > {}^1J(^{31}\text{P-}^{103}\text{Rh})\ (P\text{-}trans\text{-}N) \approx {}^1J(^{31}\text{P-}^{103}\text{Rh})\ (P\text{-}trans\text{-}S).$$

No linear or unique relationship between $\delta^{13}\text{C}$, $^1J(^{13}\text{C-}^{103}\text{Rh})$ or $^2J(^{13}\text{C-}^{31}\text{P})$, and Rh-C bond lengths or the relative *trans* influence of the donor atoms O, N or S in the bidentate ligand, in complexes of the type [Rh(L,L'-BID)(CO)(PR$_3$)], could be found.
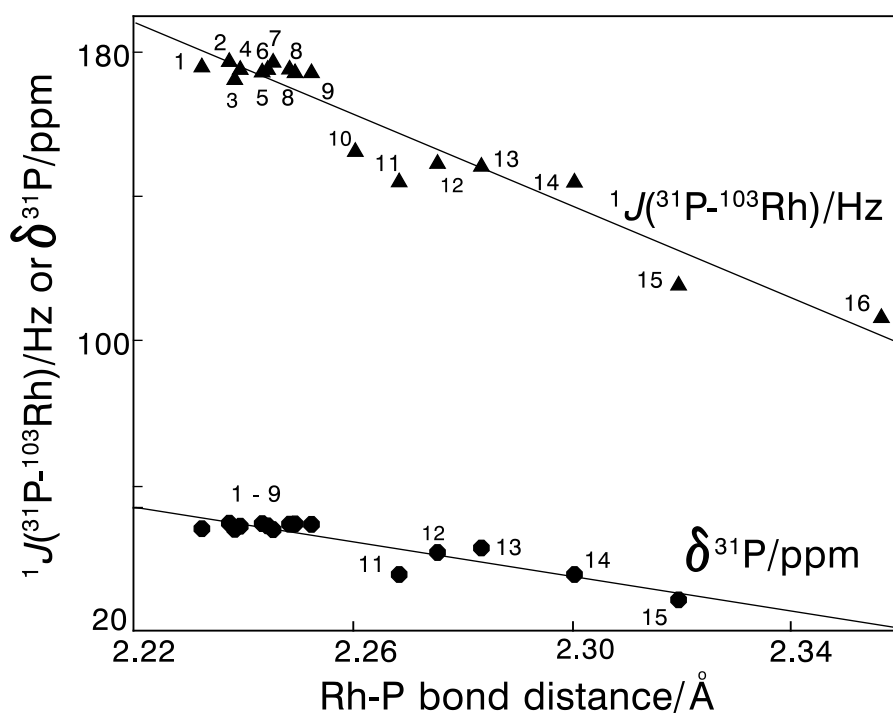
Figure 3.103: Linear relationship between the coupling constant, $^1J(^{31}\text{P-}^{103}\text{Rh})$, or the chemical shift, $\delta^{31}\text{P}$, *and* the Rh-P bond distance in various [Rh(L,L'-BID)(CO)(PR$_3$)] complexes. L,L'-BID = six-membered chelate ring with donor atoms L and L'. The numbering of complexes corresponds to that given in Table 3.79.

4 Experimental

4.1 Materials.

Solid reagents used in preparations (Merck, Aldrich and Sigma) were used without further purification. Liquid reactants and solvents were distilled prior to use; water was double distilled. Organic solvents were dried according to published methods.[1] Flash chromatography was performed on Kieselgel 60 (Merck, grain size 0.063 - 0.2 mm, eluent ether-hexane 2:3 by volume) or, if stated eluent 2, Sephadex LH-20 (Pharmacia. hexane-ethanol 6:1 by volume) utilizing an overpressure that never exceeded 100 Torr (l Torr = 1 mmHg = 133.32 Pa). Elemental analysis was performed by Canadian Microanalytical Service, Canada. Mass spectroscopy was done at the University of British Columbia, Canada. Iron analysis was by atomic adsorption as describe elsewhere.[2]

4.2 Synthesis.

4.2.1 Acetylferrocene (FcCOCH₃) {1}.

Acetylferrocene was prepared (in 81% yield) by treating ferrocene (Fc) with acetic anhydride according to a published procedure[3] with care being taken to maintain the internal temperature[4] of the reaction mixture between 100 and 105^{0}C. Recrystallisation from hexane gave a sufficiently pure product for β-diketone synthesis. Characterization data: m.p. 85^{0}C; ν_{max}(KBr)/cm^{-1} 1662 (C=O); δ_H(80 MHz, CDCl$_3$) 2,36 (3H, s CH$_3$), 4.16 (5H, s, C$_5$H$_5$), 4,47 (2H, t, C$_5$H$_4$), 4,74 (2H, t, C$_5$H$_4$); R$_f$ 0,38 (ether : hexane = 1:1).

[1] Furniss, B.S., Hannaford, A.J., Smith, P.W.G. and Tatchell, A.R., *Vogel's Textbook of Practical Organic Chemistry,* Fifth Ed., Longman Scientific & Technical, John Wiley & Sons, New York, Chapter 4, p. 395 – 469.

[2] du Plessis, W.C., Vosloo, T. and Swarts, J.C., *J.C.S. Dalton Trans.*, 2507 (1998).

[3] Bublitz, D.E. and. Rinehart, K. L., jun., in *Organic Reactions,* ed. W G. Dauben, Wiley, New York, 1969, vol.17, p. 1.

[4] Van Ryswyk, H. and Van Hecke, G.R., *J. Chem. Educ.,* **68**, 878 (1991).

4.2.2 *Methyl ferrocenoate (FcCOOMe).*

Ferrocenoic acid was prepared *via* the lithium intermediate as described elsewhere[5] and esterified by refluxing it (1.6 g, 7 mmol) in methanol (100 cm^3) in the presence of concentrated H_2SO_4 (0.04 cm^3) under nitrogen for 48 h. The resulting liquid was poured onto ice (150 g) and extracted with ether (3x100 cm^3). The combined ether extracts were washed with water, 5% aqueous $NaHCO_3$ and again water to afford the ester after removal of the dried (Na_2SO_4) solvent, the ester (1.19 g, 70%), m.p. 70 $^{\circ}$C (lit.,[6] 70 $^{\circ}$C); δ_H(80 MHz, $CDCl_3$) 3.78 (3H, s, CH_3), 4.17 (5H, s, C_5H_5). 4.35(2H, t, C_5H_4) and 4.76 (2H, t, C_5H_4).

4.2.3 *β-diketones.*

4.2.3.1   1-ferrocenyl-4,4,4-trifluorobutane-1,3-dione (Hfctfa) {3}.

Sodium ethoxide method, an adaptation of a published procedure.[7] A suspension of solid sodium ethoxide[8] (3.4 g, 50 mmol) in an ether solution (40 cm^3) of acetylferrocene (5.47 g, 24 mmol) was stirred for 15 min before the slow addition of ethyl trifluoro-acetate (6.82 g, 48 mmol), prepared, purified and dried in the same way as described for ethyl acetate[9]. The resulting orange-red precipitate was filtered after 12 h of stirring, washed with dry ether and dissolved in lukewarm (50 – 60 °C) water. The aqueous solution was filtered *without delay,* the pH immediately lowered to 2 with HCl and the product {3} extracted with ether (3 x 100 cm^3). Washing of the ether extract with water (3 x 100 cm^3), followed by drying (Na_2SO_4) and solvent removal under reduced pressure, afforded solid Hfctfa (4.06g 52%). Recrystallisation with hexane afforded spectroscopically pure Hfctfa (Found: Fe, 17.3. $C_{14}H_{14}F_3FeO_2$ requires 17.23%); m.p. 102°C (lit.,[7] 102 $^{\circ}$C); ν_{max}(KBr)/cm^{-1} 1620 (C=O); δ_H(300 MHz, $CDCl_3$) 4.20 (5H, s, enol C_5H_5), 4.65 (2H, t, enol C_5H_4), 4.85(2H, t, enol C_5H_4) and 6.07(1 H, s, enol CH).

---

[5] Goldberg, S.I., Keith, L.H. and Prokopv, T.S., *J. Org. Chem.,* **28**, 850 (1963).

[6] Schlögl, K., M*onatch. Chem.,* **88**, 601 (1957).

[7] i) Pedersen, C.J., Salem, N.J., and Weinmayr, V., *US Pat,* 2 875 223, (1959).
      ii) Weinmayr, V., *Naturwissenschaften*, **45**, 311 (1958).

[8] Furniss, B.S., Hannaford, A.J., Smith, P.W.G., and Tatchell, A.R., *Vogel's textbook of practical organic chernistry,* Longman, Harlow, 5th edn., 1989, p 634.

[9] Mann, P.G. and Saunders, B.C., *Practical Organic Chemistry,* Longman, New York, 1981, p. 95.

4.2.3.2   1-ferrocenylbutane-1,3-dione (Hfca) {4}.

Hfca was prepared in yields up to 35% according to the sodium ethoxide method as described for Hfctfa by replacing trifluoro-acetate with ethyl acetate (4.23g, 48mmol), (Found: Fe, 20.6. $C_{14}H_{14}FeO_2$ requires 20.68%); m.p. 98 ^{0}C; (lit.,[10] 97 – 97.5 ^{0}C); ν_{max}(KBr)/cm^{-1} 1620 (C=O); δ_H(300 MHz, CDCl$_3$) 2.10 (3H, s, enol CH$_3$), 2.32 (3H, s, keto CH$_3$), 3.85 (2H, s, keto CH$_2$), 4.22 (5H, s, enol C$_5$H$_5$), 4.25 (5H, s, keto C$_5$H$_5$), 4.52 (2H, t, enol C$_5$H$_4$), 4.60 (2H, t, keto C$_5$H$_4$), 4.80 (2H, t, enol C$_5$H$_4$), 4.81 (2H, t, keto C$_5$H$_4$) and 5.74(1H, s, enol CH).

4.2.3.3   1-ferrocenyl-3-phenylpropane-1,3-dione (Hbfcm) {5}.

The lithium diisopropylamide method. Rigorous Schlenk conditions were adhered to. A light yellow solution or LiNP$^i_2$ was prepared by adding *n*-butyllithium (4.21 cm^3 of a 1.6 mol dm^{-3} solution in hexane) to an ice-cooled solution of freshly distilled diisopropylamine (0.73 g, 7.2 mmol) in thf (15 cm^3). This was added to a solution of acetylferrocene (1.46 g, 6.4 mmol) in THF (l0 cm^3) and stirred at room temperature for 20 min before methyl benzoate (0.81 g, 6 mmol) dissolved in THF (10 cm^3) was added. Stirring of the resulting reaction mixture continued for 4 h before it was shaken with HCl (50 cm^3, 1 mol dm^{-3}) and immediately extracted with ether (5 x 80 cm^3). The combined ether extracts were thoroughly washed with water, dried (MgSO$_4$) and the solvent removed under reduced pressure. Flash chromatography of the residue (R$_f$ = 0.58) afforded Hbfcm (0.60g 30%), (Found: Fe, 16.6. $C_{19}H_{16}FeO_2$ requires 16.81%); m.p. 107 ^{0}C (lit.,[11] 106 - 107 ^{0}C); ν_{max}(KBr)/cm^{-1} 1640 and 1710 (C=O); δ_H(300 MHz, CDCl$_3$) 3.91(2H, s, keto CH$_2$), 4.20 (5H, s, enol C$_5$H$_5$), 4.13 (5H, s, keto C$_5$H$_5$), 4.53 (2 H, t, keto C$_5$H$_4$), 4.54 (2 H, t, enol C$_5$H$_4$), 4.85 (2 H, t, keto C$_5$H$_4$), 4.87 (2 H, t, enol C$_5$H$_4$), 6.48 (1H, s, enol CH), 7.41-7.51 and 7.88-8.11 (5H, m, C$_6$H$_5$).

4.2.3.4   1,3-diferrocenylpropane-1,3-dione (Hdfcm) {6}.

Hdfcm was prepared in yields up to 30% by the lithium diisopropylamide method under rigorous Schlenk conditions as described for Hbfcm by replacing methyl benzoate with methyl ferrocenoate (4.23g, 48mmol), (Found: Fe, 25.2. $C_{23}H_{20}Fe_2O_2$ requires 25.38%); m.p. 157 ^{0}C; ν_{max}(KBr)/cm^{-1} 1640 and 1710 (C=O); δ_H(300 MHz, CDCl$_3$) 4.19 (10H, s, 2xC$_5$H$_5$), 4.49 (4H, t, 2xC$_5$H$_4$), 4.82(4H, t, 2xC$_5$H$_4$) and 5.96(1H, s, enol CH).

---

[10] Cain, C.F., Mashburn T.A. and Hauser, C.R., *J. Org. Chem.,* **26**, 1030 (1961).

[11] Hauser, C.R. and Lindsay, J.K., *J. Org. Chem.,* **22**, 482 (1957).

4.2.3.5   2-ferrocenoyletan-1-al (Hfch) {7}.[12]

Characterization data: (Found: Fe, 21.68%, $C_{13}H_{12}FeO_2$ requires 21.81%); m.p. 104 ^{0}C; ν_{max}(KBr)/cm^{-1} 1615 (C=O); δ_H(300 MHz, CDCl$_3$) 3.79 (2H, d, keto CH$_2$), 4.23 (5H, s, enol C$_5$H$_5$), 4.24 (5H, s, keto C$_5$H$_5$), 4.53 (2H, t, keto C$_5$H$_4$), 4.57 (2H, t, enol C$_5$H$_4$), 4.59 (2H, t, keto C$_5$H$_4$), 4.81 (2 H, t, enol C$_5$H$_4$), 5.77 (1H, d, enol CH) and 7.75 (1H, m, enol CH) 9.91 (1H ,t, keto H).

4.2.4   Di-μ-chloro-bis(η-cycloocta-1,5-diene)dirhodium(I)   [Rh$_2$Cl$_2$(cod)$_2$] {9}.

The complex was prepared according to a published procedure.[13] Characterization data: m.p. 256^{0}C; 58% yield; δ_H(300 MHz, CDCl$_3$) 1.77 (4H, m, half of 4CH$_2$), 2.52 (4H, m, other half of 4CH$_2$) and 4.25 (4 H, m, 4CH).

4.2.5   [Rh(β-diketone)(cod)] complexes {10}-{15}.

The general procedure was as follows. To a stirred yellow, near saturated solution of [Rh$_2$Cl$_2$(cod)$_2$] (0.5 g, 1 mmol) in DMF (25 cm^3) was added solid β-diketone (2 mmol). After 5 min of stirring the crude product [Rh(β-diketone)(cod)] was precipitated with an excess of water, filtered off and dissolved in ether. The ether solution was washed with water, dried (MgSO$_4$) and the solvent removed under reduced pressure. Flash column chromatography gave [Rh(β-diketone)(cod)] spectroscopically pure in high yield.

(η^4-1,5-cyclooctadiene)(1-ferrocenyl-4,4,4-trifluoro-1,3-butanedionato-κ^{2}O,O')rhodium(I) [Rh(fctfa)(cod)] {10}, m.p. 188 ^{0}C; R$_f$ = 0.63; 77% yield; δ_H(300 MHz, CDCl$_3$) 1.89 (4H, m, half of aliphatic C$_8$H$_{12}$ protons), 2.53 (4H, m, other half of aliphatic C$_8$H$_{12}$ protons), 4.19 (9H, m, 4H olefinic protons of C$_8$H$_{12}$ and 5H of C$_5$H$_5$), 4.49 (2H, t, C$_5$H$_4$), 4.72 (2 H, t, C$_5$H$_4$) and 5.96 (1H, s, CH).

(η^4-1,5-cyclooctadiene)(1-ferrocenyl-1,3-butanedionato-κ^{2}O,O')rhodium(I)   [Rh(fca)(cod)] {11}, m.p. 196 ^{0}C; R$_f$ = 0.79; 53% yield; δ_H(300 MHz, CDCl$_3$) 1.87 (4H, m, half of aliphatic C$_8$H$_{12}$ protons), 2.02 (3H, t, CH$_3$), 2.51 (4H, m, other half of aliphatic C$_8$H$_{12}$ protons), 4.12 (4H,

---

[12] This complex was provided by J.C. Swarts and M.A.S. Aquino for use in this study.

[13] Chatt, J. and Venanzi, L.M., *J. Chem. Soc.,* (**A**), 4735 (1957).

m, olefinic protons of C_8H_{12}), 4.16 (5H, s, C_5H_5), 4.34 (2H, t, C_5H_4), 4.64 (2H, t, C_5H_4) and 5.62 (1H, s, CH).

(η^4-1,5-cyclooctadiene)(1-ferrocenyl-3-phenyl-1,3-propanedionato-κ^2O,O')rhodium(I) [Rh(bfcm)(cod)] {12},[14]. m.p. 203 ^{0}C; R_f = 0.78; 77% yield; δ_H(300 MHz, CDCl$_3$) 1.92 (4H, m, half of aliphatic C_8H_{12} protons), 2.55 (4H, m, other half of aliphatic C_8H_{12} protons), 4.19 (9H, m, 4 olefinic protons of C_8H_{12} and 5 H of C_5H_5), 4.39 (2H, t, C_5H_4), 4.74 (2H, t, C_5H_4), 6.29 (1H, s, CH), 7.35 – 7.45 (3H, m, C_6H_5) and 7.78 – 7.84 (2H, m, C_6H_5).

(η^4-1,5-cyclooctadiene)(1,3-diferrocenyl-1,3-propanedionato-κ^2O,O')rhodium(I) [Rh(dfcm)(cod)] {15}, m.p. > 255 ^{0}C; R_f = 0.84; 49% yield; δ_H(300 MHz, CDCl$_3$) 1.86 (4H, m, half of aliphatic C_8H_{12} protons), 2.51 (4H, m, other half of aliphatic C_8H_{12} protons), 4.10 (4H, m, olefinic protons of C_8H_{12}), 4.15 (10H, s, $2C_5H_5$), 4.33 (4H, t, half of $2C_5H_4$), 4.67 (4H, m, half of $2C_5H_4$) and 5.92 (1H, s, CH).

(η^4-1,5-cyclooctadiene)(4,4,4-trichloro-1-ferrocenyl-1,3-butanedionato-κ^2O,O')rhodium(I) [Rh(fctca)(cod)] (Hfctca = 1-ferrocenyl-4,4,4-trichlorobutane-1,3-dione) {13},[14] m.p. 188 ^{0}C; R_f = 0.73; 57% yield; δ_H(300 MHz, CDCl$_3$) 1.84 (4H, m, half of aliphatic C_8R_{12} protons), 2.49 (4H, m, other half of aliphatic C_8H_{12} protons), 4.18 (9H, m, 4H olefinic protons of C_8H_{12} and 5H of C_5H_5), 4.43 (2H, t, C_5H_4), 4.68 (2 H, t, C_5H_4) and 6.39(1H, s, CH).

(η^4-1,5-cyclooctadiene)(1-ferrocenyl-1,3-propanedionato-κ^2O,O')rhodium(I) [Rh(fch)(cod)] {14},[12] m.p. 173 ^{0}C; δ_H(300 MHz, CDCl$_3$) 1.85 (4H, m, half of aliphatic C_8R_{12} protons), 2.49 (4H, m, other half of aliphatic C_8H_{12} protons), 4.05 – 4.25 (9H, m, 4H olefinic protons of C_8H_{12} and 5H of C_5H_5), 4.36 (2H, t, C_5H_4), 4.65 (2 H, t, C_5H_4), 5.55 (1H, d, CH) and 7.88 (1H, d, CH).

4.2.6 Tetracarbonyl-μ-dichloro-dirhodium(I) [Rh$_2$Cl$_2$(CO)$_4$] {16}.

[Rh$_2$Cl$_2$(CO)$_4$] {16} was either prepared *in situ* by refluxing RhCl$_3$.3H$_2$O in DMF[15] for *ca.* 30 minutes until a light yellow colour indicated the formation of {16} or the crystalline product was

---

[14] This complex was provided by J.C. Swarts and W.C. (Ina) du Plessis for use in this study

[15] i) Varshavskii, Y.S. and Cherkasova, *Russ. J. Inorg. Chem.,* **12**, 899 (1967).

ii) Rusina, A. and Vlcek, A.A., *Nature (London),* **206**, 295 (1965).

obtained commercially. Characterization data: ν_{max}(KBr)/cm^{-1} 2010 and 2080 (C=O); δ_H(300 MHz, CDCl$_3$) 1.77 (4H, m, half of 4CH$_2$), 2.51 (4H, m, half of 4CH$_2$) and 4.25 (4H, m, 4CH).

4.2.7 [Rh(β-diketone)(CO)$_2$] complexes {17} – {20}.

4.2.7.1 Dicarbonyl(1-ferrocenyl-4,4,4-trifluoro-1,3-butanedionato-κ^{2}O,O')rhodium(I) [Rh(fctfa)(CO)$_2$] {17}.

[Rh$_2$Cl$_2$(CO)$_4$] {16} was prepared *in situ* by refluxing RhCl$_3$.3H$_2$O (0.2g, 0.76 mmol) in DMF (3 ml) for *ca.* 30 minutes. The solution was allowed to cool on ice. An equivalent amount of solid Hfctfa (0.246g, 0.76 mmol) was slowly added to a stirred solution. After 30 min of stirring the crude product [Rh(fctfa)(CO)$_2$] {17} was precipitated with an excess of water and extracted with hexane. The hexane solution was washed with water, dried (MgSO$_4$) and the solvent removed under reduced pressure to give {17} (242 mg, 66 % yield); m.p. 228 ^{0}C; ν_{max}(KBr)/cm^{-1} 2008 and 2074 (C=O); δ_H(300 MHz, CDCl$_3$) 4.21 (5H, s, C$_5$H$_5$), 4.64 (2H, t, C$_5$H$_4$), 4.86 (2H, t, C$_5$H$_4$) and 6.20 (1H, s, CH).

4.2.7.2 Dicarbonyl(1-ferrocenyl-1,3-butanedionato-κ^{2}O,O')rhodium(I) [Rh(fca)(CO)$_2$] {18}.

A solution of Hfca {4} (0.135 g, 0.50 mmol) in DMF (5 ml) was added to a solution of [Rh$_2$Cl$_2$(CO)$_4$] {16} (0.097 g, 0.25 mmol) in DMF (30 ml). The reaction mixture was stirred at room temperature for 30 min after which the crude product [Rh(fca)(CO)$_2$] {18} was precipitated with an excess of water and extracted with ether (5 x 25 ml). The ether solution was washed with water, dried (MgSO$_4$) and the solvent removed under reduced pressure. Recrystallisation with hexane afforded spectroscopically pure [Rh(fca)(CO)$_2$] {18} (96 mg, 45 % yield); m.p. 164 ^{0}C; ν_{max}(KBr)/cm^{-1} 2014 and 2068 (C=O); δ_H(300 MHz, CDCl$_3$) 2.14 (3H, s, CH$_3$), 4.17 (5H, s, C$_5$H$_5$), 4.46 (2H, t, C$_5$H$_4$), 4.77 (2H, t, C$_5$H$_4$) and 5.87 (1H, s, CH).

4.2.7.3 Dicarbonyl(1-ferrocenyl-3-phenyl-1,3-propanedionato-κ^{2}O,O')rhodium(I) [Rh(bfcm)(CO)$_2$] {19}.

This reaction was performed under Ar and in dry, freshly distilled DMF. Hbfcm {5} (0.166 g, 0.50 mmol) dissolved in dry, freshly distilled DMF (10 ml) is added to a solution of [Rh$_2$Cl$_2$(CO)$_4$] {16} (0.097 g, 0.25 mmol) in DMF (30 ml). The reaction mixture was stirred at

room temperature for 2.5 h in an Ar atmosphere. [Rh(bfcm)(CO)$_2$] {19} was precipitated with cold water (50 ml) and extracted with (distilled over Na) benzene (4 x 40 ml). The ether solution was washed with water, dried (MgSO$_4$) and the solvent removed under reduced pressure. Flash chromatography of the residue (R$_f$ = 0.70, sefadex, 4 hexane + 1 ethanol) afforded [Rh(bfcm)(CO)$_2$] {19} (93 mg, 38% yield); m.p. 205 ^{0}C; ν_{max}(KBr)/cm^{-1} 1998 and 2074 (C=O); δ_H(300 MHz, CDCl$_3$) 4.15 (5H, s, C$_5$H$_5$), 4.49 (2H, t, C$_5$H$_4$), 4.85 (2H, t, C$_5$H$_4$), 6.50 (1H, s, CH), 7.4 - 7.5 (3H, m, C$_6$H$_5$) and 7.9. (2H, m, C$_6$H$_5$).

4.2.7.4 Dicarbonyl(1,3-diferrocenyl-1,3-propanedionato-$\kappa^2 O,O'$)rhodium(I) [Rh(dfcm)(CO)$_2$] {20}

[Rh(dfcm)(cod)] {15} (210 mg, 323mmol) was dissolved in acetone (220 ml). CO was purged through the solution through a sintherglass tube under a pressure 1 cm above atmospheric pressure. [Rh(dfcm)(CO)$_2$] {20} was precipitated with cold water (100 ml), stirred for 15 min (resulting in the evolution of CO gas) and centrifuged. The precipitate {20} was washed with water, filtrated and dried in a vacuum desicator. Spectroscopically pure [Rh(dfcm)(CO)$_2$] {20} was obtained (149 mg, 77 % yield); m.p. >255 ^{0}C; ν_{max}(KBr)/cm^{-1} 2074 and 2008 (C=O); δ_H(300 MHz, CDCl$_3$) 4.18 (10H, s, C$_5$H$_5$), 4.47 (4H, t, C$_5$H$_4$), 4.83 (4H, t, C$_5$H$_4$) and 6.18 (1H, s, CH).

4.2.8   [Rh(β-diketone)(CO)(PPh$_3$)] complexes {21} – {24}.

4.2.8.1 Carbonyl(1-ferrocenyl-4,4,4-trifluoro-1,3-butanedionato-$\kappa^2 O,O'$)triphenylphosphine-rhodium(I) [Rh(fctfa)(CO)(PPh$_3$)] {21}.

A solution of PPh$_3$ (49 mg, 0.19 mmol) in hot *n*-hexane (15 ml) was added to [Rh(fctfa)(CO)$_2$] {17} (90 mg, 0.19 mmol) in *n*-hexane (30 ml) which was heated over boiling water. The resulting reaction mixture was stirred for 30 s over boiling water until no more CO gas was released and was then filtered. Crystals suitable for X-ray structure determination were obtained by slowly cooling the reaction mixture, (122 mg, 90 % yield); m.p. 256 ^{0}C; ν_{max}(KBr)/cm^{-1} 1986 (C=O); δ_H(300 MHz, CDCl$_3$) isomer 1: 3.98 (5H, s, C$_5$H$_5$), 4.06 (2H, t, C$_5$H$_4$), 4.25 (2H, t, C$_5$H$_4$), 6.09 (1H, s, CH) and 7.4 – 7.8 (15H, m, aromatic); δ_H(300 MHz, CDCl$_3$) isomer 2: 4.22 (5H, s, C$_5$H$_5$), 4.47 (2H, t, C$_5$H$_4$), 4.83 (2H, t, C$_5$H$_4$), 6.08 (1H, s, CH) and 7.4 – 7.8 (15H, m, aromatic); ratio isomer 1 : isomer 2 = 1.00 : 0.65.

4.2.8.2 Carbonyl(1-ferrocenyl-1,3-butanedionato-$\kappa^2 O,O$')triphenylphosphinerhodium(I) [Rh(fca)(CO)(PPh$_3$)] {22}.

A solution of PPh$_3$ (170 mg, 0.65 mmol) in hot *n*-hexane (15 ml) was added to [Rh(fca)(CO)$_2$] {18} (280 mg, 0.65 mmol) in hot hexane (30 ml). The reaction mixture was stirred for 60 s over boiling water until no more CO gas was released and was then filtered. [Rh(fca)(CO)(PPh$_3$)] {22} was obtained by slowly cooling the reaction mixture, (310 mg, 72 % yield); m.p. 184 ^{0}C; ν_{max}(KBr)/cm^{-1} 1980 (C=O); δ_H(300 MHz, CDCl$_3$) isomer 1: 2.19 (3H, s, CH$_3$), 3.91 (5H, s, C$_5$H$_5$), 4.08 (2H, t, C$_5$H$_4$), 4.15 (2H, t, C$_5$H$_4$), 5.78 (1H, s, CH) and 7.38 – 7.78 (15H, m, aromatic); δ_H(300 MHz, CDCl$_3$) isomer 2: 1.71 (3H, s, CH$_3$), 4.19 (5H, s, C$_5$H$_5$), 4.37 (2H, t, C$_5$H$_4$), 4.79 (2H, t, C$_5$H$_4$), 5.73 (1H, s, CH) and 7.38 – 7.78 (15H, m, aromatic); ratio isomer 1 : isomer 2 = 1.00 : 0.22

4.2.8.3 Carbonyl(1-ferrocenyl-3-phenyl-1,3-propanedionato-$\kappa^2 O,O$')triphenylphosphine-rhodium(I) [Rh(bfcm)(CO)(PPh$_3$)] {23}.

This experiment is done on dry acetone. A solution of PPh$_3$ (44 mg, 0.17 mmol) in acetone (4 ml) was added to [Rh(bfcm)(CO)$_2$] {19} (83 mg, 0.17 mmol) in acetone (15 ml). The reaction mixture was stirred until no more CO gas was released. The reaction mixture was stirred and concentrated with Ar until the first signs of milkiness. Spectroscopically pure [Rh(bfcm)(CO)(PPh$_3$)] {23} was obtained by slowly cooling the reaction mixture, (92 mg, 75 % yield); m.p. 165 ^{0}C; ν_{max}(KBr)/cm^{-1} 1977; (C=O); δ_H(300 MHz, CDCl$_3$) isomer 1: 3.92 (5H, s, C$_5$H$_5$), 4.15 (2H, t, C$_5$H$_4$), 4.26 (2H, t, C$_5$H$_4$), 6.40 (1H, s, CH) and 7 - 8 (20H, m, aromatic); (C=O); δ_H(300 MHz, CDCl$_3$) isomer 2: 4.20 (5H, s, C$_5$H$_5$), 4.40 (2H, t, C$_5$H$_4$), 4.88 (2H, t, C$_5$H$_4$), 6.43 (1H, s, CH) and 7 - 8 (20H, m, aromatic).

4.2.8.4 Carbonyl(1,3-diferrocenyl-1,3-propanedionato-$\kappa^2 O,O$')triphenylphosphinerhodium(I) [Rh(dfcm)(CO)(PPh$_3$)] {24}.

PPh$_3$ (79 mg, 0.30mmol) dissolved in hexane (20 ml) was added to [Rh(dfcm)(CO)$_2$] {20} (180 mg, 0.30mmol) dissolved in hot hexane (80 ml). CO gas was released. The excess hexane was evaporated on a rotavapor until pure [Rh(dfcm)(CO)(PPh$_3$)] {24} crystallised from the solution, (107.9 mg, 43% yield); m.p. 188 ^{0}C; ν_{max}(KBr)/cm^{-1} 1977; (C=O); δ_H(300 MHz, CDCl$_3$): 3.94 (5H, s, C$_5$H$_5$), 4.16 (2H, t, C$_5$H$_4$), 4.18 (2H, t, C$_5$H$_4$), 4.23 (5H, s, C$_5$H$_5$), 4.41 (2H, t, C$_5$H$_4$), 4.87

(2H, t, C$_5$H$_4$), 6.11 (1H, s, CH) and 7.40 – 7.51, 7.71 – 7.82 (15H, m, aromatic). Note, only one isomer with two sets of peaks for the two unequivalent ferrocene groups was obtained.

4.2.9 Carbonyl(1-ferrocenyl-4,4,4-trifluoro-1,3-butanedionato-κ^2O,O')iodomethyl-triphenylphosphinerhodium(III) [Rh(fctfa)(CO)(CH$_3$)(I)(PPh$_3$)] {25}.

MeI (1.9 g , 13.4 mmol, in excess) was added to [Rh(fctfa)(CO)(PPh$_3$)] {21} (75 mg, 0.1 mmol) dissolved in hexane at 30 °C (70 ml). N$_2$ was purged through the reaction vessel before it was sealed and left at 20 °C in the dark. After 5 days crystals suitable for X-ray structure determination were obtained from the reaction mixture, 90 % yield, m.p. 235 ^{0}C; ν_{max}(KBr)/cm^{-1} 2056 (C=O); δ_H(300 MHz, CDCl$_3$) isomer 1: 1.78 (3H, d d, CH$_3$), 4.30 (5H, s, C$_5$H$_5$ and 1H, m, C$_5$H$_4$), 4.40 (1H, m, C$_5$H$_4$), 4.48 (1H, m, C$_5$H$_4$), 4.77 (1H, m, C$_5$H$_4$), 5.31 (1H, s, CH) and 7.25 – 7.50 (15H, m, aromatic); δ_H(300 MHz, CDCl$_3$) isomer 2: 2.15 (3H, d, CH$_3$), 4.24 (5H, s, C$_5$H$_5$ and 1H, m, C$_5$H$_4$), 4.38 (1H, m, C$_5$H$_4$), 4.60 (1H, m, C$_5$H$_4$), 4.80 (1H, m, C$_5$H$_4$), 5.45 (1H, s, CH) and 7.25 – 7.50 (15H, m, aromatic). Note: Upon dissolving solid crystalline isomer 1 in CDCl$_3$ isomerization to the two isomers immediately sets in.

4.2.10 [Ir(I)(β-diketone)(cod)] complexes {27}-{34}.

4.2.10.1 [Ir(I)(β-diketonato)(cod)] complexes {27} – {31} with a non-ferrocene-containing β-diketonato ligand.

The general procedure was as follows. To a stirred solution of [Ir$_2$Cl$_2$(cod)$_2$] (0.1 g, 0.15 mmol) (chloro-1,5-cyclooctadiene iridium(I) dimer) and NaHCO$_3$ (13 mg, 0.15 mmol) in DMF (4 ml) was added an excess of β-diketone. After 15 s of stirring the crude product [Ir(β-diketone)(cod)] was **immediately** precipitated with ice water (10 ml), stirred for 5 – 10 min until the product crystallised from the solution. The product was filtered off, washed with water, filtered again and dried over P$_2$O$_5$ in a vacuum desicator. Spectroscopically pure [Ir(β-diketone)(cod)] complexes {27}-{31} were obtained up to 77 % yield.

(η^4-1,5-cyclooctadiene)(2,4-pentanedionate-κ^2O,O')iridium(I) [Ir(acac)(cod)] {27}, 92 % yield; m.p. 210 ^{0}C; δ_H(300 MHz, CDCl$_3$) 1.64 (4H, m, half of aliphatic C$_8$H$_{12}$ protons), 2.02 (6H, s, CH$_3$), 2.27 (4H, m, other half of aliphatic C$_8$H$_{12}$ protons), 3.99 (4H, m, olefinic protons of C$_8$H$_{12}$) and 5.54 (1H, s, CH).

(η^4-1,5-cyclooctadiene)(1,1,1-trifluoro-2,4-pentanedionate-κ^2O,O')iridium(I) [Ir(tfaa)(cod)]
{28}, 74% yield; δ_H(300 MHz, CDCl$_3$) 1.70 (4H, m, half of aliphatic C$_8$H$_{12}$ protons), 2.16 (3H, t, CH$_3$), 2.27 (4H, m, other half of aliphatic C$_8$H$_{12}$ protons), 4.14 (4H, m, olefinic protons of C$_8$H$_{12}$) and 5.96 (1H, s, CH).

(η^4-1,5-cyclooctadiene)(1,1,1-trifluoro-2,4-hexanedionato-κ^2O,O')iridium(I) [Ir(tfhd)(cod)]
{29}, 77% yield; m.p. 150 ^{0}C; δ_H(300 MHz, CDCl$_3$) 1.15 (3H, t, CH$_3$), 1.69 (4H, m, half of aliphatic C$_8$H$_{12}$ protons), 2.29 (4H, m, other half of aliphatic C$_8$H$_{12}$ protons), 2.42 (2H, mt, CH$_2$), 4.14 (4H, m, olefinic protons of C$_8$H$_{12}$) and 5.97 (1H, s, CH).

(η^4-1,5-cyclooctadiene)(1,1,1-trifluoro-5-methyl-2,4-hexanedionato-κ^2O,O')iridium(I)
[Ir(tfdma)(cod)] {30}, 68% yield; m.p. 118 ^{0}C; δ_H(300 MHz, CDCl$_3$) 1.14 (6H, d, CH$_3$), 1.69 (4H, m, half of aliphatic C$_8$H$_{12}$ protons), 2.29 (4H, m, other half of aliphatic C$_8$H$_{12}$ protons), 2.65 (1H, m, CH$_3$), 4.14 (4H, m, olefinic protons of C$_8$H$_{12}$) and 5.98 (1H, s, CH).

(η^4-1,5-cyclooctadiene)(1,1,1-trifluoro-5,5-dimethyl-2,4-hexanedionato-κ^2O,O')iridium(I)
[Ir(tftma)(cod)] {31}, 59% yield; m.p. 164 ^{0}C; δ_H(300 MHz, CDCl$_3$) 1.19 (9H, s, CH$_3$), 1.69 (4H, m, half of aliphatic C$_8$H$_{12}$ protons), 2.29 (4H, m, other half of aliphatic C$_8$H$_{12}$ protons), 4.14 (4H, m, olefinic protons of C$_8$H$_{12}$) and 6.13 (1H, s, CH).

4.2.10.2   (η^4-1,5-cyclooctadiene)(1-ferrocenyl-4,4,4-trifluoro-1,3-butanedionato-κ^2O,O')iridium(I) [Ir(fctfa)(cod)] {32}.

To a stirred solution of [Ir$_2$Cl$_2$(cod)$_2$] (0.2 g, 0.3 mmol) (chloro-1,5-cyclooctadiene iridium(I) dimer) in DMF (5 ml) was added solid Hfctfa (195mg, 0.6 mmol). After 30 s of stirring the crude product [Ir(fctfa)(cod)] was **immediately** precipitated with 10 ml of ice water and stirred for 5 min until the product crystallised from the solution. The crude unstable product was filtered off, washed with water, filtered again and dried over P$_2$O$_5$ in a vacuum desicator, (352 mg, 94% yield); m.p. 138 ^{0}C; δ_H(300 MHz, CDCl$_3$) 1.70 (4H, m, half of aliphatic C$_8$H$_{12}$ protons), 2.32 (4H, m, other half of aliphatic C$_8$H$_{12}$ protons), 4.12 (4H, m, 4H olefinic protons of C$_8$H$_{12}$), 4.22 (5H, s, C$_5$H$_5$), 4.59 (2H, t, C$_5$H$_4$), 4.82 (2 H, t, C$_5$H$_4$) and 6.12 (1H, s, CH). The crude product could not be purified on a kieselgel column and had to be used within two days of preparation.

4.2.10.3 (η^4-1,5-cyclooctadiene)(1-ferrocenyl-1,3-butanedionato-$\kappa^2 O,O'$)iridium(I) [Ir(fca)(cod)] {33}.

To a stirred solution of [Ir$_2$Cl$_2$(cod)$_2$] (0.2 g, 0.3 mmol) (chloro-1,5-cyclooctadiene iridium(I) dimer) and NaHCO$_3$ (25 mg, 0.3 mmol) in DMF (10 ml) was added a solution of Hfca (162 mg, 0.6 mmol) in DMF (2 ml). After 15 s of stirring the crude product [Ir(fca)(cod)] was **immediately** precipitated with 10 ml of ice water and stirred for 3 – 10 min until the product crystallised from the solution. The crude, impure and unstable product was filtered off, washed with water, filtered again and dried over P$_2$O$_5$ in a vacuum desicator, (284 mg, 83% yield); m.p. 138 ^{0}C; δ_H(300 MHz, CDCl$_3$) 1.67 (4H, m, half of aliphatic C$_8$H$_{12}$ protons), 2.08 (3H, s, CH$_3$), 2.32 (4H, m, other half of aliphatic C$_8$H$_{12}$ protons), 4.00 (4H, m, olefinic protons of C$_8$H$_{12}$), 4.17 (5H, s, C$_5$H$_5$), 4.42 (2H, t, C$_5$H$_4$), 4.73 (2H, t, C$_5$H$_4$) and 5.79 (1H, s, CH). The crude product could not be purified by chromatography on kieselgel and had to be used within two days of synthesis.

4.2.10.4 (η^4-1,5-cyclooctadiene)(1-ferrocenyl-3-phenyl-1,3-propanedionato-$\kappa^2 O,O'$)iridium(I) [Ir(bfcm)(cod)] {34}.

To a stirred solution of [Ir$_2$Cl$_2$(cod)$_2$] (0.22 g, 0.33 mmol) (chloro-1,5-cyclooctadiene iridium(I) dimer, Strem Chemicals) and NaHCO$_3$ (25 mg, 0.3 mmol) in DMF (10 ml) was added a solution of Hfca (200 mg, 0.6 mmol) in DMF (5 ml). After 15 s of stirring the crude product [Ir(bfcm)(cod)] was **immediately** precipitated with 10 ml of ice water, stirred for 3 – 10 min until the product crystallised from the solution. The impure crude product was filtered off, washed with water, filtered again and dried over P$_2$O$_5$ in a vacuum desicator, (250 mg, 66% yield); m.p. 218 ^{0}C; δ_H(300 MHz, CDCl$_3$) 1.72 (4H, m, half of aliphatic C$_8$H$_{12}$ protons), 2.35 (4H, m, other half of aliphatic C$_8$H$_{12}$ protons), 4.11 (4H, m, 4 olefinic protons of C$_8$H$_{12}$), 4.20 (5 H, s, C$_5$H$_5$), 4.46 (2H, t, C$_5$H$_4$), 4.83 (2H, t, C$_5$H$_4$), 6.46 (1H, s, CH), 7.39 – 7.60 (3H, m, C$_6$H$_5$) and 7.85 – 8.00 (2H, m, C$_6$H$_5$). The crude compound was not stable and had to be used within two days of synthesis. A sample was purified on a short kieselgel column. Most of the product was fixated on the column, but if a short (100 mm) column was packed and eluted under pressure (100 mm Hg), a *very* small fraction of pure [Ir(bfcm)(cod)] was obtained (< 15 mg, 4% yield). This purified sample was stable for longer than 3 months.

4.2.11 Ir(III) complexes.

4.2.11.1 **Dichloro(η^4-1,5-cyclooctadiene)(1-ferrocenyl-4,4,4-trifluoro-1,3-butanedionato-κ^2O,O')iridium(III) [IrCl$_2$(fctfa)(cod)] {35}.**

To a stirred solution of [Ir$_2$Cl$_2$(cod)$_2$] (0.1 g, 0.15 mmol) (chloro-1,5-cyclooctadiene iridium(I) dimer) in DMF (3 ml) was added a solution of Hfctfa (97 mg, 0.3 mmol) in DMF (3 ml). After 30 min of stirring the crude product [IrCl$_2$(fctfa)(cod)] was precipitated with ice water (2 ml), extracted with ether (200 ml), washed with water, dried (MgSO$_4$) and the solvent removed under reduced pressure. Flash column chromatography (R$_f$ = 0.30 (eluent ether-hexane 2:3 by volume) afforded {35}, (32.3 mg, 16 % yield); m.p. 248 ^{0}C; δ_H(300 MHz, CDCl$_3$) 2.24 (4H, m, half of aliphatic C$_8$H$_{12}$ protons), 2.97 (4H, m, other half of aliphatic C$_8$H$_{12}$ protons), 4.35 (5H, s, C$_5$H$_5$), 4.64 (2H, t, C$_5$H$_4$), 4.83 (2 H, t, C$_5$H$_4$), 5.79 (4H, m, 4H olefinic protons of C$_8$H$_{12}$) and 6.13 (1H, s, CH).

4.2.11.2 **Dichloro(η^4-1,5-cyclooctadiene)(1-ferrocenyl-1,3-butanedionato-κ^2O,O')iridium(III) [IrCl$_2$(fca)(cod)] {36}.**

To a stirred solution of [Ir$_2$Cl$_2$(cod)$_2$] (0.1 g, 0.15 mmol) (chloro-1,5-cyclooctadiene iridium(I) dimer) in DMF (3 ml) was added a solution of Hfca (81 mg, 0.3 mmol) in DMF (3 ml). After 45 min of stirring the crude product [IrCl$_2$(fca)(cod)] was precipitated with concentrated NaCl (10 ml) and filtered. Flash column chromatography (R$_f$ = 0.25 (eluent benzene-hexane 7:1 by volume) afforded {36}, (31.9 mg, 17 % yield); m.p. 231 ^{0}C; δ_H(300 MHz, CDCl$_3$) 2.21 (3H, s, CH$_3$), 2.26 (4H, m, half of aliphatic C$_8$H$_{12}$ protons), 2.96 (4H, m, other half of aliphatic C$_8$H$_{12}$ protons), 4.30 (5H, s, C$_5$H$_5$), 4.44 (2H, t, C$_5$H$_4$), 4.75 (2H, t, C$_5$H$_4$), 5.72 (4H, m, olefinic protons of C$_8$H$_{12}$) and 5.84 (1H, s, CH).

4.2.11.3 **Dichloro(η^4-1,5-cyclooctadiene)(1-ferrocenyl-3-phenyl-1,3-propanedionato-κ^2O,O')iridium(III) [IrCl$_2$(bfcm)(cod)] {37}.**

To a stirred solution of [Ir$_2$Cl$_2$(cod)$_2$] (0.1 g, 0.15 mmol) (chloro-1,5-cyclooctadiene iridium(I) dimer) in DMF (3 ml) was added a solution of Hbfcm (100 mg, 0.3 mmol) in DMF (3 ml). After 20 min of stirring the crude product [IrCl$_2$(bfcm)(cod)] was precipitated with concentrated NaCl (10 ml) and filtered. Flash column chromatography (R$_f$ = 0.46 (eluent ether-hexane 2:3 by volume) afforded {37}, (18 mg, 9.5 % yield); m.p. 195 ^{0}C; δ_H(300 MHz, CDCl$_3$) 2.29 (4H, m,

half of aliphatic C_8H_{12} protons), 2.99 (4H, m, other half of aliphatic C_8H_{12} protons), 4.32 (5 H, s, C_5H_5), 4.48 (2H, t, C_5H_4), 4.84 (2H, t, C_5H_4), 5.80 (4H, m, 4 olefinic protons of C_8H_{12}), 6.44 (1H, s, CH), 7.37 – 7.56 (3H, m, C_6H_5) and 7.84 – 7.89 (2H, m, C_6H_5).

4.2.11.4   Dichloro(η^4-1,5-cyclooctadiene)(1,3-diferrocenyl-1,3-propanedionato-κ^2O,O')iridium(III)   [IrCl$_2$(dfcm)(cod)] {38}.

To a stirred solution of [Ir$_2$Cl$_2$(cod)$_2$] (0.1 g, 0.15 mmol) (chloro-1,5-cyclooctadiene iridium(I) dimer) in DMF (3 ml) was added a solution of Hdfcm (132 mg, 0.3 mmol) in DMF (3 ml). After 45 min of stirring the crude product [IrCl$_2$(dfcm)(cod)] was precipitated with concentrated NaCl (10 ml) and filtered. Flash column chromatography (R_f = 0.35 (eluent benzene-hexane 7:1 by volume) afforded {38}, (12.7 mg, 5 % yield); m.p. > 255 ^{0}C; δ_H(300 MHz, CDCl$_3$) 2.29 (4H, m, half of aliphatic C_8H_{12} protons), 3.00 (4H, m, other half of aliphatic C_8H_{12} protons), 4.33 (10H, s, 2C_5H_5), 4.44 (4H, t, half of 2C_5H_4), 4.67 (4H, m, half of 2C_5H_4), 5.73 (4H, m, olefinic protons of C_8H_{12}) and 6.13 (1H, s, CH).

4.2.11.5   [Ir(β-diketonato)(CH$_3$)(I)(cod)] complexes.

The general procedure was as follows. An excess MeI was added to [Ir(β-diketonate)(cod)] (100mg) {27}, {32} and {33} dissolved in acetone (30 ml). The reaction vessel was sealed for 60 min. [Ir(β-diketonate)(CH$_3$)(I)(cod)] crystallised from the reaction mixture as the acetone was allowed to evaporate. Characterization data are as follows.

(η^4-1,5-cyclooctadiene)iodomethyl(2,4-pentanedionate-κ^2O,O')iridium(III)

[Ir(acac)(CH$_3$)(I)(cod)] {39}, 39% yield; m.p. 229 ^{0}C; δ_H(300 MHz, CDCl$_3$) 1.92 (2H, m, quarter of aliphatic C_8H_{12} protons), 2.01 (6H, s, CH$_3$ β-diketone), 2.19 (2H, m, quarter of aliphatic C_8H_{12} protons), 2.22 (3H, s, CH$_3$), 2.62 (2H, m, quarter of aliphatic C_8H_{12} protons), 3.11 (2H, m, quarter of aliphatic C_8H_{12} protons), 4.21 (2H, m, half of olefinic protons of C_8H_{12}), 5.21 (2H, m, other half of olefinic protons of C_8H_{12}) and 5.61 (1H, s, CH).

(η^4-1,5-cyclooctadiene)iodomethyl(1-ferrocenyl-4,4,4-trifluoro-1,3-butanedionato-κ^2O,O')iridium(III) [Ir(fctfa)(CH$_3$)(I)(cod)] {40}, Flash column chromatography (R_f = 0.38 (eluent ether-hexane 2:3 by volume) afforded 22% yield; m.p. 220 ^{0}C; δ_H(300 MHz, CDCl$_3$) 1.95 (2H, m, quarter of aliphatic C_8H_{12} protons), 2.22 (2H, m, quarter of aliphatic C_8H_{12} protons),

2.31 (3H, s, CH$_3$), 2.66 (2H, m, quarter of aliphatic C$_8$H$_{12}$ protons), 3.17 (2H, m, quarter of aliphatic C$_8$H$_{12}$ protons), 4.28 (2H, m, half of olefinic protons of C$_8$H$_{12}$), 4.41 (5 H, s, C$_5$H$_5$), 4.59 (2H, t, C$_5$H$_4$), 4.74 (2H, t, C$_5$H$_4$), 5.33 (2H, m, other half of olefinic protons of C$_8$H$_{12}$) and 6.15 (1H, s, CH).

(η^4-1,5-cyclooctadiene)iodomethyl(1-ferrocenyl-1,3-butanedionato-κ^2O,O')iridium(III)

[Ir(fca)(CH$_3$)(I)(cod)] {41}, 33% yield; m.p. 221 ^{0}C; δ_H(300 MHz, CDCl$_3$) 1.96 (2H, m, quarter of aliphatic C$_8$H$_{12}$ protons), 2.06 (3H, s, CH$_3$ β-diketone), 2.23 (2H, m, quarter of aliphatic C$_8$H$_{12}$ protons), 2.27 (3H, s, CH$_3$), 2.63 (2H, m, quarter of aliphatic C$_8$H$_{12}$ protons), 3.16 (2H, m, quarter of aliphatic C$_8$H$_{12}$ protons), 4.21 (2H, m, half of olefinic protons of C$_8$H$_{12}$), 4.33 (5 H, s, C$_5$H$_5$), 4.40 (2H, t, C$_5$H$_4$), 4.67 (2H, m, C$_5$H$_4$), 5.25 (2H, m, other half of olefinic protons of C$_8$H$_{12}$) and 5.87 (1H, s, CH).

4.3   Spectroscopic, kinetic and pK$_a$ measurements.

NMR measurements at 289 K were recorded on a Bruker Advance DPX 300 NMR spectrometer [^{1}H (300 MHz), ^{13}C (75.476 MHz) and ^{31}P (121.497 MHz)]. The chemical shifts are reported relative to SiMe$_4$ (0 ppm) for the ^{1}H spectra and relative to 85% H$_3$PO$_4$ (0 ppm) for the ^{31}P spectra (positive shifts downfield). The ^{13}C chemical shift is referenced to CDCl$_3$ as internal standard, δ^{13}C = 77.04 ppm.

Kinetic measurements were monitored on a Hitachi 270-50 infrared spectrometer, a GBC-916 UV/visible spectrometer and a Bruker Advance DPX 300 NMR spectrometer [^{1}H (300MHz) and ^{31}P{^{1}H} (121.497 MHz)] for slow reactions and on a Durrum D110 stopped flow instrument for the fast reactions.

The activation parameters ΔH* (activation enthalpy) and ΔS* (activation entropy), for the oxidative addition and substitution reactions were determined from the least-squares fits of the reaction rate constants *vs.* temperature data according to the Arrhenius equation, **Equation 4.1**, or rewritten in linear form as **Equation 4.2**. The activation free energy ΔG* = ΔH* - TΔS*.

Equation 4.1:
$$k = \frac{RT}{Nh} e^{\frac{-\Delta H^*}{RT}} e^{\frac{\Delta S^*}{R}}$$

Equation 4.2:
$$\ln \frac{k}{T} = -\frac{\Delta H^*}{RT} + \frac{\Delta S^*}{R} + \ln \frac{R}{Nh}$$

h = Planck constant = 6.625 x 10^{-34} Js, N = Avogadro's number = 6.023 x 10^{23} mol^{-1}, R = universal gas constant = 8.314 J mol^{-1} K^{-1}

4.3.1 Oxidative addition reactions.

Oxidative addition reactions were monitored on the IR (by monitoring formation and disappearance of the carbonyl peaks), UV/visible (by monitoring the change in absorbance at the specified wavelength) and NMR (by monitoring the change in integration units of the specified signals) spectrophotometers. All kinetic measurements were monitored under pseudo-first-order conditions with [MeI] seven to 10000 times the concentration of the [Rh(β-diketonate)(CO)(PPh$_3$)] complex in the specified solution.   The concentration [Rh(β-diketonate)(CO)(PPh$_3$)] $\cong$ 0.0004 mol dm^{-3} for UV/visible measurements and $\cong$ 0.025 mol dm^{-3} for IR and NMR measurements. Kinetic measurements under pseudo-first-order conditions for different concentrations of a [Rh(β-diketonate)(CO)(PPh$_3$)] complex, for a constant [MeI] confirmed that the concentration [Rh(β-diketonate)(CO)(PPh$_3$)] did not influence the value of the observed kinetic rate constant. The observed first-order rate constants were obtained from least-squares fits of absorbance *vs* time data.[16] For reactions exhibiting biphasic kinetics, the linear portion of the plot plot ln(A$_t$-A1) *vs*. time of gives rate constants for the second stage (k$_3$). The intercept x and slope k$_3$ allowed the modified plot of ln(A1-A$_t$+xexp(-k$_3$t)) *vs*. time, t, to be carried out. The slope yielding rate constants k$_{1obs}$ for the first stage (A$_t$ = absorbance at time t, A1 = absorbance at t = ∞).

4.3.2 Substitution kinetics.

Substitution reaction rate constants were obtained by following the formation of the reaction product of [M(β-diketonate)(cod)] (M = Rh, Ir) with 1,10 phenantroline at the specified

---

[16] MINSQ, Least squares parameter Estimation, Version 3.12, MicroMath, 1990.

wavelength, in the specified solvent, using a Durrum stopped-flow spectrophotometer, model D-10. The concentration of the [M(β-diketonate)(cod)] complexes were $0.00007 - 0.0010$ mol dm^{-3} with an excess of at least seven fold of phenanthroline ($0.0005 - 0.050$ mol dm^{-3}) for all runs in order to achieve pseudo-first-order reaction conditions. Kinetic measurements under pseudo-first-order conditions for different concentrations of a [M(β-diketonate)(cod)] complex, for a constant [MeI] confirmed that the concentration [M(β-diketonate)(cod)] did not influence the value of the observed kinetic rate constant. The observed first-order rate constants were obtained from least-squares fits of absorbance *vs* time data.[16] First-order plots were obtained for at least two half-lives.

4.3.3 Acid dissociation constant determinations.

The pK$_a$ values were determined by measuring the absorbance at different pH during an acid-base titration in water or acetonitrile-water mixtures, 1:9 by volume, $\mu = 0.100$ mol dm^{-3} (NaClO$_4$) at 21.0(1) ^{0}C. β-Diketone concentrations were where possible less than 0.2 mmol dm^{-3}. A linear response by the pH meter (Hanna instruments model HI 9321), fitted with a glass electrode, was ensured by calibration with commercial buffers (Sigma) at pH = -log α_H = 4.01, 7.00 and 12.00 respectively, α_H = activity of H$^+$. A test pK$_a$ determination was then performed by titrating the well characterized compound acetylacetone with sodium hydroxide. A least squares fit of the obtained UV absorbance/pH data for this titration using **Equation 4.3**, utilising the fitting program MINSQ,[16] resulted in a pK$_a$ of 8.95(8) in water. This was within experimental error the same as the best available published pK$_a$ for acetylacetone in water (8.878(5) when $\mu = 1$ mol dm^{-3} and 8.98 when $\mu = 0.0172$ mol dm^{-3}).[17] It was therefore concluded that the electrode was calibrated to measure hydrogen ion activity under the conditions used. It is not expected that the electrode would behave differently for any of the other pK$_a$ determinations because only pK$_a$ values of a series of β-diketones were determined. The pK$_a$ values were determined by measuring the UV absorbance/pH data with titration from high to low pH and a least squares fit of the absorbance/pH data using **Equation 4.3**.

---

[17] Martell, A.E., *Stability Constants of Metal-Ion Complexes,* The Chemical Society, London, Special Publication No. 25, 3rd edn., part II, 1971, p. 365.

Equation 4.3:
$$A_T = \frac{A_{HA}10^{-pH} + A_A 10^{-pK_a}}{10^{-pH} + 10^{-pK_a}}$$

with A_T = total absorbance, A_{HA} the absorbance of the β-diketone in the protonated form and A_A the absorbance of the β-diketone in the deprotonated (basic) form.

4.4 Electrochemistry.

Measurements on the specified concentrations (mmol dm^{-3}) of solutions of the complexes in acetonitrile containing 0.100 mol dm^{-3} tetra-*n*-butylammonium hexafluorophosphate (Fluka, electrochemical grade) as supporting electrolyte were conducted under a blanket of purified argon at 25.0 ^{0}C utilizing a BAS model CV-27 voltammograph[18] interfaced with a personal computer. A three-electrode cell, which utilized a Pt auxiliary electrode, a Pt (surface area 0.03142 cm^2) or a glassy carbon (surface area 0.0707 cm^2) working electrode, and a Ag/Ag$^+$ (0.0100 mol dm^{-3} AgNO$_3$) reference electrode[19] mounted on a Luggin capillary was used.[20] A salt bridge containing 0.1 mol dm^{-3} TBAPF$_6$/CH$_2$Cl$_2$ was used with the reference electrode for measurements in CH$_2$Cl$_2$ as solvent. Data, uncorrected for junction potentials, were collected with an Adalab-PC^{TM} and Adapt^{TM} data acquisition kit (Interactive Microwave, Inc.) with locally developed software, and analyzed with Hyperplot (JHM International, Inc.). All temperatures were kept constant to within 0.5^{0}C. Successive experiments under the same experimental conditions, shown that all formal reduction and oxidation potentials were reproduceable within 3 mV.

Bulk electrolysis was carried out on the BAS CV-27 voltammograph[18] at 25.0(1) °C. A three-electrode cell, which utilized a Pt wire auxiliary electrode (isolated from the sample by means of a salt bridge with 0.1 mol dm^{-3} TBAPF$_6$/CH$_3$CN), a glassy carbon working electrode (electro-

---

[18] *BAS CV-27 Voltammograph Instruction Manuel*, Bioanalytical Systems Inc., West Lafayette, Indiana (1994).

[19] Sawyer, D.T. and Roberts, J.L., Jr., *Experimental electrochemistry for chemists,* Wiley, New York. 1974. p.54.

[20] Evans, D.H., O'Connell, K.M., Peterson, R.A and Kelly, M.J., *J. Chem. Educ.* **60**, 291 (1983); Kissinger, PT. and Heineman, W.R., *J. Chem. Educ.* **60**, 702 (1983); van Benschoten, J.J., Lewis, J.Y. and Heineman, W.R*., J. Chem. Educ*. **60,** 772 (1983); Sawyer D.T. and Roberts, J.L., Jr., *Experimental electrochemistry for chemists*, Wiley, New York. 1974, p. 118; Mabbott, G.A., *J. Chem. Educ.* **60,** 697 (1983).

active area 3 cm^2) and a Ag/Ag$^+$ (0.0100 mol dm^{-3}, AgNO$_3$ in 0.1 mol dm^{-3} TBAPF$_6$/CH$_3$CN) reference electrode mounted on a Luggin capillary were employed. Current readings and the integrated current (coulombs) were recorded manually from the coulometer function at a different time t.

4.5 Crystallography.

4.5.1 Structure determination of Hfctfa.

Crystals of Hfctfa were obtained by recrystallizing from acetone-hexane (1:5 by volume). A dark red crystal was mounted on a glass fiber and intensity data were collected on a Rigaku AFC5R diffractometer using graphite monochromated Cu-Kα radiation and a rotating anode generator. Cell constants and an orientation matrix for data collection were obtained from a least-squares refinement using the setting angles of 25 carefully centered reflections in the range 62.88° < 2θ < 74.41°. Data were corrected for Lorentz and polarization effects. A correction for secondary extinction was applied. The structure was solved by direct methods[21] and expanded using Fourier techniques[22]. The non-hydrogen atoms were refined anisotropically. Hydrogen atoms were included but not refined. The locations of H10 and H11 (chapter 3 paragraph 3.8.1) were estimated from a difference Fourier synthesis. Neutral atom scattering factors were taken from Cromer and Waber.[23] Anomalous dispersion effects were included in F$_{calc}$;[24] the values for Δf' and Δf'' were those of Creagh and McAuley.[25] The values for the mass attenuation coefficients

[21] Altomare, A., Cascarano, M., Giacovazzo, C. and Guagliardi, A., *J. Appl. Crystallogr*., **26**, 343 (1993).

[22] Beurskens, P.T., Admiraal, G., Beurskens, G., Bosman, W.P., de Gelder, R., Israel, I. and Smits, J.M.M., *The DIRDIF-94 program system. Technical Report of the Crystallography Laboratory*, University of Nijmegen, The Netherlands, 1994.

[23] Cromer, D.T. and Waber, J.T., *International tables for X-ray crystallography*, **Vol. IV**, The Kynoch Press, Birmingham, Table 2.2 A, 1974.

[24] Ibers, J.A. and Hamilton, W.C., *Acta Cryst*., **17**, 781 (1964).

[25] Creagh, D.C. and McAuley, W.J., *International tables for crystallography,* **Vol. C**, Edited by A.J.C. Wilson, Kluwer Academic Publishers, Boston, Table 4.2.6.8, 1992. p. 219 - 222.

are those of Creagh and Hubell.[26] All calculations were performed using the teXsan[27] crystallographic software package of the Molecular Structure Corporation. Crystallographic detail is reported in paragraph 3.8.1, chapter 3. The final fractional coordinates are given in appendix C and refinement parameters are reported in paragraph 3.8.1, chapter 3.

4.5.2   *Structure determination of [Rh(fctfa)(CO)₂].*

Crystals of [Rh(fctfa)(CO)₂] were obtained by recrystallization from hot hexane by slowly cooling the reaction mixture. A dark red block crystal having approximate dimentions of 0.10 x 0.18 x 0.22 mm was mounted on a glass fiber and intensity data were collected on a Rigaku AFC5R diffractometer using graphite monochromated Mo-Kα radiation and a rotating anode generator. Cell constants and an orientation matrix for data collection were obtained from a least-squares refinement using the setting angles of 25 carefully centered reflections in the range $28.44° < 2\theta < 36.52°$. Data were corrected for Lorentz and polarization effects. A correction for secondary extinction was applied. The structure was solved by direct methods[28] and expanded using Fourier techniques[22]. The non-hydrogen atoms were refined anisotropically, while the rest were refined isotropically.   Hydrogen atoms were included but not refined.   Neutral atom scattering factors were taken from Cromer and Waber.[23] Anomalous dispersion effects were included in F_{calc};[24] the values for $\Delta f'$ and $\Delta f''$ were those of Creagh and McAuley.[25] The values for the mass attenuation coefficients are those of Creagh and Hubell.[26] All calculations were performed using the teXsan[27] crystallographic software package of the Molecular Structure Corporation. Crystallographic detail is reported in paragraph 3.8.2 chapter 3. The final fractional coordinates are given in appendix C and refinement parameters are reported in paragraph 3.8.2 chapter 3.

---

[26] Creagh, D.C. and Hubbell, J.H., *International tables for crystallography,* **Vol. C**, Edited by A.J.C. Wilson, Kluwer Academic Publishers, Boston, Table 4.2.4.3, p.200 - 206.

[27] *TeXan for windows: crystal structure analysis package*. Molecular Structure Corporation, The Woodlands, Tex. 1997.

[28] Sheidrick, G.M., *SHELXS86, in: Crystallographic Computing 3,* (Eds G.M. Sheldrick, C. Kruger and R. Goddard), Oxford University Press, pp.175-189 (1985).

4.5.3   *Structure determination of [Rh(fctfa)(CO)(PPh₃)].*

Crystals of [Rh(FcTFA)(CO)(PPh₃)] were obtained by recrystallization from hot hexane by slowly cooling the reaction mixture. The density was determined by flotation in sodium iodide solution. A crystal of dimensions 0.25 x 0.15 x 0.30 mm was used for data collection on an Enraf-Nonius CAD-4F diffractometer with graphite-monochromated Mo $K\alpha$ radiation. The $\omega/2\theta$-scan technique was used with variable scan width $\Delta\omega = (0.43 + 0.34\tan\theta)°$, scan speed 5.49° min^{-1} in ω and a maximum scan time of 60 s per reflection. The unit cell parameters were determined from least-squares refinement of 25 reflections with $6 < \theta < 18°$ (total measuring range $3 < \theta < 30°$). Empirical absorption corrections[29] were applied with minimum and maximum correction factors of 0.94 and 1.00 respectively. The mean intensity of three standard reflections, measured over 7200 s of X-ray exposure time, varied from the initial value by <-1%. All possible reflections with $(\sin\theta)/\lambda < 0.70$ Å^{-1} in the range $0 < h < 14$, $-17 < k < 17$, $-18 < l < 18$ were measured, giving 7733 unique reflections of which 6083 were considered observed [$I > 3.0\sigma(I)$]. The structure was solved by the heavy-atom method using *SHELXS86*[30] and was subjected to anisotropic full-matrix least-squares refinement on F (a total of 380 parameters refined) using *SHELXS76*[31]. The H-atom positions were calculated riding on the adjacent C atoms assuming C-H = 1.08 Å, and were refined with an overall temperature factor. Neutral-atom scattering factors were taken from Cromer & Mann[32] and anomalous-dispersion corrections for rhodium from *International Tables for X-ray Crystallography.*[33] Final $R = 0.045$ and wR = 0.044 (unit weights), $(\Delta\rho)_{max} = 0.66$, $(\Delta\rho)_{min} = -0.41$ eÅ^{-3} and $(\Delta/\sigma)_{max} = 0.35$. S was not calculated. The final fractional coordinates are given in appendix C and selected geometrical parameters in chapter 3 paragraph 3.8.3.[34]

[29] North, A.C.T., Phillips, D.C. and Matthews,, F.S. *Acta Cryst.,* **A24**, 352-359.

[30] Sheldrick, G.M., *Acta Cryst.,* **A46,** 467, (1990).

[31] Sheldrick, G.M., *SHELX*76, Program for crystal structure determination, University of Chambridge, England, 1976.

[32] Cromer, D.T. & Mann, J., *Acta. Cryst.,* **A24,** 321 (1968).

[33] *International Tables for X-ray Crystallography,* Vol. III, 1962, p.216.

[34] Johnson, C.K. *ORTEP*II, Report ORNL-5138, Oak Ridge National Laboratory, Tennessee, USA 1976.

4.5.4   *Structure determination of [Rh(fctfa)(CH₃)(I)(CO)(PPh₃)].*

Crystals of [Rh(fctfa)(CH₃)(I)(CO)(PPh₃)] were obtained during the work-up in the synthesis of the compound from hexane as described in 4.2.9 page 292. The density was determined by flotation in sodium iodide solution. A crystal of dimensions 0.075 x 0.150 x 0.650 mm was used for data collection on a Syntex P-1 diffractometer with Nb filtered, Mo $K\alpha$ radiation. The $\omega/2\theta$-scan technique was used with variable scan width $\Delta\omega = (0.43 + 0.34\tan\theta)°$, scan speed 5.49° min⁻¹ in ω and a maximum scan time of 60 s per reflection. The unit cell parameters were determined from least-squares refinement of 25 reflections with $15 < \theta < 20°$ (total measuring range $3 < \theta < 25°$). Empirical absorption corrections[35] were applied with minimum and maximum correction factors of 0.4529 and 0.7413 respectively. The mean intensity of three standard reflections, measured over 7200 s of X-ray exposure time, varied from the initial value by <-1%. All possible reflections with $(\sin\theta)/\lambda < 0.59$ Å⁻¹ in the range $-12 < h < 12, 0 < k < 18, 0 < l < 24$ were measured, giving 4420 unique reflections of which 4414 were considered observed [$I > 2.0\sigma(I)$]. The structure was solved by the heavy-atom method using *SHELXS86*[30] and was subjected to anisotropic full-matrix least-squares refinement on F (a total of 380 parameters refined) using *SHELXS93*[36]. The H-atom positions were calculated riding on the adjacent C atoms assuming C-H = 0.930 Å, and were refined with an overall temperature factor. Neutral-atom scattering factors were taken from Cromer & Mann[32] and anomalous-dispersion corrections for rhodium from *International Tables for X-ray Crystallography*[37] Final $R = 0.0588$ and wR = 0.1692 (unit weights), $(\Delta\rho)_{max} = 1.841$, $(\Delta\rho)_{min} = -1.087$ eÅ⁻³ and $(\Delta/\sigma)_{max} = -0.745$. The high value of the maximum residual electron density $(\Delta\rho)_{max}$ of 1.841 is due to irrelevant peaks near the heavy atoms Rh and Ir. The final fractional coordinates are given in appendix C and selected geometrical parameters in chapter 3 paragraph 3.8.4.[34]

---

[35] Akselrud, L.G., Grin, Yu. N., Zavalii, P. Yu., Pacharsky, V.K. and Fundamensky, V.S., *CSD-universal program package for single crystal and/or powder structure data refinement,* XII European Crystallographic Meeting, Moscow, August 1989, Collected Abstracts, v.**3**, p. 155.

[36] Sheldrick, G.M., *SHELX*93, Program for crystal structure determination, University of Göttingen, Germany, 1993.

[37] Wilson, A.J.C., ed., *International Tables for X-ray Crystallography,* Volume **C**, Kluver Academic Publishers, Dortrecht, 1992.
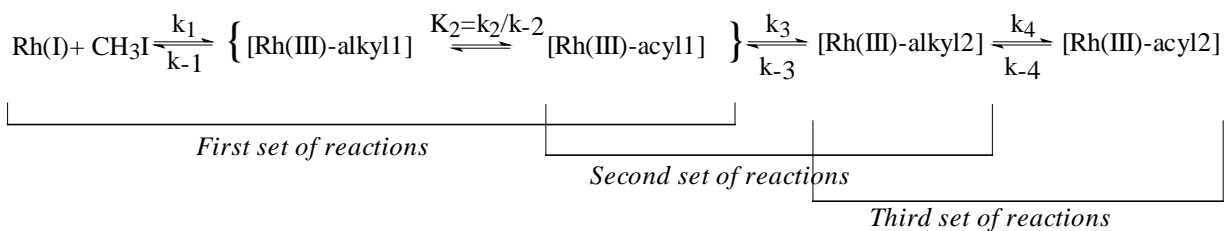
5 Summary.

Synthetic routes to prepare new β-diketonato rhodium(I) complexes of the type [Rh(FcCOCHCOR)(CO)$_2$] and [Rh(FcCOCHCOR)(CO)(PPh$_3$)] with Fc = ferrocenyl and R = Fc, C$_6$H$_5$, CH$_3$ and CF$_3$ have been developed and optimized. Optimized synthetic routes to complexes of the type [Ir(R'COCHCOR)(cod)], with R' = Fc and R = C$_6$H$_5$, CH$_3$ and CF$_3$, or with R' = CF$_3$ and R = CH$_2$CH$_3$, CH(CH$_3$)$_2$ and C(CH$_3$)$_3$ have also been developed. For the iridium complexes, short synthetic times (< 30 s) were especially important. NMR studies on FcCOCH$_2$COR indicate that enolization in a direction away from the ferrocenyl group always dominates. This observation was explained utilizing the solved crystal structure of FcCOCH$_2$COCF$_3$. The crystal structure of [Rh(fctfa)(CO)$_2$] was also solved.

From ^{1}H and ^{31}P NMR studies, it is clear that for complexes of the type [Rh(β-diketonato)(CO)(PPh$_3$)] with an unsymmetrical β-diketonato ligand, at least two main isomers exist in solution. For the (FcCOCHCOCF$_3$)$^-$ complex, the isomer that should dominate based on electronic considerations (χ_{Fc} = 1.87, χ_{Fc} = 3.01), is the isomer with PPh$_3$ *trans* to the ferrocenyl group. However, the structure determination of [Rh(fctfa)(CO)(PPh$_3$)] indicated that *crystallization energy*, rather than electronic or steric influences of the ferrocenyl group, resulted in crystallization of the isomer where PPh$_3$ is *cis* to the ferrocenyl group.

The chemical kinetics of oxidative addition of CH$_3$I to [Rh(FcCOCHCOR)(CO)(PPh$_3$)] has been studied in detail utilizing IR, UV/visible, ^{1}H NMR and ^{31}P NMR techniques. The NMR studies revealed that the rate of oxidative addition of iodomethane to the different [Rh(FcCOCHCOR)(CO)(PPh$_3$)] isomers was the same. Three definite sets of reactions involving at least two Rh(III)-alkyl and two Rh(III)-acyl species, as shown in the reaction sequence below, were observed. For the first time a complete general reaction sequence for the oxidative addition of iodomethane to complexes of the type [Rh(β-diketonate)(CO)(PPh$_3$)] could be provided. The same reaction sequence was demonstrated to be valid for bidentate ligands other than β-diketonates as well. All previously reported reaction sequences are just special cases of the following reaction sequence:

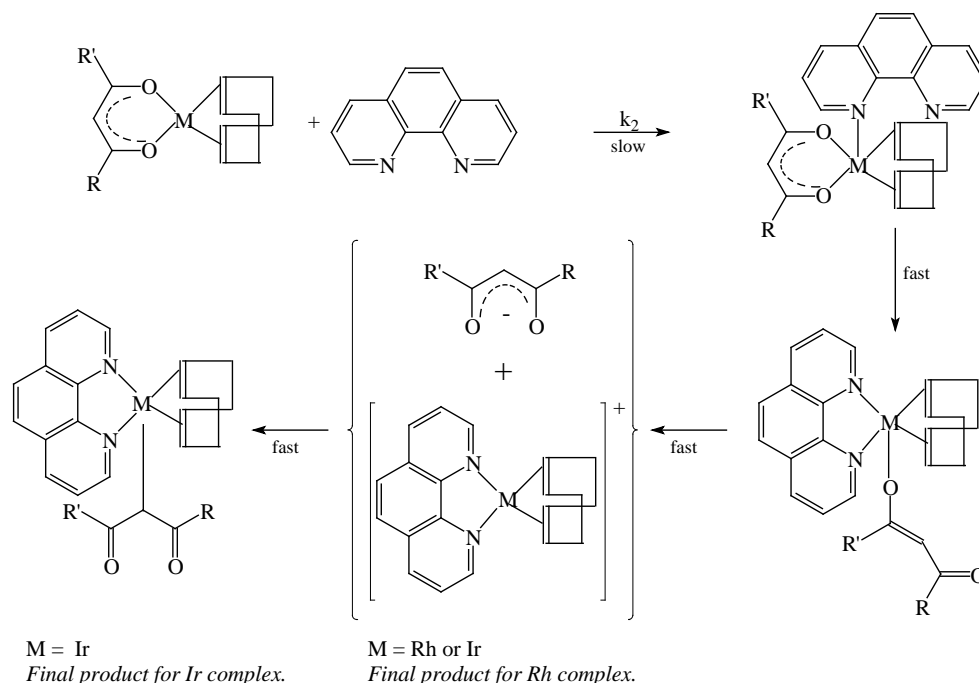$$\text{Rh(I)}+ \text{CH}_3\text{I} \underset{k_{-1}}{\overset{k_1}{\rightleftharpoons}} \left\{ \text{[Rh(III)-alkyl1]} \underset{}{\overset{K_2=k_2/k_{-2}}{\rightleftharpoons}} \text{[Rh(III)-acyl1]} \right\} \underset{k_{-3}}{\overset{k_3}{\rightleftharpoons}} \text{[Rh(III)-alkyl2]} \underset{k_{-4}}{\overset{k_4}{\rightleftharpoons}} \text{[Rh(III)-acyl2]}$$

First set of reactions

Second set of reactions

Third set of reactions

All rate constants except k_2 and k_{-2} were determined. The equilibrium K_2 was found to be fast enough in the CF_3 complex to be maintained during Rh(I) depletion. For the other complexes (R = Fc, C_6H_5 and CH_3), the equilibrium K_2 could not be maintained in full during the Rh(I) disappearance. In all cases investigated, K_2 could be maintained during the formation of the Rh(III)-alkyl2 species. This study also describes for the first time how to successfully determine the rate of conversion from Rh(III)-alkyl2 to Rh(III)-acyl2 species. A crystal structure determination of [Rh(fctfa)(CO)(PPh$_3$)(CH$_3$)(I)] provided an example of the structure of a Rh(III)-alkyl2 complex.

^{1}H and ^{31}P NMR studies further showed that all rhodium-containing complexes in the above mentioned reaction scheme, are actually composed of at least two main isomers, that is Rh(I)A $\overset{K_{c1}}{\rightleftharpoons}$ Rh(I)B, Rh(III)-alkyl 1A $\overset{K_{c2}}{\rightleftharpoons}$ Rh(III)-alkyl 1B, Rh(III)-acyl 1A $\overset{K_{c3}}{\rightleftharpoons}$ Rh(III)-acyl 1B, Rh(III)-alkyl 2A $\overset{K_{c4}}{\rightleftharpoons}$ Rh(III)-alkyl 2B, Rh(III)-acyl 2A $\overset{K_{c5}}{\rightleftharpoons}$ Rh(III)-acyl 2B. Values for K_{c1}, K_{c2}, K_{c3}, K_{c4} and K_{c5} were determined for the CF_3- and CH_3-complexes.

It was shown that the relative rates of oxidative addition of iodomethane to the [Rh(R'COCHCOR)(CO)(PPh$_3$)] complexes are dependant on the sum of the group electronegativities of the groups R' and R on the β-diketonato ligand (R'COCHCOR)$^-$, as well as the pK$_a$ of the free β-diketones.

The chemical kinetic study of the substitution of the β-diketonato ligand with 1,10-phenanthroline from [Rh(FcCOCHCOH)(cod)] and [Ir(FcCOCHCOR)(cod)] (R= CF$_3$, CH$_3$ and C$_6$H$_5$) showed that the rate of substitution becomes faster when the group electronegativity of the R groups increases. This tendency is, as expected, exactly the opposite to what was observed during oxidative addition. A general reaction mechanism for both Rh and Ir complexes is presented below. In the case of the *rhodium* complexes, the *last fast step was not observed,* and the final reaction product during the substitution reactions involving rhodium complexes, is the four coordinate complex [Rh(phen)(cod)]$^+$. For the iridium complexes the final reaction product

is the five coordinate species [Ir(C^3-β-diketonato)(phen)(cod)]. It is interesting to note that in the case of the iridium complexes, the β-diketonato coordination mode changed from κO,κO' to σ-C^3.

M = Ir
Final product for Ir complex.

M = Rh or Ir
Final product for Rh complex.

In an additional study the effect of bulkiness of R substituents on the rate of the β-diketonato substitution with 1,10-phenanthroline in complexes of the type [Ir(CF$_3$COCHCOR)(cod)] with R = CH$_3$, CH$_2$CH$_3$, CH(CH$_3$)$_2$ and C(CH$_3$)$_3$ was determined. No clear-cut steric retardation could be identified. All substitution reactions were independent of a solvent step implying the general substitution rate law

$$\text{Rate} = (k_s + k_2[\text{phen}]) [M(\beta\text{-diketonato})(\text{cod})] \text{ simplifies to}$$
$$\text{Rate} = k_2[\text{phen}][M(\beta\text{-diketonato})(\text{cod})]$$

where k_s (≈ 0) is the rate constant indicating solvent participation.

The cyclic voltammetry study of all the ferrocene-containing β-diketonato complexes of rhodium(I) and iridium(I) synthesized, exhibited a single electrochemically reversible couple corresponding to the formal reduction potential of the ferrocenyl group of the β-diketonato ligand coordinated to the rhodium or iridium complexes, as well as an electrochemically irreversible anodic oxidation peak which corresponds to the oxidation of the Rh and Ir. Bulk electrolysis showed that Rh(I) was oxidized to Rh(III), while Ir(I) was only oxidized to Ir(II). Except for the case of [Rh(β-diketonato)(CO)$_2$], the rhodium oxidation wave was always at potentials slightly less positive (*c.a.* 100 mV) than the oxidation wave of the ferrocenyl group. For the dicarbonyl complexes, oxidation of rhodium(I) occurred at potentials at least 470 mV more positive than

ferrocenyl oxidation. The Rh(III) reduction was observed at potentials at least 1000 mV more negative than the Rh(I) oxidation. This is consistent with the large amount of work that has to be performed in switching from four coordinate rhodium(I) complexes to six coordinate rhodium(III) complexes and back again. For all complexes studied, the formal reduction potentials of the ferrocenyl group and the oxidation potentials of rhodium or iridium became more positive when R substituents on the β-diketonato ligand became more electron-withdrawing. It was also shown that a linear relationship exists between the sum of the electronegativities of the groups R' and R on the β-diketonato ligand (R'COCHCOR)$^-$ and the formal oxidation potentials of the electrochemical irreversible rhodium and iridium centra to which the β-diketonato ligands are coordinated.

The ^{31}P NMR study on different six-membered chelate complexes, [Rh(L,L'-BID)(CO)(PPh$_3$)] and related Rh(III) complexes, indicated a general decrease in the coupling constant $^1J(^{31}$P-^{103}Rh) (in Hz), as the Rh-P bond length (in Å), determined by X-ray crystallography, increases. L,L'-BID is a bidentate ligand with donor atoms L and L', such as the β-diketonatos fctfa, tfhd, tftma, sacac *etc.* Utilizing the available results this relationship was quantified as

$$d(\text{Rh-P}) = -0.0014(1) \times {}^1J({}^{31}\text{P-}{}^{103}\text{Rh}) + 2.49(2),$$

with the Rh-P bond lengths, d(Rh-P), varying between 2.23 Å and 2.36 Å.

The electron density on the Rh(I) and Ir(I) metal centres was manipulated over a wide range by changing the R group on the coordinated ligand (FcCOCHCOR)$^-$ from the highly electron donating Fc group ($\chi_{Fc} = 1.87$) to C$_6$H$_5$, ($\chi_{Fc} = 2.21$) to CH$_3$($\chi_{Fc} = 2.34$) to the strongly electron withdrawing CF$_3$ group ($\chi_{Fc} = 3.01$). The effect of the different R groups on the β-diketonato ligand (FcCOCHCOR)$^-$ coordinated to the rhodium(I) and iridium(I) complexes was not only observed in kinetic rate constants, formal reduction potentials of the ferrocenyl group and the oxidation potential of Rh(I) or Ir(I), but also in physical quantities such as pK$_a$-values, IR stretching frequencies, and crystallographic bond lengths.

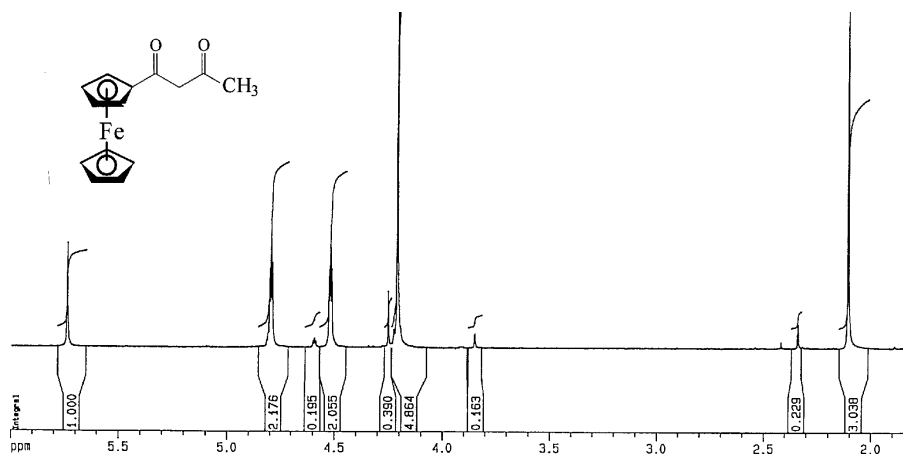The first two publications that partially describe results of this study includes:

1   du Plessis, W.C., Erasmus, J.C., Lamprecht, G.J., Conradie, J., Cameron, T.S., Aquino, M.A.S. and Swarts, J.C., *Can. J. Chem.*, **77**, 378 (1999).

2   Lamprecht, G.J., Swarts, J.C., Conradie, J., and Leipoldt, J.G., *Acta Cryst.*, **C49**, 82 (1993).
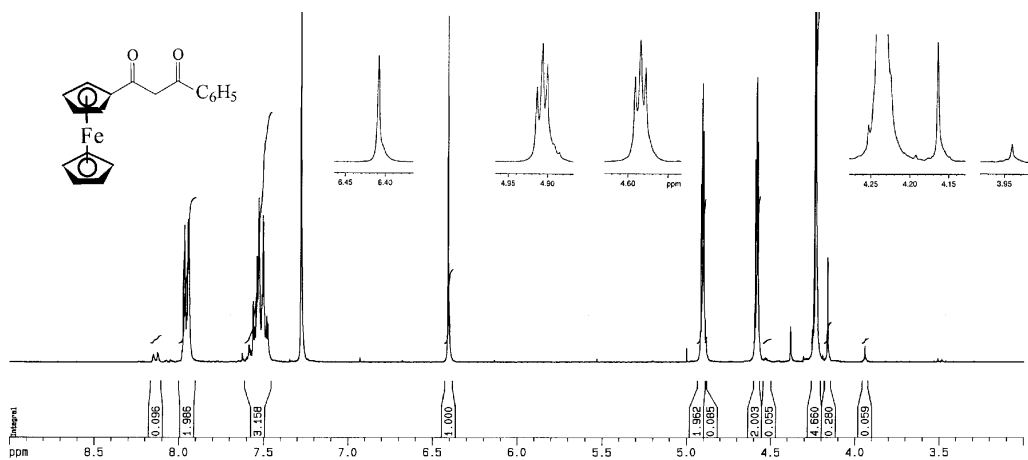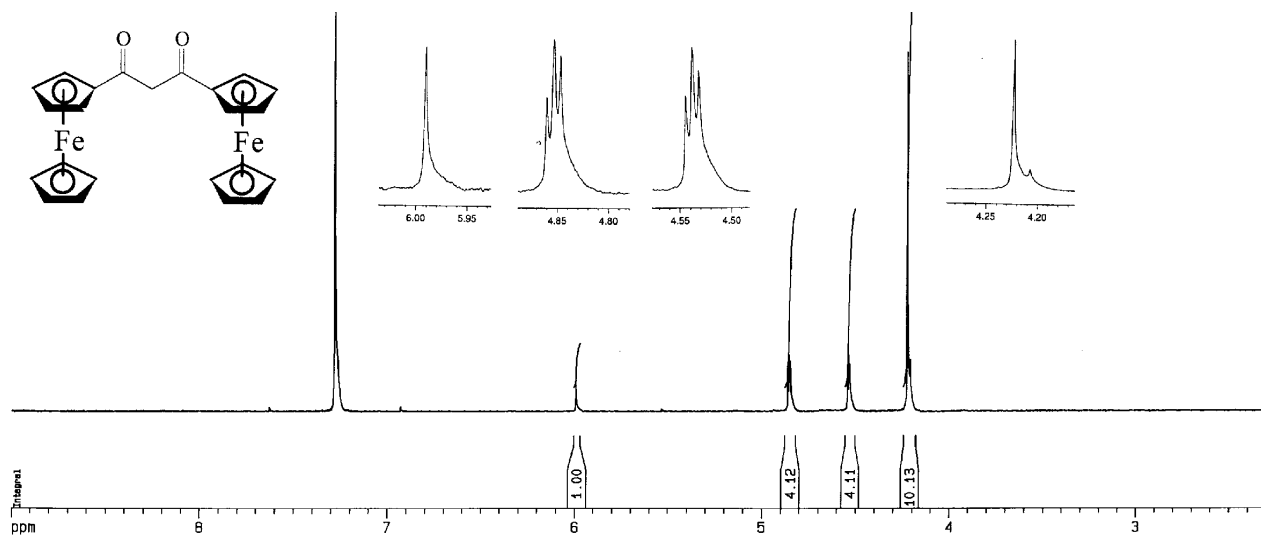
A ¹H NMR
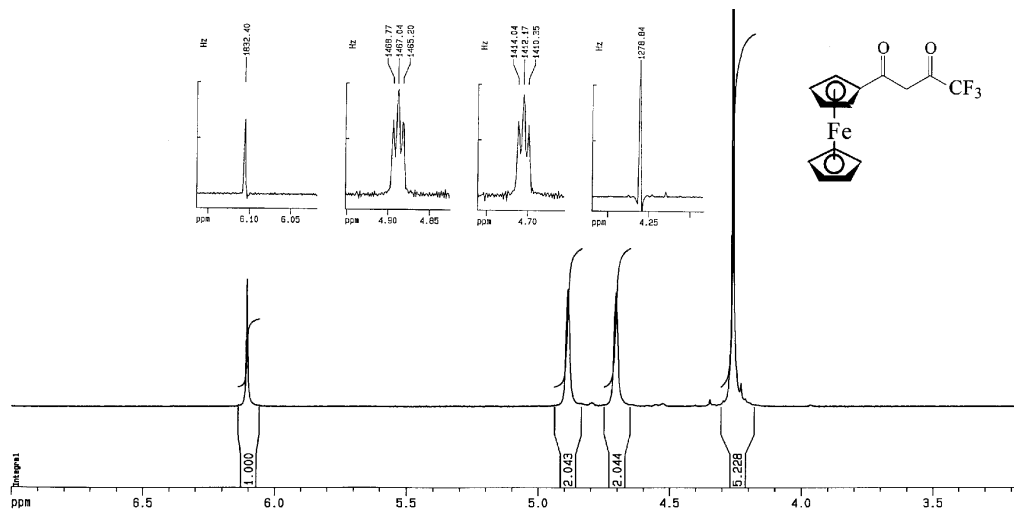
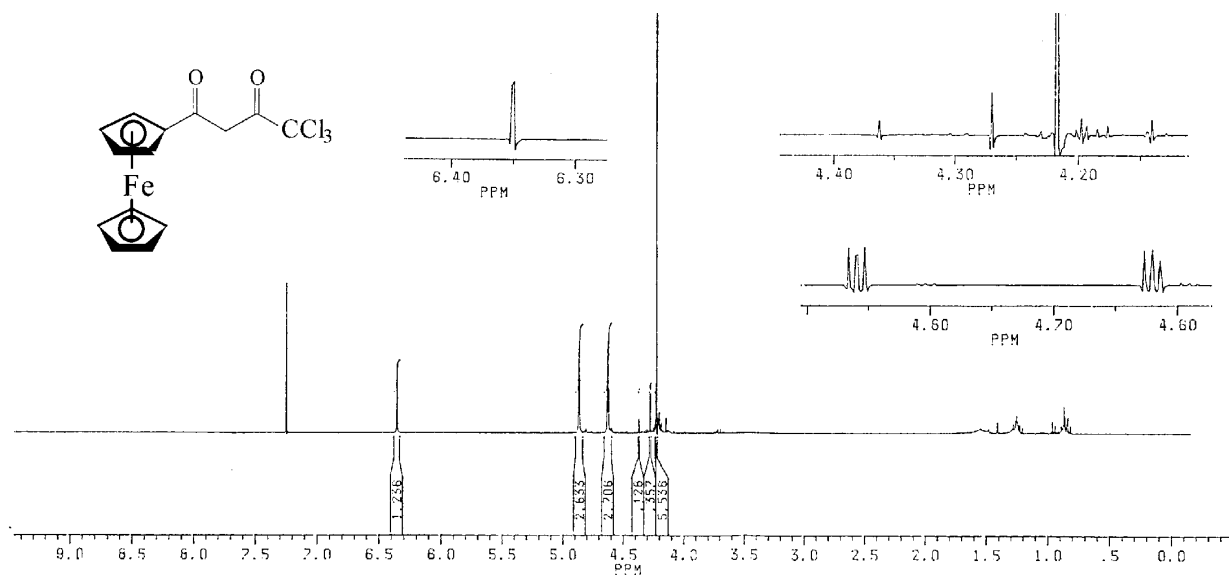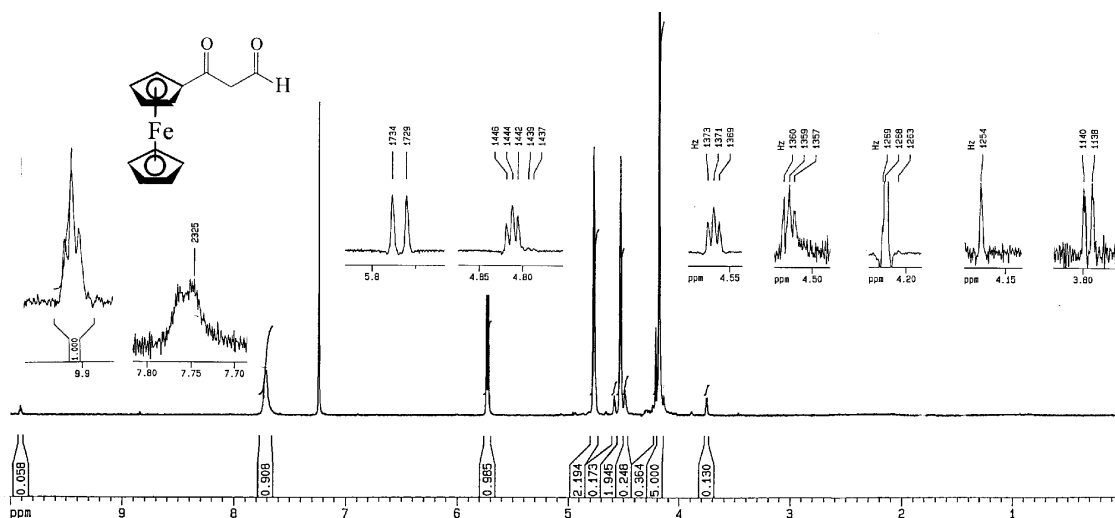**Spectrum 1: Hfctfa**

Spectrum 2: Hfca

Spectrum 3: Hbfcm

^{1}H NMR

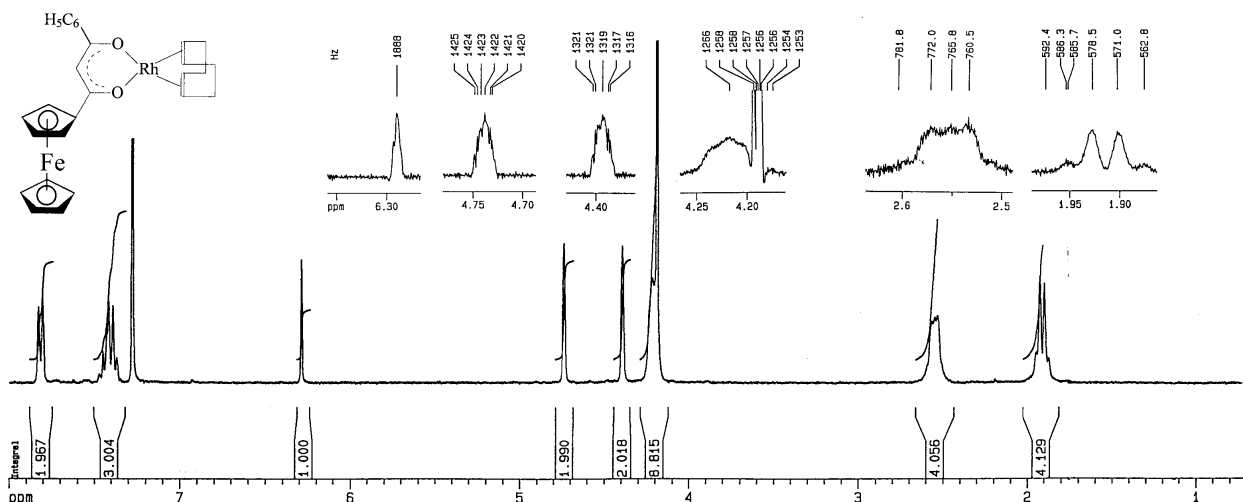**Spectrum 4: Hdfcm**

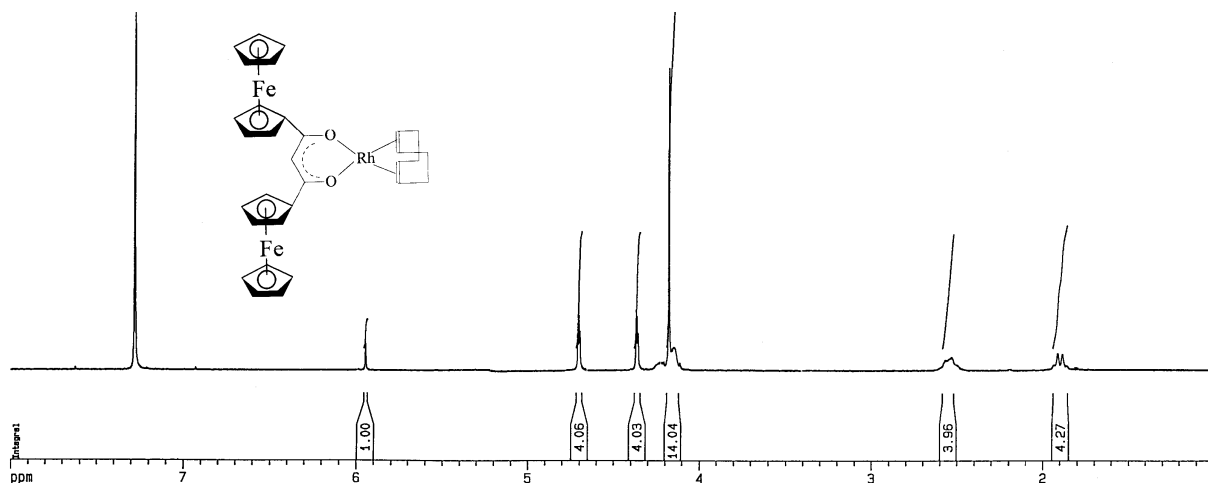**Spectrum 5: Htftca**

Spectrum 6: Hfch
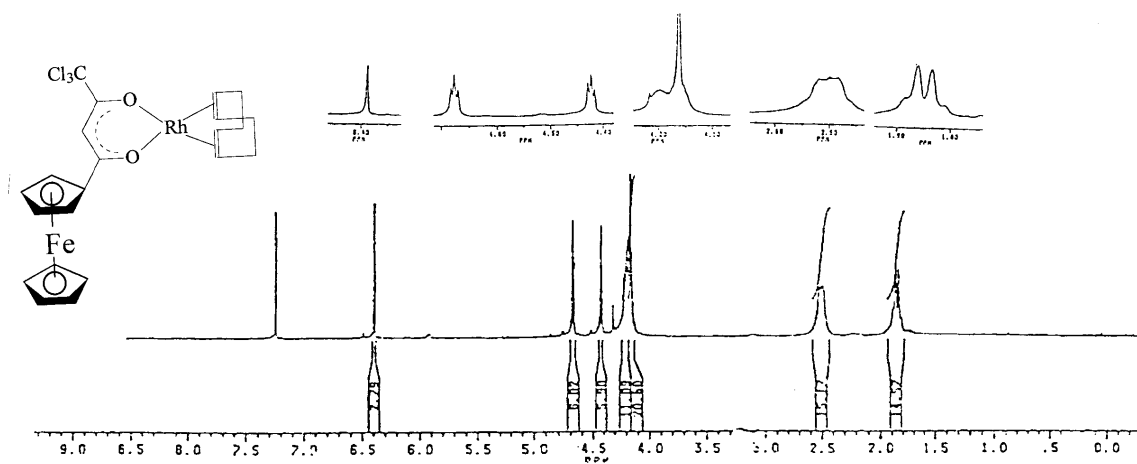
310
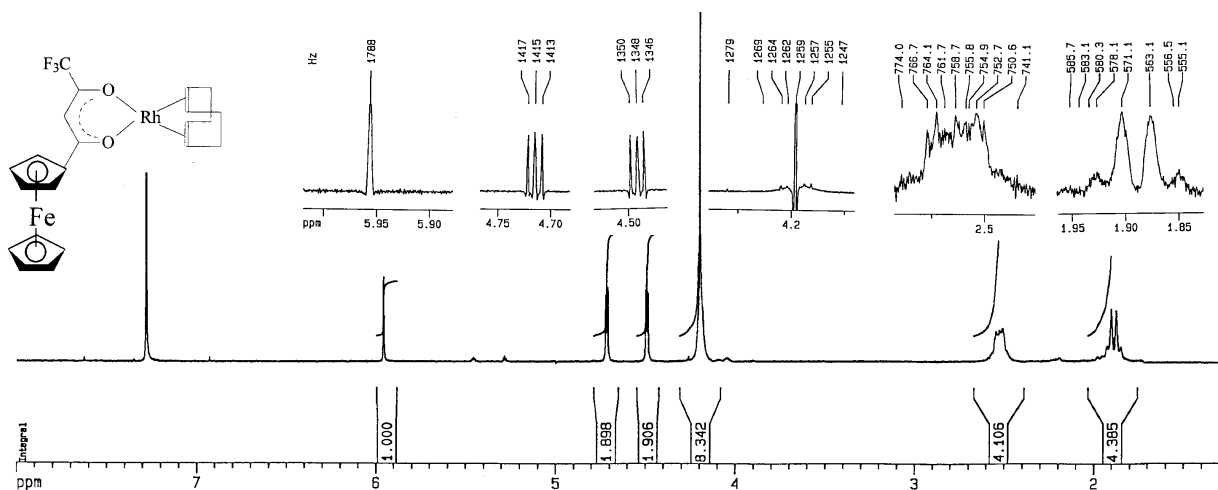
Spectrum 7: [Rh(fctfa)(cod)]
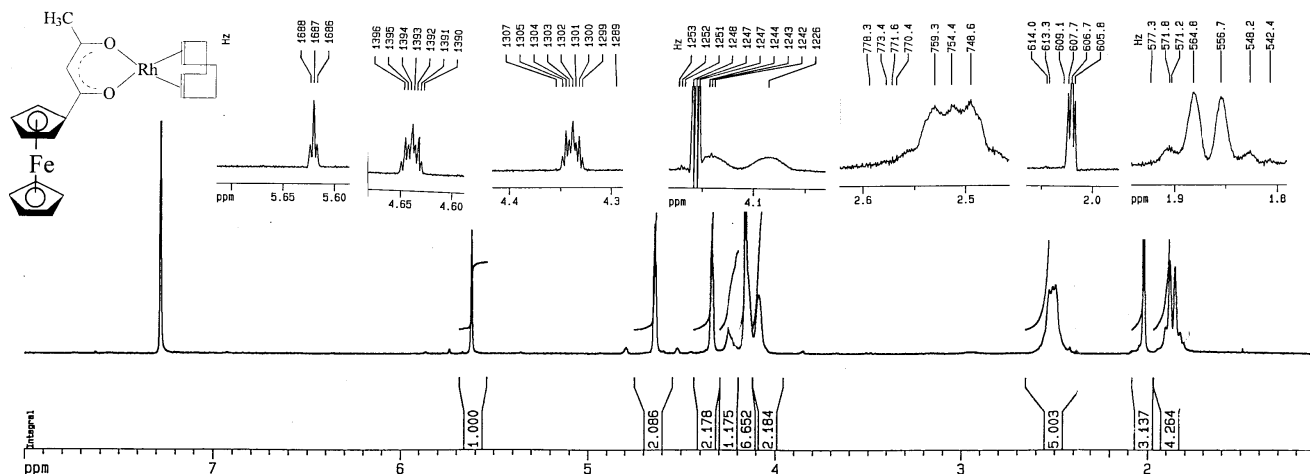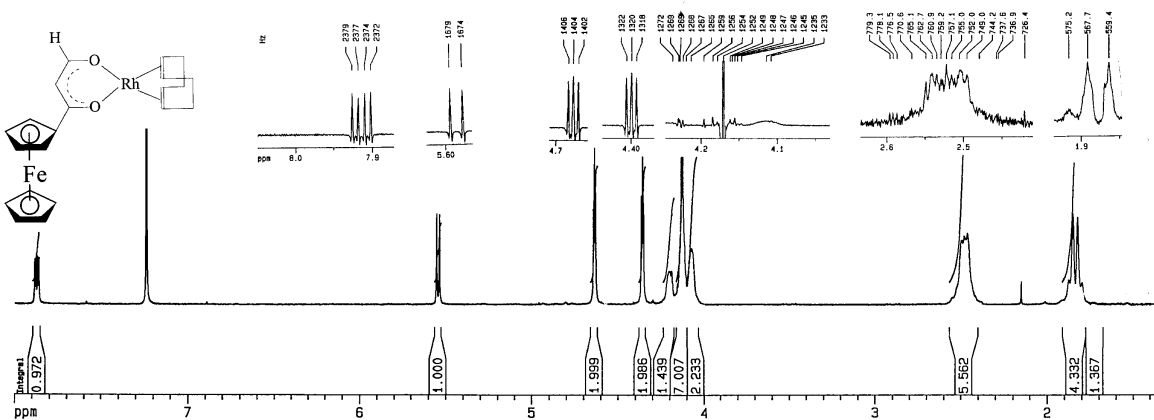

Spectrum 8: [Rh(fca)(cod)]

Spectrum 9: [Rh(bfcm)(cod)]

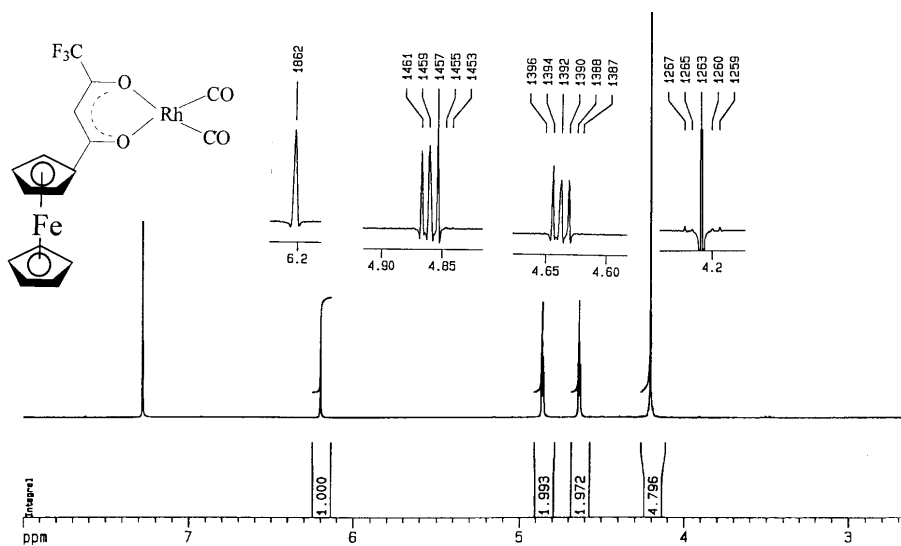**Spectrum 10: [Rh(dfcm)(cod)]**

Spectrum 11: [Rh(fctca)(cod)]

Spectrum 12: [Rh(fch)(cod)]

Spectrum 13: [Rh(fctfa)(CO)₂]
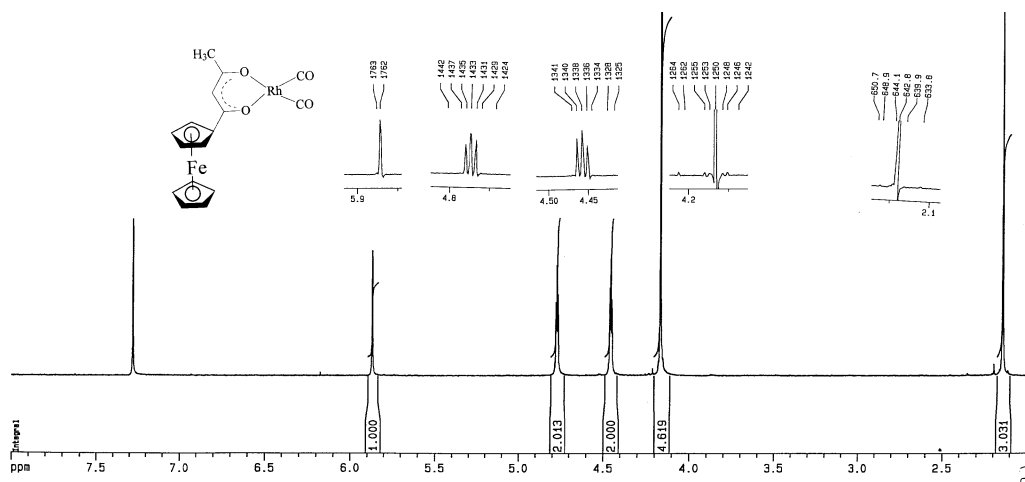
Spectrum 14: [Rh(fca)(CO)₂]
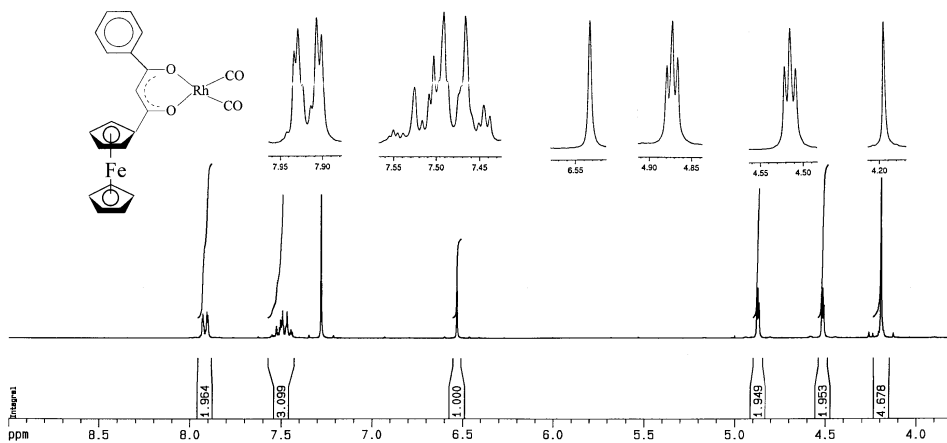
Spectrum 15: [Rh(bfcm)(CO)₂]
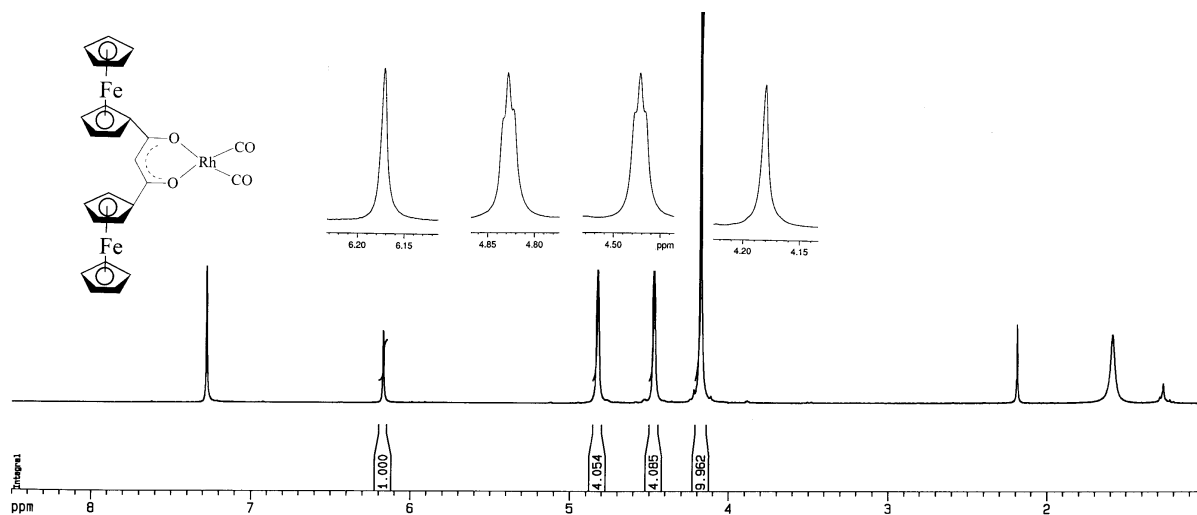
Spectrum 16: [Rh(dfcm)(CO)₂]
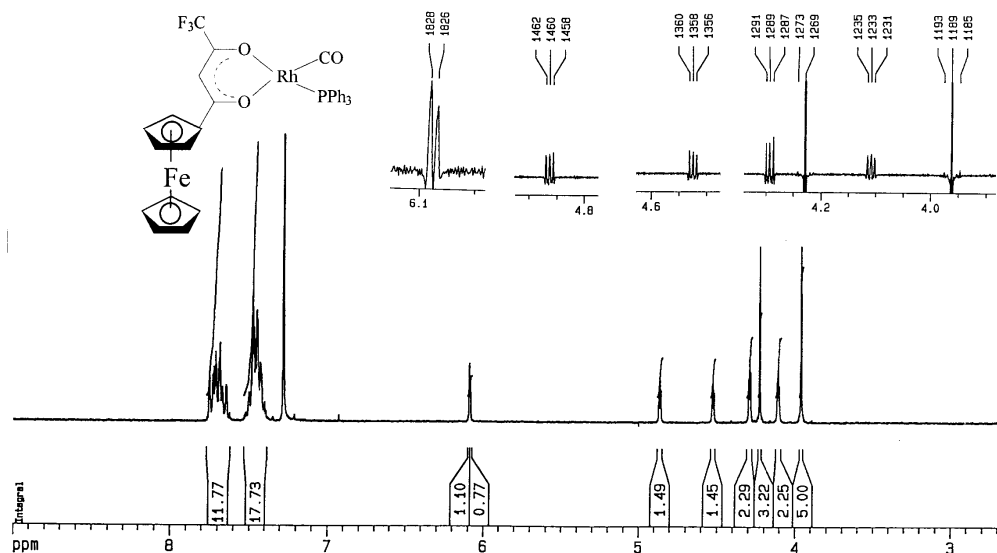
Spectrum 17: [Rh(fctfa)(CO)(PPh)₃]
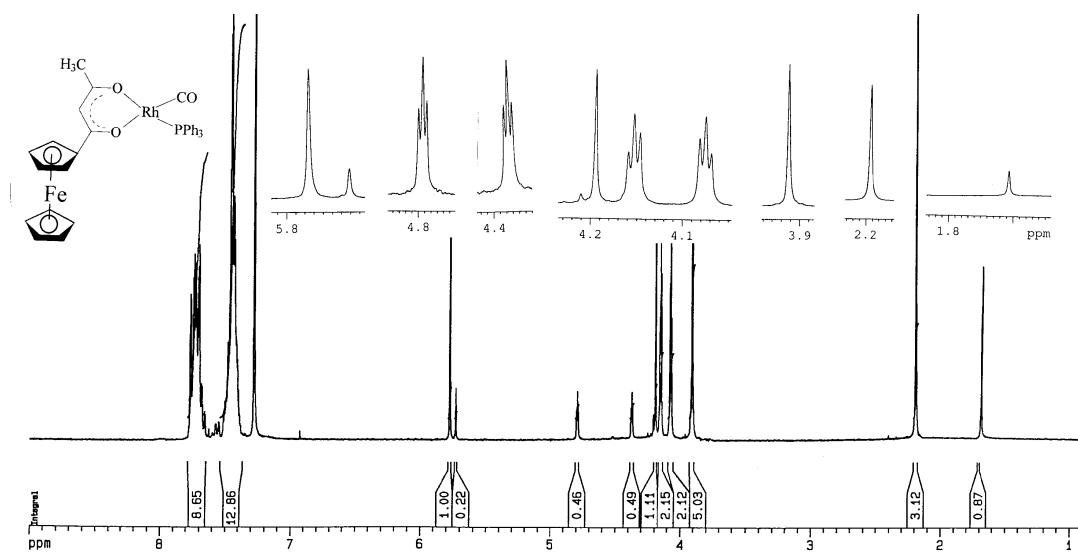
Spectrum 18: [Rh(fca)(CO)(PPh)₃]
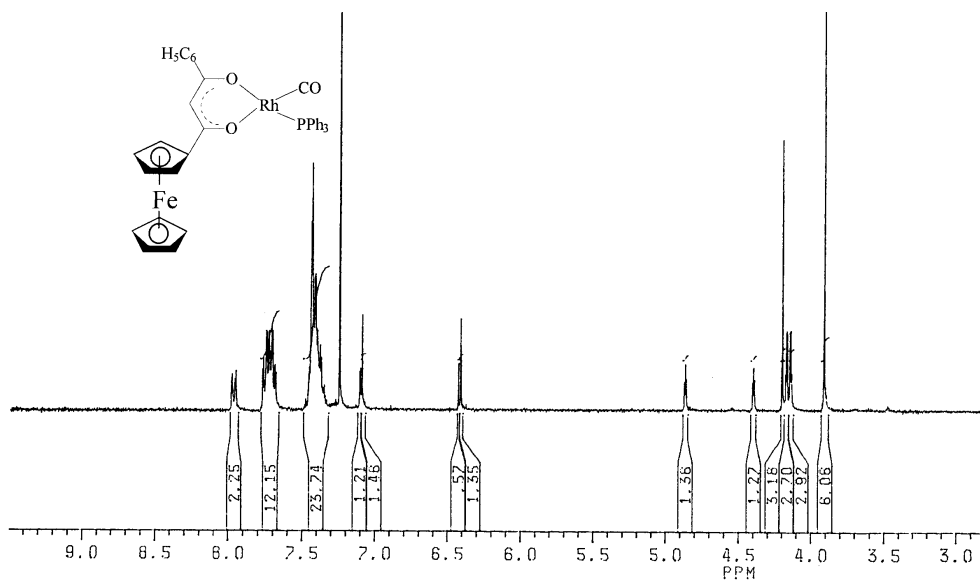
Spectrum 19: [Rh(bfcm)(CO)(PPh)₃]
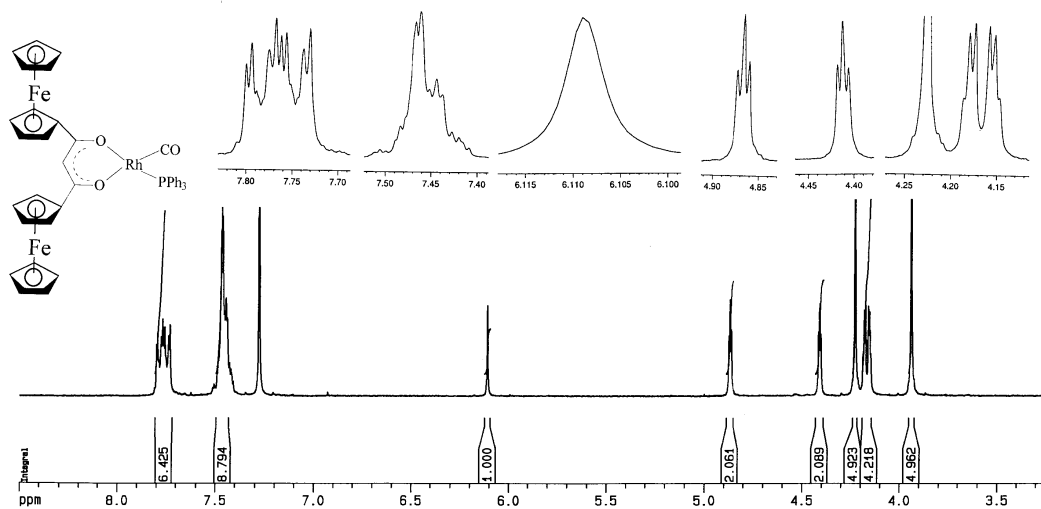
Spectrum 20: [Rh(dfcm)(CO)(PPh)₃]
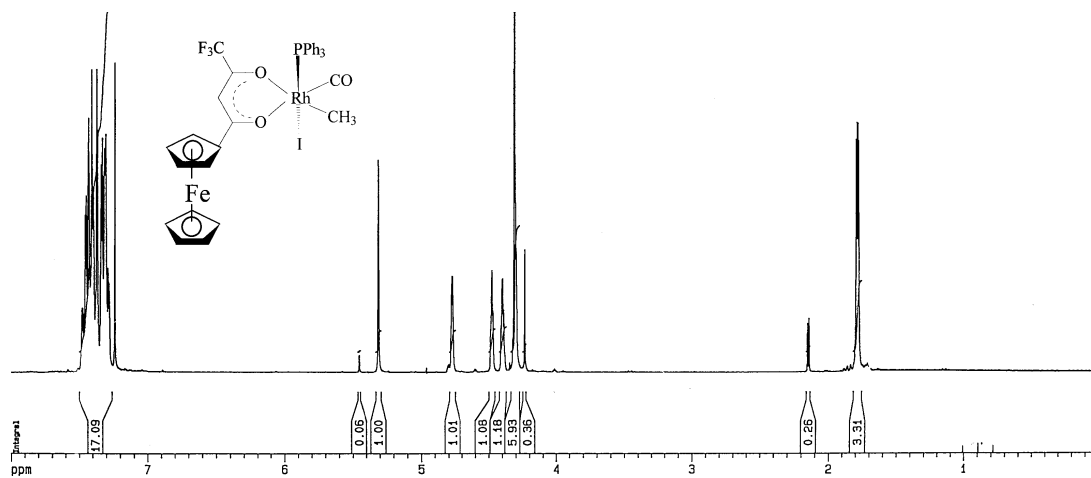
Spectrum 21: [Rh(fctfa)(CO)(PPh)₃(CH₃)(I)]
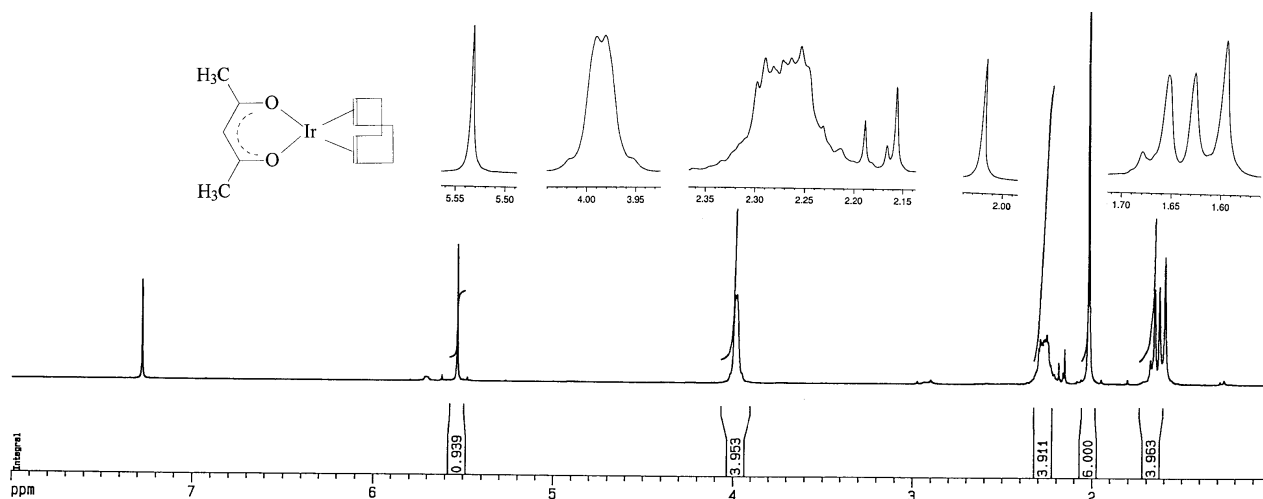
Spectrum 22: [Ir(acac)(cod)]
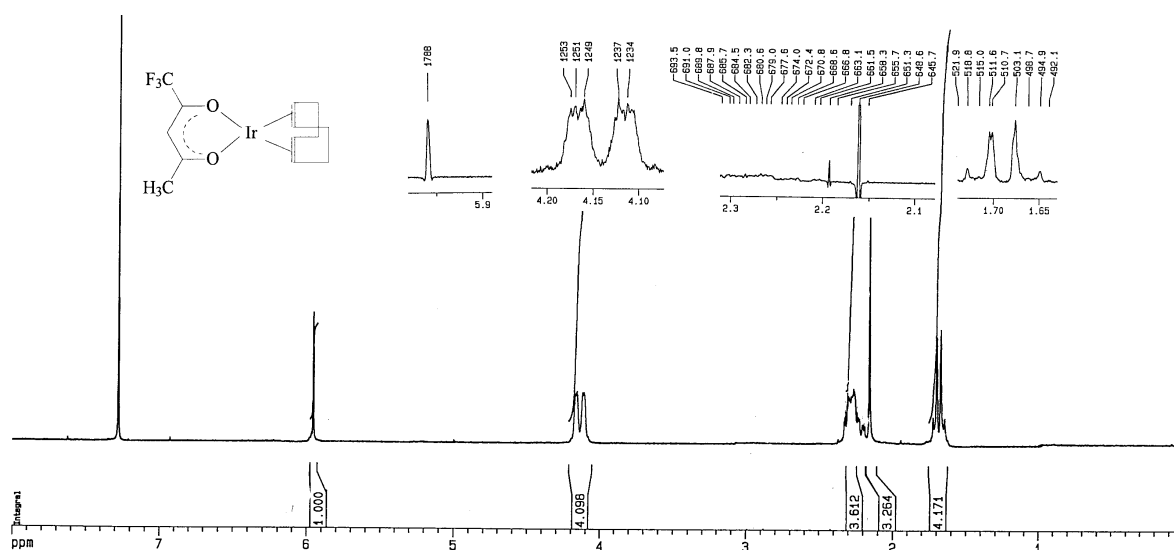
Spectrum 23: [Ir(tfaa)(cod)]
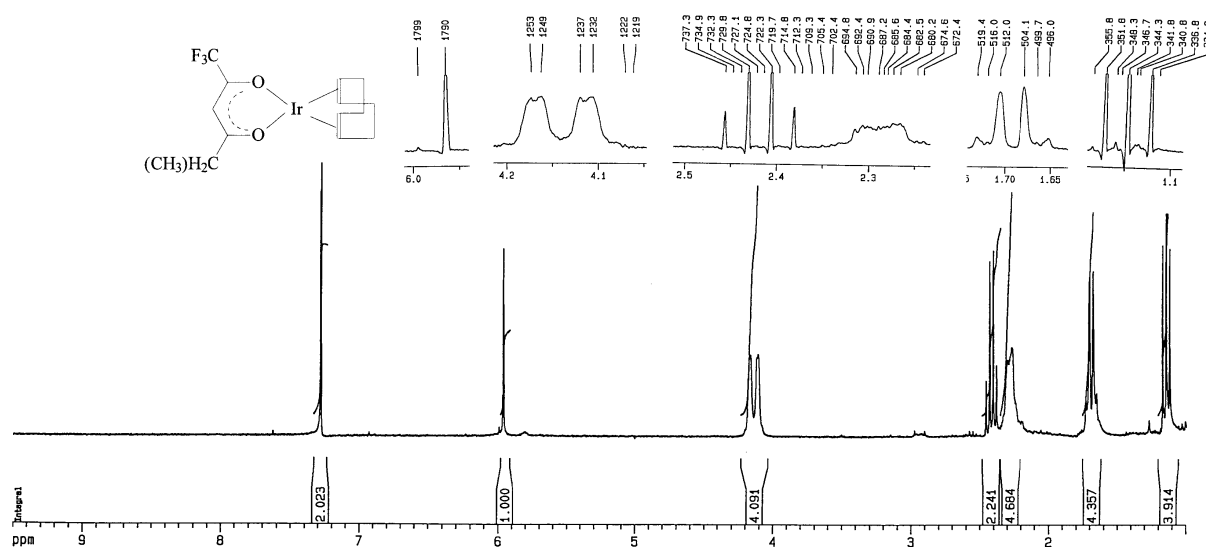
Spectrum 24: [Ir(tfhd)(cod)]

316
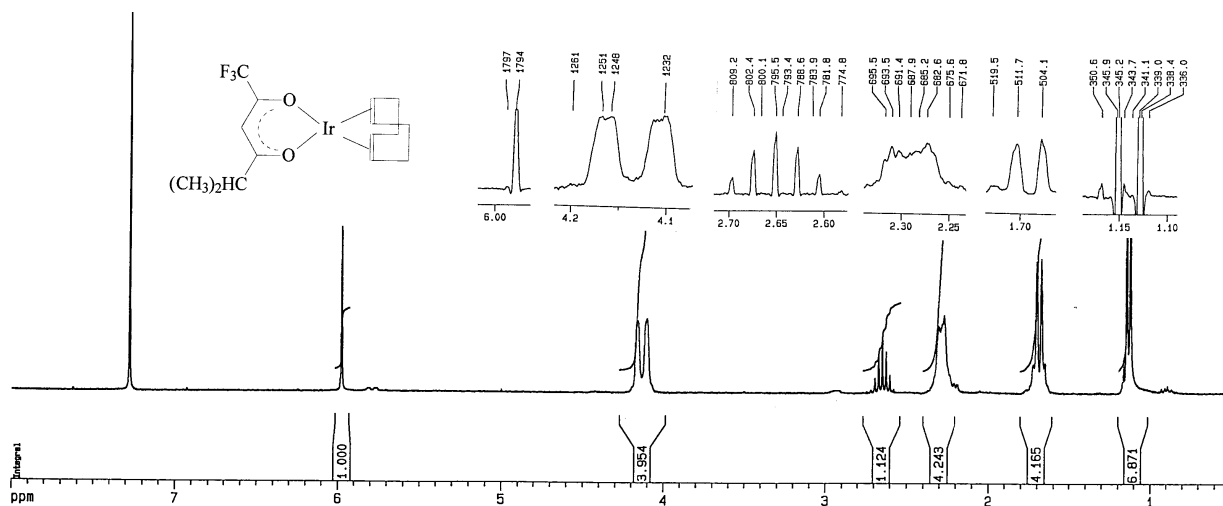
Spectrum 25: [Ir(tfdma)(cod)]
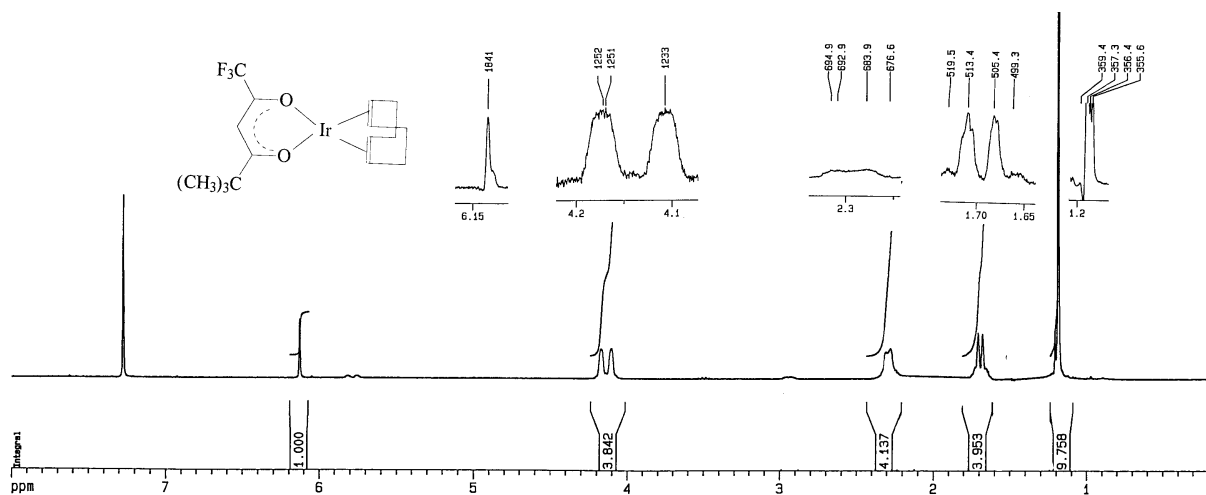
Spectrum 26: [Ir(tftma)(cod)]
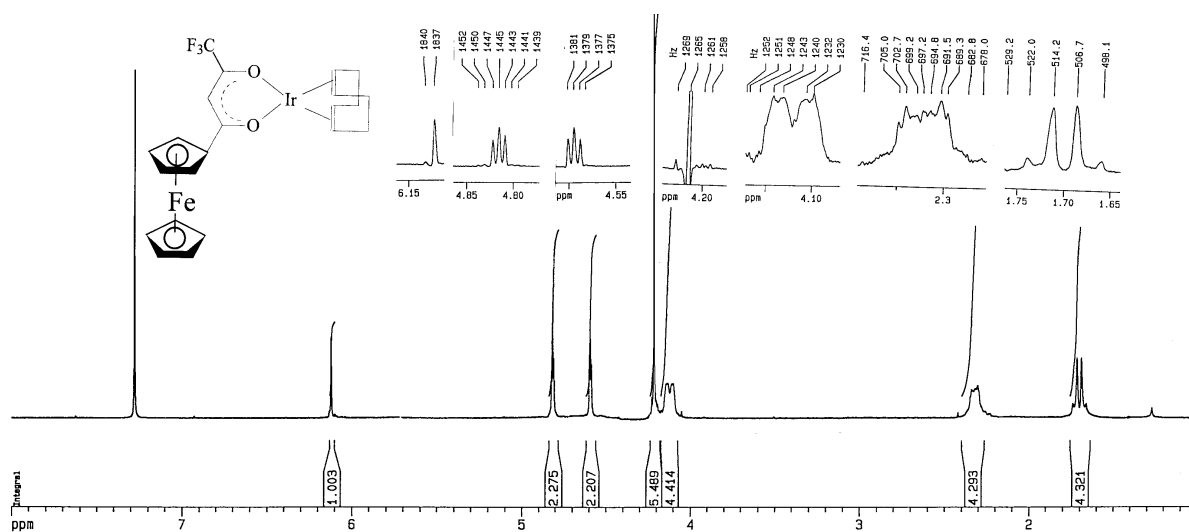
Spectrum 27: [Ir(fctfa)(cod)]
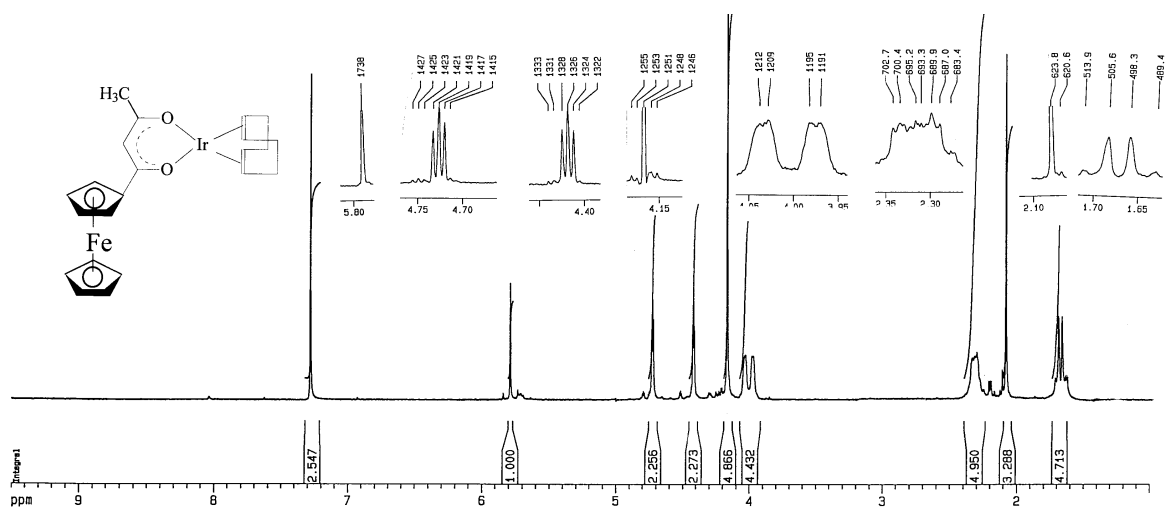
Spectrum 28: [Ir(fca)(cod)]
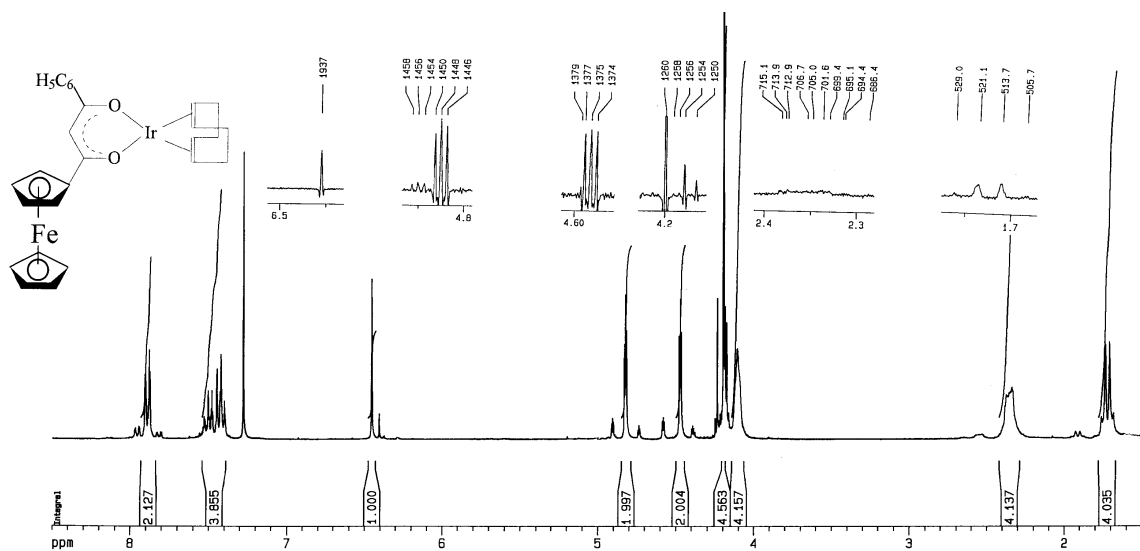
Spectrum 29: [Ir(bfcm)(cod)]
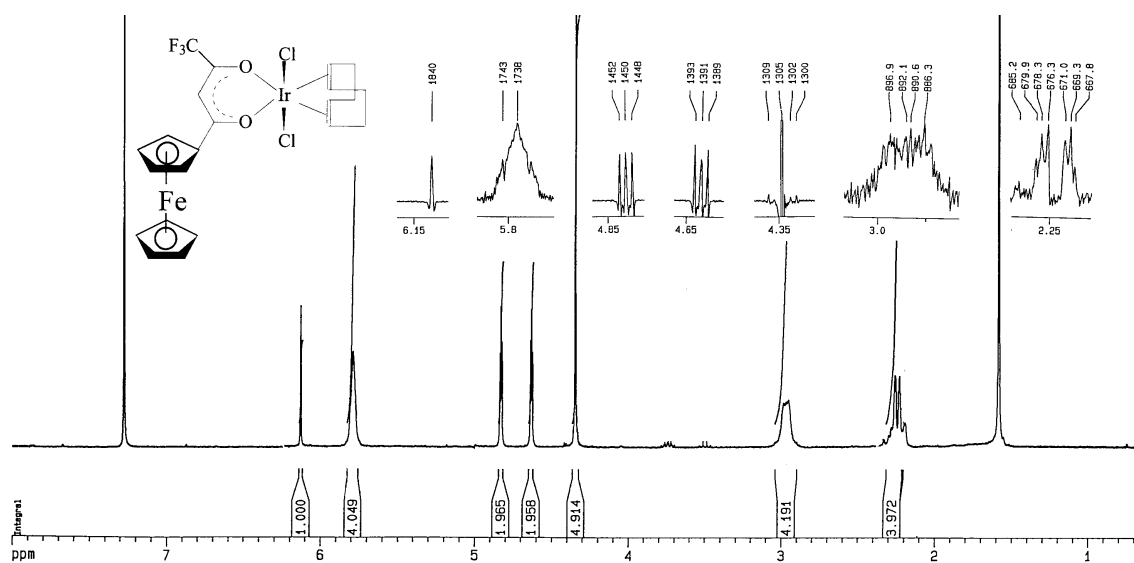
Spectrum 30: [Ir(Cl)₂(fctfa)(cod)]

318
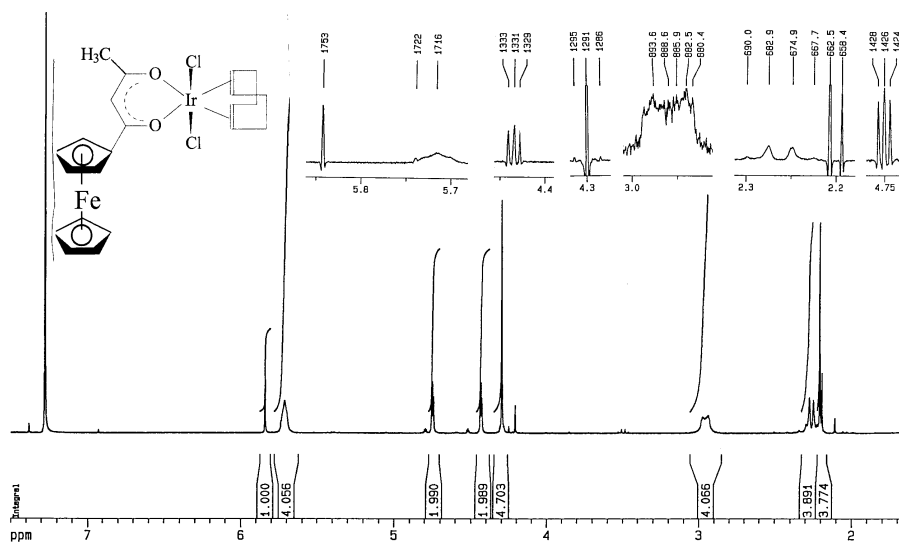
Spectrum 31: [Ir(Cl)$_2$(fca)(cod)]
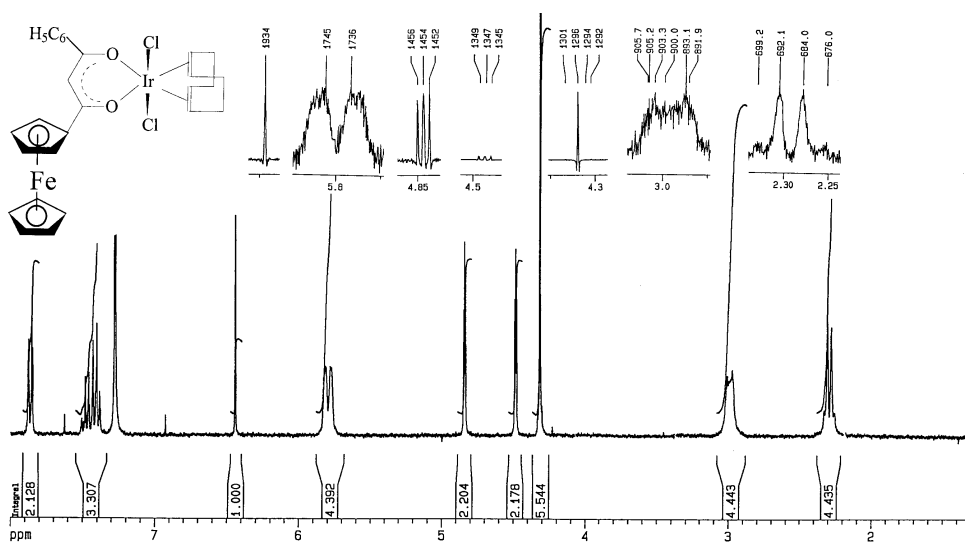
Spectrum 32: [Ir(Cl)$_2$(bfcm)(cod)]
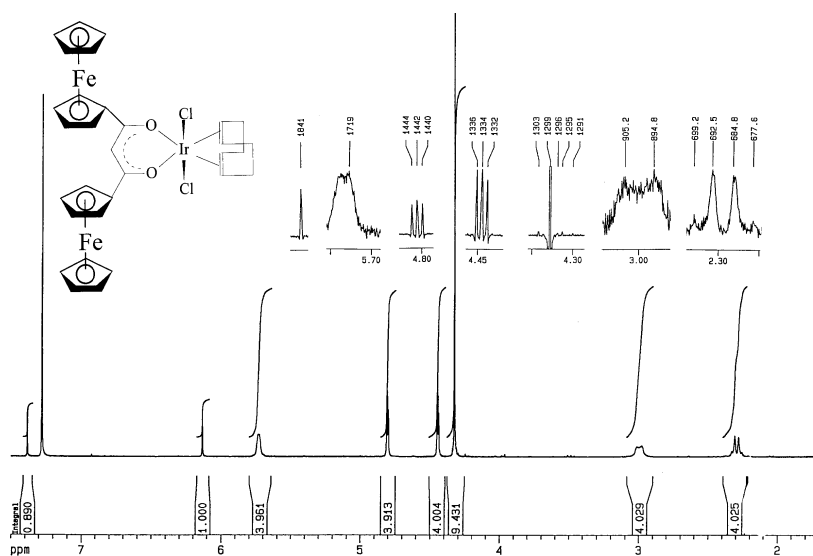
Spectrum 33: [Ir(Cl)$_2$(dfcm)(cod)]
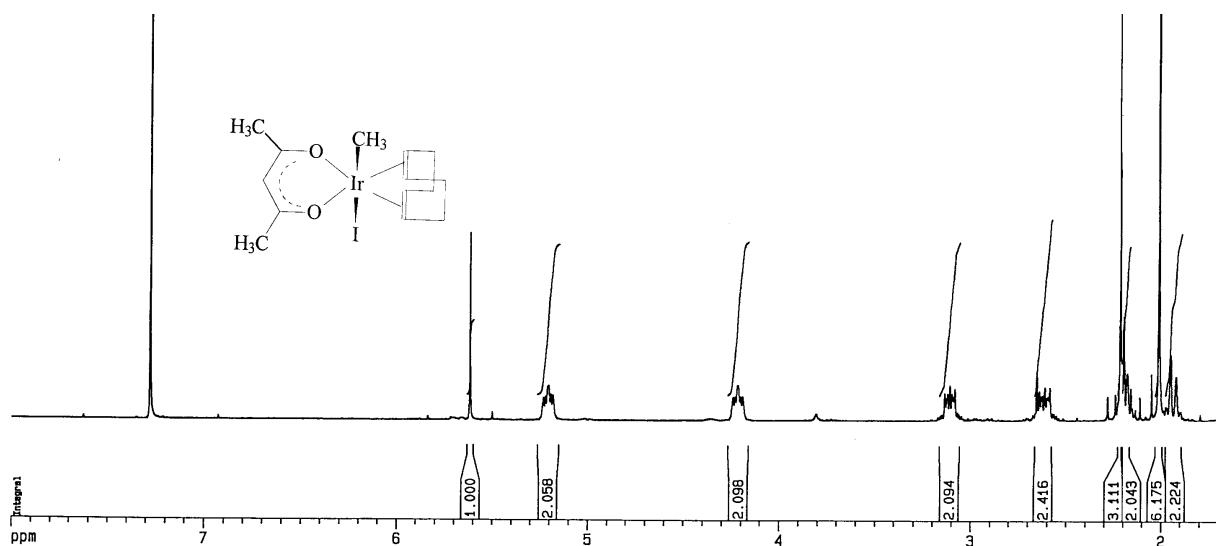
Spectrum 34: [Ir(CH₃)(I)(acac)(cod)]
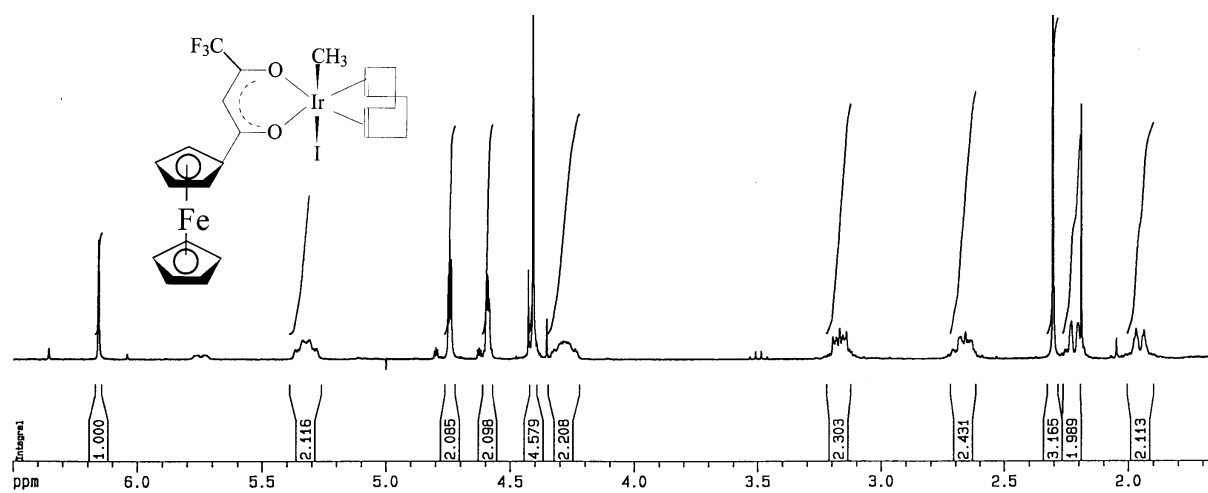
Spectrum 35: [Ir(CH₃)(I)(fctfa)(cod)]
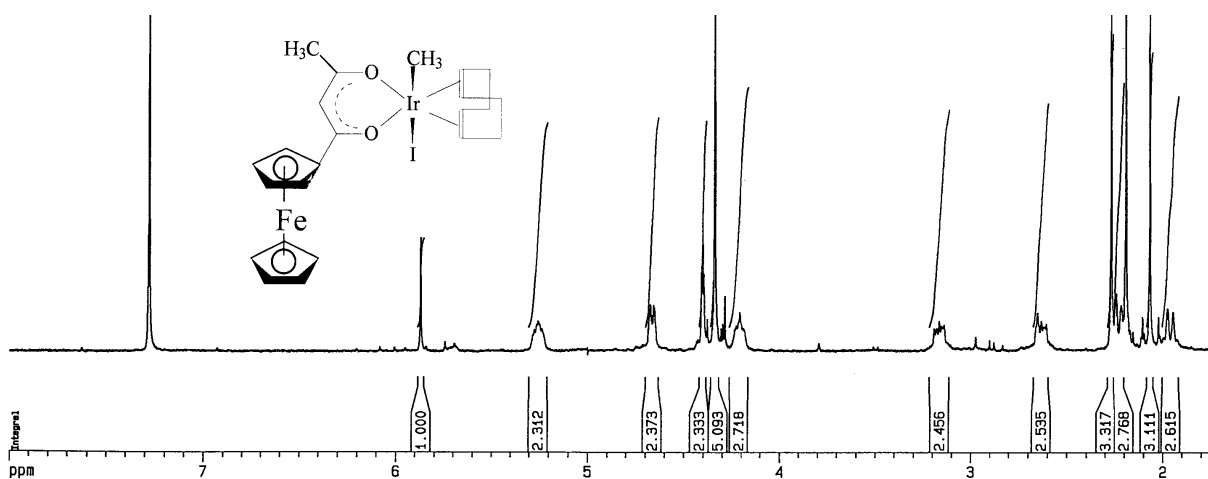
Spectrum 36: [Ir(CH₃)(I)(fca)(cod)]

ppm 195.004

171.982
171.507
171.033

ppm 120.062

116.335

93.729
93.701

ppm | 195 | 190 | 175 | 170 | ppm | 120 | 115 | 110 | 105 | 100 | 95

ppm

77.8526
77.4292
77.0056

75.7285

74.1650

71.2692
70.7904
70.2818
70.0039
69.5994

solvent CDCl₃ ⟶

ppm | 80 | 75 | 70
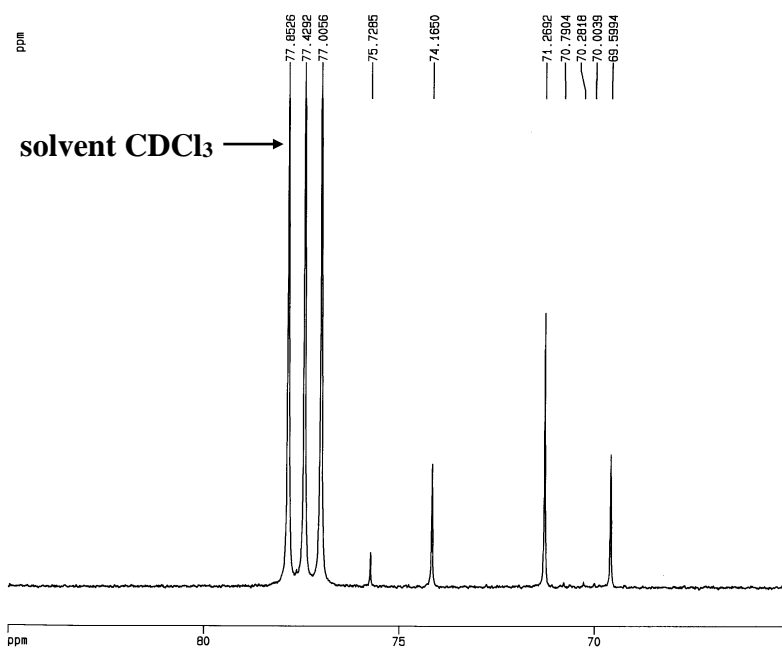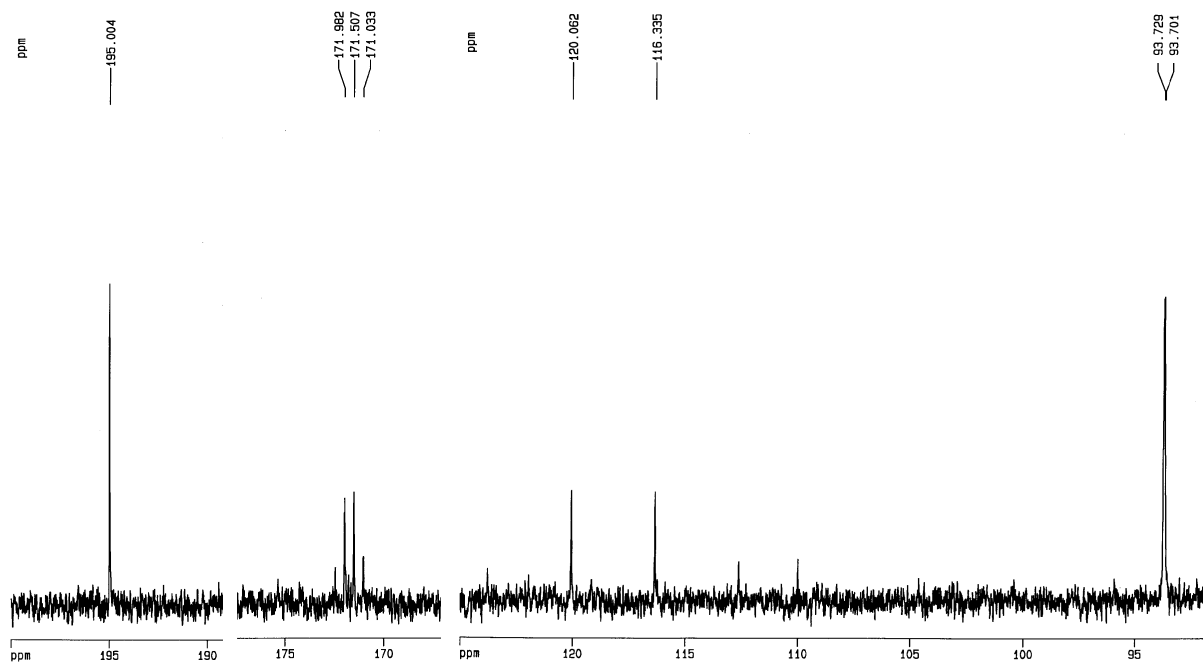
Spectrum 1: ^{13}C NMR spectrum of Hfctfa in CDCl₃.
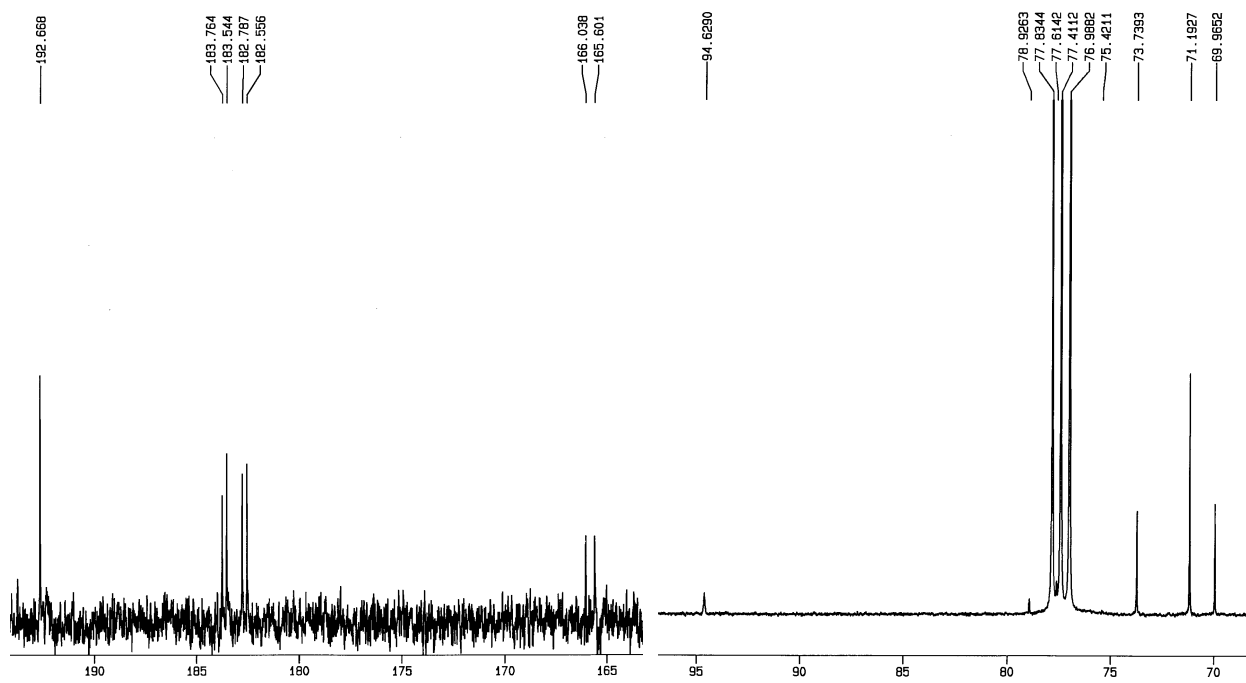
Spectrum 2: ^{13}C NMR spectrum of [Rh(fctfa)(CO)$_2$].
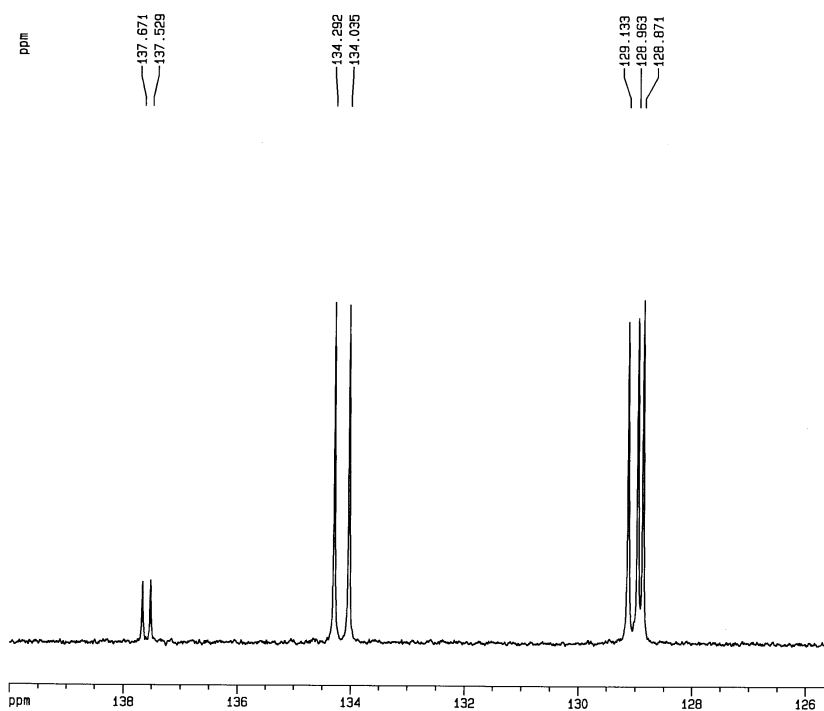
Spectrum 3: ^{13}C of free PPh$_3$.

322
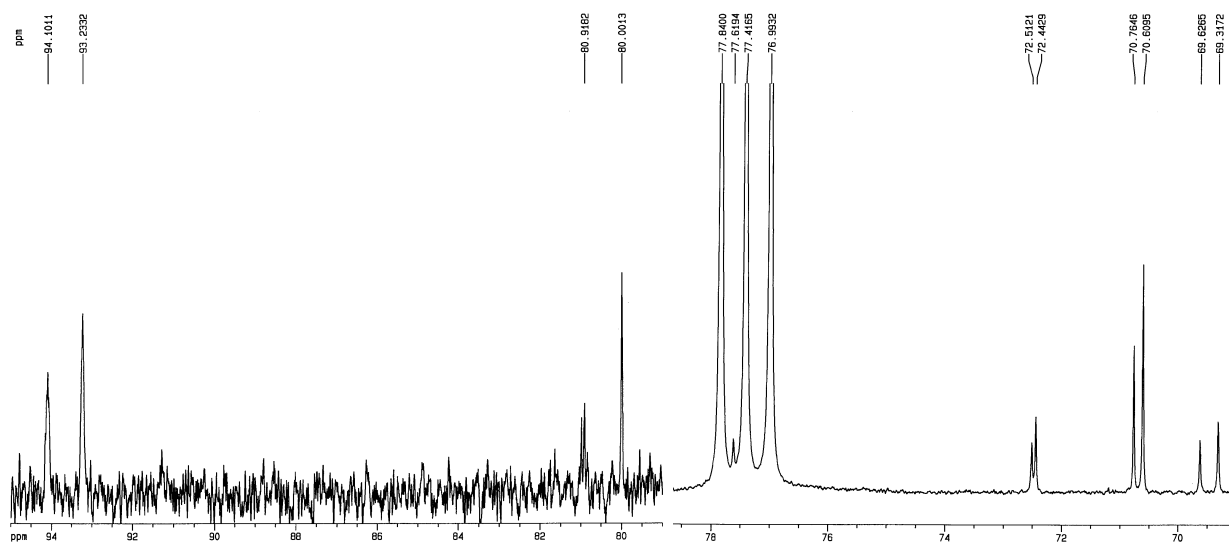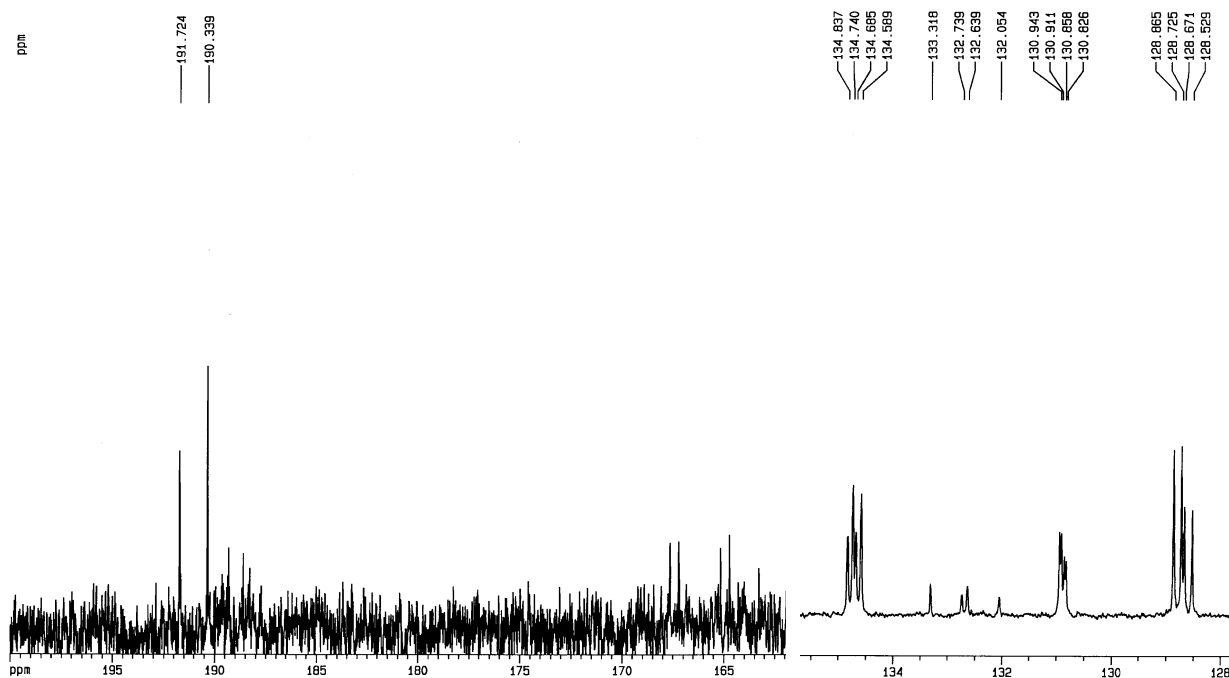
Spectrum 4: ^{13}C NMR spectrum of [Rh(fctfa)(CO)(PPh)$_3$].
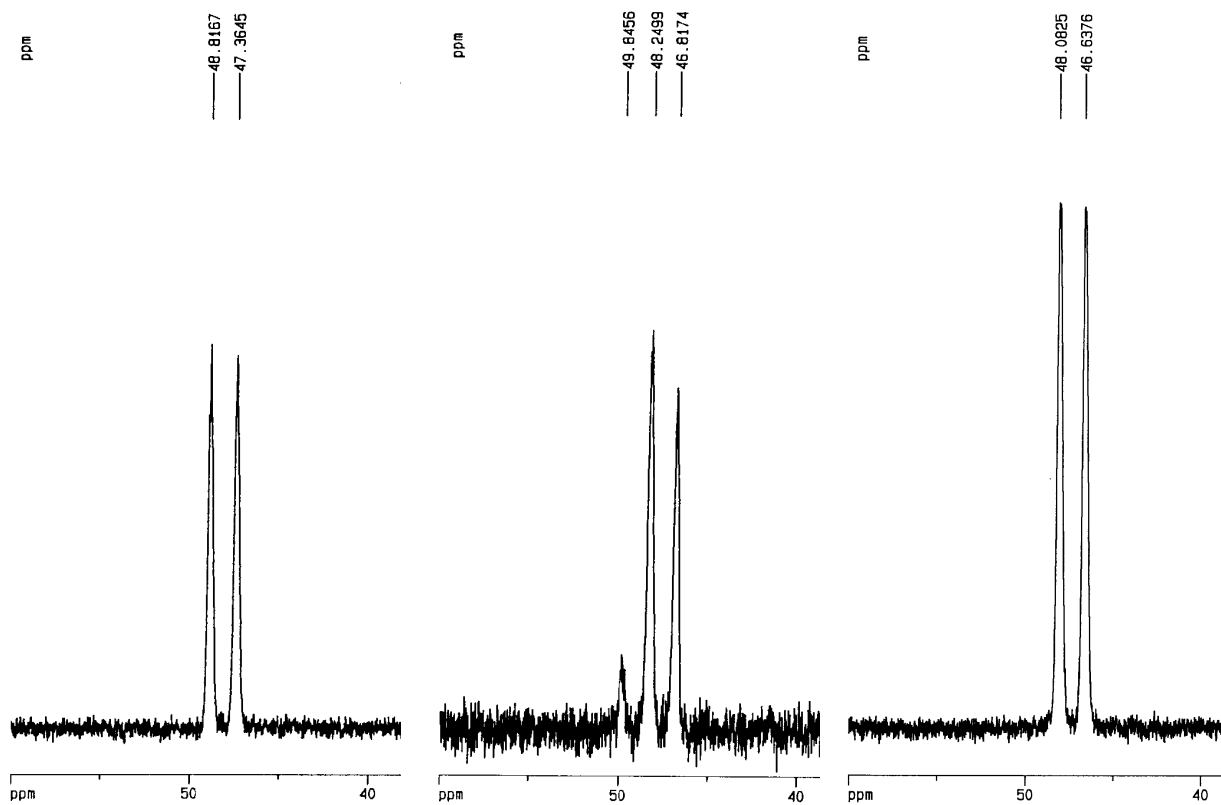
Spectrum 5: ^{31}P NMR [Rh(fctfa)(CO)(PPh₃)], [Rh(fca)(CO)(PPh₃)], [Rh(dfcm)(CO)(PPh₃)].
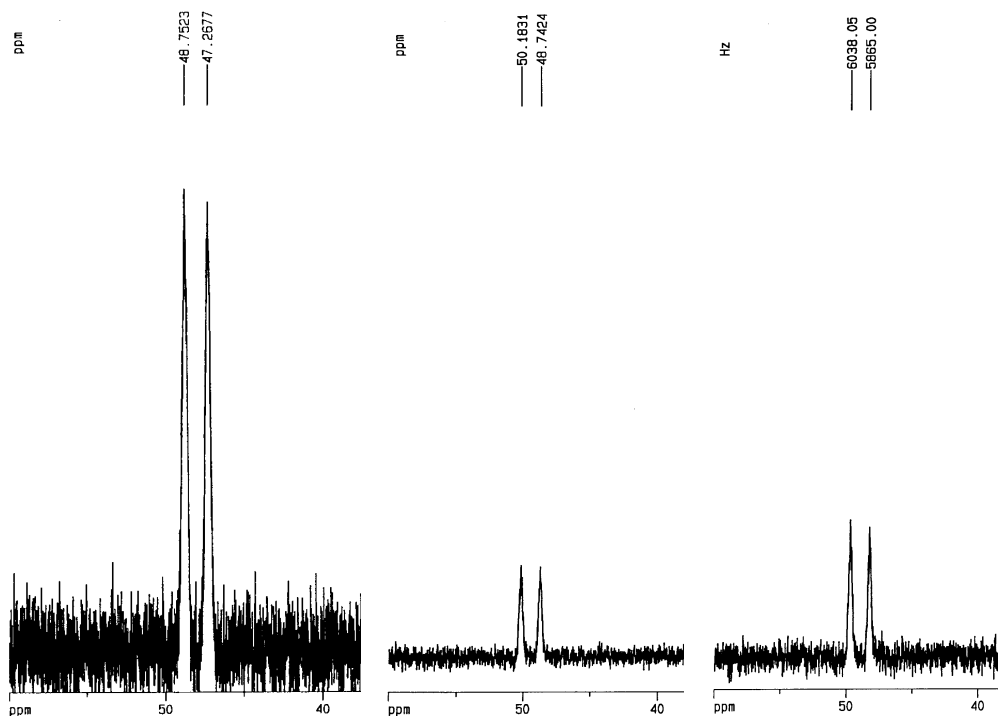
Spectrum 6: ^{31}P NMR [Rh(tta)(CO)(PPh₃)], [Rh(bzaa)(CO)(PPh₃)], [Rh(acac)(CO)(PPh₃)].

324
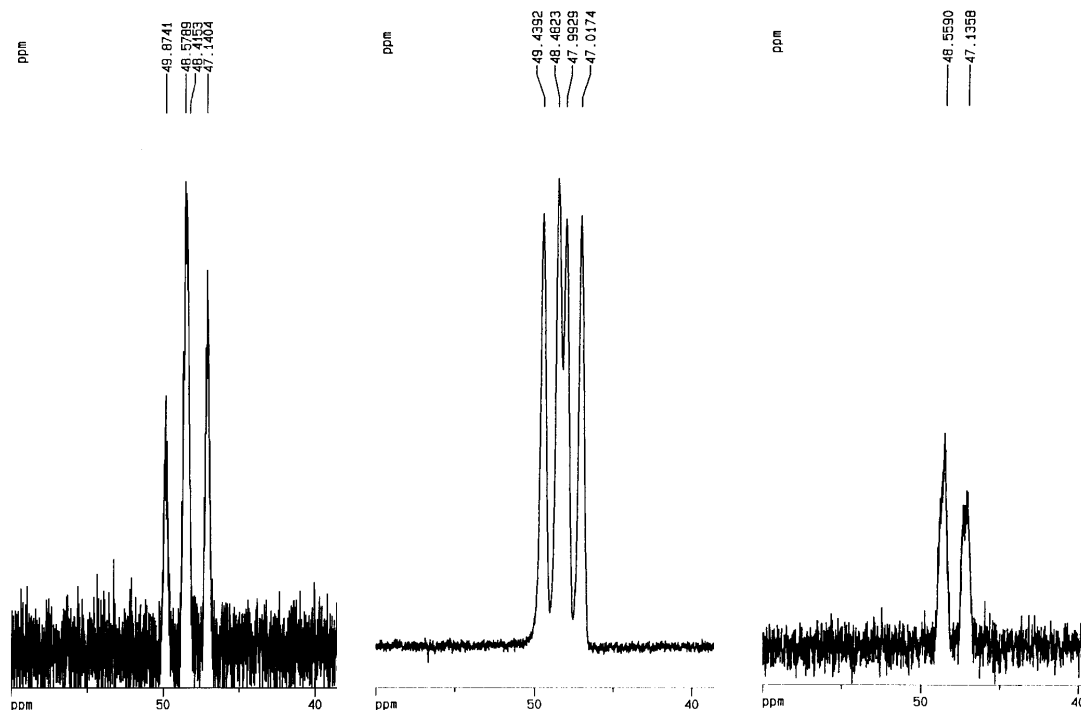
Spectrum 7: ^{31}P NMR [Rh(tfhd)(CO)(PPh₃)], [Rh(tfdma)(CO)(PPh₃)], [Rh(tftma)(CO)(PPh₃)].
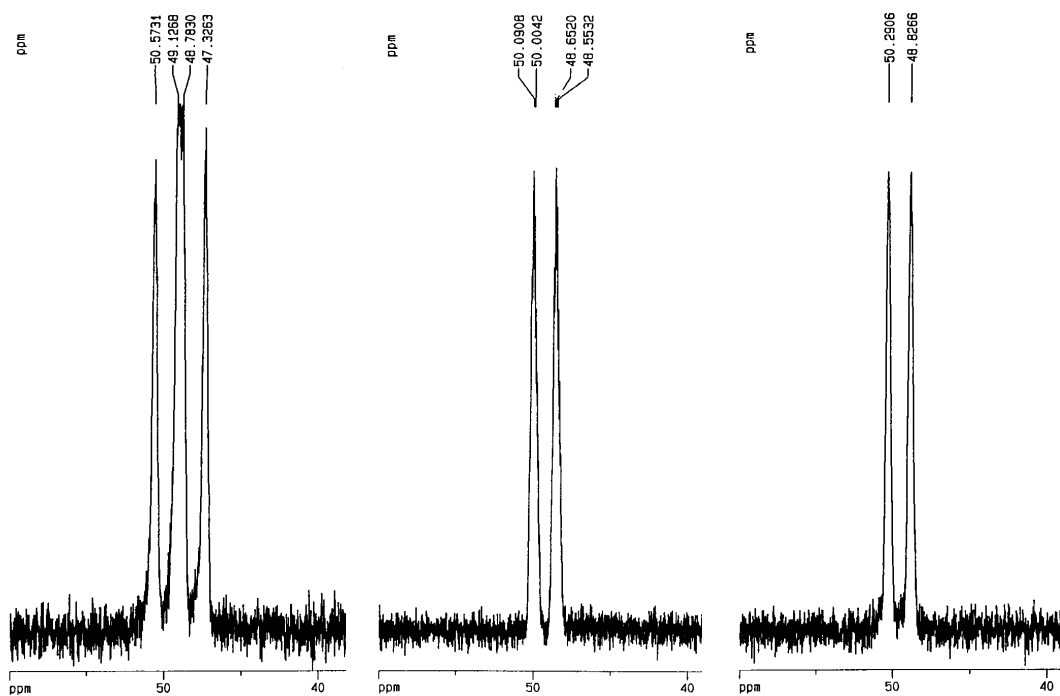
Spectrum 8: ^{31}P NMR: [Rh(tfba)(CO)(PPh₃)], [Rh(ba)(CO)(PPh₃)], [Rh(dbm)(CO)(PPh₃)]
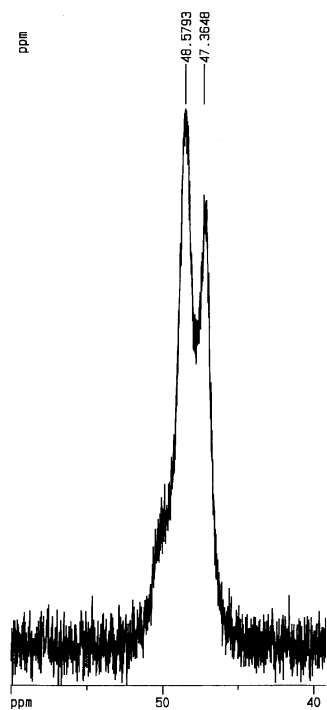
Spectrum 9: ³¹P NMR: [Rh(tfaa)(CO)(PPh₃)]

Spectrum 10: ³¹P NMR spectrum of [Rh(fctfa)(CO)(PPh₃)(CH₃)(I)].

Spectrum 9: ^{31}P NMR: [Rh(tfaa)(CO)(PPh$_3$)]
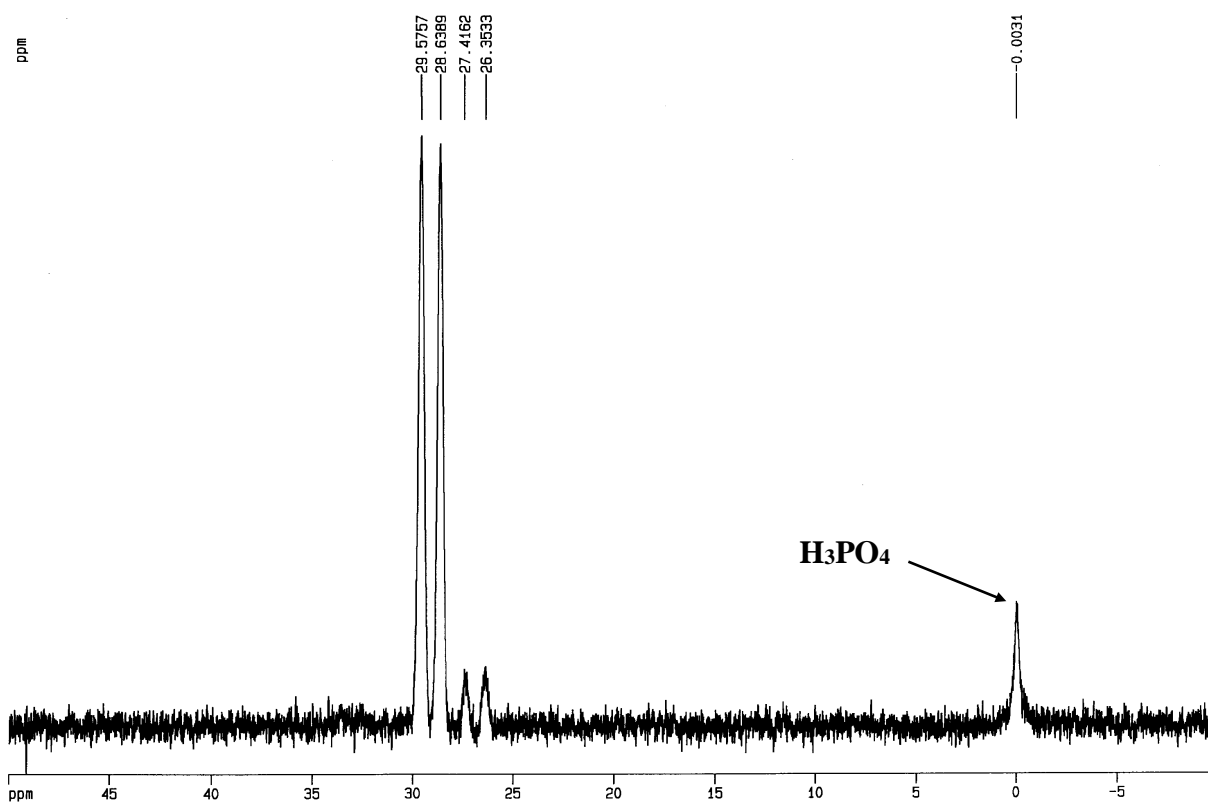
Spectrum 10: ^{31}P NMR spectrum of [Rh(fctfa)(CO)(PPh$_3$)(CH$_3$)(I)].

Listed atomic coordinates and anisotropic displacement parameters.

B.1 Hfctfa.

Atomic coordinates and B_{iso}/B_{eq} and occupancy of Hfctfa with e.s.d.'s in parentheses.

atom	x	y	z	B_{eq}	occ	atom	x	y	z	B_{eq}
Fe(1)	1.1961(1)	0.12047(6)	0.65776(3)	4.00(1)		C(9)	1.2240(8)	0.1695(5)	0.7510(2)	6.0(1)
F(1)	1.4402(8)	0.3313(5)	0.3945(3)	9.3(2)	0.600	C(10)	1.0954(7)	0.2619(5)	0.7183(2)	6.0(1)
F(2)	1.371(1)	0.5133(6)	0.4317(3)	11.3(2)	0.600	C(11)	1.0020(6)	0.1893(4)	0.5277(2)	4.43(9)
F(3)	1.1938(9)	0.4475(9)	0.3518(2)	11.7(2)	0.600	C(12)	1.1655(5)	0.2499(4)	0.4884(2)	4.10(9)
F(4)	1.206(1)	0.5193(8)	0.3842(5)	11.0(3)	0.400	C(13)	1.1049(6)	0.3456(4)	0.4479(2)	4.6(1)
F(5)	1.289(1)	0.3360(9)	0.3518(4)	9.9(3)	0.400	C(14)	1.2726(7)	0.4097(5)	0.4048 2)	5.8(1)
F(6)	1.455(1)	0.419(1)	0.4258(4)	11.9(3)	0.400	H(1)	1.4013	0.0401	0.5521	6.199
O(1)	0.7994(4)	0.2278(3)	0.5252(1)	5.67(7)		H(2)	1.3797	-0.1205	0.6427	7.581
O(2)	0.9063(4)	0.3944(3)	0.4409(1)	6.38(8)		H(3)	0.9977	-0.1107	0.6886	7.062
C(1)	1.0632(6)	0.0848(4)	0.5709(2)	4.17(9)		H(4)	0.7696	0.0538	0.6256	6.418
C(2)	1.2748(7)	0.0236(4)	0.5777(2)	5.2(1)		H(5)	1.1849	0.3837	0.6411	6.500
C(3)	1.2618(8)	-0.0661(5)	0.6283(2)	6.4(1)		H(6)	1.5597	0.2736	0.6463	6.556
C(4)	1.0481(8)	-0.0599(5)	0.6537(2)	6.0(1)		H(7)	1.5564	0.1141	0.7367	6.957
C(5)	0.9213(7)	0.0309(5)	0.6186(2)	5.3(1)		H(8)	1.1757	0.1158	0.7851	7.310
C(6)	1.2288(7)	0.3173(4)	0.6703(2)	5.6(1)		H(9)	0.9448	0.2844	0.7270	7.174
C(7)	1.4373(7)	0.2568(5)	0.6736(2)	5.5(1)		H(10)	1.3224	0.2193	0.4949	3.801
C(8)	1.4352(7)	0.1676(5)	0.7236(2)	5.8(1)		H(11)	0.8107	0.3178	0.4702	3.801

$B_{eq} = 8/3\ \pi^2(U_{11}(aa*)^2 + U_{22}(bb*)^2 + U_{33}(cc*)^2 + 2U_{12}(aa*bb*)\cos\gamma + 2U_{13}(aa*cc*)\cos\beta + 2U_{23}(bb*cc*)\cos\alpha)$

Anisotropic displacement parameters of Hfctfa with e.s.d.'s in parentheses.

atom	U_{11}	U_{22}	U_{33}	U_{12}	U_{13}	U_{23}
Fe(1)	0.0553(3)	0.0606(3)	0.0362(2)	0.0010(4)	-0.0001(2)	-0.0031(4)
F(1)	0.085(3)	0.101(4)	0.171(5)	0.022(3)	0.072(3)	0.027(4)
F(2)	0.203(6)	0.112(5)	0.116(4)	-0.063(4)	0.062(4)	-0.023(4)
F(3)	0.090(4)	0.299(9)	0.057(3)	0.028(5)	-0.004(3)	0.063(4)
F(4)	0.088(5)	0.098(6)	0.23(1)	0.014(5)	0.048(6)	0.093(6)
F(S)	0.130(6)	0.162(8)	0.084(5)	-0.020(6)	0.041(5)	-0.009(6)
F(6)	0.059(4)	0.23(1)	0.158(7)	-0.073(5)	-0.059(4)	0.101(7)
O(1)	0.051(2)	0.098(2)	0.067(2)	0.009(2)	0.004(1)	0.015(2)
O(2)	0.055(2)	0.099(2)	0.088(2)	0.015(2)	0.002(1)	0.036(2)
C(1)	0.061(2)	0.058(3)	0.040(2)	0.013(2)	-0.005(2)	-0.009(2)
C(2)	0.084(3)	0.076(3)	0.038(2)	0.025(3)	0.001(2)	-0.010(2)
C(3)	0.100(3)	0.073(3)	0.069(3)	0.021(3)	-0.012(3)	-0.002(3)
C(4)	0.095(3)	0.067(3)	0.064(3)	-0.010(3)	-0.010(3)	0.002(2)
C(5)	0.059(3)	0.081(3)	0.062(2)	-0.010(2)	-0.005(2)	0.001(3)
C(6)	0.081(3)	0.065(3)	0.065(3)	0.009(3)	-0.015(2)	-0.008(2)
C(7)	0.064(3)	0.082(3)	0.063(3)	-0.013(3)	-0.008(2)	0.000(3)
C(8)	0.076(3)	0.090(4)	0.054(2).	0.005(3)	-0.020(2)	-0.012(2)
C(9)	0.092(3)	0.087(4)	0.048(2)	-0.002(3)	0.010(2)	-0.007(2)
C(10)	0.061(3)	0.094(3)	0.072(3)	0.008(3)	0.007(2)	-0.041(3)
C(11)	0.058(2)	0.071(3)	0.039(2)	0.004(2)	-0.007(2)	-0.008(2)
C(12)	0.041(2)	0.071(3)	0.044(2)	0.009(2)	-0.009(2)	-0.003(2)
C(13)	0.050(2)	0.077(3)	0.047(2)	0.009(2)	-0.003(2)	-0.004(2)
C(14)	0.058(3)	0.098(4)	0.064(3)	0.011(3)	0.005(2)	0.004(3)

The general temperature factor expression;
$\exp(-2\pi^2(a*^2U_{11}h^2 + b*^2U_{22}k^2 + c*^2U_{33}l^2 + 2a*b*U_{12}hk + 2a*c*U_{13}hl + 2b*c*U_{23}kl))$

B.2 [Rh(fctfa)(CO)₂].

Atomic coordinates and B_{iso}/B_{eq} and occupancy of [Rh(fctfa)(CO)$_2$] with e.s.d.'s in parentheses.

atom	x	y	z	B_{eq}	occ
Rh(1)	0.42680(6)	0.36313(4)	-0.16031(6)	3.36(2)	
Fe(1)	0.3051(1)	0.09153(7)	-0.1186(1)	3.53(3)	
O(1)	0.6144(7)	0.3572(4)	0.0020(7)	7.1(2)	
O(2)	0.4275(6)	0.5141(4)	-0.1414(6)	6.1(2)	
O(3)	0.4232(5)	0.2583(3)	-0.1699(5)	3.8(2)	
O(4)	0.2964(5)	0.3687(3)	-0.2672(5)	4.3(2)	
C(1)	0.155(1)	0.0986(8)	-0.107(1)	6.6(4)	
C(2)	0.213(1)	0.1514(8)	-0.049(1)	7.9(5)	
C(3)	0.289(1)	0.120(1)	0.025(1)	8.6(6)	
C(4)	0.279(1)	0.049(1)	0.012(1)	7.6(5)	
C(5)	0.194(1)	0.0363(7)	-0.065(1)	7.5(5)	
C(6)	0.3734(6)	0.1477(5)	-0.2159(6)	2.8(2)	
C(7)	0.3099(7)	0.0950(5)	-0.2700(7)	3.5(2)	
C(8)	0.3501(8)	0.0312(5)	-0.2287(7)	3.8(2)	
C(9)	0.4351(8)	0.0448(4)	-0.1479(7)	3.6(2)	
C(10)	0.4476(6)	0.1156(5)	-0.1419(6)	3.3(2)	
C(11)	0.5430(9)	0.3597(5)	-0.0612(8)	4.7(3)	
C(12)	0.4265(8)	0.4569(5)	-0.1472(7)	4.2(3)	
C(13)	0.3568(8)	0.2220(5)	-0.2259(7)	3.6(2)	
C(14)	0.2700(7)	0.2480(5)	-0.2929(7)	4.1(2)	
C(15)	0.2483(7)	0.3156(5)	-0.3069(7)	4.1(2)	
F(1)	0.098(1)	0.2843(4)	-0.4296(9)	7.7(4)	0.720
F(2)	0.1660(9)	0.3820(6)	-0.4446(9)	7.7(3)	0.720
F(3)	0.0828(9)	0.3645(6)	-0.3239(7)	7.7(3)	0.720
F(4)	0.155(2)	0.304(2)	-0.479(2)	7.997	0.280
F(5)	0.121(3)	0.390(1)	-0.392(2)	7.997	0.280
F(6)	0.065(2)	0.291(1)	-0.363(2)	7.997	0.280
C(16a)	0.1438(6)	0.3368(4)	-0.3793(6)	7.700	0.720
C(16b)	0.142(2)	0.325(1)	-0.389(2)	7.997	0.280
H(1)	0.1001	0.1045	-0.1642	7.837	
H(2)	0.2026	0.1992	-0.0589	9.558	
H(3)	0.3388	0.1421	0.0756	10.390	
H(4)	0.3224	0.0153	0.0487	9.129	
H(5)	0.1662	-0.0076	-0.0849	9.006	
H(6)	0.2519	0.1015	-0.3233	4.139	
H(7)	0.3248	-0.0128	-0.2511	4.623	
H(8)	0.4756	0.0118	-0.1060	4.290	
H(9)	0.4991	0.1386	-0.0944	3.716	
H(10)	0.2238	0.2161	-0.3307	4.916	

$B_{eq} = 8/3 \ \pi^2(U_{11}(aa^*)^2 + U_{22}(bb^*)^2 + U_{33}(cc^*)^2 + 2U_{12}(aa^*bb^*)\cos\gamma + 2U_{13}(aa^*cc^*)\cos\beta + 2U_{23}(bb^*cc^*)\cos\alpha)$

Anisotropic displacement parameters of [Rh(fctfa)(CO)$_2$] with e.s.d.'s in parentheses.

atom	U_{11}	U_{22}	U_{33}	U_{12}	U_{13}	U_{23}
Rh(1)	0.0425(4)	0.0387(4)	0.0437(5)	-0.0102(4)	0.0015(3)	-0.0044(4)
Fe(1)	0.0448(8)	0.0434(8)	0.0459(9)	-0.0041(7)	0.0079(7)	-0.0016(7)
O(1)	0.085(6)	0.068(5)	0.098(7)	-0.011(5)	-0.029(5)	-0.003(5)
O(2)	0.071(5)	0.041(4)	0.109(7)	-0.003(4)	-0.010(5)	-0.001(4)
O(3)	0.058(4)	0.030(3)	0.053(4)	-0.010(3)	0.001(3)	0.002(3)
O(4)	0.053(4)	0.043(4)	0.056(4)	0.002(3)	-0.016(3)	-0.004(4)
C(1)	0.077(9)	0.09(1)	0.082(9)	-0.021(9)	0.015(8)	-0.017(9)
C(2)	0.12(1)	0.09(1)	0.11(1)	0.03(1)	0.07(1)	0.02(1)
C(3)	0.11(1)	0.16(2)	0.07(1)	-0.04(1)	0.05(1)	-0.06(1)
C(4)	0.09(1)	0.12(1)	0.08(1)	0.01(1)	0.033(9)	0.03(1)
C(5)	0.09(1)	0.066(9)	0.15(1)	-0.016(8)	0.07(1)	0.014(9)
C(6)	0.027(5)	0.047(6)	0.030(5)	-0.002(4)	-0.000(4)	0.000(4)
C(7)	0.043(6)	0.048(6)	0.037(6)	-0.000(5)	-0.002(5)	-0.006(5)
C(8)	0.067(7)	0.037(6)	0.044(6)	-0.000(5)	0.016(6)	-0.015(5)
C(9)	0.055(6)	0.034(5)	0.039(6)	0.001(5)	-0.008(5)	0.010(5)
C(10)	0.030(5)	0.058(6)	0.030(6)	-0.006(4)	-0.016(4)	0.002(4)
C(11)	0.076(8)	0.036(5)	0.063(8)	-0.016(6)	0.002(7)	-0.004(6)
C(12)	0.053(6)	0.038(6)	0.063(7)	-0.019(5)	0.004(5)	-0.014(5)
C(13)	0.063(7)	0.033(5)	0.039(6)	-0.019(5)	0.007(5)	-0.007(4)
C(14)	0.042(6)	0.041(6)	0.059(7)	-0.008(4)	-0.022(5)	-0.003(5)
C(15)	0.043(6)	0.053(7)	0.048(6)	0.002(5)	-0.021(5)	0.001(5)

The general temperature factor expression:

$$\exp(-2\pi^2(a^{*2}U_{11}h^2 + b^{*2}U_{22}k^2 + c^{*2}U_{33}l^2 + 2a^*b^*U_{12}hk + 2a^*c^*U_{13}hl + 2b^*c^*U_{23}kl))$$

B.3 [Rh(fctfa)(CO)(PPh$_3$)]

Anisotropic thermal parameters (x 10^3) for [Rh(fctfa)(CO)(PPh$_3$)] with e.s.d.'s in parentheses.

ATOM	U_{11}	U_{22}	U_{33}	U_{23}	U_{13}	U_{12}
Rh	33.3(1)	34.6(1)	59.1(2)	14.3(1)	14.7(1)	12.6(1)
Fe	45.8(3)	42.6(3)	47.3(3)	15.8(3)	15.3(3)	15.8(3)
P	35.7(5)	31.1(4)	47.5(6)	12.0(4)	12.6(4)	11.0(4)
O(1)	41(1)	42(1)	55(2)	7(1)	13(1)	16(1)
O(2)	44(2)	49(2)	80(2)	17(2)	21(2)	23(1)
C(51)	37(2)	36(2)	47(2)	13(2)	12(2)	10(1)
C(1)	47(2)	37(2)	52(2)	17(2)	20(2)	15(2)
C(31)	37(2)	40(2)	46(2)	18(2)	13(2)	14(1)
C(5)	40(2)	50(2)	70(3)	19(2)	12(2)	14(2)
C(15)	56(2)	43(2)	51(2)	15(2)	13(2)	21(2)
O(3)	49(2)	83(3)	90(3)	18(2)	-2(2)	19(2)
C(3)	54(2)	43(2)	81(3)	25(2)	37(2)	29(2)
C(32)	51(2)	45(2)	66(3)	23(2)	25(2)	24(2)
C(36)	55(2)	36(2)	66(3)	15(2)	27(2)	12(2)
C(12)	59(3)	47(2)	53(3)	15(2)	24(2)	17(2)
C(11)	50(2)	37(2)	49(2)	14(2)	18(2)	15(2)
C(41)	51(2)	34(2)	42(2)	9(2)	14(2)	17(2)
C(56)	60(3)	53(3)	55(3)	20(2)	8(2)	15(2)
C(53)	62(3)	39(2)	67(3)	10(2)	21(2)	10(2)
C(33)	53(3)	67(3)	74(3)	32(3)	31(2)	31(2)
C(43)	103(4)	60(3)	57(3)	21(2)	35(3)	29(3)
C(42)	63(3)	52(2)	48(2)	14(2)	19(2)	20(2)
C(2)	54(2)	47(2)	67(3)	17(2)	25(2)	26(2)
C(14)	53(3)	54(2)	56(3)	20(2)	9(2)	20(2)
C(54)	52(3)	50(3)	71(3)	-5(2)	5(2)	7(2)

C(46)	57(3)	62(3)	53(3)	20(2)	16(2)	29(2)
C(44)	115(5)	74(4)	50(3)	26(3)	22(3)	48(4)
C(13)	61(3)	51(2)	47(2)	17(2)	15(2)	13(2)
C(52)	55(2)	39(2)	49(2)	14(2)	17(2)	12(2)
C(34)	46(2)	70(3)	65(3)	30(3)	23(2)	16(2)
C(35)	58(3)	47(2)	68(3)	18(2)	24(2)	4(2)
F(3)	131(4)	149(4)	290(7)	81(5)	153(5)	86(4)
C(45)	84(4)	86(4)	61(3)	26(3)	13(3)	49(3)
C(23)	93(4)	43(2)	78(4)	23(3)	27(3)	12(3)
C(22)	78(4)	77(4)	123(5)	65(4)	53(4)	47(3)
F(2)	218(6)	232(6)	208(6)	141(5)	134(5)	200(6)
F(1)	121(4)	177(5)	189(5)	-68(4)	-2(3)	112(4)
C(25)	86(4)	68(3)	72(4)	34(3)	41(3)	23(3)
C(55)	63(3)	77(4)	51(3)	11(3)	-4(2)	19(3)
C(4)	69(4)	75(4)	112(5)	24(4)	41(4)	45(3)
C(24)	57(3)	71(3)	96(4)	44(3)	31(3)	19(3)
C(21)	72(4)	87(4)	77(4)	54(3)	4(3)	8(3)

Fractional coordinates $(x10^4)$ and equivalent isotropic thermal parameters $(\text{Å}^2 x10^3)$ for [Rh(fctfa)(CO)(PPh$_3$)] with e.s.d.'s in parentheses.

ATOM	x/a	y/b	z/c	U_{eq}	ATOM	x/a	y/b	z/c	U_{eq}
Rh	2093.5(3)	3117.7(3)	858.9(3)	43.31(7)	H(14)	8765(5)	5857(4)	4891(4)	86(3)*
Fe	7035.5(6)	6926.9(5)	4045.9(5)	45.8(1)	C(54)	829(5)	-1837(4)	-2567(5)	70(1)
P	3176.1(10)	1860.1(8)	334.6(9)	39.3(2)	H(54)	289(5)	-2698(4)	-3255(5)	86(3)*
O(1)	3825(3)	4066(2)	2235(2)	49(1)	C(46)	5167(5)	1664(4)	1950(4)	56(1)
O(2)	1175(3)	4287(3)	1546(3)	58(1)	H(46)	5961(5)	2037(4)	1597(4)	86(3)*
C(51)	2223(4)	382(3)	-801(3)	42(1)	C(44)	4530(7)	851(5)	3282(4)	76(2)
C(1)	4030(4)	4978(3)	3079(3)	45(1)	H(44)	4827(7)	591(5)	3963(4)	86(3)*
C(31)	4753(4)	2489(3)	-31(3)	41(1)	C(13)	7292(5)	6659(4)	5505(4)	56(1)
C(S)	626(5)	2296(4)	-392(4)	56(1)	H(13)	7939(5)	7318(4)	6321(4)	86(3)*
C(15)	6564(5)	5150(4)	3781(4)	51(1)	C(52)	2042(5)	-689(3)	-651(4)	50(1)
H(15)	6562(5)	4463(4)	3057(4)	86(3)*	H(52)	2459(5)	-659(3)	166(4)	86(3)*
O(3)	-309(4)	1803(4)	-1189(3)	83(1)	C(34)	7210(5)	3500(5)	-516(4)	60(1)
C(3)	1729(5)	5112(4)	2504(4)	54(1)	H(34)	8169(5)	3895(5)	-699(4)	86(3)*
C(32)	5325(5)	1760(4)	-653(4)	51(1)	C(35)	6658(5)	4231(4)	94(4)	62(1)
H(32)	4812(5)	791(4)	-950(4)	86(3)*	H(35)	7187(5)	5199(4)	391(4)	86(3)*
C(36)	5425(5)	3738(4)	333(4)	54(1)	F(3)	-366(5)	5022(5)	2901(6)	169(2)
H(36)	4987(5)	4321(4)	801(4)	86(3)*	C(45)	5530(7)	1345(5)	2840(5)	75(1)
C(12)	5865(5)	6422(4)	5003(4)	54(1)	H(45)	6617(7)	1488(5)	3188(5)	86(3)*
H(12)	5235(5)	6873(4)	5367(4)	86(3)*	C(23)	8097(7)	8706(4)	4376(5)	75(1)
C(11)	5401(4)	5480(3)	3929(3)	46(1)	H(23)	8620(7)	9419(4)	5188(5)	86(3)*
C(41)	3772(4)	1498(3)	1517(3)	43(1)	C(22)	6686(6)	8318(5)	3758(6)	78(2)
C(56)	1700(5)	327(4)	-1851(4)	60(1)	H(22)	5925(6)	8676(5)	4005(6)	86(3)*
H(56)	1832(5)	1150(4)	-1988(4)	86(3)*	F(2)	283(6)	6129(6)	2117(5)	166(2)
C(53)	1340(5)	-1793(4)	-1526(4)	61(1)	F(1)	1269(5)	6832(5)	3770(5)	191(2)
H(53)	1195(5)	-2617(4)	-1389(4)	86(3)*	C(25)	7687(7)	1190(5)	2769(5)	73(1)
C(33)	6552(5)	2269(5)	-897(4)	60(1)	H(25)	7839(7)	6522(5)	2121(5)	86(3)*
H(33)	6985(5)	1696(5)	-1384(4)	86(3)*	C(55)	1005(5)	-783(5)	-2736(4)	72(1)
C(43)	3150(7)	686(5)	2863(4)	73(1)	H(55)	602(5)	-318(5)	-3558(4)	86(3)*
H(43)	2364(7)	298(5)	3215(4)	86(3)*	C(4)	759(6)	5742(6)	2841(6)	82(2)
C(42)	2766(5)	1019(4)	1986(4)	56(1)	C(24)	8706(6)	8009(5)	3159(5)	72(1)
H(42)	1684(5)	906(4)	1868(4)	86(3)*	H(24)	9787(6)	8093(5)	4010(5)	86(3)*
C(2)	3027(5)	5499(4)	3250(4)	55(1)	C(21)	6442(6)	7372(6)	2752(5)	82(2)
H(2)	3302(5)	6253(4)	4019(4)	86(3)*	H(21)	5460(6)	6880(6)	2088(5)	86(3)*
G(14)	7726(5)	5884(4)	4751(4)	56(1)	-	-	-	-	-

* isotropic temperature factor.

$$U_{eq} = \frac{1}{3}\sum_i \sum_j U_{ij} a_i^* a_j^* (a_i a_j)$$

B.4 [Rh(fctfa)(CO)(PPh₃)(CH₃)I].

Atomic coordinates (x 10^4) and equivalent isotropic displacement parameters (A^2 x 10^3) for [Rh(fctfa)(CO)(PPh₃)(CH₃)I] with e.s.d.'s in parentheses. $U_{eq} = \frac{1}{3} \sum_i \sum_j U_{ij} a_i^* a_j^* (a_i a_j)$.

Atom	x	y	z	U_{eq}	Atom	x	y	z	U_{eq}
Rh	5270(1)	3502(1)	3695(1)	42(1)	C(24)	9483(9)	2946(8)	1851(6)	87(3)
I	7703(1)	3928(1)	3971(1)	64(1)	C(25)	8958(11)	3670(11)	2163(6)	106(5)
Fe	7813(1)	3281(1)	1388(1)	57(1)	C(31)	2901(7)	2588(5)	2708(3)	47(2)
P	3188(2)	3123(1)	3502(1)	43(1)	C(32)	2602(8)	1701(5)	2664(4)	63(2)
F(1)	7610(12)	938(9)	4198(9)	97(5)	C(33)	2489(9)	1270(7)	2066(5)	74(3)
F(2)	7350(3)	348(10)	3252(6)	144(8)	C(34)	2669(8)	1724(7)	1506(5)	72(3)
F(3)	5960(2)	357(13)	3918(12)	139(8)	C(35)	2948(8)	2606(7)	1533(4)	68(2)
O(1)	5596(5)	3359(3)	2711(2)	47(1)	C(36)	3086(7)	3043(6)	2140(4)	55(2)
O(2)	5842(5)	2146(3)	3839(2)	52(1)	C(41)	2119(7)	4051(5)	3549(4)	54(2)
O(3)	4865(8)	3956(5)	5067(3)	85(2)	C(42)	1981(9)	4394(7)	4172(4)	72(2)
C(1)	6096(6)	2710(5)	2444(3)	44(2)	C(43)	1213(9)	5130(8)	4247(5)	83(3)
C(2)	6495(8)	1921(6)	2753(4)	60(2)	C(44)	614(9)	5501(7)	3712(6)	82(3)
C(3)	6355(8)	1706(5)	3399(4)	53(2)	C(45)	755(9)	5174(6)	3107(5)	74(2)
C(4)	6851(13)	829(6)	3664(5)	80(3)	C(46)	1503(7)	4447(6)	3019(4)	57(2)
C(5)	5035(8)	3752(6)	4555(4)	56(2)	C(51)	2605(7)	2339(5)	4083(3)	53(2)
C(6)	4858(9)	4811(5)	3469(4)	63(2)	C(52)	3407(9)	1803(6)	4482(4)	63(2)
C(11)	6225(7)	2819(6)	1735(4)	56(2)	C(53)	2908(10)	1184(6)	4885(4)	68(2)
C(12)	5986(8)	3601(8)	1367(4)	70(3)	C(54)	1679(11)	1098(7)	4911(5)	82(3)
C(13)	6334(11)	3466(11)	727(5)	96(4)	C(55)	878(10)	1617(8)	4525(5)	85(3)
C(14)	6775(12)	2609(10)	683(5)	95(4)	C(56)	1320(9)	2247(7)	4112(5)	72(2)
C(15)	6721(9)	2182(7)	1294(4)	69(2)	F(11)	8050(3)	690(4)	3560(3)	200(3)
C(21)	8809(11)	4345(8)	1662(8)	105(4)	F(12)	6620(14)	650(4)	4160(2)	360(6)
C(22)	9253(11)	4023(7)	1093(6)	88(3)	F(13)	6320(5)	221(19)	3280(4)	190(3)
C(23)	9635(9)	3185(8)	1195(6)	81(3)					

Hydrogen coordinates (x 10^4) and isotropic displacement parameters (A^2 x 10^3) for [Rh(fctfa)(CO)(PPh₃)(CH₃)I].

ATOM	x	y	z	U_{eq}	ATOM	x	y	z	U_{eq}
H(2)	6885	1509	2500	95(7)	H(33)	2292	673	2046	95(7)
H(61)	4285	4702	3200	95(7)	H(34)	2601	1434	1104	95(7)
H(62)	4617	5138	3748	95(7)	H(35)	3046	2916	1147	95(7)
H(63)	5415	5050	3288	95(7)	H(36)	3301	3637	2158	95(7)
H(12)	5653	4119	1525	95(7)	H(42)	2398	4136	4539	95(7)
H(13)	6279	3880	389	95(7)	H(43)	1118	5360	4662	95(7)
H(14)	7061	2355	308	95(7)	H(44)	100	5987	3760	95(7)
H(15)	6958	1605	1394	95(7)	H(45)	342	5442	2743	95(7)
H(21)	8469	4902	1715	95(7)	H(46)	1585	4228	2598	95(7)
H(22)	9284	4335	702	95(7)	H(52)	4266	1863	4476	95(7)
H(23)	9951	2821	881	95(7)	H(53)	3440	820	5143	95(7)
H(24)	9693	2405	2043	95(7)	H(54)	1366	684	5192	95(7)
H(25)	8753	3706	2597	95(7)	H(55)	23	1544	4542	95(7)
H(32)	2475	1389	3045	95(7)	H(56)	772	2604	3857	95(7)

Anisotropic displacement parameters (A^2 x 10^3) for [Rh(fctfa)(CO)(PPh$_3$)(CH$_3$)I] with e.s.d.'s in parentheses. The anisotropic displacement factor exponent takes the form:

$$\exp(-2\pi^2(a^{*2}U_{11}h^2 + b^{*2}U_{22}k^2 + c^{*2}U_{33}l^2 + 2a^*b^*U_{12}hk + 2a^*c^*U_{13}hl + 2b^*c^*U_{23}kl))$$
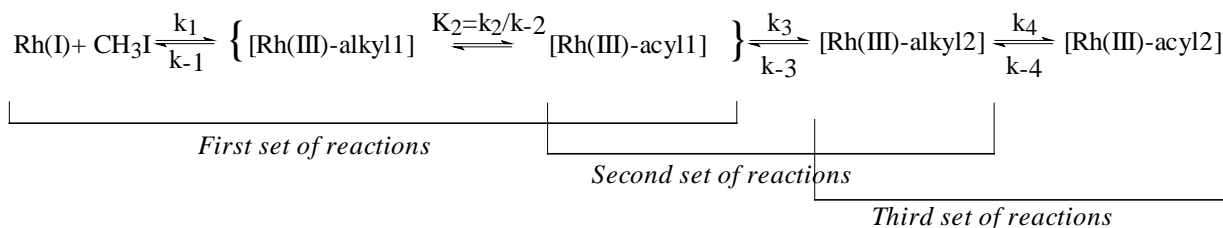
ATOM	U_{11}	U_{22}	U_{33}	U_{23}	U_{13}	U_{12}
Rh	53(1)	38(1)	34(1)	1(1)	9(1)	-2(1)
I	62(1)	74(1)	55(1)	2(1)	1(1)	-16(1)
Fe	59(1)	67(1)	48(1)	-3(1)	18(1)	-5(1)
P	54(1)	43(1)	35(1)	1(1)	11(1)	-1(1)
F(1)	107(8)	84(8)	96(12)	17(6)	-19(8)	14(5)
F(2)	270(2)	91(9)	73(7)	4(6)	26(11)	113(13)
F(3)	161(13)	73(10)	179(19)	51(11)	-6(13)	-39(10)
O(1)	51(3)	52(3)	40(3)	4(2)	13(2)	0(2)
O(2)	66(3)	40(3)	51(3)	4(2)	13(2)	1(2)
O(3)	113(6)	94(5)	46(4)	-16(3)	2(3)	15(4)
C(1)	45(4)	53(4)	34(3)	-2(3)	6(3)	-3(3)
C(2)	77(5)	56(5)	49(4)	-7(4)	21(4)	1(4)
C(3)	71(5)	40(4)	50(4)	-5(3)	10(4)	0(3)
C(4)	133(10)	49(5)	60(6)	1(5)	21(6)	17(6)
C(5)	58(5)	53(4)	56(5)	-6(4)	1(4)	7(4)
C(6)	80(6)	45(4)	66(5)	5(4)	10(4)	-8(4)
C(11)	55(4)	74(5)	38(4)	-6(4)	11(3)	-13(4)
C(12)	56(5)	110(8)	45(4)	21(5)	10(4)	13(5)
C(13)	88(7)	159(13)	42(5)	22(7)	15(5)	-14(8)
C(14)	107(8)	138(11)	43(5)	-26(6)	23(5)	-43(8)
C(15)	73(6)	84(6)	53(5)	-24(5)	20(4)	-24(5)
C(21)	76(7)	68(7)	171(14)	-31(8)	14(8)	-12(5)
C(22)	83(7)	82(7)	103(8)	12(6)	39(6)	-15(6)
C(23)	63(6)	80(7)	104(8)	5(6)	34(5)	12(5)
C(24)	71(6)	97(8)	93(8)	13(7)	6(5)	-13(6)
C(25)	77(7)	168(14)	75(7)	-36(8)	17(6)	-44(8)
C(31)	51(4)	51(4)	41(4)	1(3)	13(3)	0(3)
C(32)	82(6)	51(4)	60(5)	-13(4)	24(4)	-10(4)
C(33)	82(6)	69(6)	74(6)	-25(5)	22(5)	-12(5)
C(34)	61(5)	94(7)	63(6)	-31(5)	10(4)	2(5)
C(35)	61(5)	103(8)	42(4)	5(5)	17(4)	4(5)
C(36)	61(5)	59(5)	44(4)	3(4)	4(3)	7(4)
C(41)	55(4)	46(4)	60(5)	-6(4)	8(4)	-3(3)
C(42)	82(6)	76(6)	57(5)	-12(5)	4(4)	17(5)
C(43)	75(6)	96(8)	79(7)	-35(6)	17(5)	11(6)
C(44)	61(5)	66(6)	120(9)	-33(6)	5(6)	0(5)
C(45)	72(6)	63(5)	86(7)	-7(5)	-6(5)	8(5)
C(46)	60(5)	58(5)	52(4)	-3(4)	3(4)	0(4)
C(51)	66(5)	55(4)	39(4)	-3(3)	20(3)	-11(4)
C(52)	75(6)	67(5)	51(5)	9(4)	26(4)	-7(4)
C(53)	83(6)	64(5)	60(5)	18(4)	20(4)	0(5)
C(54)	109(9)	69(6)	71(6)	3(5)	37(6)	-30(6)
C(55)	71(6)	108(9)	81(7)	9(6)	27(5)	-27(6)
C(56)	69(6)	87(6)	64(5)	16(5)	20(4)	-18(5)
F(11)	90(2)	290(6)	210(5)	150(4)	-20(2)	50(3)
F(12)	910(18)	110(3)	100(3)	90(3)	250(7)	290(7)
F(13)	220(4)	32(12)	310(8)	-20(3)	-50(5)	-14(19)

332

Abstract.

Synthetic routes to prepare new Rh(I)-β-diketonate complexes [Rh(FcCOCHCOR)(CO)$_2$] and [Rh(FcCOCHCOR)(CO)(PPh$_3$)] with Fc = ferrocenyl and R = Fc, C$_6$H$_5$, CH$_3$ and CF$_3$ have been developed and optimized. Optimized synthetic routes to iridium(I) complexes, [Ir(R'COCHCOR)(cod)], with R' = Fc and R = C$_6$H$_5$, CH$_3$ and CF$_3$, or with R' = CF$_3$ and R = CH$_2$CH$_3$, CH(CH$_3$)$_2$ and C(CH$_3$)$_3$ have also been developed.

^{1}H and ^{31}P NMR studies indicated that for complexes of the type [Rh(β-diketonato)(CO)(PPh$_3$)] with an unsymmetrical β-diketonato ligand, at least two main isomers exist in solution. The structure of one isomer of [Rh(fctfa)(CO)(PPh$_3$)], as well as crystal structures of FcCOCH$_2$COCF$_3$, [Rh(fctfa)(CO)$_2$] and [Rh(fctfa)(CO)(PPh$_3$)(CH$_3$)(I)] were solved.

The chemical kinetics of the oxidative addition of iodomethane to [Rh(FcCOCHCOR)(CO)(PPh$_3$)] has been studied utilizing IR, UV/visible, ^{1}H NMR and ^{31}P NMR techniques. The NMR studies revealed that the rate of oxidative addition of iodomethane to the different [Rh(FcCOCHCOR)(CO)(PPh$_3$)] isomers was the same. A complete general reaction sequence for the oxidative addition of iodomethane to all [Rh(bidentate ligand)(CO)(PPh$_3$)] complexes is:

$$Rh(I) + CH_3I \underset{k_{-1}}{\overset{k_1}{\rightleftarrows}} \left\{ [Rh(III)\text{-alkyl1}] \overset{K_2=k_2/k_{-2}}{\rightleftharpoons} [Rh(III)\text{-acyl1}] \right\} \underset{k_{-3}}{\overset{k_3}{\rightleftarrows}} [Rh(III)\text{-alkyl2}] \underset{k_{-4}}{\overset{k_4}{\rightleftarrows}} [Rh(III)\text{-acyl2}]$$

First set of reactions

Second set of reactions

Third set of reactions

^{1}H and ^{31}P NMR studies further showed that all rhodium-containing complexes in the above mentioned reaction scheme, are actually composed of at least two main isomers, that is Rh(I)A $\overset{K_{c1}}{\square}$ Rh(I)B, Rh(III)-alkyl 1A $\overset{K_{c2}}{\square}$ Rh(III)-alkyl 1B, Rh(III)-acyl 1A $\overset{K_{c3}}{\square}$ Rh(III)-acyl 1B, Rh(III)-alkyl 2A $\overset{K_{c4}}{\square}$ Rh(III)-alkyl 2B, Rh(III)-acyl 2A $\overset{K_{c5}}{\square}$ Rh(III)-acyl 2B.

The kinetics of substitution of the β-diketonato ligand with 1,10-phenanthroline from [Rh(FcCOCHCOH)(cod)] and [Ir(FcCOCHCOR)(cod)] (R= CF$_3$, CH$_3$ and C$_6$H$_5$) showed that

the rate of substitution becomes faster when the group electronegativity of the R groups increases. This tendency is, as expected, exactly the opposite to what was observed during oxidative addition. A general reaction mechanism for both Rh and Ir complexes was presented. An additional study on the rate of the β-diketonato substitution with 1,10-phenanthroline in complexes of the type [Ir(CF$_3$COCHCOR)(cod)] with R = CH$_3$, CH$_2$CH$_3$, CH(CH$_3$)$_2$ and C(CH$_3$)$_3$ showed that the size of R does not hamper the rate of substitution. All substitution reactions were independent of a solvent step.

The cyclic voltammetry study of all the ferrocene-containing β-diketonato complexes of rhodium(I) and iridium(I) synthesized, exhibited a single electrochemically reversible redox couple corresponding to the formal reduction potential of the ferrocenyl group of the β-diketonato ligand coordinated to the rhodium or iridium complexes, as well as an electrochemically irreversible anodic oxidation peak which corresponds to the oxidation of the metal = Rh or Ir.

The ^{31}P NMR study on different six-membered chelate complexes, [Rh(L,L'-BID)(CO)(PPh$_3$)], and related Rh(III) complexes, indicated a general decrease in coupling constants $^1J(^{31}$P-^{103}Rh) as the Rh-P bond length, determined by X-ray crystallography, increases according to the relationship d(Rh-P) = -0.0014(1) x $^1J(^{31}$P-^{103}Rh) + 2.49(2). The Rh-P bond lengths, d(Rh-P), varied between 2.23 Å and 2.36 Å.

The electron density on the Rh(I) and Ir(I) metal centres was manipulated over a wide range by changing the R group on the coordinated ligand (FcCOCHCOR)$^-$ from the highly electron donating Fc group (χ_{Fc} = 1.87) to C$_6$H$_5$, (χ_{C6H5} = 2.21) to CH$_3$(χ_{CH3} = 2.34) to the strongly electron withdrawing CF$_3$ group (χ_{CF3} = 3.01). The effect of the different R groups on the β-diketonato ligand (FcCOCHCOR)$^-$ coordinated to the rhodium(I) and iridium(I) complexes was not only observed in kinetic rate constants, but also in formal reduction potentials of the ferrocenyl group, the oxidation potential of Rh(I) or Ir(I), pK$_a$-values, IR stretching frequencies, and crystallographic bond lengths.
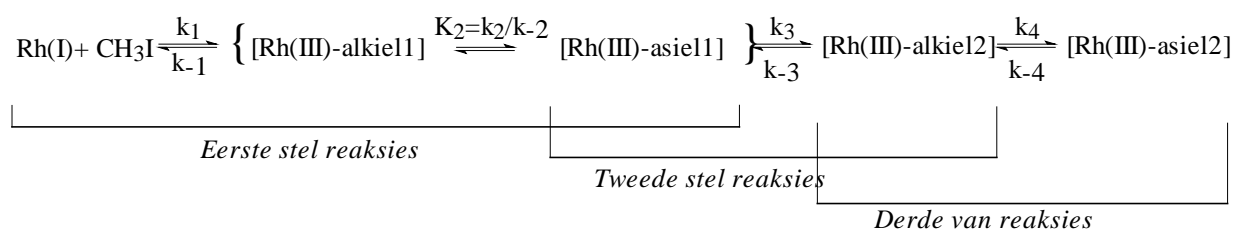
Key words.

Opsomming.

Sintese-tegnieke om nuwe Rh(I)-β-diketonato komplekse [Rh(FcCOCHCOR)(CO)$_2$] en [Rh(FcCOCHCOR)(CO)(PPh$_3$)] met Fc = ferroseniel en R = Fc, C$_6$H$_5$, CH$_3$ and CF$_3$ te berei, is ontwikkel en geoptimiseer. Geoptimiseerde sintese-tegnieke vir die bereiding van iridium(I) komplekse, [Ir(R'COCHCOR)(cod)], met R' = Fc en R = C$_6$H$_5$, CH$_3$ en CF$_3$, of met R' = CF$_3$ en R = CH$_2$CH$_3$, CH(CH$_3$)$_2$ en C(CH$_3$)$_3$, is ook ontwikkel.

^{1}H- en ^{31}P-KMR-studies van die komplekse [Rh(β-diketonato)(CO)(PPh$_3$)] wat 'n asimmetriese β-diketonato-ligand bevat, het aangetoon dat daar ten minste twee isomere van hierdie komplekse in oplossing bestaan. Die kristalstruktuur van een van die isomere van [Rh(fctfa)(CO)(PPh$_3$)], asook die kristalstrukture van FcCOCH$_2$COCF$_3$, [Rh(fctfa)(CO)$_2$] en [Rh(fctfa)(CO)(PPh$_3$)(CH$_3$)(I)] is opgeklaar.

Die oksidatiewe addisie van metieljodied aan [Rh(FcCOCHCOR)(CO)(PPh$_3$)] is deur middel van infra-rooi, UV/sigbaar, ^{1}H-KMR en ^{31}P-KMR-spektroskopie ondersoek. Die KMR-studies het getoon dat die tempo van oksidatiewe addisie van metieljodied aan die verskillende [Rh(FcCOCHCOR)(CO)(PPh$_3$)] isomere, dieselfde was. Die voorgestelde algemene reaksieskema vir die oksidatiewe addisie van metieljodied aan [Rh(bidentate-ligand)(CO)(PPh$_3$)] komplekse is:

$$\text{Rh(I)}+ \text{CH}_3\text{I} \underset{k_{-1}}{\overset{k_1}{\rightleftharpoons}} \left\{ \text{[Rh(III)-alkiel1]} \underset{}{\overset{K_2=k_2/k_{-2}}{\rightleftharpoons}} \text{[Rh(III)-asiel1]} \right\} \underset{k_{-3}}{\overset{k_3}{\rightleftharpoons}} \text{[Rh(III)-alkiel2]} \underset{k_{-4}}{\overset{k_4}{\rightleftharpoons}} \text{[Rh(III)-asiel2]}$$

Eerste stel reaksies

Tweede stel reaksies

Derde van reaksies

Die ^{1}H- en ^{31}P-KMR-studies het verder aangetoon dat alle rodiumbevattende komplekse in bogenoemde reaksieskema uit minstens twee isomere bestaan, naamlik Rh(I)A $\overset{K_{c1}}{\square}$ Rh(I)B, Rh(III)-alkiel 1A $\overset{K_{c2}}{\square}$ Rh(III)-alkiel 1B, Rh(III)-asiel 1A $\overset{K_{c3}}{\square}$ Rh(III)-asiel 1B, Rh(III)-alkiel 2A $\overset{K_{c4}}{\square}$ Rh(III)-alkiel 2B, Rh(III)-asiel 2A $\overset{K_{c5}}{\square}$ Rh(III)-asiel 2B.

Resultate van die substitusiekinetika van [Rh(FcCOCHCOH)(cod)] en [Ir(FcCOCHCOR)(cod)] (R= CF$_3$, CH$_3$ and C$_6$H$_5$) met 1,10-fenantrolien, het aangetoon dat die tempo van substitusie toegeneem het namate die groepelektronegatiwiteit van die R-groepe toegeneem het. Soos verwag, is hierdie tendens die teenoorgestelde as wat in die geval van oksidatiewe addisie waargeneem is. 'n Algemene reaksieskema vir beide rodium en iridium komplekse is voorgestel. 'n Addisionele studie van die tempo van substitusie van die β-diketonato-ligand met 1,10-fenantrolien in komplekse van die tipe [Ir(CF$_3$COCHCOR)(cod)] met R = CH$_3$, CH$_2$CH$_3$, CH(CH$_3$)$_2$ en C(CH$_3$)$_3$, het aangetoon dat die grootte van R nie die tempo van substitusie vertraag nie. Alle substitusiereaksies was onafhanklik van 'n oplosmiddelroete.

Die sikliese voltammetriese studie van alle gesintetiseerde ferroseen-bevattende β-diketonato-komplekse van rodium(I) en iridium(I), het 'n elektrochemies omkeerbare redox koppel bevat, wat ooreengestem het met die formele reduksiepotensiaal van die ferrosenielgroep van die β-diketonato-ligand gekoördineer aan die rodium of iridium komplekse, asook 'n chemies onomkeerbare anodiese oksidasiepotensiaal, wat ooreengestem het met die oksidasie van rodium of iridium.

Die ^{31}P-KMR-studie van verskillende seslid chelaatkomplekse, [Rh(L,L'-BID)(CO)(PPh$_3$)], en verwante Rh(III) komplekse, het 'n algemene afname in die koppelingskonstante $^1J(^{31}$P-^{103}Rh) getoon namate die kristallografies bepaalde Rh-P bindingslengtes toegeneem het, met die lineêre verwantskap d(Rh-P) = -0.0014(1) x $^1J(^{31}$P-^{103}Rh) + 2.49(2). Die Rh-P bindingslengtes, d(Rh-P), het tussen 2.23 Å en 2.36 Å gewissel.

Die elektrondigtheid op die Rh(I) and Ir(I) metaalsentra is oor 'n groot gebied gevarieër deur die R-groep op die gekoördineerde (FcCOCHCOR)$^-$ ligand te wissel vanaf die sterk elektrondonerende Fc-groep (χ$_{Fc}$ = 1.87), na C$_6$H$_5$, (χ$_{C6H5}$ = 2.21), na CH$_3$ (χ$_{CH3}$ = 2.34), en na die sterk elektrononttrekkende CF$_3$-groep (χ$_{CF3}$ = 3.01). Die invloed van die verskillende R-groepe op die gekoördineerde β-diketonato-ligand (FcCOCHCOR)$^-$ aan die rodium(I) and iridium(I) komplekse, is nie alleenlik in die kinetiese tempokonstantes waargeneem nie, maar ook in die formele reduksiepotensiale van die ferrosenielgroep, die oksidasiepotensiaal van Rh(I) of Ir(I), pK$_a$-waardes, karbonielstrekkingsfrekwensies, en kristallografies bepaalde bindingslengtes.